TRANSACTIONS
OF THE ASME
Series E

Journal of APPLIED MECHANICS

December 1959

DYNAMICS • VIBRATIONS • ELASTICITY • LUBRICATION AND WEAR
RHEOLOGY • FRACTURES • STRUCTURES • HYDRAULICS • AERODYNAMICS
INTERNAL FLOW • MECHANICAL PROPERTIES OF METALS • THERMODYNAMICS
TURBULENCE • HEAT TRANSFER • COMPUTING DEVICES AND METHODS
BOUNDARY LAYERS • AEROELASTICITY • EXPERIMENTAL STRESS ANALYSIS

Published Quarterly by
THE AMERICAN SOCIETY OF MECHANICAL ENGINEERS

TRANSACTIONS
OF THE ASME
Series E

EDITORIAL DEPARTMENT

Editor, J. J. JAKLITSCH, JR.
Consulting Editor, LEO BLOSSETT
Art Editor, ROBERT GALFORD
Production, HELEN R. WILSON

APPLIED MECHANICS DIVISION

Chairman, W. PRAGER
Secretary, S. D. RATOSKY
Technical Editor, D. C. DRUCKER
Technical Editor, J. KESTIN
Acting Technical Editor, P. V. MACNEIL
Honorary Editor, ANNIE M. ARGERSLEV

OFFICERS OF THE ASME

President, G. B. WARREN
Secretary, O. B. SCHIER, II
Treasurer, E. J. KATES
Assistant Treasurer, H. J. RAMEY

PUBLICATIONS COMMITTEE

Chairman, JOSEPH GEIS
E. S. A. SHROTZKI
HENDLEY H. BLACKMON
R. D. MINDLIN
MARTIN SOLAND
Junior Representatives
A. T. WUSKA
A. S. GOLDSTEIN

REGIONAL ADVISORY BOARD

Region I, GUY L. FAUSKE
Region II, GLENN R. FRYLING
Region III, F. J. HEINZE
Region IV, FRANCIS C. SMITH
Region V, H. M. CATHER
Region VI, C. B. EARLE
Region VII, M. POPOVICH
Region VIII, LARS HELANDER

Published quarterly by The American Society of Mechanical Engineers. Publication office at 20th and Northampton Streets, Easton, Pa. The editorial departments is located at the headquarters of the Society, 29 West Thirty-Ninth Street, New York 18, N. Y. Cable address, "Mechanast," New York. Price $3.00 a copy, $10.00 annually to members, $6.50 a copy, $17.00 annually. Add 30 cents for postage to all countries outside the United States and Canada. Changes of address must be received at Society headquarters seven weeks before they are to be effective on the mailing list. Please send old as well as new address. . . . By-Laws. The Society shall not be responsible for statements or opinions advanced in papers or . . . printed in its publications (B13, Par. 4). . . . Second-class mail privileges authorized at Easton, Penna. . . . This publication is authorized to be mailed at the special rates of postage prescribed by Section 132.122 . . . © Copyright, 1959, by The American Society of Mechanical Engineers. Reprints from this publication may be made on condition that full credit be given the Transactions of the ASME, Series E—Journal of Applied Mechanics, and the author, and that date of publication be stated.

TRANSACTIONS OF THE ASME
is indexed by the Engineering Index, Inc.

Journal of
APPLIED MECHANICS

VOLUME 26 • SERIES E • NUMBER 4

December 1959

CONTENTS

TECHNICAL PAPERS

477 **Boundary-Layer Solution for a Flow in a Diverging Passage Having a Swirl Component**
M. A. Sinbel

485 **Slow Rotatory Motion of a Circular Disk About One of Its Diameters in a Viscous Fluid**
R. P. Kanwal

488 **Thermal Stresses Owing to a Hot Spot in a Rectangular Strip**
C. W. Nelson

491 **Impact and Moving Loads on a Slightly Curved Elastic Half Space**
A. C. Eringen and J. C. Samuels

499 **Stability of Forced Oscillations With Nonlinear Second-Order Terms**
Chi-Neng Shen

503 **On Inertia Effects in a Transient Thermoelastic Problem**
Eli Sternberg and J. G. Chakravorty

510 **Coupled Torsional and Longitudinal Vibrations of a Thin Bar**
R. C. Di Prima

513 **Production of Rotation in a Confined Liquid Through Translational Motion of the Boundaries**
R. R. Berlot

517 **Nonlinear Creep Deformations of Columns of Rectangular Cross Section**
H. H. Bleich and O. W. Dillon, Jr.

526 **Forced Vibrations of a Circular Plate**
Herbert Reismann

528 **On the Propagation of Shock Waves in a Nonhomogeneous Elastic Medium**
Eli Sternberg and J. G. Chakravorty

537 **The Frequency of Flexural Vibration of Rectangular Orthotropic Plates With Clamped or Supported Edges**
R. F. S. Hearmon

541 **Axially Symmetric Extensional Vibrations of a Circular Disk With a Concentric Hole**
O. G. Gustafsson and T. R. Kane

546 **Analysis of a Nonlinear Mechanical System With Three Degrees of Freedom**
S. A. Hovanessian

549 **Stresses in an Ellipsoidal Rotor in a Centrifugal Force Field**
M. A. Goldberg and Michael Sadowsky

553 **Carrying Capacity of Elastic-Plastic Shells With Various End Conditions**
Burton Paul

561 **Extensional Vibrations of Elastic Plates**
R. D. Mindlin and M. A. Medick

570 **Triaxial Tension at the Head of a Rapidly Running Crack in a Plate**
J. M. Frankland

573 **Viscous Flow Through Tubes of Multiply Connected Cross Sections**
F. A. Gaydon and H. Nuttall

577 **On the Accuracy of Some Shell Solutions**
G. D. Galletly and J. R. M. Radok

584 **The Drag on Spheres and Cylinders in a Stream of Dust-Laden Air**
Thomas Gillespie and A. W. Gunter

587 **Elastic Flexible Cable in Plane Motion Under Tension**
Wen-Hsiung Li

594 **Incremental Stress-Strain Law Applied to Work-Hardening Plastic Materials**
Chintsun Hwang

CONTENTS

599 **On the Plastic Flow of Coulomb Solids Beyond Original Failure**
A. W. Jenike and R. T. Shield

603 **The Free Vibrations of Grillages**
J. P. Ellington and H. McCallion

608 **Piping Flexibility Analysis by Stiffness Matrix**
L. H. Chen

613 **A Photoelastic Approach to Transient Stress Problems Employing Low-Modulus Materials**
J. W. Dally, W. F. Riley, and A. J. Durelli

621 **Rupture Characteristics of Safety Diaphragms**
N. A. Weil

625 **Bending of Isosceles Right Triangular Plates**
H. J. Fletcher

629 **Developments in the Application of the Grid Method to Dynamic Problems**
A. J. Durelli, J. W. Dally, and W. F. Riley

635 **The Solution of Elastic Stability Problems With the Electric Analog Computer**
J. H. Shields and R. H. MacNeal

643 **Symmetric Vortex Separation on Circular Cylinders and Cones**
A. E. Bryson

649 **Thermoelastic Problem for a Transversely Isotropic Hollow Sphere Embedded in an Elastic Medium**
J. Nowinski

651 **Transient Analysis of Stress-Wave Penetration in Plates**
Norman Davids

661 **Transverse Flexure of a Semi-Infinite Thin Plate Containing an Infinite Row of Circular Holes**
O. Tamate

666 **Fundamental Frequency of a Thin, Flat, Circular Plate Simply Supported Along a Circle of Arbitrary Radius**
R. Y. Bodine

BRIEF NOTES

669 Flexure of Cylindrically Aeolotropic Plate — *R. L. Thorkildsen and W. H. Hoppmann, II*

672 Heat Transfer From a Nonisothermal Disk — *J. P. Hartnett*

673 Harmonic Analysis of Crank-and-Rocker Mechanisms — *F. Freudenstein*

675 Deflection Curve of a Simply Supported Beam — *D. Gospodnetic*

676 On Plane-Stress Solution of a Compressible Wedge — *A. Kalnins*

678 An Application of a Reciprocal Theorem — *F. L. DiMaggio and H. H. Bleich*

679 Simple Thickness-Shear Modes of Vibration of Plates — *Yi-Yuan Yu*

681 The Nonlinear Conical Spring — *R. Schmidt and G. Wempner*

683 On the Calculation of Shallow Shells — *W. Flügge and D. A. Conrad*

685 A Solution of the Steady Linear Heat-Flow Equation — *R. P. Stein*

686 Bending of Thin Rectangular Plates — *M. N. Keshava Rao*

DISCUSSION

689 Discussion of previously published papers by *Y-T Chou and E. Saibel; J. N. Goodier, W. E. Jahsman, and E. A. Ripperger; I. R. Whiteman; V. C. Liu; K. E. Bisshopp*

BOOK REVIEWS

696 Plastic Design of Steel Frames

696 Introduction to Nuclear Engineering

696 Subsonic Gas Dynamics

697 Handbook of Physics

697 Jet Propulsion Engines

697 Stress and Strain Analysis

698 Nuclear Engineering Handbook

698 Classical Mechanics

698 Sound Pulses

TRANSACTIONS OF THE ASME Series B

Journal of ENGINEERING FOR INDUSTRY

Volume 81 • Series B • Number 4

CONTENTS FOR NOVEMBER, 1959

281 Dynamic Problems Associated With Satellite Orbit Control, by B. W. Augenstein. (59—Av-4)

289 Study of Machinability of Metals, by H. Takeyama and E. Usui. (58—A-161)

293 Four-Bar Linkages—Approximate Synthesis, by W. W. Worthley and R. T. Hinkle. (58—A-130)

301 A Theory for the Effect of Mean Stress on Fatigue of Metals Under Combined Torsion and Axial Load or Bending, by W. N. Findley. (58—A-61)

307 An Analysis of Critical Stresses and Mode of Failure of a Wire Rope, by W. L. Starkey and H. A. Cress. (58—A-63)

317 An Application of Statistics to the Dimensioning of Machine Parts, by M. F. Spotts. (58—A-44)

323 The Dynamic Analysis and Design of Relatively Flexible Cam Mechanisms Having More Than One Degree of Freedom, by R. C. Johnson. (58—A-192)

332 Power Heat Balance Considerations in Design and Operation of Industrial Plants, by J. L. Hudson. (58—A-166)

339 Influence of Hot and Cold Storage-Loads on the Refrigerated-Space Temperature of a Cooling Complex, by C. F. Kayan. (58—A-165)

348 Development and Uses of a New Line of Vibratory Feeders and Unit Vibrators, by A. F. Israelson. (59—SA-33)

353 A Mechanical Time-Delay Device Sensitive to Centrifugal Fields, by J. R. Baumgarten, R. Cohen, and A. S. Hall, Jr. (59—SA-9)

TRANSACTIONS OF THE ASME Series A

Journal of
ENGINEERING FOR POWER
Volume 81 • Series A • Number 4

CONTENTS FOR OCTOBER, 1959

361 The Aerodynamic Approach to Furnace Design, by J. H. Chesters. (58-A-72)
371 Use of Flow Models for Boiler-Furnace Design, by R. W. Curtis and L. E. Johnson. (58-A-120)
380 Use of Models for Studying Pulverized-Coal Burner Performance, by G. C. Whitney. (58-A-95)
383 Basic Principles of Combustion-Model Research, by A. A. Putnam and E. W. Ungar. (58-A-73)
389 A New Performance Criterion for Steam-Turbine Regenerative Cycles, by J. Kenneth Salisbury. (58-A-205)
403 Power Test Code Thermometer Wells, by J. W. Murdock. (58-A-176)
417 Flow-Induced Noise in Heat Exchangers, by A. A. Putnam. (58-A-103)
423 The Effect of Fuel Types and Admission Method Upon Combustion Efficiency, by H. N. McManus, Jr., W. E. Ibele, and T. E. Murphy. (58-A-128)
428 Torsion of a Prismatical Bar Whose Section Is a Crescent, by F. Sisto. (59-GTP-6)
433 The Transient Response of Gas-Turbine-Plant Heat Exchangers—Regenerators, Intercoolers, Precoolers, and Ducting, by A. L. London, F. R. Biancardi, and J. W. Mitchell. (59-GTP-5)
449 Stresses in Hollow Cylinders Due to Asymmetrical Heat Generation, by Harry Kraus and George Sonnemann.

TRANSACTIONS OF THE ASME Series C

Journal of
HEAT TRANSFER
Vol. 81 • Series C • No. 4

CONTENTS FOR NOVEMBER, 1959

253 Dynamic Response of Heat Exchangers Having Internal Heat Sources—Part III, by V. S. Arpaci and J. A. Clark. (58—SA-39)
267 Heating and Cooling Air and Carbon Dioxide in the Thermal Entrance Region of a Circular Duct With Large Gas to Wall Temperature Differences, by Helmut Wolf. (59—SA-15)
280 Turbulent Fow in a Circular Tube With Arbitrary Internal Heat Sources and Wall Heat Transfer, by R. Siegel and E. M. Sparrow. (59—SA-19)
291 Laminar Condensation Heat Transfer on a Horizontal Cylinder, by E. M. Sparrow and J. L. Gregg. (59—SA-13)
297 The Use of Thin Films for Increasing Evaporation and Condensation Rates in Process Equipment, by E. L. Lustenader, R. Richter, and F. J. Neugebauer. (59—SA-30)
308 Some General Considerations of the Heating of Satellites, by A. J. Eggers, Jr., T. J. Wong, and R. E. Slye.
315 The Penetration of Planetary Atmospheres, by Carl Gazley, Jr. (59—Av-27)
323 Thermodynamic Properties of Helium at Low Temperatures and High Pressures, by D. B. Mann and R. B. Stewart. (59—HT-19)
327 Radiation Fin Efficiency for One-Dimensional Heat Flow in a Circular Fin, by R. L. Chambers and E. V. Somers. (59—HT-8)

TRANSACTIONS OF THE ASME Series D

Journal of
BASIC ENGINEERING
Vol. 81 • Series D • No. 4

CONTENTS FOR DECEMBER, 1959

433 Applications of Computer and Model Studies to Problems Involving Hydraulic Transients, by I. W. McCaig and F. H. Jonker. (58—A-101)
446 Large Water-Level Displacements in the Simple Surge Tank, by A. W. Marris. (58—A-29)
455 Experience in the Use of the Gibson Method of Water Measurement for Efficiency Tests of Hydraulic Turbines, by N. R. Gibson. (58—A-78)
488 Free Discharge Through a Turbine Distributor, Case, and Draft Tube, by R. A. Sutherland. (58—A-76)
493 Symposium on Welded Spiral Cases From the Manufacturer's Viewpoint. (58—A-60)
505 Dériaz Type Reversible Pump-Turbine Installation at Sir Adam Beck-Niagara Forebay Pumped Storage Project, by A. E. Aeberli. (58—A-77)
521 Reversible Pump-Turbines for Sir Adam Beck-Niagara Pumping-Generator Station, by P. Dériaz and J. G. Warnock. (58—A-108)
534 Some Hydraulic Features of Puntledge Generating Plant, by A. W. Lash and R. E. Passmore. (58—A-100)
543 Application of Boundary-Layer Theory in Turbomachinery, by H. Schlichting.
552 Radial Equilibrium in Supersonic Compressors, by A. G. Hammitt and S. M. Bogdonoff. (58—A-110)
559 Résumé of the Supersonic-Compressor Research at NACA Lewis Laboratory, by W. W. Wilcox, E. R. Tysl, and M. J. Hartmann. (58—A-177)
569 Application and Analysis of a Computer Control System, by Irving Lefkowitz and D. P. Eckman. (58—A-281)
578 The Response of Pneumatic Transmission Lines to Step Inputs, by C. B. Schuder and R. C. Binder. (58—A-136)
585 A General Approach to the Practical Solution of Creep Problems, by A. Mendelson, M. H. Hirschberg, and S. S. Manson. (58—A-98)
599 Multiaxial Creep Studies on Inconel at 1500 F, by C. R. Kennedy, W. O. Harms, and D. A. Douglas. (58—A-193)
610 Creep-Rupture Strength of Austenitic Cr-Ni-Mo Steels in Sheet and Bar Form, by G. V. Smith, F. Garofalo, R. W. Whitmore, and R. R. Burt. (58—A-102)
617 Correlation of High Temperature Creep and Rupture Data, by Hans Conrad. (58—A-96)
629 Comparison of Parameter Methods for Extrapolating High-Temperature Data, by R. M. Goldhoff. (58—A-121)
645 Tests on Deflection of Flat Oval Bourdon Tubes, by G. Kardos. (58—A-67)
651 Bending and Stretching of Corrugated Diaphragms, by R. F. Dressler. (58—A-62)
660 Electromagnetic Flowmeter Primary Elements, by V. P. Head. (58—A-126)
669 The Distribution of Contact Pressures in the Rolling of Metals, by C. W. MacGregor and R. B. Palme. (58—A-260)
681 The Effects of Friction in the Rolling of Metals, by M. D. Stone.

Boundary-Layer Solution for a Flow in a Diverging Passage Having a Swirl Component

M. A. SINBEL[1]
Assistant Director of Pipelines, General Petroleum Authority, Cairo, Egypt

In this paper a solution is given to estimate the boundary-layer thickness owing to translational and rotational motion. The solution is an attempt to derive the boundary-layer equations when the main stream possesses both swirl and axial velocity. The development of the boundary layer in a conical duct is influenced by centrifugal action in addition to the pressure and viscous forces. The boundary-layer momentum integral equations are derived and presented herein for a set of spherical polar co-ordinates. The solution has been carried out for laminar flow. A turbulent form of the solution can be obtained by the introduction of the mixing-length theory. A numerical solution is carried out to make a comparison between the estimated and actual measured values.

Derivation of the Equations

The equations of steady motion of a viscous fluid which flows symmetrically with respect to the axis $\theta = 0$ are in spherical polar co-ordinates

$$u\frac{\partial u}{\partial R} + \frac{v}{R}\frac{\partial u}{\partial \theta} - \frac{w^2}{R} - \frac{v^2}{R} = -\frac{1}{\rho}\left(\frac{\partial p}{\partial R}\right) + \nu\left(\nabla^2 u - \frac{2u}{R^2} - \frac{2}{R^2}\frac{\partial v}{\partial \theta} - \frac{2v\cot\theta}{R^2}\right) \quad (1)$$

and

$$u\frac{\partial w}{\partial R} + \frac{v}{R}\frac{\partial w}{\partial \theta} + \frac{uw}{R} + \frac{uw\cot\theta}{R} = \nu\left(\nabla^2 w - \frac{w}{R^2\sin^2\theta}\right) \quad (2)$$

where

R = distance of a point from origin which is taken at the vertex of the cone
θ = angle which radius vector makes with axis
u = radial velocity
v = component of velocity in axial plane perpendicular to R
w = component of velocity perpendicular to axial planes
p = pressure
ρ = density
ν = kinematic viscosity

and the pressure is given by

$$\frac{p}{\rho} = -\tfrac{1}{2}\frac{C^2}{R^2\sin^2\theta} + \text{const} \quad (3)$$

therefore

$$\frac{1}{\rho}\frac{\partial p}{\partial R} = \frac{C^2}{R^3\sin^2\theta} \quad (4)$$

If the boundary layer is thin compared with R some terms may be neglected, as shown by Taylor, and the approximate forms are

$$u\frac{\partial u}{\partial R} + \frac{v}{R}\frac{\partial u}{\partial \theta} + \frac{C^2}{R^3\sin^2\theta} - \frac{w^2}{R} = \frac{\nu}{R^2}\frac{\partial^2 u}{\partial \theta^2} \quad (5)$$

$$u\frac{\partial w}{\partial R} + \frac{v}{R}\frac{\partial w}{\partial \theta} + \frac{uw}{R} = \frac{\nu}{R^2}\frac{\partial^2 w}{\partial \theta^2} \quad (6)$$

The full equation of continuity is

$$\frac{\partial u}{\partial R} + \frac{2u}{R} + \frac{1}{R}\frac{\partial v}{\partial \theta} = 0 \quad (7)$$

From the equations of motion (5) and (6) in which the boundary layer is assumed to have a definite thickness δ, variations in $\sin\theta$ in the boundary layer may be neglected and $\sin\theta$ taken as $\sin\alpha$ (5) then becomes

$$\int u\frac{\partial u}{\partial R}\,d\theta + \int \frac{v}{R}\frac{\partial u}{\partial \theta}\,d\theta + \int\left(\frac{C^2}{R^3\sin^2\theta} - \frac{w^2}{R}\right)d\theta = \frac{\nu}{R^2}\left[\frac{\partial u}{\partial \theta}\right]_{\theta=\alpha} \quad (8)$$

From the equation of continuity

$$\int \frac{v}{R}\frac{\partial u}{\partial R}\,d\theta = \frac{1}{R}\,[uv]_{\alpha-\delta/R}^{\alpha} + \int\left(u\frac{\partial u}{\partial R} + \frac{2u^2}{R}\right)d\theta \quad (9)$$

In the present problem at $\theta = \alpha$, $u = 0$; and at $\theta = \alpha - \delta/R$, $u = U$.

Again from the equation of continuity (7)

$$\int_{\alpha-\delta/R}^{\alpha}\left(R\frac{\partial u}{\partial R} + 2u\right)d\theta = (v)_{\alpha-\delta/R} \quad (10)$$

From (8) and (10)

$$\frac{\nu}{R^2}\left[\frac{\partial u}{\partial \theta}\right]_{\theta=\alpha} = 2\int u\frac{\partial u}{\partial R}\,d\theta + 2\int\frac{u^2}{R}\,d\theta + \int\left(\frac{C^2}{R^3\sin^2\theta} - \frac{w^2}{R}\right)d\theta - \frac{U}{R}\int_{\alpha-\delta/R}^{\alpha}\left(R + \frac{\partial u}{\partial R} + 2u\right)d\theta \quad (11)$$

---

[1] Lecturer, Faculty of Engineering, Ain Shams University, Abbasia, Cairo, Egypt.

Presented at the West Coast Conference of the Applied Mechanics Division, Stanford, Calif., September 9–11, 1959, of THE AMERICAN SOCIETY OF MECHANICAL ENGINEERS.

Discussion of this paper should be addressed to the Secretary, ASME, 29 West 39th Street, New York, N. Y., and will be accepted until January 10, 1960, for publication at a later date. Discussion received after the closing date will be returned.

NOTE: Statements and opinions advanced in papers are to be understood as individual expressions of their authors and not those of the Society. Manuscript received at ASME Applied Mechanics Division, December 9, 1957. Paper No. 59—APMW-14.

This may thus be called the longitudinal momentum integral.

In the same way, the transverse momentum integral obtained from (6) is

$$\int u\frac{\partial w}{\partial R}\,d\theta + \int \frac{v}{R}\frac{\partial w}{\partial \theta}\,d\theta + \int \frac{wu}{R}\,d\theta = \frac{\nu}{R^2}\left[\frac{\partial w}{\partial \theta}\right]_{\theta=\alpha} \quad (12)$$

Using the equation of continuity (7), therefore

$$\int \frac{v}{R}\frac{\partial w}{\partial \theta}\,d\theta = \frac{1}{R}\,[vw]_{\alpha-\delta/R}^{\alpha} + \int\left(w\frac{\partial u}{\partial R} + \frac{2uw}{R}\right)d\theta$$

From the boundary conditions at $\theta = \alpha$, $w = 0$; and at $\theta = \alpha - \delta/R$,

$$(vw)_{\alpha-\delta/R} = \frac{C}{R\sin\alpha}(v)_{\alpha-\delta/R}$$

$$\therefore \int \frac{v}{R}\frac{\partial w}{\partial \theta}\,d\theta = -\frac{C}{R^2\sin\alpha}(v)_{\alpha-\delta/R} + \int\left(w\frac{\partial u}{\partial R} + \frac{2uw}{R}\right)d\theta \quad (13)$$

Substituting (13) for the second term in (12),

$$\frac{\nu}{R^2}\left(\frac{\partial w}{\partial \theta}\right)_{\theta=\alpha} = 3\int\frac{uw}{R}\,d\theta + \int\frac{\partial}{\partial R}(uw)d\theta - \frac{C}{R^2\sin\alpha}\int_{\alpha-\delta/R}^{\alpha}\left(R\frac{\partial u}{\partial R} + 2u\right)d\theta \quad (14)$$

These longitudinal and transverse momentum integrals pertain to a laminar boundary layer in which $\partial u/\partial t$ is zero. In a turbulent boundary layer $\partial u/\partial t$ is not zero, although it may be represented by the stress to which it gives rise. Accordingly, a new term proportional to the square of the velocity gradient in the longitudinal and transverse directions is introduced. The factor of proportionality is called the mixing length similar to Prandtl's definition of mixing length. The mixing length in a turbulent flow represents a value proportional to the motion of molar volume of fluid across the direction of basic flow.

The formula $\tau = \rho l^2(du/dy)^2$ was first given by Prandtl in his theory of the mixing length, assuming a special kind of mechanism for the turbulent exchange of momentum. According to Prandtl, in the case when the shearing stress across the boundary layer is constant, the mixing length is determined by the distance from the wall. As a first approximation, he assumed the mixing length simply to be proportional to this distance. Here u denotes the resultant velocity and the expression is not applicable to its components. In Cartesian co-ordinates the shear stress, in the case of turbulent boundary layers, consists of two terms (the mean value of viscous stress plus the apparent shearing stress due to turbulence)

$$\tau = \mu\frac{\partial u_m}{\partial y} + \rho l^2\left(\frac{\partial u_m}{\partial y}\right)^2$$

The first term is important only for the very small distance from the boundary. In the same way the left-hand side of equations (11) and (14) is adjusted; the first $(\nu/R^2)(\partial u/\partial\theta)_{\theta=\alpha}$ becomes, adding the apparent shear stress due to turbulence,

$$\frac{1}{R^2}\left[\nu\frac{\partial u}{\partial\theta} + \frac{l^2}{\delta}\left(\frac{\partial u}{\partial\theta}\right)^2\right] \therefore \frac{1}{R^2}\left[\nu\frac{\partial u}{\partial\theta} + \frac{l^2}{\delta}\left(\frac{\partial u}{\partial\theta}\right)^2\right]$$

$$= 2\int u\frac{\partial u}{\partial R}\,d\theta + 2\int\frac{u^2}{R}\,d\theta + \int\left(\frac{C^2}{R^2\sin^2\theta} - \frac{w^2}{R}\right)d\theta - \frac{U}{R}\int_{\alpha-\delta/R}^{\alpha}\left(R\frac{\partial u}{\partial R} + 2u\right)d\theta \quad (15)$$

The left-hand side of equation (14) becomes, after adding the apparent shear stress due to turbulence,

$$\frac{1}{R^2}\left[\nu\frac{\partial w}{\partial\theta} + \frac{l^2}{\delta}\left(\frac{\partial w}{\partial\theta}\right)^2\right]$$

Therefore

$$\frac{1}{R^2}\left[\nu\frac{\partial w}{\partial\theta} + \frac{l^2}{\delta}\left(\frac{\partial w}{\partial\theta}\right)^2\right] = 3\int\frac{uw}{R}\,d\theta + \int\frac{\partial}{\partial R}(uw)d\theta - \frac{C}{R^2\sin\alpha}\int_{\alpha-\delta/R}^{\alpha}\left(R\frac{\partial u}{\partial R} + 2u\right)d\theta \quad (16)$$

Equations (15) and (16), by assuming a suitable form for the distribution of velocity through the boundary layer, are

$$u = \frac{CE}{R\sin\alpha}f(\eta)$$

where $f(\eta)$ is assumed here to take a quadric form

$$f(\eta) = a\eta + b\eta^2 + c\eta^3 + d\eta^4$$

Also

$$w = \frac{C}{R\sin\alpha}\varphi(\eta)$$

where

$$\varphi(\eta) = a'\eta + b'\eta^2 + c'\eta^3 + d'\eta^4$$

and

$$\eta = \frac{R(\alpha-\theta)}{\delta}$$

and varies from 0 to 1 through the boundary layer.

The boundary conditions are $u = w = 0$, at $\theta = \alpha$, i.e., at $\eta = 0$, and

$$u = U,\quad w = \frac{C}{R\sin\alpha},\quad \frac{\partial u}{\partial\theta} = 0,\quad \frac{\partial w}{\partial\theta} = 0$$

at $\theta = (\alpha - \delta)/R$, i.e., at $\eta = 1$.

The two variables E and δ determine the boundary layer at any point so that E and δ are functions of R only and can be determined by using the momentum integrals (15) and (16).

The values of $\partial u/\partial R$ and $\partial(uw)/\partial R$ which occur in the momentum integrals must be expressed first in terms of the variables δ, E, and η, hence

$$\frac{\partial u}{\partial R} = \frac{C}{\sin\alpha}\left[\left(\frac{1}{R}\frac{dE}{dR} - \frac{E}{R^2}\right)f + \frac{E}{R^2}\left(1 - \frac{R}{\delta}\frac{d\delta}{dR}\right)\eta\frac{df}{d\eta}\right]$$

and

$$\frac{\partial}{\partial R}(uw) = \frac{C^2}{\sin^2\alpha}\left[f\varphi\left(\frac{1}{R^2}\frac{\partial E}{\partial R} - \frac{2E}{R^3}\right) + \frac{E}{R^3}\left(1 - \frac{R}{\delta}\frac{d\delta}{dR}\right)\eta\frac{d}{d\eta}(f\varphi)\right]$$

Before these values are inserted in the momentum integrals, the variable of integration is changed from $d\theta$ to $-(\delta/R)d\eta$, with the boundary conditions at $\eta = 0, f = 0$, and at $\eta = 1, f = 1, \varphi = 1$,

therefore

$$\int_0^1 \eta f \frac{df}{d\eta}\, d\eta = {}^1/_2 - {}^1/_2 \int_0^1 f^2 d\eta$$

Also

$$\int_0^1 \eta \frac{d}{d\eta}(f\varphi)d\eta = 1 - \int_0^1 f\varphi d\eta$$

and

$$\int_0^1 \eta \frac{d}{d\eta} f\, d\eta = 1 - \int_0^1 f d\eta$$

The right-hand side of equation (16) becomes

$$= {}^1/_2 \frac{\delta^2}{R^2}\left[-\int \frac{2C^2 f\varphi}{R\sin^2\alpha\delta}\frac{dE}{dR}\, d\eta - \frac{2EC^2}{R\sin^2\alpha\delta^2}\frac{d\delta}{dR}\int_0^1 f\varphi d\eta + \int \frac{2C^2 f}{R\sin^2\alpha\delta}\frac{dE}{dR}\, d\eta + \frac{2EC^2}{R\sin^2\alpha\delta^2}\frac{d\delta}{dR}\int_0^1 f d\eta\right]$$

and equation (16) itself becomes

$$-E\frac{\nu\sin\alpha}{C}\left(\frac{d\varphi}{d\eta}\right) - E\frac{l^2}{\delta^2}\left(\frac{d\varphi}{d\eta}\right)^2 = -{}^1/_2\frac{\delta^2}{R^2}\left(\int_0^1 f\varphi d\eta - \int_0^1 f d\eta\right)\left(R\frac{dE^2}{dR} + \frac{RE^2}{\delta^2}\frac{d\delta^2}{dR}\right) \quad (17)$$

Now considering the equation (15) in the same way

$$-E\frac{\nu\sin\alpha}{C}\left(\frac{df}{d\eta}\right) - \frac{E^2 l^2}{\delta^2}\left(\frac{df}{d\eta}\right)^2 = \frac{\delta^2}{R^2}\left\{\int_0^1 f^2 d\eta\left[-R\frac{dE^2}{dR} + E^2 - \frac{RE^2}{2\delta^2}\frac{d\delta^2}{dR}\right] - 1 + \int_0^1 \varphi^2 d\eta + \int_0^1 f d\eta\left[\frac{R}{2}\frac{dE^2}{dR} + \frac{E^2 R}{2\delta^2}\frac{d\delta^2}{dR}\right]\right\} \quad (18)$$

To reduce (17) and (18) to nondimensional form, the length along the generator from the vertex to the point at which the boundary layer may be supposed to start may be taken as R_0. The nondimensional variables are then

$$R_1 = R/R_0$$

$$\delta_1 = \frac{\delta}{R_0}\left(\frac{C}{\nu\sin\alpha}\right)^{1/2}$$

$$L^2 = l^2/\delta^2$$

As stated by Prandtl,[2] since the sign of du/dy and the sign of τ are required to change together, the formula connecting stress with velocity gradient is better written as

$$\tau = \rho l\left|\frac{du}{dy}\right|\left(l\frac{du}{dy}\right)$$

[2] Prandtl, "Aerodynamic Theory," vol. 3, Springer, Berlin, 1935, p. 130.

Now equation (17) becomes

$$-ER_1\left[\left(\frac{\partial\varphi}{\partial\eta}\right) + L_2\frac{C}{\nu\sin\alpha}\left|\frac{d\varphi}{d\eta}\right|\left(L_2\frac{d\varphi}{d\eta}\right)\right] = -{}^1/_2\,\delta_1^2\left[\frac{dE^2}{dR_1} + \frac{E^2}{\delta_1^2}\frac{d\delta_1^2}{dR_1}\right]\left[-\int_0^1 f d\eta + \int_0^1 f\varphi d\eta\right] \quad (19)$$

In the same way equation (18) becomes

$$-ER_1\left[\left(\frac{df}{d\eta}\right) + EL_1\frac{C}{\nu\sin\alpha}\left|\frac{df}{d\eta}\right|\left(L_1\frac{df}{d\eta}\right)\right] = -\delta_1^2\left[\int_0^1 f^2 d\eta\left(\frac{dE^2}{dR_1} - \frac{E^2}{R_1} + \frac{E^2}{2\delta_1^2}\frac{d\delta_1^2}{dR_1}\right) + \frac{1}{R_1}\left(1 - \int_0^1 \varphi^2 d\eta\right) - {}^1/_2\int_0^1 f d\eta\left(\frac{dE^2}{dR_1} + \frac{E^2}{\delta_1^2}\frac{d\delta_1^2}{dR_1}\right)\right] \quad (20)$$

Now the particular forms of f and φ have to be considered

$$\int_0^1 f d\eta = \left[\frac{a\eta^2}{2} + \frac{b\eta^3}{3} + \frac{c\eta^4}{4} + \frac{d\eta^5}{5}\right]_0^1 = \frac{a}{2} + \frac{b}{3} + \frac{c}{4} + \frac{d}{5} = G$$

$$\int_0^1 f^2 d\eta = \frac{a^2}{3} + \frac{ab}{2} + \frac{b^2 + 2ac}{5} + \frac{ad + bc}{3} + \frac{2bd + c^2}{7} + \frac{cd}{4} + \frac{d^2}{9} = h$$

$$\int_0^1 \varphi^2 d\eta = \frac{a'^2}{3} + \frac{a'b'}{2} + \frac{b'^2 + 2a'c'}{5} + \frac{a'd' + b'c'}{3} + \frac{2b'd' + c'^2}{7} + \frac{c'd'}{4} + \frac{d'^2}{9} = M$$

$$\int_0^1 f\varphi d\eta = \frac{aa'}{3} + \frac{ab' + a'b}{4} + \frac{bb' + ac' + a'c}{5} + \frac{ad' + a'd + bc' + b'c}{6} + \frac{bd' + b'd + cc'}{7} + \frac{cd' + c'd}{8} + \frac{dd'}{9} = N$$

$$\frac{df}{d\eta} = a + 2b\eta + 3c\eta^2 + 4d\eta^3$$

At $\eta = 0$,

$$\frac{df}{d\eta} = a$$

$$\frac{d\varphi}{d\eta} = a' + 2b'\eta + 3c'\eta^2 + 4d'\eta^3$$

At $\eta = 0$,

$$\frac{d\varphi}{d\eta} = a'$$

Putting $df/d\eta$ at $\eta =$ any value from 0 to 1 $= n$ and $d\varphi/d\eta = m$, n varies from a to $a + 2b + 3c + 4d$ as η varies from 0 to 1; m varies from a' to $a' + 2b' + 3c' + 4d'$ as η varies from 0 to 1. At the wall, the ratio of $df/d\eta$ to $d\varphi/d\eta$ is equal to E.

Equation (19) becomes

$$-ER_1\left[m + mL_2\frac{C}{\nu\sin\alpha}(mL_2)\right] = -{}^1/_2\delta_1^2(-G+N)\left(\frac{dE^2}{dR_1} + \frac{E^2}{\delta_1^2}\frac{d\delta_1^2}{dR_1}\right) \quad (20a)$$

Equation (20) becomes

$$\left[\frac{dE^2}{dR_1}\left(\frac{2h-G}{h-G}\frac{1}{E}\delta_1^2\right) + \frac{d\delta_1^2}{dR_1}E - \frac{2h}{h-G}E\frac{\delta_1^2}{R_1} + \frac{2(1-M)}{(h-G)E}\frac{\delta_1^2}{R_1}\right] = \frac{2n}{h-G}R_1\left[1 + EL_1\frac{C}{\nu\sin\alpha}(nL_1)\right] \quad (20b)$$

From (20*a*) and (20*b*)

$$\frac{dE^2}{dR_1} = \frac{2E^2}{R_1} - \frac{2(1-M)}{hR_1} + 2R_1\frac{E}{\delta_1^2}\left[\frac{n(N-G)\left\{1 + EL_1\frac{C}{\nu\sin\alpha}(nL_1)\right\}}{h(N-G)} - \frac{m(h-G)\left\{1 + L_2\frac{C}{\nu\sin\alpha}(mL_2)\right\}}{h(N-G)}\right] \quad (20c)$$

It was found experimentally that the term for the shear stress resulting from laminar flow is negligible compared to the turbulent stress except at the wall, so that equations (20*b*) and (20*c*) can be put in the form

$$\frac{dE^2}{dR_1} = \frac{2E^2}{R_1} - \frac{2(1-M)}{hR_1} + 2R_1\frac{E}{\delta_1^2}\left\{\frac{n(N-G)EL_1\frac{C}{\nu\sin\alpha}(nL_1) - m(h-G)L_2\frac{C}{\nu\sin\alpha}(mL_2)}{h(N-G)}\right\} \quad (20d)$$

and

$$2m\frac{R_1}{(N-G)}L_2\frac{C}{\nu\sin\alpha}(mL_2) = \frac{\delta_1^2}{E}\frac{dE^2}{dR_1} + E\frac{d\delta_1^2}{dR_1} \quad (20e)$$

since L_1 is in the direction of the radial motion and L_2 in the direction of the whirl motion. Therefore

$$\frac{\overline{L_1}}{\overline{L_2}} = E$$

The values of L_1 and L_2 are equal also at the wall $n/m = E$ for the special case when $f(\eta) = \varphi(\eta)$.

Introducing these relations in equations (20*d*) and (20*e*),

$$\frac{dE^2}{dR_1} - \left(\frac{2E^2}{R_1} - \frac{2(1-M)}{hR_1}\right) = 2R_1\frac{E}{\delta_1^2}\frac{C}{\nu\sin\alpha}n^2L_1^2\frac{E-(1/E^2)}{h} \quad (20f)$$

and

$$L_1^2 = \frac{\nu\sin\alpha}{C}\frac{E(h-G)}{2n^2R_1}\left(\delta_1^2\frac{dE^2}{dR_1} + E^2\frac{d\delta_1^2}{dR_1}\right) \quad (20g)$$

Check With Taylor's and Binnie's Work

Before solving the two equations (20*b*) and (20*c*), a check is made with the work done by Binnie and Harris in their solution for the boundary layer for swirling liquid flow through a nozzle.

Binnie assumed the same function for both the radial velocity u and the component of the velocity perpendicular to the axial planes; i.e.,

$$u = G(R)\varphi(\eta)$$

$$w = \frac{C}{R\sin\alpha}\varphi(\eta)$$

where he assumes $\varphi(\eta)$ to take either the form $\varphi(\eta) = 2\eta - \eta^2$ or $\varphi(\eta) = 2\eta - 2\eta^3 + \eta^4$.

From our assumption that u and w take the forms

$$u = \frac{CE}{R\sin\alpha}f(\eta)$$

and

$$w = \frac{C}{R\sin\alpha}\varphi(\eta)$$

we notice that to reduce our formula to those given by Binnie $f(\eta) = \varphi(\eta)$ also

$$\frac{CE}{R\sin\alpha} = G(R)$$

i.e.,

$$E = G(R)\frac{R\sin\alpha}{C}$$

Binnie gives another function

$$F(R) = \frac{1}{\rho}\frac{\partial p}{\partial R}$$

therefore

$$F(R) = \frac{C^2}{R^3\sin^3\alpha}$$

In reducing his formula to the nondimensional form, Binnie assumes two other functions:

$$f(R_1) = F(R)\frac{R_0^3\sin^3\alpha}{C^2}$$

and

$$g(R_1) = G(R)\frac{R_0\sin\alpha}{C}$$

Therefore

$$E = g(R_1)\frac{C}{R_0\sin\alpha}\frac{R\sin\alpha}{C} = g(R_1)R_1$$

$$\frac{dE^2}{dR_1} = 2g(R_1)\frac{dg}{dR_1}R_1^2 + 2R_1g^2$$

also

$$\frac{f}{g} = \frac{1}{g}\frac{C^2}{R^3\sin^2\alpha}\frac{R_0^3\sin^2\alpha}{C^2} = \frac{1}{gR_1^2}$$

We now employ the functions assumed by Binnie for the expressions for φ with the particular form of $\varphi = 2\eta - \eta^3$

$$\int_0^1\varphi^2d\eta = 0.53, \quad \int_0^1\varphi d\eta = 0.6, \quad \left[\frac{d\varphi}{d\eta}\right]_{\eta=0} = 2$$

Binnie considered the laminar case only, so the terms in equations

(20a) and (20b) which contain the mixing length are omitted; hence

$$2m\frac{R_1}{(h-G)} = \frac{\delta_1^2}{E}\frac{dE^2}{dR_1} + E\frac{d\delta_1^2}{dR_1}$$

and

$$2n\frac{R}{(h-G)} = \frac{dE^2}{dR_1}\left(\frac{2h-G}{h-G}\frac{1}{E}\delta_1^2\right) + \frac{d\delta_1^2}{dR_1}E - \frac{2h}{h-G}E\frac{\delta_1^2}{R_1} + \frac{2(1-M)}{(h-G)E}\frac{\delta_1^2}{R_1}$$

$$m = n = \left(\frac{d\varphi}{d\eta}\right)_{\eta=0} = 2$$

for Binnie's assumption

$$h = \int_0^1 f^2 d\eta = M = \int_0^1 \varphi^2 d\eta = N = \int_0^1 f\varphi d\eta$$

$$\int_0^1 f d\eta = \int_0^1 \varphi d\eta = 0.6$$

The first equation reduces to

$$-\frac{2}{0.134\delta_1^2} = \frac{dg}{dR_1} + \frac{g}{R_1} + \frac{g}{2\delta_1^2}\frac{d\delta_1^2}{dR_1} \simeq -\frac{15}{\delta_1^2}$$

which is the equation given by Binnie.

The second equation reduces to

$$\frac{30}{\delta_1^2} = \frac{g}{\delta_1^2}\frac{d\delta_1^2}{dR_1} - 6\frac{dg}{dR_1} + 2\frac{g}{R_1} + \frac{8}{gR_1^2} - \frac{15f}{g}$$

which is the second equation given by Binnie.

In another case he replaced the velocity distribution by another form

$$\varphi = 2\eta - 2\eta^3 + \eta^4$$

His two equations were of the form

$$\frac{17.02}{\delta_1^2} = \frac{g}{2\delta_1^2}\frac{d\delta_1^2}{dR_1} + \frac{dg}{dR_1} + \frac{g}{R_1}$$

$$\frac{34.04}{\delta_1^2} = \frac{g}{\delta_1^2}\frac{d\delta_1^2}{dR_1} - 7.915\frac{dg}{dR_1} + \frac{2g}{R_1} + \frac{9.915}{gR_1^2} - 17.02\frac{f}{g}$$

Taylor considered the case with pure swirl. His two functions for the velocity distributions were

$$f(\eta) = \eta - 2\eta^3 + \eta^5$$

and

$$\varphi(\eta) = 2\eta - \eta^3$$

His two equations were of the form

$$\frac{dE^2}{dR_1} = -\frac{98}{R_1} + \frac{2E^2}{R_1} - \frac{330E^2R_1}{E\delta_1^2}$$

$$\frac{d}{dR_1}(E\delta_1^2) = \frac{49E\delta_1^2}{E^2R_1} - \frac{E\delta_1^2}{R_1} + 285\,R_1$$

Note on Experimental Procedure

Generation of Swirl. Two methods were used for introducing swirl at the entry:

(*a*) Swirl introduced by a spiral case, the side wall of which was a logarithmic spiral of 10 deg spiral angle. The width of the case was 5 in. and the diameter of the throat was 5.63 in. A bellmouth made of wax was fitted at the entrance to the diffuser, which improved the flow considerably. The spiral case was bolted directly to the working section without any length in between.

(*b*) Swirl introduced by a set of 16 stationary guide vanes made of thin sheet brass $^1/_{16}$ in. thick. The sheet was rolled to a suitable radius of 3.2025 in. The vanes are 1.83 in. long, having a chord of 3.25 in. and an angle of twist of 20 deg. The blades are set radially at the entry on an outside radius of 9 in. They are fitted on a wooden board and can be set at any convenient angle. A bellmouth, made of wax, is screwed to the wooden board, Fig. 1(*a*).

Measuring Instruments. Two cones having a concluded angle of 10° 14′ for the first cone and 14° 14′ for the second, are used for the experiment. In the first cone, traverses were taken at positions 2, 4, 6, and 8, corresponding to distances from the apex of the cone equal to 76.9, 86.1, 95.1, 104.8, and 114.4 cm, respectively.

The diameters of the ends of the test sections were 12 and 6 in., downstream; the 12-in. end carried a flange joined to a 12-in. pipe leading to a fan. For velocity measurements, a pitot cylinder together with a static tube was used. For readings near the wall, a hot-wire anemometer was used, Fig. 1(*b*).

The pitot cylinder was used for the total-head measurements. It also gave the direction of the flow. It was of the so-called cantilevered cylinder form in which the pressure holes are near the end of a protruding cylinder. The cylinder had an outside diameter of $^1/_8$ in. The two holes had an included angle of 80 deg. The cylinder was calibrated in a wind tunnel against a standard pitot tube. The accuracy of the instrument is about $^1/_2$ deg on angle and 1 per cent on velocity. The air direction in the two-dimensional case is assumed to be along the axis. The direction of rotation, when swirl is introduced, is read off an angle scale.

The coefficient of the 80-deg tube is taken to be 1.

A Prandtl static tube is used for measuring the static head. The head of the tube, which is introduced in the air current is bent

Table 1 Numerical solution (10° 14′ cone)

Station	2	4	6	8
δ (experimental) cm	1.3	1.3	1.9	2.3
C_1 m per sec	0.2979	0.2907	0.3294	0.315
δ_1^2 (experimental)	13.9472	13.5431	32.9487	52.9926
$h = \int_0^1 f^2 d\eta$ (graphical)	0.777	0.7034	0.7784	0.7509
$G = \int_0^1 f d\eta$ (graphical)	0.873	0.7974	0.8624	0.8229
$(G-h)$	0.096	0.094	0.084	0.072
E	3.101	2.6601	2.1404	1.7777
R_1	0.613	0.722	0.833	0.94
Ln	0.018809	0.014022	0.020976	0.023022
δ_1	4.6776	4.2544	5.3778	5.671
δ (calculated), cm	1.6283	1.5028	1.78	1.7917

Fig. 1(a) Stationary guide vanes for introduction of swirl

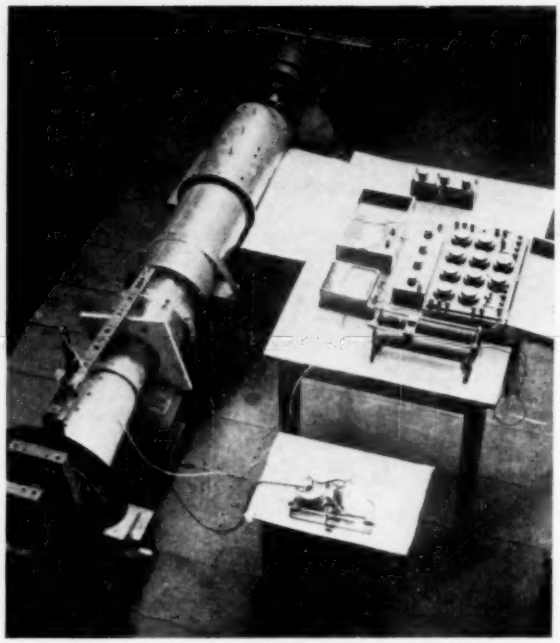

Fig. 1(b) Hot-wire anemometer and setup of experimental equipment

at right angles to face the stream and terminates in a conical plug. This form of head deflects the air only slightly and, at a short distance back from the end (3 cm), where the flow is once more sensibly parallel to the tube, four small holes are drilled. The tube has an outside diameter of 4 mm.

It was not possible to take the readings within 5-mm distance from the wall because of the size of the static tube. A hot-wire anemometer was used mainly for the readings in that region and to check to readings obtained by the afore-mentioned instruments. A variable inclination manometer was used after being calibrated against a micromanometer.

The Hot-Wire Anemometer. The two ends of a platinum wire, 1 cm long and 0.003 in. diam, are joined to two manganin supports by means of very thin locating screws. The two supports are fixed to an ebonite rod which in turn is fixed to a micrometer traversing unit having a protractor and a pointer fitted to it. Before use, wires were annealed by passing a current through them sufficient to raise their temperature to red heat for some hours. The wire is then calibrated in a jet of air which passes through an orifice of 2-in. diam. The wire is calibrated in the center of the jet against a standard pitot tube. When the hot wire is used for measurements in swirling flow, it has not been used as a yawmeter. The direction was given by the pitot cylinder. It was possible to adjust the distance between the wire and the wall down to 0.005 in.

Method of Numerical Solution. The velocity distributions for the radial component and the perpendicular component are determined experimentally. A curve is drawn for u and w against η where

$$\eta = \frac{R}{\delta}(\alpha - \theta)$$

η varies from 0 to 1 through the boundary layer. The velocity is measured at the following positions of η: $\eta = 0, 0.2, 0.4, 0.6, 0.8$, and 1.0.

An average value for E is taken through the boundary layer and it is assumed to be constant for every particular section. The nondimensional value for L (the ratio of the mixing length and the boundary-layer thickness δ) is determined semiempirically from equation (20f) as follows:

(a) From the radial and tangential-velocity distributions an estimate can be made for the translational boundary-layer thickness δ. The radial-velocity distribution curves showed a definite point of inflection at the edge of the boundary layer as seen in Fig. 2(a). The tangential-velocity curves showed a change to the free-vortex shape, Fig. 2(b). Thus the experimental value for the nondimensional boundary-layer thickness δ is calculated from

Table 2 Numerical solution (14° 14′)

Station	2	3	4	5	6
δ (experimental), cm	2.5	2.6	3.2	3.5	3.8
C, m per sec	0.2281	0.2435	0.2310	0.2277	0.2796
δ_1^2 (experimental)	59.8562	63.8161	92.281	109.0116	156.5201
$h = \int_0^1 f^2 d\eta$ (graphical)	0.5583	0.6349	0.536	0.5761	0.6416
$G = \int_0^1 f d\eta$ (graphical)	0.6588	0.7407	0.67	0.6941	0.7396
$(G - h)$	0.1005	0.1055	0.134	0.118	0.098
E	3.721	3.6873	2.9078	2.8309	2.2073
R_1	0.6349	0.7093	0.7879	0.8639	0.9423
Ln	0.0326	0.0388	0.0514	0.0575	0.0601
δ_1	6.7617	8.9604	11.76	13.077	12.375
δ (calculated), cm	2.2824	2.9163	3.9174	4.3636	3.7387

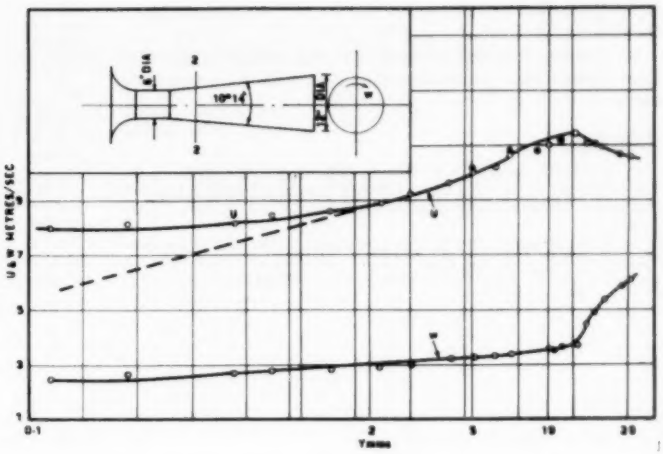

Fig. 2(a) Logarithmic plot of velocity distribution in boundary layer. Comparison of pitot and hot-wire readings.

$$\delta_1 = \frac{\delta}{R_0}\left(\frac{C}{\nu \sin \alpha}\right)^{1/2}$$

α = half the angle of the cone 5° 7′ for the first cone, and 7° 7′ for the second cone; C is the vortex constant. An average value for C is assumed for every section.

(*b*) The constants G, h, M, and N were obtained graphically by plotting the curves u/U, $1 - (u/U)$, and $(u/U)[1 - (u/U)]$ against y/δ. $h = \int f^2 d\eta$, $G = \int f d\eta$. G is the ratio of the areas under the momentum-thickness curve to the area under the displacement thickness curve. $G - h$ is the area under the momentum-thickness curves.

(*c*) $(dE^2)/(dR_1)$ is determined graphically from Fig. 3.

(*d*) $(d\delta_1{}^2 E/(dR_1)$ is determined graphically in a similar way as $(dE^2)/(dR_1)$ by plotting $\delta_1{}^2$ against R_1. Therefore

$$L^2 n^2 = \left[\frac{E^2(h - G)}{2R_1}\left(\frac{\nu \sin \alpha}{C}\right)\frac{d\delta_1{}^2}{dR_1} + \frac{E(h - G)}{2R_1}\left(\frac{\nu \sin \alpha}{C}\right)\delta_1{}^2 \frac{dE^2}{dR_1}\right]$$

from which $L^2 n^2$ is calculated.

The experimental value of $L^2 n^2$ is introduced in equation $(20g)$ and is calculated.

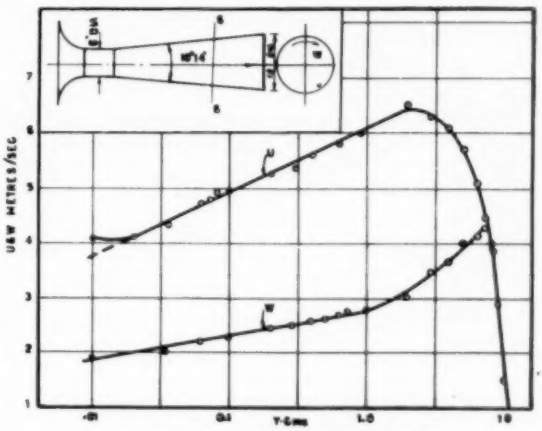

Fig. 2(b) Logarithmic plot of velocity distributions

Conclusion

The following conclusions can be drawn from the analysis of the three-dimensional solution and a comparison of the numerical results for the turbulent boundary layer.

1 It is possible to generalize the velocities in the boundary layer by use of two characteristic quantities δ_1 and E, where δ_1 is the nondimensional boundary-layer thickness and E is given by the deviation of direction of the surface drag from that of the pressure gradient.

2 The three-dimensional boundary-layer equations can take any form (hyperbolic, parabolic, and so on), depending on the shape of the velocity profiles in the boundary layer.

3 When the velocity distributions were plotted on a logarithmic scale it was noticed that the readings of the hot-wire anemometer were not sensitive in the 1-mm from-the-wall region. This can be accounted for by shifting the origin 1 mm from the wall or by assuming a suitable value for the stress at the wall

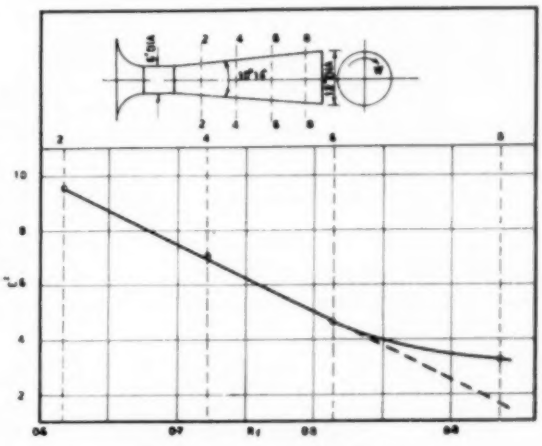

Fig. 3 Experimental E^2 against R_1

which gives rise to a value of the velocity at 1 mm near enough to the experimental value.

4 The semiempirical solution of the three-dimensional equations shows a fair quantitative agreement with the experimental values.

References

1 A. M. Binnie and D. P. Harris, "The Application of Boundary Layer Theory to Swirling Liquid Flow Through a Nozzle," *Quarterly Journal of Mechanics and Applied Mathematics*, vol. 3, part 1, 1950, p. 89.

2 J. M. Burgers, "Some Considerations on the Development of Boundary Layers in the Case of Flows Having a Rotational Component," *Nederl. Akad Van Wetenschappen*, vol. 44, 1941, pp. 12–25.

3 J. C. Cooke, "On Pohlhausen's Method With Application to a Swirl Problem of Taylor," *Journal of The Aeronautical Sciences*, vol. 19, 1952, pp. 486–490.

4 H. Peters, "Conversion of Energy in Cross-Sectional Divergences Under Different Conditions of Inflow," National Advisory Committee for Aeronautics, Technical Memorandum No. 737, 1934.

5 J. M. Roberttson and D. Ross, "Effect of Entrance Conditions on Diffuser Flow," *Transactions of the American Society of Civil Engineers*, vol. 118, 1953, pp. 1068–1091.

6 M. A. Sinbel, "Flow in Conical Passages," thesis, University of London, London, England, December, 1953.

7 G. I. Taylor, "The Boundary Layer in the Converging Nozzle of a Swirl Atomiser," *Quarterly Journal of Mechanics and Applied Mathematics*," vol. 3, part 2, 1950, p. 129.

R. P. KANWAL
Mathematics Research Center,
University of Wisconsin,
Madison, Wis.
Now Associate Professor,
Department of Mathematics,
The Pennsylvania State University,
University Park, Pa.

Slow Rotatory Motion of a Circular Disk About One of Its Diameters in a Viscous Fluid[1]

An analytic solution is presented for the case when a rigid circular plate is made to rotate about a diameter in its plane, in an infinite mass of viscous fluid. Formulas are derived for the velocity components, pressure, and the couple experienced by the disk.

THE INVESTIGATIONS regarding the motion set up in an infinite mass of viscous fluid when a circular disk is being translated edgewise as well as broadside-on have been made as a limiting case to the motion of an oblate spheroid [1].[2] The case of a steady rotation about its normal axis has been studied by Jeffery [2] as a limit to the case of an oblate spheroid rotating about its major axis. Jeffery, however, outlined an independent approach in terms of certain dual integral equations for this particular mode of motion of the disk but could not give a complete analysis. These integral equations are a special case of the integral equations which have been discussed subsequently by Titchmarsh [3] and Busbridge [4]. It is a matter of simple verification that all the afore-mentioned three modes of motion of the disk can be solved by the use of the dual integral equations as pointed out by Jeffery for the case of one of these modes of motion. In fact, Gupta [5] has recently discussed the case of its broadside-on translation by this method.

There is a fourth mode of motion of the disk; namely, its steady rotation about a diameter in its plane. This case does not appear to have been discussed so far. The reason apparently is that it cannot be analyzed as a limiting process to the motion of an oblate spheroid. The purpose of this paper is to provide a solution for this case by the use of the integral equations mentioned previously. The accuracy of our results has been checked by employing certain limit processes to the solution of the corresponding problem in elastostatics recently solved by Bycroft [6].

Equations of Motion and Their Solution

After neglecting the second-order terms, the Navier-Stokes equations governing the steady flow of a viscous fluid in cylindrical co-ordinates are [7]

$$\mu\left(\nabla^2 u - \frac{u}{r^2} - \frac{2}{r^2}\frac{\partial v}{\partial \theta}\right) = \frac{\partial p}{\partial r}, \tag{1}$$

$$\mu\left(\nabla^2 v + \frac{2}{r^2}\frac{\partial u}{\partial \theta} - \frac{v}{r^2}\right) = \frac{1}{r}\frac{\partial p}{\partial \theta}, \tag{2}$$

$$\mu\nabla^2 w = \frac{\partial p}{\partial z}. \tag{3}$$

The equation of continuity is

$$\frac{\partial u}{\partial r} + \frac{u}{r} + \frac{1}{r}\frac{\partial v}{\partial \theta} + \frac{\partial w}{\partial z} = 0 \tag{4}$$

From the equations (1–4) we get after some appropriate differentiation and addition

$$\nabla^2 p = 0, \tag{5}$$

where

$$\nabla^2 = \frac{\partial^2}{\partial r^2} + \frac{1}{r}\frac{\partial}{\partial r} + \frac{1}{r^2}\frac{\partial^2}{\partial \theta^2} + \frac{\partial^2}{\partial z^2}. \tag{6}$$

The appropriate stresses required in the analysis are

$$p_{zz} = -p + 2\mu\frac{\partial w}{\partial z},$$

$$p_{rz} = \mu\left(\frac{\partial u}{\partial z} + \frac{\partial w}{\partial r}\right), \tag{7}$$

$$p_{\theta z} = \mu\left(\frac{1}{r}\frac{\partial w}{\partial \theta} + \frac{\partial v}{\partial z}\right).$$

The disk coincides with the plane $z = 0$. In view of the symmetry it will be sufficient to consider the region above the disk; i.e., the region $z \geq 0$.

Let us start with finding an appropriate solution of equation (5). The solution is to be such that (*a*) it vanishes at infinity; (*b*) it is equal but opposite in sign at a point $(r, \theta + \pi, z)$ to that at the point (r, θ, z). We may therefore put

$$p = 2\mu\alpha^2 B(\alpha) F(r) e^{-\alpha z} \sin\theta, \tag{8}$$

where $B(\alpha)$ is a constant. The reason for the constant $2\mu\alpha^2$ appearing in (8) will become clear shortly. Equation (5) then becomes

$$\frac{d^2F}{dr^2} + \frac{1}{r}\frac{dF}{dr} + \left(\alpha^2 - \frac{1}{r^2}\right)F = 0. \tag{9}$$

The required solution of this equation is

$$F = J_1(\alpha r). \tag{10}$$

Thus from (8) we get

$$p = 2\mu\alpha^2 B(\alpha) e^{-\alpha z} J_1(\alpha r) \sin\theta. \tag{11}$$

[1] This work was sponsored by the U. S. Army under Contract No. DA-11-022-ORD-2059 with the University of Wisconsin.

[2] Numbers in brackets designate References at end of paper.

Presented at the West Coast Conference of the Applied Mechanics Division, Stanford, Calif., September 9–11, 1959, of THE AMERICAN SOCIETY OF MECHANICAL ENGINEERS.

Discussion of this paper should be addressed to the Secretary, ASME, 29 West 39th Street, New York, N. Y., and will be accepted until January 10, 1960, for publication at a later date. Discussion received after the closing date will be returned.

NOTE: Statements and opinions advanced in papers are to be understood as individual expressions of their authors and not those of the Society. Manuscript received by ASME Applied Mechanics Division, October 9, 1958. Paper No. 59—APMW-6.

Putting this value of p in equation (3), we see that w is given by the relation

$$\nabla^2 w = 2\alpha^2 B(\alpha) e^{-\alpha z} J_1(\alpha r) \sin\theta, \tag{12}$$

Its complementary solution is found, as before, to be

$$w = \alpha A(\alpha) e^{-\alpha z} J_1(\alpha r) \sin\theta, \tag{13}$$

while the particular solution is, as can be easily verified,

$$w = [\alpha B(\alpha) + \alpha^2 B(\alpha) z] e^{-\alpha z} J_1(\alpha r) \sin\theta, \tag{14}$$

Thus the complete solution for w is

$$w = [\alpha A(\alpha) + \alpha B(\alpha) + \alpha^2 B(\alpha) z] e^{-\alpha z} J_1(\alpha r) \sin\theta. \tag{15}$$

In order to find the complementary solutions of equations (1) and (2) we put

$$u = -A(\alpha) e^{-\alpha z} \frac{\partial g(r)}{\partial r} \sin\theta,$$
$$v = -A(\alpha) e^{-\alpha z} \frac{g(r)}{r} \cos\theta, \tag{16}$$

and find as above that

$$g(r) = J_1(\alpha r).$$

Similarly the particular solutions of (1) and (2) are, respectively,

$$u = -\alpha B(\alpha) z e^{-\alpha z} \frac{\partial J_1(\alpha r)}{\partial r} \sin\theta,$$

and

$$v = -\alpha B(\alpha) z e^{-\alpha z} \frac{J_1(\alpha r)}{r} \cos\theta. \tag{17}$$

Thus the complete solutions for u and v are

$$u = -[A(\alpha) + \alpha B(\alpha) z] e^{-\alpha z} \frac{\partial J_1(\alpha r)}{\partial r} \sin\theta,$$
$$v = -[A(\alpha) + \alpha B(\alpha) z] e^{-\alpha z} \frac{J_1(\alpha r)}{r} \cos\theta. \tag{18}$$

The constants appearing in the relations (8), (15), and (18) have been so adjusted as to satisfy the equation of continuity (4).

In view of the symmetry of the problem and the fact that the fluid is viscous, we require that $u = 0 = v$ in the plane of the disk; i.e., $z = 0$. This gives $A = 0$ and we have finally

$$u = -\alpha B(\alpha) z e^{-\alpha z} \frac{\partial J_1(\alpha r)}{\partial r} \sin\theta, \tag{19}$$

$$v = -\alpha B(\alpha) z e^{-\alpha z} \frac{J_1(\alpha r)}{r} \cos\theta, \tag{20}$$

$$w = [\alpha B(\alpha) + \alpha^2 B(\alpha) z] e^{-\alpha z} J_1(\alpha r) \sin\theta, \tag{21}$$

$$p = 2\mu\alpha^2 B(\alpha) e^{-\alpha z} J_1(\alpha r) \sin\theta, \tag{22}$$

and

$$p_{zz}|_{z=0} = -2\mu\alpha^2 B(\alpha) J_1(\alpha r) \sin\theta. \tag{23}$$

We generalize our solution by integrating the expression for u, v, and w with respect to α from 0 to ∞. The boundary conditions in the plane of the disk become

$$w = \omega_0 r \sin\theta, \quad r \leqslant r_0,$$
$$p_{zz}|_{z=0} = 0, \quad r > r_0, \tag{24}$$

where r_0 is the radius of the disk and ω_0 is its angular velocity. These boundary conditions yield the dual integral equations

$$\int_0^\infty \alpha B(\alpha) J_1(\alpha r) d\alpha = \omega_0 r, \quad r \leq r_0,$$
$$\int_0^\infty \alpha^2 B(\alpha) J_1(\alpha r) d\alpha = 0, \quad r > r_0. \tag{25}$$

The solution is [3, 6]

$$B(\alpha) = \frac{4\omega_0 r_0}{\pi\alpha^2}\left[\frac{\sin\alpha r_0}{\alpha r_0} - \cos\alpha r_0\right], \tag{26}$$

and thus

$$p_{zz}|_{z=0} = \frac{-8\mu\omega_0 r_0 \sin\theta}{\pi}\int_0^\infty \left[\frac{\sin\alpha r_0}{\alpha r_0} - \cos\alpha r_0\right] J_1(\alpha r) d\alpha$$
$$= \frac{-8\mu\omega_0 r \sin\theta}{\pi(r_0^2 - r^2)^{1/2}}. \tag{27}$$ [8]

The couple required to maintain the motion is

$$T = \left[2\int_0^{r_0}\int_0^{2\pi} p_{zz} r^2 \sin\theta dr\, d\theta\right]$$
$$= \frac{-16\mu\omega_0}{\pi}\int_0^{2\pi}\sin^3\theta d\theta \int_0^{r_0}\frac{r^3}{(r_0^2 - r^2)^{1/2}} dr$$
$$= -\frac{32}{3}\mu\omega_0 r_0^3. \tag{28}$$

Evaluation of w in Plane $z = 0$

From formulas (21) and (26) we see that

$$w|_{z=0} = \frac{4\omega_0 r_0}{\pi}\sin\theta\int_0^\infty\left(\frac{\sin\alpha r_0}{\alpha^2 r_0} - \frac{\cos\alpha r_0}{\alpha}\right) J_1(\alpha r) d\alpha. \tag{29}$$

We introduce two dimensionless quantities; viz.,

$$W = \frac{w}{\omega_0 r_0}\bigg|_{z=0}, \quad R = \frac{r}{r_0}. \tag{30}$$

From equation (29) we get

$$W = \frac{4}{\pi}(I_1 - I_2)\sin\theta, \tag{31}$$

where

$$I_1 = \int_0^\infty \frac{\sin\alpha r_0}{\alpha^2 r_0} J_1(\alpha r) d\alpha, \tag{32}$$

and

$$I_2 = \int_0^\infty \frac{\cos\alpha r_0}{\alpha} J_1(\alpha r) d\alpha. \tag{33}$$

Now the value of I_2 is known and is given as [8]

$$I_2 = \begin{cases} 0 & \text{for } R \leq 1, \\ \cos\left\{\sin^{-1}\dfrac{1}{R}\right\} & \text{for } R \geq 1. \end{cases} \tag{34}$$

To evaluate I_1 we use the relation

$$\frac{J_1(xt)}{x} = \int_0^1 t J_0(xt) dt, \tag{35}$$

and get

$$I_1 = R\int_0^1 t\,dt\int_0^\infty \frac{\sin \alpha r}{\alpha} J_0(\alpha r t)d\alpha. \tag{36}$$

But [8]

$$\int_0^\infty \frac{\sin \alpha r_0}{\alpha} J_0(\alpha r t)d\alpha = \begin{cases} \dfrac{\pi}{2} & \text{for } t \le \dfrac{1}{R}, \\ \sin^{-1}\dfrac{1}{Rt} & \text{for } t \ge \dfrac{1}{R}. \end{cases} \tag{37}$$

Therefore for $R \le 1$

$$I_1 = R\int_0^1 \frac{\pi}{2}\,t dt = \frac{\pi}{4}R. \tag{38a}$$

For $R \ge 1$

$$I_1 = R\left\{\int_0^{\frac{1}{R}} \frac{\pi}{2}\,t dt + \int_{1/R}^1 t\sin^{-1}\frac{1}{Rt}\,dt\right\} = \frac{R}{2}\sin^{-1}\frac{1}{R} + \frac{(R^2-1)^{1/2}}{2R}. \tag{38b}$$

Finally from (31), (34), and (38) we have

$$W = \frac{4}{\pi}(I_1 - I_2)\sin\theta = \begin{cases} R\sin\theta & \text{for } R \le 1, \\ \dfrac{4}{\pi}\left[\dfrac{R}{2}\sin^{-1}\dfrac{1}{R} + \dfrac{(R^2-1)^{1/2}}{2R} - \cos\left(\sin^{-1}\dfrac{1}{R}\right)\right]\sin\theta & \text{for } R \ge 1 \end{cases}. \tag{39}$$

The first part of the foregoing solution is just the boundary condition (24).

Here a word about shearing stresses will be in order. If we calculate the shear stress from the values of u, v, w given by equations (19–21), their value is zero. It should, however, be noted that if one were to write the answer for the problem for both positive and negative z, some of the z in the equations would be replaced by $|z|$. It would emerge from this that the shear stresses are not odd functions of z. A careful investigation of the implications of the formulas for the shear stresses would probably then reveal that, despite the fact these formulas contain a factor $|z|$, the limit of these stresses as z tends to zero would not be zero.

Some of our results can be checked. Bycroft [6] has recently solved the problem of the equilibrium of a rigid circular plate on a semi-infinite elastic space where he has discussed all the four modes of equilibrium. Now there is a well-known limit process by which the results in elastostatics can be compared with those in viscous incompressible fluids where the flow is governed by linearized Navier-Stokes equations. We will describe it briefly for our particular case. When a rigid circular disk resting on a semi-infinite elastic stratum (i.e., $z > 0$) is made to rotate about a diameter in its plane, the equations of equilibrium in Love's notation are [9]:

$$(\lambda+2\mu)\frac{\partial\Delta}{\partial r} - \frac{2\mu}{r}\frac{\partial\tilde{\omega}_r}{\partial\theta} + 2\mu\frac{\partial\tilde{\omega}_\theta}{\partial z}, \tag{40}$$

$$(\lambda+2\mu)\frac{1}{r}\frac{\partial\Delta}{\partial\theta} - 2\mu\frac{\partial\tilde{\omega}_r}{\partial z} + 2\mu\frac{\partial\tilde{\omega}_z}{\partial r}, \tag{41}$$

$$(\lambda+2\mu)\frac{\partial\Delta}{\partial z} - \frac{2\mu}{r}\frac{\partial}{\partial r}(r\tilde{\omega}_\theta) + \frac{2\mu}{r}\frac{\partial\tilde{\omega}_r}{\partial\theta}, \tag{42}$$

where

$$2\tilde{\omega}_\theta = \left\{\frac{\partial u}{\partial z} - \frac{\partial w}{\partial r}\right\},$$
$$2\tilde{\omega}_r = \left\{\frac{1}{r}\frac{\partial w}{\partial\theta} - \frac{\partial v}{\partial z}\right\}, \tag{43}$$
$$2\tilde{\omega}_z = \frac{1}{r}\left\{\frac{\partial(rv)}{\partial r} - \frac{\partial u}{\partial\theta}\right\},$$

and Δ is given by the left-hand side of the equation (4). The solutions of these equations will tend to the equations for our problem under the following limiting process [10]:

$$\lambda \to \infty, \quad \Delta \to 0, \quad \text{such that } \lambda\Delta \to -p$$

We can compare two of our main results, namely (8) and (28). Now the solutions given by Bycroft for Δ and the couple T acting on the side of the disk which is in contact with the elastic stratum are, respectively,

$$\Delta = \frac{\mu}{(\lambda+\mu)}C_1(\alpha)e^{-\alpha z}J_1(\alpha r)\sin\theta, \tag{44}$$

C_1 being a constant and

$$T = \frac{16\omega_0\mu(\lambda+\mu)r_0^3}{3(\lambda+3\mu)}, \tag{45}$$

where ω_0 is the angle of rotation in this case.

From (44) it is clear that as $\lambda \to \infty$, $\Delta \to 0$ and $\lambda\Delta \to -p$, with $C_1(\alpha) = 2\alpha^2 B(\alpha)$; and from (45) it is clear that $T \to (16/3)\omega_0\mu r_0^3$, which is just half of the value of the couple in our problem, as indeed it should be.

References

1 H. Lamb, "Hydrodynamics," Dover Publications, 1945, p. 605.

2 G. B. Jeffery, "On the Steady Rotation of a Solid of Revolution in a Viscous Fluid," Proceedings of the London Mathematical Society, vol. 14, 1915, p. 327.

3 E. C. Titchmarsh, "Theory of Fourier Integrals," Oxford University Press, 1937, p. 337.

4 I. W. Busbridge, "Dual Integral Equations," Proceedings of the London Mathematical Society (2), vol. 44, 1938, p. 115.

5 S. C. Gupta, "Slow Broadside Motion of a Flat Plate in a Viscous Liquid," *Zeitschrift für angewandte Mathematik und Physik*, vol. 8, 1957, p. 257.

6 G. N. Bycroft, "Forced Vibrations of a Rigid Circular Plate on a Semi-Infinite Elastic Space and on an Elastic Stratum," Philosophical Transactions of Royal Society, London, vol. 248, 1956, p. 327.

7 "Modern Developments in Fluid Dynamics," edited by S. Goldstein, Oxford University Press, 1938, chapter 3.

8 G. N. Watson, "Theory of Bessel Functions," Cambridge University Press, second edition, 1944, p. 405.

9 A. E. H. Love, "Mathematical Theory of Elasticity," Dover Publications, New York, N. Y., 1944.

10 B. R. Seth, "Generalized Singular Points With Applications to Flow Problems," Proceedings of the Indian Academy of Sciences, vol. 40A, 1955, p. 25.

Thermal Stresses Owing to a Hot Spot in a Rectangular Strip

C. W. NELSON

Associate Professor,
Division of Engineering Design,
University of California, Berkeley, Calif.
Mem. ASME
Now with IBM Engineering Laboratory,
Endicott, N. Y.

The thermal stresses for the plane-stress problem of a circular hot spot in an infinitely long straight strip of rectangular cross section are derived by a Fourier integral approach. The hot spot is located on the longitudinal center line of the strip, and its radius is such that the boundary of the hot spot is tangent to both edges of the strip. The temperature may be any function of the radius within the hot spot and is assumed to have a constant value (zero) throughout the rest of the strip. Numerical values are given for the stresses on the edges and both center lines of the strip for a particular case.

IT IS the purpose of this note to present some results for the thermal stresses in the plane-stress problem of a circular hot spot in an infinitely long straight strip of rectangular cross section. The hot spot is located on the longitudinal center line of the strip, as shown in Fig. 1, and its radius is such that the boundary of the hot spot is tangent to both edges of the strip.

The temperature inside the hot spot is denoted by T, where T is any function of r only and r is the radial co-ordinate or distance from the center of the hot spot. The temperature outside the hot spot is assumed to be constant and no loss of generality results if the datum of temperature is so chosen as to make this constant zero. The linear coefficient of thermal expansion, α, is assumed to be constant.

The solution of the problem was obtained by starting with the known solution[1] for the stresses due to the same hot spot in an infinite plate. Next, a strip of width $2a$ was assumed to be cut from the infinite plate without disturbing the stress system. This required the maintenance of normal and shearing stresses on both edges of the infinite strip. Finally, the stresses due to removing the normal and shearing stresses on the edges of the strip were added to the stresses for the infinite plate to obtain the total stresses for the problem of Fig. 1.

For an infinite plate with temperature, T, any function of r, the known stresses[1] transformed to rectangular co-ordinates for convenience in the present problem are

$$\sigma_{x1} = -\frac{E\alpha T y^2}{x^2 + y^2} - \frac{E\alpha(x^2 - y^2)}{(x^2 + y^2)^2} \int_0^r T(\lambda)\lambda d\lambda \qquad (1)$$

$$\sigma_{y1} = -\frac{E\alpha T x^2}{x^2 + y^2} + \frac{E\alpha(x^2 - y^2)}{(x^2 + y^2)^2} \int_0^r T(\lambda)\lambda d\lambda \qquad (2)$$

$$\tau_{xy1} = \frac{E\alpha T xy}{x^2 + y^2} - \frac{2E\alpha xy}{(x^2 + y^2)^2} \int_0^r T(\lambda)\lambda d\lambda \qquad (3)$$

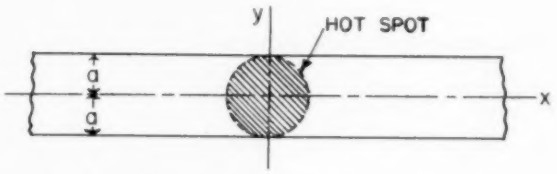

Fig. 1 Infinitely long rectangular strip with a hot spot

where E is Young's modulus, λ is a dummy variable of integration, and the subscript 1 denotes that these are the stresses for an infinite plate and only part of the stresses for the problem of Fig. 1. For the case of a hot spot of radius a, i.e., when $T = 0$ for $r > a$, Equations (1) to (3) are still applicable for the stresses in the infinite plate.

If a strip of width $2a$ with edges $y = \pm a$ is assumed to be cut from the infinite plate containing the hot spot without disturbing the stress system as given by Equations (1) to (3), this requires the maintenance of boundary stresses

$$(\sigma_{y_1})_{y=\pm a} = \frac{CE\alpha(x^2 - a^2)}{(x^2 + a^2)^2} \qquad (4)$$

$$(\tau_{xy_1})_{y=\pm a} = \mp\frac{2CE\alpha ax}{(x^2 + a^2)^2} \qquad (5)$$

on the edges of the strip. In Equations (4) and (5), C is a constant given by

$$C = \int_0^a T(\lambda)\lambda d\lambda \qquad (6)$$

When the boundary stresses given by Equations (4) and (5) are removed from the edges of the strip, the additional stresses thus produced may be found by the well-established Fourier integral procedure[2] and, when these stresses are added to the

[1] S. Timoshenko and J. N. Goodier, "Theory of Elasticity," McGraw-Hill Book Company, Inc., New York, N. Y., second edition, 1951, pp. 406–408.

Contributed by the Applied Mechanics Division and presented at the Annual Meeting, Atlantic City, N. J., November 29–December 4, 1959, of THE AMERICAN SOCIETY OF MECHANICAL ENGINEERS.

Discussion of this paper should be addressed to the Secretary, ASME, 29 West 39th Street, New York, N. Y., and will be accepted until January 10, 1960, for publication at a later date. Discussion received after the closing date will be returned.

NOTE: Statements and opinions advanced in papers are to be understood as individual expressions of their authors and not those of the Society. Manuscript received by ASME Applied Mechanics, March 17, 1958. Paper No. 59—A-8.

[2] L. N. G. Filon, "On an Approximate Solution for the Bending of a Beam of Rectangular Cross Section Under Any System of Loads, With Special Reference to Points of Concentrated or Discontinuous Loading," *Philosophical Transactions of The Royal Society of London*, England, vol. 201, series A, 1903, p. 63.

Other references dealing with the application of the Fourier-integral method to straight-beam problems are given in the Bibliography of the paper: C. W. Nelson, C. J. Ancker, Jr., and Ning-Gau Wu, "The Stresses in a Flat Curved Bar Due to Concentrated Radial Loads," JOURNAL OF APPLIED MECHANICS, vol. 19, TRANS. ASME, vol. 74, 1952, pp. 529–536.

stresses with subscript 1, the total stresses for the problem of Fig. 1 are found to be

$$\sigma_x = \sigma_{x1} + \frac{E\alpha C}{4a^2} \int_0^\infty \frac{\left[(3w + we^{-w} - w^2)\cosh\frac{wy}{2a} + \frac{w^2y}{a}\sinh\frac{wy}{2a}\right]}{\sinh w + w}\cos\frac{wx}{2a}\,dw \quad (7)$$

$$\sigma_y = \sigma_{y'} + \frac{E\alpha C}{4a^2} \int_0^\infty \frac{\left[(w - we^{-w} + w^2)\cosh\frac{wy}{2a} - \frac{w^2y}{a}\sinh\frac{wy}{2a}\right]}{\sinh w + w}\cos\frac{wx}{2a}\,dw \quad (8)$$

$$\tau_{xy} = \tau_{xy1} + \frac{E\alpha C}{4a^2} \int_0^\infty \frac{\left[(w + we^{-w} - w^2)\sinh\frac{wy}{2a} + \frac{w^2y}{a}\cosh\frac{wy}{2a}\right]}{\sinh w + w}\sin\frac{wx}{2a}\,dw \quad (9)$$

where w is a dummy variable of integration.

Obviously, the evaluation of the stresses by means of Equations (7) to (9) and (1) to (3) is about as simple for one distribution of temperature within the hot spot as it is for some other. However, in order to show some numerical results, a specific temperature distribution must be assumed and the following results are based on the assumption that the temperature has a constant value T_0 throughout the hot spot and, of course, is zero everywhere else in the strip.

The stresses were computed along the top edge of the strip, the vertical center line, and the horizontal center line, by means of the following equations obtained from Equations (7) to (9):

$$(\sigma_x)_{y=+a} = \frac{E\alpha T_0}{2}\int_0^\infty \frac{w\cosh\frac{w}{2}\cos\frac{wx}{2a}\,dw}{\sinh w + w} \quad (10)$$

$$(\sigma_x)_{x=0} = -\frac{E\alpha T_0}{2} + \frac{E\alpha T_0}{8} \int_0^\infty \frac{\left[(3w + we^{-w} - w^2)\cosh\frac{wy}{2a} + \frac{w^2y}{a}\sinh\frac{wy}{2a}\right]}{\sinh w + w}\,dw \quad (11)$$

$$(\sigma_y)_{x=0} = -\frac{E\alpha T_0}{2} + \frac{E\alpha T_0}{8} \int_0^\infty \frac{\left[(w - we^{-w} + w^2)\cosh\frac{wy}{2a} - \frac{w^2y}{a}\sinh\frac{wy}{2a}\right]}{\sinh w + w}\,dw \quad (12)$$

$$(\sigma_x)_{y=0} = (\sigma_{x1})_{y=0} + \frac{E\alpha T_0}{8}\int_0^\infty \frac{3w + we^{-w} - w^2}{\sinh w + w}\cos\frac{wx}{2a}\,dw \quad (13)$$

$$(\sigma_y)_{y=0} = (\sigma_{y'})_{y=0} + \frac{E\alpha T_0}{8}\int_0^\infty \frac{w - we^{-w} + w^2}{\sinh w + w}\cos\frac{wx}{2a}\,dw \quad (14)$$

The foregoing are the only nonzero stresses at the three locations investigated since σ_y and τ_{xy} are zero on the edges of the strip and τ_{xy} is also zero on both center lines of the strip.

The infinite integrals required in Equations (10) to (14) were evaluated by expanding the numerator of each integrand in a Maclaurin series in powers of w, except that the factor e^{-w} occurring in the numerators of some of the integrands was not expanded. Thus each integral was expressed as a series of integrals of the type

$$\mathrm{I}_k = \frac{1}{2(k!)}\int_0^\infty \frac{w^k dw}{\sinh w + w} \quad (15)$$

or

$$\mathrm{II}_k = \frac{1}{2(k!)}\int_0^\infty \frac{w^k e^{-w} dw}{\sinh w + w} \quad (16)$$

The integrals I_k and II_k are two of the four Howland's integrals and tables of values of these integrals are available.[3,4] The convergence of each series of Howland's integrals was improved by application of a Kummer transformation.[5] For example, one of the integrals required in Equations (13) and (14) is

$$\int_0^\infty \frac{w\cos\frac{wx}{2a}\,dw}{\sinh w + w} = 2\mathrm{I}_1 - 6\mathrm{I}_2\left(\frac{x}{2a}\right)^2 + 10\mathrm{I}_3\left(\frac{x}{2a}\right)^4 - \ldots \quad (17)$$

and the series in the right member of this equation converges poorly as x approaches $2a$. By use of a Kummer transformation, Equation (17) can be replaced by

$$\int_0^\infty \frac{w\cos\frac{wx}{2a}\,dw}{\sinh w + w} = \frac{2\left[1 - \left(\frac{x}{2a}\right)^2\right]}{\left[1 + \left(\frac{x}{2a}\right)^2\right]^2} - \left[2(1 - \mathrm{I}_1) - 6(1 - \mathrm{I}_2)\left(\frac{x}{2a}\right)^2 + 10(1 - \mathrm{I}_3)\left(\frac{x}{2a}\right)^4 - \ldots\right] \quad (18)$$

and the series in the right member of Equation (18) converges well for $x = 2a$ with poor convergence as x approaches $4a$.

The values of σ_x along the top or bottom of the strip are given in Table 1 and shown graphically in Fig. 2. Values of σ_x and σ_y along the vertical center line of the strip are given in Table 2 and plotted in Fig. 3. Values of σ_x and σ_y along the horizontal center line of the strip are given in Table 3 and plotted in Fig. 4. It

[3] C. B. Ling and C. W. Nelson, "On Evaluation of Howland's Integrals," *Annals of Academia Sinica*, 1955, pp. 45–50 (Taiwan, China).

[4] Chih-Bing Ling, "Stresses in a Perforated Strip," JOURNAL OF APPLIED MECHANICS, vol. 24, TRANS. ASME, vol. 79, 1957, pp. 365–375. There is one typographical error in the Howland's integrals tabulated in this reference. This error is in the value of I_7 for which the correct value is $\mathrm{I}_7 = 0.972699$ which is the value given in the reference under footnote 3.

[5] Konrad Knopp, "Theory and Application of Infinite Series," Blackie and Son Limited, London and Glasgow, first edition, 1928, or second edition, 1951.

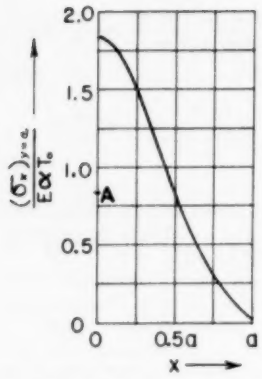

Fig. 2 Variation of σ_x along edges of bar; point A shows value of $(\sigma_x)_{y=a}/(E\alpha T_0)$ just inside boundary of hot spot

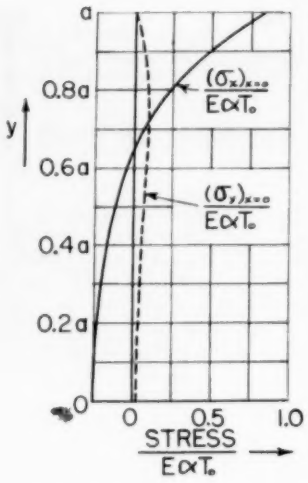

Fig. 3 Variation of σ_x and σ_y along vertical center line of hot spot

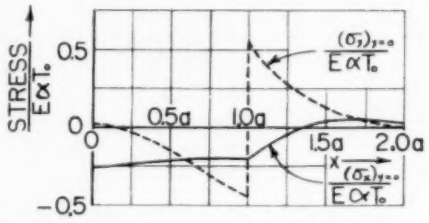

Fig. 4 Variation of σ_x and σ_y along horizontal center line of strip

Table 1 Values of σ_x along top or bottom edge of strip shown in Fig. 1

x	$\frac{(\sigma_x)_{y=a}}{E\alpha T_0}$
0	1.8350
$0.2a$	1.6200
$0.5a$	0.8525
$1.0a$	0.0168

Table 2 Values of σ_x and σ_y along vertical center line of strip, $x = 0$

y	$\frac{(\sigma_x)_{x=0}}{E\alpha T_0}$	$\frac{(\sigma_y)_{x=0}}{E\alpha T_0}$
a	0.8350	0
$0.8a$	0.2322	0.0873
$0.6a$	−0.0417	0.0768
$0.4a$	−0.1736	0.0494
$0.2a$	−0.2346	0.0285
0	−0.2525	0.0210

should be noted that the value of $(\sigma_x)_{y=\pm a}$ in Fig. 2 (outside the hot spot) is 1.8350 $E\alpha T_0$ while the value of $(\sigma_x)_{y=\pm a}$ in Fig. 3 (inside the hot spot) is 0.8350 $E\alpha T_0$. The latter value is indicated by point A in Fig. 2 in order to call attention to this discontinuity in σ_x.

Table 3 Values of σ_x and σ_y along horizontal center line of strip, $y = 0$

x	$\frac{(\sigma_x)_{y=0}}{E\alpha T_0}$	$\frac{(\sigma_y)_{y=0}}{E\alpha T_0}$
0	−0.2525	0.0210
$0.2a$	−0.2453	−0.0105
$0.4a$	−0.2276	−0.0962
$0.6a$	−0.2088	−0.2131
$0.8a$	−0.1982	−0.3350
$1.0a$	−0.2012	−0.4416[a] / 0.5584[b]
$1.2a$	−0.0652	0.3253
$1.6a$	0.0276	0.0922
$2.0a$	0.0333	0.0120

[a] Inside the hot spot.
[b] Outside the hot spot.

The numerical results in Tables 1, 2, and 3 confirm the natural expectation that the greatest stress for the problem of Fig. 1, with $T = T_0$ throughout the hot spot, is σ_x at the top or bottom of the hot spot. The value of this maximum stress is found to be 1.8350 $E\alpha T_0$, considerably greater than the value $E\alpha T_0$ which would occur at the same point due to heating a narrow strip along the line $x = 0$ to a temperature T_0 above the temperature of the rest of the bar.

Impact and Moving Loads on a Slightly Curved Elastic Half Space[1]

A. C. ERINGEN
Professor,
Division of Engineering Sciences,
Purdue University,
Lafayette, Ind.

J. C. SAMUELS
Assistant Professor,
Division of Engineering Sciences,
Purdue University,
Lafayette, Ind.

Two-dimensional Fourier transforms are employed to treat the two-dimensional dynamic problem of elastic half space having a slightly wavy boundary. The various boundary curves considered include square and triangular bumps and holes, and sinusoidal and periodic boundaries. The number of different types of surface loadings considered are: (a) *Normal tractions and zero shear,* (b) *impulsive normal tractions and zero shear,* (c) *suddenly applied normal tractions and zero shear,* (d) *concentrated normal load and zero shear,* (e) *concentrated impulsive load and zero shear,* (f) *pulsating normal load and zero shear,* (g) *moving loads,* (h) *pulsating moving loads,* (i) *vertical and horizontal loads,* (j) *moving vertical loads. Stress and displacement components for special cases of the loads described in* (a, c, f, *and* g) *acting on a sinusoidal boundary lead to a solution which requires evaluation of a single indefinite integral. Closed-form results are given for a uniform pulsating pressure load.*

THE problem of dynamical and moving loads on a wavy boundary is of considerable practical and theoretical interest. The waves produced by moving vehicles, impact, and other types of dynamical loads on a foundation having a wavy surface fall into this category. Applications also may be found in the field of geophysics and in the oil industry. The problem in its realistic form is a formidable one. By assuming that the boundary is slightly curved, however, it is possible to give a treatment. This, of course, is the case in the problem of the semi-infinite plane with a boundary curve which is almost but not quite straight. A number of important problems, for example, the sinusoidal boundary having a long wave length, naturally fall into this category.

The equations for a two-dimensional isotropic, elastic body with zero body forces, subjected to dynamical loads on the wavy surface, are solved. In a number of cases, it is found that a closed-form solution is possible.

[1] The work contained in this paper was sponsored by the Office of Naval Research.

Contributed by the Applied Mechanics Division and presented at the Annual Meeting, Atlantic City, N. J., November 29–December 4, 1959, of THE AMERICAN SOCIETY OF MECHANICAL ENGINEERS.

Discussion of this paper should be addressed to the Secretary, ASME, 29 West 39th Street, New York, N. Y., and will be accepted until January 10, 1960, for publication at a later date. Discussion received after the closing date will be returned.

NOTE: Statements and opinions advanced in papers are to be understood as individual expressions of their authors and not those of the Society. Manuscript received by ASME Applied Mechanics Division, May 12, 1958. Paper No. 59—A-2.

Formulation of Problem

The equations of motion in rectangular co-ordinates x, y, and time t for a two-dimensional, homogeneous, isotropic, elastic body having zero body forces are

$$\frac{\partial \sigma_x}{\partial x} + \frac{\partial \tau_{xy}}{\partial y} = \rho \frac{\partial^2 u}{\partial t^2}, \quad \frac{\partial \tau_{xy}}{\partial x} + \frac{\partial \sigma_y}{\partial y} = \rho \frac{\partial^2 v}{\partial t^2} \tag{1}$$

Here σ_x, σ_y, τ_{xy} are the stress components; u, v are the displacement components, and ρ is the mass density per unit volume. The stress and displacement components are related to each other by Hooke's law:

$$\sigma_x = \lambda \left(\frac{\partial u}{\partial x} + \frac{\partial v}{\partial y} \right) + 2\mu \frac{\partial u}{\partial x},$$

$$\sigma_y = \lambda \left(\frac{\partial u}{\partial x} + \frac{\partial v}{\partial y} \right) + 2\mu \frac{\partial v}{\partial y},$$

$$\tau_{xy} = \mu \left(\frac{\partial v}{\partial x} + \frac{\partial u}{\partial y} \right) \tag{2}$$

where λ and μ are Lamé's elastic constants.

Nomenclature

x, y = rectangular co-ordinates
t = time
ξ, ζ, κ, η_1, η_2 = Fourier-transform variables
λ, μ = Lame constants
c_1 = velocity of irrotational waves
c_2 = velocity of equivoluminal waves
σ_x, σ_y, τ_{xy} = components of stress tensor
σ_n = traction normal to boundary
τ_n = traction tangential to boundary
ϵ = perturbation parameter
$\sigma_i (i = 0, 1, 2, \ldots)$ = coefficient of ϵ^i in expansion of σ_n
$\tau_i (i = 0, 1, 2, \ldots)$ = coefficient of ϵ^i in expansion of τ_n
σ_v, σ_h = vertical and horizontal components of surface traction
u, v = components of displacement vector
ϕ, ψ = displacement potential functions
$f(x)$ = equation of boundary surface
$\bar{F}(\eta)$ = one-dimensional Fourier transform of a function $F(x)$
$\bar{F}(\xi, \zeta)$ = two-dimensional Fourier transform of a function $F(x, t)$
V_0 = velocity of moving load
V = V_0/c_1
$2\pi/r$ = wave length of sinusoidal boundary
$\omega/(2\pi c_1)$ = frequency of pulsating surface load

If we introduce two functions $\phi(x, y, t)$ and $\psi(x, y, t)$ such that

$$u = \frac{\partial \phi}{\partial x} + \frac{\partial \psi}{\partial y}, \quad v = \frac{\partial \phi}{\partial y} - \frac{\partial \psi}{\partial x} \tag{3}$$

equations (2) become

$$\sigma_x = \lambda \nabla^2 \phi + 2\mu \left(\frac{\partial^2 \phi}{\partial x^2} + \frac{\partial^2 \psi}{\partial x \partial y} \right), \quad \sigma_y = \lambda \nabla^2 \phi + 2\mu \left(\frac{\partial^2 \phi}{\partial y^2} - \frac{\partial^2 \psi}{\partial x \partial y} \right),$$
$$\tau_{xy} = \mu \left(2 \frac{\partial^2 \phi}{\partial x \partial y} - \frac{\partial^2 \psi}{\partial x^2} + \frac{\partial^2 \psi}{\partial y^2} \right), \quad \nabla^2 \phi \equiv \frac{\partial^2 \phi}{\partial x^2} + \frac{\partial^2 \phi}{\partial y^2} \tag{4}$$

By introducing (3) and (4) into (1), we find that they are satisfied if ϕ and ψ are the solutions of the wave equations

$$\frac{\partial^2 \phi}{\partial \tau^2} = \nabla^2 \phi, \quad \beta^2 \frac{\partial^2 \psi}{\partial \tau^2} = \nabla^2 \psi \tag{5}$$

where

$$\beta^2 = c_1^2/c_2^2 = (\lambda + 2\mu)/\mu, \quad c_1^2 = (\lambda + 2\mu)/\rho, \quad c_2^2 = \mu/\rho, \quad \tau = c_1 t \tag{6}$$

The equation of the wavy boundary, Fig. 1, may be written in the form

$$y = \epsilon f(x), \quad \epsilon \ll 1 \tag{7}$$

where ϵ represents a small perturbation parameter which, for example, may be selected as the ratio of the height of the highest hill to the smallest wave length, or in some other fashion.

The boundary conditions read: At $y = \epsilon f(x)$,

$$\sigma_n = \sigma_x n_x^2 + 2\tau_{xy} n_x n_y + \sigma_y n_y^2$$
$$\tau_n = (\sigma_x - \sigma_y) n_x n_y + \tau_{xy}(n_y^2 - n_x^2) \tag{8}$$

where σ_n and τ_n are prescribed functions at the boundary curve, and n_x and n_y are the components of the inner unit normal which are given by

$$n_x = -\epsilon f'(1 + \epsilon^2 f'^2)^{-1/2}, \quad n_y = (1 + \epsilon^2 f'^2)^{-1/2} \tag{9}$$

where the prime represents differentiation with respect to x; i.e., $f' \equiv df/dx$. We now substitute (9) into (8) and expand the result into a power series in ϵ. Neglecting the terms containing ϵ^n for $n \geq 3$, we obtain:

$$\sigma_n = \sigma_y - 2\epsilon f' \tau_{xy} + \epsilon^2 f'^2 (\sigma_x - \sigma_y) + 0(\epsilon^3)$$
$$\tau_n = \tau_{xy} + \epsilon f'(\sigma_y - \sigma_x) - 2\epsilon^2 f'^2 \tau_{xy} + 0(\epsilon^3) \tag{10}$$

The problem is now reduced to finding solutions of (5) which vanish at $y = \infty$ and satisfy (10) at the boundary $y = \epsilon f(x)$.

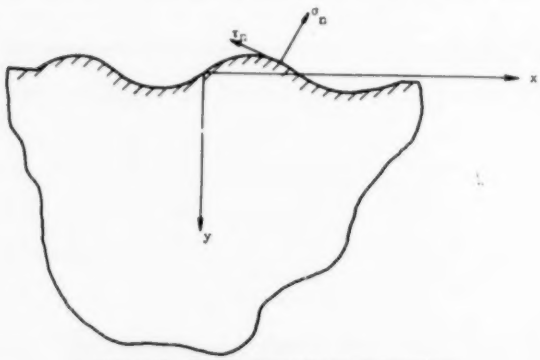

Fig. 1 Elastic half space with wavy boundary

The General Solution

To find the solution of (5), we introduce two-dimensional Fourier transforms

$$\bar{\phi}(\xi, y, \zeta) = \frac{1}{2\pi} \int\int_{-\infty}^{\infty} \phi(x, t, \tau) \exp\,[i(\xi x + \zeta \tau)] dx d\tau \tag{11}$$

and a similar one for ψ. The inverse of (11) is given by

$$\phi(x, y, \tau) = \frac{1}{2\pi} \int\int_{-\infty}^{\infty} \bar{\phi}(\xi, y, \zeta) \exp\,[-i(\xi x + \zeta \tau)] d\xi d\zeta \tag{12}$$

If we now apply (11) to (5), we obtain

$$d^2\bar{\phi}/dy^2 = p^2 \bar{\phi}, \quad d^2\bar{\psi}/dy^2 = q^2 \bar{\psi}$$
$$p = (\xi^2 - \zeta^2)^{1/2}, \quad q = (\xi^2 - \beta^2 \zeta^2)^{1/2} \tag{13}$$

Solutions of (13) vanishing at $y = \infty$ have the forms

$$\bar{\phi} = Ae^{-py}, \quad \bar{\psi} = Be^{-qy} \tag{14}$$

The stress and the displacement components are now obtained by using (14) in (12) and the result in (4) and (3).

$$\sigma_x/2\mu = \frac{1}{2\pi} \int\int_{-\infty}^{\infty} (a_1 A e^{-py} + b_1 B e^{-qy}) E d\xi d\zeta$$
$$\sigma_y/2\mu = \frac{1}{2\pi} \int\int_{-\infty}^{\infty} (a_2 A e^{-py} + b_2 B e^{-qy}) E d\xi d\zeta \tag{15}$$
$$\tau_{xy}/2\mu = \frac{1}{2\pi} \int\int_{-\infty}^{\infty} (a_4 A e^{-py} + b_3 B e^{-qy}) E d\xi d\zeta$$

$$u = -\frac{1}{2\pi} \int\int_{-\infty}^{\infty} (i\xi A e^{-py} + qB e^{-qy}) E d\xi d\zeta$$
$$v = -\frac{1}{2\pi} \int\int_{-\infty}^{\infty} (pA e^{-py} - i\xi B e^{-qy}) E d\xi d\zeta \tag{16}$$

where

$$a_1 = -\left(\xi^2 + \frac{\lambda}{2\mu} \zeta^2 \right), \quad b_1 = i\xi(\xi^2 - \beta^2 \zeta^2)^{1/2}$$
$$a_2 = \xi^2 - {}^1/_2 \beta^2 \zeta^2, \quad b_2 = -b_1, \quad b_3 = a_2$$
$$a_3 = i\xi(\xi^2 - \zeta^2)^{1/2}, \quad E \equiv \exp[-i(\xi x + \zeta \tau)] \tag{17}$$

The functions $A(\xi, \zeta)$ and $B(\xi, \zeta)$ in (14) to (16) will be determined from the boundary conditions (10). To this end, we substitute (15) into (10). Hence,

$$\sigma_n/2\mu = \frac{1}{2\pi} \int\int_{-\infty}^{\infty} \{A[a_2 - 2\epsilon f' a_3 + \epsilon^2 f'^2 (a_1 - a_2)] e^{-\epsilon pf} + B[b_2 - 2\epsilon f' b_3 + \epsilon^2 f'^2 (b_1 - b_2)] e^{-\epsilon qf}\} E d\xi d\zeta$$
$$\tau_n/2\mu = \frac{1}{2\pi} \int\int_{-\infty}^{\infty} \{A[a_3 + \epsilon f'(a_2 - a_1) - 2\epsilon^2 f'^2 a_3] e^{-\epsilon pf} + B[b_3 + \epsilon f'(b_2 - b_1) - 2\epsilon^2 f'^2 b_3] e^{-\epsilon qf}\} E d\xi d\zeta \tag{18}$$

We write

$$\sigma_n = \sigma_0 + \epsilon\sigma_1 + \epsilon^2\sigma_2 + \ldots, \qquad \tau_n = \tau_0 + \epsilon\tau_1 + \epsilon^2\tau_2 + \ldots$$

$$A = A_0 + \epsilon A_1 + \epsilon^2 A_2 + \ldots, \qquad B = B_0 + \epsilon B_1 + \epsilon^2 B_2 + \ldots \tag{19}$$

$$e^{-\epsilon pf} = 1 - \epsilon pf + {}^1/_2\epsilon^2 p^2 f^2 - \ldots, \text{ etc.}$$

Substituting (19) into (18) and equating the coefficients of the powers of ϵ, we obtain:

$$\frac{1}{2\pi}\iint_{-\infty}^{\infty}(a_2A_0 + b_2B_0)Ed\xi d\zeta = \sigma_0/2\mu$$

$$\frac{1}{2\pi}\iint_{-\infty}^{\infty}(a_3A_0 + b_3B_0)Ed\xi d\zeta = \tau_0/2\mu \tag{20}$$

$$\frac{1}{2\pi}\iint_{-\infty}^{\infty}(a_2A_1 + b_2B_1)Ed\xi d\zeta = \frac{\sigma_1}{2\mu} + \frac{1}{2\pi}\iint_{-\infty}^{\infty}[A_0(pfa_2 + 2f'a_3) + B_0(qfb_2 + 2f'b_3)]Ed\xi d\zeta$$

$$\frac{1}{2\pi}\iint_{-\infty}^{\infty}(a_3A_1 + b_3B_1)Ed\xi d\zeta = \frac{\tau_1}{2\mu} + \frac{1}{2\pi}\iint_{-\infty}^{\infty}\{A_0[pfa_3 + f'(a_1 - a_2)] + B_0[qfb_3 + f'(b_1 - b_2)]\}Ed\xi d\zeta \tag{21}$$

$$\frac{1}{2\pi}\iint_{-\infty}^{\infty}(a_2A_2 + b_2B_2)Ed\xi d\zeta = \frac{\sigma_2}{2\mu} + \frac{1}{2\pi}\iint_{-\infty}^{\infty}\{A_1(pfa_2 + 2f'a_3) + B_1(qfb_2 + 2f'b_3) - A_0[{}^1/_2p^2f^2a_2 + 2pff'a_3 + f'^2(a_1 - a_2)] - B_0[{}^1/_2q^2f^2b_2 + 2qff'b_3 + f'^2(b_1 - b_2)]\}Ed\xi d\zeta$$

$$\frac{1}{2\pi}\iint_{-\infty}^{\infty}(a_3A_2 + b_3B_2)Ed\xi d\zeta = \frac{\tau_2}{2\mu} + \frac{1}{2\pi}\iint_{-\infty}^{\infty}\{A_1[pfa_3 + f'(a_1 - a_2)] + B_1[qfb_3 + f'(b_1 - b_2)] - A_0[{}^1/_2p^2f^2a_3 + pff'(a_1 - a_3) - 2f'^2a_3] - B_0[{}^1/_2q^2f^2b_3 + qff'(b_1 - b_2) - 2f'^2b_3]\}E\,d\xi\,d\zeta \tag{22}$$

Equations (20) to (22) are, respectively, the coefficients of 1, ϵ, and ϵ^2 in (18). Consistent with (10), we ignore terms in (18) with order higher than ϵ^2.

We note that equations (20) are the boundary conditions for the case of a flat boundary. Thus (21) and (22) represent the first and second-order corrections that would be needed when the boundary curve is not a straight line but a wavy one. From (20), we solve for A_0 and B_0 by taking the Fourier transforms of both sides. Hence,

$$a_2A_0 + b_2B_0 = \bar{\sigma}_0/2\mu, \quad a_3A_0 + b_3B_0 = \bar{\tau}_0/2\mu \tag{23}$$

or

$$A_0 = (2\mu D)^{-1}(b_3\bar{\sigma}_0 - b_2\bar{\tau}_0), \quad B_0 = (2\mu D)^{-1}(-a_3\bar{\sigma}_0 + a_2\tau_0), \quad D = a_2b_3 - a_3b_2 \tag{24}$$

The quantities A_0 and B_0, so determined, may be substituted into the integrals on the right of (21) to evaluate these integrals. But, since we leave the form of $f(x)$ general, we cannot solve for A_1 and B_1 from these integral equations in their present forms. Thus, we introduce a Fourier-integral representation of $f(x)$ into these integrals; i.e., we write

$$f(x) = \frac{1}{2\pi}\int_{-\infty}^{\infty}\bar{f}(\eta)e^{-i\eta x}d\eta, \quad f'(x) = -\frac{i}{2\pi}\int_{-\infty}^{\infty}\eta\bar{f}(\eta)e^{-i\eta x}d\eta$$

$$\bar{f}(\eta) = \int_{-\infty}^{\infty}f(x)e^{i\eta x}dx \tag{25}$$

Let us, for instance, consider the first of (21) and introduce (25) into the right-hand side of this equation.

$$\frac{1}{2\pi}\iint_{-\infty}^{\infty}(a_2A_1 + b_2B_1)Ed\xi d\zeta = \frac{\sigma_1}{2\mu} + \frac{1}{4\pi^2}\iiint_{-\infty}^{\infty}[A_0(pa_2 - 2i\eta a_3) + B_0(qb_2 - 2i\eta b_3)]\bar{f}(\eta)\exp[-i(\xi x + \zeta\tau) - i\eta x]d\xi d\zeta d\eta \tag{26}$$

If we set $\xi + \eta = \kappa$, $d\xi = d\kappa$, then the triple integral on the right of this equation becomes

$$\frac{1}{4\pi^2}\iiint_{-\infty}^{\infty}[A_0(pa_2 - 2i\eta a_3) + B_0(qb_2 - 2i\eta b_3)]^{\xi=\kappa-\eta}\bar{f}(\eta)\exp[-i(\kappa x + \zeta\tau)]d\kappa d\zeta d\eta \tag{27}$$

If we replace ξ by κ on the left of (26) and use (27) on the right, the integrals on both sides become double Fourier integrals. We now can take the Fourier transforms of both sides and obtain

$$a_2A_1 + b_2B_1 = \frac{\bar{\sigma}_1}{2\mu} + \frac{1}{2\pi}\int_{-\infty}^{\infty}[A_0(pa_2 - 2i\eta a_3) + B_0(qb_2 - 2i\eta b_3)]^{\xi=\kappa-\eta}\bar{f}(\eta)d\eta \tag{28}$$

A similar procedure applied to the second of (21) gives

$$a_3A_1 + b_3B_1 = \frac{\bar{\tau}_1}{2\mu} + \frac{1}{2\pi}\int_{-\infty}^{\infty}\{A_0[pa_3 - i\eta(a_1 - a_2)] + B_0[qb_3 - i\eta(b_1 - b_2)]\}^{\xi=\kappa-\eta}\bar{f}(\eta)d\eta \tag{29}$$

The solution of (28) and (29) gives:

$$A_1(\kappa, \zeta) = [2\mu\, D(\kappa, \zeta)]^{-1}[b_3(\kappa, \zeta)(\bar{\sigma}_1 + \bar{s}_1) - b_2(\kappa, \zeta)(\bar{\tau}_1 + \bar{I}_1)]$$
$$B_1(\kappa, \zeta) = [2\mu\, D(\kappa, \zeta)]^{-1}[-a_3(\kappa, \zeta)(\bar{\sigma}_1 + \bar{s}_1) + a_2(\kappa, \zeta)(\bar{\tau}_1 + \bar{I}_1)] \tag{30}$$

where

$$\bar{\sigma}_1 \equiv \bar{\sigma}_1(\kappa, \zeta), \quad \bar{\tau}_1 \equiv \bar{\tau}_1(\kappa, \zeta)$$

and

$$\mathfrak{z}_1(\kappa, \zeta)/2\mu = \frac{1}{2\pi}\int_{-\infty}^{\infty} [L_1(A_0, B_0, \eta)]^{\xi=\kappa-\eta} \bar{f}(\eta)d\eta$$
$$\mathfrak{l}_1(\kappa, \zeta)/2\mu = \frac{1}{2\pi}\int_{-\infty}^{\infty} [M_1(A_0, B_0, \eta)]^{\xi=\kappa-\eta} \bar{f}(\eta)d\eta \quad (31)$$

$$L_1(A_0, B_0, \eta) = A_0(pa_2 - 2i\eta a_3) + B_0(qb_2 - 2i\eta b_3)$$
$$M_1(A_0, B_0, \eta) = A_0[pa_2 - i\eta(a_1 - a_3)] + B_0[qb_2 - i\eta(b_1 - b_3)] \quad (32)$$

It is now clear that the same procedure may be used to solve for A_2 and B_2 from (22). The result follows:

$$A_2(\kappa, \zeta) = [2\mu\, D(\kappa, \zeta)]^{-1}[b_2(\kappa, \zeta)(\delta_2 + \mathfrak{z}_2) - b_2(\kappa, \zeta)(\bar{\tau}_2 + \mathfrak{l}_2)]$$
$$B_2(\kappa, \zeta) = [2\mu\, D(\kappa, \zeta)]^{-1}[-a_2(\kappa, \zeta)(\delta_2 + \mathfrak{z}_2) + a_2(\kappa, \zeta)(\bar{\tau}_2 + \mathfrak{l}_2)] \quad (33)$$

where $\delta_2 \equiv \delta_2(\kappa, \zeta), \quad \bar{\tau}_2 \equiv \bar{\tau}_2(\kappa, \zeta)$

and

$$\mathfrak{z}_2(\kappa, \zeta)/2\mu = \frac{1}{2\pi}\int_{-\infty}^{\infty} [L_1(A_1, B_1, \eta)]^{\xi=\kappa-\eta} \bar{f}(\eta)d\eta + \frac{1}{4\pi^2}\iint_{-\infty}^{\infty} [L_2(A_0, B_0, \eta_1, \eta_2)]^{\xi=\kappa-\eta_1-\eta_2} \bar{f}(\eta_1)\bar{f}(\eta_2)d\eta_1 d\eta_2$$
$$\mathfrak{l}_2(\kappa, \zeta)/2\mu = \frac{1}{2\pi}\int_{-\infty}^{\infty} [M_1(A_1, B_1, \eta)]^{\xi=\kappa-\eta} \bar{f}(\eta)d\eta + \frac{1}{4\pi^2}\iint_{-\infty}^{\infty} [M_2(A_0, B_0, \eta_1, \eta_2])]^{\xi=\kappa-\eta_1-\eta_2} \bar{f}(\eta_1)\bar{f}(\eta_2)d\eta d\eta_2 \quad (34)$$

where

$$L_2(A_0, B_0, \eta_1, \eta_2) = A_0[-{}^1\!/_2 p^2 a_2 + 2ipa_3\eta_1 + (a_1 - a_2)\eta_1\eta_2] + B_0[-{}^1\!/_2 q^2 b_2 + 2iqb_3\eta_1 + (b_1 - b_2)\eta_1\eta_2]$$
$$M_2(A_0, B_0, \eta_1, \eta_2) = A_0[-{}^1\!/_2 p^2 a_3 + ip(a_1 - a_2)\eta_1 - 2a_3\eta_1\eta_2] + B_0[-{}^1\!/_2 q^2 b_3 + iq(b_1 - b_2)\eta_1 - 2b_3\eta_1\eta_2] \quad (35)$$

This completes the problem formally. Given the boundary curve $y = \epsilon f(x)$, we can calculate A and B in terms of the boundary values of the normal and tangential tractions σ_n and τ_n, by using (19), (24), and (30)–(35), up to and including the terms of the order ϵ^2. Equations (15) and (16) can then be used to calculate the stress and the displacement components.

In the following, we first consider certain special types of boundary curves $\epsilon f(x)$ and then special cases of σ_n and τ_n-distributions.

Some Special Boundary Curves

A few special boundary curves of interest are shown in Figs. 2–4. We will give $\bar{f}(\eta)$ in each of these cases.

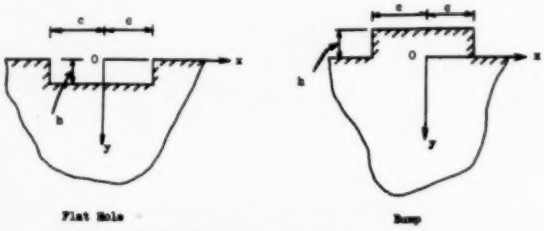

Fig. 2 Boundaries with a flat hole or a bump

Flat Bump or Flat Hole, Fig. 2. In this case, we have

$$\epsilon f(x) = \begin{cases} h & \text{for } |x| < c \\ 0 & \text{for } |x| > c \end{cases} \quad (36)$$

For $h > 0$, we have a hole, and for $h < 0$, we have a bump. We select $\epsilon = h/2c \ll 1$, and using (25), we obtain:

$$\bar{f}(\eta) = (4c/\eta)\sin \eta c \quad (37)$$

Let us note, however, that this type of boundary violates the assumption concerning the smallness of the slope of the boundary curve, at the points $x = \pm c$, since at these points $f' = \pm\infty$. It is believed, however, that the results are still valid away from these points.

A Triangular Hill or a Triangular Hole, Fig. 3. In this case, we have

$$\epsilon f(x) = \begin{cases} h(1 + x/c) & \text{for } -c \le x \le 0 \\ h(1 - x/c) & \text{for } 0 \le x \le c \\ 0 & \text{for } |x| > c \end{cases} \quad (38)$$

It is a hill or a hole according to whether $h > 0$ or $h < 0$. Equation (25) gives

$$\bar{f}(\eta) = 4\eta^{-2}(1 - \cos \eta c), \quad \epsilon = h/2c \quad (39)$$

Sinusoidal Wavy Boundary, Fig. 4. In this case, we have

$$\epsilon f(x) = h \sin rx \quad (40)$$

Equation (25) formally gives

$$\bar{f}(\eta) = -i\pi^2 r^{-1}[\delta(-r - \eta) - \delta(r - \eta)], \quad \epsilon = hr/\pi \quad (41)$$

where δ represents the Dirac delta function which has the formal properties that

$$\delta(u) = \begin{cases} \infty & \text{for } u = 0 \\ 0 & \text{for } u \neq 0 \end{cases}, \quad F(x) = \int_{-\infty}^{\infty} F(u)\,\delta(u - x)du \quad (42)$$

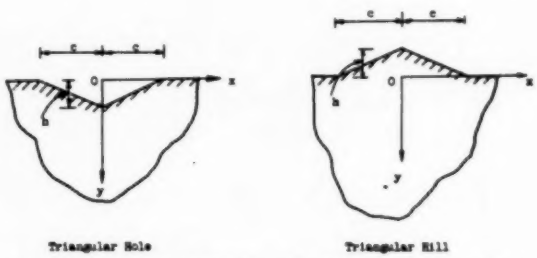

Fig. 3 Boundaries with a triangular hole or a triangular hill

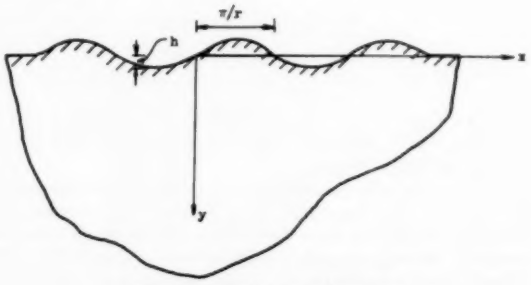

Fig. 4 Sinusoidal wavy boundary

In obtaining (41), we used the formal relation[2]

$$2\pi\delta(u) = \int_{-\infty}^{\infty} e^{-iuz}dx \tag{43}$$

We note that the present case is by far the most interesting of all three. Moreover, in this case, we can readily evaluate the integrals appearing in the expressions (31) and (34), by using the properties of $\delta(u)$ expressed by (42). The result is

$$\begin{aligned}
I_1(\kappa, \zeta)/2\mu &= (\pi/2ir)[L_1(A_0, B_0, \mp r)]_{\xi=\kappa-r}^{\xi=\kappa+r} \\
I_1(\kappa, \zeta)/2\mu &= (\pi/2ir)[M_1(A_0, B_0, \mp r)]_{\xi=\kappa-r}^{\xi=\kappa+r} \\
I_2(\kappa, \zeta)/2\mu &= (\pi/2ir)[L_1(A_1, B_1, \mp r)]_{\xi=\kappa-r}^{\xi=\kappa+r} \\
&\quad - (\pi^2/4r^2)[L_2(A_0, B_0, \mp r, -r)]_{\xi=\kappa}^{\xi=\kappa+2r} \\
&\quad - (\pi^2/4r^2)[L_2(A_0, B_0, \pm r, r)]_{\xi=\kappa}^{\xi=\kappa-2r} \\
I_2(\kappa, \zeta)/2\mu &= (\pi/2ir)[M_1(A_1, B_1, \mp r)]_{\xi=\kappa-r}^{\xi=\kappa+r} \\
&\quad - (\pi^2/4r^2)[M_2(A_0, B_0, \mp r, -r)]_{\xi=\kappa}^{\xi=\kappa+2r} \\
&\quad - (\pi^2/4r^2)[M_2(A_0, B_0, \pm r, r)]_{\xi=\kappa}^{\xi=\kappa-2r}
\end{aligned} \tag{44}$$

In these equations, the upper sign goes with the upper value of ξ and the lower sign with the lower value.

The case of a more general periodic boundary curve can be treated in a similar fashion by taking

$$\epsilon f(x) = \sum_n h_n \sin nrx$$

which gives

$$\epsilon\bar{f}(\xi) = -i\pi \sum_n h_n[\delta(-nr - \xi) - \delta(nr - \xi)]$$

Here

$$h_n = \epsilon k_n, \quad k_n = 0(1)$$

We may select ϵ in such a way that the slope $\epsilon f'$ is not large. This imposes a condition on h_n. The calculation of $I_1, \ldots, I_2$ is similar to the one given previously. We shall, however, not pursue this further, but go on to the consideration of special types of surface tractions.

Some Special Types of Loading

A few special types of boundary loading are of fundamental interest. In the following, we calculate A_0 and B_0. The coefficients $A_1, \ldots, B_2$ are calculated in terms of A_0 and B_0 through the general expressions (30)–(35). In the case of the special types of boundary curves studied in the previous section, we use the equations developed therein.

Normal Tractions and Zero Shear. In this case, we have

$$\sigma_n = N(x, \tau), \quad \tau_n = 0 \tag{45}$$

Hence,

$$\sigma_0 = N(x, \tau), \quad \sigma_1 = \sigma_2 = \ldots = \tau_0 = \tau_1 = \ldots = 0$$

Equations (24) give

$$A_0 = (2\mu D)^{-1}b_2\bar{N}(\xi, \zeta), \quad B_0 = -(2\mu D)^{-1}a_2\bar{N}(\xi, \zeta) \tag{46}$$

[2] All of these relations can be justified in a distribution sense. See, for instance, L. Schwartz, "Theorie des Distributions," Herman and Company, Paris, France, vols. 1 and 2, 1950.

Impulsive Normal Tractions and Zero Shear. This is obtained from (46) by taking $N(x, \tau) = N(x)\,\delta(\tau)$. Hence,

$$A_0 = (4\pi\mu D)^{-1}b_2\bar{N}(\xi), \quad B_0 = -(4\pi\mu D)^{-1}a_2\bar{N}(\xi) \tag{47}$$

In case the normal load is a uniform pressure p_0, we substitute

$$\bar{N}(\xi) = -2\pi p_0\delta(\xi) \tag{48}$$

Suddenly Applied Normal Load and Zero Shear. This type of load is expressed by $\sigma_s = \tau_s = 0$, except:

$$\sigma_0 = \begin{cases} N(x) & \text{for} \quad \tau > 0 \\ 0 & \text{for} \quad \tau < 0 \end{cases} \tag{49}$$

To determine δ_0, we introduce Heisenberg's delta function

$$\delta_+(u) = {}^1/_2\delta(u) - \frac{1}{2\pi iu} \tag{50}$$

Then,

$$\int_{-\infty}^{\infty} \delta_+(\zeta)e^{-i\xi\tau}\,d\zeta = {}^1/_2 + \frac{1}{\pi}\int_0^{\infty} \frac{\sin \zeta\tau}{\zeta}\,d\zeta = \begin{cases} 1 & \text{for} \quad \tau > 0 \\ 0 & \text{for} \quad \tau < 0 \end{cases} \tag{51}$$

The function on the right may be used to obtain the Fourier transform of (49).

$$\sigma_0 = \bar{N}(\xi)\delta_+(\zeta) \tag{52}$$

If the load $N(x)$ is a uniform pressure, we use (48) for $\bar{N}(\xi)$.

Concentrated Normal Load and Zero Shear. In (45), by taking $N(x, \tau) = N(\tau)\,\delta(x)$, we obtain the case of time-dependent concentrated load acting at the origin of the co-ordinates. Hence,

$$A_0 = (4\pi\mu D)^{-1}b_2\bar{N}(\zeta), \quad B_0 = -(4\pi\mu D)^{-1}a_2\bar{N}(\zeta) \tag{53}$$

Concentrated Impulse Load and Zero Shear. If further we take $N(\tau) = N_0\delta(\tau)$, (53) reduces to

$$A_0 = (4\pi\mu D)^{-1}b_2N_0, \quad B_0 = -(4\pi\mu D)^{-1}a_2N_0 \tag{54}$$

The concentrated load is applied at the origin of the co-ordinates impulsively.

Pulsating Normal Load and Zero Shear. In this case, we have (45) with

$$N(x, \tau) = N(x)\sin\omega\tau \tag{55}$$

which leads to

$$\begin{aligned}
A_0 &= (4i\mu D)^{-1}b_2\bar{N}(\xi)[\delta(-\omega - \zeta) - \delta(\omega - \zeta)] \\
B_0 &= -(4i\mu D)^{-1}a_2\bar{N}(\xi)[\delta(-\omega - \zeta) - \delta(\omega - \zeta)]
\end{aligned} \tag{56}$$

If, further, the normal load is concentrated at the origin of the co-ordinates, then $N(x) = N_0\delta(x)$. Hence $\bar{N}(\xi) = N_0$ must be substituted into (56). If the normal load is a uniformly distributed pressure p_0, we use (48).

Moving Loads. Moving normal and tangential stresses may be represented by

$$\sigma_n = \sigma(s - V\tau), \quad \tau_n = \tau(s - V\tau), \quad V = V_0/c_1 \tag{57}$$

where s is the arc length along the boundary curve and V_0 is the load velocity tangential to the boundary curve.

For s, we have

$$s = \int_0^x (1 + \epsilon^2f'^2)^{1/2}dx = x + \frac{\epsilon^2}{2}\int_0^x f'^2dx + 0(\epsilon^4) \tag{58}$$

Using (58) in (57) and expanding the result into a Taylor series about $(x - V\tau)$, we shall have

$$\sigma_n = \sigma(x - V\tau) + {}^1/_2\epsilon^2\sigma'(x - V\tau)\int_0^x f'^2dx + 0(\epsilon^4)$$
$$\tau_n = \tau(x - V\tau) + {}^1/_2\epsilon^2\tau'(x - V\tau)\int_0^x f'^2dx + 0(\epsilon^4) \quad (59)$$

If the load is a concentrated type, then we write

$$\sigma(x - V\tau) = P\delta(x - V\tau), \quad \tau(x - V\tau) = Q\delta(x - V\tau) \quad (60)$$

where P and Q are the magnitudes of the normal and tangential force components.

From (59), it is clear that

$$\sigma_0 = \sigma(x - V\tau), \quad \sigma_1 = 0, \quad \sigma_2 = {}^1/_2\sigma_0'\int_0^x f'^2dx$$
$$\tau_0 = \tau(x - V\tau), \quad \tau_1 = 0, \quad \tau_2 = {}^1/_2\tau_0'\int_0^x f'^2dx \quad (61)$$

In the subsequent analysis, we need the Fourier transforms of (61). Thus,

$$\bar{\sigma}_0 = \frac{1}{2\pi}\int\int_{-\infty}^{\infty}\sigma(x - V\tau)\exp[i(\xi x + \zeta\tau)]dx\,d\tau$$

Upon writing $x - V\tau = \alpha$, this becomes

$$\bar{\sigma}_0 = \bar{\sigma}(\xi)\delta(\xi V + \zeta), \quad \bar{\tau}_0 = \bar{\tau}(\xi)\delta(\xi V + \zeta) \quad (62)$$

where we used (43). The inclusion of $\bar{\sigma}_2$, $\bar{\tau}_2$ and the retention of the terms of the order of ϵ^2 in the analysis require much effort for a relatively small return. Therefore, in the analysis of a moving load, they will be ignored. If we assume that the surface load is moving with a constant horizontal velocity, we find that all $\sigma_i = \tau_i = 0$ except σ_0 and τ_0, and the latter are given by (61).

Pulsating, Moving Loads. In this case, we have

$$\sigma_0 = \sigma(x - V\tau)\sin\omega\tau, \quad \tau_0 = \sigma(x - V\tau)\sin\omega\tau \quad (63)$$

excluding the terms of the order of ϵ^2.

$$\bar{\sigma}_0 = (-i/2)\bar{\sigma}(\xi)[\delta(\omega + \xi V + \zeta) - \delta(-\omega + \xi V + \zeta)] \quad (64)$$

and a similar expression for $\bar{\tau}_0$.

Vertical and Horizontal Loads. When the vertical and the horizontal components of the tractions, σ_v and σ_h, are given, we express σ_n and τ_n in terms of these tractions by

$$\sigma_n = \sigma_h n_x + \sigma_v n_y, \quad \tau_n = \sigma_h n_y - \sigma_v n_x \quad (65)$$

Upon using (9) and expanding the result into powers of ϵ, we obtain

$$\sigma_n = \sigma_v - \epsilon f'\sigma_h - {}^1/_2\epsilon^2 f'^2\sigma_v + 0(\epsilon^3)$$
$$\tau_n = \sigma_h + \epsilon f'\sigma_v - {}^1/_2\epsilon^2 f'^2\sigma_h + 0(\epsilon^3) \quad (66)$$

It is now clear that

$$\sigma_0 = \sigma_v, \quad \sigma_1 = -f'\sigma_h, \quad \sigma_2 = -{}^1/_2 f'^2\sigma_v$$
$$\tau_0 = \sigma_h, \quad \tau_1 = f'\sigma_v, \quad \tau_2 = -{}^1/_2 f'^2\sigma_h \quad (67)$$

Thus we have

$$\bar{\sigma}_0 = \bar{\sigma}_v, \quad \bar{\tau}_0 = \bar{\sigma}_h \quad (68)$$

To obtain $\bar{\sigma}_1$, we write the Fourier transform of $(f'\sigma_h)$ and use (25). Hence,

$$\bar{\sigma}_1 = \frac{i}{4\pi^2}\int\int\int_{-\infty}^{\infty}\eta\bar{f}(\eta)\sigma_h(x, \tau)\exp[i(\xi x - \eta x + \zeta\tau)]dx d\tau d\eta$$

If we now substitute $\xi - \eta = \kappa$, this expression reads

$$\bar{\sigma}_1 = -\frac{i}{2\pi}\int_{-\infty}^{\infty}(\xi - \kappa)\bar{f}(\xi - \kappa)\bar{\sigma}_h(\kappa, \zeta)d\kappa \quad (69)$$

An expression for $\bar{\tau}_1$ follows from (69) by taking $-\bar{\sigma}_v$ for $\bar{\sigma}_h$. Fourier transforms of σ_2 and τ_2 are calculated in a similar fashion. The result is

$$\bar{\sigma}_2 = \frac{1}{8\pi^2}\int\int_{-\infty}^{\infty}\eta(\xi - \eta - \kappa)\bar{f}(\eta)\bar{f}(\xi - \eta - \kappa)\bar{\sigma}_v(\kappa, \zeta)d\eta\,d\kappa \quad (70)$$

and a similar expression for $\bar{\tau}_2$.

Moving Vertical Loads. This follows from (67) by taking $\sigma_h = 0$, and

$$\sigma_0 = \sigma_v(x - V\tau), \quad \sigma_1 = 0$$
$$\tau_0 = 0, \quad \tau_1 = f'(x)\sigma_v(x - V\tau) \quad (71)$$

We ignore the terms of the order of ϵ^2 and higher. The Fourier transform of σ_0 is identical to (62), while that of τ_1 is:

$$\bar{\tau}_1 = (i/2\pi)(\xi + \zeta/V)\bar{\sigma}_v(-\zeta/V)\bar{f}(\xi + \zeta/V) \quad (72)$$

where σ_v is a concentrated load and using $\sigma_v = p\delta(x - V\tau)$, we find

$$\bar{\sigma}(\xi) = p \quad (73)$$

When the boundary is sinusoidal, (40) will be used in (72), leading to

$$\bar{\tau}_1 = (\pi/2r)(\xi + V^{-1}\zeta)[\delta(\xi + V^{-1}\zeta + r) - \delta(\xi + V^{-1}\zeta - r)]\bar{\sigma}_v(-\zeta/V) \quad (74)$$

If further the load is a vertical concentrated load, we find

$$\bar{\tau}_1 = (\pi p/2r)(\xi + V^{-1}\zeta)[\delta(\xi + V^{-1}\zeta + r) - \delta(\xi + V^{-1}\zeta - r)] \quad (75)$$

Many other types of loads are possible. However, they are excluded here since the method of treatment is now made clear.

Stress and Displacement Components

Once the constants A and B are determined, the stress and displacement components are calculated from equations (15) and (16). It is found that the various integrations reduce to single integrals in the following special cases concerning the sinusoidal boundary: (*a*) Pulsating normal concentrated load, (*b*) moving concentrated load, and (*c*) suddenly applied pressure. The expressions for the stress and displacement components have been obtained as single integrals in these cases but are not presented here as they are unduly long and can be obtained readily, if desired, by using the results of the two preceding sections.

One case, which is of particular interest because of its simplicity, is the uniform pulsating pressure on a sinusoidal boundary. Although this case is not as important practically as some others, nevertheless it provides an easy case for numerical calculations and permits us to get an insight into how the boundary irregularities influence the solution to the problem.

For a uniform pulsating pressure on a sinusoidal boundary, we have the results of the preceding subsection "Pulsating Normal Load and Zero Shear" with $\sigma_i = \tau_i = 0$ for all i except

$$\bar{\sigma}_0 = \overline{N}(\xi, \zeta) = -2\pi p_0\delta(\xi)[\delta(-\omega - \zeta) - \delta(\omega - \zeta)] \quad (76)$$

This value may be used to determine A_0, B_0, A_1, and B_1. These are then used in (15) and (16) to get the stress and displacement components

$$\sigma_x/p_0 = -\frac{\lambda}{\lambda+2\mu}\sin\omega(y+\tau) + [\epsilon/D(-r,\omega)]$$
$$\Big\{P\Big[-\pi\omega r^{-1}\Big(r^2+\frac{\lambda}{2\mu}\omega^2\Big)(r^2-{}^1/_2\beta^2\omega^2)\cos\omega\tau$$
$$-2\pi r\beta^{-2}\Big(r^2+\frac{\lambda}{2\mu}\omega^2\Big)(r^2-\beta^2\omega^2)^{1/2}\sin\omega\tau\Big]$$
$$+Q[\pi\omega r(r^2-\omega^2)^{1/2}(r^2-\beta^2\omega^2)^{1/2}\cos\omega\tau$$
$$+2\pi r\beta^{-2}(r^2-{}^1/_2\beta^2\omega^2)(r^2-\beta^2\omega^2)^{1/2}\sin\omega\tau]\Big\}\sin rx$$

$$\sigma_y/p_0 = -\sin\omega\tau - [\epsilon/D(-r,\omega)]$$
$$\{P[-\pi\omega r^{-1}(r^2-{}^1/_2\beta^2\omega^2)^2\cos\omega\tau$$
$$+2\pi r\beta^{-2}(r^2-{}^1/_2\beta^2\omega^2)(r^2-\beta^2\omega^2)^{1/2}\sin\omega\tau]$$
$$+Q[\pi\omega r(r^2-\beta^2\omega^2)^{1/2}(r^2-\omega^2)^{1/2}\cos\omega\tau$$
$$-2\pi r\beta^{-2}(r^2-{}^1/_2\beta^2\omega^2)(r^2-\beta^2\omega^2)^{1/2}\sin\omega\tau]\}\cos rx \qquad (77)$$

$$\tau_{xy}/p_0 = [\epsilon/D(-r,\omega)]$$
$$\{P[-\pi\omega(r^2-\omega^2)^{1/2}(r^2-{}^1/_2\beta^2\omega^2)\cos\omega\tau$$
$$-2\pi r^2\beta^{-2}(r^2-\omega^2)^{1/2}(r^2-\beta^2\omega^2)^{1/2}\sin\omega\tau]$$
$$+Q[\pi\omega(r^2-\omega^2)^{1/2}(r^2-{}^1/_2\beta^2\omega^2)\cos\omega\tau$$
$$+2\pi\beta^{-2}(r^2-{}^1/_2\beta^2\omega^2)^2\sin\omega\tau]\}\cos rx$$

$$(2\mu/p_0)u = [\epsilon/D(-r,\omega)]\{P[\pi\omega(r^2-{}^1/_2\beta^2\omega^2)\cos\omega\tau$$
$$+2\pi r^2\beta^{-2}(r^2-\beta^2\omega^2)^{1/2}\sin\omega\tau]$$
$$+Q[-\pi\omega(r^2-\omega^2)^{1/2}(r^2-\beta^2\omega^2)^{1/2}\cos\omega\tau$$
$$-2\pi\beta^{-2}(r^2-{}^1/_2\beta^2\omega^2)(r^2-\beta^2\omega^2)^{1/2}\sin\omega\tau]\}\cos rx$$

$$(2\mu/p_0)v = 2\beta^{-2}\omega^{-1}\cos\omega(y+\tau) + [\epsilon/D(-r,\omega)]$$
$$\{P[-\pi\omega r^{-1}(r^2-{}^1/_2\beta^2\omega^2)(r^2-\omega^2)^{1/2}\cos\omega\tau$$
$$-2\pi r\beta^{-2}(r^2-\beta^2\omega^2)^{1/2}(r^2-\omega^2)^{1/2}\sin\omega\tau]$$
$$+Q[\pi r\omega(r^2-\omega^2)^{1/2}\cos\omega\tau$$
$$+2\pi r\beta^{-2}(r^2-{}^1/_2\beta^2\omega^2)\sin\omega\tau]\}\sin rx$$

$$P = \exp[-y(r^2-\omega^2)^{1/2}],\quad Q = \exp[-y(r^2-\beta^2\omega^2)^{1/2}]$$

From equations (77) we note the following interesting results:

The perturbation terms consist of standing waves in the x-direction. We may consider these as waves propagating to the left and right with propagation velocity $v/c_1 = \omega/r$. Thus the disturbances generated by the surface undulations are propagated to the left and right with a frequency-dependent propagation velocity $v/c_1 = \omega/r$, where ωc_1 is the frequency of the pulsating pressure.

If $0 \leq \omega/r < 1/\beta$, then the perturbation is exponentially attenuated in the y-direction; therefore they are confined to the neighborhood of the surface. When $1/\beta < \omega/r < 1$, the perturbation term multiplied by Q begins to propagate downward with a frequency-dependent propagation velocity $v/c_1 = \omega(\beta^2\omega^2 - r^2)^{-1/2}$ and when $1 < \omega/r < \infty$, the perturbation term containing P also begins to propagate downward with propagation velocity $v/c_1 = \omega(\omega^2 - r^2)^{-1/2}$.

Since each perturbation term contains the factor $D(-r,\omega)$ in the denominator, we can expect singular behavior when it vanishes. It vanishes when the velocity of propagation of the disturbances is equal to the velocity of propagation of Rayleigh waves in the medium. This condition prevails when the wave length of the surface corrugations is equal to the wave length of the Rayleigh wave having frequency ωc_1.

The amplitudes of the pertubation terms are plotted in Fig. 5 for materials satisfying Poisson's condition ($\lambda = \mu$) and $y = 0$ (approximately at the surface). The correction terms for u, v, and σ_x show a resonance at $\omega = 0.531\,r$; that is, when the corrugation wave length is equal to that of the Rayleigh wave frequency ωc_1. We are led to expect something of this sort from the foregoing discussion. The amplitude of the correction to the shear-stress component is independent of the load frequency while the normal stress σ_y grows continually with frequency. The results in Fig. 5 are computed from the formulas:

$$u = 0 + \epsilon H_u(\theta)\cos(\omega\tau - \phi_0)\cos rx$$
$$v = (p_0/3\mu\omega)\cos\omega\tau + \epsilon H_v(\theta)\cos(\omega\tau - \phi_0)\sin rx$$
$$\sigma_x = -\Big(\frac{\lambda p_0}{\lambda+2\mu}\Big)\sin\omega\tau + \epsilon H_x(\theta)\cos(\omega\tau - \phi_1)\sin rx \qquad (78)$$
$$\sigma_y = -p_0\sin\omega\tau + \epsilon H_y(\theta)\cos\omega\tau\sin rx$$
$$\tau_{xy} = 0 + \epsilon H_{xy}(\theta)\sin\omega\tau\cos rx$$

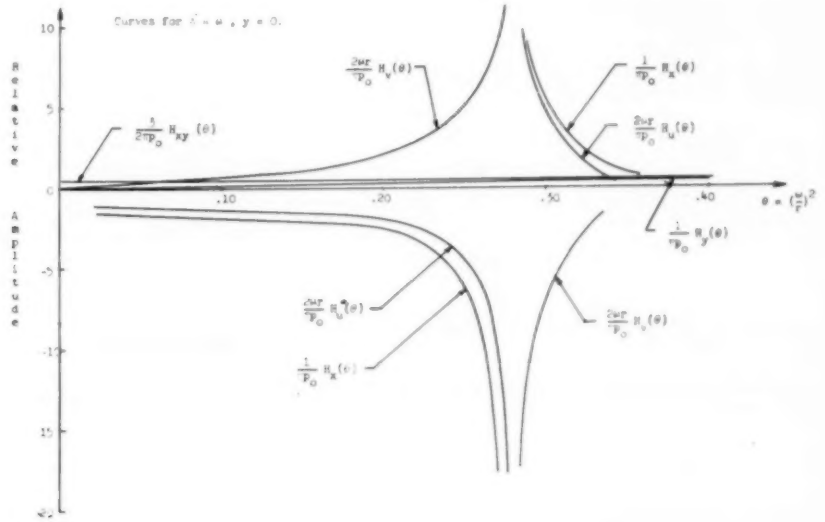

Fig. 5 Variation of amplitude of correction term with frequency for uniformly pulsating load on a sinusoidal boundary

where

$$(2\mu r/\pi p_0)H_u(\theta) = \{\theta[1 - {}^3/_8\theta - (1 - 3\theta)^{1/2}(1 - \theta)^{1/2}]^2 + (1 - 3\theta)\theta^2\}^{1/2}/D(\theta)$$

$$(2\mu r/\pi p_0)H_v(\theta) = -[{}^9/_4\theta^2(1 - \theta) + {}^4/_3[(1 - \theta)^{1/2}(1 - 3\theta)^{1/2} - (1 - {}^3/_2\theta)]^2\}^{1/2}/D(\theta)$$

$$(1/\pi p_0)H_\sigma(\theta) = \left\{\theta[(1 - 3\theta)^{1/2}(1 - \theta)^{1/2} - \left(1 + \frac{\theta}{2}\right)(1 - {}^3/_8\theta)]^2 + {}^{16}/_3\theta^2(1 - 3\theta)\right\}^{1/2} \Big/ D(\theta)$$

$$(1/\pi p_0)H_y(\theta) = \theta^{1/2}, \quad ({}^3/_2\pi p_0)H_{xy}(\theta) = 1$$

$$D(\theta) = (1 - {}^3/_2\theta)^2 - [(1 - 3\theta)(1 - \theta)]^{1/2}$$

$\theta = (\omega/r)^2$, $0 \leq \theta \leq {}^1/_3$ for solution vanishing at $y = \infty$.
ϕ_0, ϕ_1, and ϕ_2 are phase angles.

The resonance phenomena found in the analysis should be interpreted only as a tendency for the quantities u, v, and σ_x to become large as surface corrugations wave length approaches the Rayleigh surface wave length. Since the analysis is based on the assumption that the perturbations are small, the validity of this result must await experimental verification or a more exact theory.

Surface Waves

As in the case of Rayleigh surface waves for the flat boundary, we may investigate the possibility of surface wave propagations in the case of a slightly curved boundary.[3] This is accomplished by setting $\sigma_n = \tau_n = 0$ on the boundary. According to (19), this implies that $\sigma_0 = \sigma_1 = \tau_0 = \tau = \ldots = 0$.

From (23), we find that

$$D = a_2b_3 - a_3b_2 = 0, \quad B_0 = -a_2A_0/b_2 \tag{79}$$

or, according to (17),

$$D(\xi, \zeta) = (\zeta^2 - {}^1/_2\beta^2\zeta^2)^2 - \xi^2(\xi^2 - \zeta^2)^{1/2}(\xi^2 - \beta^2\zeta^2)^{1/2} = 0 \tag{80}$$

The roots of (80) give the Rayleigh surface wave velocities, as is well known. Using the conditions $\sigma_1 = \tau_1 = 0$, through (30) to (32), we obtain

$$A_1(\kappa, \zeta) = \frac{1}{2\pi D(\kappa, \zeta)} \int_{-\infty}^{\infty} A_0(\kappa, -\eta\zeta)\bar{f}(\eta) \left[\{(\kappa^2 - {}^1/_2\beta^2\zeta^2)[(\kappa + -\eta)^2 + -{}^1/_2\beta^2\zeta^2] - \kappa(\kappa - \eta)(\kappa^2 - \beta^2\zeta^2)^{1/2}[(\kappa - \eta)^2 - \zeta^2]^{1/2}\} \times \{[(\kappa - \eta)^2 - \zeta^2]^{1/2} - [(\kappa - \eta)^2 - \beta^2\zeta^2]^{1/2}\} - \frac{\lambda + \mu}{\mu}\eta\zeta^2\kappa(\kappa^2 - \beta^2\zeta^2)^{1/2}\right] d\eta$$

$$B_1(\kappa, \zeta) = \frac{i}{2\pi D(\kappa, \zeta)} \int_{-\infty}^{\infty} A_0(\kappa - \eta, \zeta)\bar{f}(\eta) \left[\{-\kappa(\kappa^2 - \zeta^2)^{1/2}[(\kappa - \eta)^2 - {}^1/_2\beta^2\zeta^2] + (\kappa - \eta)(\kappa^2 - {}^1/_2\beta^2\zeta^2)[(\kappa - \eta)^2 - \zeta^2]^{1/2}\} \times \{[(\kappa - \eta)^2 - \zeta^2]^{1/2} - [(\kappa - \eta)^2 - \beta^2\zeta^2]^{1/2}\} + \frac{\lambda + \mu}{\mu}\eta\zeta^2(\kappa^2 - {}^1/_2\beta^2\zeta^2)\right] d\eta \tag{81}$$

(81) (cont.)

for a general boundary shape. For the sinusoidal boundary, (41) may be used to simplify (81) to

$$A_1(\kappa, \zeta) = \frac{\pi}{2irD(\kappa, \zeta)} \left[\{(\kappa^2 - {}^1/_2\beta^2\zeta^2)[(\kappa + r)^2 - {}^1/_2\beta^2\zeta^2] - \kappa(\kappa + r)(\kappa^2 - \beta^2\zeta^2)^{1/2}[(\kappa + r)^2 - \zeta^2]^{1/2}\} \times \{[(\kappa + r)^2 - \zeta^2]^{1/2} - [(\kappa + r)^2 - \beta^2\zeta^2]^{1/2}\} A_0(\kappa + r, \zeta) - \{[\kappa^2 - {}^1/_2\beta^2\zeta^2)[(\kappa - r)^2 - {}^1/_2\beta^2\zeta^2] - \kappa(\kappa - r)(\kappa^2 - \beta^2\zeta^2)^{1/2}[(\kappa - r)^2 - \zeta^2]^{1/2}\} \times \{[(\kappa - r)^2 - \zeta^2]^{1/2} - [(\kappa - r)^2 - \beta^2\zeta^2]^{1/2}\} A_0(\kappa - r, \zeta) + \frac{\lambda + \mu}{\mu} r\zeta^2\kappa(\kappa^2 - \beta^2\zeta^2)^{1/2}[A_0(\kappa + r, \zeta) + A_0(\kappa - r, \zeta)]\right]$$

$$B_1(\kappa, \zeta) = \frac{\pi}{2rD(\kappa, \zeta)} \left[\{-\kappa[\kappa^2 - \zeta^2)^{1/2}[(\kappa + r)^2 - {}^1/_2\beta^2\zeta^2] + (\kappa + r)(\kappa^2 - {}^1/_2\beta^2\zeta^2)[(\kappa + r)^2 - \zeta^2]^{1/2}\} \times \{[(\kappa + r)^2 - \zeta^2]^{1/2} - [(\kappa + r)^2 - \beta^2\zeta^2]^{1/2}\} A_0(\kappa + r, \zeta) + \{\kappa(\kappa^2 - \zeta^2)^{1/2}[(\kappa - r)^2 - {}^1/_2\beta^2\zeta^2] - (\kappa - r)(\kappa^2 - {}^1/_2\beta^2\zeta^2)[(\kappa - r)^2 - \zeta^2]^{1/2}\} \times \{[(\kappa - r)^2 - \zeta^2]^{1/2} - [(\kappa - r)^2 - \beta^2\zeta^2]^{1/2}\} A_0(\kappa - r, \zeta) - \frac{\lambda + \mu}{\mu} r\zeta^2 (\kappa^2 - {}^1/_2\beta^2\zeta^2)[A_0(\kappa + r, \zeta) + A_0(\kappa - r, \zeta)]\right] \tag{82}$$

Several points of interest may be observed. From the appearance of $D(\kappa, \zeta)$, which in view of (79) is zero, in the denominator, one may think at first that $A_0 = 0$ must be true, making a surface wave propagation impossible. However, substitution of A_1 and B_1 into expression (21) will show that $D(\kappa, \zeta)$ will cancel out, and (21) will be satisfied without any restriction on A_0. Thus in a half space of slightly curved boundary there exist Rayleigh surface waves of arbitrary amplitude. These waves travel to the right and left from the source point as is apparent from the occurrence of $\kappa - \zeta$ and $\kappa + \zeta$ in the foregoing expression. The velocity of these waves is the same as for the half space having a flat boundary.

Acknowledgment

The authors are indebted to Mr. John W. Dunkin for his extreme care in checking the analysis.

[3] The authors are indebted to a referee for suggesting this portion of the analysis.

CHI-NENG SHEN
Associate Professor
of Mechanical Engineering,
Rensselaer Polytechnic Institute,
Troy, N. Y.
Assoc. Mem. ASME

Stability of Forced Oscillations With Nonlinear Second-Order Terms

A solution is obtained for forced oscillations with nonlinear second-order terms. The stability of this solution is given by its variational equation. The boundary of stability is analyzed by both the perturbation and continued fraction methods. The amplitude of oscillation with damping terms is also determined by the iteration procedure.

THE tanks of the form shown in Fig. 1 are used to provide an example of a system with nonlinear second-order terms, where a linear feedback controller is used to control a two-capacity process. The volume of a parabolic tank is expressed as

$$V_2 = C_2(y_2 + \alpha y_2^2) \tag{1}$$

where y_2 is the height of liquid above the plane of symmetry and C_2 is a constant.

The differential equations which define the behavior of the control system may be written as

$$R_2R_dC_1C_2\frac{d^2}{dt^2}(y_2 + \alpha y_2^2) + R_dC_2\frac{d}{dt}(y_2 + \alpha y_2^2) + (R_2 + R_d)C_1\frac{dy_2}{dt} + (1 + kR_d)y_2 = R_dF + C_1R_2\frac{dy_d}{dt} + y_d \tag{2}$$

where the R and C are resistances and capacities of the system, respectively. If the inflow F or the level y_d is subjected to a sinusoidal disturbance, then Equation (2), after necessary change of variables, becomes

$$\frac{d^2}{dt^2}(Y + \beta Y^2) + M_n\frac{d}{dt}(Y + \beta Y^2) + M_1\frac{dY}{dt} + Y = G\cos(pt - \phi) \tag{3}$$

where the quantities β, M_n, M_1, G, p, and ϕ are all parameters.

The object of this paper is to find periodic solutions of Equation (3) by various approximate methods.

Solution by Iteration Method[1]

To start with a specialized form of Equation (3), the following equation is to be considered:

$$\frac{d^2}{dt^2}(Y + \beta Y^2) + Y = \beta G_0\cos pt, \quad \text{where} \quad G = \beta G_0 \tag{4}$$

Transposing all the terms with β to the right-hand side and introducing p^2Y on both sides of the equation, Equation (4) takes the following form for the nth-order iteration:

$$\frac{d^2}{dt^2}Y_n + p^2Y_n = -\frac{d^2}{dt^2}(\beta Y_{n-1}^2) + (p^2 - 1)Y_{n-1} + \beta G_0\cos pt \tag{5}$$

This is a recurrence formula linking the nth and $(n - 1)$th approximations, where $Y_n = 0$ for $n < 0$. The sequence $Y_0, Y_1 \ldots$ is now considered, where Y_n satisfies Equation (5). Here it is convenient to start the iteration process with $p^2 = 1$, $\beta = 0$. For the zero-order iteration of Y, Equation (5) has the solution

$$Y_0 = A\cos pt + C\sin pt \tag{6}$$

The term $C\sin pt$ would eventually be zero in the next step of the iteration process. It is therefore convenient to omit it here.[2] The equation for the first-order iteration is

$$\frac{d^2}{dt^2}Y_1 + p^2Y_1 = [(p^2 - 1)A + \beta G_0 + 0.75p^2\beta A^3]\cos pt + 2.25p^2\beta A^3\cos 3pt \tag{7}$$

The system by Equation (7) also has a natural frequency of $Y_1 = A\cos pt$. If the coefficient of $\cos pt$ in Equation (7) were not zero the particular solution would have a term of the type $Ct\sin pt$, which is not periodic. Since periodic solutions alone are of interest, the coefficient of $\cos pt$ is equal to zero, thus the frequency p after the first iteration is

$$p^2 = \frac{1 - \beta G_0/A}{1 + 0.75\beta A^2} \tag{8}$$

[2] Footnote 1, p. 86.

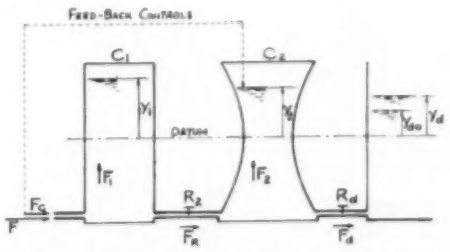

Fig. 1 Single nonlinear capacity of two-capacity process

[1] See similar treatment of iteration procedure in "Nonlinear Vibrations in Mechanical and Electrical Systems," by J. J. Stoker, Interscience Publishers, New York, N. Y., 1950.

Contributed by the Applied Mechanics Division and presented at the Annual Meeting, Atlantic City, N. J., November 29–December 4, 1959, of THE AMERICAN SOCIETY OF MECHANICAL ENGINEERS.

Discussion of this paper should be addressed to the Secretary, ASME, 29 West 39th Street, New York, N. Y., and will be accepted until January 10, 1960, for publication at a later date. Discussion received after the closing date will be returned.

NOTE: Statements and opinions advanced in papers are to be understood as individual expressions of their authors and not those of the Society. Manuscript received by ASME Applied Mechanics Division, May 21, 1958. Paper No. 59—A-19.

Since the coefficient of the cosine term is zero in Equation (7), the solution may be written as

$$Y_1 = A_1 \cos pt + B \cos 3pt, \tag{9}$$

where

$$B = -{}^1/_{32}\beta A^3$$

The term $A_1 \cos pt$ represents the free vibration with some arbitrary amplitude A_1 to be assigned. We may choose for A_1 the value of A for the first approximation $Y_0 = A \cos pt$. These steps will also be followed for further approximations.

The frequency p after the second iteration becomes

$$p^2 = \frac{1 - G/A}{1 + 0.75\beta A^2 - 0.375(0.75\beta A^2)^2 + 0.281(0.75\beta A^2)^3} \tag{10}$$

The amplitude A is plotted versus frequency p in Fig. 2 for $\beta = +4/300$ and in Fig. 3 for $\beta = -4/300$. The choice of any particular value for β in no way limits the generality of the treatment. The discussion of this statement may be found in a previous paper[3] by the author.

If the disturbance G decreases and finally approaches zero as its limit, the frequency p gradually becomes the natural frequency of the system. It is therefore possible to check the curves for $G = 0$ in Figs. 2 and 3 versus the exact natural frequencies obtained by elliptic integrals.[4] The values computed from Equation (10) are close approximations to the exact solutions at moderate amplitudes although they deviate slightly from the exact solution at extremely large amplitudes.

If G is sufficiently large, there is a range of frequencies for which no solution exists when β is negative. This can be found from Fig. 3.

[3] Chi-Neng Shen, "On the Solution of a Differential Equation with Nonlinearity Appearing in the Second Derivative of Combined Linear and Cubic Terms," *Quarterly of Applied Mathematics*, vol. 15, 1957, p. 16.

[4] Ibid., p 21.

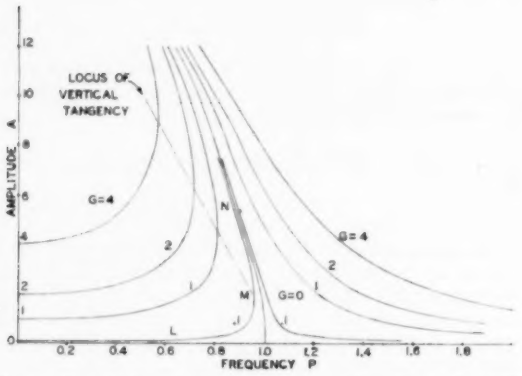

Fig. 2 Sinusoidal response for positive nonlinearity $\beta = 4/300$

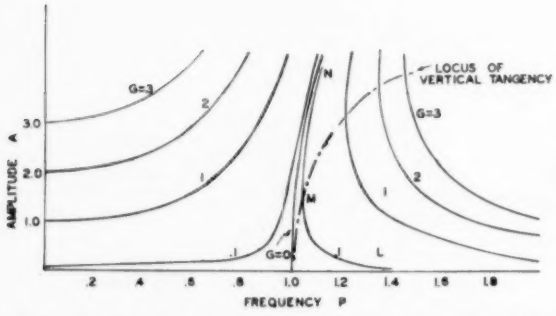

Fig. 3 Sinusoidal response for negative nonlinearity $\beta = -4/300$

The Linear Variational Equation

The solution by Equations (9) and (10) for the nonlinear differential Equation (4) may not be stable. Under an infinitesimal disturbance, a stable system will gradually return to its original amplitude and frequency. Let $Y(t)$ and $Y(t) + \delta Y(t)$ be two slightly different solutions of the differential equations. By substituting the value of $Y + \delta Y$ for Y in Equation (4), and by neglecting $(\delta Y)^2$ and $(\delta Y)^3$, which are infinitesimals of higher order, Equation (4) takes the form,

$$\frac{d^2}{dt^2}(Y + \beta Y^3) + Y + \frac{d^2}{dt^2}(\delta Y) + \frac{d^2}{dt^2}(3\beta Y^2 \delta Y) + \delta Y = G \cos pt \tag{11}$$

By subtracting Equation (4) from Equation (11), the linear variational differential equation in δY is

$$\frac{d^2}{dt^2}[(1 + 3\beta Y^2)\delta Y] + \delta Y = 0 \tag{12}$$

The solution of δY should be bounded for a stable solution of Y. The linear variational equation in W is

$$\frac{d^2W}{dt^2} + \frac{W}{1 + 3\beta Y^2} = 0 \tag{13}$$

where

$$W = (1 + 3\beta Y^2)\delta Y \tag{13a}$$

provided

$$1 + 3\beta Y^2 \neq 0 \tag{13b}$$

It also can be shown that δY is bounded provided W is bounded. Using Y_1 for Y, squaring Y_1 from Equation (9), and neglecting the terms $\cos 4\,pt$ and $\cos 6\,pt$, we have

$$Y^2 = 0.5(A^2 + B^2) + 0.5(A^2 + 2AB) \cos 2pt \tag{14}$$

Finally, by letting $z = 2pt$, Equation (13) can be written in a convenient form as

$$\frac{d^2W}{dz^2} + \frac{W}{S + C \cos z} = 0, \tag{15}$$

where

$$S = 4p^2[1 + 1.5\beta(A^2 + B^2)], \tag{16}$$

and

$$C = 4p^2[1.5\beta(A^2 + 2AB)] \tag{17}$$

Equation (15) is the key variational equation to be solved in the next section for the stability of the system.

Boundary of Stability by Perturbation Method[5]

Equation (15) has a period of 4π and 2π. The stable regions are joining together at the points

$$1/S = n^2/4, \quad C = 0 \tag{18}$$

[5] Loc. cit., Stoker.[1]

where $n = 1, 2, 3, \ldots$ = any positive integer.

As C approaches zero, the periodic solutions of Equation (15) are

$$W = \sin nz/2 \quad \text{and} \quad W = \cos nz/2 \tag{19}$$

For small values of C it is assumed that both $W(z, C)$ and $S(C)$ can be expanded in power series of C:

$$W = W_0 + CW_1 + C^2W_2 + \ldots + C^iW_i + \ldots \tag{20}$$

$$S = S_0 + CS_1 + C^2S_2 + \ldots + C^iS_i + \ldots \tag{21}$$

where S_i are constants and W_i are functions of z.

Substitution of Equations (20) and (21) into Equation (15) yields the following relation:

$$(S_0 + CS_1 + C^2S_2 + \ldots + C\cos z)\left(\frac{d^2W_0}{dz^2} + C\frac{d^2W_1}{dz^2} + C^2\frac{d^2W_2}{dz^2} + \ldots\right) + (W_0 + CW_1 + C^2W_2 + \ldots) = 0 \tag{22}$$

By collecting coefficients of like powers of C and setting to zero the resulting expressions, and by rearranging terms of W_i, the iteration procedure may be outlined as

$$\frac{d^2W_0}{dz^2} + \frac{W_0}{S_0} = 0, \tag{23}$$

$$\frac{d^2W_1}{dz^2} + \frac{W_1}{S_0} = -\frac{(S_1 + \cos z)}{S_0}\frac{d^2W_0}{dz^2}, \tag{24}$$

and

$$\frac{d^2W_2}{dz^2} + \frac{W_2}{S_0} = -\frac{S_2}{S_0}\frac{d^2W_0}{dz^2} - \frac{(S_1 + \cos z)}{S_0}\frac{d^2W_1}{dz^2} \tag{25}$$

The following list shows the various branches of curves of S versus C by their perturbation method.

$$\begin{aligned} &n = 1, \quad W_0 = \cos 0.5z, \quad S = 4 - 0.5C + 9C^2/128 \\ &n = 1, \quad W_0 = \sin 0.5z, \quad S = 4 + 0.5C + 9C^2/128 \end{aligned} \tag{26}$$

$$\begin{aligned} &n = 2, \quad W_0 = \cos z, \quad S = 1 + C^2/3 \\ &n = 2, \quad W_0 = \sin z, \quad S = 1 + C^2/3 \end{aligned} \tag{27}$$

$$\begin{aligned} &n = 3, \quad W_0 = \cos 1.5z, \quad S = 4/9 + 207C^2/256 \\ &n = 3, \quad W_0 = \sin 1.5z, \quad S = 4/9 + 207C^2/256 \end{aligned} \tag{28}$$

Equations (26) give the boundary of stability of the steady-state solutions. It can be shown that the regions between these two curves are unstable.

Boundary of Stability by Continued Fractions

Equation (15) may be transformed again into the following form by letting $S = 1/v^2$ and $C = 2\gamma/v^2$; thus

$$(1 + 2\gamma\cos z)\frac{d^2W}{dz^2} + v^2W = 0 \tag{29}$$

Recently Equation (29) was solved in detail for the case $2\gamma < 1$.[6] The boundary of stability of the solution is expressed in continued fractions as

$$1 - v^2 - \cfrac{\gamma^2}{1 - (v^2/4) - \left\{\gamma^2/[1 - (v^2/9) - \ldots]\right\}} = 0 \tag{30}$$

also,

$$1 \pm \gamma - 4v^2\cfrac{\gamma^2}{1 - (4v^2/9) - \left\{\gamma^2/[1 - (4v^2/25) - \ldots]\right\}} = 0 \tag{31}$$

These continued fractions yield a family of curves of v versus γ. The corresponding values of S versus C may thus be found as plotted in Fig. 4. Note that the unstable regions branch out from $S = 4$ and $C = 0$. For small values of C the solution obtained by using the perturbation method of the previous section checks very well with the exact method of continued fractions that was obtained from the work of Cambi.[6]

Stability of Forced Oscillations

The aim of this section is to outline the necessary synthesis based on the previous analysis. Suppose the magnitude of the disturbance G is given. We may start with Equation (10) and Equation (9) to determine the frequency p and the third harmonic B for a set of assumed amplitudes A as already shown in Figs. 2 and 3. The two parameters S and C of the variational equation may be computed by Equations (16) and (17) for the same set of A. Then C may be plotted versus S as shown in Fig. 5 for $G = 0.1$ and $\beta = \pm 4/300$. The shaded areas are stable regions redrawn from Fig. 4. These branches of the curves MN are unstable while the curves LM are stable. The point M may also be traced in either Fig. 2 or Fig. 3 where it indicates the point of tangency of a vertical tangent to the curve.

The locus of vertical tangents may be obtained by differentiating p with respect to A of Equation (10) and setting this result equal to zero. This yields the value of G in terms of A. If this value of G is substituted into Equation (10) the frequency p_t of the locus of the points of tangency from the vertical tangents can be expressed in terms of A as follows:

$$p_t^2 = \frac{1}{1 + 3(0.75\beta A^2) - 1.875(0.75\beta A^2)^2 + 2(0.75\beta A^2)^3} \tag{32}$$

If p_t is substituted for p in Equations (16) and (17) a single locus of C versus S may be obtained. For small values of G, this curve lies on the boundary of stability as shown by MM in Fig. 5. This locus is also plotted in Figs. 2 and 3.

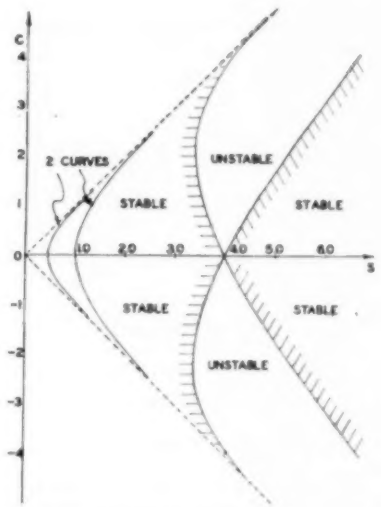

Fig. 4 Stability of continued fraction; shaded area stable region

[6] Enzo Cambi, "The Simplest Form of Second-Order Linear Differential Equation, With Periodic Coefficient," *Proceedings of The Royal Society of Edinburgh*, Section A, vol. 63, 1949–50, pp. 27–51.

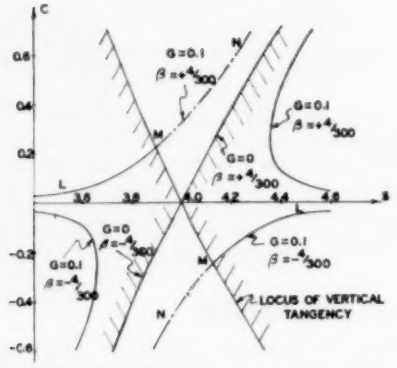

Fig. 5 Stability of forced oscillation; shaded area stable region

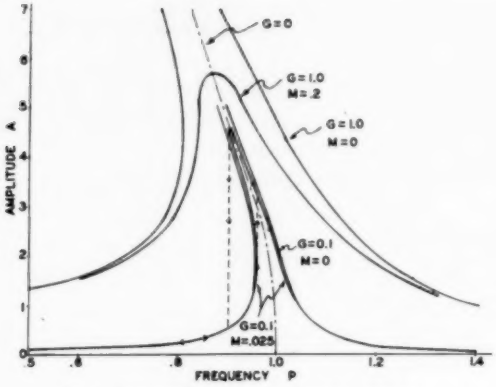

Fig. 6 Sinusoidal response with damping term

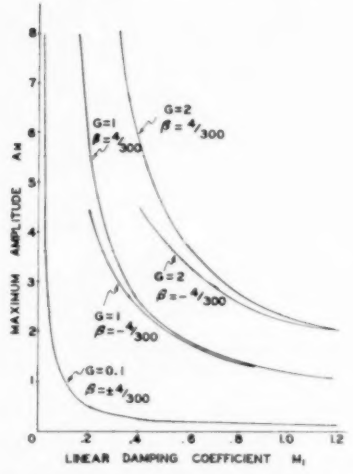

Fig. 7 Maximum amplitude under damping

Solution With Damping Terms

An examination of the general Equation (3) indicates that M_n and M_1 are nonlinear and linear damping coefficients, respectively. For convenience Equation (2) may be rearranged in the following form:

$$\frac{d^2}{dt^2}(Y + \beta Y^3) + M\frac{d}{dt}(Y + \mu Y^3) + Y = G_1 \cos pt + G_2 \sin pt, \quad (33)$$

where

$$M = M_n + M_1, \quad (34)$$

$$\mu = \beta M_n/(M_n + M_1), \quad (35)$$

$$G_1 = G \cos \phi, \quad (36)$$

$$G_2 = G \sin \phi \quad (37)$$

The iteration method may also be used here as previously given in the section, "Solution by Iteration Method," if Equation (33) may be written as

$$\frac{d^2Y_n}{dt^2} + p^2Y_n = -\frac{d^2}{dt^2}(\beta Y_{n-1}^3) - M\frac{d}{dt}(Y_{n-1} + \mu Y_{n-1}^3) + (p^2 - 1)Y_{n-1} + G_1 \cos pt + G_2 \sin pt, \quad (38)$$

where Y_n = nth iteration of Y.

For a periodic solution on the first-order iteration of Equation (38) the necessary conditions are that

$$(0.75)\beta p^2 A^3 + (p^2 - 1)A + G_1 = 0, \quad (39)$$

and

$$MpA[1 + (0.75)\mu A^2] + G_2 = 0 \quad (40)$$

For the first-order iteration, Equation (38) has a particular solution of the form,

$$Y_{1p} = B \cos 3pt + C \sin 3pt, \quad (41)$$

where

$$B = -(9/32)\beta A^3, \quad (42)$$

and

$$C = -(3M/32p)\mu A^3 \quad (43)$$

Thus the first iterated value of Y becomes,

$$Y_1 = A \cos pt + B \cos 3pt + C \sin 3pt \quad (44)$$

We may fix our attention here on a case where $M_n = 0$ and the linear damping coefficient M_1 is not zero. Then $M = M_1$, and $\mu = 0$. With the same procedure on the second iterationt he frequency p^2 may be formulated as follows:

$$p^2 = \{(2\phi - M_1^2) \pm [(2\phi - M_1^2)^2 - 4\phi^2(1 - G^2/A^2)]^{1/2}\}/2\phi^2 \quad (45)$$

where

$$\phi = 1 + 0.75\beta A^2 - 0.375(0.75\beta A^2)^2 + 0.281(0.75\beta A^2)^3$$

It also can be shown that the amplitude A is reduced substantially within the "nonlinear resonance" region. In Fig. 6 the curves are for $G = 1.0$, $M_1 = 0.2$, and $G = 0.1$, $M_1 = 0.025$. A jump phenomenon is shown as indicated by the arrows on one curve.

The maximum value of A may be found by differentiating p^2 with respect to A^2 and equating its reciprocal to zero. This maximum occurs at the points where the two roots of Equation (45) are equal to each other. This can be done by setting to zero the value under the radical of Equation (45), thus

$$M_1^2 = 2\phi[1 - (1 - G^2/A_m^2)^{1/2}] \quad (46)$$

These maximum amplitudes are given in Fig. 7 for $G = 0.1$, 1.0, and 2.0.

On Inertia Effects in a Transient Thermoelastic Problem[1]

ELI STERNBERG

Professor of Mechanics,
Division of Applied Mathematics,
Brown University, Providence, R. I.
Assoc. Mem. ASME

J. G. CHAKRAVORTY

Research Associate,
Division of Applied Mathematics,
Brown University, Providence, R. I.

This paper is concerned with the dynamic treatment of a transient thermoelastic problem for a semi-infinite medium which is constrained against transverse displacements and is exposed to a uniform time-dependent heating (or cooling) of its entire plane boundary. The stress distribution appropriate to this problem, in the event that the surface temperature is a step-function of time, was previously established by Danilovskaya [1][2] and by Mura [2]. In the present investigation the accompanying displacements are determined in closed form. In addition, an exact closed solution, in terms of error functions, is obtained for the case in which the time-dependence of the given surface temperature is of the ramp-type. The ensuing field of thermal stress is compared with the corresponding quasi-static stress distribution, with a view toward a quantitative assessment of the accompanying inertia effects as influenced by the rate at which the temperature of the boundary is altered. The results indicate that the conclusions reached in [1] and [2] are in need of essential modification once the assumption of an instantaneous change of the surface temperature is abandoned.

Introduction

The conventional quasi-static approach to thermoelastic problems in the presence of time-dependent temperature fields (and under stationary loading conditions) rests on the assumption that the inertia terms may be neglected in the governing field equations. This hypothesis, which goes back to Duhamel [3], is known to yield useful results in a wide variety of applications. It is evident, however, that the quality of the approximation must depend both on the size of the relevant intrinsic inertia parameters and on the nature of the time variations inherent in the temperature distribution. If, in particular, the temperature field exhibits sufficiently steep time-gradients, the dynamic effects disregarded in the traditional treatment of the problem may be expected to become significant. Moreover, when the inertia terms are taken into account, the entire character of the problem is altered: the process of transmission of the thermal stresses is then no longer purely diffusive but involves the propagation of elastic waves.

The first attempt to examine inertia effects in a transient thermoelastic problem is apparently due to Danilovskaya [1] (1950). The particular problem considered in [1] concerns an elastic half space that is free from loading and is subjected to a suddenly applied, and thereafter steadily maintained, uniform change of the surface temperature over its entire plane boundary. Throughout the interior of the medium, the temperature-distribution is assumed to obey the heat-conduction equation, in the absence of thermoelastic coupling.[3] The ensuing thermal stresses are determined rigorously within classical elastokinetics in [1], on the assumption that the body is constrained against lateral displacements. More recently, Mura [2] independently arrived at the same results, while Danilovskaya [4] generalized her previous solution to accommodate convective boundary conditions. None of the investigations cited so far includes the determination of the accompanying thermal displacements. The conclusions reached in [1] and [2] involve qualitative, and sizable quantitative, inertia corrections, which invalidate Duhamel's hypothesis for the problem discussed there.

In the following we return to Danilovskaya's original problem and obtain the missing displacements in closed form. The main objective of the present investigation, however, is the study of a modified problem in which the boundary of the half space undergoes a linear rise (or fall) in temperature during a finite time interval, after which the surface is held at constant temperature. An exact closed solution, in terms of error functions, appropriate to such a "ramp-type" boundary condition, is reached and compared with the corresponding quasi-static solution. This comparison aims at a quantitative appraisal of the inertia effects in their dependence upon the rate of heating (or cooling) of the boundary. The results—which are no longer confined to the physically unrealistic limiting case represented by an instantaneous change in the temperature of the boundary—suggest that the dynamic effects induced by a gradual heating or cooling of the boundary are substantially different from those encountered in [1] and [2], even at extremely high, but finite, time-gradients of the surface temperature.

Inertia terms have been taken into account in several thermoelastic investigations since the appearance of Danilovskaya's original paper [1]. Thus Boley [5] and Boley and Barber [6] studied thermally induced beam and plate vibrations. A particularly important contribution to the subject under discussion is due to Nowacki [7] who obtained several closed exact solutions to the (uncoupled) three-dimensional thermoelastic equations of motion, corresponding to a time-dependent heat source in the

[1] The results communicated in this paper were obtained in the course of an investigation conducted under Contract Nonr 562(25) with the Office of Naval Research, Department of the Navy, Washington, D. C.

[2] Numbers in brackets designate References at end of paper.

[3] It should be pointed out that the term "thermoelasticity" is reserved by some authors to describe the study of processes which are governed by the coupled field equations; in the present paper the term is applied in its narrower connotation.

Presented at the Summer Conference of the Applied Mechanics Division, Troy, N. Y., June 18–20, 1959, of THE AMERICAN SOCIETY OF MECHANICAL ENGINEERS.

Discussion of this paper should be addressed to the Secretary, ASME, 29 West 39th Street, New York, N. Y., and will be accepted until January 10, 1960, for publication at a later date. Discussion received after the closing date will be returned.

NOTE: Statements and opinions advanced in papers are to be understood as individual expressions of their authors and not those of the Society. Manuscript received by ASME Applied Mechanics Division, May 21, 1958. Paper 59—APM-9.

interior of a medium which occupies the entire space.[4] We also mention a purely formal dynamic treatment by Ignaczak [8] of the thermoelastic problem for the half space, in the presence of a time-dependent heat source at the boundary. Finally, we draw attention to recent investigations[5] of thermoelastic coupling effects, although the primary aim of these studies is unrelated to the main purpose of the present paper.

Governing Equations. Statement of Problem

Let (x, y, z) be Cartesian co-ordinates and consider an elastic medium occupying the half space $x \geq 0$. Suppose that the body is subjected to a time-dependent temperature field of the form

$$T = T(x, t) \tag{1}$$

and is constrained to the uniaxial motion characterized by the displacement field

$$u_x = u(x, t), \quad u_y = u_z = 0. \tag{2}$$

The displacement-stress relations of the classical theory of elasticity then reduce to

$$\sigma_x = \frac{2\mu}{1-2\nu}\left[(1-\nu)\frac{\partial u}{\partial x} - (1+\nu)\alpha T\right],$$
$$\sigma_y = \sigma_z = \frac{2\mu}{1-2\nu}\left[\nu\frac{\partial u}{\partial x} - (1+\nu)\alpha T\right], \tag{3}$$

where $(\sigma_x, \sigma_y, \sigma_z)$ are the components of normal stress, and the Cartesian components of shear stress vanish identically. Here μ, ν, and α designate the shear modulus, Poisson's ratio, and the coefficient of thermal expansion, respectively. If the body forces are absent, the equations of motion, at present, degenerate into the single equation

$$\frac{\partial \sigma_x}{\partial x} = \rho\frac{\partial^2 u}{\partial t^2}, \tag{4}$$

in which ρ denotes the mass density.

Substitution for σ_x in (4) from the first of (3) yields the displacement equation of motion

$$\frac{\partial^2 u}{\partial x^2} = \frac{1}{c^2}\frac{\partial^2 u}{\partial t^2} + \frac{(1+\nu)\alpha}{1-\nu}\frac{\partial T}{\partial x}, \tag{5}$$

provided c is the velocity of irrotational waves, given by

$$c^2 = \frac{2(1-\nu)\mu}{(1-2\nu)\rho}. \tag{6}$$

On the other hand, elimination of u between (4) and the first of (3) leads to the stress equation of motion

$$\frac{\partial^2 \sigma_x}{\partial x^2} = \frac{1}{c^2}\frac{\partial^2 \sigma_x}{\partial t^2} + \frac{\rho(1+\nu)\alpha}{1-\nu}\frac{\partial^2 T}{\partial t^2}. \tag{7}$$

We assume that the temperature field (1) obeys the (uncoupled) heat-conduction equation, whence

$$\kappa\frac{\partial^2 T}{\partial x^2} = \frac{\partial T}{\partial t}, \tag{8}$$

where κ is the thermal diffusivity.

The initial condition for the independent heat-conduction problem is taken as

$$T(x, 0) = 0 \quad (0 < x < \infty), \tag{9}$$

while two distinct types of boundary conditions are to be considered. For an instantaneous heating of the boundary (Danilovskaya's case),

$$T(0, t) = h(t)T_0, \tag{10}$$

in which T_0 is a constant and $h(t)$ designates the Heaviside step-function defined by

$$h(t) = 0 \quad \text{for} \quad -\infty < t < 0, \quad h(t) = 1 \quad \text{for} \quad 0 < t < \infty. \tag{11}$$

Alternatively, for a ramp-type heating of the boundary,

$$T(0, t) = f(t), \tag{12}$$

with

$$f(t) = 0 \quad \text{for} \quad -\infty < t \leq 0,$$
$$f(t) = \frac{T_0}{t_0}t \quad \text{for} \quad 0 \leq t \leq t_0, \tag{13}$$
$$f(t) = T_0 \quad \text{for} \quad t_0 \leq t < \infty,$$

where $T_0 \gtrless 0$ and $t_0 > 0$ are constants. Finally, we adjoin the regularity requirement

$$T(x, t) \to 0 \text{ as } x \to \infty. \tag{14}$$

If the medium is initially at rest, the thermal displacements and stresses arising from the temperature field $T(x, t)$ are governed by the initial conditions

$$u(x, 0) = 0, \quad \left[\frac{\partial u}{\partial t}\right]_{(x,0)} = 0 \quad (0 < x < \infty), \tag{15}$$

while the corresponding boundary condition, appropriate to vanishing surface tractions, appears as

$$\sigma_x(0, t) = 0 \tag{16}$$

and is to be supplemented by the regularity requirement

$$u(x, t), \quad \sigma_x(x, t), \quad \sigma_y(x, t) \to 0 \quad \text{as} \quad x \to \infty. \tag{17}$$

At this stage it is expedient to introduce dimensionless variables. Thus, we let

$$a = \frac{\kappa}{c} = \kappa\left[\frac{(1-2\nu)\rho}{2(1-\nu)\mu}\right]^{1/2}, \tag{18}$$

and define a dimensionless x-co-ordinate and time by means of

$$\xi = \frac{x}{a}, \quad \tau = \frac{\kappa t}{a^2}, \tag{19}$$

setting, in particular,

$$\tau_0 = \frac{\kappa t_0}{a^2}. \tag{20}$$

Next, we define a dimensionless temperature and displacement as well as dimensionless components of stress, through

$$\varphi = \frac{T}{T_0}, \qquad \hat{u} = \frac{1-\nu}{(1+\nu)\alpha T_0}\frac{u}{a},$$
$$\hat{\sigma}_x = \frac{1-2\nu}{2(1+\nu)\alpha T_0}\frac{\sigma_x}{\mu}, \quad \hat{\sigma}_y = \frac{(1-2\nu)(1-\nu)}{2(1+\nu)\alpha T_0}\frac{\sigma_y}{\mu}. \tag{21}$$[6]

With reference to this notation, and in view of (8), (9), the

[4] The dependence on time assumed in [7] includes the Dirac delta-function, the Heaviside step-function, and the sinusoidal pulse.

[5] See, for example, Deresiewicz [9], [10], which contain specific references.

[6] Since $\sigma_z = \sigma_y$, we omit any further reference to σ_z.

temperature problem reduces to the determination of a function $\varphi(\xi, \tau)$ which satisfies

$$\frac{\partial^2 \varphi}{\partial \xi^2} = \frac{\partial \varphi}{\partial \tau}, \tag{22}$$

and conforms to the initial condition

$$\varphi(\xi, 0) = 0 \quad (0 < \xi < \infty). \tag{23}$$

Moreover, by virtue of (10) to (13), we have the boundary condition

$$\varphi(0, \tau) = h(\tau), \tag{24}$$

in case of a sudden temperature application, or

$$\varphi(0, \tau) = \phi(\tau) \tag{25}$$

with

$$\begin{aligned} \phi(\tau) &= 0 \quad \text{for} \quad -\infty < \tau \leq 0, \\ \phi(\tau) &= \tau/\tau_0 \quad \text{for} \quad 0 \leq \tau \leq \tau_0, \\ \phi(\tau) &= 1 \quad \text{for} \quad \tau_0 \leq \tau < \infty, \end{aligned} \tag{26}$$

in case of a ramp-type heating. In either case, the regularity condition (14) now becomes

$$\varphi(\xi, \tau) \to 0 \quad \text{as} \quad \xi \to \infty. \tag{27}$$

Once φ has been found, the associated thermal displacements and stresses, in view of (3), (5), (15), (16), (17), (19), and (21), may be obtained by solving

$$\frac{\partial^2 \hat{u}}{\partial \xi^2} = \frac{\partial^2 \hat{u}}{\partial \tau^2} + \frac{\partial \varphi}{\partial \xi}, \tag{28}$$

$$\hat{\sigma}_x = \frac{\partial \hat{u}}{\partial \xi} - \varphi, \quad \hat{\sigma}_y = \nu \frac{\partial \hat{u}}{\partial \xi} - (1 - \nu)\varphi = \nu \hat{\sigma}_x - (1 - 2\nu)\varphi, \tag{29}$$

subject to the initial conditions

$$\hat{u}(\xi, 0) = 0, \quad \left[\frac{\partial \hat{u}}{\partial \tau}\right]_{(\xi, 0)} = 0 \quad (0 < \xi < \infty), \tag{30}$$

the boundary condition

$$\hat{\sigma}_x(0, \tau) = 0, \tag{31}$$

and the regularity conditions

$$\hat{u}(\xi, \tau), \quad \hat{\sigma}_x(\xi, \tau), \quad \hat{\sigma}_y(\xi, \tau) \to 0 \quad \text{as} \quad \xi \to \infty. \tag{32}$$

Suppose that $\varphi(\xi, \tau)$, in addition to satisfying (23), meets

$$\left[\frac{\partial \varphi}{\partial \tau}\right]_{(\xi, 0)} = 0 \quad (0 < \xi < \infty). \tag{33}$$

In this event, (3), (7), (30) imply that the stress $\hat{\sigma}_x(\xi, \tau)$ admits the alternative characterization through

$$\frac{\partial^2 \hat{\sigma}_x}{\partial \xi^2} = \frac{\partial^2 \hat{\sigma}_x}{\partial \tau^2} + \frac{\partial^2 \varphi}{\partial \tau^2}, \tag{34}$$

together with the initial conditions

$$\hat{\sigma}_x(\xi, 0) = 0, \quad \left[\frac{\partial \hat{\sigma}_x}{\partial \tau}\right]_{(\xi, 0)} = 0 \quad (0 < \xi < \infty), \tag{35}$$

the boundary condition (31), and the regularity requirement for $\hat{\sigma}_x$ contained in (32).

[7] Observe that the second of (29) merely serves to determine $\hat{\sigma}_y$ after $\hat{\sigma}_x$ has been established.

Sudden Heating of the Boundary. Reconsideration of Danilovskaya's Problem

The well-known solution[8] to the heat-conduction problem governed by (22), (23), (24), and (27) is given by

$$\varphi(\xi, \tau) = \psi(\theta), \quad \theta = \frac{\xi}{2\sqrt{\tau}} \quad (\tau > 0), \tag{36}$$

provided $\psi(\theta)$ designates the complementary error function defined through

$$\psi(\theta) \equiv \operatorname{erfc}(\theta) = \frac{2}{\sqrt{\pi}} \int_\theta^\infty \exp(-\lambda^2) d\lambda. \tag{37}$$

For future convenience, we recall here that

$$\psi(-\theta) = 2 - \psi(\theta), \quad \psi(0) = 1, \quad \psi(\theta) \to 0 \quad \text{as} \quad \theta \to \infty, \tag{38}$$

and cite the power-series development

$$\psi(\theta) = 1 - \frac{2}{\sqrt{\pi}} \sum_{n=0}^{\infty} \frac{(-1)^n \theta^{2n+1}}{(2n+1)\underline{|n}}, \tag{39}$$

as well as the semiconvergent expansion, valid as $\theta \to \infty$,

$$\psi(\theta) = \frac{\exp(-\theta^2)}{\theta\sqrt{\pi}} \left[\sum_{n=0}^{m} \frac{(-1)^n \underline{|2n}}{\underline{|n}(2\theta)^{2n}} + O(\theta^{-2m-2})\right] \quad (m = 0, 1, 2, \ldots). \tag{40}$$

Evidently, (36) is consistent with (33).

In treating the associated thermoelastic problem, Danilovskaya [1] employs the formulation through (34), (35), (31), (32) and does not consider the displacement field. In contrast, Mura [2] takes (28) to (32) as his starting point, but subsequently avoids the explicit determination of the displacements to which we turn our attention presently.

Thus, let

$$U(\xi, s) \equiv \mathfrak{L}\{\hat{u}(\xi, \tau)\} = \int_0^\infty \exp(-s\tau)\hat{u}(\xi, \tau) d\tau, \tag{41}$$

whence $U(\xi, s)$ is the Laplace transform, with respect to τ, of the displacement $\hat{u}(\xi, \tau)$, s being the transform-parameter. Applying the Laplace transform to (28), and bearing in mind the initial conditions (30) as well as the temperature field (36), we reach the ordinary differential equation

$$\frac{d^2 U}{d\xi^2} - s^2 U = -\frac{1}{\sqrt{s}} \exp(-\xi\sqrt{s}) \tag{42}$$

which, by virtue of (24), (29), (30), and (32), is subject to the boundary and regularity conditions

$$\left[\frac{dU}{d\xi}\right]_{(0, s)} = \frac{1}{s}, \quad U(\xi, s) \to 0 \quad \text{as} \quad \xi \to \infty. \tag{43}$$

The boundary-value problem characterized by (42), (43) has the solution,

$$U(\xi, s) = U_1(\xi, s) + U_2(\xi, s), \tag{44}$$

with

$$U_1(\xi, s) = \frac{\exp(-\xi s)}{s(1 - s)}, \quad U_2(\xi, s) = \frac{\exp(-\xi\sqrt{s})}{s^{3/2}(s - 1)}. \tag{45}$$

The inversion of U_1 is elementary[9] and yields

[8] See, for example, Carslaw and Jaeger [11], p. 247.

[9] See, for example, [12], p. 241, No. 1, and p. 242, No. 9.

$$\hat{u}_1(\xi, \tau) \equiv \mathfrak{L}^{-1}\{U_1(\xi, s)\} = h(\tau - \xi)[1 - \exp(\tau - \xi)], \quad (46)$$

where h again is the Heaviside step-function defined in (11). With a view toward inverting U_2, we note on the basis of Doetsch [13] (page 76, no. 20) that

$$\hat{u}_2(\xi, \tau) \equiv \mathfrak{L}^{-1}\{U_2(\xi, s)\} = \int_0^\infty g(\xi, \lambda)\chi(\tau, \lambda)d\lambda, \quad (47)$$

provided

$$\chi(\tau, \lambda) = \frac{1}{\sqrt{(\pi\tau)}} \exp(-\lambda^2/4\tau), \quad (48)$$

while

$$g(\xi, \tau) \equiv \mathfrak{L}^{-1}\{G(\xi, s)\}, \quad G(\xi, s) = \frac{\exp(-\xi s)}{s^2(s^2 - 1)}. \quad (49)$$

The inversion of G, in turn, presents no difficulties. In fact, [12] (page 241, no. 1, and page 230, no. 8) after a convolution, lead to

$$g(\xi, \tau) = h(\tau - \xi)[\sinh(\tau - \xi) - \tau + \xi]. \quad (50)$$

Substituting (50) in (47), and carrying out the integration, one obtains

$$\hat{u}_2(\xi, \tau) = \xi\psi(\theta) - 2(\tau/\pi)^{1/2} \exp(-\theta^2) + \frac{1}{2}\beta(\xi, \tau), \quad (51)$$

where θ and $\psi(\theta)$, as before, are given by (36) and (37), whereas

$$\beta(\xi, \tau) = \exp(\tau - \xi)\psi(\theta - \sqrt{\tau}) - \exp(\tau + \xi)\psi(\theta + \sqrt{\tau}). \quad (52)^{10}$$

In addition to β, it is expedient to introduce an auxiliary function γ, defined through

$$\gamma(\xi, \tau) \equiv -\frac{\partial\beta}{\partial\xi} = \exp(\tau - \xi)\psi(\theta - \sqrt{\tau}) + \exp(\tau + \xi)\psi(\theta + \sqrt{\tau}). \quad (53)^{10}$$

From (41), (44), (46), and (51), now follows

$$\hat{u}(\xi, \tau) = h(\tau - \xi)[1 - \exp(\tau - \xi)] + \xi\psi(\theta) - 2(\tau/\pi)^{1/2} \exp(-\theta^2) + \frac{1}{2}\beta(\xi, \tau), \quad (54)$$

while (29), in conjunction with (36), (53), (54), yields

$$\hat{\sigma}_x(\xi, \tau) = h(\tau - \xi) \exp(\tau - \xi) - \frac{1}{2}\gamma(\xi, \tau),$$
$$\hat{\sigma}_y(\xi, \tau) = \nu\hat{\sigma}_x(\xi, \tau) - (1 - 2\nu)\psi(\theta). \quad (55)$$

This completes the solution of the dynamic thermoelastic problem under consideration, for the case in which the surface temperature is a step-function of time. It is readily confirmed that the formal results (36), (54), (55) satisfy all relevant field equations, as well as the pertinent initial, boundary, and regularity conditions. Also, the stresses (55) agree with the corresponding results in [1] and [2].

Those terms in (54), (55), which contain the Heaviside function $h(\tau - \xi)$ as a multiplier, indicate the presence of a plane shock-wave which, as is seen from (18), (19), propagates with the velocity c of irrotational waves given by (6); the remaining terms are diffusive in character. The wave-front issues from the boundary and at all times remains parallel to the boundary. While $\hat{u}$ in (54) is continuous, as required by the physical continuity of the material, the stresses (55) exhibit finite jump-discontinuities at the wave-front. Specifically,

$$\hat{\sigma}_x(\xi, \xi+) - \hat{\sigma}_x(\xi, \xi-) = 1,$$
$$\hat{\sigma}_y(\xi, \xi+) - \hat{\sigma}_y(\xi, \xi-) = \nu. \quad (56)$$

We consider next the quasi-static displacements and stresses corresponding to the temperature field (36), which are characterized by (28), (29), (31), (32) provided the acceleration term in (28) is deleted. The solution to this simple problem has the form

$$\hat{u}(\xi, \tau) = \xi\psi(\theta) - 2(\tau/\pi)^{1/2} \exp(-\theta^2),$$
$$\hat{\sigma}_x(\xi, \tau) = 0, \quad \hat{\sigma}_y(\xi, \tau) = -(1 - 2\nu)\psi(\theta) \ (\tau > 0). \quad (57)$$

Thus, $\hat{\sigma}_x$ vanishes identically in the quasi-static solution.

According to (24), (31), and the second of (29),

$$\hat{\sigma}_y(0, \tau) = -(1 - 2\nu)h(\tau) \quad (58)$$

applies equally to (55) and (57), so that the boundary values of $\hat{\sigma}_y$ exhibit no inertia effects. Finally, one may verify with the aid of (38), (39), (40) that

$$\varphi(\xi, \tau) \to 1 \quad \text{as} \quad \tau \to \infty, \quad (59)$$

and that

$$\hat{\sigma}_x(\xi, \tau) \to 0, \quad \hat{\sigma}_y(\xi, \tau) \to -(1 - 2\nu) \quad \text{as} \quad \tau \to \infty, \quad (60)$$

hold both for the dynamic and quasi-static solution. Consequently, the stresses tend to the same steady-state values in both solutions; in contrast, the dynamic and quasi-static displacements grow beyond bounds as $\tau \to \infty$.

Solution for Ramp-Type Heating

We turn now to the case of a ramp-type heating (or cooling) of the free surface, in which the boundary condition (24) is to be replaced with (25). The dynamic solution to this modified thermoelastic problem may be obtained from the corresponding solution established in the preceding section by means of the Duhamel integral. To this end, let $S_0(\xi, \tau)$ and $S(\xi, \tau)$ denote the dynamic solutions appropriate to (24) and (25), respectively. Then,

$$S(\xi, \tau) = \int_0^\tau \frac{d}{d\lambda}[\phi(\lambda)]S_0(\xi, \tau - \lambda)d\lambda, \quad (61)^{11}$$

in which ϕ is given by (26). From (61), (26), we draw

$$S = S'(\xi, \tau) \equiv \frac{1}{\tau_0}\int_0^\tau S_0(\xi, \tau - \lambda)d\lambda \quad (0 \le \tau < \tau_0),$$
$$S = S'(\xi, \tau) - S'(\xi, \tau - \tau_0) \quad (0 \le \tau_0 < \infty). \quad (62)$$

Moreover, (62) clearly remain valid if $S_0(\xi, \tau)$ and $S(\xi, \tau)$ are interpreted to stand for the respective quasi-static solution[12] belonging to (24) and (25).

All of the integrals represented by the right member of the first of (62) can be evaluated in closed form, in terms of elementary and error functions. Since the results thus obtained are amenable to direct verification, the tedious and voluminous details of the underlying computations will be omitted.

From (62), (36) we ultimately reach the temperature distribution for the modified problem in the form

[10] Note that the arguments of ψ in (52), (53) are $\theta + \sqrt{\tau}$ or $\theta - \sqrt{\tau}$, as indicated.

[11] Note that S and S_0 here represent "vectors" with the appropriate components φ, u, $\hat{\sigma}_x$, and $\hat{\sigma}_y$.

[12] The temperature fields are, of course, the same in the dynamic and the quasi-static case.

$$\left.\begin{aligned}\varphi = \varphi'(\xi,\tau) &\equiv \frac{1}{\tau_0}\left[\left(\tau+\frac{\xi^2}{2}\right)\psi(\theta)\right.\\ &\qquad \left.-\,\xi\,(\tau/\pi)^{1/2}\exp\,(-\theta^2)\right] \quad (0\le\tau\le\tau_0),\\ \varphi &= \varphi'(\xi,\tau)-\varphi'(\xi,\tau-\tau_0) \quad (\tau_0\le\tau<\infty).\end{aligned}\right\} \tag{63}$$

The associated dynamic displacements follow from (62) and (54). In this manner one is eventually led to

$$\left.\begin{aligned}\hat{u} = \hat{u}'(\xi,\tau) &\equiv \frac{1}{\tau_0}\left\{h(\tau-\xi)[1+\tau-\xi\right.\\ &\qquad -\exp(\tau-\xi)]+\frac{1}{2}\beta(\xi,\tau)\\ &\qquad -\frac{1}{3}\,(6+4\tau+\xi^2)(\tau/\pi)^{1/2}\exp\,(-\theta^2)\\ &\qquad \left.+\frac{1}{6}\,\xi(6+6\tau+\xi^2)\psi(\theta)\right\} \quad (0\le\tau\le\tau_0),\\ \hat{u} &= \hat{u}'(\xi,\tau)-\hat{u}'(\xi,\tau-\tau_0) \quad (\tau_0\le\tau<\infty).\end{aligned}\right\} \tag{64}$$

The stresses belonging to (64) are most conveniently obtained with the aid of (29). Thus,

$$\left.\begin{aligned}\hat{\sigma}_x = \hat{\sigma}_x'(\xi,\tau) &\equiv \frac{1}{\tau_0}\left\{h(\tau-\xi)[\exp(\tau-\xi)-1]\right.\\ &\qquad \left.+\psi(\theta)-\frac{1}{2}\,\gamma(\xi,\tau)\right\} \quad (0\le\tau\le\tau_0),\\ \hat{\sigma}_x &= \hat{\sigma}_x'(\xi,\tau)-\hat{\sigma}_x'(\xi,\tau-\tau_0) \quad (\tau_0\le\tau<\infty),\\ \hat{\sigma}_y &= \nu\hat{\sigma}_x(\xi,\tau)-(1-2\nu)\varphi(\xi,\tau) \quad (0\le\tau<\infty),\end{aligned}\right\} \tag{65}$$

where φ is, in the present instance, given by (63).

The foregoing fields of temperature, displacement, and stress depend continuously on ξ and τ, throughout $0\le\xi<\infty, 0\le\tau<\infty$. On the other hand, the space and time derivatives of $\hat{u}$, $\hat{\sigma}_x$, $\hat{\sigma}_y$ in (64), (65) display jump discontinuities both at $\tau=\xi$ and at $\tau=\xi+\tau_0$; these discontinuities are evidently propagated with the velocity c of irrotational waves, given by (6).

The first of (57), in conjunction with (62), yields the quasi-static displacements for the modified problem, while the corresponding stresses then follow from (29). The results of this computation are

$$\left.\begin{aligned}\hat{u} = \hat{u}'(\xi,\tau) &\equiv \frac{1}{\tau_0}\left[\xi\left(\tau+\frac{1}{6}\,\xi^2\right)\psi(\theta)\right.\\ &\qquad \left.-\frac{1}{3}\,(\tau/\pi)^{1/2}(\xi^2+4\tau)\,\exp\,(-\theta^2)\right] \quad (0\le\tau\le\tau_0),\\ \hat{u} &= \hat{u}'(\xi,\tau)-\hat{u}'(\xi,\tau-\tau_0) \quad (\tau_0\le\tau<\infty),\\ \hat{\sigma}_x(\xi,\tau) &= 0, \quad \hat{\sigma}_y(\xi,\tau) = -(1-2\nu)\varphi(\xi,\tau)\\ &\qquad\qquad (0\le\tau<\infty),\end{aligned}\right\} \tag{66}$$

in which φ is once more given by (63).

In place of (58) we now have

$$\hat{\sigma}_y(0,\tau) = -(1-2\nu)\phi(\tau) \quad (0\le\tau<\infty), \tag{67}$$

with ϕ defined by (26), valid for both (65) and (66). The limit relations (59), (60) continue to hold for the dynamic and the quasi-static solution of the modified problem. Finally, both of these solutions evidently fulfill

$$S(\xi,\tau)\to S_0(\xi,\tau) \quad \text{as} \quad \tau_0\to 0. \tag{68}$$

Numerical Results. Discussion

The numerical evaluation of the solutions derived in the pre-

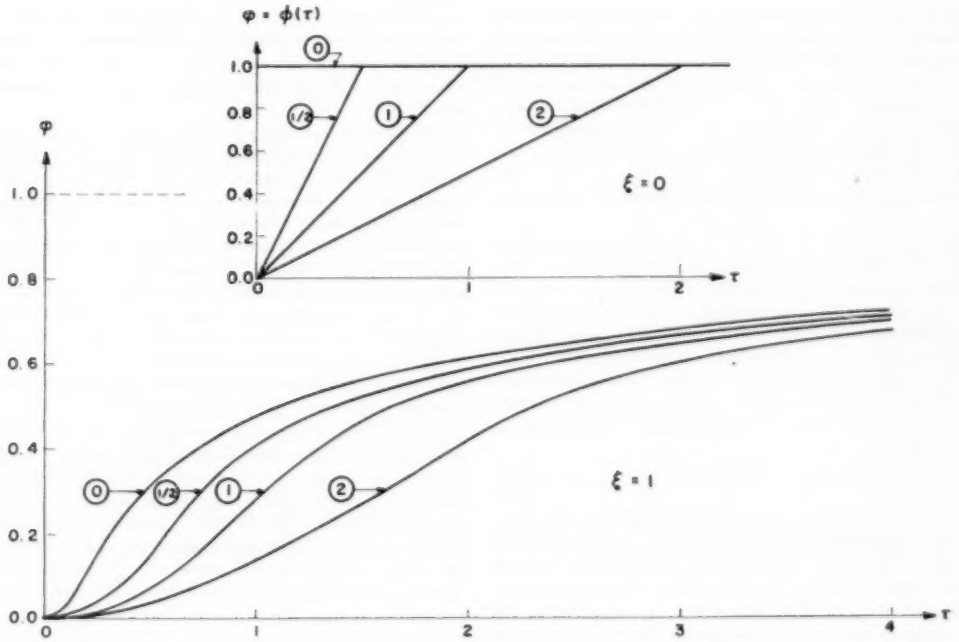

Fig. 1 Time-dependence of φ at $\xi = 0$ and $\xi = 1$ for various values of τ_0

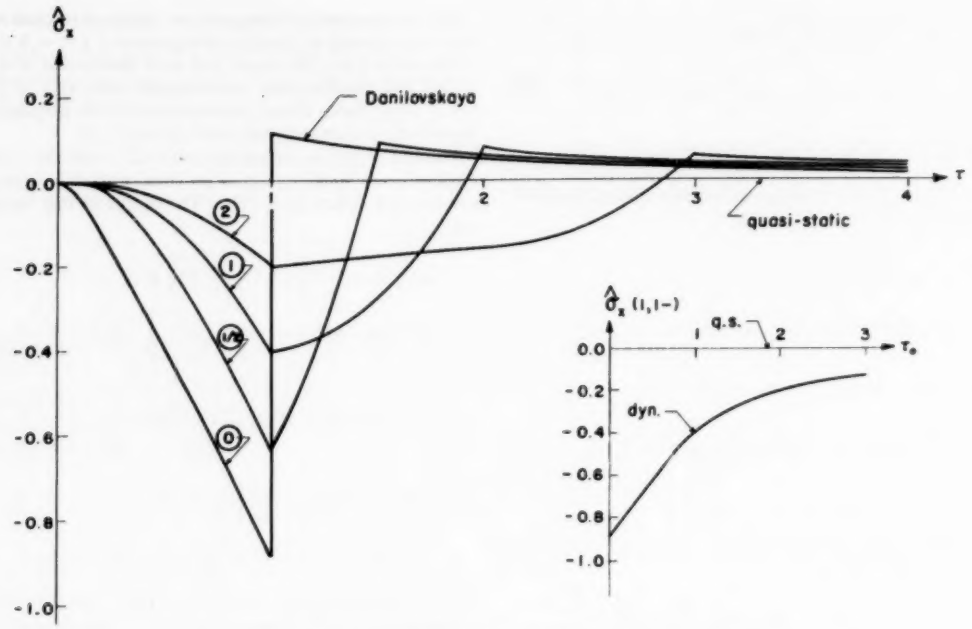

Fig. 2 Time-dependence of $\hat{\sigma}_x$ at $\xi = 1$ for various values of τ_0

ceding sections is readily accomplished with the aid of available tables [14] of the error function.

Fig. 1 shows the time-dependence of the dimensionless temperature $\varphi(\xi, \tau)$ at the boundary $\xi = 0$ and at the interior plane $\xi = 1$, for $\tau_0 = 1/2, 1, 2$, as well as for the limiting case $\tau_0 = 0$ which corresponds to an instantaneous heating of the surface. The curves belonging to $\xi = 0$, of course, merely illustrate the boundary condition (25).

Fig. 2 depicts the dimensionless stress $\hat{\sigma}_x$, which is independent of ν, as a function of τ at the level $\xi = 1$, for the same values of τ_0 underlying Fig. 1. The presence of a nonvanishing $\hat{\sigma}_x$ is entirely due to inertia effects, this stress being identically zero in the quasi-static solution. When $\tau_0 = 0$ (Danilovskaya's case), $\hat{\sigma}_x(1, \tau)$ exhibits a jump-discontinuity at $\tau = 1$, as predicted by (56); for $\tau_0 > 0$, the curves under discussion are continuous but display discontinuities of slope at $\tau = 1$ and $\tau = 1 + \tau_0$. Regardless of the value of τ_0, $\hat{\sigma}_x(1, \tau)$ tends to the steady-state value zero as $\tau \to \infty$.

The peak-values of $\hat{\sigma}_x(1, \tau)$, at $\tau = 1$, decline rapidly with increasing τ_0, as is evident from the inset diagram in Fig. 2. Thus the peak-value appropriate to $\tau_0 = 3$ is found to be less than 14 per cent of the peak-value corresponding to $\tau_0 = 0$. In order to render this comparison meaningful, it is essential to establish the relation between the dimensionless time τ and the physical time t for an actual material. To this end, we consider structural steel and use the approximate values $\nu = 1/3$, $\mu = 7.55 \times 10^{11}$ dynes/cm², $\rho = 7.85$ gm/cm³, $\kappa = 0.12$ cm²/sec. Equations (18) and (19) now yield

$$a = 1.93 \times 10^{-7} \text{ cm}, \quad t = (3.12 \times 10^{-13})\tau \text{ sec}. \qquad (69)$$

Consequently, $\tau_0 = 3$, in the case of steel, implies that the time-interval during which the surface temperature is raised or lowered is of the order of 10^{-12} sec. Nevertheless, even such an exceedingly rapid heating or cooling of the boundary reduces the maximum magnitude of $\hat{\sigma}_x(1, \tau)$ by 86 per cent as compared to the maximum value in the event of an instantaneous temperature change.

We turn, finally, to the discussion of the transverse normal stress. In this connection, we recall that the surface-values of $\hat{\sigma}_y$ are free from inertia effects. In Fig. 3, $\hat{\sigma}_y(\xi, \tau)$ is plotted as a function of τ for $\xi = 1$, $\tau_0 = 0, 1/2, 1, 2$, and $\nu = 1/3$. The curves in the upper part of this figure, refer to the dynamic values, given by (55), (65); those in the lower portion are based on the quasi-static values in (57), (66). Both families of curves asymptotically approach the common steady-state value $-1/3$, as $\tau \to \infty$. The quasi-static curves represent analytic functions of τ for $0 < \tau < \infty$. In contrast, the corresponding dynamic curves have discontinuous slopes at $\tau = 1$, $\tau = 1 + \tau_0$, if $\tau_0 > 0$, whereas the curve appropriate to $\tau_0 = 0$ exhibits the jump-discontinuity described in the last of (56).

The effect of variations in τ_0 upon $\hat{\sigma}_y$ at $\xi = 1$, $\tau = 1-$, is illustrated by the inset diagram in Fig. 3. It is seen that the dynamic and the quasi-static value of $\hat{\sigma}_y(1, 1-)$ diminish very rapidly as τ_0 is increased. Indeed, one finds that $\tau_0 = 10^{13}$, which corresponds to approximately 3.12 sec for steel,[13] yields a reduction of $\hat{\sigma}_y(1, 1-)$ from -0.46 and -0.16 at $\tau_0 = 0$ (Danilovskaya's values) to 0.23×10^{-13} and 0.093×10^{-13}, in the dynamic and quasi-static case, respectively. Both of these reduced values are, in turn, insignificantly small compared to the steady-state value of $\hat{\sigma}_y$. It should be emphasized, however, that the ratio of the quasi-static to the dynamic value of $\hat{\sigma}_y(1, 1-)$, which reflects the error arising from the neglect of the inertia terms, is independent of τ_0 for $\tau_0 > 1$, and is given by 0.41.

In conclusion, we draw attention to the fact that the particular problem underlying this investigation suffers from two deficiencies as a means for studying the validity of Duhamel's hypothesis. Thus, the artificial constraint of the body to the one-dimensional motion assumed in (2), results in a severe degeneracy of the quasi-static stress distribution, as evidenced by the vanishing of the primary normal stress σ_x. Next, the absence of a characteristic length in the problem under consideration obscures the influence upon the dynamic effects sought of the size of the

[13] See Equations (69).

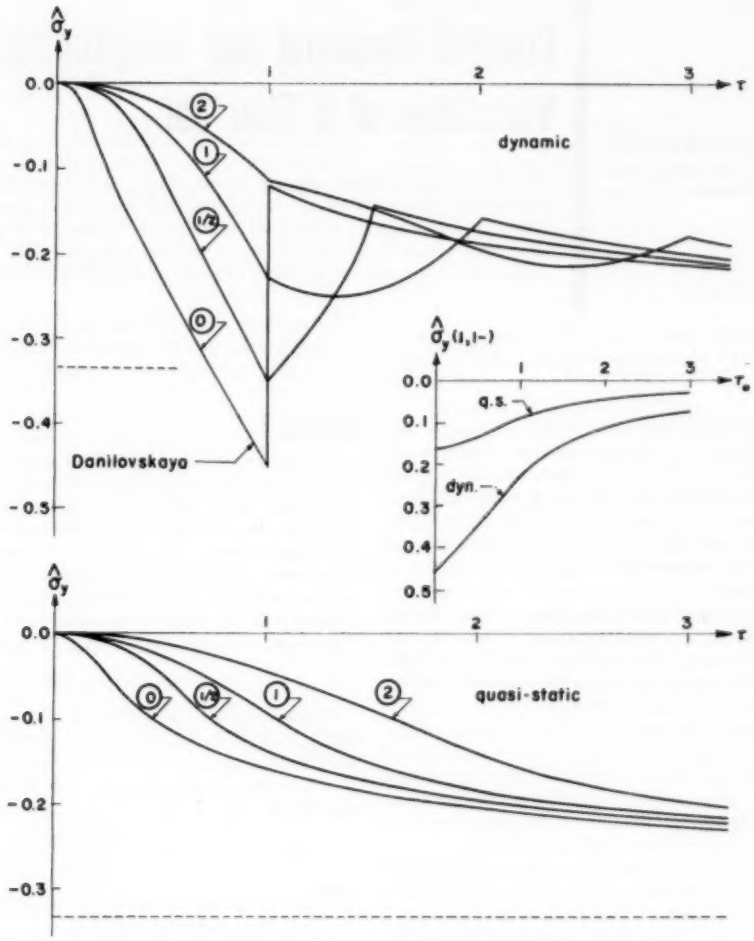

Fig. 3 Time-dependence of $\hat{\sigma}_y$ at $\xi = 1$ for various values of τ_0 ($\nu = 1/3$)

intrinsic inertia parameters, which remain hidden in the dimensionless time and distance scales.

Acknowledgment

The authors are greatly indebted to Prof. B. Budiansky of Harvard University who proposed the subject of this investigation and made valuable suggestions concerning the discussion of the results obtained.

References

1 V. I. Danilovskaya, "Thermal Stresses in an Elastic Half-Space Due to a Sudden Heating of Its Boundary" (in Russian), *Prikladnaya Matematika i Mekhanika*, vol. 14, 1950, p. 316.

2 T. Mura, "Thermal Strain and Stresses in Transient State," Proceedings of the Second Japan Congress of Applied Mechanics, vol. 9, 1952.

3 J. M. C. Duhamel, "Second Mémoire sur les Phénomènes Thermomécaniques," *J. de l'École Polytechnique*, vol. 15, 1837.

4 V. I. Danilovskaya, "On a Dynamical Problem of Thermoelasticity" (in Russian). *Prikladnaya Matematika i Mekhanika*, vol. 16, 1952, p. 341.

5 B. A. Boley, "Thermally Induced Vibrations of Beams," *Journal of the Aeronautical Sciences*, vol. 23, 1956, p. 179.

6 B. A. Boley and A. D. Barber, "Dynamic Response of Beams and Plates to Rapid Heating," JOURNAL OF APPLIED MECHANICS, vol. 24, TRANS. ASME, vol. 79, 1957, p. 413.

7 W. Nowacki, "A Dynamical Problem of Thermoelasticity," *Nadb. Arch. Mech. Stos.*, vol. 9, 1957, p. 325.

8 J. Ignaczak, "Thermal Displacements in an Elastic Semi-Space Due to a Sudden Heating of the Boundary Plane," *Nadb. Arch. Mech. Stos.*, vol. 9, 1957, p. 395.

9 H. Deresiewicz, "Plane Waves in a Thermoelastic Solid," *Journal of the Acoustical Society of America*, vol. 29, 1957, p. 204.

10 H. Deresiewicz, "Solution of the Equations of Thermoelasticity," Proceedings of the Third U. S. National Congress of Applied Mechanics, ASME, 1958, pp. 287–291.

11 H. S. Carslaw and J. C. Jaeger, "Conduction of Heat in Solids," Clarendon Press, Oxford, 1947.

12 Staff of the Bateman Manuscript Project, "Tables of Integral Transforms—I," McGraw-Hill Book Company, Inc., New York, N. Y., 1954.

13 G. Doetsch, "Tabellen zur Laplace-Transformation und Anleitung zum Gebrauch," Springer, Berlin, 1947.

14 Tables of Probability Functions, vol. 1, New York, W. P. A., 1941.

Coupled Torsional and Longitudinal Vibrations of a Thin Bar[1]

R. C. Di PRIMA

Associate Professor of Mathematics, Rensselaer Polytechnic Institute, Troy, N. Y.

The effect of pretwist on the natural frequencies of coupled torsional-longitudinal oscillations of thin bars is studied. It is found that the natural frequencies of oscillations which consist primarily of torsional motion may be considerably increased depending upon the thinness of the bar, and the amount of pretwist. The natural frequencies of oscillations which consist primarily of longitudinal motion are not significantly altered.

It is well known that when a thin bar is under torsion there is a slight decrease in distance between cross sections. A normal stress is thus produced in each longitudinal fiber which is not parallel to the axis of the bar; and hence there is a stress component which produces an additional torque. It has been shown that for straight bars this is a higher order effect and can be neglected except for comparatively large angles of twist in bars of thin cross section.[2]

If the bar is pretwisted (but not prestressed), the same reasoning leads to a first-order correction in the torque predicted by the classical Saint Venant theory. This correction may be considerable depending upon the amount of initial twist, the form of the cross section, and the material of the bar.[3]

Thus for a pretwisted bar there is a coupling between longitudinal and torsional motion which in general should not be neglected. This coupling effect is analyzed in this paper using a "beam-type" theory. The natural frequencies of coupled longitudinal-torsional oscillations of a thin bar are computed and compared with the natural frequencies of uncoupled motion.

Recently Reissner and Washizu[4] have considered the effect of pretwist on the natural frequencies of torsional oscillations of a beam of narrow cross section. Their analysis is based on a variational principle for the linear theory of shallow shells which is the appropriate specialization of a general variational principle for stresses and deformations. The results of this paper are in agreement with those given by Reissner and Washizu.

Analysis

Consider a thin bar of length l, described by an axis (x-axis) which is the locus of centroids of cross-sectional planes taken normal to the plane, Fig. 1. Let the bar be pretwisted about this axis by an amount $\tau(x)$ radians; τ is measured positive in a clockwise direction with increasing x. It is assumed that the bar is not prestressed. Consider an element of the bar of length dx and a longitudinal fiber a distance r from the axis of the bar. This fiber forms a helix of radius r and spiral angle βr where $\beta = d\tau/dx$. The length of this fiber (aa' in Fig. 1) is given by

$$ds_0 \cong \left\{1 + (r\beta)^2\right\}^{1/2} dx \tag{1}$$

Corresponding to an applied elastic torque each cross section will be rotated through an angle $\theta(x)$, where θ is measured in the same manner as τ. It is assumed that $d\theta/dx$ is small compared to β. The strain in the fiber aa' due to this rotation can be expressed as

$$\epsilon = \frac{ds - ds_0}{ds_0} + \epsilon_0, \tag{2}$$

where

$$ds \cong \left\{1 + \left(r\beta + r\frac{d\theta}{dx}\right)^2\right\}^{1/2} dx, \tag{3}$$

and ϵ_0 is the strain due to the decrease in distance between two cross sections. Here $\epsilon_0 > 0$ implies tension and $\epsilon_0 < 0$ implies compression. Substituting for ds in Equation (2), neglecting $r^2\beta^2$ against 1, and quadratic terms in $d\theta/dx$ gives[5]

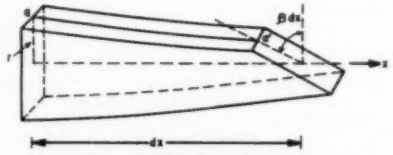

GEOMETRY OF PRETWISTED BEAM

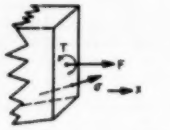

STRESS RESULTANTS

Fig. 1

[1] This work was partially supported by the Office of Naval Research, contract No. Nonr 1866(02), Harvard University, and by the Air Force Office of Scientific Research of the Air Research and Development Command, under contract No. AF 18(600)-1586, Rensselaer Polytechnic Institute.

[2] S. Timoshenko, "Strength of Materials—Vol. II," D. Van Nostrand Company, Inc., New York, N. Y., 2nd edition, 1941, pp. 298–304.

[3] Chen Chu, "The Effect of Initial Twist on the Torsional Rigidity, of Thin Prismatic Bars and Tubular Members," Proceedings of The First U. S. National Congress of Applied Mechanics, 1951, pp. 265–269.

[4] E. Reissner and K. Washizu, "On Torsional Vibrations of a Beam with a Small Amount of Pretwist," *Journal of the Japan Society of Aeronautical Engineers*, vol. 5, 1957, pp. 330–335.

Contributed by the Applied Mechanics Division and presented at the Annual Meeting, Atlantic City, N. J., November 29–December 4, 1959, of The American Society of Mechanical Engineers.

Discussion of this paper should be addressed to the Secretary, ASME, 29 West 39th Street, New York, N. Y., and will be accepted until January 10, 1960, for publication at a later date. Discussion received after the closing date will be returned.

Note: Statements and opinions advanced in papers are to be understood as individual expressions of their authors and not those of the Society. Manuscript received by ASME Applied Mechanics Division, March 31, 1958. Paper No. 59—A-18.

[5] Throughout this paper terms in $d\theta/dx$ which would lead to higher order corrections have been neglected. Thus when $\beta = 0$, our results for ϵ, the longitudinal stress, the resultant torque, and resultant longitudinal force will reduce to those given by the classical theory.

$$\epsilon = r^2\beta \frac{d\theta}{dx} + \epsilon_0 \tag{4}$$

The corresponding normal stress, $\sigma = E\epsilon$ (where E is Young's modulus), has components $\sigma \cos(r\beta)$ and $\sigma \sin(r\beta)$ parallel to the axis of the bar and in the cross section of the bar, respectively. In accord with the assumptions on order of magnitude, $d\theta/dx$ has been neglected in computing the angle of inclination. If T and F are the resultant torque and resultant longitudinal force acting across a cross section, Fig. 1, then

$$F = \int_A \sigma \, dA, \quad T = GJ \frac{d\theta}{dx} + \int_A r(r\beta\sigma)dA \tag{5}$$

Here A denotes the area of the cross section, G the shear modulus and J the torsional rigidity predicted by the classical theory. The terms $\cos r\beta$ and $\sin r\beta$ have been replaced by 1 and $r\beta$, respectively.

Substituting for σ in Equations (5), noting that $\epsilon_0 = du/dx$ where $u(x)$ is the displacement in the positive x-direction, and carrying out the necessary integrations gives

$$F = EA \frac{du}{dx} + EI_0\beta \frac{d\theta}{dx},$$
$$T = (GJ + EI_2\beta^2) \frac{d\theta}{dx} + EI_0 \frac{du}{dx}, \tag{6}$$

where

$$I_0 = \int_A r^2 dA; \quad I_2 = \int_A r^4 dA$$

It should be noted that if $\beta = 0$, i.e., the bar is not pretwisted, Equations (6) uncouple, and we obtain the well-known classical equations

$$F = EA \, du/dx, \text{ and } T = GJ \, d\theta/dx$$

The Eigenvalue Problem

The equations of equilibrium for simple harmonic motion are

$$\frac{dF}{dx} + \rho A\omega^2 u = 0, \quad \frac{dT}{dx} + \rho I_\theta \omega^2 \theta = 0, \tag{7}$$

where ρ is the density, and the period of the motion is $2\pi/\omega$. Substituting for F and T from Equations (6) gives

$$E \frac{d}{dx}\left\{A \frac{du}{dx}\right\} + \rho A\omega^2 u = -E \frac{d}{dx}\left\{I_0\beta \frac{d\theta}{dx}\right\},$$
$$\frac{d}{dx}\left\{(GJ + EI_2\beta^2) \frac{d\theta}{dx}\right\} + \rho I_\theta \omega^2 \theta = -E \frac{d}{dx}\left\{I_0\beta \frac{du}{dx}\right\} \tag{8}$$

The boundary conditions for a free-free beam are $F = T = 0$ at the ends. Using Equations (6) these conditions become

$$du/dx = d\theta/dx = 0 \tag{9}$$

at $x = 0$ and $x = l$. For a cantilevered beam the boundary conditions at $x = 0$ are replaced by $u = \theta = 0$.

From now on we shall restrict ourselves to the case of bars of constant cross section and constant β. For the free-free beam the boundary conditions (9) suggest a solution of the form

$$u = B \cos \frac{n\pi x}{l}, \quad \theta = C \cos \frac{n\pi x}{l}, \tag{10}$$
$$n = 1, 2, \ldots$$

Substituting in Equations (8), and setting the determinant of the coefficients of B and C equal to zero leads to the following equation for ω:

$$\{\omega^2 - \omega_L^2\}\{\omega^2 - (1 + \gamma)\omega_T^2\} - K\omega_L^2\omega_T^2 = 0, \tag{11}$$

where $\omega_T^2 = GJn^2\pi^2/\rho I_\theta l^2$, $\omega_L^2 = En^2\pi^2/\rho l^2$ are the squares of the natural frequencies of uncoupled torsional and longitudinal oscillations, respectively, and $\gamma = EI_2\beta^2/GJ$ and $K = EI_0^2\beta^2/GJA$. Since, $\omega_T^2 \ll \omega_L^2$, it follows from Equation (11) that

$$\omega_1^2 = (1 + \gamma)\omega_T^2 + \frac{K\omega_L^2\omega_T^2}{\omega_1^2 - \omega_L^2},$$
$$\sim (1 + \gamma - K)\omega_T^2, \tag{12}$$

for the primarily torsional frequency. The primarily longitudinal frequency follows in the same manner

$$\omega_2^2 = \omega_L^2 + \frac{K\omega_L^2\omega_T^2}{\omega_2^2 - (1 + \gamma)\omega_T^2} \sim \omega_L^2 + K\omega_T^2,$$
$$\sim \omega_L^2 \tag{13}$$

The exact solution of Equation (11) indicates that the approximate formulas just given for ω_1^2 and ω_2^2 are quite accurate. Computations have been carried out using Equation (11) for the case of a bar of rectangular cross section of width $2b$ and depth $2h$, for depth-to-width ratios of 1/10, 1/15, and 1/20. The torsional rigidity, J, was computed from the formula $J = 4k_1Ah^2$ where $k_1 = 0.312$ for $h/b = 1/10$, and 1/3 for $h/b = 1/15$ and 1/20.[6] Also Poisson's ratio which appears in the ratio E/G was taken to be 1/3. In Fig. 2, $\lambda_T = \omega_1/\omega_T$ has been plotted as a function of βb for the three values of h/b.

The results are in close agreement with the approximate

[6] S. Timoshenko and J. N. Goodier, "Theory of Elasticity," McGraw-Hill Book Company, Inc., New York, N. Y., second edition, 1951, pp. 277–278.

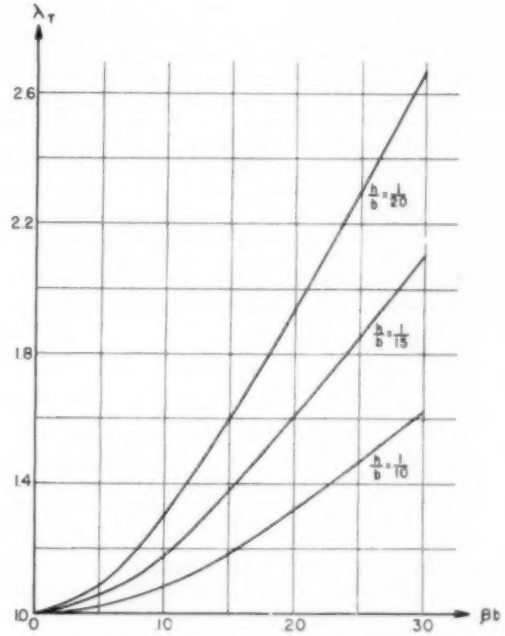

Fig. 2 $\lambda_T = \left(\frac{\rho I_\theta^2 \omega^2}{GJn^2\pi^2}\right)^{1/2}$ versus βb

formula given by Equation (12). It is clear from Fig. 2 that for any mode the effect of initial pretwist is to raise the "torsional" natural frequency (and, depending upon h/b and βb, by a considerable amount). On the other hand, the maximum percentage charge in ω_2/ω_L for the range of h/b and βb considered here was less than 1.5 per cent. Thus the "longitudinal" natural frequency is practically unaltered by pretwisting.

It is interesting to note that if longitudinal inertia is neglected in Equation (8) the bar has an effective GJ given by

$$GJ_{eff} = GJ\{1 + \gamma - K\} = GJ\left\{1 + \frac{EI_2\beta^2}{GJ} - \frac{EI_0{}^2\beta^2}{GJA}\right\}, \quad (14)$$

which is the same as the result given in Equation (12). For a bar of narrow cross section the foregoing equation reduces to

$$GJ_{eff} = GJ\left\{1 + {}^4/_{30}(1 + \nu)\left(\frac{b}{h}\right)^2(\beta b)^2\right\}, \quad (15)$$

where terms $0(h^2/b^2)$ have been neglected and ν denotes Poisson's ratio. This expression for the effective torsional rigidity differs from that given by Reissner and Washizu[4] only in that they have a $1 - \nu$ in the denominator instead of a $1 + \nu$ in the numerator.

Finally, a suitable solution for the cantilevered beam is

$$u = B \sin (n\pi x/2l), \quad \theta = C \sin (n\pi x/2l), \quad n = 1, 3, 5 \ldots$$

The analysis for this case is identical with that for the free-free beam, and it is only necessary to replace n by $n/2$ with n ranging over the odd integers to make the results from the free-free beam applicable to the cantilevered beam.

Acknowledgment

The author would like to express his appreciation to Prof. Bernard Budiansky for suggesting this problem, and for his helpful comments. He is also indebted to the referee for calling the author's attention to the work of Reissner and Washizu and for his suggestions which aided considerably in revising this paper.

Production of Rotation in a Confined Liquid Through Translational Motion of the Boundaries

R. R. BERLOT[1]
Energy Research Division,
Electro-Optical Systems, Inc.,
Pasadena, Calif.

The motion of a fluid contained in a cylindrical tank driven laterally to its axis is analyzed in terms of a combination of surface waves and a two-dimensional combined vortex. Nonlinearities are introduced by analogy with the motions of a set of spherical pendulums. The results of theory and experiment agree within the limits of experimental error and the approximations of the theory.

THE response of confined liquids to external driving forces is of interest in connection with the control of large liquid-propellant rockets in which the motion of the liquids is an important consideration in the stabilization of the autopilot. For stability analysis, it has been customary to neglect the nonlinear terms in the Navier-Stokes equation on the supposition that the motions to be studied were infinitesimally small. It also has been assumed that the viscous terms could be dropped for the reason, as Lamb [1][2] has indicated, that for slightly viscous fluids the viscous effects are confined to a narrow region in the vicinity of the boundary. In the course of experiments designed to check the linear inviscid theory, it was observed that, when a periodic linear motion was applied to the boundaries in a direction normal to the gravity vector, the liquid responded with an oscillatory motion about a single nodal line normal to the plane containing the gravity vector and the vector describing the linear motion of the boundaries, provided the driving frequency was sufficiently far removed from the natural frequency of oscillation. However, when the driving frequency was in the neighborhood of the natural frequency, the liquid departed from planar motion and a rotational wave was observed to wash around the boundaries. Upon cessation of the driving motion of the boundaries, it was observed, by dropping bits of paper into the liquid, that rotation was present. The phenomenon is not predicted by linear, inviscid theory, and it is the purpose of this paper to indicate the mechanism whereby the rotation was produced in the liquid.

Theory

The idea of representing the degrees of freedom of a confined liquid with a free surface by a set of spring-mass systems was first introduced, to the author's knowledge, by Graham and Rodríguez [2], who applied it to a rectangular fuel tank. Gleghorn [3] employed the same analogy to describe the motion of fluid in a cylindrical tank. Kachigan [4] and Schmitt [5] replaced the spring-mass systems by a set of simple pendulums. With either analogy, the technique consisted in solving Laplace's equation for the velocity potential in co-ordinates appropriate to the boundaries and formulating the expression for the fluid kinetic energy from which the masses of the pendulums or spring-mass systems could be extracted. The lengths of the pendulum suspensions, or the spring constants of the spring-mass systems were then chosen to yield the natural frequencies of the liquid degrees of freedom.

Since these treatments all started with the assumption that the fluid velocity was entirely derivable from a scalar potential function, the possibility of describing rotational motion was excluded *ab initio*. Furthermore, the form chosen for the scalar potential function provided no means for the fluid to carry angular momentum. On the other hand, since, away from resonance, the fluid degrees of freedom appeared to be adequately represented by a set of pendulums, and since, in the vicinity of resonance, the fluid motion departed from the plane of drive, as indeed a conical pendulum would, it seemed that it should be possible to sustain the pendulum analogy in both regions by generalizing the mathematical description of the fluid motion to include rotation and angular momentum. This is done in the following paragraphs.

For the purpose of this paper, it is sufficient to restrict consideration to a circular cylinder whose axis is parallel to the gravity vector. The cylinder is terminated on the bottom by a plane surface perpendicular to the axis and is filled to a depth h, with an inviscid, incompressible fluid of density ρ. We shall indicate the solution for the linearized equations first and subsequently introduce the nonlinearities phenomenologically.

The linearized momentum equation for an incompressible, inviscid fluid is

$$\partial\bar{q}/\partial t = \bar{a} - \nabla P/\rho, \tag{1}$$

where

$\bar{q}$ = fluid-velocity vector
P = fluid pressure
$\bar{a}$ = external acceleration vector
ρ = fluid density
t = time

Expressing both the fluid velocity and external acceleration vectors in terms of a scalar and a vector potential [6],

$$\bar{q} = -\nabla\phi + \nabla\times\bar{\sigma}, \tag{2}$$

$$\bar{a} = -\nabla\Omega + \nabla\times\bar{\varepsilon}, \tag{3}$$

yields

[1] Formerly with Space Technology Laboratories, Los Angeles, Calif.

[2] Numbers in brackets designate References at end of paper.

Contributed by the Applied Mechanics Division and presented at the Annual Meeting, Atlantic City, N. J., November 29–December 4, 1959, of THE AMERICAN SOCIETY OF MECHANICAL ENGINEERS.

Discussion of this paper should be addressed to the Secretary, ASME, 29 West 39th Street, New York, N. Y., and will be accepted until January 10, 1960, for publication at a later date. Discussion received after the closing date will be returned.

NOTE: Statements and opinions advanced in papers are to be understood as individual expressions of their authors and not those of the Society. Manuscript received by ASME Applied Mechanics Division, May 22, 1958. Paper No. 59—A-15.

$$\nabla(P/\rho - \partial\phi/\partial t + \Omega) = \nabla \times (\bar{s} - \partial\bar{\sigma}/\partial t) \quad (4)$$

We shall consider solutions of Equation (4) for which

$$\bar{s} - \partial\bar{\sigma}/\partial t = \nabla\xi \quad (5)$$

where ξ is an arbitrary scalar function of the co-ordinates and time. Then we obtain

$$P/\rho - \partial\phi/\partial t + \Omega = F(t) = 0, \quad (6)$$

since the arbitrary function of time, $F(t)$, may be absorbed in the definition of the zero value of ϕ.

In references [4] and [5], the masses and lengths of the pendulums were given, respectively, as

$$m_i = 2\pi\rho R^2 \tanh k_i h/k_i(k_i^2R^2 - 1), \quad (7)$$

and

$$l_i = 1/k_i \tanh k_i h \quad (8)$$

We shall show that these same expressions result when we include a vortex in the linearized description of the fluid motion.

Thus we write as the expression for the scalar velocity potential for fluid contained in a right-hand cylinder and subjected to a constant acceleration (or gravitational field) along the axis (z-direction) and a time-dependent acceleration perpendicular to the axis (x-direction),

$$\phi = K\theta + \sum_{i=1}^{\infty} J_1(k_i r)(A_i \sinh k_i z + B_i \cosh k_i z) \cos\theta, \quad (9)$$

where r, θ, and z are cylindrical co-ordinates. (This is essentially the form for the velocity potential used in reference [3], except that the vortex term, $K\theta$, was not included.) The condition that the normal velocity component shall vanish at the solid boundaries is

$$-\partial\phi/\partial n + \text{curl}_n\, \bar{\sigma} = 0, \quad (10)$$

where n is the direction normal to the solid boundaries. It may be noted that the vortex term in Equation (9) does not enter into the satisfaction of the solid boundary conditions. To avoid a singularity at $r = 0$, we shall introduce a two-dimensional combined vortex through the following stream function, ψ:

$$\psi = \frac{\zeta}{4}(a^2 - r^2) \quad \text{for} \quad r < a, \quad (11)$$

$$\psi = \frac{\zeta a^2}{2} \ln(r/a) \quad \text{for} \quad r > a. \quad (12)$$

This function yields the same velocity in the θ-direction as the velocity potential, $K\theta$ (with a proper choice of K), for $r > a$, namely

$$q_\theta = \zeta a^2/2r, \quad (13)$$

while for $r < a$ we obtain

$$q_\theta = \zeta r/2 \quad (14)$$

No velocity terms are contributed by ψ to either the r or z-direction. Thus neither the irrotational nor the rotational vortex term enters the solid boundary conditions.

At the fluid-free surface the pressure is independent of time. We would like to make use of Equation (6) to satisfy this condition but we must first assure ourselves that the requirement given by Equation (5) is met. Let us assume that all the external forces are conservative. Then $\bar{s} = 0$. Equation (10) now requires that

$$\bar{\sigma} = \int \nabla\, \xi dt + f(r, \theta, z), \quad (15)$$

where f is an arbitrary function. Now the part of the velocity with a nonvanishing curl is given by Equation (14), and it can be shown that this term would result from the following form for $\bar{\sigma}$:

$$\bar{\sigma} = \bar{r}_1 \zeta r z/2, \quad (16)$$

where $\bar{r}_1$ is a unit vector in the radial direction. Thus, if we take $\nabla\xi = 0$ in Equation (15) and let f be given by Equation (16), the pressure will be given by Equation (6).

Thus we have shown that the vortex terms do not enter into the satisfaction of the free surface or solid boundary conditions, which determine A_i and B_i of Equation (9). If we assume K of Equation (9) to be independent of time, the pressure, given by Equation (6), will be unaffected by the vortex terms. Thus the expressions for the pendulum masses and lengths will be unchanged by the inclusion of vortex items.

This development has been entirely linear up to this point. We shall now assume that the previously omitted nonlinearities can be reintroduced to some extent by considering the pendulums to be free to swing about the point of suspension in any direction and applying Euler's equations to describe their motion. This procedure has been carried out, for a single pendulum, on both a digital [8] and an analog [9] computer and the results have been compared [10] with those obtained experimentally. The results will be discussed following a brief description of the experimental equipment.

In setting up an analogy between the fluid vortex motion and the rotary motion of a conical or spherical pendulum, we have at our disposal from Equations (11) and (12) two constants, namely, ζ and a. We may employ the two functions which specify the rotation, angular momentum, and rotational kinetic energy to evaluate these constants, requiring that the energy and momentum be the same for the set of pendulums as for the fluid. The rotational kinetic energy for the set of pendulums, E_p, is given by

$$E_p = \sum_{i=1}^{\infty} (m_i/2) i^2 \omega^2 l_i^2 (1 - g^2/\omega^4 i^4 l_i^4) \quad (17)$$

The angular momentum is

$$H_p = \omega \sum_{i=1}^{\infty} i m_i l_i^2 (1 - g^2/l_i^2 i^4 \omega^4) \quad (18)$$

The corresponding quantities, as obtained from the fluid stream function of ψ, are

$$E_f = \frac{\pi\rho h}{4} \zeta^2 a^4 (1/4 + \ln R/a), \quad (19)$$

$$H_f = 2\pi\rho h \zeta a^2 (R^2/4 - a^2/8) \quad (20)$$

Equating E_p to E_f and H_p to H_f, and eliminating ζ yields

$$\ln R/a = \pi\rho h(2R^2 - a^2)/8 \sum_{i=1}^{\infty} i(m_i l_i^2 - m_i g^2/\omega^4 i^4) - 1/4 \quad (21)$$

If $k_i h$ is greater than 1.84, we may approximate the summations to within 5 per cent by taking $\tanh k_i h$ equal to unity. Then, from Equation (21) by neglecting a^2 with respect to $2R^2$, we obtain

$$a/R = 1.28 e^{-3.7h/R(1 - 3.4g^2/\omega^4 R^2)} \quad (22)$$

The smallness of a/R as given by Equation (22) for $h \approx R$, justifies the neglect of a^2. Using Equations (17), (19), and (22) we may obtain ζ as

$$\zeta = 35.6\omega(R/h)(1 - 3.4g^2/\omega^4 R^2) e^{7.4h/R(1 - 3.4g^2/\omega^4 R^2)} \quad (23)$$

It may be noted that these expressions break down for shallow fluid levels ($h \to 0$), for in such cases the pendulum lengths l_i, and

hence also the energy as given by Equation (17), go to infinity. Equating the moment due to centrifugal force to that due to gravity, we obtain for the angle θ, between the pendulum suspension length and the gravity vector,

$$\cos\theta = g/\omega^2 l_i \tag{24}$$

From this we see that as l_i approaches infinity, θ approaches $\pi/2$, and we may conclude that the theory breaks down because the assumption of infinitesimal free-surface oscillations has been violated. We also see, from Equation (17), that since the kinetic energy cannot be negative, there is a threshold frequency below which rotary motion is not possible [11]; namely,

$$\omega_{th} = \left[\left|\sum_{i=1}^{\infty}(m_i g^2/i^2)\Big/\sum_{i=1}^{\infty}(m_i l_i^2 i^2)\right|\right]^{1/4} \tag{25}$$

Experiments

The experimental equipment is shown in Fig. 1. It consisted of a lucite tank of 1 ft diam, rigidly held on a four-wheel carriage. The carriage wheels were grooved, and rolled on a pair of inverted V-tracks. The carriage was driven by a rigid link attached to a $^1/_4$-hp U. S. Electric Motors Varidrive, Type VA-GD, through a set of pulleys and belts. The maximum driving frequency which could be attained with the equipment was about 1.2 cycles per sec. The maximum carriage displacement was 1 in. peak to peak. The experiments reported here were run with water at a depth of 1 ft. (Some additional experiments were run with glycerine, but time did not permit a sufficient amount of useful data to be taken.) The wave height of the water was measured in the direction of the drive and at 90 deg to it by means of impedance bridges. One leg of each bridge consisted of a pair of 0.001-in. nichrome wires taped to the tank wall extending down into the water. As a wave changed the water level at the wires, the bridge was unbalanced, and the bridge output was fed into a 20-kc Consolidated Electrodynamics amplifier system. The signals were recorded on a Consolidated Electrodynamics oscillograph tape, the timing lines of which served as a measure of the frequency. The carriage displacement was measured with a Schaevitz linear differential transformer and recorded on the same tape.

Results and Discussion

The digital and analog-computer studies of the response of a pendulum to a driving force in a single direction revealed the presence of boundaries between the regions where the oscillations of the pendulum are confined to the plane of the external driving force, and the regions where rotary motion results from the planar driving force. Similar boundaries were observed in the fluid experiments. A measure of the validity of the pendulum analogy may be expected to be its success in predicting the experimentally observed boundaries. A comparison of the experimental with the computed boundaries is presented in Fig. 2. It appears that the lower boundary is predicted fairly well up to the largest value of input amplitude used in the computations. The upper boundary appears to be predicted, within experimental error, for input amplitudes up to about 0.1 in. peak to peak. For large input amplitudes, the calculated boundary occurs at lower driving frequencies than the observed boundary. A possible reason for the greater success of the analogy at the lower boundary is the fact that only one pendulum, that with the lowest natural frequency, was used in the computations, and the upper boundary would be expected to be influenced by the second pendulum. Figs. 3 and 4 present the fundamental component of both the experimental wave height and the computed pendulum displacement with a linear second-order system for comparison. It may be seen that the experimental results deviate more from

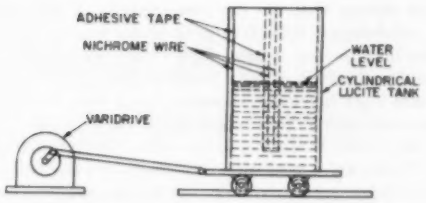

Fig. 1 Schematic of experimental equipment

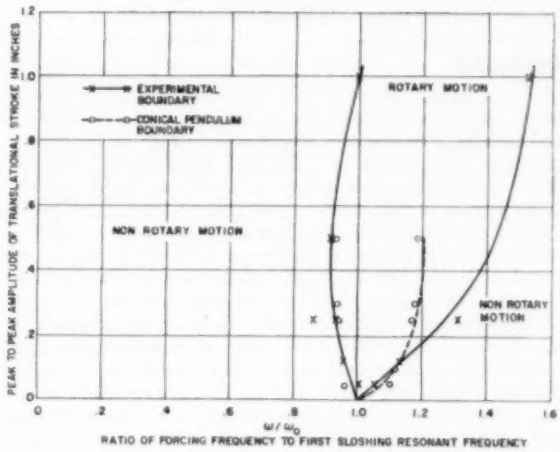
EXPERIMENTAL BOUNDARY
CONICAL PENDULUM BOUNDARY
ROTARY MOTION
NON ROTARY MOTION
NON ROTARY MOTION
PEAK TO PEAK AMPLITUDE OF TRANSLATIONAL STROKE IN INCHES
ω/ω0
RATIO OF FORCING FREQUENCY TO FIRST SLOSHING RESONANT FREQUENCY

Fig. 2 Comparison of experimental and conical pendulum model regions of rotary sloshing

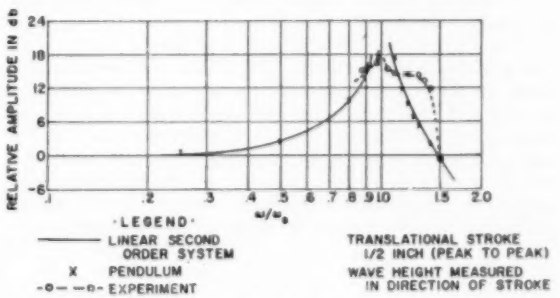

Fig. 3 Comparison of experimental and pendulum model frequency responses

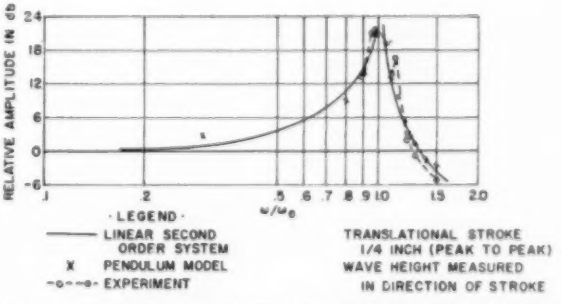

Fig. 4 Comparison of experimental and pendulum model frequency responses

the linear system than do the computations of the pendulum motion, exhibiting a secondary peak above the first resonance. This also may be due to the effect of the equivalent "second pendulum" in the fluid, which was not included in the calculation. Figs. 2 and 3 are frequency responses which were obtained both experimentally and on the computers by allowing the transients due to the initial conditions to die down before readings were taken. There was a noticeable difference between the time required for these transients to die out on the computers as compared with the fluid experiments. The experimental time was considerably shorter. This might have been due to coupling between the pendulums, allowing energy to be transferred to higher frequencies where it would be dissipated more rapidly.

Conclusions

The agreement between theory and experiment indicates that the analogy between the motions of the fluid degrees of freedom, and those of a set of spherical pendulums, which was suggested by the analysis, has some basis in fact. It is suggested that the mechanism whereby rotation was produced in the liquid, which it is the purpose of this paper to explain, may be stated as follows: When the liquid is driven in a single plane in a region around one of the natural frequencies of surface waves, oscillatory motion of the liquid about a nodal line perpendicular to the driving plane is unstable. Therefore, any slight departure of the center of gravity of the fluid from the plane containing the axis of the cylinder and the driving vector will, by the action of centrifugal force, be amplified until an equilibrium is reached between the action of centrifugal force and that of gravity. The center of gravity of the liquid will move in an orbit about the axis of the cylinder and the angular momentum will be carried by a vortex. This would be true even for an ideal fluid; however, the velocity of the fluid would tend to infinity as the axis of the cylinder was approached. In an actual fluid, the slightest viscosity would result in appreciable viscous stresses in the neighborhood of the axis, and rotational flow would be produced.

It is recognized that the nonlinear pendulum analogy has not been established quantitatively. To do this would require comparing the theoretical velocity distribution, given by Equations (9), (13), (14), (22), and (23), with experiments. Such experiments were not within the scope of the equipment used by the author. Further experiments, including some with liquids of greater viscosity, would be desirable for establishing quantitative measures of validity of the pendulum analogy. It may be expected that as the viscosity is increased the combined vortex velocity distribution assumed in Equations (13) and (14) should become less valid. Another effect of increasing viscosity should be narrowing of the region in which rotational motion is stable and the appearance of a threshold input amplitude below which rotational motion cannot be induced. Such effects were observed in the laboratory working with pure glycerine and also on the computers when damping was introduced; however, no quantitative comparison is presently available between the experimental and computer results. For liquids of very small viscosity, it is expected that the velocity distribution away from the vortex filament and the boundary layer should be given fairly well by the theory developed here.

As with any analogy, this one should break down somewhere. The utility of the linear analogy has already been established in autopilot stability studies. The justification for the nonlinear analogy approach is the fact that exact solutions to the nonlinear Navier-Stokes equations do not appear imminent.

References

1 H. Lamb, "Hydrodynamics," Dover Publications, Inc., New York, N. Y., 6th edition, 1945.

2 E. W. Graham, "The Characteristics of Fuel Motion Which Affect Airplane Dynamics," Douglas Aircraft Company, Santa Monica, Calif., Report SM-14212, November, 1951.

3 G. J. Gleghorn, "Motion of Fuel of Fluid in a Cylindrical Tank," Space Technology Laboratories Memorandum, February, 1956.

4 K. Kachigan, "Forced Oscillations of a Fluid in a Cylindrical Tank," Convair Report ZU-7-046, October, 1955.

5 A. F. Schmitt, "Forced Oscillations in a Cylindrical Tank Undergoing Both Translation and Rotation," Convair Report ZU-7-069, October, 1956.

6 The inclusion of a vector potential in the expression for the fluid velocity was a technique employed by K. M. Case and W. C. Parkinson to treat oscillations of a viscous fluid in their paper "Damping of Surface Waves in an Incompressible Liquid," *Journal of Fluid Mechanics*, vol. 2, 1957, p. 172.

7 V. L. Streeter, "Fluid Dynamics," McGraw-Hill Book Company, Inc., New York, N. Y., 1948.

8 B. A. Troesch, "Pendulum Analogy," Space Technology Laboratories Memorandum GM 42.4-4, November, 1957.

9 J. V. Howell, "Motion of a Conical Pendulum," Space Technology Laboratories Memorandum GM 42.4-4, November, 1957.

10 R. R. Berlot and L. E. Freed, "Comparison of Experimental Sloshing Results With Spherical Pendulum Theory," Space Technology Laboratories Memorandum GM 42.6-54, January, 1956.

11 L. E. Freed, "Stability of Motion of Conical Pendulums," Space Technology Laboratories Memorandum GM 45.3-434, October, 1957. Freed has examined the converse problem of the possible regions of planar motion and concludes that regions exist, centered about the natural frequencies of free oscillation, in which purely planar forced oscillations are not stable.

Nonlinear Creep Deformations of Columns of Rectangular Cross Section[1]

H. H. BLEICH
Professor of Civil Engineering, Director, Institute of Flight Structures, Columbia University, New York, N. Y. Mem. ASME

O. W. DILLON, JR.[2]
Assistant Professor, Department of Civil Engineering, Johns Hopkins University, Baltimore, Md.

Creep deformations of columns of rectangular cross section are studied for the case of materials following the nonlinear law $\dot{\epsilon} = (1/E)\dot{\sigma} + \lambda\sigma^k$. *The essential point of the paper is the following: The time rate of the curvature* $\dot{\kappa}$ *of an element of a bar loaded by a constant force* P *and an increasing bending moment* $M(t)$ *has bounds, which depend on* P *and on the instantaneous values of* M *and* $\dot{M}$, *but not on the history of* M. *In combination with the collocation method, this permits the formulation of ordinary differential equations for upper and lower bounds on the deformations. Closed solutions for the critical time are obtained for one bound, while the other requires numerical integration. The bounds which are a function of the initial eccentricity are reasonably close and are presented in tables and graphs. By qualitative reasoning it is further shown that the location of the actual critical time with respect to the two bounds is governed by the ratio of the column load* P *and the nominal Euler buckling load* P_E *of the column if it were elastic.*

SOLUTIONS for the problem of creep buckling of nonlinearly viscoelastic columns are available in relatively simple form if the cross section is an H-section consisting of only two chords. For the case of the creep law (1) selected in this paper the displacements and the critical time are determined in closed form in reference [1].[3] The analogous problem for columns of rectangular cross section considered here is much more complicated, and existing treatments are either approximate or purely numerical ones.

A simple approximate solution [2] converts rectangular sections into equivalent H-sections and then applies the results of [1]. A more powerful approach, using a variational method, is presented in [3]. It has, however, certain limitations which will be discussed in the light of the present work. In addition, a purely numerical procedure [4] is available.

The crucial point of the method used in this paper is the recognition that the time rate of curvature of an element of a column has bounds which depend on the bending moment M and its rate of change $\dot{M}$ at a given instant, but not on the previous history of M. Using these bounds on the rate of curvature, and employing the collocation method, ordinary nonlinear differential equations are obtained, from which bounds for the critical time can be computed. The changes in the character of the stress distribution with time, which make the problem so complex, are eliminated from the analysis by the use of the bounds on the rate of curvature.

Derivation of Differential Equations

Stress-Strain Rate Relation. This paper is based on the constant-temperature, one-dimensional, nonlinear viscoelastic relation:

$$\dot{\epsilon} = \frac{\dot{\sigma}}{E} + \lambda\sigma^k \tag{1}$$

where k is an odd integer and $\dot{\epsilon}$ and σ are the strain rate and stress, respectively. Both are positive for compression. The fluidity λ is assumed constant and E is the elastic modulus. The parame-

[1] The work reported here was sponsored by the Office of Naval Research, U. S. Navy, under contract Nonr 266(34), Project Nr-64-417.

[2] Formerly Research Assistant, Institute of Flight Structures, Columbia University, New York, N. Y.

[3] Numbers in brackets designate References at end of paper.

Contributed by the Applied Mechanics Division and presented at the Annual Meeting, Atlantic City, N. J., November 29–December 4, 1959, of THE AMERICAN SOCIETY OF MECHANICAL ENGINEERS.

Discussion of this paper should be addressed to the Secretary, ASME, 29 West 39th Street, New York, N. Y., and will be accepted until January 10, 1960, for publication at a later date. Discussion received after the closing date will be returned.

NOTE: Statements and opinions advanced in papers are to be understood as individual expressions of their authors and not those of the Society. Manuscript received by ASME Applied Mechanics Division, May 28, 1958. Paper No. 59—A-1.

Nomenclature

b = width of column
E = Young's modulus
h = thickness of column
$I = \frac{bh^3}{12}$ = moment of inertia
k = exponent in viscoelastic law, Equation (1)
L = length of column
n = parameter in Equation (3)
M = bending moment with respect to axis at $\zeta = 0$
P = longitudinal force
t_{cr} = critical time
x = longitudinal co-ordinate, Fig. 1
$z = z(x)$ = deflection of column
z = deflection at center of column
z_0 = initial deflection at center of column
$\dot{\epsilon}$ = strain rate
λ = viscous constant in Equation (1)
σ = stress
$\sigma_0 = \frac{P}{hb}$ = mean stress
$\sigma_E = \frac{\pi^2 E h^2}{12L^2}$ = Euler buckling stress
κ = curvature of column
ζ = nondimensional co-ordinate in cross section, Fig. 1
τ = nondimensional time, Equation (13)
τ_{cr} = critical value of τ
$\cdot$ = differentiation with respect to time

ter k is of order 3 for aluminum and 5 for stainless steel [5]. The results obtained from Equation (1) can be extended to the case where k is an even integer by using

$$\dot{\epsilon} = \frac{\dot{\sigma}}{E} + \lambda|\sigma^{k-1}|\sigma \tag{1a}$$

which relations assume that the material properties in tension and compression are the same. No derivations based on Equation (1a) will be presented, but some results for even integral k are given in the next section.

Curvature of an Element of a Column. Consider an element of a column of rectangular cross section, Fig. 1, loaded by a force P. The deflection z will increase from an initial[4] value z_0 and will be a function of the time t and of the co-ordinate x. The element will be subjected to the direct force P and the bending moment

$$M = \left(z + \frac{h}{2}\right) P$$

where M is referred to the axis $\zeta = 0$ on the convex side of the column, Fig. 1. Inertia forces are not considered.

Neglecting terms of higher order, the curvature κ of the column is $\kappa = -z''$ and

$$\dot{\kappa} = -\dot{z}'' \tag{2}$$

where primes indicate derivatives with respect to the co-ordinate x. Making the conventional assumption that plane sections before bending remain plane after bending, the rate of curvature $\dot{\kappa}$ can be expressed as a function of $\dot{M}$ and of the stress distribution $\sigma(\zeta, t)$. The foregoing assumption furnishes the relation

$$\dot{\epsilon} = \dot{\kappa}h(\zeta - n) \tag{3}$$

where n is a parameter defining the location of the instantaneous center of rotation of the plane of the cross section. Substitution of Equation (3) into Equation (1) gives:

$$\dot{\kappa}h(\zeta - n) = \frac{\dot{\sigma}}{E} + \lambda\sigma^k \tag{4}$$

Integration of this equation over the cross section, once in its present form and once after multiplication by ζ, furnishes two equations for $\dot{\kappa}$ and n. Noting

$$\int_0^1 \dot{\sigma}d\zeta = 0, \quad bh^2\int_0^1 \zeta\dot{\sigma}d\zeta = \dot{M} \quad \text{and} \quad I = \frac{bh^3}{12},$$

the rate of curvature $\dot{\kappa}$ can be expressed by eliminating n:

$$\dot{\kappa} = \frac{\dot{M}}{EI} + \frac{12\lambda}{h}\int_0^1 (\zeta - \tfrac{1}{2})\sigma^k d\zeta \tag{5}$$

Bounds for the Rate of Curvature $\dot{\kappa}$. Visualize the element of the column under the action of the constant compressive force P and the bending moment M, if this moment is also constant. The curvature κ will increase but with a steadily decreasing rate as shown in Fig. 2. After a long time the curvature rate will approach a value $\dot{\kappa}_\infty$ which can be obtained from purely viscous relations, while the initial value $\dot{\kappa}_0$ requires the use of viscoelastic Equation (1). The actual rate of curvature at any time t is bounded

$$\dot{\kappa}_0(M, P) \geq \dot{\kappa}(M, P) \geq \dot{\kappa}_\infty(M, P)$$

Next, consider the element again to be loaded by the constant force P and the same moment M as before, but let the moment at $t = t_1$ be increased to a value M_1. At $t = t_1$ there will be a sudden increase in curvature (due to elastic effects), Fig. 2(a). Thereafter the curvature will increase, but with a decreasing rate $\dot{\kappa}$ which will reach an asymptotic value $\dot{\kappa}_\infty(M_1, P)$. Consider further the history of the element if the force P and the larger moment M_1 had been applied immediately at $t = 0$; the response for this case being shown in dashed lines in Fig. 2(a). The initial rate of curvature $\dot{\kappa}_0(M_1, P)$ due to M_1 and P will be greater than the actual rate $\dot{\kappa}(M_1, P)$, which in turn will be larger than the asymptotic rate $\dot{\kappa}_\infty(M_1, P)$, or

$$\dot{\kappa}_0(M_1, P) \geq \dot{\kappa}(M_1, P) \geq \dot{\kappa}_\infty(M_1, P)$$

If the increase in moment from M to M_1 is infinitesimal, $M_1 = M + dM$, and occurs during a time dt, the inequality applies also

Fig. 2 Time history of curvature (P = const, M = const)

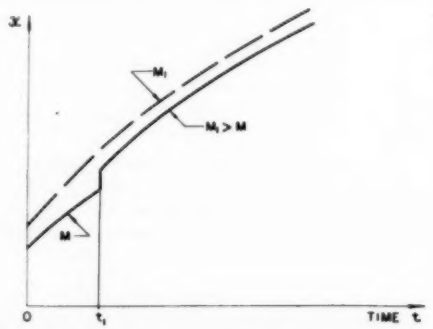

Fig. 2(a) Time history of curvature (P = const, M not const)

[4] Note that z_0 is the deflection at the instant $t = 0$, not the deflection in the unloaded state.

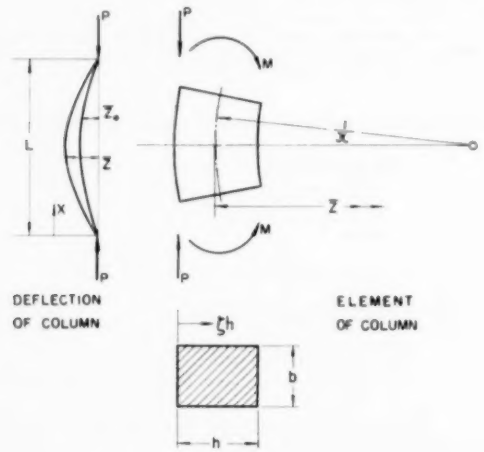

Fig. 1

while the moment increases, provided the elastic part of the curvature rate $(1/EI)\dot{M}$ is added to the bounds

$$\dot{\kappa}_0(M, P) + \frac{\dot{M}}{EI} \geq \dot{\kappa}(M, P) \geq \frac{\dot{M}}{EI} + \dot{\kappa}_\infty(M, P) \qquad (6)$$

where the subscript 1 has been omitted. This equation applies quite generally for any element under the action of a constant compressive force and an increasing moment, and the inequality (6) is therefore applicable to the problem of creep buckling. The existence of the inequality is demonstrated in Appendix 1 in a simple manner for rectangular cross sections under the action of a bending moment $M(t)$ for $P = 0$. In the general case $P \neq 0$ it is shown to be true for a simplified cross section consisting of three elements. The generalization to a rectangular section leads to difficulties because the column transient stress states are then very cumbersome to describe analytically. Appendix 1 therefore makes the inequality only plausible for the column of rectangular section. A general proof, presumably, should attempt to use basic principles to avoid these difficulties.

Replacing the actual rate of curvature $\dot{\kappa}$ in the deformation analysis by the larger rate $\dot{\kappa}_0 + \dot{M}/EI$, the column will appear to collapse sooner, giving a lower bound for the critical time; the reverse applies if the asymptotic rate of curvature $\dot{\kappa}_\infty + \dot{M}/EI$ is used. As both bounds are functions of P and M only, Equations (2), (3), (5) lead to a partial differential equation for the deflection of the form $\dot{z}'' = f(z)$. Assuming the shape of the deflected column to be sinusoidal[5] at all times,

$$z = z \sin \frac{\pi x}{L} \qquad (7)$$

collocation at the center $x = L/2$ leads to an ordinary differential equation for the deflection z at the center of the column.

The values of $\dot{\kappa}_0$ and κ_∞ which are required to form these differential equations are determined in Appendixes 2 and 3, and both are found to be inherently nonlinear functions of z. The expression for $\dot{\kappa}_\infty$ is in parametric form such that in this case a differential equation for z cannot be written explicitly; instead, a differential equation for the parameter n is obtained from which the critical time can be determined.

Differential Equations. Noting

$$\frac{\pi^2 \dot{z}}{L^2} = \dot{\kappa} \quad \text{and} \quad \dot{M} = P\dot{z} \equiv bh\sigma_0\dot{z}$$

the differential equation giving the lower bound on the critical time is obtained by replacing $\dot{\kappa}$ by its upper bound $\dot{\kappa}_0 + \dot{M}/EI$ according to Equation (6); substituting $\dot{\kappa}_0$ from Equation (37) (Appendix 2) results after rearrangement in

$$\frac{\dot{z}}{h} = \frac{\lambda\sigma_0 k_E}{\sigma_E - \sigma_0} \sum_{i=1}^{(k+1)/2} \frac{1}{2(2i+1)} \binom{k}{2i-1} \left(6\,\frac{z}{h}\right)^{2i-1} \qquad (8)$$

where

$$\sigma_E = \frac{\pi^2 EI}{bhL^2} = \frac{\pi^2 Eh^2}{12L^2} \qquad (9)$$

and the symbol $\binom{k}{2i-1}$ is the binomial coefficient.

To obtain the upper bound on the critical time, $\dot{\kappa}$ is similarly replaced by the lower bound $\dot{\kappa}_\infty + \dot{M}/EI$. Using Equation (43) (Appendix 3) gives

$$\frac{\dot{z}}{h} = \frac{\lambda\sigma_0^k E \left(\frac{k+1}{k}\right)^k}{12(\sigma_E - \sigma_0)A^k} \qquad (10)$$

where A is a function of the nondimensional parameter n,

$$A(n) \equiv (1-n)^{(k+1)/k} - n^{(k+1)/k} \qquad (11)$$

and z is defined by Equation (42) (Appendix 3) as function of n. Differentiation of Equation (42) with respect to time gives

$$\frac{\dot{z}}{h} = \frac{k}{2k+1}\dot{n} + \frac{k+1}{2k+1}\left[\frac{k+1}{k}\frac{n^{1/k}\dot{n}}{A} - \frac{n^{(k+1)/k}\dot{A}}{A^2}\right] \qquad (12)$$

which will be used to eliminate $\dot{z}$.

Solution of the Differential Equations

Lower Bound for the Critical Time. Introducing a nondimensional time τ by the definition

$$\tau = \frac{kE\lambda\sigma_0^k}{\sigma_E - \sigma_0}\, t \qquad (13)$$

Equation (8) can be written in the form

$$\frac{d}{d\tau}\left(\frac{z}{h}\right) - \left(\frac{z}{h}\right) - B_3\left(\frac{z}{h}\right)^3 - B_5\left(\frac{z}{h}\right)^5 - B_7\left(\frac{z}{h}\right)^7 \ldots = 0 \qquad (14)$$

where the coefficients $B_i = 0$ if $i > k$. Separation of variables and expansion in partial fractions permits integration in closed form.

An analysis for even k, based on Equation (1a), leads also to differential equations of the type (14) as long as no tension stresses occur, i.e., for $z \leq h/6$. For larger values of z (and even k) an equation of the type

$$\frac{d}{d\tau}\left(\frac{z}{h}\right) - B_0 - B_2\left(\frac{z}{h}\right)^2 \ldots\ldots\ldots\ldots = 0 \qquad (15)$$

can be derived. Tables 1 and 2 give the respective values of the coefficients B for $k = 3$ to 7.

Table 1 Coefficients B_i in equation (14)

k	B_3	B_5	B_7
3	7.2	0	0
4	21.6	0	0
5	43.2	111	0
6	72.0	555	0
7	108.0	1667	2220

Table 2 Coefficients B_i in equation (15)

k	B_0	B_2	B_4	B_6
4	0.0625	6.75	27.0	0
6	0.0417	11.25	270.0	486.0

Excluding $k = 1$, the solutions of Equation (14) with the initial condition $\tau = 0$ for $z = z_0$ indicate infinite values of the deflection for some finite value of the nondimensional time, called τ_{cr}; expressions for τ_{cr} are given in Table 3 for $k = 3$ to 7. Expressions for the deflection z as function of τ are easily obtained but have not been listed; a typical response is shown in Fig. 3 for $k = 3$, $z_0/h = 0.02$.

[5] This assumption is frequently made in treatments of creep buckling problems, even for simpler geometries [1].

Upper Bound for the Critical Time. After elimination of $\dot{z}$ between Equations (10) and (12) and introduction of the nondimensional time τ defined by Equation (13), the variables can be separated. Using the initial condition $\tau = 0$ for $n = n_0$, where n_0 is the value of the parameter n corresponding to the initial eccentricity z_0, τ is obtained as a function of n:

$$\tau = \frac{12k}{2k+1}\left(\frac{k}{k+1}\right)^k \left[k\int_{n_0}^{n} A^k dn + \frac{(k+1)^2}{k}\int_{n_0}^{n} A^{k-1}n^{1/k}dn - (k+1)\int_{A_0}^{A} n^{(k+1)/k}A^{k-2}\,dA\right] \tag{16}$$

$A \equiv A(n)$ is defined by Equation (11), and $A_0 = A(n_0)$.

Equation (42) in Appendix 3, relating z and n, indicates that as z increases from the initial value z_0 to $z \to \infty$, the parameter n also increases from the initial value $n_0 < 1/2$ and becomes $n = 1/2$ in the limit $z \to \infty$. Equation (16) gives therefore τ_{cr} if the upper limits of integration are $n = 1/2$ and $A(1/2) = 0$, respectively.

After repeated integration by parts and regrouping, τ_{cr} becomes

$$\tau_{cr} = \frac{12k}{(2k+1)(k-1)}\left(\frac{k}{k+1}\right)^k \left[(k+1)\left(1 - n_0 + \frac{n_0^{(k+1)/k}}{A_0}\right)A_0^k - 2(2k+1)\int_{n_0}^{1/2} A^k dn\right] \tag{17}$$

The integral in Equation (17) could be integrated in closed form. However, the large number of terms resulting from the expansion of the integrand into partial fractions makes the closed-form solution very cumbersome, and the values of the integral were obtained by numerical integration.

The numerical results for the upper bound on τ_{cr} obtained in this manner for $k = 3$, 5, and 7 are shown in Fig. 4, together with the lower bounds for τ_{cr} computed from Table 3.

The time history of the deflection z can be obtained by determining as first step τ as a function of n from an expression quite similar to Equation (17). The numerical computations for this purpose do not require integrations beyond those necessary to find τ_{cr} as a function of z_0/h. As the next and final step the values of z/h as functions of n are found from Equations (42), and the result cross-plotted. A typical response is shown in Fig. 3.

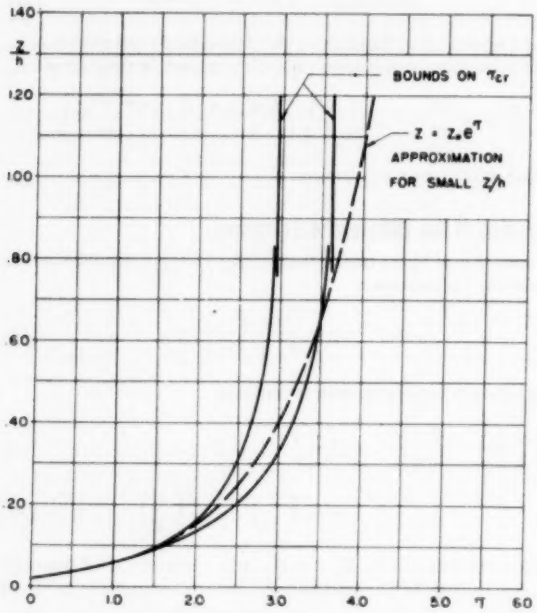

Fig. 3 Bounds on deflection z/h ($k = 3$, $z_0/h = 0.020$)

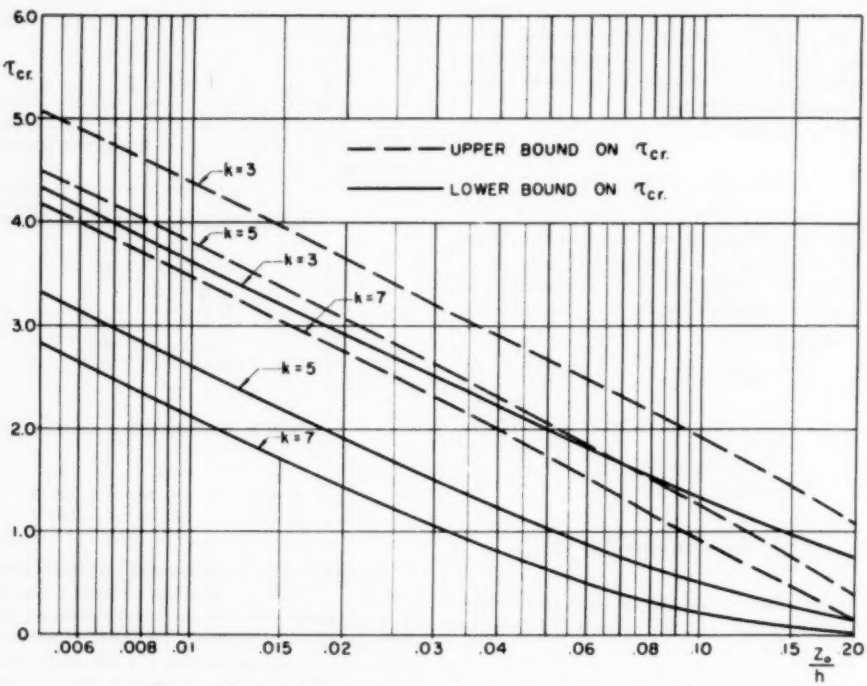

Fig. 4 Bounds for nondimensional critical time τ_{cr} as function of z_0/h

Table 3 Expressions for lower bound on τ_{cr}

k	
3	$0.5 \ln \left(1 + \frac{h^2}{7.2 z_0^2}\right)$
4[a]	$0.5 \ln \left(1 + \frac{h^2}{21.6 z_0^2}\right) - 0.034$
5	$0.25 \ln \left(1 + \frac{h^2}{2.57 z_0^2} + \frac{h^4}{111 z_0^4}\right) - 0.285 \ln \frac{222(z_0/h)^2 + 81.0}{222(z_0/h)^2 + 5.4}$
6[a]	$0.25 \ln \left(1 + \frac{h^2}{7.75 z_0^2} + \frac{h^4}{556 z_0^4}\right) - 0.320 \ln \frac{1110(z_0/h)^2 + 128.4}{1110(z_0/h)^2 + 15.6} - 0.004$
7	$0.50 \ln \left(1 + \frac{h^2}{89.9 z_0^2}\right) + 0.00065 \ln \frac{(z_0/h)^2 + 0.680}{(z_0/h)^2 + 0.0594} - 0.01264 \ln \frac{(z_0/h)^2 + 0.0594}{(z_0/h)^2 + 0.1115}$

[a] For $z_0/h \leq 1/6$.

Table 4 Coefficients C in equation (18)

k	For lower bound	For upper bound
3	0.987	0.26
4	1.57	0.56[a]
5	1.95	0.81
6	2.26	1.02[a]
7	2.45	1.16

[a] Obtained by parabolic interpolations from the values of C for odd k.

Approximations for Small Initial Eccentricities z_0/h. Examination of the various expressions for the bounds on τ_{cr} in Table 3 and in Equation (17) shows that for small values of z_0/h asymptotic approximations of the form

$$\tau_{cr} \simeq \ln \frac{h}{z_0} - C \tag{18}$$

apply, where the value of the constant C depends on the particular case considered, Table 4. The fact that the first term of (18) is identical for the upper and lower bounds, without an additional coefficient, results from the fact that the expressions for the limits $\dot{\kappa}_0$ and $\dot{\kappa}_\infty$ of the curvatures for small values of z become identical, as pointed out in Appendix 3 after Equation (38),

Fig. 4 shows the bounds for τ_{cr} as function of $\ln(z_0/h)$, and Equation (18) requires that for small z_0/h, the curves approach a set of parallel lines; this is indeed the case. It appears from Fig. 4 that the approximation (18) may be used with very good results if $z_0/h \leq 0.015$.

The deflection z/h as a function of τ also can be approximated as long as z/h remains small; in this case the nonlinear terms in Equation (14) may be dropped with the result $z/z_0 = e^\tau$. The identical result is obtained from Equations (10) and (12) for the other bound. This approximation is also indicated in Fig. 3, showing the upper and lower bounds on the response z/h for a typical case.

Estimate of Location of τ_{cr} Between Bounds. The bounds for the nondimensional critical time are solely functions of k and of the initial eccentricity z_0/h; all the other parameters of the problem appear only through Equation (13) when the nondimensional τ_{cr} is converted into the actual time t_{cr}. It is important to realize, however, that the value of the parameter τ_{cr}—if the problem is solved exactly—is not just a function of z_0/h but also of some of the additional basic parameters now only entering through Equation (13). The spread between the bounds is therefore an indication of the effect, or better of the additional effect, of these basic parameters. By purely qualitative considerations it will be shown that the location of the actual value τ_{cr} between the bounds is a function of the parameter $\tau_{cr}(\sigma_E - \sigma_0)/\sigma_0$.

Consider what situation is necessary to make the lower bound (based on the linear stress distribution) a good approximation. At the instant of loading there will be a linear stress distribution; whether this distribution will remain close to linear as time goes by will depend on the rate of additional loading versus the rate of relaxation of the stresses. During any short element of time the stress-strain law (1) may be linearized and one can determine an "instantaneous relaxation time T,"

$$T = 1/kE\lambda\sigma^{k-1} \tag{19}$$

which is a function of the instantaneous stress σ. Unless the values of T for "pertinent" stress levels σ are small versus the critical time t_{cr} of collapse, the stress distribution must remain nearly linear and τ_{cr} must lie close to the lower bound. A difficulty in the foregoing reasoning lies in the question of selecting the "pertinent" stress level. From curves like Fig. 3, showing the time history of the deflection z, one can conclude that for small original eccentricities most of the lifetime of a column is spent in the range of small z/h where the stresses σ differ not too much from σ_0. However, it is not proper to use $\sigma \approx \sigma_0$ because wherever this holds the terms $\dot{\kappa}_0$ and $\dot{\kappa}_\infty$ are practically identical and the responses $z(t)$ in this range are therefore identical anyway.[6] The important range which influences the critical time occurs at slightly larger values of z/h where $\dot{\kappa}_0$ and $\dot{\kappa}_\infty$ begin to differ; for such values z/h the stress σ will exceed σ_0 on the compression side of the column and as the larger stress governs the relaxation in case of the nonlinear law (1), a value

$$\sigma \simeq \sigma_0/\beta \tag{20}$$

must be used, where β is somewhat smaller than unity. (No exact determination is possible, of course.)

The time T, Equation (19), should be compared with the lifetime $\bar{t}$ of the column measured from the instant when the values $\dot{\kappa}_0$ and $\dot{\kappa}_\infty$ begin to differ. Fig. 3 indicates that this occurs for $k = 3$ for $z/h \simeq 0.15$, and examination for the cases $k = 5, 7$ indicates noticeable deviation at $z/h = 0.10$ and 0.05, respectively. This permits determination of $\bar{t}$.

The lower bound will be a good approximation if $\bar{t}$ is not larger than T, because the stresses then have not had time to relax. Expressing $\bar{t}$ by means of Equation (13) in terms of a nondimensional time $\bar{\tau}$ one finds after cancellation

$$\bar{\tau} \frac{\sigma_E - \sigma_0}{\sigma_0} \leq \beta^{k-1} \tag{21}$$

where the value $\bar{\tau}$ for the lower bound is to be used.

By a similar reasoning it may be concluded that the upper bound will be a close approximation if the time $\bar{t}$ is very much larger than T,

$$\bar{\tau} \frac{\sigma_E - \sigma_0}{\sigma_0} \gg \beta^{k-1} \tag{21a}$$

where the upper bound value $\bar{\tau}$ is to be used.

The order of magnitude of the value β and $\bar{\tau}$ can be estimated from the foregoing values z/h defining where $\dot{\kappa}_0$ and $\dot{\kappa}_\infty$ begin to differ. For $k = 3$ to 7 one may use $\beta^{k-1} \simeq 0.2$, while $\bar{\tau}$ for both bounds is of the order unity, $\bar{\tau} \simeq 1$, and Equations (21) become

[6] See the comment after Equation (44), Appendix 3.

$\sigma_E \leq 1.2\sigma_0$ and $\sigma_E \gg 1.2\sigma_0$, respectively. The lower bound will therefore be a good approximation only in the rare case that the average stress σ_0 amounts to more than 80 per cent of the elastic buckling stress σ_E of the column. On the other hand, the upper bound will be a good approximation whenever σ_0 is very much smaller than σ_E, say $\sigma_0/\sigma_E < 0.2$.

Obviously, there are intermediate cases where neither of the two inequalities is clearly satisfied and the foregoing qualitative considerations are of no help. But even in such cases it is useful to know that the actual value should not be expected to be close to either bound.

The afore-mentioned reasoning indicates also that a plotting of test results versus τ_{cr} should indicate a band of scatter between the bounds; this scatter could be resolved by using the additional parameter σ_E/σ_0. It is interesting to note that this scatter should not exist in case of sections consisting of two chords as treated in [1], and the additional parameter enters only in rectangular (or other solid) sections.

Discussion and Conclusions

Results Obtained. The values of upper and lower bounds on the critical time for columns of rectangular cross section were determined for the nonlinear creep law, Equation (1), in the range $k = 3$ to 7. The results in terms of a nondimensional critical time τ_{cr} defined by

$$\tau_{cr} = \frac{kE\lambda\sigma_0^k}{\sigma_E - \sigma_0} t_{cr} \qquad (13)$$

are plotted for odd values of k in Fig. 4 in the range $0.005 \leq z_0/h \leq 0.20$ of initial eccentricities. For the important range of small eccentricities the bounds may be determined from the asymptotic expressions

$$\tau_{cr} = \ln \frac{h}{z_0} - C \qquad (18)$$

where the values of the coefficient C are given in Table 4.

The definition (13) of the nondimensional time differs from the one in [1] in the inclusion of the factor k. This definition reduces the sensitivity of τ_{cr} as function of k and facilitates interpolation.

The spread between the bounds varies; it is not too large for small initial eccentricities, but becomes quite large for $z_0/h > 0.10$. It is therefore important that it be possible to locate the actual value of τ_{cr} between the bounds—at least in a qualitative manner—by means of the inequalities (21) through consideration of the parameter σ_0/σ_E. If this parameter is larger than 0.8, the lower bound on τ_{cr} will be a good approximation, while the upper bound on τ_{cr} will be close if the foregoing parameter is less than 0.2.

The derivation of the inequalities (21) shows that the spread between the bounds is caused by the physical fact that the nondimensional critical time τ_{cr} is not solely a function of z_0/h, but depends also on other parameters. The spread between the bounds is a measure of the effect which these other parameters may have, and it is one of the merits of the present theory that it clearly shows this effect. In case of the widely studied simplified section consisting of two chords, the effect of the other parameters disappears, and τ_{cr} is solely a function of z_0/h.

Comparison With Other Theories Giving Results in Closed Form. Two other approaches are available which give results in closed form. By converting the rectangular cross section into an "equivalent" two-chord section and applying the results of [1] one can obtain at least a crude aproximation for τ_{cr}. More recently a more refined method, reference [3], using a "variational" approach has been developed. Distributions of stress and strain rates containing arbitrary parameters are assumed and an appropriate expression is varied. Applying the method to the column, reference [3] uses linear expressions only, resulting in differential equations[7] which are quite similar to Equation (14) obtained in this paper for the lower bound on the critical time:

$$\frac{d}{d\tau}\left(\frac{z}{h}\right) - \frac{z}{h} - c_3 B_3 \left(\frac{z}{h}\right)^3 - c_5 B_5 \left(\frac{z}{h}\right)^5 - c_7 B_7 \left(\frac{z}{h}\right)^7 \cdots\cdots\cdots = 0 \qquad (22)$$

The coefficients B_i are those occurring in Equation (14) while the modifying coefficients c_i have the values $c_3 = 3/4$, $c_5 = 5/8$, $c_7 = 35/64$. All values c_i being less than unity, the variational method always gives values τ_{cr} which are larger than the lower bounds in Fig. 4.

The results of this paper and those of the equivalent section and variational method can be conveniently compared in the range of small z_0/h where all approaches lead to expressions of the form (18) such that it is sufficient to compare the numerical values of C shown in Table 5 and the respective values in Table 4.

Table 5 Coefficients C in equations (18)

	According to	
k	Variational method	Equivalent section method
3	0.844	0.693
5	1.76	1.65
7	2.35	2.28

The values C in Table 5 lie between the bounds given in Table 4, providing a check on the present theory. The latter is superior, however, because it indicates and allows for the dependency of τ_{cr} on parameters in addition to z_0/h. The fact that the variational method gives a result which is really no better than the equivalent-section approach, is due to the assumption of linear stress and strain distributions which can only lead to a rough approximation. A remedy lies in the use of a refined stress distribution, but the complexity of the resulting differential equations appears to make this impracticable.

Comparison With Result of a Numerical Procedure [4]. For the case $k = 3$, the critical time was determined in [4] for rectangular sections by numerical integration without assumptions on the character of the stress distribution, but still using the collocation method.

For example, the numerical integration gives a critical time $t_{cr} = 155$ min for the case illustrated[8] in Fig. 3 of reference [4]; the corresponding nondimensional value is $\tau_{cr} = 4.64$, while the upper and lower bounds according to Equation (18) and Table 4 are 4.36 and 3.63, respectively. The result of the numerical procedure lies slightly, but definitely, outside the bounds determined in this paper; this contradiction requires explanation.

On examination, the authors have come to the conclusion that the discrepancy is due to the fact that the numerical procedure gives a result which is not a critical time in the sense used in this paper, and the values should not be compared. Reference [4] utilizes a standard finite difference forward integration in time [Equation (13) of the reference]; the finite-difference process employed leads to increasing—but never infinite—displacements or stresses, and the value of t_{cr} obtained in [4] is solely one where the displacements become large. No approximation of a critical

[7] The equation was derived by the authors using the method of reference [3].

[8] The data are $k = 3$, $E = 7.4 \times 10^6$ psi, $1/\lambda = 298 \times 10^{14}$ min. lb^3/in.^{6}, $\sigma_0/\sigma_E = 0.70$, $z_0/h = 0.0096$. When computing the foregoing value t_{cr}, allowance was made for a printing error in Fig. 3 of reference [4]. According to a communication from the authors, the relation for the time parameter should read $\tau = t/234.6$.

time in the sense used here can be obtained on this basis (It should be noted that reference [4] is essentially an application of the procedure developed in reference [6], where the unsuitability of integration using equal increments of t to determine a critical time is clearly stated.)[9]

The authors feel, therefore, that the apparent contradiction with the results of reference [4] does not cast doubt on the results of their work.

Conclusion

A method has been presented which permits determination of upper and lower bounds for the critical time of rectangular columns of viscoelastic material following the nonlinear law, Equation (1). The numerical results, giving limits on t_{cr} as function of the initial eccentricity z_0/h, are presented in Fig. 4 and Tables 3 and 4.

A criterion is given, Equations (21), permitting an estimate near which of the bounds the actual value of the critical time can be expected.

When applying the results to physical situations, it obviously must be kept in mind that the bounds obtained in this paper are based on the assumptions underlying the analysis. In recent work, references [7, 8], efforts have been made to unify the conventional theory of eccentric buckling and that of creep buckling for H-type sections. In cases where the interaction effect with inelastic buckling is of consequence, the limits for the critical time found in this paper would of course require modification.

References

1 Joseph Kempner, "Creep Bending and Buckling of Nonlinearly Viscoelastic Columns," NACA TN 3137, January, 1954.

2 Sharad Patel, Joseph Kempner, Burton Erickson, and A. H. Mobassery, "Correlation of Creep-Buckling Tests With Theory," NACA RM 56C20, May, 1956.

3 J. L. Sanders, Jr., H. G. McComb, Jr., and F. R. Schlechte, "A Variational Theorem for Creep With Applications to Plates and Columns," NACA TN 4003, May, 1957.

4 Sharad Patel and V. D. Wagle, "Creep Buckling of Rectangular Section Columns," Polytechnic Institute of Brooklyn, Brooklyn, N. Y., PIBAL Report No. 358, June, 1957.

5 H. H. Bleich, "On the Analysis of Non-Linear Viscoelastic Structures With Temperature Gradients," ONR Contract Nonr 266(34) Technical Report No. 3, Columbia University, New York, N. Y., June, 1957.

6 Charles Libove, "Creep Buckling Analysis of Rectangular-Section Columns," NACA TN 2956, June, 1953.

[9] Quoting from reference [6], p. 12: "A step-by-step solution of equation (23) on the basis of equal increments of t' should therefore not be attempted. Rather, the solution should be carried forward on the basis of equal increments in μ. . ."

7 N. J. Hoff, "Creep Buckling," *Aeronautical Quarterly*, vol. 7, 1956, pp. 1–20.

8 I. N. Rabotnov and S. A. Shesterikov, "Stability of a Bar or Plate in the Presence of Creep," *Prikladnaya Matematika i Mekhanika*, vol. 21, 1957, pp. 406–412.

APPENDIX 1

Bounds on Rate of Deformation

Consider an element of a bar of a nonlinear viscoelastic material, obeying the law Equation (1), under the action of a direct force P and a bending moment $M(t)$ as indicated in Fig. 1. The curvature rate $\dot{\kappa}(t)$ for this bar as a function of the stress at an instant is given by Equation (5).

Rectangular Cross Section, Bending Only. Without loss of generality, consider only an element of a beam of unit depth, $h = 1$, and unit width, $b = 1$, subjected to a bending moment $M(t)$ which does not decrease with time, $\dot{M} \geq 0$. The stress distribution will be antisymmetric such that only one half the beam $1/2 \leq \zeta \leq 1$ need be considered. The nature of the combined loading and relaxation process is such that the stress distribution $\sigma(\zeta)$ will be as shown in Fig. 5(*a*). The stress σ must be positive and monotonically increasing. If compared with the elastic distribution σ_e which has the same bending moment, there must be just one intersection as indicated in Fig. 5(*a*). This fact is sufficient to prove that the actual curvature rate is less than the initial value $\dot{\kappa}_0$.

The difference of the curvature rates produced by the two distributions is, using Equation (5)

$$\dot{\kappa}_0 - \dot{\kappa} = \frac{24\lambda}{h}\int_0^{1/2} u\sigma_e^k du - \frac{\dot{M}}{EI} - \frac{24\lambda}{h}\int_0^{1/2} u\sigma^k du \quad (23)$$

where $u = \zeta - 1/2$.

Combining the two integrals it is to be proved that:

$$\int_0^{1/2} u(\sigma_e - \sigma)(\sigma_e^{k-1} + \sigma_e^{k-2}\sigma \ldots . \sigma^{k-1})du \geq 0 \quad (24)$$

The two stress distributions pertain to the same bending moment, hence:

$$\int_0^{1/2} u(\sigma_e - \sigma)du = \int_0^{1/2} f du = 0 \quad (25)$$

where $f = u(\sigma_e - \sigma)$. This equation states that the positive and negative portions of Fig. 5(*b*) must be equal. Equation (24) requires integration over the product of f and an increasing positive term in the brackets, making the inequality (24) obvious.

In an identical manner, the relative shapes of the stress dis-

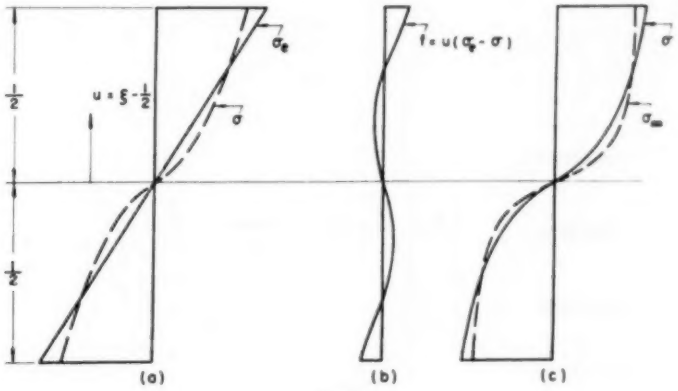

Fig. 5

tribution $\sigma(u)$ and of $\sigma_\infty(u)$ in Fig. 5(*c*) permit the conclusion:

$$\int_0^{1/2} u\sigma^k du - \int_0^{1/2} u\sigma_\infty{}^k du \geq 0 \tag{26}$$

and one can conclude finally that for the case of bending considered here

$$\dot{\kappa}_0 + \frac{\dot{M}}{EI} \geq \dot{\kappa} \geq \dot{\kappa}_\infty + \frac{\dot{M}}{EI} \tag{27}$$

where $\dot{\kappa}_0$ and $\dot{\kappa}_\infty$ are the rates obtained from Equation (5) with $\dot{M} = 0$ if the actual stresses σ are replaced by the elastic stress σ_e and the long term (i.e., purely viscous) distribution, σ_∞, respectively.

It must be emphasized that the proof just given applies for uniform temperature, i.e., when λ is constant, and that the restriction $\dot{M} \geq 0$ is necessary because unusual residual-stress patterns may otherwise be obtained for which Equation (27) would not be valid.

Column With Combined Bending and Compression. The stress distributions which may occur in an element of a rectangular bar under a constant compressive load P and an increasing moment $M(t)$ are of a much greater variety than the ones in the previous case, and it has not been possible to generalize the proof presented in the foregoing. The following proof is restricted to a simplified cross section consisting of three concentrated elements which carry the direct load, and which are connected by shear webs.

The cross section is taken to be symmetric as shown in Fig. 6(*a*). Without further loss of generality the distance between the chords, and the area of the inner chord are made equal to unity. The areas of the outer flanges are taken as α. If an elastic beam of such a section is subjected to a force P and moment M, the straight-line stress distribution of Fig. 6(*b*) will result. Without loss of generality, let $P = 1 + 2\alpha$, and the respective stresses in the three chords are:

$$s_1 = 1 - \mu, \quad s_2 = 1, \quad s_3 = 1 + \mu \tag{28}$$

where $\mu = \mu(M)$.

Consider next the nonlinear viscoelastic bar and stress distributions which may occur therein. The relaxation process requires stress distributions of one of the two types indicated in Fig. 6(*c*), such that

$$\sigma_3 > |\sigma_1|, \quad 2\sigma_2 > \sigma_1 + \sigma_3 \tag{29}$$

where positive stress indicates compression. All stress distributions having the resultant force $P = 1 + 2\alpha$ and the moment M can be expressed by the linear distribution S and one parameter Δ:

$$\begin{aligned} \sigma_1 &= S_1 - \Delta = 1 - \mu - \Delta \\ \sigma_2 &= S_2 + 2\alpha\Delta = 1 + 2\alpha\Delta \\ \sigma_3 &= S_3 - \Delta = 1 + \mu - \Delta \end{aligned} \tag{30}$$

The stress distributions which may occur during relaxation are contained in the foregoing equations but are restricted by equations (29) which require:

$$0 \leq \Delta \leq 1 \tag{31}$$

as may be seen by substitution. Actually, the values Δ which may occur are further restricted to lie between 0 for the elastic stress distribution, and a value $\Delta_\infty(k, P, M) < 1$ for the long-term distribution.

It is now possible to compare the deformation rates of the elastic stress distribution S and any other distribution σ. The generalization of the integral in Equation (5) for an arbitrary cross section is obviously $\int(\zeta - 1/2)\sigma^k dA$ to be taken over the entire area. For the present case

$$\int(\zeta - 1/2)s^k dA - \int(\zeta - 1/2)\sigma^k dA = \alpha \sum_i \binom{k}{i} \mu^i[1 - (1 - \Delta)^{k-i}] \tag{32}$$

where the sum is to be taken over-all odd values of $i \leq k$ and $\binom{k}{i}$ denotes the binomial coefficient. Since by definition $\mu > 0$, and $\Delta < 1$, the sum contains positive terms only, and it is proved that $(\dot{M}/EI) + \dot{\kappa}_0 \geq \dot{\kappa}$.

Similarly, two stress distributions σ_1 and σ_2 for which $\Delta_1 < \Delta_2$ may be compared, with the result:

$$\int(\zeta - 1/2)\sigma_1{}^k dA - \int(\zeta - 1/2)\sigma_2{}^k dA = \alpha \sum_i \binom{k}{i} \mu^i[(1 - \Delta_1)^{k-i} - (1 - \Delta_2)^{k-i}] \tag{33}$$

As mentioned after equation (31), physically possible stress distributions must be such that $0 \leq \Delta < \Delta_\infty < 1$. Let $\sigma_2 = \sigma_\infty$ and $\Delta_2 = \Delta_\infty$, and equation (33) proves $\dot{\kappa} > (\dot{M}/EI) + \dot{\kappa}_\infty$ and the existence of the bounds.

APPENDIX 2

Derivation of $\dot{\kappa}_0$

To obtain the term $\dot{\kappa}_0$ in the upper bound Equation (6) for the rate of curvature $\dot{\kappa}$, the elastic stress σ_e and $\dot{M} = 0$ are to be substituted into Equation (5):

$$\dot{\kappa}_0 = \frac{12\lambda}{h} \int_0^1 (\zeta - 1/2)\sigma_e{}^k d\zeta \tag{34}$$

The collocation method being used, only the value of the moment at the center of the column ($x = L/2$) is required; from Equation (7)

$$M = P\left(z + \frac{h}{2}\right) \tag{35}$$

and

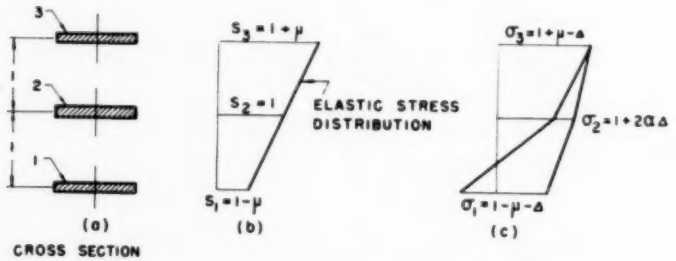

Fig. 6

$$\sigma_z = \sigma_0\left[1 + 12\,\frac{z}{h}\left(\zeta - \frac{1}{2}\right)\right] \tag{36}$$

where $\sigma_0 = P/(bh)$. After integration,

$$\dot{\kappa}_0 = \frac{12\lambda\sigma_0^k}{h}\sum_{i=1}^{(k+1)/2}\frac{1}{2(2i+1)}\binom{k}{2i-1}\left(\frac{6z}{h}\right)^{2i-1} \tag{37}$$

where k is inherently odd.

A derivation of $\dot{\kappa}_0$ for even k, based on Equation (1*a*), leads to a similar expression for $\dot{\kappa}_0$, but with an upper limit $k/2$ for the sum, provided $z < h/6$ such that $\sigma_z > 0$ everywhere.

APPENDIX 3

Derivation of $\dot{\kappa}_\infty$

The lower bound on the rate of curvature Equation (6) contains $\dot{\kappa}_\infty$, the long-time curvature rate when $\dot{M} = 0$. The stresses σ_∞ are those in a purely viscous material where

$$\dot{\epsilon} = \lambda\sigma_\infty^k$$

Expressing the strain rate $\dot{\epsilon}$ by means of Equation (3)

$$\sigma_\infty = \left(\frac{h\dot{\kappa}_\infty}{\lambda}\right)^{1/k}(\zeta - n)^{1/k} \tag{38}$$

The load and moment on the cross section at $x = L/2$ are

$$\frac{P}{bh} = \sigma_0 = \int_0^1 \sigma d\zeta = \left(\frac{h\dot{\kappa}_\infty}{\lambda}\right)^{1/k}\int_0^1 (\zeta - n)^{1/k}d\zeta$$

$$= \left(\frac{h\dot{\kappa}_\infty}{\lambda}\right)^{1/k}\frac{k}{k+1}\left[(1-n)^{(k+1)/k} - n^{(k+1)/k}\right] \tag{39}$$

$$\frac{M}{bh^2} = \int_0^1 \zeta\sigma d\zeta = \left(\frac{h\dot{\kappa}_\infty}{\lambda}\right)^{1/k}\int_0^1 \zeta(\zeta - n)^{1/k}d\zeta$$

$$= \left(\frac{h\dot{\kappa}_\infty}{\lambda}\right)^{1/k}\frac{k}{2k+1}\left[(1-n)^{(2k+1)/k} + n^{(2k+1)/k}\right] + n\sigma_0 \tag{40}$$

where use has been made of the fact that k is an odd integer. Equations (39), (40), and $M = P(z + h/2)$ permit the expression of the deflection z as a function of the parameter n. Using the abbreviation

$$A(n) \equiv (1-n)^{(k+1)/k} - n^{(k+1)/k} \tag{41}$$

one obtains the result

$$\frac{z}{h} = \frac{1}{2(2k+1)} + \left(\frac{k}{2k+1}\right)n + \left(\frac{k+1}{2k+1}\right)\left(\frac{n^{(k+1)/k}}{A}\right) \tag{42}$$

$$\dot{\kappa}_\infty = \frac{\lambda\sigma_0^k\left(\dfrac{k+1}{k}\right)^k}{hA^k} \tag{43}$$

Equations (42), (43) define $\dot{\kappa}_\infty$ as a function of z, since both are functions of the parameter n.

The parameter n can be eliminated readily in the limiting case $n \to -\infty$, which implies that the deflection z is small, resulting in the linear relation

$$\lim_{n\to-\infty}\dot{\kappa}_\infty = \frac{12\lambda k\sigma_0^k}{h^2}\,z \tag{44}$$

It is of considerable importance that this linear term is identical with the linear term of the expression (37) for $\dot{\kappa}_0$; it indicates that for small deflections the two limits for the rate of curvature are close together, and in consequence the limits for the critical time obtained are of the same order of magnitude; if this were not the case, the approach used in this paper would be quite useless.

HERBERT REISMANN

The Martin Company,
Denver Division,
Littleton, Colo.

Forced Vibrations of a Circular Plate

A solution is presented for the response of a clamped, circular plate to the action of an arbitrarily placed, harmonically oscillating, transverse, concentrated force. The method may be extended to a variety of loading and boundary conditions and can also be applied to ring-shaped plates.

THE earliest consideration of the subject of transverse vibrations of circular plates seems to be due to Poisson [1][1] whose work is restricted to the case of radial symmetry. Kirchhoff [2] gave the general solution of the problem of free vibrations, and later authors such as Rayleigh [3], Prescott [4], Warren [5], Roberson [6], Sneddon [7], and others considered various special cases of free and forced vibrations. It is the object of this paper to find the response of a clamped, thin, circular plate to the action of a harmonically oscillating, transverse, concentrated force. The approach taken here is based on classical techniques and utilizes the concept of a singularity solution.

In the subsequent development we shall neglect the effect of damping, although the same approach can be adapted to account for its presence.

Formulation and Solution

We consider the transverse vibration of a thin plate due to the action of an oscillatory concentrated load $F \cos pt$. For small deformations, the deflection surface of the plate $\omega(\rho, \theta, t)$ must satisfy the differential equation of motion (3)

$$\nabla^4\omega + \frac{m}{\lambda^4 D}\frac{\partial^2\omega}{\partial t^2} = 0 \tag{1}$$

as well as the boundary conditions imposed at the circular edge. In addition, the deflection function must display a singularity at the load point $r_1 = 0$ dictated by the following equilibrium condition:

$$F \cos pt = \lim_{r_1 \to 0} \int_0^{2\pi} Q_r r_1 d\theta + \lim_{r_1 \to 0} \int_0^{r} \int_0^{2\pi} m \frac{\partial^2\omega}{\partial t^2} r_1 dr_1 d\theta \tag{2}$$

where the radial shear force per unit length of circumference is given by [8]

$$Q_r = D\lambda^3 \frac{\partial}{\partial\rho_1}\left[\frac{1}{\rho_1}\frac{\partial}{\partial\rho_1}\left(\rho_1 \frac{\partial\omega}{\partial\rho_1}\right)\right]$$

A particular solution of Equation (1) is

$$\omega_1 = WK_0(\rho_1) \cos pt \tag{3}$$

and using this expression we note that

$$\lim_{r_1 \to 0} \int_0^{2\pi} Q_r r_1 d\theta = \lim_{\rho_1 \to 0} F\rho_1 K_1(\rho_1) \cos pt = F \cos pt$$

$$\lim_{r_1 \to 0} \int_0^{r_1} \int_0^{2\pi} m \frac{\partial^2\omega}{\partial t^2} r_1 dr_1 d\theta = \lim_{\rho_1 \to 0} F[1 - \rho_1 K_1(\rho_1)] \cos pt = 0$$

Thus it has been shown that the singularity solution, Equation (3), satisfies the required equilibrium condition, Equation (2). Moreover, by direct substitution it can be shown that Equation (3) satisfies the differential Equation (1). It represents the steady-state response of an infinite elastic plate to a harmonically oscillating, transverse, concentrated load. In what follows we shall chose the reference line $\theta = 0$ to be the radial line through the load point. It should be noted that generality is not lost by this choice.

The general solution of Equation (1) is derived in reference [3]. For a plate which deflects symmetrically with respect to its diameter ($\theta = 0, \pi$) it is (neglecting free vibrations)

$$\frac{\omega_2}{\cos pt} = R_0 + 2\sum_{n=1}^{\infty} R_n \cos n\theta \tag{4}$$

where

$$R_n = A_n J_n(\rho) + B_n I_n(\rho) + C_n Y_n(\rho) + D_n K_n(\rho)$$

Since the general solution, Equation (4), is expressed as an infinite trigonometric series, it is convenient to express the particular solution in a similar form. With the notation indicated in Fig. 1,

$$\rho_1^2 = \rho^2 + \delta^2 - 2\delta\rho \cos\theta$$

[1] Numbers in brackets designate References at end of paper.

Contributed by the Applied Mechanics Division and presented at the Annual Meeting, Atlantic City, N. J., November 29–December 4, 1959, of THE AMERICAN SOCIETY OF MECHANICAL ENGINEERS.

Discussion of this paper should be addressed to the Secretary, ASME, 29 West 39th Street, New York, N. Y., and will be accepted until January 10, 1960, for publication at a later date. Discussion received after the closing date will be returned.

NOTE: Statements and opinions advanced in papers are to be understood as individual expressions of their authors and not those of the Society. Manuscript received by ASME Applied Mechanics Division, June 10, 1958. Paper No. 59—A-9.

Nomenclature

ω = deflection of median surface
p = frequency
t = time
D = flexural rigidity of plate = $(Eh^3)/[12(1 - \nu^2)]$
E = Young's modulus
h = plate thickness
ν = Poisson's ratio
λ^4 = frequency parameter = mp^2/D
ρ = dimensionless radial co-ordinate = λr
δ = dimensionless radius of load circle = λb
η = dimensionless radius of plate = λa
θ = angular co-ordinate
F = amplitude of concentrated load
q = load intensity
W = load parameter = $-F/(2\pi\lambda^2 D)$
Q_r = radial shearing force per unit length
J_n = Bessel function of first kind
I_n = Bessel function of second kind
Y_n = modified Bessel function of first kind
K_n = modified Bessel function of second kind
$\nabla^2 = \frac{\partial^2}{\partial\rho^2} + \frac{1}{\rho}\frac{\partial}{\partial\rho} + \frac{1}{\rho^2}\frac{\partial^2}{\partial\theta^2}$

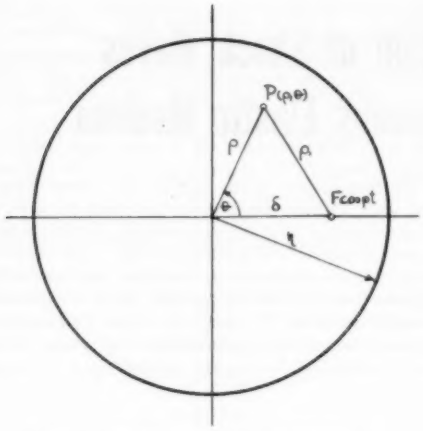

Fig. 1 Plan view—eccentrically loaded plate

Applying Neumann's addition theorem for modified Bessel functions of the second kind [8] we obtain, for $\rho < \delta$

$$\frac{\omega_1}{W \cos pt} = K_0(\rho_1) = K_0(\delta)I_0(\rho) + 2\sum_{n=1}^{\infty} K_n(\delta)I_n(\rho)\cos n\theta \tag{5a}$$

for $\rho > \delta$

$$\frac{\omega_1}{W \cos pt} = K_0(\rho_1) = I_0(\delta)K_0(\rho) + 2\sum_{n=1}^{\infty} I_n(\delta)K_n(\rho)\cos n\theta \tag{5b}$$

For a plate clamped at the boundary it is required that (in dimensionless form):

$$\omega(\eta, \theta) = 0 \tag{6a}$$

$$\left(\frac{\partial \omega}{\partial \rho}\right)_{(\eta,\theta)} = 0 \tag{6b}$$

The complete solution $\omega = \omega_1 + \omega_2$ must satisfy Equation (6); in addition, it is required that the slope and deflection at the center of the plate remain finite. Thus $C_n = D_n = 0$, and upon substituting the complete solution as given by the superposition of Equations (4) and (5*b*) into the boundary condition, Equations (6), we obtain identities in θ giving rise to a system of two equations in two unknowns·

$$A_nJ_n(\eta) + B_nI_n(\eta) = -I_n(\delta)K_n(\eta)$$

$$A_nJ_n'(\eta) + B_nI_n'(\eta) = -I_n(\delta)K_n'(\eta)$$

Solving

$$A_n = I_n(\delta)\,\frac{I_n(\eta)K_n'(\eta) + I_n'(\eta)K_n(\eta)}{J_n(\eta)I_n'(\eta) - J_n'(\eta)I_n(\eta)}$$

$$B_n = I_n(\delta)\,\frac{K_n(\eta)J_n'(\eta) + K_n'(\eta)J_n(\eta)}{J_n(\eta)I_n'(\eta) - J_n'(\eta)I_n(\eta)}$$

Table 1

ρ	$-R_0$	$-R_1$	$-R_2$	$-R_3$	$-R_4$
0	1.25721	0	0	0	0
0.2	1.25852	0.03738	0.00449	0.00019	0
0.4	1.26267	0.07395	0.01807	0.00202	0.00010
0.6	1.27011	0.10899	0.04087	0.00708	0.00193
0.8	1.28863	0.14173	0.07348	0.01692	0.00548

Thus the complete solution for the time-dependent deflection of a clamped circular plate under the action of a concentrated oscillating load $F \cos pt$ at $(\delta, 0)$ is conveniently expressed as

$$\frac{\omega}{W \cos pt} = K_0(\rho^2 + \delta^2 - 2\delta\rho\cos\theta)^{1/2} + R_0 + \sum_{n=1}^{\infty} R_n \cos n\theta$$

$$R_n = A_nJ_n(\rho) + B_nI_n(\rho) \tag{7}$$

valid for $0 \le \theta \le 2\pi, \quad 0 \le \rho \le \eta$.

A computation was carried out for a plate with $\delta = 1/2$, $\eta = 1$, and Table 1 gives an indication of the rate of convergence of the infinite series, Equation (7), for this case.

Generalization

The method developed can be extended to obtain exact solutions for harmonically oscillating load distributions of an arbitrary nature. Let $\omega_I = \omega_I(\rho, \theta;\ \delta, \phi)\cos pt$ be the response of a circular plate harmonically forced by a unit concentrated load at (δ, ϕ). Then the response of the same plate subjected to the distributed load $q(\rho, \theta)\cos pt$ is given by

$$\frac{\omega}{\cos pt} = \omega_0(\rho, \theta) = \int_0^{\eta}\int_0^{2\pi} q(\rho, \theta)\omega_I(\rho, \theta;\ \delta, \phi)\delta d\delta d\phi$$

where ω_I may be considered as the influence function.

Although the solution in this paper is given for a clamped plate, the technique is applicable to a variety of boundary conditions. In addition, because of the nature of the solution, ring plates, i.e., plates with two concentric circular boundaries, also come within the scope of this analysis.

References

1 S. D. Poisson, "Sur le Mouvement des Corps Elastiques," *Memoires de l'Academie Royale des Sciences de l'Institut de France*, vol. 8, 1829, p. 545.

2 G. Kirchhoff, "Über das Gleichgewicht und die Bewegung einer Elastischen Scheibe," *Journal für die reine und angewandte Mathematik* (Crelle), vol. 40, 1850, p. 51.

3 Lord Rayleigh, "Theory of Sound," Dover Publications, New York, N. Y., first American edition, 1945.

4 J. Prescott, "Applied Elasticity," Dover Publications, New York, N. Y., first American edition, 1946.

5 A. G. Warren, "Free and Forced Oscillations of Thin Bars, Flexible Disks, and Annuli," *London, Edinburgh, and Dublin Philosophical Magazine*, series 7, vol. 9, 1930, pp. 881–901.

6 R. E. Roberson, "Transverse Vibrations of a Free Circular Plate Carrying Concentrated Mass," JOURNAL OF APPLIED MECHANICS, vol. 18, TRANS. ASME, vol. 73, 1951, pp. 280–282.

7 I. N. Sneddon, "Fourier Transforms," McGraw-Hill Book Company, Inc., New York, N. Y., 1951.

8 A. Gray, G. B. Mathews, and T. M. McRobert, "Bessel Functions," Macmillan and Company, Limited, London, England, 1931.

ELI STERNBERG
Professor of Mechanics,
Division of Applied Mathematics,
Brown University, Providence, R. I.
Assoc. Mem. ASME

J. G. CHAKRAVORTY
Research Associate,
Division of Applied Mathematics,
Brown University, Providence, R. I.

On the Propagation of Shock Waves in a Nonhomogeneous Elastic Medium[1]

This paper is concerned with the propagation of shock waves in a nonhomogeneous isotropic plate of infinite extent and arbitrary thickness. The plate has a transverse cylindrical hole at which uniform shearing tractions are suddenly applied and thereafter steadily maintained; the body is otherwise free from loading. It is assumed that the shear modulus of the material is proportional to an arbitrary—not necessarily integral—power of the radial distance from the axis of the hole, while no restriction is placed upon the (continuous) radial variation of Young's modulus. The solution obtained, which is discussed in detail, constitutes a generalization of results reached by Goodier and Jahsman [1],[2] who considered the present problem for a homogeneous medium.

Introduction

In a recent paper, Goodier and Jahsman [1] studied the propagation of shock waves in an isotropic, *homogeneous* elastic plate of infinite extent and arbitrary thickness, which has a transverse cylindrical hole. The "rotary" motion considered in [1] arises from shearing tractions, uniformly distributed over the boundary of the opening and acting parallel to the faces of the plate; these tractions are suddenly applied and thereafter steadily maintained.[3] The body is otherwise free from loading.

It is the object of the present paper to extend the investigation contained in [1] to a class of inhomogeneous elastic materials, in the hope that the corresponding solutions may be of interest beyond their immediate context; the results reached here are apt to enhance the understanding of more general wave-propagation phenomena associated with continuously inhomogeneous elastic media.[4]

With a view toward a description of the type of inhomogeneity underlying this investigation, let (r, θ, z) be circular cylindrical co-ordinates and let the plate under consideration occupy the region $a \leq r < \infty$, $|z| \leq d/2$, a being the radius of the hole and d the plate thickness. If E and μ, respectively, denote Young's modulus and the shear modulus of the material, we assume that

$$E = E(r), \quad \mu = \mu_0 \left(\frac{r}{a}\right)^{\alpha} \left(\alpha \gtrless 0\right), \tag{1}$$

in which μ_0 is the value of μ at the hole. Thus the shear modulus is taken proportional to an arbitrary power of the radial distance from the axis of the opening, while no restriction is placed upon the (continuous) radial variation of Young's modulus. The variation of Poisson's ratio follows from (1) since we adhere to the assumption of isotropy. In order to shorten the analysis, we shall regard the mass density as constant. It should be emphasized, however, that the admission of a power law for the density—analogous to that stipulated for μ, but involving an exponent which may be distinct from α—introduces no essential complications.

In dealing with the special case $\alpha = 0$, appropriate to the homogeneous medium, Goodier and Jahsman [1] made use of an operational scheme originated by Kromm [3] in connection with the allied problem in which the hole is subjected to a suddenly rising uniform radial pressure (or radial velocity).[5] If $\alpha \neq 2$, Kromm's procedure may be extended to the present generalized problem. Thus, as in [1] and [3], one is led to integral equations of Volterra's first kind for the nonvanishing cylindrical component of displacement, stress, and particle velocity.[6] The numerical solution of these integral equations, with the aid of approximately equivalent systems of linear algebraic equations, is readily accomplished for every $\alpha \neq 2$; it necessitates, in fact, no greater volume of computations than is encountered when $\alpha = 0$, and has been carried out here to determine the stress distribution for $\alpha = 1$. Moreover, the formulas for the instantaneous position and velocity of the wave front of the ensuing diverging cylindrical shock wave remain elementary for all choices of the "stiffness exponent" α. The same applies to the formulas for the peak values of the stress and particle velocity at the wave front.

For the exceptional case $\alpha = 2$, we deduce an exact *explicit* solution in integral representation and again discuss the stress distribution numerically. Finally, we find that there exists an infinite sequence of α-values which gives rise to exact solutions in closed form and in terms of elementary functions. Two members of this sequence, which correspond to $\alpha = -2/3$ and $\alpha = 10$, are determined explicitly and discussed in detail.

The character of the solution is found to depend on whether $\alpha < 2$ or $\alpha > 2$. For $\alpha < 2$, the values of stress and particle velocity at the wave front decline monotonically as the shock

---

[1] The results presented in this paper were obtained in the course of an investigation conducted under Contract Nonr 56225 with the Office of Naval Research, Department of the Navy, Washington, D. C.

[2] Numbers in brackets designate References at end of paper.

[3] The companion case, in which a rotary velocity is suddenly imposed at the hole, is also treated in [1].

[4] See [2] for a comprehensive bibliography on the subject of wave propagation in nonhomogeneous media. The investigations cited in [2] aim primarily at layered media rather than at media with continuously varying properties; they are, moreover, confined to surface waves in semi-infinite bodies.

Presented at the West Coast Conference of the Applied Mechanics Division, Stanford, Calif., September 9–11, 1959, of The American Society of Mechanical Engineers.

Discussion of this paper should be addressed to the Secretary, ASME, 29 West 39th Street, New York, N. Y., and will be accepted until January 10, 1960, for publication at a later date. Discussion received after the closing date will be returned.

Note: Statements and opinions advanced in papers are to be understood as individual expressions of their authors and not those of the Society. Manuscript received by ASME Applied Mechanics Division, June 10, 1958. Paper No. 59—APMW-17.

[5] In view of the title of [1], it may be worth mentioning that Kromm's solution [3] involves the approximative assumption of generalized plane stress, whereas the plane-stress character of the results in [1] is a rigorous consequence of the three-dimensional field equations.

[6] The integral equation for the displacement is not included in [1].

wave progresses. The solution asymptotically approaches the steady equilibrium state in which the stress distribution is statically determinate and, hence, independent of α. In contrast, for $\alpha > 2$, the stress at the wave front increases steadily and beyond bounds during the *finite* time in which the wave here reaches infinity. In this instance, the solution fails to approach a steady state and ceases to be physically significant once the entire body is stressed, the stresses at infinity having become unbounded.

Formulation of Problem—Governing Equations

The problem described in the preceding section is characterized by an axisymmetric displacement field of pure torsion, appropriate to a purely rotary motion. With reference to the cylindrical co-ordinates (r, θ, z) introduced earlier, we thus have

$$u_r = u_z = 0, \quad u_\theta = u(r, t), \tag{2}$$

where (u_r, u_θ, u_z) are the cylindrical components of displacement and t is the time. Equations (2), in conjunction with the displacement-stress relations of the linear theory of isotropic elastic media, now yield the shear stress

$$s_{r\theta} = s(r, t) = \mu\left(\frac{\partial u}{\partial r} - \frac{u}{r}\right), \tag{3}$$

whereas all remaining cylindrical components of stress vanish identically. The shear modulus μ is, for the time being, assumed to be an arbitrary function[7] of r. The equations of motion here reduce to the single equation

$$\frac{\partial s}{\partial r} + \frac{2s}{r} = \gamma\,\frac{\partial^2 u}{\partial t^2}, \tag{4}[8]$$

in which γ designates the (constant) mass density.

In stating the initial and boundary conditions, we cite merely those requirements which are not automatically satisfied by virtue of (2). The relevant initial conditions are then given by

$$u(r, 0) = 0, \quad \left[\frac{\partial u}{\partial t}\right]_{(r,\,0)} = 0 \quad (a < r < \infty), \tag{5}$$

while the nontrivial boundary condition becomes

$$s(a, t) = h(t)s_0 \quad (-\infty < t < \infty), \tag{6}$$

where s_0 is a constant and $h(t)$ is the Heaviside step function, defined by

$$h(t) = 1 \text{ for } t > 0, \quad h(t) = 0 \quad \text{for} \quad t < 0. \tag{7}$$

Since the tractions at infinity are to vanish, we adjoin the regularity condition

$$s(r, t) \to 0 \quad \text{as} \quad r \to \infty. \tag{8}$$

The problem under consideration, therefore, reduces to the solution of (3), (4) for the displacement $u(r, t)$ and the shear stress $s(r, t)$, subject to conditions (5), (6), (8). Moreover, the present formulation of the problem is rigorous within the *three-dimensional* linear theory.[5]

At this stage, it is expedient to introduce dimensionless variables. To this end, we define a dimensionless radial co-ordinate and time by means of the relations

$$\rho = \frac{r}{a}, \quad \tau = \frac{c_0 t}{a} \tag{9}$$

where

$$c_0 = (\mu_0/\gamma)^{1/2}, \quad \mu_0 = \mu(a), \tag{10}$$

whence c_0 is the velocity of shear waves in a *homogeneous* medium whose shear modulus coincides with the local value of μ at the boundary of the hole. Next, we define a dimensionless shear modulus, displacement, and stress through

$$\hat{\mu} = \frac{\mu}{\mu_0}, \quad \hat{u} = \frac{\mu_0 u}{s_0 a}, \quad \hat{s} = \frac{s}{s_0}. \tag{11}$$

Equations (3), (4), with the aid of (9), (10), (11), become

$$\hat{s} = \hat{\mu}\left(\frac{\partial \hat{u}}{\partial \rho} - \frac{\hat{u}}{\rho}\right), \tag{12}$$

$$\frac{\partial \hat{s}}{\partial \rho} + \frac{2\hat{s}}{\rho} = \frac{\partial^2 \hat{u}}{\partial \tau^2}, \tag{13}$$

and substitution for $\hat{s}$ from (12) into (13) leads to the displacement equation of motion in the dimensionless form

$$\frac{\partial^2 \hat{u}}{\partial \rho^2} + \left(1 + \frac{\rho}{\hat{\mu}}\,\frac{d\hat{\mu}}{d\rho}\right)\left[\frac{1}{\rho}\,\frac{\partial \hat{u}}{\partial \rho} - \frac{\hat{u}}{\rho^2}\right] = \frac{1}{\hat{\mu}}\,\frac{\partial^2 \hat{u}}{\partial \tau^2}. \tag{14}$$

The partial differential equation (14) is analytically tractable if

$$\hat{\mu} = \rho^\alpha \quad \left(\alpha \gtrless 0\right), \tag{15}$$

α being a constant, in which case the coefficient of the term in brackets is constant. This motivates the particular choice of $\mu(r)$ announced in (1).

We shall assume, henceforth, that (15) holds and, consequently, replace (14), (12) with

$$\frac{\partial^2 \hat{u}}{\partial \rho^2} + (1 + \alpha)\left(\frac{1}{\rho}\,\frac{\partial \hat{u}}{\partial \rho} + \frac{\hat{u}}{\rho^2}\right) = \frac{1}{\rho^\alpha}\,\frac{\partial^2 \hat{u}}{\partial \tau^2}, \tag{16}$$

$$\hat{s} = \rho^\alpha\left(\frac{\partial \hat{u}}{\partial \rho} - \frac{\hat{u}}{\rho}\right) \tag{17}$$

By virtue of (9), (10), (11), conditions (5), (6), (8) may be written as

$$\hat{u}(\rho, 0) = 0, \quad \left[\frac{\partial \hat{u}}{\partial \tau}\right]_{(\rho,\,0)} = 0 \quad (1 < \rho < \infty), \tag{18}$$

$$\hat{s}(1, \tau) = h(\tau) \quad (-\infty < \tau < \infty), \tag{19}$$

$$\hat{s}(\rho, \tau) \to 0 \quad \text{as} \quad \rho \to \infty. \tag{20}$$

Thus we need to determine the solution of (16) which conforms to (18) and is such that the stress (17) meets (19), (20).

Solution of the Associated Equilibrium Problem

In the equilibrium problem associated with the foregoing problem of motion, u and s are independent of the time. In place of (19) and (20) we now have

$$\hat{s}(1) = 1, \quad \hat{s}(\rho) \to 0 \quad \text{as} \quad \rho \to \infty, \tag{21}$$

as the governing (time-independent) boundary and regularity conditions. Equation (16) now reduces to the displacement equation of equilibrium

$$\frac{d^2 \hat{u}}{d\rho^2} + (1 + \alpha)\left(\frac{1}{\rho}\,\frac{d\hat{u}}{d\rho} - \frac{\hat{u}}{\rho^2}\right) = 0. \tag{22}$$

which is an ordinary differential equation of the Euler type, while (17) becomes

[7] We require merely that this function be positive and continuously differentiable for $a \leq r < \infty$, while postponing the particular choice of $\mu(r)$ appearing in (1).

[8] The body forces are assumed to vanish.

$$\hat{s} = \rho^{\alpha}\left(\frac{d\hat{u}}{d\rho} - \frac{\hat{u}}{\rho}\right). \tag{23}$$

The solution of (22) which conforms to (21), in view of (23), is given by

$$\hat{u} = -\frac{\rho^{-\alpha-1}}{2+\alpha} \quad (\alpha \neq -2), \quad \hat{u} = \rho \log \rho \quad (\alpha = -2), \tag{24}$$

and from (24), (23) follows

$$\hat{s} = \rho^{-2}, \tag{25}$$

regardless of the particular value of α.

We note that the displacement (24) tends to zero as $\rho \to \infty$ only if[9] $\alpha > -1$. Next, we observe that the stress distribution given by (25) is independent of the stiffness exponent α. This conclusion, which at first sight may seem surprising, is self-evident; the stresses, in the present case, are statically determinate, whence (25) is immediate from elementary equilibrium considerations. More explicitly, (13) here passes over into the stress equation of equilibrium

$$\frac{d\hat{s}}{d\rho} + \frac{2\hat{s}}{\rho} = 0 \tag{26}$$

which, together with (21), implies (25) directly. The stress field determined by (25), according to (12), remains compatible and (25) continues to hold, even if (15) is replaced with an *arbitrary* radial variation $\hat{\mu}(\rho)$ of the shear modulus, provided $\hat{\mu}(\rho)$ is continuously differentiable for $1 \leq \rho < \infty$ and $\hat{\mu}^{-1}(\rho)$ is sufficiently well behaved as $\rho \to \infty$.

Application of the Laplace Transform—Classification of the Stiffness Exponent

Returning to the dynamic problem which constitutes our main objective, we now remove the time dependence from the governing field equations and boundary conditions with the aid of the Laplace transform. To this end, let the Laplace transform, with respect to τ, of a function $f(\rho, \tau)$ be $F(\rho, p)$, whence

$$F(\rho, p) = L[f(\rho, \tau)] = \int_0^{\infty} e^{-p\tau} f(\rho, \tau) d\tau, \tag{27}[10]$$

in which p is the transform parameter. In particular, let

$$\left.\begin{aligned} U(\rho, p) &= L[\hat{u}(\rho, \tau)], \\ S(\rho, p) &= L[\hat{s}(\rho, \tau)], \\ V(\rho, p) &= L[\hat{v}(\rho, \tau)], \end{aligned}\right\} \tag{28}$$

where

$$\hat{v}(\rho, \tau) = \frac{\partial \hat{u}}{\partial \tau} \tag{29}$$

is the particle velocity. Applying the Laplace transform to (16), (17), (19), (20), and taking into account the initial conditions (18), we reach the field equations

$$\frac{d^2U}{d\rho^2} + \frac{(1+\alpha)}{\rho}\frac{dU}{d\rho} - \left[\frac{1+\alpha}{\rho^2} + \frac{p^2}{\rho^{\alpha}}\right] U = 0, \tag{30}$$

$$S = \rho^{\alpha}\left[\frac{dU}{d\rho} - \frac{U}{\rho}\right], \tag{31}$$

together with the boundary condition

$$S(1, p) = \frac{1}{p}, \tag{32}$$

and the regularity condition

$$S(\rho, p) \to 0 \quad \text{as} \quad \rho \to \infty. \tag{33}$$

Moreover,

$$V(\rho, p) = pU(\rho, p). \tag{34}$$

If $\alpha \neq 2$, (30) is reducible to a modified Bessel equation and has the general solution

$$U(\rho, p) = A_1\rho^{-\alpha/2} I_n\left(\frac{p\rho^{\beta}}{\beta}\right) + A_2\rho^{-\alpha/2} K_n\left(\frac{p\rho^{\beta}}{\beta}\right), \tag{35}$$

where I_n and K_n are the modified Bessel functions of the first and second kind, of order n, while

$$\beta = 1 - \frac{\alpha}{2}, \quad n = \frac{2+\alpha}{2-\alpha}. \tag{36}$$

The coefficients A_1, A_2 appearing in (35) are arbitrary functions of p and are to be determined consistent with (32), (33).

On the other hand, for $\alpha = 2$ ($\beta = 0$), (30) is an equation of the Euler type, whose complete solution is given by

$$U = A_1\rho^{m_1} + A_2\rho^{m_2}, \quad m_{1,2} = -1 \pm (4 + p^2)^{1/2}. \tag{37}$$

The character of the solution (35) depends on whether β is positive or negative and hence on whether $\alpha < 2$ or $\alpha > 2$. This leads us to distinguish between, and deal separately with, the following three fundamental cases:

$$\left.\begin{aligned} &\text{Case 1} \\ &\qquad -\infty < \alpha < 2 \quad (0 < \beta < \infty, \quad -1 < n < \infty); \\ &\text{Case 2} \\ &\qquad \alpha = 2 \quad (\beta = 0); \\ &\text{Case 3} \\ &\qquad 2 < \alpha < \infty \quad (-\infty < \beta < 0, \quad -\infty < n < -1). \end{aligned}\right\} \tag{38}$$

Solution for Case 1. Generalization of Kromm's Scheme

Since $\beta > 0$ in the case under consideration, the argument of the Bessel functions entering (35) is positive for $p > 0$ and tends to infinity as $\rho \to \infty$. Applying conditions (32), (33) to (35), we obtain, by virtue of (31) and the recursion formulas appropriate to the modified Bessel functions[11]

$$U(\rho, p) = -K_n\left(\frac{p\rho^{\beta}}{\beta}\right)\left[p^2\rho^{\alpha/2} K_{n+1}\left(\frac{p}{\beta}\right)\right]^{-1}, \tag{39}$$

$$S(\rho, p) = K_{n+1}\left(\frac{p\rho^{\beta}}{\beta}\right)\left[pK_{n+1}\left(\frac{p}{\beta}\right)\right]^{-1}, \tag{40}$$

while (39), (34) imply

$$V(\rho, p) = -K_n\left(\frac{p\rho^{\beta}}{\beta}\right)\left[p\rho^{\alpha/2} K_{n+1}\left(\frac{p}{\beta}\right)\right]^{-1}. \tag{41}$$

Unfortunately, the explicit inversion of (39), (40), (41), in a

[9] For $\alpha < -1$, the displacement field is unbounded as $\rho \to \infty$, and its physical significance becomes questionable. In this connection, attention also should be drawn to the discontinuous dependence of $\hat{u}$ on α, at $\alpha = -2$.

[10] Throughout this paper, image functions are designated by capital letters, while the corresponding lower-case letters are used to denote their respective antecedents.

[11] See Watson [4], p. 79.

form suitable for numerical computations, appears to be prohibitive, in general.[13] For this reason, we extend Kromm's scheme of solution [3], which Goodier and Jahsman [1] adapted to the present problem for a homogeneous medium ($\alpha = 0$). Thus, let

$$\Phi \equiv e^{p/\beta} K_{n+1}\left(\frac{p}{\beta}\right), \tag{42}$$

$$\Psi_1 \equiv \frac{1}{p}\,\Psi_2(\rho, p), \tag{43}$$

$$\Psi_2 \equiv \frac{1}{p}\, e^{p/\beta} K_{n+1}\left(\frac{p\rho^\beta}{\beta}\right) \tag{44}$$

$$\Psi_3 \equiv \frac{-\rho^{-\alpha/2}}{p}\, e^{p/\beta} K_n\left(\frac{p\rho^\beta}{\beta}\right). \tag{45}$$

With these definitions, (39), (40), (41) may be written as

$$\left.\begin{aligned} U(\rho, p)\Phi(p) &= \Psi_1(\rho, p), \\ S(\rho, p)\Phi(p) &= \Psi_2(\rho, p), \\ V(\rho, p)\Phi(p) &= \Psi_3(\rho, p) \end{aligned}\right\} \tag{46}$$

From (46), (28), and the convolution theorem, follow

$$\int_0^\tau \hat{u}(\rho, \xi)\varphi(\tau - \xi)d\xi = \psi_1(\rho, \tau), \tag{47}$$

$$\int_0^\tau \hat{s}(\rho, \xi)\varphi(\tau - \xi)d\xi = \psi_2(\rho, \tau), \tag{48}$$

$$\int_0^\tau \hat{v}(\rho, \xi)\varphi(\tau - \xi)d\xi = \psi_3(\rho, \tau), \tag{49}$$

in which $\varphi(\tau)$, $\psi_i(\rho, \tau)$ are the antecedents of $\Phi(p)$, $\Psi_i(\rho, p)$ $(i = 1, 2, 3)$ with respect to the Laplace transform. Equations (47), (48), (49) are three integral equations of Volterra's first kind for the desired unknown functions $\hat{u}(\rho, \tau)$, $\hat{s}(\rho, \tau)$, and $\hat{v}(\rho, \tau)$.

The determination of the kernel $\varphi(\tau)$ and of the right-hand members $\psi_i(\rho, \tau)$ $(i = 1, 2, 3)$ in (47), (48), (49), may be effected by recourse to available inverse Laplace transforms and to elementary properties of the transform.[13] Thus (42), with the aid of [7],[14] yields after some manipulation,

$$\varphi(\tau) = \frac{h(\tau)\beta}{2(\omega^2 - 1)^{1/2}}\left[(\omega + \sqrt{\omega^2 - 1})^{n+1} + (\omega - \sqrt{\omega^2 - 1})^{n+1}\right], \tag{50}[16]$$

where

$$\omega = \beta\tau + 1 \tag{51}$$

Equations (44), (45), in view of [5],[16] ultimately give

$$\psi_2(\rho, \tau) = \frac{h(\tau - \delta)}{2(n+1)\rho^2}\left[(\omega + \sigma)^{n+1} - (\omega - \sigma)^{n+1}\right], \tag{52}$$

provided

$$\delta = \frac{\rho^\beta - 1}{\beta} \tag{53}$$

and

$$\sigma = (\omega^2 - \rho^{2\beta})^{1/2}; \tag{54}$$

$$\psi_2(\rho, \tau) = \frac{h(\tau - \delta)}{2n\rho^{n+1}}\left[(\omega - \sigma)^n - (\omega + \sigma)^n\right] \quad \text{for} \quad n \neq 0 \quad (\alpha \neq -2), \tag{55}$$

$$\psi_2(\rho, \tau) = -h(\tau - \delta)\rho \log\left(\frac{\omega + \sigma}{\rho^2}\right) \quad \text{for} \quad n = 0 \quad (\alpha = -2). \tag{56}$$

Finally, by (43),

$$\psi_1(\rho, \tau) = \int_0^\tau \psi_2(\rho, \xi)d\xi, \tag{57}$$

and a tedious computation, based on (57), (55), (56), eventually leads to

$$\psi_1(\rho, \tau) = \frac{h(\tau - \delta)}{2\beta n(n^2 - 1)\rho^{n+1}}\left[(\omega - n\sigma)(\omega + \sigma)^n - (\omega + n\sigma)(\omega - \sigma)^n\right] \quad \text{for} \quad n \neq 0, 1 \ (\alpha \neq -2, 0), \tag{58}$$

$$\psi_1(\rho, \tau) = \frac{h(\tau - \delta)\rho}{2}\left[\sigma - \omega \log\left(\frac{\omega + \sigma}{\rho^2}\right)\right] \quad \text{for} \quad n = 0 \quad (\alpha = -2), \tag{59}$$

$$\psi_1(\rho, \tau) = \frac{h(\tau - \delta)}{2\rho}\left[\rho^2 \log\left(\frac{\omega + \sigma}{\rho}\right) - \omega\sigma\right] \quad \text{for} \quad n = 1 \quad (\alpha = 0). \tag{60}$$

This completes the derivation of the integral equations (47), (48), (49). For the special case $\alpha = 0$, (48) and (49) reduce to the corresponding results in [1].[8] The kernel function $\varphi(\tau)$, given by (50), is seen to possess an integrable singularity at $\tau = 0$. Furthermore, the integral of $\varphi(\tau)$ is found to be elementary. Indeed, Equation (50), after several changes of the variable of integration, yields

$$\int_\eta^\tau \varphi(\tau - \xi)d\xi = \frac{h(\tau - \eta)}{2(n+1)}\left[(\zeta + \sqrt{\zeta^2 - 1})^{n+1} - (\zeta - \sqrt{\zeta^2 - 1})^{n+1}\right], \tag{61}$$

with

$$\zeta = \beta(\tau - \eta) + 1, \tag{62}$$

as may be verified directly.

The solution of (47), (48), (49), in analytical form, becomes feasible only for an exceptional sequence of α-values[13] which will be discussed later on. For arbitrary α $(-\infty < \alpha < 2)$, the values of $\hat{u}(\rho, \tau)$, $\hat{s}(\rho, \tau)$, and $\hat{v}(\rho, \tau)$, may be found by the usual numerical process.[17] Thus, each integral equation is replaced with an (approximately) equivalent finite system of linear algebraic equations, obtained by regarding the unkown function as piecewise constant over the range of the integration, and by making use of (61). Fortunately, the volume of computations so encountered is no greater than in the special instance of the homogeneous medium. The numerical values of $\hat{s}(\rho, \tau)$ for $\alpha = 1$, presented at the end of the paper, were established in this manner.

We turn now to certain general conclusions which may be drawn from the integral equations (47), (48), (49). Since each of the right-hand members has the factor $h(\tau - \delta)$, it follows that

$$\hat{u}(\rho, \tau) = \hat{s}(\rho, \tau) = \hat{v}(\rho, \tau) = 0 \quad \text{for} \quad \tau < \delta \tag{63}[18]$$

---

[13] As will be shown later, there exists an infinite sequence of α-values for which the inverse transforms may be determined in closed form and in terms of elementary functions.

[13] See, for example, Doetsch [5] or Churchill [6]. A more extensive tabulation of inverse Laplace transforms is contained in [7].

[14] Reference [7], p. 278, no. 18.

[15] Recall (7).

[16] Reference [5], p. 139, no. 21, and p. 138, no. 18.

[17] See [3] for details of this scheme.

[18] The lower limit of integration in (47), (48), (49) may be replaced by δ because of (63).

and, according to (53), $\delta \to \infty$ as $\rho \to \infty$ because $\beta > 0$ in Case 1. This confirms the presence of a diverging cylindrical shock wave which issues from the cylindrical boundary and progresses toward infinity in infinite time. If ρ and τ, momentarily, denote the instantaneous radius of the wave front and the time at which this radius is attained, (63), (53), (51), imply

$$\rho = (\beta\tau + 1)^{1/\beta} = \omega^{1/\beta}, \quad \tau = \frac{\rho^\beta - 1}{\beta} = \delta. \tag{64}$$

The (dimensionless) velocity of the wave front is, therefore, given by

$$\hat{w} \equiv \frac{d\rho}{d\tau} = \rho^{\alpha/2} = \omega^{\frac{1-\beta}{\beta}} = \sqrt{\hat{\mu}}, \tag{65}$$

in which (15) has been used. Consequently, as was to be expected, the instantaneous velocity of the wave front coincides with the velocity of shear waves in a homogeneous medium, which has the same mass density, and whose shear modulus has the value of $\mu(\rho)$ at the instantaneous position of the wave front. In particular, $\hat{w}$ increases or decreases with ρ and τ, depending on whether $\alpha > 0$ or $\alpha < 0$.

Of special interest are the values of the displacement, stress, and particle velocity at the wave front. These values may be determined by noting, on the basis of (47), (48), (49), that

$$\left.\begin{aligned} \hat{u}(\rho, \delta+) &= \lim_{\epsilon \to 0} \frac{\psi_1(\rho, \delta + \epsilon)}{\Pi}, \\ \hat{s}(\rho, \delta+) &= \lim_{\epsilon \to 0} \frac{\psi_2(\rho, \delta + \epsilon)}{\Pi}, \\ \hat{v}(\rho, \delta+) &= \lim_{\epsilon \to 0} \frac{\psi_3(\rho, \delta + \epsilon)}{\Pi}. \end{aligned}\right\} \tag{66}$$

if

$$\Pi = \int_\delta^{\delta+\epsilon} \varphi(\delta + \epsilon - \xi) d\xi. \tag{67}$$

Carrying out this lengthy limit process with the aid of (51) to (61), and bearing in mind (63), (64), one arrives at

$$\hat{u}_* \equiv \hat{u}(\rho, \delta+) = \hat{u}(\omega^{1/\beta-}, \tau) = 0, \tag{68}$$

$$\hat{s}_* \equiv \hat{s}(\rho, \delta+) = \hat{s}(\omega^{1/\beta-}, \tau) = \rho^{\alpha/4 - 1/2} = \omega^{-1/2}, \tag{69}$$

$$\hat{v}_* \equiv \hat{v}(\rho, \delta+) = \hat{v}(\omega^{1/\beta-}, \tau) = -\rho^{-\alpha/4 - 1/2} = -\omega^{1/2 - 1/\beta}. \tag{70}$$

Equation (68) is consistent with the physical requirement that the displacements remain continuous throughout the body at all times. As seen from (69), (70), the shear stress and the particle velocity suffer finite jump discontinuities at the wave front. The peak value of $\hat{s}$ decreases as the wave progresses, since $\alpha < 2$ at present; the particle speed $|\hat{v}|$, at the wave front, increases or decreases according as $\alpha < -2$ or $\alpha > -2$.

Finally, we observe that (48) is met by the equilibrium stress (25) in the limit as $\tau \to \infty$; i.e., in the steady state. Similarly, the equilibrium values of $\hat{u}(\rho, \tau)$, appearing in (24), satisfy (47), provided[9] $\alpha \neq -2$.

The foregoing conclusions agree with the results given in [1] if the medium is assumed to be homogeneous ($\alpha = 0$).

Solution for Case 2

Referring to (38), we note that $\alpha = 2$ and $\beta = 0$ in the present case. The general solution of the transformed displacement equation of motion is now given by (37) which, on invoking (31), (32), (33), yields

$$U(\rho, p) = -\frac{\exp\,[-\lambda(4 + p^2)^{1/2}]}{\rho p[2 + (4 + p^2)^{1/2}]}, \tag{71}$$

where

$$\lambda = \log \rho \tag{72}$$

With a view toward the inversion of (71), we recall the general formula[10]

$$F[(p^2 + 1)^{1/2}] = L\left\{f(\tau) - \int_0^\tau f[(\tau^2 - \xi^2)^{1/2}] J_1(\xi) d\xi\right\}, \tag{73}$$

in which J_1 is the Bessel function of the first kind, of order one. With the aid of (73) and of elementary results in Laplace transform theory, we find from (71), (72) after trivial manipulations,

$$\hat{u}(\rho, \tau) = \frac{h(\tau - \lambda)}{2\rho}\left[-1 + \rho^2 e^{-2\tau} + 2\rho^2 \int_0^\tau \int_0^{2(\xi^2 - \lambda^2)^{1/2}} \exp\left\{-\sqrt{(2\xi)^2 - \eta^2}\right\} J_1(\eta) d\eta d\xi\right] \tag{74}$$

The corresponding shear stress and particle velocity follow from (74) through (17) and (29):

$$\hat{s}(\rho, \tau) = h(\tau - \lambda)\left[1 - 2\lambda \int_0^{2(\tau^2 - \lambda^2)^{1/2}} \frac{J_1(\xi)}{\sqrt{\xi^2 + (2\lambda)^2}} d\xi\right], \tag{75}$$

$$\hat{v}(\rho, \tau) = h(\tau - \lambda)\rho\left[\int_0^{2(\tau^2 - \lambda^2)^{1/2}} \exp\left\{-\sqrt{(2\tau)^2 - \xi^2}\right\} J_1(\xi) d\xi - e^{-2\tau}\right]. \tag{76}$$

This completes the solution for Case 2. Substitution into (16) to (20) confirms that (74), (75), (76) satisfy the governing field equations, as well as the initial and boundary conditions. The representation (74) of $\hat{u}$, which involves an iterated integral, is unwieldy for numerical purposes. On the other hand, the simple integrals appearing in (75), (76) are readily accessible to numerical evaluation. Such tabulations have been carried out for the integral in (75), and the corresponding results for $\hat{s}$ will be presented in a subsequent section.

An inspection of the foregoing solution reveals that (63), previously derived for Case 1 ($\alpha < 2$), remains valid in Case 2 ($\alpha = 2$), if δ is replaced by λ. Also, according to (53), (72), (36),

$$\lambda \equiv \log \rho = \lim_{\alpha \to 2} \delta. \tag{77}$$

The cylindrical shock wave, as in Case 1, progresses to infinity in infinite time. In place of (64), we now have

$$\rho = e^\tau, \quad \tau = \log \rho = \lambda, \tag{78}$$

if τ, once more, is the time in which the wave front attains the radius ρ. The velocity of the wave front obeys

$$\hat{w} \equiv \frac{d\rho}{d\tau} = \rho = e^\tau = \sqrt{\hat{\mu}}, \tag{79}$$

while $\hat{u}$, $\hat{s}$, and $\hat{v}$ at the wave front are evidently given by

$$\hat{u}_* \equiv \hat{u}(\rho, \lambda+) = \hat{u}(e^{\tau-}, \tau) = 0, \tag{80}$$

$$\hat{s}_* \equiv \hat{s}(\rho, \lambda+) = \hat{s}(e^{\tau-}, \tau) = 1, \tag{81}$$

$$\hat{v}_* \equiv \hat{v}(\rho, \lambda+) = \hat{v}(e^{\tau-}, \tau) = -1/\rho = -e^{-\tau}. \tag{82}$$

[9] See [7], p. 227, no. 5.

[10] See [7], p. 227, no. 5.

Equations (78), (79), (80), (81), (82) coincide with (64), (65), (68), (69), (70), if in the latter equations we proceed to the limit as $\alpha \to 2$ ($\beta \to 0$). This reflects the continuous transition from Case 1 to Case 2. For future reference, it is essential to notice from (81) that the peak values of the stress $\hat{s}$ at the front of the wave remain constant for $\alpha = 2$.

Lastly, we consider the limit of the present solution as $\tau \to \infty$. By (28), (71),

$$\lim_{\tau \to \infty} \hat{u}(\rho, \tau) = \lim_{p \to 0+} pU(\rho, p) = -\frac{1}{4\rho^2} \tag{83}$$[20]

whereas (75), in view of Watson's identity[21]

$$\int_0^\infty \frac{J_1(\xi)}{[\xi^2 + (2\lambda)^2]^{1/2}}\, d\xi = I_{1/2}(\lambda) K_{1/2}(\lambda), \tag{84}$$

implies

$$s(\rho, \tau) \to \rho^{-2} \quad \text{as} \quad \tau \to \infty. \tag{85}$$

Thus $\hat{u}$ and $\hat{s}$, in Case 2, again tend to the equilibrium values (24), (25) in the steady state.

Solution for Case 3

Here $\alpha > 2$ and $\beta < 0$, as announced in the classification (38). Consequently, the argument $p\rho^\beta \beta^{-1}$ of the modified Bessel functions I_n and K_n in (35) is negative for $p > 0$, so that neither function is real-valued in the present case; furthermore, in contrast to Case 1, the argument now tends to zero as $\rho \to \infty$. Since both $I_n(z)$ and $K_n(z)$ have (linearly independent) singularities at $z = 0$, the general solution (35) or (30) cannot be adapted to the regularity requirement (33) in Case 3; hence, (20) cannot hold; i.e., $\hat{s}(\rho, \tau)$ no longer tends to zero *at all times* as $\rho \to \infty$. This pathological behavior of the solution when $\alpha > 2$ is suggested already by the behavior of $\hat{s}(\rho, \tau)$ in the transition Case 2 ($\alpha = 2$), as manifest in (81).

Therefore we are compelled to abandon (33) and to relax (20) accordingly; the latter condition is now required to hold merely for a finite time interval following the start of the motion. This leaves us with the single boundary condition (32), which is insufficient to determine uniquely the values of both $A_1(p)$ and $A_2(p)$ in (35). One finds, however, that unless $A_1 = 0$, (35) fails to give rise to a diverging wave in the physical domain; on these grounds, the functions of the first kind are inadmissible in (35).

Setting A_1 equal to zero, and proceeding as in Case 1, we are formally led once again to the integral equations (47), (48), (49). Moreover, the kernel $\varphi(\tau)$ and the right-hand members $\psi_i(\rho, \tau)$ ($i = 1, 2, 3$), retain their previous definitions, given in (50), (52), (55), (58), and one arrives, as before, at the conclusions (63), (64), (65), (68), (69), (70).

We now show that the validity of the foregoing results, in Case 3, is confined to the time interval

$$0 < \tau < \tau_\infty, \quad \tau_\infty = -1/\beta > 0 \tag{86}$$

To this end, we note from (53) that

$$\hat{\delta} \to \tau_\infty \quad \text{as} \quad \rho \to \infty \tag{87}$$

Equivalently, (65), (36) imply (if $\alpha > 2$),

$$\int_1^\infty \frac{d\xi}{\hat{u}(\xi)} = \int_1^\infty \xi^{-\alpha/2} d\xi = -1/\beta = \tau_\infty, \tag{88}$$

while from (69), at present,

$$\hat{s}(\rho, \hat{\delta}+) \to \infty \quad \text{as} \quad \rho \to \infty \tag{89}$$

According to (88), in Case 3, the velocity of the wave front increases so rapidly as its radius grows, that the wave reaches infinity in the *finite* time τ_∞. Also, as is evident from (89), the value of the stress $\hat{s}$ at the front of the wave increases steadily and beyond bounds as the wave spreads to infinity; i.e., as $\tau \to \tau_\infty$. The motion, in the case under consideration, fails to approach the steady equilibrium state. Indeed, for $\tau > \tau_\infty$ the stresses at infinity have become unbounded and the foregoing results cease to be physically significant.

The solution of the integral equations characterizing $\hat{u}$, $\hat{s}$, and $\hat{v}$, for arbitrary values of α in the range $2 < \alpha < \infty$, may be accomplished by the same numerical scheme to which we referred in connection with Case 1. The functions $\varphi(\tau - \xi)$ and $\psi_i(\rho, \tau)$ ($i = 1, 2, 3$), appearing in (47), (48), (49), are found to be purely imaginary in Case 3, for the time-range (86). This observation is consistent with the real-valuedness of the physical unknowns.

A Class of Elementary Solutions in Closed Form

Let $\alpha \neq 2$ (Case 1 or Case 2), so that (39) represents the Laplace transform of the displacement $\hat{u}(\rho, \tau)$. Moreover, recall that when n is half an odd integer, i.e.,

$$n = k + 1/2 \quad (k = 0, \pm 1, \pm 2, \ldots), \tag{90}$$

the modified Bessel functions of the second kind degenerate into the elementary functions given by[22]

$$K_{k+1/2}(z) = \left(\frac{\pi}{2z}\right)^{1/2} e^{-z} \sum_{m=0}^{k} \frac{|k+m}{|m\,|k-m\,(2z)^m} \quad (k \geq 0), \tag{91}$$

$$K_{-n}(z) = K_n(z) \quad (n \text{ arbitrary}). \tag{92}$$

Thus, if n in (39) obeys (90), the determination of $\hat{u}(\rho, \tau)$ from $U(\rho, p)$ reduces to the determination of the inverse of a rational function and may be carried out in closed form, in terms of elementary functions. Consequently, also $\hat{s}(\rho, \tau)$ and $\hat{v}(\rho, \tau)$, which follow from $\hat{u}(\rho, \tau)$ by means of (23) and (29), admit similar representations.

In view of (90), (36), the infinite aggregate of elementary, closed solutions here referred to corresponds to the sequence of stiffness exponents,

$$\alpha = \frac{2(2k-1)}{3+2k} \quad (k = 0, \pm 1, \pm 2, \ldots) \tag{93}$$

For the convenience of the reader, we include Table 1 which displays the initial members of the sequence (93).

Table 1 Initial members of sequence (93)

k	0	1	−1	2	−2	3	−3	4	−4
α	−2/3	2/5	−6	6/7	10	10/9	14/3	14/11	18/5

As illustrative examples, we now present explicitly the closed solutions appropriate to $\alpha = -2/3$ and $\alpha = 10$, which belong to Case 1 and Case 3, respectively. Since the underlying computations are entirely elementary, the final results may be cited without intermediate detail.

Solution for $\alpha = -2/3$:

$$\left.\begin{aligned} \hat{u}(\rho, \tau) &= h(\tau - \hat{\delta})\, \frac{3}{4}\, \rho^{-1/3} \left\{ \exp\left[-\frac{4}{3}(\tau - \hat{\delta})\right] - 1 \right\}, \\ s(\rho, \tau) &= h(\tau - \hat{\delta}) \left\{ (\rho^{-2/3} - \rho^{-2}) \exp\left[-\frac{4}{3}(\tau - \hat{\delta})\right] + \rho^{-2} \right\}, \\ \hat{v}(\rho, \tau) &= -h(\tau - \hat{\delta}) \rho^{-1/3} \exp\left[-\frac{4}{3}(\tau - \hat{\delta})\right], \end{aligned}\right\} \tag{94}$$

[20] Note that the existence of the first limit is assumed.

[21] See [4], p. 435.

[22] See [4], p. 79 and p. 80.

where h, as before, is the Heaviside step function and

$$\delta = \frac{3}{4}\left(\rho^{\frac{4}{3}} - 1\right); \tag{95}$$

$$\hat{u}(\rho, \delta+) = 0, \quad \hat{s}(\rho, \delta+) = \rho^{-\frac{4}{3}}, \quad \hat{v}(\rho, \delta+) = -\rho^{-\frac{1}{3}}, \tag{96}$$

$$\hat{u}(\rho, \tau) \to -\frac{3}{4}\rho^{-\frac{1}{3}}, \quad \hat{s}(\rho, \tau) \to \rho^{-2} \quad \text{as} \quad \tau \to \infty. \tag{97}$$

Solution for $\alpha = 10$:

$$\left.\begin{aligned} \hat{u}(\rho, \tau) &= h(\tau - \delta)\,[2\rho(\tau - \delta)^2 - \rho^{-2}(\tau - \delta)\,], \\ \hat{s}(\rho, \tau) &= h(\tau - \delta)\rho^2, \\ \hat{v}(\rho, \tau) &= h(\tau - \delta)\,[4\rho(\tau - \delta) - \rho^{-2}], \end{aligned}\right\} \tag{98}$$

where

$$\delta = \frac{1}{4}\left(1 - \rho^{-4}\right); \tag{99}$$

$$\hat{u}(\rho, \delta+) = 0, \quad \hat{s}(\rho, \delta+) = \rho^2, \quad \hat{v}(\rho, \delta+) = -\rho^{-2}, \tag{100}$$

$$\delta \to 1/4 \quad \text{as} \quad \rho \to \infty, \tag{101}$$

and the solution is valid for $0 < \tau < 1/4$.

It is readily confirmed by substitution and inspection that the preceding two solutions indeed satisfy the governing field equations (16), (17), the initial conditions (18), the boundary condition (19), and the regularity requirement (20). One also may verify easily that both solutions satisfy the integral equations (47), (48), (49). Finally, the particular results just cited, evidently conform to the general conclusions reached earlier for Cases 1 and 3.

Numerical Results—Discussion

In this section we consider illustrative numerical results based on the foregoing solutions. For the sake of brevity, the discussion will be confined to the space and time dependence of the dimensionless shear stress $\hat{s}(\rho, \tau)$, corresponding to various choices of the stiffness exponent α in (1).

Figs. 1, 2 refer to $\alpha = -2/3$ and thus to a plate the shear modulus of which diminishes steadily with increasing distance from the axis of the hole. Fig. 1 displays $\hat{s}$ as a function of ρ for $\tau = 4, 8, 12$, together with the steady-state limit as $\tau \to \infty$; Fig. 2 exhibits the dependence upon τ of $\hat{s}$ for $\rho = 1, 4, 8, 12$. The graphs under consideration were obtained by evaluation of the elementary closed solution (94). The analogous results for the homogeneous medium ($\alpha = 0$), appearing in Figs. 2, 3, were taken from [1] and have been included here for purposes of comparison.[23]

The qualitative behavior of the stress distribution appropriate

[23] The authors are indebted to Professor J. N. Goodier and Dr. W. E. Jahsman for their permission to reproduce these two figures.

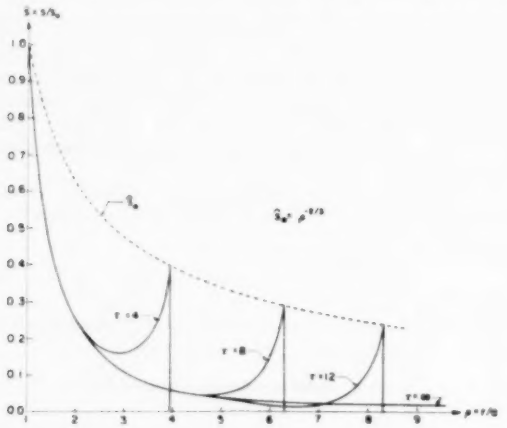

Fig. 1 $\alpha = -2/3$. Stress as a function of position at various times.

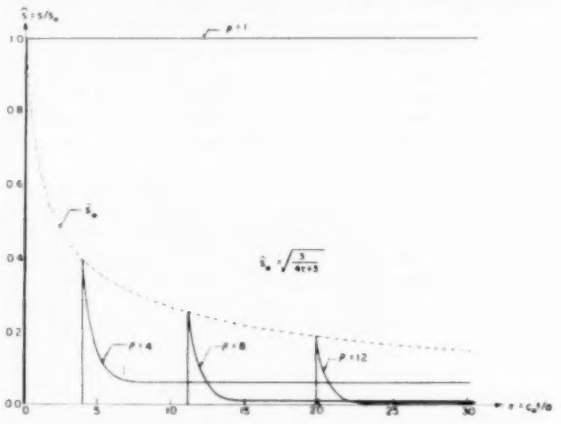

Fig. 2 $\alpha = -2/3$. Stress as a function of time at various positions.

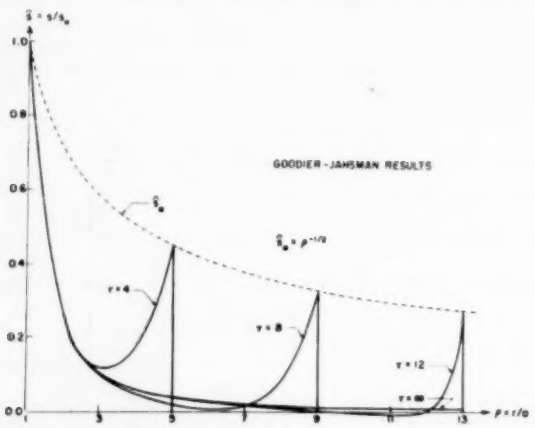

Fig. 3 $\alpha = 0$. Stress as a function of potision at various times.

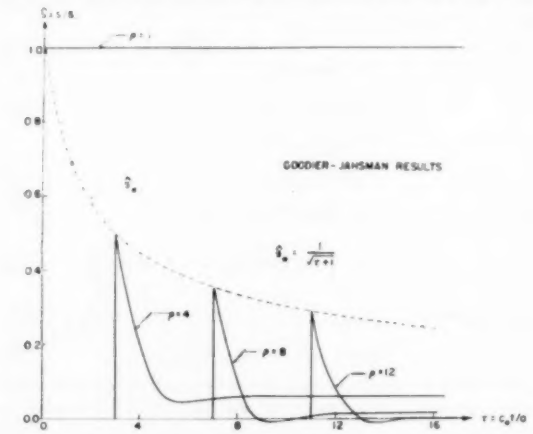

Fig. 4 $\alpha = 0$. Stress as a function of time at various positions.

to $\alpha = -2/3$ is quite similar to that characteristic of $\alpha = 0$. As seen from Fig. 1 and Fig. 3, for fixed finite τ, $\hat{s}(\rho, \tau)$ decreases sharply from its boundary value of unity and—at first following closely the steady-state curve—attains a minimum from which it rises to the peak-value $\hat{s}_*$ at the wave front. The material ahead of the wave front is unstressed. On the other hand, Fig. 2 and Fig. 4 indicate that for fixed $\rho\,(\rho > 1)$ the plate remains free from stress until the shock wave reaches the location in question. At that moment $\hat{s}$ instantaneously reaches the peak value $\hat{s}_*$ and thereafter declines almost monotonically (except for a slight dip) toward the respective steady-state asymptote. In accordance with the general formula (69), the peak-values $\hat{s}_*$—which lie on the dashed curves—decay more rapidly for $\alpha = -2/3$ than for $\alpha = 0$.

Fig. 5 corresponds to $\alpha = 1$; that is, to a plate whose shear modulus increases in direct proportion to ρ. The curves shown here, which depict $\hat{s}$ as a function of τ for $\rho = 4, 8, 12$, are based on the numerical solution of the integral equation (48). In com-

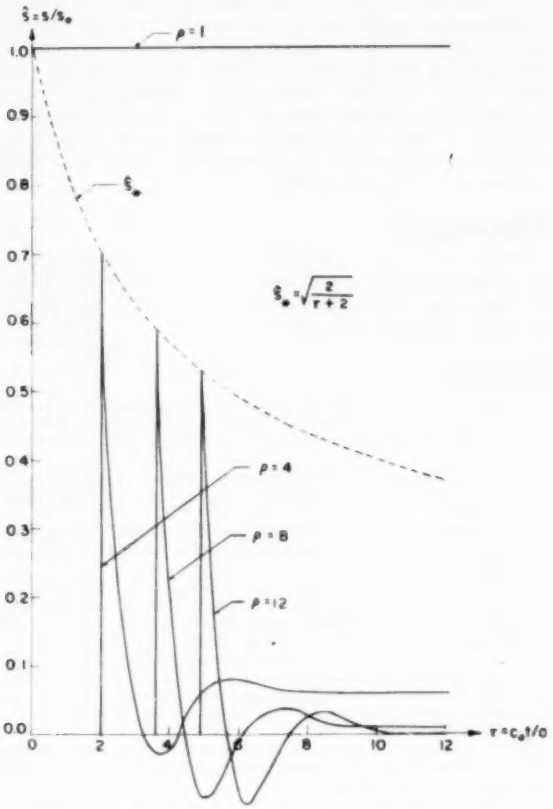

Fig. 5 $\alpha = 1$. Stress as a function of time at various positions.

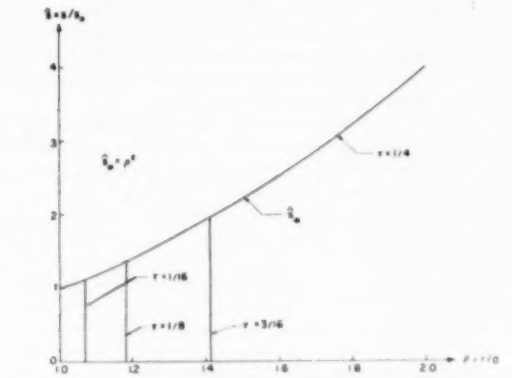

Fig. 7 $\alpha = 10$. Stress as a function of position at various times.

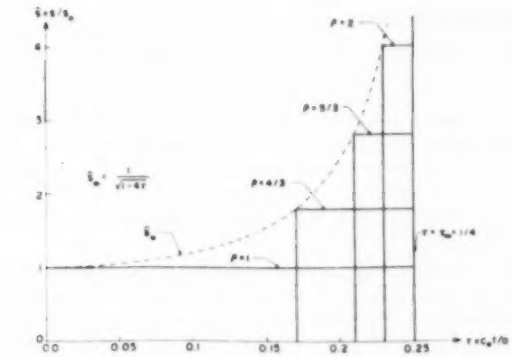

Fig. 8 $\alpha = 10$. Stress as a function of time at various positions.

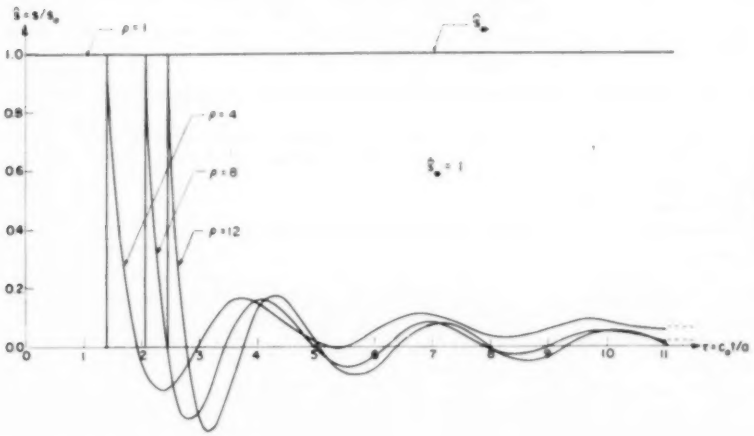

Fig. 6 $\alpha = 2$. Stress as a function of time at various positions.

paring these curves with their counterparts in Fig. 2 and Fig. 4, we observe notably that $\hat{s}$ now undergoes one pronounced oscillation before asymptotically approaching the appropriate steady-state value.

All of the graphs discussed so far are illustrative of Case 1 ($\alpha < 2$). In contrast, Fig. 6 describes Case 2 ($\alpha = 2$). The numerical results underlying this figure are analogous to those appearing in Figs. 2, 4, and were reached from the integral representation (75). This necessitated the numerical evaluation of the definite integral in (75), which was carried out with the aid of an IBM 650 electronic computer. We observe that in the present transition case the peak values $\hat{s}_*$ remain constant, as predicted by (81). Furthermore, the stress at a fixed interior point, after an initial drop, now oscillates *indefinitely* (with decreasing amplitude) about its steady-state equilibrium value.

Case 3 ($\alpha > 2$) is exemplified by Figs. 7, 8 which belong to $\alpha = 10$. The corresponding closed elementary solution (98) happens to be severely degenerate. Fig. 7 shows the variation with ρ of the shear stress at times $\tau = 1/16, 1/8, 3/16$, and $1/4$. The portions of these curves which lie behind the wavefront overlap and all lie on the limiting parabola $\hat{s} = \rho^2$, which is fully realized at $\tau = \tau_\infty = 1/4$. As pointed out in the general discussion of Case 3, for $\tau \geq \tau_\infty$ the front of the wave has reached infinity and the stresses have become unbounded, whence the validity of the solution is confined to the finite time interval $0 \leq \tau < \tau_\infty$. Fig. 8 indicates the response, as far as $\hat{s}$ is concerned, at various positions in the plate. Evidently, this response, in the particular example under consideration, is a step function of time at any fixed point of the body.

Concluding Remarks

The investigation presented in this paper admits certain generalizations, and extensions to related problems, which it may be useful to mention. Specifically, the restriction to a constant mass density can be relaxed at the expense of merely trivial complications. Suppose not only the shear modulus μ but also the density γ, obeys a power law; i.e.,

$$\gamma = \gamma_0 \left(\frac{r}{a}\right)^\kappa \quad \left(\kappa \gtrless 0\right) \tag{102}$$

In this event, γ in (10) needs to be replaced by γ_0. The governing field equations (16), (17) then remain unaltered, except that the exponent α in the right-hand member of (16) now becomes $\alpha - \kappa$. Clearly, the succeeding developments remain applicable with only minor modifications.

Next, suppose that instead of the boundary condition (6), which corresponds to a suddenly rising shear load, we have

$$\left[\frac{\partial u}{\partial t}\right]_{(a,\,t)} = h(t)v_0, \tag{103}$$

which represents a suddenly imposed tangential velocity of the boundary. This more elementary problem, which Goodier and Jahsman [1] solved for the homogeneous medium, permits a strictly analogous treatment.

Similarly, the generalized plane stress solutions, due to Kromm [3], of the companion problems in which the cylindrical boundary is subjected to a *radial* pressure (or a radial velocity), are tractable by the present means if $\mu(r)$ and $\gamma(r)$ are again given by power laws, *provided Poisson's ratio is constant*. Finally, the same applies—under analogous inhomogeneity assumptions—to the problem of the infinite medium with a *spherical cavity*, the boundary of which is subjected to a sudden radial pressure (or velocity). This problem, for a homogeneous body, was apparently solved first by Jeffreys [8].[24]

Acknowledgment

The authors are indebted to Mr. J. J. Kalker, Research Associate in the Division of Applied Mathematics at Brown University, who supervised those numerical computations which were carried out on the IBM 650 electronic computer.

References

1 J. N. Goodier and W. E. Jahsman, "Propagation of a Sudden Rotary Disturbance in an Elastic Plate in Plane Stress," JOURNAL OF APPLIED MECHANICS, vol. 23, TRANS. ASME, vol. 78, 1956, p. 284.

2 W. A. Ewing, W. S. Jardetzky, and F. Press, "Elastic Waves in Layered Media," McGraw-Hill Book Company, Inc., New York, N. Y., 1957.

3 A. Kromm, "Zur Ausbreitung von Stosswellen in Kreislochscheiben," *Zeitschrift für angewandte Mathematik und Mechanik*, vol. 28, 1948, pp. 104 and 297.

4 G. N. Watson, "Treatise on the Theory of Bessel Functions," The Macmillan Company, New York, N. Y., second edition, 1945.

5 G. Doetsch, "Tabellen zur Laplace-Transformation und Anleitung zum Gebrauch," Springer, Berlin, Germany, 1947.

6 R. V. Churchill, "Modern Operational Mathematics in Engineering," McGraw-Hill Book Company, Inc., New York, N. Y., 1944.

7 Staff of the Bateman Manuscript Project, A. Erdélyi, Editor, "Tables of Integral Transforms," vol. 1, McGraw-Hill Book Company, Inc., New York, N. Y., 1954.

8 H. Jeffreys, "On the Cause of Oscillatory Movement in Seismograms," *Monthly Notices*, Royal Astronautical Society, Geophysical Supplement, vol. 2, 1931, p. 410.

[24] Jeffrey's solution, which is in closed form, has since been rediscovered by various subsequent authors.

R. F. S. HEARMON

Officer in Charge,
Physics Section,
Forest Products Research Laboratory,
Princes Risborough,
Aylesbury, Bucks, England

The Frequency of Flexural Vibration of Rectangular Orthotropic Plates With Clamped or Supported Edges

The Rayleigh method, using characteristic beam functions appropriate to the boundary conditions, is applied to derive closed formulas for the frequencies of vibration of orthotropic plates under any combination of clamped or supported edges.

Theory

WARBURTON [1][1] has derived approximate expressions for the frequencies of all the modes of vibration of isotropic plates subjected to any combination of free, supported, or clamped edges. He applied the Rayleigh method, assuming that the deflections of the plates could be represented by suitable characteristic functions satisfying the boundary conditions [1, 2], and that the nodal lines were approximately parallel to the sides of the plates.

In the present paper, Warburton's treatment is extended to the "specially orthotropic" plate with any of its edges either clamped or supported; i.e., to a plate made of a material possessing three mutually perpendicular axes of elastic symmetry, two of which lie in the plane of the plate parallel to the respective sides, Fig. 1. The third symmetry axis is normal to the other two and is therefore perpendicular to the plane of the plate. The thickness of the plate and its deflection are assumed small; under these conditions, a two-dimensional treatment applies, and the elastic properties in the third symmetry direction do not enter into the problem.

[1] Numbers in brackets designate References at end of paper.

Presented at the Summer Conference of the Applied Mechanics Division, Troy, N. Y., June 18–20, 1959, of THE AMERICAN SOCIETY OF MECHANICAL ENGINEERS.

Discussion of this paper should be addressed to the Secretary, ASME, 29 West 39th Street, New York, N. Y., and will be accepted until January 10, 1960, for publication at a later date. Discussion received after the closing date will be returned.

NOTE: Statements and opinions advanced in papers are to be understood as individual expressions of their authors and not those of the Society. Manuscript received by ASME Applied Mechanics Division, June 12, 1958. Paper No. 59—APM-8.

It is possible to extend Warburton's treatment to orthotropic plates with free edges, but free edges are not discussed in the present paper, partly because the characteristic functions only satisfy the boundary conditions approximately for a free edge [1], and partly because inclusion of free edges would somewhat complicate the derivation and presentation of the results.

Warburton expresses the deflection w of a point (x, y) on the plate as a function of time and position by the equation

$$w = W \sin \omega t = K\theta(x)\phi(y) \sin \omega t, \tag{1}$$

where K is a constant and $\theta(x)$, $\phi(y)$ are functions which satisfy the boundary conditions.

Appropriate functions are

(a) Simply supported at $x = 0$, $x = a$:

$$\theta(x) = \sin \frac{(m-1)\pi x}{a} = \sin \frac{\gamma_0 x}{a}, \tag{2}$$

where $\gamma_0 = (m-1)\pi$ for all values of $m (m \geq 2)$.

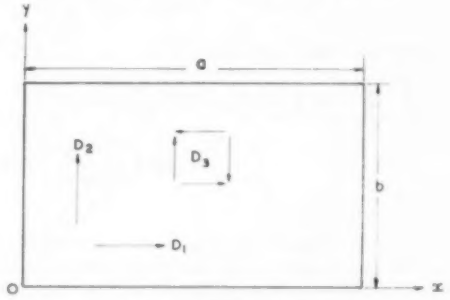

Fig. 1 Diagram of plate

Nomenclature

a = length of side of plate parallel to Ox, Fig. 1
b = length of side of plate parallel to Oy, Fig. 1
$D_1 = E_1h^3/12\mu$
$D_2 = E_2h^3/12\mu$
$D_3 = D_4 + 2D_5$
$D_4 = E_1\nu_{21}h^3/12\mu$
$D_5 = G_{12}h^3/12$
} flexural and torsional rigidities of plate
E_1 = Young's modulus in bending in Ox-direction
E_2 = Young's modulus in bending in Oy-direction
G_{12} = rigidity modulus for shear stresses in Ox and Oy-directions
h = plate thickness
m = number of nodal lines, including edges, perpendicular to Ox $(m \geq 2)$
n = number of nodal lines, including edges, perpendicular to Oy $(n \geq 2)$
t = time
T = maximum kinetic energy
V = maximum potential energy
w = transverse displacement of a point on plate
$\mu = 1 - \nu_{21}\nu_{12}$
ρ = density of plate material (mass per unit volume)
ν_{21} = Poisson's ratio corresponding with compressive strain in Ox-direction, extensional strain in Oy-direction for tension in Oy-direction
ω = circular frequency ($= 2\pi \times$ frequency)

Other symbols are defined in the text as they occur.

(*b*) Clamped at $x = 0$, supported at $x = a$:

$$\theta(x) = \cosh\frac{\gamma_1 x}{a} - \cos\frac{\gamma_1 x}{a} - \alpha_1\left(\sinh\frac{\gamma_1 x}{a} - \sin\frac{\gamma_1 x}{a}\right), \quad (3)$$

where to sufficient accuracy, $\alpha_1 = 1$, and $\gamma_1 = (m - {}^1/_4)\pi$ for all values of $m(m \geqslant 2)$.

(*c*) Clamped at $x = 0$, $x = a$:

$$\theta(x) = \cosh\frac{\gamma_2 x}{a} - \cos\frac{\gamma_2 x}{a} - \alpha_2\left(\sinh\frac{\gamma_2 x}{a} - \sin\frac{\gamma_2 x}{a}\right), \quad (4)$$

where $\alpha_2 = 0.982$, $\gamma_2 = 4.730$ for $m = 2$, and to sufficient accuracy $\alpha_2 = 1$, $\gamma_2 = (m - {}^1/_2)\pi$ for all other values of $m(m \geqslant 3)$.

Equations (3) and (4) are in the form used by Young and Felgar [2], with the notation slightly modified.

Analogous expressions hold for $\phi(y)$; for instance, if the plate is clamped at $y = 0$ and supported at $y = b$,

$$\phi(y) = \cosh\frac{\epsilon_1 y}{b} - \cos\frac{\epsilon_1 y}{b} - \sinh\frac{\epsilon_1 y}{b} + \sin\frac{\epsilon_1 y}{b}, \quad (5)$$

where $\epsilon_1 = (n - {}^1/_4)\pi$ for all values of $n(n \geqslant 2)$.

The maximum potential energy of bending corresponds with $\sin^2\omega t = 1$ and is [3, 4]

$$V = \frac{1}{2}\int_0^a\int_0^b\left[D_1\left(\frac{\partial^2 W}{\partial x^2}\right)^2 + D_2\left(\frac{\partial^2 W}{\partial y^2}\right)^2 + 2D_4\frac{\partial^2 W}{\partial x^2}\frac{\partial^2 W}{\partial y^2} + 4D_5\left(\frac{\partial^2 W}{\partial x\partial y}\right)^2\right]dxdy, \quad (6)$$

where the D are the principal rigidities (see Nomenclature). For supported and clamped edges, W is always zero at the edges, and [5]

$$\int_0^a\int_0^b\left[\frac{\partial^2 W}{\partial x^2}\frac{\partial^2 W}{\partial y^2} - \left(\frac{\partial^2 W}{\partial x\partial y}\right)^2\right]dxdy = 0.$$

Thus Equation (6) can be simplified to

$$V = \frac{1}{2}\int_0^a\int_0^b\left[D_1\left(\frac{\partial^2 W}{\partial x^2}\right)^2 + D_2\left(\frac{\partial^2 W}{\partial y^2}\right)^2 + 2D_4\left(\frac{\partial^2 W}{\partial x\partial y}\right)^2\right]dxdy, \quad (7)$$

where $D_4 = D_4 + 2D_5$.

In an isotropic material, $D_1 = D_2 = D_4$ and Equation (7) reduces to the known equation for the strain energy of a bent isotropic plate subject to the condition $W = 0$ at all points along the edges.

The maximum kinetic energy corresponds with $\cos^2\omega t = 1$ and

$$T = \frac{\rho h\omega^2}{2}\int_0^a\int_0^b W^2 dxdy. \quad (8)$$

Thus equating maximum kinetic and potential energies from (7) and (8)

$$\rho h\omega^2 = \frac{\int_0^a\int_0^b\left[D_1\left(\frac{\partial^2 W}{\partial x^2}\right)^2 + D_2\left(\frac{\partial^2 W}{\partial y^2}\right)^2 + 2D_3\left(\frac{\partial^2 W}{\partial x\partial y}\right)^2\right]dxdy}{\int_0^a\int_0^b W^2 dxdy}, \quad (9)$$

and the frequencies are obtained by substituting the expression for W appropriate to the boundary conditions, Equations (1) to (5), in Equation (9). The definite integrals can be evaluated by standard methods, or simply by referring to the list prepared by Felgar [6]. It is then found that the equations for the frequencies can be put in the general form

$$\rho h\omega^2 = \frac{A^4 D_1}{a^4} + \frac{B^4 D_2}{b^4} + \frac{2CD_3}{a^2 b^2}. \quad (10)$$

and the values of A, B, and C for any combination of clamped (c) and supported (s) edges, and for any values of m and n, are set out in Table 1; the equation for a plate with all edges supported (Case 6) coincides with the known exact solution [4].

Table 1 Frequency equations

$$\rho h\omega^2 = \frac{A^4 D_1}{a^4} + \frac{B^4 D_2}{b^4} + \frac{2C D_3}{a^2 b^2}$$

$\gamma_0 = (m-1)\pi$ $\quad \gamma_1 = (m-\frac{3}{4})\pi$ $\quad \gamma_2 = (m-\frac{1}{2})\pi$

$\epsilon_0 = (n-1)\pi$ $\quad \epsilon_1 = (n-\frac{3}{4})\pi$ $\quad \epsilon_2 = (n-\frac{1}{2})\pi$

s = Supported Edge $\quad$ c = Clamped Edge

Boundary Conditions	A	B	C	m	n
1	4·730	4·730	151·3	2	2
	4·730	ϵ_2	$12{\cdot}30\epsilon_2(\epsilon_2-2)$	2	3,4,5,· ·
	γ_2	4·730	$12{\cdot}30\gamma_2(\gamma_2-2)$	3,4,5,· ·	2
	γ_2	ϵ_2	$\gamma_2\epsilon_2(\gamma_2-2)(\epsilon_2-2)$	3,4,5,· ·	3,4,5,· ·
2	4·730	ϵ_1	$12{\cdot}30\epsilon_1(\epsilon_1-1)$	2,3,4,· ·	2
	γ_2	ϵ_1	$\gamma_2\epsilon_1(\gamma_2-2)(\epsilon_1-1)$	2,3,4,· ·	3,4,5,· ·
3	4·730	ϵ_0	$12{\cdot}30\epsilon_0^2$	2	2,3,4,· ·
	γ_2	ϵ_0	$\gamma_2\epsilon_0^2(\gamma_2-2)$	3,4,5,· ·	2,3,4,· ·
4	γ_1	ϵ_1	$\gamma_1\epsilon_1(\gamma_1-1)(\epsilon_1-1)$	2,3,4,· ·	2,3,4,· ·
5	γ_1	ϵ_0	$\gamma_1\epsilon_0^2(\gamma_1-1)$	2,3,4,· ·	2,3,4,· ·
6	γ_0	ϵ_0	$\gamma_0^2\epsilon_0^2$	2,3,4,· ·	2,3,4,· ·

Discussion

For the fundamental mode of a plate with all edges clamped ($m = n = 2$), Equation (10) becomes

$$\rho h\omega^2 = 501\left(\frac{D_1}{a^4} + \frac{D_2}{b^4} + \frac{0.605D_3}{a^2b^2}\right). \quad (11)$$

A previous investigation of this case [7], assuming

$$w = Kx^2y^2(a-x)^2(b-y)^2\sin\omega t$$

gave

$$\rho h\omega^2 = 504\left(\frac{D_1}{a^4} + \frac{D_2}{b^4} + \frac{0.571D_3}{a^2b^2}\right). \quad (12)$$

Table 2 Values of λ^2

Case number	1	2	3	4	5	6
λ^2 Equation (13)	41.01	37.56	35.41	20.72	18.60	9.375
λ^2 Huffington	...	...	35.40	...	18.59	9.375

Table 3 Values of λ^2 and d. Fundamental mode of square plates.

$D_1/D_3 \rightarrow$	1/3		3		1/3		3	
	Case 1				Case 2			
$D_2/D_3 \downarrow$	λ^2	d	λ^2	d	λ^2	d	λ^2	d
1/3	6.53	+1.5	20.24	−1.9	5.43	+1.3	19.13	−2.2
3	20.24	−1.9	33.94	−2.7	11.94	−2.9	25.64	−3.5
	Case 3				Case 4			
1/3	4.54	−0.2	18.24	−2.5	4.34	+1.3	10.85	−3.3
3	7.21	−0.8	20.91	−2.5	10.85	−3.3	17.36	−5.0

Equation (12) also was obtained independently by Lekhnitskiĭ [4]; the agreement between Equations (11) and (12) is satisfactory.

Huffington and Hoppmann [8] have given the transcendental frequency equations for a number of cases in which two opposite sides are supported, and Huffington [9] has supplied the results of numerical computations based on the solutions of these equations, for a plate of maple 5-ply wood having, in the present conventions,

$$a/b = 1/2, \quad D_2/D_3 = 4.810, \quad D_1/D_3 = 1.543.$$

In order to compare Huffington's results with those obtained from Equation (10) in conjunction with Table 1, it is convenient to introduce the quantity λ^2 where

$$\lambda^2 = \rho h \omega^2 a^2 b^2 / \pi^4 D_3,$$

or, substituting for $\rho h \omega^2$ from Equation (10):

$$\lambda^2 = \frac{1}{\pi^4}\left(\frac{A^1 b^2 D_1}{a^2 D_3} + \frac{B^1 a^2 D_2}{b^2 D_3} + 2C\right). \qquad (13)$$

Values of λ^2, calculated from (13) for all six cases represented in Table 1, are given in Table 2, and compared with Huffington's values (suitably converted) for the three cases having opposite edges supported.

In spite of the approximate nature of the Rayleigh method, the values obtained are in close agreement with Huffington's; in Case 6 (all edges supported), both methods lead to the exact solution.

The fundamental frequencies of vibration of square orthotropic plates have been calculated for various boundary conditions by Kanazawa and Kawai [10]. They do not obtain closed formulas for the frequencies, but describe a method of successive approximations which appears to involve rather troublesome calculations in each individual case. They tabulate the first approximation to λ^2 for the boundary conditions 1, 2, 3, 4, and for D_1/D_3, D_2/D_3 equal to 1/3, 1/2, 1, 2, 3. All their calculations have been checked using Equation (13) and Table 1, but it is sufficient for comparative purposes to quote the values corresponding to D_1/D_3, D_2/D_3 equal to 1/3 and 3. The values of λ^2 in Table 3 are those obtained from Equation (13), and d is the percentage difference between these values and those of Kanazawa and Kawai (positive values of d mean that the estimate from Equation (13) is the greater).

Kanazawa and Kawai appear to have tabulated the values of λ^2 corresponding to Cases 3 and 4 against the wrong boundary conditions, and this error was corrected before the comparisons leading to the values of d, Table 3, were made. Examination of Table 3 shows that the differences tend to be positive by about 1 per cent for the lowest values of D_1/D_3 and D_2/D_3, and negative by 2 to 5 per cent for the highest values of D_1/D_3 and D_2/D_3. As is well known, the Rayleigh method yields frequencies which are too high, and the estimates of Kanazawa and Kawai are therefore slightly better than those from Equation (13) at low D_1/D_3, D_2/D_3, whereas at high D_1/D_3, D_2/D_3 the reverse is true. Values of D_1/D_3, D_2/D_3 both less than unity are, however, unrealistic because, in approximate terms, they would involve the shear modulus of the material being higher than both the Young's moduli.

Gumenyuk [12] has published closed formulas, obtained by a finite-difference method, for the flexural frequencies of orthotropic plates under the boundary conditions 1–6, Table 1. His equations corresponding to Cases 2 and 5 cannot be put into the same form as Equation (10), but on converting the remainder, it appears that Gumenyuk's values of A and B are generally lower than those obtained here, whereas the values of C are generally higher. It is not possible to comment further on these results, since details of the derivations are not given in the paper so far seen [12].

As a final illustration of the use of Equation (13), values of λ for plywood plates having $D_2/D_3 = 4.810$, $D_1/D_3 = 1.543$ have been

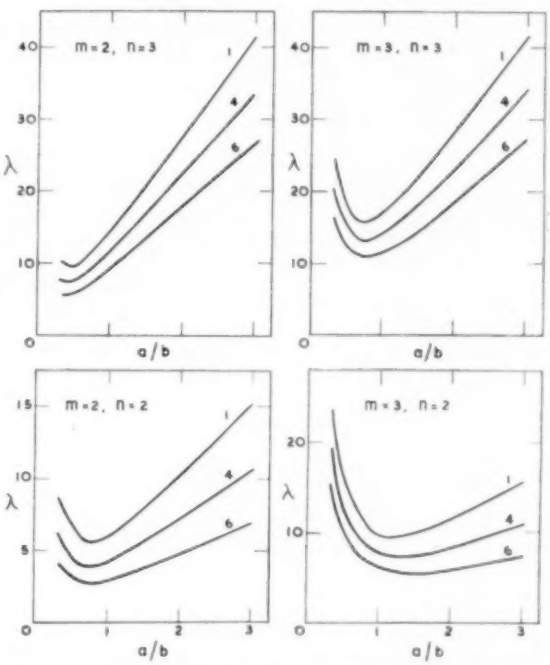

Fig. 2 Values of λ as affected by boundary conditions and ratio a/b maple 5-ply; $D_1/D_3 = 1.543$, $D_2/D_3 = 4.810$

calculated for various ratios a/b up to 3, for $m = n = 2$; $m = 2$, $n = 3$; $m = 3$, $n = 2$; $m = n = 3$; and for the boundary conditions 1, 4, and 6. The results are plotted in Fig. 2. In practice, the frequencies will be influenced by the occurrence of shear and rotatory inertia effects [11], which are ignored in deriving Equation (10), and, in addition, the assumed boundary conditions can seldom be realized exactly in experimental work [7]. Nevertheless, the curves of Fig. 2 should show approximately the trend in frequency with change in boundary conditions, shape of plate, and order of mode, and owing to the closed nature of Equation (10) the calculations could be extended to plates with other dimensions, boundary conditions, and elastic properties if such information were required.

The estimates of the frequencies can be improved by applying the Ritz modification of the Rayleigh method. The labor involved, however, would be considerable; moreover, previous experience with the Rayleigh-Ritz procedure [7] suggests that it would not yield simple closed formulas, and that the gain in accuracy would be slight. For these reasons, no attempt has been made to apply the Ritz method to the present problem.

Acknowledgment

The work described in the paper was carried out as part of the program of the Forest Products Research Board, and is published by permission of the Department of Scientific and Industrial Research.

References

1 G. B. Warburton, "The Vibration of Rectangular Plates," *Proceedings of The Institution of Mechanical Engineers*, vol. 168, 1954, pp. 371–384.

2 D. Young and R. P. Felgar, Jr., "Tables of Characteristic Functions Representing Normal Modes of Vibration of a Beam," The University of Texas Publication, No. 4913, Bureau of Engineering Research, Engineering Research Series, No. 44, 1949.

3 H. W. March, "Flat Plates of Plywood Under Uniform or Concentrated Loads," United States Department of Agriculture, Forest Products Laboratory, Report No. 1312, March, 1942.

4 S. G. Lekhnitskiĭ, "Anizotropnye Plastinki," *Gos. Izd. Tekh-Teoret. Lit.*, Moscow-Leningrad, 2nd edition, 1957.

5 D. M. A. Leggett, "The Buckling of a Square Panel Under Shear When One Pair of Edges is Clamped, and the Other Pair is Simply Supported," Aeronautical Research Council Reports and Memoranda No. 1991, 1941.

6 R. P. Felgar, Jr., "Formulas for Integrals Containing Characteristic Functions of a Vibrating Beam," The University of Texas, Bureau of Engineering Research, Circular No. 14, 1950.

7 R. F. S. Hearmon, "The Fundamental Frequency of Vibration of Rectangular Wood and Plywood Plates," *Proceedings of the Physical Society of London*, vol. 58, 1946, pp. 78–92.

8 N. J. Huffington, Jr., and W. H. Hoppmann II, "On the Transverse Vibrations of Rectangular Orthotropic Plates," JOURNAL OF APPLIED MECHANICS, vol. 25, TRANS. ASME, vol. 80, 1958, pp. 389–395.

9 N. J. Huffington, Jr., Private communication, January 20, 1958.

10 T. Kanazawa and T. Kawai, "On the Lateral Vibration of Anisotropic Rectangular Plates (Studied by Integral Equation)," *Proceedings of the Second Japan National Congress for Applied Mechanics*, 1952, pp. 333–338.

11 R. D. Mindlin, A. Schacknow, and H. Deresiewicz, "Flexural Vibrations of Rectangular Plates," JOURNAL OF APPLIED MECHANICS, vol. 23, TRANS. ASME, vol. 78, 1956, pp. 430–436.

12 V. S. Gumenyuk, "Determination of the Lowest (Fundamental) Frequency of Free Vibration of Orthotropic Plates," *Prikladnaya Mekhanika, Akad. Nauk Ukrainskoĭ R. S. R.*, vol. 2, 1956, pp. 224–226.

O. G. GUSTAFSSON
Research Engineer,
SKF Industries, Inc.
Philadelphia, Pa.

T. R. KANE
Associate Professor
of Mechanical Engineering,
University of Pennsylvania,
Philadelphia, Pa.
Mem. ASME

Axially Symmetric Extensional Vibrations of a Circular Disk With a Concentric Hole[1]

In a paper by T. R. Kane and R. D. Mindlin,[2] a two-dimensional theory was developed for high-frequency extensional vibrations of elastic, isotropic plates. This theory is now used to study vibrations of a circular disk with a concentric hole.

LOW-FREQUENCY extensional vibrations of a thin plate can be described satisfactorily by the equations of the theory of generalized plane stress. In order to deal with low-frequency vibrations of thick plates or with high-frequency vibrations of thin plates, it is necessary to use equations which make adequate provision for the phenomenon of coupling between extensional and thickness modes of motion. Such equations have been presented.[2] In the present paper they are used to study axially symmetric, extensional vibrations of a circular disk with a concentric hole.

First a résumé of the relevant equations of the plate theory is given. This is followed by the derivation of a frequency equation, a number of limiting cases of which are presented. Finally, the manner in which the frequency spectrum may be computed is described.

Plate Displacements, Stresses, and Equations of Motion

Letting r, θ, z be cylindrical co-ordinates, and considering only motions symmetrical with respect to the z-axis, the components of displacement u_r, u_θ, u_z in a plate bounded by the planes $z = \pm h$ are assumed to be given to sufficient approximation by[2]

$$u_r = v_r(r, t)$$

$$u_\theta = 0$$

$$u_z = zh^{-1}v_z(r, t)$$

In the case of free vibrations of circular frequency ω, v_r, and v_z may be expressed in terms of two independent displacement potentials, $\phi_1(r)$ and $\phi_2(r)$,

$$v_r = \frac{\partial\phi_1}{\partial r} + \frac{\partial\phi_2}{\partial r} \qquad (1)$$

$$v_z = \sigma_1\phi_1 + \sigma_2\phi_2$$

These potentials are governed by the equations of motion

$$\left(\frac{d^2}{dr^2} + \frac{1}{r}\frac{d}{dr} + \delta_i^2\right)\phi_i = 0, \quad i = 1, 2 \qquad (2)$$

Boundary conditions, sufficient to insure a unique solution, are obtained by specifying, on the edge of the plate, the plate stresses, defined as

$$N_r = \int_{-h}^{h} \sigma_r dz$$

$$N_{r\theta} = \int_{-h}^{h} \tau_{r\theta} dz$$

$$R_r = \int_{-h}^{h} \tau_{rz} z dz$$

These are related to the displacements v_r and v_z by

$$N_r = 2h\left[(\lambda + 2G)\frac{dv_r}{dr} + \lambda\frac{v_r}{r} + \kappa\lambda\frac{v_z}{h}\right]$$

$$N_{r\theta} = 0 \qquad (3)$$

$$R_r = \frac{2Gh^2}{3}\frac{dv_z}{dr}$$

In the foregoing equations

$$\sigma_i = \frac{h(\lambda + G)}{\kappa\lambda}\left(\delta_i^2 - \frac{\omega^2}{c_1}\right), \quad i = 1, 2 \qquad (4)$$

$$\delta_i^2 = \frac{3\kappa^2}{2\beta h^2}\left[(\alpha + \beta)\frac{\omega^2}{\tilde{\omega}^2} - 1 - (-1)^i\psi\right], \quad i = 1, 2 \qquad (5)$$

$$\psi = \left\{\left[(\alpha + \beta)\frac{\omega^2}{\tilde{\omega}^2} - 1\right]^2 + 4\alpha\beta\frac{\omega^2}{\tilde{\omega}^2}\left(1 - \frac{\omega^2}{\tilde{\omega}^2}\right)\right\}^{1/2} \qquad (6)$$

$$\alpha = c_1^2/c_2^2, \quad \beta = c_2^2/c_3^2 \qquad (7)$$

$$c_1^2 = (\lambda + 2G)/\rho, \quad c_2^2 = G/\rho, \quad c_3^2 = \frac{4G(\lambda + G)}{\rho(\lambda + 2G)} \qquad (8)$$

$$\tilde{\omega}^2 = \frac{\pi^2(\lambda + 2G)}{4h^2\rho} \qquad (9)$$

$$\kappa^2 = \pi^2/12 \qquad (10)$$

λ and G are Lame's constants of elasticity; ρ is the mass density of the plate material; α and β are dimensionless constants which depend only on the value of Poisson's ratio ν; $\tilde{\omega}$ is the frequency corresponding to the first mode of pure thickness vibration of an infinite plate.

---

[1] A thesis, presented to the Faculty of the School of Mechanical Engineering of The University of Pennsylvania in partial fulfillment of the requirements for the degree of Master of Science.

[2] T. R. Kane and R. D. Mindlin, "High-Frequency Extensional Vibrations of Plates," JOURNAL OF APPLIED MECHANICS, vol. 23, TRANS. ASME, vol. 78, 1956, pp. 277–283.

Contributed by the Applied Mechanics Division and presented at the Annual Meeting, Atlantic City, N. J., November 29–December 4, 1959, of THE AMERICAN SOCIETY OF MECHANICAL ENGINEERS.

Discussion of this paper should be addressed to the Secretary, ASME, 29 West 39th Street, New York, N. Y., and will be accepted until January 10, 1960, for publication at a later date. Discussion received after the closing date will be returned.

NOTE: Statements and opinions advanced in papers are to be understood as individual expressions of their authors and not those of the Society. Manuscript received by ASME Applied Mechanics Division, June 16, 1958. Paper No. 59—A-32.

Solution of Equations of Motion

For a circular disk of radius a, with a concentric hole of radius b, the solutions of Equations (2) are

$$\phi_1 = A_1 J_0(\delta_1 r) + B_1 Y_0(\delta_1 r)$$
$$\phi_2 = A_2 J_0(\delta_2 r) + B_2 Y_0(\delta_2 r)$$

where J_0 and Y_0 are Bessel functions of the first and second kind, and A_1, A_2, B_1, B_2 are constants. Hence from Equations (1),

$$v_r = -A_1\delta_1 J_1(\delta_1 r) - B_1\delta_1 Y_1(\delta_1 r) - A_2\delta_2 J_1(\delta_2 r) - B_2\delta_2 Y_1(\delta_2 r)$$
$$v_z = A_1\sigma_1 J_0(\delta_1 r) + B_1\sigma_1 Y_0(\delta_1 r) + A_2\sigma_2 J_0(\delta_2 r) + B_2\sigma_2 Y_0(\delta_2 r)$$

Traction-free edges at $r = a$ and $r = b$ are obtained by setting the components of stress given in Equations (3) equal to zero at $r = a$ and $r = b$. This results in the following four simultaneous, homogeneous equations in A_1, A_2, B_1, B_2:

$$\begin{aligned} C_1A_1 + C_2A_2 + C_3B_1 + C_4B_2 &= 0 \\ C_5A_1 + C_6A_2 + C_7B_1 + C_8B_2 &= 0 \\ C_9A_1 + C_{10}A_2 + C_{11}B_1 + C_{12}B_2 &= 0 \\ C_{13}A_1 + C_{14}A_2 + C_{15}B_1 + C_{16}B_2 &= 0 \end{aligned} \tag{11}$$

where

$$C_1 = J_1(\gamma) - \frac{\alpha\eta\gamma}{\beta} J_0(\gamma)$$

$$C_2 = J_1(\xi\gamma) - \frac{\alpha\eta\gamma}{\beta\xi} J_0(\xi\gamma)$$

$$C_3 = Y_1(\gamma) - \frac{\alpha\eta\gamma}{\beta} Y_0(\gamma)$$

$$C_4 = Y_1(\xi\gamma) - \frac{\alpha\eta\gamma}{\beta\xi} Y_0(\xi\gamma)$$

$$C_5 = J_1(\zeta\gamma) - \frac{\alpha\eta\zeta\gamma}{\beta} J_0(\zeta\gamma)$$

$$C_6 = J_1(\zeta\xi\gamma) - \frac{\alpha\eta\zeta\gamma}{\beta\xi} J_0(\zeta\xi\gamma)$$

$$C_7 = Y_1(\zeta\gamma) - \frac{\alpha\eta\zeta\gamma}{\beta} Y_0(\zeta\gamma)$$

$$C_8 = Y_1(\zeta\xi\gamma) - \frac{\alpha\eta\zeta\gamma}{\beta\xi} Y_0(\zeta\xi\gamma)$$

$$C_9 = J_1(\gamma)$$

$$C_{10} = \frac{\xi^2 - 2\eta}{1 - 2\eta} J_1(\xi\gamma)$$

$$C_{11} = Y_1(\gamma)$$

$$C_{12} = \frac{\xi^2 - 2\eta}{1 - 2\eta} Y_1(\xi\gamma)$$

$$C_{13} = J_1(\zeta\gamma)$$

$$C_{14} = \frac{\xi^2 - 2\eta}{1 - 2\eta} J_1(\zeta\xi\gamma)$$

$$C_{15} = Y_1(\zeta\gamma)$$

$$C_{16} = \frac{\xi^2 - 2\eta}{1 - 2\eta} Y_1(\zeta\xi\gamma)$$

(12)

In these equations

$$\xi^2 = \frac{\delta_2}{\delta_1} \tag{13}$$

$$\gamma = \delta_1 a \tag{14}$$

$$\zeta = \frac{b}{a} \tag{15}$$

$$\eta = \frac{\omega^2}{2c_1^2\delta_1^2} = \beta \frac{\omega^2}{\bar{\omega}^2} \left[(\alpha + \beta) \frac{\omega^2}{\bar{\omega}^2} - 1 + \psi \right]^{-1} \tag{16}$$

Examination of Equations (5) and (13) shows that ξ is real for $\omega/\bar{\omega} > 1$ and imaginary for $\omega/\bar{\omega} < 1$. It is therefore convenient to introduce the real quantity

$$\bar{\xi} = -i\xi$$

for the frequency range $\omega/\bar{\omega} < 1$, with

$$i = (-1)^{1/2}$$

Equations (12) may then be written in the following alternate form:

$$C_1 = J_1(\gamma) - \frac{\alpha\eta\gamma}{\beta} J_0(\gamma)$$

$$C_2 = iJ_1(i\bar{\xi}\gamma) - \frac{\alpha\eta\gamma}{\beta\bar{\xi}} J_0(i\bar{\xi}\gamma)$$

$$C_3 = Y_1(\gamma) - \frac{\alpha\eta\gamma}{\beta} Y_0(\gamma)$$

$$C_4 = H_1^{(1)}(i\bar{\xi}\gamma) + \frac{\alpha\eta\gamma}{\beta\bar{\xi}} iH_0^{(1)}(i\bar{\xi}\gamma)$$

$$C_5 = J_1(\zeta\gamma) - \frac{\alpha\eta\zeta\gamma}{\beta} J_0(\zeta\gamma)$$

$$C_6 = iJ_1(i\zeta\bar{\xi}\gamma) - \frac{\alpha\eta\zeta\gamma}{\beta\bar{\xi}} J_0(i\zeta\bar{\xi}\gamma)$$

$$C_7 = Y_1(\zeta\gamma) - \frac{\alpha\eta\zeta\gamma}{\beta} Y_0(\zeta\gamma)$$

$$C_8 = H_1^{(1)}(i\zeta\bar{\xi}\gamma) + \frac{\alpha\eta\zeta\gamma}{\beta\bar{\xi}} iH_0^{(1)}(i\zeta\bar{\xi}\gamma)$$

$$C_9 = J_1(\gamma)$$

$$C_{10} = \frac{-\bar{\xi}^2 - 2\eta}{1 - 2\eta} iJ_1(i\bar{\xi}\gamma)$$

$$C_{11} = Y_1(\gamma)$$

$$C_{12} = \frac{-\bar{\xi}^2 - 2\eta}{1 - 2\eta} H_1^{(1)}(i\bar{\xi}\gamma)$$

$$C_{13} = J_1(\zeta\gamma)$$

$$C_{14} = \frac{-\bar{\xi}^2 - 2\eta}{1 - 2\eta} iJ_1(i\zeta\bar{\xi}\gamma)$$

$$C_{15} = Y_1(\zeta\gamma)$$

$$C_{16} = \frac{-\bar{\xi}^2 - 2\eta}{1 - 2\eta} H_1^{(1)}(i\zeta\bar{\xi}\gamma)$$

(17)

where $H^{(1)}$ is the Hankel function of the first kind.

The frequency equation is obtained from Equations (11), by setting the determinant of the coefficients of A_1, A_2, B_1, B_2 equal to zero:

$$\begin{vmatrix} C_1 & C_2 & C_3 & C_4 \\ C_5 & C_6 & C_7 & C_8 \\ C_9 & C_{10} & C_{11} & C_{12} \\ C_{13} & C_{14} & C_{15} & C_{16} \end{vmatrix} = 0 \tag{18}$$

Limiting Cases

Before proceeding to the detailed solution of Equation (18), it is helpful to study a number of limiting cases.

Small Hole. In this case $b \ll a$ so that $\zeta \approx 0$. Now, for small x

$$J_0(x) \approx 1$$

$$J_1(x) \approx x/2$$

$$Y_0(x) \approx (2/\pi) \log x$$

$$Y_1(x) \approx -2/\pi x$$

Hence for small values of ζ, those of Equations (12) which contain ζ become

$$C_5 \approx \zeta\gamma\left(\frac{1}{2} - \frac{\alpha\eta}{\beta}\right)$$

$$C_6 \approx \zeta\gamma\left(\frac{\xi}{2} - \frac{\alpha\eta}{\beta\xi}\right)$$

$$C_7 \approx -\frac{2}{\pi\zeta\gamma}$$

$$C_8 \approx -\frac{2}{\pi\zeta\xi\gamma}$$

$$C_{13} \approx \zeta\gamma/2$$

$$C_{14} \approx \frac{\zeta\xi\gamma(\xi^2 - 2\eta)}{2(1 - 2\eta)}$$

$$C_{15} \approx -2/\pi\zeta\gamma$$

$$C_{16} \approx -\frac{2(\xi^2 - 2\eta)}{\pi\zeta\xi\gamma(1 - 2\eta)}$$

Inserting these expressions in Equation (18), the frequency equation, for $\zeta \approx 0$, becomes

$$\frac{1 - \xi^2}{(1 - 2\eta)\xi^2\gamma}(C_1C_{10} - C_2C_9) = 0$$

This equation has real, positive roots only when

$$C_1C_{10} - C_2C_9 = 0$$

or, using Equations (12), when

$$\frac{\beta}{\alpha} - \frac{\eta\gamma}{\xi}\frac{J_0(\xi\gamma)}{J_1(\xi\gamma)} = \frac{\xi^2 - 2\eta}{1 - 2\eta}\left[\frac{\beta}{\alpha} - \eta\gamma\frac{J_0(\gamma)}{J_1(\gamma)}\right]$$

This, as it should be, is the frequency equation for a solid circular disk, as given previously.[2] For the first two modes of motion, values of $\omega/\bar{\omega}$ versus a/h satisfying this equation are plotted (for $\nu = 0.3$) as curves I and II in Fig. 1.

Large Hole. As b approaches a, ζ approaches unity and can be written as

$$\zeta = 1 - \epsilon$$

where $\epsilon \ll 1$.

Now, for small ϵ

$$P_0(\zeta x) \approx P_0(x) + \epsilon x P_1(x)$$

$$P_1(\zeta x) \approx (1 + x)P_1(x) - \epsilon x P_0(x)$$

where $P = J$, Y and $x = \gamma$, $\xi\gamma$.

Thus those of Equations (12) which contain ζ can be written as

$$C_5 = (1 + \epsilon_1)J_1(\gamma) - \frac{\alpha\eta\gamma}{\beta}(1 + \epsilon_3)J_0(\gamma)$$

$$C_6 = (1 + \epsilon_1)J_1(\xi\gamma) - \frac{\alpha\eta\gamma}{\beta\xi}(1 + \epsilon_4)J_0(\xi\gamma)$$

$$C_7 = (1 + \epsilon_1)Y_1(\gamma) - \frac{\alpha\eta\gamma}{\beta}(1 + \epsilon_3)Y_0(\gamma)$$

$$C_8 = (1 + \epsilon_1)Y_1(\xi\gamma) - \frac{\alpha\eta\gamma}{\beta\xi}(1 + \epsilon_2)Y_0(\xi\gamma) \tag{19}$$

$$C_{13} = (1 + \epsilon)J_1(\gamma) - \epsilon\gamma J_0(\gamma)$$

$$C_{14} = \frac{\xi^2 - 2\eta}{1 - 2\eta}[(1 + \epsilon)J_1(\xi\gamma) - \epsilon\xi\gamma J_0(\xi\gamma)]$$

$$C_{15} = (1 + \epsilon)Y_1(\gamma) - \epsilon\gamma Y_0(\gamma)$$

$$C_{16} = \frac{\xi^2 - 2\eta}{1 - 2\eta}[(1 + \epsilon)Y_1(\xi\gamma) - \epsilon\xi\gamma Y_0(\xi\gamma)]$$

where, neglecting second-degree terms in ϵ,

$$\epsilon_3 = \epsilon\left(\frac{\beta}{\alpha\eta} - 1\right)$$

$$\epsilon_4 = \epsilon\left(1 - \frac{\alpha}{\beta}\eta\gamma^2\right) \tag{20}$$

$$\epsilon_2 = \epsilon\left(\frac{\beta\xi^2}{\alpha\eta} - 1\right)$$

Equation (18) now becomes

$$(C_1C_{11} - C_3C_9)(C_1'C_{11}' - C_3'C_9') = 0 \tag{21}$$

where C_1, C_3, C_9, and C_{11} are given by Equations (12) and

$$C_1' = \frac{(1 - \xi^2)(\epsilon_1 - \epsilon_3)}{(1 - 2\eta)(1 + \epsilon_1)}J_1(\xi\gamma) - \frac{\alpha\eta\gamma(\epsilon_2 - \epsilon_3)}{\beta\xi(1 + \epsilon_1)}J_0(\xi\gamma)$$

$$C_3' = \frac{(1 - \xi^2)(\epsilon_1 - \epsilon_3)}{(1 - 2\eta)(1 + \epsilon_1)}Y_1(\xi\gamma) - \frac{\alpha\eta\gamma(\epsilon_2 - \epsilon_3)}{\beta\xi(1 + \epsilon_1)}Y_0(\xi\gamma) \tag{22}$$

$$C_9' = \frac{(\xi^2 - 1)\epsilon\beta}{(1 - 2\eta)(1 + \epsilon)\alpha\eta}J_1(\xi\gamma) - \frac{\epsilon\gamma(\xi^2 - 2\eta)(\xi^2 - 1)}{\xi(1 - 2\eta)(1 + \epsilon)}J_0(\xi\gamma)$$

$$C_{11}' = \frac{(\xi^2 - 1)\epsilon\beta}{(1 - 2\eta)(1 + \epsilon)\alpha\eta}Y_1(\xi\gamma) - \frac{\epsilon\gamma(\xi^2 - 2\eta)(\xi^2 - 1)}{\xi(1 - 2\eta)(1 + \epsilon)}Y_0(\xi\gamma)$$

Thus from Equations (12)

$$C_1C_{11} - C_3C_9 = \frac{\alpha\eta\gamma}{\beta}\left[J_1(\gamma)Y_0(\gamma) - J_0(\gamma)Y_1(\gamma)\right] \quad (23)$$

and from Equations (22) and (20), for $\epsilon \approx 0$

$$C_1'C_{11}' - C_3'C_9' = \frac{(\xi^2 - 1)}{(1 - 2\eta)}\left[\xi^2\frac{\beta}{\alpha\eta} + (\xi^2 - 2\eta + 1)\left(\frac{\alpha}{\beta}\eta\gamma^2 - 2\right)\right] [J_1(\xi\gamma)Y_0(\xi\gamma) - J_0(\xi\gamma)Y_1(\xi\gamma)] \quad (24)$$

Examination of the expressions (23) and (24) shows that the roots of equation

$$\xi^2\frac{\beta}{\alpha\eta} + (\xi^2 - 2\eta + 1)\left(\frac{\alpha}{\beta}\eta\gamma^2 - 2\right) = 0$$

are the only real, positive roots of Equation (21). By using Equations (13)–(16) together with Equations (5)–(10), this becomes

$$\omega^4 - \omega^2\frac{E}{(1 - \nu^2)\rho}\left[\frac{1}{a^2} + \frac{\pi^2}{4h^2}\right] + \frac{\pi^2E^2}{4(1 - \nu^2)a^2h^2\rho^2} = 0 \quad (25)$$

which is the frequency equation for the lowest modes ($n = 1/2$) of symmetrical, extensional vibrations of a thin cylindrical shell.[3] This result, which is unrestricted as regards the ratio a/h, shows once again (see footnote 2, section 10) that the plate theory contains equations valid for very thick plates. Curves III and IV in Fig. 1 shows $\omega/\bar{\omega}$ versus a/h as obtained from Equation (25).

Thin Plate, Low Frequencies. For $a/h \gg 1$ and $\omega/\bar{\omega} \ll 1$ Equations (13), (14), and (16) reduce approximately to

$$\xi^2 = -\frac{\bar{\omega}^2}{\alpha\beta\omega^2}$$

$$\gamma = \frac{a\omega}{c_3} \quad (26)$$

$$\eta = \frac{1}{2\alpha}$$

Hence for small $\omega/\bar{\omega}$, ξ is a large imaginary quantity.

Now, for large x

$$J_0(ix) \approx (2\pi x)^{-1}e^x$$

$$iH_0^{(1)}(ix) \approx \left(\frac{2}{\pi x}\right)^{1/2}e^{-x}$$

$$iJ_1(ix) \approx -(2\pi x)^{-1}e^x$$

$$H_1^{(1)}(ix) \approx -\left(\frac{2}{\pi x}\right)^{1/2}e^{-x}$$

Thus those of Equations (17) which contain $\bar{\xi}$ can be written approximately as

$$C_2 = -(2\pi\bar{\xi}\gamma)^{-1/2}e^{\bar{\xi}\gamma}$$

$$C_4 = -\left(\frac{2}{\pi\bar{\xi}\gamma}\right)^{1/2}e^{-\bar{\xi}\gamma}$$

$$C_6 = -(2\pi\zeta\bar{\xi}\gamma)^{-1/2}e^{\zeta\bar{\xi}\gamma}$$

$$C_8 = -\left(\frac{2}{\pi\zeta\bar{\xi}\gamma}\right)^{1/2}e^{-\zeta\bar{\xi}\gamma}$$

$$C_{10} = \bar{\xi}^2(2\pi\bar{\xi}\gamma)^{-1/2}e^{\bar{\xi}\gamma}$$

$$C_{12} = \bar{\xi}^2\left(\frac{2}{\pi\bar{\xi}\gamma}\right)^{1/2}e^{-\bar{\xi}\gamma}$$

$$C_{14} = \bar{\xi}^2(2\pi\zeta\bar{\xi}\gamma)^{-1/2}e^{\zeta\bar{\xi}\gamma}$$

$$C_{16} = \bar{\xi}^2\left(\frac{2}{\pi\zeta\bar{\xi}\gamma}\right)^{1/2}e^{-\zeta\bar{\xi}\gamma}$$

Inserting these expressions in Equation (18), the frequency equation for large values of $\bar{\xi}$ becomes

$$(C_1C_7 - C_3C_5)\zeta^{-1/2}\sinh(1 - \zeta) = 0$$

or

$$C_1C_7 - C_3C_5 = 0 \quad (27)$$

where [see Equations (17) and (26)]

$$C_1 = J_1\left(\frac{a\omega}{c_3}\right) - \frac{a\omega}{2\beta c_3}J_0\left(\frac{a\omega}{c_3}\right)$$

$$C_3 = Y_1\left(\frac{a\omega}{c_4}\right) - \frac{a\omega}{2\beta c_3}Y_0\left(\frac{a\omega}{c_3}\right)$$

$$C_5 = J_1\left(\frac{\zeta a\omega}{c_3}\right) - \frac{\zeta a\omega}{2\beta c_3}J_0\left(\frac{\zeta a\omega}{c_3}\right) \quad (28)$$

$$C_7 = Y_1\left(\frac{\zeta a\omega}{c_3}\right) - \frac{\zeta a\omega}{2\beta c_3}Y_0\left(\frac{\zeta a\omega}{c_3}\right)$$

Table 1 Computed frequencies of first two modes of vibration of circular disk with concentric hole, $\zeta = 0.5$

			First Mode			
a/h	3.80	2.53	1.49	0.99	0	
$\omega/\bar{\omega}$	0.2	0.3	0.5	0.7	0.863	
			Second Mode			
a/h	4.88	3.87	2.08	1.25	0.80	0.65
$\omega/\bar{\omega}$	0.7	0.8	0.9	0.95	1.1	1.3

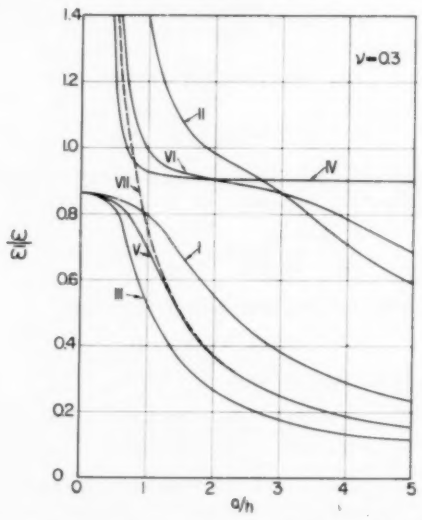

Fig. 1 Curves I–VI show frequencies of first two modes of axially symmetric extensional vibrations of circular disk with concentric hole according to equations of this paper for $\zeta = 0$ (Curves I- and II), for $\zeta = 1$ (Curves III and IV), for $\zeta = 0.5$ (Curves V and VI). Curve VII shows frequencies of first mode according to theory of generalized plane stress for $\zeta = 0.5$.

[3] A. E. H. Love, "Theory of Elasticity," fourth edition, Cambridge University Press, Cambridge, England, 1927, p. 546.

It may be verified that Equation (27) is precisely the frequency equation obtained when this problem is solved in terms of the theory of generalized plane stress. Curve VII in Fig. 1 represents this result.

Thin Ring. When ζ approaches 1 in Equations (28), Equation (27) becomes the frequency equation for a thin ring. C_4 and C_7 then approaches the values given by Equations (19) and the positive, real solutions of the frequency equation are found by solving the equation

$$\epsilon_0 = \epsilon_1 \tag{29}$$

where ϵ_0 and ϵ_1 are given by Equations (20).

From Equations (20), (26), and (29), one then finds that

$$\omega = (E/\rho a^2)^{1/2}$$

which agrees with the frequency predicted in Timoshenko[4] for the lowest mode of radial vibration of a thin circular ring.

[4] S. Timoshenko, "Vibration Problems in Engineering," D. Van Nostrand Company, Inc., New York, N. Y., third edition, 1955, p. 426.

Computation of Frequencies

The complete frequency spectrum may be computed in the same manner as for a solid circular disk.[2]

From Equations (14) and (16), noting that $\tilde{\omega} = \pi c_1/2h$

$$\frac{a}{h} = \frac{\gamma\tilde{\omega}}{\pi\omega}(8\eta)^{1/2} \tag{30}$$

α and β depend only on Poisson's ratio ν, while ξ and η depend only on ν and $\omega/\tilde{\omega}$. Hence a choice of ν and $\omega/\tilde{\omega}$ reduces the expressions (12) or (17) to transcedental functions of γ and ζ only. Thus for a given ζ, each root γ of Equation (18) corresponds to a value of a/h in accordance with Equation (30).

Results of computations for the first two modes ($\nu = 0.3$, $\zeta = 0.5$) are shown in Table 1 and illustrated by curves V and VI in Fig. 1.

Analysis of a Nonlinear Mechanical System With Three Degrees of Freedom

S. A. HOVANESSIAN[1]

Assistant in Engineering, and Junior Research Engineer, University of California, Los Angeles, Calif.

In recent years the methods of solution of nonlinear vibratory systems with one degree of freedom have been extended to the solution of nonlinear systems with two degrees of freedom. For these systems, the steady-state amplitude equations can be obtained by several methods, such as perturbation and the iteration method introduced by Duffing. In this paper the amplitude-frequency equations for a nonlinear mechanical system with three degrees of freedom are obtained, using Duffing's method for obtaining the steady-state amplitude equations [1].[2] *The steady-state response curves of two nonlinear mechanical systems, each having three degrees of freedom, are given.*

Derivation of Steady-State Amplitude Equations

CONSIDER the mechanical system with three degrees of freedom as shown in Fig. 1. A periodic driving force is applied to mass m_3. The springs are all nonlinear with cubic nonlinearity. Hence an extension or contraction of any one of the springs from the position of equilibrium will give rise to a restoring force, expressed by the following equation:

$$R = kq \pm \epsilon q^3 \tag{1}$$

where

R = restoring force
k = coefficient of linear term
ϵ = coefficient of cubic term
q = extension or contraction of spring from position of equilibrium

This relationship between the restoring force R and the displacement from the position of equilibrium q is shown in Fig. 2. In Equation (1) the positive sign refers to a hardening spring and the negative sign specifies a softening spring.

In the case of hardening springs ($\epsilon > 0$), the equations of motion of the system of Fig. 1, from Newton's second law of motion, can be written as follows:

$$m_1\ddot{x}_1 + k_1(x_1 + \mu_1 x_1^3) - k_2[(x_2 - x_1) + \mu_2(x_2 - x_1)^3] = 0 \tag{2a}$$

$$m_2\ddot{x}_2 + k_2[(x_2 - x_1) + \mu_2(x_2 - x_1)^3] - k_3[(x_3 - x_2) + \mu_3(x_3 - x_2)^3] = 0 \tag{2b}$$

$$m_3\ddot{x}_3 + k_3[(x_3 - x_2) + \mu_3(x_3 - x_2)^3] = F_0 \cos \omega t \tag{2c}$$

where

$$\mu_1 = \frac{\epsilon_1}{k_1}, \quad \mu_2 = \frac{\epsilon_2}{k_2}, \quad \mu_3 = \frac{\epsilon_3}{k_3}$$

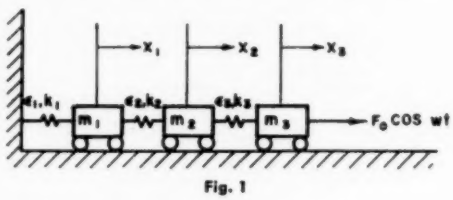

Fig. 1

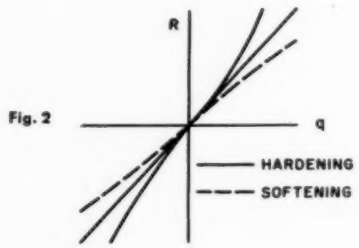

Fig. 2

m = mass
x_i = displacement of mass m_i from position of equilibrium
$F_0 \cos \omega t$ = applied periodic force
ω = angular frequency of applied force
t = time

The dots indicate derivatives with respect to time.

Summation of Equations (2*a*), (2*b*), and (2*c*), and summation of (2*a*) and (2*b*), together with Equation (2*a*), results in Equations (3*a*), (3*b*) and (3*c*), respectively.

$$m_1\ddot{x}_1 + m_2\ddot{x}_2 + m_3\ddot{x}_3 + k_1(x_1 + \mu_1 x_1^3) = F_0 \cos \omega t \tag{3a}$$

$$m_1\ddot{x}_1 + m_2\ddot{x}_2 + k_1(x_1 + \mu_1 x_1^3) - k_3[(x_3 - x_2) + \mu_3(x_3 - x_2)^3] = 0 \tag{3b}$$

$$m_1\ddot{x}_1 + k_1(x_1 + \mu_1 x_1^3) - k_2[(x_2 - x_1) + \mu_2(x_2 - x_1)^3] = 0 \tag{3c}$$

Following Duffing's iterative method [2, 3] we assume the following equations as a first approximation for the solution of (3):

$$\begin{aligned} x_1 &= A \cos \omega t \\ x_2 &= B \cos \omega t \\ x_3 &= C \cos \omega t \end{aligned} \tag{4}$$

In these equations A, B, and C are the values of the steady-state amplitudes of the motion. Substituting Equations (4) in Equations (3) and using the trigonometric identity,

---

[1] Now Research Engineer, California Research Corporation, La Habra Laboratory, La Habra, Calif.

[2] Numbers in brackets designate References at end of paper.

Presented at the Summer Conference of the Applied Mechanics Division, Troy, N. Y., June 18–20, 1959, of THE AMERICAN SOCIETY OF MECHANICAL ENGINEERS.

Discussion of this paper should be addressed to the Secretary, ASME, 29 West 39th Street, New York, N. Y., and will be accepted until January 10, 1960, for publication at a later date. Discussion received after the closing date will be returned.

NOTE: Statements and opinions advanced in papers are to be understood as individual expressions of their authors and not those of the Society. Manuscript received by ASME Applied Mechanics Division, June 19, 1958. Paper No. 59—APM-29.

$$\cos^3 \omega t = \frac{\cos 3\omega t}{4} + \frac{3}{4} \cos \omega t,$$

three equations are obtained involving the amplitudes of the vibrations. Equating the coefficients of the cos ωt-terms in these equations to zero gives the following set of algebraic relations between the amplitudes of steady-state vibrations (this assumes the cos 3 ωt-terms can be neglected [2, 3]):

$$-Am_1\omega^2 + k_1A + {}^3/_4k_1\mu_1A^3 - Bm_2\omega^2 - Cm_3\omega^2 = F_0 \quad (5a)$$

$$-Am_1\omega^2 + k_1A + {}^3/_4k_1\mu_1A^3 - Bm_2\omega^2 - k_2(C - B) - {}^3/_4k_2\mu_2(C - B)^3 = 0 \quad (5b)$$

$$-Am_1\omega^2 + k_1A + {}^3/_4k_1\mu_1A^3 - k_2(B - A) - {}^3/_4k_2\mu_2(B - A)^3 = 0 \quad (5c)$$

Setting $m_2 = m_3$, the foregoing equations after some algebraic manipulations can be written:

$$(B - A)^3 + {}^4/_3\frac{1}{\mu_2}(B - A) - {}^4/_3\frac{1}{k_2\mu_2}(K) = 0 \quad (6a)$$

$$(C - B)^3 + {}^4/_3\frac{1}{\mu_3}(C - B) + {}^4/_3\frac{m_2\omega^2}{k_2\mu_3}(B - A) - {}^4/_3\frac{1}{k_2\mu_2}(K - Am_2\omega^2) = 0 \quad (6b)$$

$$2A + (C - B) + 2(B - A) + \frac{F_0}{m_2\omega^2} = \frac{K}{m_2\omega^2} \quad (6c)$$

where

$$K = -Am_1\omega^2 + k_1A + {}^3/_4k_1\mu_1A^3 \quad (6d)$$

Equations (6) form the basis of the graphical solution for the values of the steady-state amplitudes, the description of which follows.

Given the physical constants of the system, for a particular value of ω (angular frequency of the impressed force), Equation (6d) gives K as a function of A. By calculating the values of K for several values of A and solving the cubic Equation (6a),[3] for these values of K, the corresponding values of $(B - A)$ are obtained. Using the values of $(B - A)$ thus obtained, K previously found, and solving cubic Equation (6b), $(C - B)$ can be obtained as a function of A. Now, since the values of $(B - A)$, $(C - B)$, and K are known as a function of A, the right and the left sides of Equation (6c) can be plotted against A. The intersections of these two curves give the correct values of A. Since we already have obtained $(B - A)$ and $(C - B)$ as a function of A, we can easily find the magnitudes of the amplitudes B and C.

The foregoing method can be extended to the solution of nonlinear systems, with cubic nonlinearity, having more than three degrees of freedom. The driving force can be applied to any one of the masses with minor adjustments in the derivation of the amplitude Equations (4).

Solution of the Three-Degrees-of-Freedom System

Case 1. In this numerical example all masses are considered to be equal and the springs are all nonlinear hardening with cubic nonlinearity.

[3] The cubic Equations (6a) and (6b) will have only one real root for hardening spring systems, and this root is used in the subsequent calculations.

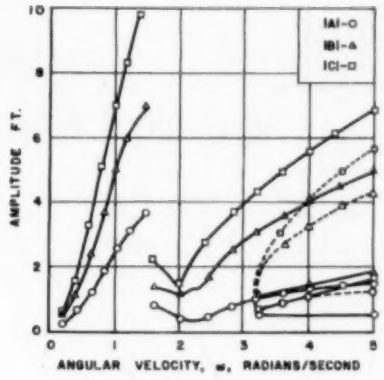

Fig. 3

Referring to Fig. 1, let us assume the following constants for the system:[4]

$$m_1 = m_2 = m_3 = 1 \text{ lb-sec}^2/\text{ft}$$

$$k_1 = k_2 = k_3 = 1 \text{ lb per ft}, \quad \epsilon_1 = \epsilon_2 = \epsilon = 1 \text{ pcf}$$

$$\mu_1 = \mu_2 = \mu_3 = 1\,\frac{1}{\text{ft}^2}, \quad F_0 = 0.20 \text{ lb}$$

Substituting the foregoing values in the amplitude-frequency Equations (6), and following the method of solution previously outlined, we will obtain the response curves given in Fig. 3. From this figure it is seen that the response curves rise sharply up to an angular frequency ω of about 1.5 radian per sec. For values of ω slightly greater than this, the amplitudes decrease with increasing ω until a minimum is reached at $\omega \approx 2.0$. Beyond this point the amplitudes increase monotonically with ω. Hence, within the range of ω-values shown, there are only two "peaks." Since the system considered here possesses three degrees of freedom, comparison with systems having two degrees of freedom [5, 6, 7], would lead one to expect response curves with three peaks. If the range of the calculations were extended to larger values of ω, it is possible that a third peak might be observed. For each value of $\omega > 3.2$ there are three values of the amplitudes. The dashed lines in Fig. 3 correspond to unstable regions of the response curves [8].

Case 2. In the present example the first mass is considered to be larger than the other two equal masses. The first spring is considered to be linear while the other two are nonlinear hardening springs, with cubic nonlinearity.

Referring to Fig. 1, let us assume the following constants for the system[4]:

$$m_1 = 2 \text{ lb-sec}^2/\text{ft}, \; m_2 = m_3 = 1 \text{ lb-sec}^2/\text{ft}$$

$$k_1 = 1 \text{ lb per ft}, \; k_2 = k_3 = 2 \text{ lb per ft}$$

$$\epsilon_1 = 0 \text{ pcf}, \quad \epsilon_2 = \epsilon_3 = 1 \text{ pcf}$$

$$\mu_1 = 0, \quad \mu_2 = \mu_3 = {}^1/_2\ 1/\text{ft}^2, \; F_0 = 0.20 \text{ lb}$$

Substituting the foregoing values in the amplitude-frequency Equations (6) and solving the resulting equations for the values of the amplitudes, as outlined previously, gives the response

[4] Stoker [2] points out that in applying Duffing's method the values of the coefficients of nonlinear terms ϵ should be small. But in the present example the rather large values of ϵ are chosen as an aid in arithmetical manipulation.

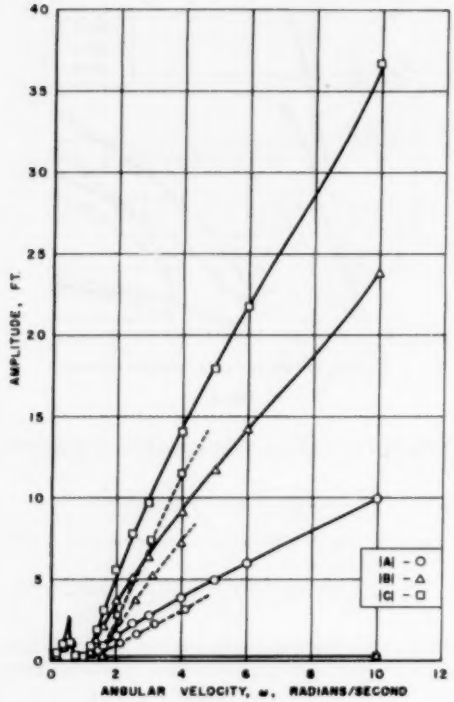

Fig. 4

curves of Fig. 4. From this figure it is observed that within the range of $0 < \omega < 10$ radians per sec two peaks exist—one at $\omega \approx 0.5$ and the second starting at $\omega \approx 1.7$ radian per sec. Since the first peak is small, the direction of bending of the response curves, at this value of ω, is not known. Starting from the value of $\omega \approx 1.6$ radian per sec the response curves start to rise and bend toward the right, as expected for the case of hardening springs. For values of $\omega > 1.8$ radian per sec there are always three values of the amplitudes corresponding to each value of ω. The unstable regions of the response curves are partially shown by dashed lines.

Acknowledgment

The author wishes to acknowledge the invaluable assistance of Prof. Louis A. Pipes during the progress of this work. He is also indebted to Dr. Elmer L. Dougherty of California Research Corporation for assistance in the preparation of the final manuscript.

References

1 R. M. Rosenberg, discussion of "Harmonic Oscillations of Nonlinear Two-Degree of Freedom Systems," JOURNAL OF APPLIED MECHANICS, vol. 22, TRANS. ASME, vol. 77, 1955, pp. 602–603.

2 J. J. Stoker, "Nonlinear Vibrations," Interscience Publishers, Inc., New York, N. Y., 1950.

3 B. Katz, "Analysis of a Nonlinear Mechanical System," MSc thesis, University of California, Los Angeles, Calif., 1956.

4 S. A. Hovanessian, "Nonlinear Vibrations With Three Degrees of Freedom," PhD dissertation, University of California, Los Angeles, Calif., 1958.

5 T. C. Huang, "Harmonic Oscillations of Nonlinear Two-Degree-of-Freedom Systems," JOURNAL OF APPLIED MECHANICS, vol. 22, TRANS. ASME, vol. 77, 1955, pp. 107–110.

6 F. R. Arnold, "Steady-State Behavior of Systems Provided With Nonlinear Dynamic Absorbers," JOURNAL OF APPLIED MECHANICS, vol. 22, TRANS. ASME, vol. 77, 1955, pp. 487–492.

7 C. P. Atkinson, "Electronic Analog Computer Solutions of Nonlinear Vibratory Systems of Two Degrees of Freedom," JOURNAL OF APPLIED MECHANICS, vol. 23, TRANS. ASME, vol. 78, 1956, pp. 629–634.

8 K. Klotter, "A Comprehensive Stability Criterion for Forced Vibrations in Nonlinear Systems," JOURNAL OF APPLIED MECHANICS, vol. 20, TRANS. ASME, vol. 75, 1953, pp. 9–12.

M. A. GOLDBERG
Research Engineer,
Grumman Aircraft Engineeering Corp.,
Bethpage: L. I., N. Y.

MICHAEL SADOWSKY
Professor, Department of Mechanics,
Rensselaer Polytechnic Institute,
Troy, N. Y.
Mem. ASME

Stresses in an Ellipsoidal Rotor in a Centrifugal Force Field[1]

This paper contains an exact solution for the stress distribution in an elastic ellipsoid rotating about a free axis. The surface of the body is free from boundary stresses. The stresses are expressed with the use of 12 coefficients which have been tabulated for 209 ellipsoids of different shapes. General diagrams give the maximum values of stresses as functions of two shape ratios.

THE stress field in a rotating ellipsoid was first examined by Chree.[2,3] He was mainly concerned with oblate spheroids of slight eccentricity for geophysical applications.

Statement of Problem

The problem consists of the determination of the stresses in a homogeneous, isotropic, elastic ellipsoid

$$f(x, y, z) \equiv \frac{x^2}{b^2} + \frac{y^2}{c^2} + \frac{z^2}{a^2} = 1 \qquad (c \leq b) \tag{1}$$

of mass density ρ rotating with constant angular velocity ω about the z-axis. The surface of the body is to be free from boundary stresses.

Construction of Solution by Superposition

The actual field of centrifugal body force is $\omega^2\rho(x\bar{i} + y\bar{j})$. To avoid clumsy algebra, we multiply it by $8(1 - \nu)/(\omega^2\rho)$ switching to a fictitious body force $8(1 - \nu)(x\bar{i} + y\bar{j})$. Stresses computed in the fictitious field will have to be multiplied by $(\omega^2\rho)/[8(1 - \nu)]$ for actualization. An elastic stress field derivable from displacements and equilibrating with the fictitious body force is

$$\begin{aligned}
\sigma_x &= -(3 - 2\nu)x^2 - (1 + 2\nu)y^2 \\
\sigma_y &= -(1 + 2\nu)x^2 - (3 - 2\nu)y^2 \\
\sigma_z &= -4\nu(x^2 + y^2) \\
\tau_{xy} &= -2(1 - 2\nu)xy \\
\tau_{xz} &= \tau_{yz} = 0
\end{aligned} \tag{2}$$

For the removal of boundary stresses due to (2) we will use three types of basic solutions derivable from three independent potential functions[4] φ, ϑ, and λ:

First Basic Solution.[5]

$$2G(u, v, w) = \text{grad } \varphi \tag{3}$$

$$\sigma_x = \varphi_{zz};\ \sigma_y = \varphi_{yy};\ \sigma_z = \varphi_{zz}$$
$$\tau_{xy} = \varphi_{xy};\ \tau_{yz} = \varphi_{yz};\ \tau_{zx} = \varphi_{zx} \tag{4}$$

Second Basic Solution.

$$G(u, v, w) = \text{curl } (0, 0, \vartheta) \tag{5}$$

$$\sigma_x = 2\vartheta_{xy};\ \sigma_y = -2\vartheta_{xy};\ \sigma_z = 0 \tag{6}$$

$$\tau_{xy} = \vartheta_{yy} - \vartheta_{xx};\ \tau_{yz} = -\vartheta_{zx};\ \tau_{zx} = \vartheta_{yz}$$

Third Basic Solution.

$$2G(u, v, w) = \text{grad } (z\lambda) - 4(1 - \nu)(0, 0, \lambda) \tag{7}$$

$$\sigma_x = z\lambda_{xz} - 2\nu\lambda_z;\ \sigma_y = z\lambda_{yz} - 2\nu\lambda_z;\ \sigma_z = z\lambda_{zz} - 2(1 - \nu)\lambda_z \tag{8}$$

$$\tau_{xy} = z\lambda_{xy};\ \tau_{yz} = z\lambda_{yz} - (1 - 2\nu)\lambda_y;\ \tau_{zx} = z\lambda_{zz} - (1 - 2\nu)\lambda_x$$

The potential functions φ, ϑ, λ will be selected using the standard spherical forms

$$r^n P_n^m(\cos\theta)\cos m\phi \text{ and } r^n P_n^m(\cos\theta)\sin m\phi \tag{9}$$

in which P_n^m is the symbol for the associated Legendre function of the first kind and

$$\begin{aligned}
x &= r\sin\theta\cos\phi \\
y &= r\sin\theta\sin\phi \\
z &= r\cos\theta
\end{aligned} \tag{10}$$

The centrifugal field (2) produces residual stresses on the boundary. We will remove them by polynomial basic solutions (3–8). As suggested by (2), the removing polynomials for the stresses should be of degree 2, and the normal stresses should be even functions in x, y, z. These requests limit the acceptable basic solutions to the following:

First Basic type. Acceptable φ functions:

$$\left.\begin{matrix} [r^2 P_2^0(p)] \\ [1/6\ r^2 P_2^2(p)\cos 2\phi] \end{matrix}\right\} \tag{11}$$

---

[1] The work reported here is a part of the doctoral dissertation of M. A. Goldberg at Rensselaer Polytechnic Institute.

[2] C. Chree, "The Stresses and Strains in Isotropic Solid Ellipsoids in Equilibrium Under Bodily Forces Derivable From a Potential of the Second Degree," *Proceedings of the Royal Society*, London, England, vol. 58, 1895, p. 39.

[3] J. Prescott, "Applied Elasticity," Dover Publications, New York, N. Y., first American edition, 1946, pp. 332–345.

[4] M. A. Sadowsky and E. Sternberg, "Stress Concentration Around an Ellipsoidal Cavity in an Infinite Body Under Arbitrary Plane Stress Perpendicular to the Axis of Revolution of Cavity," JOURNAL OF APPLIED MECHANICS, vol. 14, TRANS. ASME, vol. 69, 1947, p. A-191.

[5] Subscripts attached to functions which originally bear no subscripts denote partial derivatives; e.g.,

$$\varphi_{xy} = \frac{\partial^2\varphi}{\partial x\,\partial y}$$

Contributed by the Applied Mechanics Division and presented at the Annual Meeting, Atlantic City, N. J., November 29–December 4, 1959, of THE AMERICAN SOCIETY OF MECHANICAL ENGINEERS.
Discussion of this paper should be addressed to the Secretary, ASME, 29 West 39th Street, New York, N. Y., and will be accepted until January 10, 1960, for publication at a later date. Discussion received after the closing date will be returned.
NOTE: Statements and opinions advanced in papers are to be understood as individual expressions of their authors and not those of the Society. Manuscript received by ASME Applied Mechanics, June 20, 1958. Paper No. 59—A-4.

$$\left.\begin{aligned} &{}^3/_4 A_1 r^4 P_4^0(p) \\ &{}^1/_{80} B_1 r^4 P_4^2(p) \cos 2\phi \\ &\frac{1}{1260} C_1 r^4 P_4^4(p) \cos 4\phi \end{aligned}\right\} \tag{12}$$

Second Basic Type. Acceptable ϑ function:

$$^1/_{80} A_2 r^4 P_4^2(p) \sin 2\phi \tag{13}$$

Third Basic Type. Acceptable λ functions:

$$[^1/_2 r P_1^0(p)] \tag{14}$$

$$\left.\begin{aligned} &{}^1/_2 A_3 r^2 P_2^0(p) \\ &{}^1/_{20} B_3 r^2 P_2^2(p) \cos 2\phi \end{aligned}\right\} \tag{15}$$

The bracketed solutions (11) and (14) have uniform (constant) stress fields. We drop them and introduce instead the uniform field in the form

$$\sigma_x = A_0, \quad \sigma_y = B_0, \quad \sigma_z = C_0$$
$$\tau_{xy} = \tau_{yz} = \tau_{zx} = 0 \tag{16}$$

The solution of the problem (S) is now set up as a superposition:

$$(S) = (2) + (16) + (12) + (13) + (15) \tag{17}$$

9 unknown coefficients are involved; i.e.,

$$A_0, B_0, C_0; \ A_1, B_1, C_1; \ A_2; \ A_3, B_3 \tag{18}$$

An evaluation of stresses in (S) in dimensionless form shows that they are of the following form:

$$\frac{\sigma_x}{\sigma_0} = K_{1x}\left(1 - \frac{x^2}{b^2}\right) - K_{2x}\frac{y^2}{c^2} - K_{3x}\frac{z^2}{a^2}$$

$$\frac{\sigma_y}{\sigma_0} = K_{1y}\left(1 - \frac{y^2}{c^2}\right) - K_{2y}\frac{x^2}{b^2} - K_{3y}\frac{z^2}{a^2}$$

$$\frac{\sigma_z}{\sigma_0} = K_{1z}\left(1 - \frac{z^2}{a^2}\right) + K_{2z}\frac{x^2}{b^2} + K_{3z}\frac{y^2}{c^2} \tag{19}$$

$$\frac{\tau_{xy}}{\sigma_0} = -\frac{K_1}{2(1-\nu)}\frac{xy}{b^2}$$

$$\frac{\tau_{yz}}{\sigma_0} = -\frac{K_2}{2(1-\nu)}\frac{yz}{b^2}$$

$$\frac{\tau_{zx}}{\sigma_0} = -\frac{K_3}{2(1-\nu)}\frac{xz}{b^2}$$

in which the 12 coefficients

$$K_{1x}, K_{2x}, K_{3x}, K_{1y}, K_{2y}, K_{3y},$$
$$K_{1z}, K_{2z}, K_{3z}, K_1, K_2, K_3 \tag{20}$$

are dimensionless numbers depending linearly on the set (18) and

$$\sigma_0 = 2(1-\nu)b^2 \tag{21}$$

is the average value of σ_x on the central section $x = 0$ of the ellipsoid.

Boundary Conditions

We have from (1)

$$\frac{\partial f}{\partial x} = \frac{2x}{b^2}, \quad \frac{\partial f}{\partial y} = \frac{2y}{c^2}, \quad \frac{\partial f}{\partial z} = \frac{2z}{a^2} \tag{22}$$

Hence the boundary conditions for a free surface read

$$\sigma_x \frac{x}{b^2} + \tau_{xy}\frac{y}{c^2} + \tau_{zx}\frac{z}{a^2} = 0$$

$$\tau_{yx}\frac{x}{b^2} + \sigma_y \frac{y}{c^2} + \tau_{yz}\frac{z}{a^2} = 0 \tag{23}$$

$$\tau_{zx}\frac{x}{b^2} + \tau_{zy}\frac{y}{c^2} + \sigma_z \frac{z}{a^2} = 0$$

The stresses in (19) are composed of terms quadratic in x, y, z with the exception of 3 constant terms K_{1x}, K_{1y}, K_{1z}. For ex-

Table 1 Coefficients for K_{1x}, K_{2x}, and K_{3x} for various shape ratios

δ_1 \ δ_2	K_{1x} .1	.4	.7	1.0	K_{2x} .1	.4	.7	1.0	K_{3x} .1	.4	.7	1.0
.1	1.344	1.478	1.651	1.715	.030	.430	.950	1.140	1.349	1.481	1.651	1.719
.4	1.350	1.480	1.649	1.715	.030	.422	.921	1.096	1.369	1.499	1.674	1.762
.7	1.324	1.446	1.606	1.680	.029	.400	.848	.998	1.266	1.385	1.575	1.722
1.0	1.259	1.373	1.518	1.593	.027	.369	.748	.881	1.010	1.123	1.323	1.495
2.0	1.098	1.190	1.282	1.325	.025	.293	.567	.697	.368	.467	.561	.603
4.0	1.031	1.098	1.175	1.207	.023	.254	.551	.671	.101	.138	.149	.156
10.0	1.010	1.070	1.147	1.174	.020	.259	.563	.672	.020	.022	.023	.025

Table 2 Coefficients for K_{1y}, K_{2y}, and K_{3y} for various shape ratios

δ_1 \ δ_2	K_{1y} .1	.4	.7	1.0	K_{2y} .1	.4	.7	1.0	K_{3y} .1	.4	.7	1.0
.1	.013	.236	.809	1.715	.000	.069	.465	1.140	.015	.237	.810	1.719
.4	.013	.237	.813	1.715	.000	.067	.454	1.096	.013	.239	.830	1.762
.7	.014	.243	.824	1.680	.001	.075	.453	.998	.014	.256	.882	1.722
1.0	.014	.255	.828	1.593	.002	.094	.451	.881	.015	.285	.901	1.495
2.0	.016	.268	.720	1.325	.005	.124	.369	.697	.019	.306	.550	.603
4.0	.017	.217	.606	1.207	.007	.082	.299	.671	.021	.147	.159	.156
10.0	.016	.179	.566	1.174	.006	.049	.280	.672	.017	.025	.025	.025

clusive use on the surface (1) we homogenize those constant terms into quadratic terms by (1). Then the left members in (23) appear as homogeneous polynomials of the third degree. Cancellation of common factors leaves (23) in quadratic terms only. Equating to zero the coefficients of the 6 linearly independent terms $x^2, \ldots\ldots yz, \ldots\ldots$ leads to a nonhomogeneous 9 by 9 linear system possessing a unique solution for (18). The 90 coefficients of the system depend quadratically on all 3, a, b, c and linearly on Poisson's ratio ν. The values of the 12 coefficients (20) depend only on 2 shape ratios

$$\delta_1 = \frac{b}{a} \quad \text{and} \quad \delta_2 = \frac{c}{b} \tag{24}$$

and on ν.

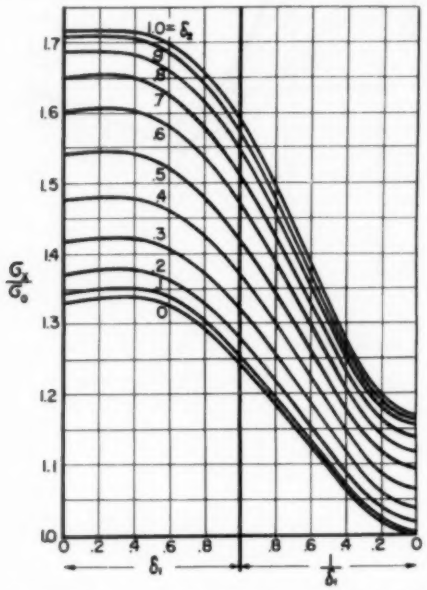

Fig. 1 Dimensionless stress σ_x/σ_0 at center for various shape ratios

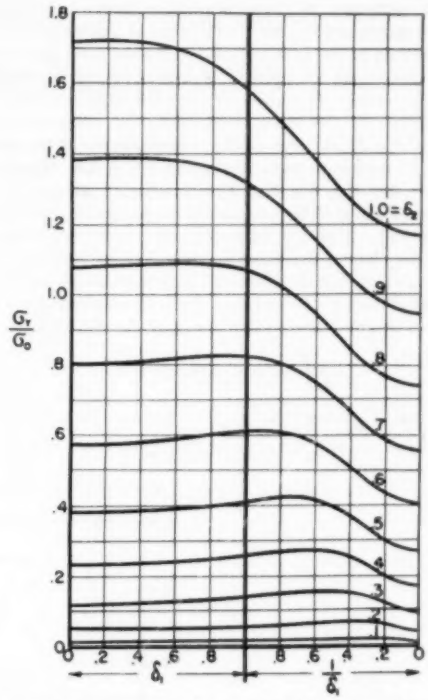

Fig. 2 Dimensionless stress σ_y/σ_0 at center for various shape ratios

Table 3 Coefficients for K_{1z}, K_{2z}, and K_{3z} for various shape ratios

	K_{1z}				K_{2z}				K_{3z}			
δ_1 \ δ_2	.1	.4	.7	1.0	.1	.4	.7	1.0	.1	.4	.7	1.0
.1	.103	.162	.286	.420	-.387	-.447	-.619	-.840	-.013	-.201	-.527	-.840
.4	.045	.106	.212	.299	-.164	-.217	-.387	-.598	-.014	-.201	-.470	-.598
.7	-.034	.022	.091	.086	.152	.103	-.028	-.171	-.014	-.189	-.334	-.171
1.0	-.078	-.032	-.022	-.101	.327	.282	.217	.202	-.014	-.155	-.127	.202
2.0	-.057	-.060	-.133	-.180	.239	.241	.309	.361	-.012	-.000	.220	.361
4.0	-.017	-.044	-.060	-.066	.075	.104	.125	.131	-.008	.071	.117	.131
10.0	-.003	-.010	-.011	-.011	.014	.021	.022	.023	.003	.020	.022	.023

Table 4 Coefficients for K_1, K_2, and K_3 for various shape ratios

	K_1				K_2				K_3			
δ_1 \ δ_2	.1	.4	.7	1.0	.1	.4	.7	1.0	.1	.4	.7	1.0
.1	1.840	1.467	.980	.805	.001	-.001	-.003	-.006	-.004	-.004	-.005	-.006
.4	1.848	1.481	1.016	.866	.007	-.021	-.051	-.067	-.027	-.025	-.034	-.067
.7	1.813	1.465	1.061	.954	-.033	-.115	-.167	-.059	.080	.085	.043	-.059
1.0	1.725	1.406	1.078	.998	-.129	-.261	-.209	.141	.349	.350	.272	.141
2.0	1.503	1.246	1.001	.879	-.384	-.338	.485	1.011	1.022	1.012	1.009	1.011
4.0	1.411	1.182	.873	.750	-.549	.616	1.272	1.471	1.302	1.344	1.437	1.471
10.0	1.386	1.136	.817	.703	-.166	1.340	1.546	1.609	1.386	1.468	1.572	1.609

Results

The 9 by 9 system was solved for a complete range of shape ratios δ_1 and δ_2 with $\nu = 0.3$. This was accomplished with a high-speed IBM-650 electronic computer at Rensselaer Polytechnic Institute. The primary aim was a numerical determination of the set (20) of the 12 coefficients K. A total of 2508 values has been tabulated to 6 significant figures. An excerpt of the tabulation drastically reduced in size is reproduced as Tables 1–4. The original computation covers 209 different shapes of triaxial ellipsoids, the excerpt covers 28. The ultimate aim of the computation was a determination of the stress field within an ellipsoid and an analysis of the dependence of the stresses on the shape ratios δ_1 and δ_2. All numerical work was done for $\nu = 0.3$. The tabulations show that K_{1x}, K_{2x}, K_{3x}, K_{1y}, K_{2y}, K_{3y} are all positive. By (19) we conclude that the maxima of σ_x and σ_y are at the center of the ellipsoid. Figs. 1 and 2 show them; each curve holds for a given δ_2, the plotting is against δ_1. Fig. 3 gives the value of σ_x at the center, which may, but does not have to be the maximum of σ_x within the ellipsoid. Indeed, as there is no resultant force in the z-direction on any plane section $z = z_0$ of the ellipsoid, we have

$$\iint \sigma_z(x, y, z_0)dx\,dy = 0 \tag{25}$$

By (19) and (1), this gives

$$4K_{1z} + K_{2z} + K_{3z} = 0 \tag{26}$$

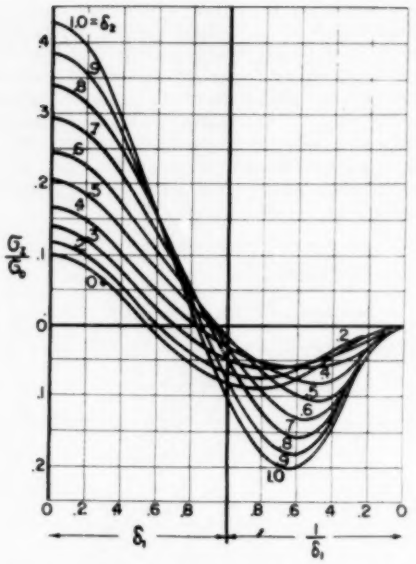

Fig. 3 Dimensionless stress σ_x/σ_0 at center for various shape ratios

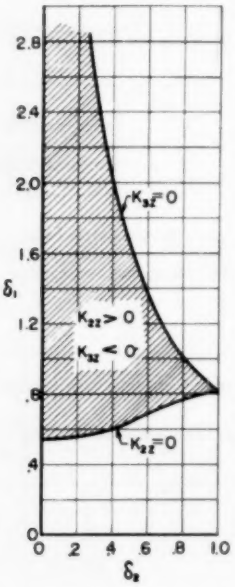

Fig. 4 (*Right*) Region (shaded) for which maximum stress σ_x is on surface of ellipsoid

Fig. 5 (*Left*) Profiles of σ_x on x = 0, 1, 2, 3, and 4 for spheroid a = 5, $b = c = 1$

which shows that K_{1x}, K_{2x}, and K_{3x} are never all of the same sign. The distribution of positive and negative values is rather individualistic here, as seen from the tables. If K_{2x} and K_{3x} are opposite in sign, then one of them is alike with K_{1x}, and by (19) the absolute maximum of σ_x is on the surface of the ellipsoid at the ends of the corresponding ("alike") axis at $[\pm b, 0, 0]$ or $[0, \pm c, 0]$. Fig. 4 shows the region in the δ_1, δ_2-plane where this happens. If K_{2x} and K_{3x} are alike in sign, they are opposite to K_{1x} by (26) and the absolute maximum of σ_x by (19) is at the center of the ellipsoid. This is always the case with a spheroid $b = c$, since the tables show that for $\delta_2 = 1$, $K_{2x} = K_{3x}$. Fig. 5 gives extra details on σ_x for a spheroid.

An analytical investigation (prior to numerical methods of orientation) has revealed the existence of just one ellipsoid which is in a state of plane stress ($\sigma_x = \tau_{xz} = \tau_{xy} = 0$); namely, a spheroid $\delta_2 = 1$ with

$$\delta_1^2 = \frac{4\nu(1 + \nu)}{(1 - \nu)(3 + \nu)} \tag{27}$$

giving $\delta_1 = 0.822$ for $\nu = 0.3$.

Acknowledgment

The authors are indebted to the Rensselaer Polytechnic Institute Computer Laboratory for the gratuitous use of their facilities, and to Messrs. W. J. Knapp, W. G. McClintock, and A. Gross for their assistance. A computation of numerical results on standard desk calculators would have required about 2 years. This time was reduced to 4 weeks through the use of an IBM-650.

Carrying Capacity of Elastic-Plastic Shells With Various End Conditions, Under Hydrostatic Compression[1]

BURTON PAUL
Assistant Professor,
Division of Engineering,
Brown University,
Providence, R. I.
Assoc. Mem. ASME

This paper considers the influence of the beam-column effect on the carrying capacity of hydrostatically loaded elastic-plastic cylindrical shells. Specific problems considered include shells with clamped ends, simply supported ends, and a combination thereof. It is shown that in all cases considered there exist two characteristic modes of failure corresponding, respectively, to long and short shells where the terms "long" and "short" are unambiguously defined. Detailed results are presented graphically along with general conclusions useful for design purposes.

THE methods of limit analysis have been used with increasing frequency in the past decade to determine the carrying capacities of beams, frames, rings, plates, and shells. It is implicit in such analyses that the equations of equilibrium be referred to undeformed configurations. Such an approach must necessarily omit the so-called beam-column effect which tends to weaken structures in the presence of compressive loadings.

In an earlier paper [1][2] the beam-column effect[3] was introduced into the equations of equilibrium for a hydrostatically loaded, simply supported cylindrical shell made of an elastic, perfectly plastic material. The references of that paper supply the background for the present one. It was found that a fully plastic mode of collapse existed for short shells, and the associated carrying capacity was computed for a wide range of shell parameters. Although no uniqueness theorem exists for such problems the collapse mode found satisfied all required boundary conditions as well as a modified plastic potential-flow law and the equations of equilibrium. In particular, it was shown in a numerical example that the contained elastic-plastic deformation becomes indefinitely large as the load increases from zero toward the predicted fully plastic carrying capacity. In the present paper, the analysis will be extended in several directions.

In [1] the carrying capacity was determined for short, simply supported shells. The numerical results given in that report, however, covered a range of shell parameters which extended slightly beyond the range of validity of the solution. As pointed out in [1], this amounted to a slight extension or distortion of the yield condition used. In the present paper this approximation will be dispensed with and it will be seen that the solution given in [1] is valid for short shells only, and another solution is valid for long shells. The two words long and short will be defined precisely, and it will be shown that all simply supported shells fit into one or the other category.

The shell with both ends clamped, besides being of great interest for its own sake, represents a typical bay in a long shell reinforced at regular intervals by rigid reinforcing rings. The fully plastic collapse mode for such shells will be determined in this paper. It will be seen that two types of solutions, corresponding to long and short shells, respectively, exist in this case too. These two types of solution again cover the entire range of shell parameters.

As an illustration of the generality of the techniques employed for clamped and simply supported shells, an example will be given of a shell having mixed boundary conditions; i.e., one end clamped and the other simply supported. It is found that the general characteristics of the previous solutions are preserved in this case where two types of solutions are seen to cover the entire range of long and short shells with boundary conditions of the type specified.

It is of interest that all long shells of the three types investigated have the same carrying capacity. This common carrying capacity is the same as that for a shell with free ends, where collapse is due entirely to membrane forces.

In this paper only radially symmetric modes of deformation are considered; therefore all dependent variables are functions of a single co-ordinate measured along the axis of the shell. The deformations found satisfy all kinematic boundary conditions, provide a non-negative rate of energy dissipation, and are related to the stress resultants by the plastic potential-flow law associated with a given singular yield condition; that is, the velocity fields are kinematically admissible in the sense of limit analysis [2]. The stress-resultant fields associated with each of the problems considered will be seen to satisfy all boundary conditions on stress, the equations of equilibrium (including the beam-column effect of the axial load), and the given yield condition. Following the nomenclature of limit analysis, a stress field satisfying these three requirements will be referred to in this paper as a statically admissible stress field.

Although the solutions which follow are both kinematically and statically admissible, there is no assurance that the carrying capacities so determined are unique. The possibility does exist that the collapse mechanisms visualized can never be developed in the actual shell owing to the constraints of the elastic region in the era of contained plastic deformation which must in reality

---

[1] The work reported upon in this paper was done at the Polytechnic Institute of Brooklyn, and was sponsored by the Office of Naval Research.

[2] Numbers in brackets designate References at end of paper.

[3] The tendency of the bending moment produced by the axial forces acting on the radial displacements to produce further displacements, and ultimately collapse, will for brevity be referred to as "beam-column effect."

Presented at the Summer Conference of the Applied Mechanics Division, Troy, N. Y., June 18–20, 1959, of THE AMERICAN SOCIETY OF MECHANICAL ENGINEERS.

Discussion of this paper should be addressed to the Secretary, ASME, 29 West 39th Street, New York, N. Y., and will be accepted until January 10, 1960, for publication at a later date. Discussion received after the closing date will be returned.

NOTE: Statements and opinions advanced in papers are to be understood as individual expressions of their authors and not those of the Society. Manuscript received by ASME Applied Mechanics Division, June 23, 1958. Paper No. 59—APM-16.

precede collapse. Thus some mode of collapse other than the one visualized may actually prevail.

If the carrying capacities found in this paper are below the lowest known elastic buckling loads (as they are shown to be for a wide variety of simply supported shells in [1]), they represent possible improved upper bounds on the actual carrying capacities. The possibility does exist that even lower carrying capacities are associated with different (possibly asymmetric) modes of plastic collapse. It should be noted that the solution given provides a lower value of collapse load than does the solution of the analogous purely elastic beam-column problem, primarily because the lever arms (radial deflections) on which the axial forces act have been increased by the plastic component of radial deflection.

The notation and basic equations are essentially the same as those of [1], but are restated in section 1 in order to make this paper reasonably self-contained. Sections 2 and 3 deal with shells having clamped ends and simply supported ends, respectively. The distinction between long and short shells of both types is pointed out. Section 4 deals with shells having one end simply supported and the other end clamped. Both the rigid-plastic collapse load and the elastic-plastic carrying capacity are determined. Finally in Section 5 the results are evaluated and consideration is given to reinforcement by rigid rings.

1 Notation and Basic Equations

A circular cylindrical shell has the dimensions indicated in Fig. 1, and is made of an elastic perfectly plastic material having modulus of elasticity E, Poisson's ratio ν, and tensile yield stress Y. The bending moment per unit length produced by axial stress is M_x; the axial and circumferential forces per unit length are given by N_x and N_ϕ, respectively. The corresponding curvature and strains are κ_x, ϵ_x, ϵ_φ. The inward radial deflection is represented by w, and the axial co-ordinate x is measured from a suitably chosen origin. The shell is assumed to be submersed in a uniform hydrostatic-pressure field of magnitude p. Therefore, the loading consists of a pressure p acting over the lateral surface of the cylinder and an axial compressive force $p\pi a^2$ uniformly distributed over the end cross sections.

The following dimensionless variables prove convenient:

Kinematic variables:	Dynamic variables:
$c^2 = (L/a)(L/h)$	$n_x = N_x/N_0 = N_x/2Yh$
$b^2 = \frac{1}{2}(Y/E)(a/L)^2$	$m_x = M_x/M_0 = M_x/Yh^2$ (1)
$y = x/L;\ (\ )' = \partial(\ )/\partial y$	$n_\phi = N_\phi/N_0 = N_\phi/2Yh$
$W = (E/Y)(w/a)$	$P = (1/2)(p/Y)(a/h)$

Within the spirit of thin-wall, small-deformation theory of shells the governing equations of equilibrium are[4]

$$n_x = -P/2, \quad m_x''/2c^2 + 2n_x b^2 W'' + n_\phi + P = 0 \qquad (2)$$

Within the elastic range the stresses and strains are related by Hooke's law:

$$e_\phi = -W = n_\phi - \nu n_x, \qquad (3)$$

$$\kappa = -W''/2c^2 = (3/4)(1 - \nu^2)m_x \qquad (4)$$

Although Hooke's law can be used to find ϵ_x in terms of n_ϕ and n_x, this relationship will prove to be unnecessary for the problem under consideration.

The relationship between the stress and moment resultants for a plastic point in the shell has been discussed by Onat [4] and Hodge [5]. The yield surface may be approximated by a polyhedron bounded by twelve planes in the space of the stress resultants (m_x, n_x, n_φ). This surface represents the true yield surface for an idealized sandwich cross section, or a linearization of the true yield surface for a uniform section, based upon Tresca's maximum-shear-stress criterion of yielding.

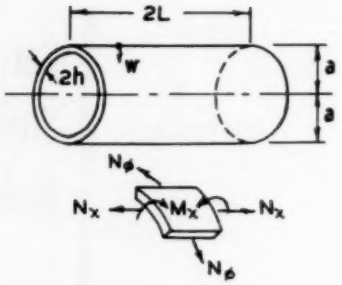

Fig. 1 Dimensions and co-ordinates

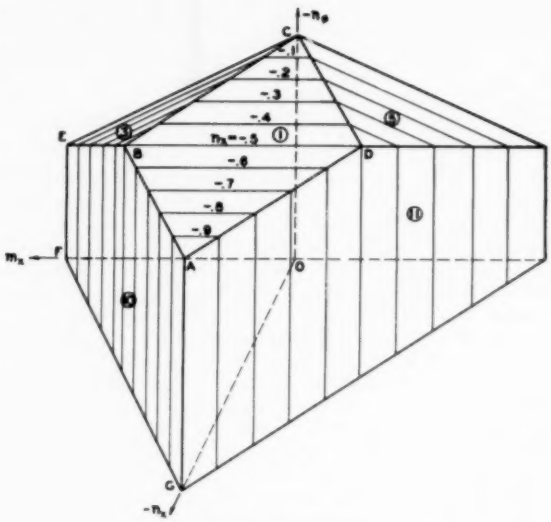

Fig. 2 Yield surface

Fig. 2 shows that part of the yield surface for which $n_x \leq 0$ and $n_\varphi \leq 0$. Five of the twelve bounding planes of the entire surface are shown. Level curves for various negative values of n_x are indicated. Table 1 [5] gives the equation of each face shown in Fig. 2.

Table 1 Equations of yield surface

Face	Equation
1	$-n_\phi = 1$
3	$n_x - 2n_\phi + m_x = 2$
5	$n_x - 2n_\phi - m_x = 2$
10	$-n_x + m_x = 1$
11	$-n_x - m_x = 1$

In what follows, only completely plastic modes of deformation will be considered so that all points of the shell must correspond to some point in the space (m_x, n_x, n_ϕ) which lies on the yield surface. If each strain component is divided into an elastic and plastic part, the plastic potential-flow law states that the plastic part of a suitably chosen strain-rate vector is parallel to the exterior normal to the yield surface at the corresponding stress

[4] Reference [3], p. 536.

point. Wherever the normal is not uniquely defined, e.g., at edges such as AB or vertexes such as B in Fig. 2, the plastic-strain-rate vector may lie anywhere in between the normals of the intersecting surfaces at that point. The elastic part of the strain rate still is given by the differentiated form of Hooke's law.

It develops that the pertinent portions of the yield surface for the problem under consideration are the points on the plane $n_\varphi = -1$. This plane is indicated as $ABCD$ in Fig. 2. If the stress point corresponds to an interior point of this plane it will be said to be in plastic regime 1. In regime 1 the flow law [5] requires that

$$\dot{\kappa}^p = \dot{\epsilon}_x{}^p = 0 \tag{5ab}$$

$$\dot{\epsilon}_\phi{}^p \leq 0 \tag{6}$$

where a dot signifies differentiation with respect to any monotonically increasing function of time, and the superscript p refers to the plastic component of strain rate. The total curvature is

$$\dot{\kappa} = \dot{\kappa}^e + \dot{\kappa}^p \tag{7}$$

where the superscripts e refer to the elastic component of curvature given by Equation (4). Upon integration of Equation (7) and use of (5a) and (4) one obtains

$$W^e = -(3/2)c^2(1 - \nu^2)m_x + F(y) \tag{8}$$

where $F(y)$ is an arbitrary function of y alone. If a cross section of the shell goes directly from the elastic state into regime 1, without first entering any other regime, continuity of W^e requires that $F(y) = 0$, so that in regime 1 the relevant relations are given by Equation (4) and

$$n_\varphi = -1; \quad e_\varphi < 0 \tag{9a, b}$$

Equation (4) implies that W' is continuous in regime 1. The condition on $\dot{\epsilon}_x{}^p$ may be used to determine the axial displacement. Since this displacement is irrelevant to this problem it will not be considered explicitly.

As the loading progresses it turns out that certain cross sections of the shell move onto the intersections of the plane $ABCD$ with the faces 10 and 11. Points corresponding to the line AB will be said to be in regime 1–10, and points corresponding to the line AD will be said to be in plastic regime 1–11. For a point in regime 1–10 or 1–11 the slope W' need not be continuous. A discontinuity in W' will be referred to as a plastic-hinge circle. Therefore, the condition of continuous slope is replaced by the condition that the cross section be in regime 1–10 or 1–11, i.e., that

$$m_x - n_x = 1, \quad \text{or} \quad -m_x - n_x = 1 \tag{10a, b}$$

Equation (9a) stipulates that a point lies somewhere on the extended plane $ABCD$ in the stress-resultant space but does not insure that the point in question lies within the square $ABCD$. It will be seen, in the present problem, that $n_x < -1/2$. Therefore, a necessary and sufficient condition for the stress point to be on the yield surface in regimes 1, 1–10 or 1–11, is

$$-(1 + n_x) \leq m_x \leq 1 + n_x \tag{11}$$

When Equation (4) is combined with the equilibrium equations (2) the following relationship is obtained:

$$m_x'' + k^2 m_x = 2c^2(1 - P), \tag{12}$$

where

$$k^2 = 3(1 - \nu^2)b^2c^4P \tag{13}$$

Equation (12) is valid only in regime 1, but not necessarily valid in either regime 1–10, or 1–11.

Physical reasoning requires that m_x, m_x', and W be continuous at all points of the shell. Furthermore, symmetry requires that if the origin of x is located at the middle cross section of the shell, and conditions of support at both ends are the same,

$$m_x'(0) = 0 \tag{14}$$

Upon integration of Equation (12) subject to Equation (14) it is found that

$$m_x = C_1 \cos ky + 2(c^2/k^2)(1 - P) \tag{15}$$

where C_1 is a constant of integration.

2 Shells With Ends Built In

It will prove convenient in this section and in the immediately following section to measure the co-ordinate x from the middle cross section.

A first step in the determination of a statically admissible stress distribution is a tentative hypothesis regarding the plastic regime corresponding to various parts of the shell. A heuristic argument is presented in [5] which indicates that at least for small values of c^2 a rigid-plastic shell will be entirely in regime 1 except for the middle and end cross sections which will be in regimes 1–10 and 1–11, respectively. Adopting this same argument provisionally for the present problem, Equations (10a, b) provide two additional boundary conditions which may be substituted into Equation (15) to give

$$C_1 = (1 - P/2) - (2c^2/k^2)(1 - P) \tag{16}$$

$$P = \frac{(1 - \cos k) + (k^2/2c^2)(1 + \cos k)}{(1 - \cos k) + (k^2/4c^2)(1 + \cos k)} \tag{17}$$

Equation (17) is transcendental in P and may be solved numerically to give P as a function of the parameters c^2 and b^2. It may be observed that, for a rigid-plastic material, E approaches infinity, and hence b tends to zero. In this limiting case

$$P = (2 + c^2)/(1 + c^2) = P_0{}^b \tag{18}$$

where $P_0{}^b$ is the rigid-plastic collapse load for a shell with ends built in [5]. It also should be noted that P, as given by Equation (17), is always greater than unity and decreases monotonically from $P_0{}^b$ to unity as k varies from zero to π. Fig. 3 shows two curves, each consisting of a cosine term plus a constant term and satisfying all required boundary conditions on $m(y)$. These curves show that Inequality (11) is satisfied if $0 \leq k \leq \pi$ and violated for $\pi \leq k$. Inequality (11) also may be satisfied for the particular values $k = \pi + 2n\pi$ ($n = 1, 2, \ldots$) in which case Equation (17) reduces to $P = 1$.

A kinematically admissible velocity field is obtained by noting that for P given by Equation (17) the moment distribution is a function of y alone so that Equation (4) can be differentiated to give

$$\dot{W}^e = 0 \tag{19}$$

Upon integration of (19) subject to the boundary condition

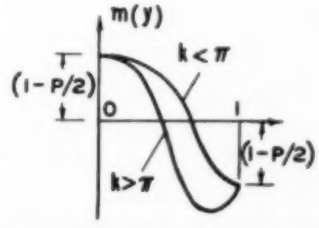

Fig. 3 Schematic of moment distribution

$\dot{W}(1) = 0$, the velocity distribution is found to be given by

$$\dot{W} = \dot{W}_0(1 - y) \tag{20}$$

where $\dot{W}_0$ is the central deflection. If $\dot{W}_0 \geq 0$ the velocity distribution satisfies all conditions for kinematic admissibility.

Thus a collapse load has been found which is associated with a statically admissible stress distribution and a kinematically admissible velocity distribution for clamped shells having $0 \leq k \leq \pi$. Such shells will be referred to hereinafter as short shells; all other clamped shells will be referred to as long shells.

It has been seen already that for certain discrete values of k, admissible stress and velocity fields can be associated with the collapse load $P = 1$. It will now be shown that if $P = 1$, admissible (though not necessarily unique) stress and velocity fields can be associated with all long shells.

In order to construct a statically admissible moment field for long shells let it be assumed that a central portion of the shell, $0 \leq y \leq v$, where v is to be determined, is at the vertex B, of Fig. 2. The remainder of the shell may then be assumed to be in regime 1, except for the ends which are at vertex D. Therefore

$$P = -n_\varphi = 1, \tag{21}$$

$$m = {}^1/_2 \quad (0 \leq y \leq v), \tag{22}$$

$$m = {}^1/_2 \cos k(y - v) \qquad (v \leq y \leq 1), \tag{23}$$

Equation (22) satisfies the equilibrium equations (2) if $W'' = 0$ for $0 \leq y \leq v$, and Equation (23) satisfies the equilibrium equation (12) valid in regime 1. It is to be noted that continuity of m and m' has been enforced at $y = v$. The boundary condition $m(1) = -{}^1/_2$ is satisfied if $\cos k(1 - v) = -1$, or

$$k(1 - v) = \pi(1 + 2n) \quad n = 0, 1, 2, \ldots \tag{24}$$

In order to have $v \geq 0$, the additional requirement $2n \leq (k/\pi) - 1$ must be enforced. Since n is not uniquely specified, neither is the moment distribution. Fig. 4(a, b) illustrates the ambiguity in moment distribution associated with the choices $n = 0$, 1, for the special case $3\pi \leq k \leq 5\pi$. It is obvious from Fig. 4 that Inequality (11) is satisfied and the stress field is statically admissible.

In order to construct a kinematically admissible velocity field it is necessary to note that substitution of Equations (21) and (22) into the equilibrium equations (2) loads to

$$W'' = 0 \quad (0 \leq y \leq v) \tag{25}$$

Equation (25) implies continuity of slope throughout the central region. Therefore plastic hinges can appear only at $v \leq y$ wherever $m = \pm{}^1/_2$. Observing that $\dot{W}'' = 0$ within regime 1 and $\dot{W}(1) = 0$, kinematically admissible velocity fields may be associated with the corresponding moment fields of Fig. 4, as illustrated in Fig. 5.

In addition to the ambiguity in moment distribution associated with the choice of integer n, an alternative possibility for a statically admissible moment distribution is given by the assumption that the center is in the regime 1 and the ends in regime D; that is,

$$\begin{aligned} m_x &= {}^1/_2 \cos ky \qquad (0 \leq y \leq v) \\ m_x &= -{}^1/_2 \qquad (v \leq y \leq 1) \\ v &= (2n + 1)\pi/k; \quad -n_\phi = P = 1; \quad (2n + 1) \leq \pi/k \end{aligned} \tag{26}$$

Fig. 6(a) shows an alternate possibility for a shell having the same dimensions as the shell of Fig. 4. It is assumed that $n = 0$ [compare with Fig. 4(a)]. It may be verified that a kinematically admissible velocity field, with a hinge circle at $y = 0$, may be associated with this stress field. For example, see Fig. 6(b), and compare with the alternate velocity field shown in Fig. 5(a).

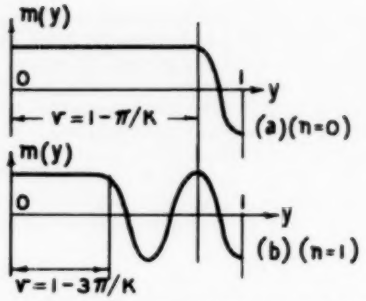

Fig. 4 Admissible moment fields for $3\pi \leq k \leq 5\pi$

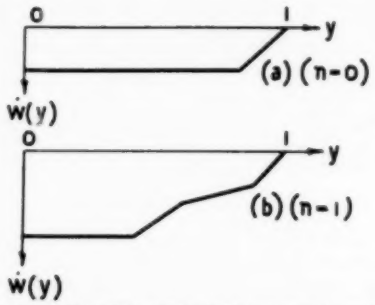

Fig. 5 Admissible velocity fields associated with Fig. 4(a), (b)

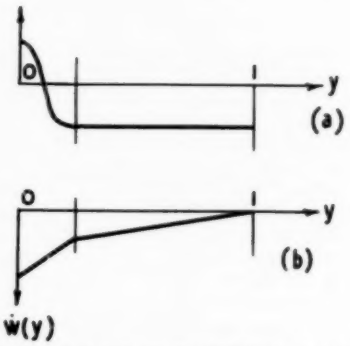

Fig. 6 Alternate moment and velocity fields for $3\pi \leq k \leq 5\pi$ ($n = 0$)

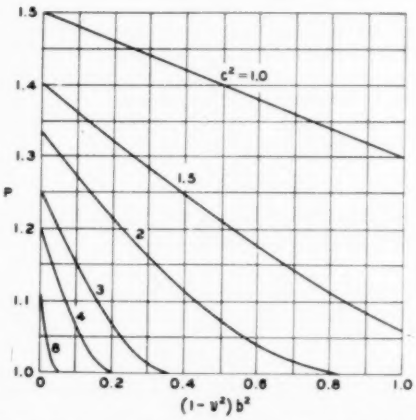

Fig 7 Elastic-plastic carrying capacity for shells with clamped ends

The significant point is that all of these various stress and moment fields which are admissible for long shells predict the same value of P; viz., $P = 1$.

In summary, a built-in shell is called long or short accordingly as the parameter

$$\gamma^2 = 3(1 - \nu^2)b^2c^4 = (3/2)(1 - \nu^2)(Y/E)(L/h)^2 \qquad (27)$$

is greater or less than $(\pi)^2$. For long shells $P = 1$; for short shells P is given by Equation (17) or Fig. 7.

3 Simply Supported Shells

If the boundary condition (10b) is replaced by $m(1) = 0$, it can easily be seen that a suitable moment field for a simply supported shell is given by Equations (15), (16) and

$$P = \frac{(k^2/2c^2 - 1)\cos k + 1}{(k^2/4c^2 - 1)\cos k + 1} \qquad (28)$$

Equation (28) has been derived already in detail in [1] where it was noted that as $E \to \infty$

$$P \to (2 + 2c^2)/(1 + 2c^2) = P_0^s$$

where P_0^s is the collapse load for a simply supported, rigid-plastic cylinder.

It may be shown that the collapse load predicted by Equation (28) decreases monotonically from P_0^s to unity as k increases from zero to $\pi/2$. In [1] it was assumed that for values of k slightly greater than $\pi/2$ Equation (28) would still provide a reasonable first approximation to the carrying capacity, which would then be less than 1. This is equivalent to a modification of the yield surface by allowing the face 10 to extend slightly beyond the line EB in Fig. 2. In the present paper this approximation will not be necessary since it will be shown that for $\pi/2 \leq k$ the carrying capacity $P = 1$ can be associated with statically and kinematically admissible stress and velocity fields.

The fact that the statically admissible solution of this paper predicts a higher carrying capacity (for $k \geq \pi/2$) than does the statically inadmissible solution of reference [1], illustrates the fact that the theorems of limit analysis are invalid when significant changes in geometry occur.

A statically admissible stress field is given by Equations (21, 22, 23) if the boundary condition $m(1) = 0$ is enforced. Substitution of this boundary condition into Equation (23) leads to

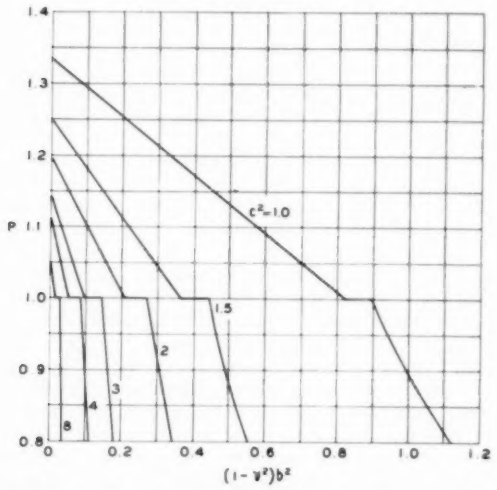

Fig. 8 Elastic-plastic carrying capacity for simply supported shells

$$k(1 - \nu) = \pi/2(1 + 2n) \qquad n = 0, 1, 2, \ldots \qquad (29)$$

The restriction $2n \leq (2k/\pi) - 1$ must be observed in order that $v \geq 0$. By reasoning similar to that of the previous section it may be shown that kinematically admissible velocity fields can be associated with the stress fields described in the foregoing. Simply supported shells may be classified as long or short accordingly as the parameter γ^2, defined by Equation (27) is greater or less than $(\pi/2)^2$. For long shells $P = 1$; for short simply supported shells P is given by Equation (28) or Fig. 8.

The lower branches of the curves shown in Fig. 8 represent the asymmetric elastic buckling load computed by Batdorf [6].

4 Shells With Mixed Boundary Conditions

The techniques of the previous section can be applied to problems of somewhat greater complexity. As an example the case of a shell simply supported at one end and clamped at the other end will be considered. It will prove convenient in this section to place the origin of the co-ordinate x at the simply supported cross section and to consider x increasing in the direction of the built-in cross section.

As a first step toward the solution of the elastic-plastic problem it is desirable to solve the rigid-plastic problem. The previous solutions suggest that an admissible stress field may be obtained by assuming the entire shell in regime 1 except for the built-in cross section which is in regime 1–11 and some intermediate cross section $y = u$ which is in regime 1–10. Thus the boundary conditions may be formulated as

$$m(0) = 0; \quad m(u) = 1 - P/2; \quad m'(u) = 0; \quad m(2) = -1 + P/2 \qquad (30a,b,c,d)$$

Equation (30c) is a necessary requirement for the stress point corresponding to $y = u$ to remain on the yield surface. For a rigid-plastic material no deformation occurs until the full collapse load is reached, consequently the term multiplied by W^* in the equation of equilibrium (2) may be omitted. After substitution of $n_\phi = -1$ into the equilibrium equation one obtains an ordinary linear differential equation of second order, which may easily be integrated. The four boundary conditions (30) are sufficient to determine the two constants of integration as well as u and P. The final equations are

$$u = 2(\sqrt{2} - 1) = 0.828 \qquad (31)$$

$$P = (2 + 2u^2c^2)/(1 + 2u^2c^2) = P_0^m \qquad (32)$$

$$m = c^2(1 - P)(y^2 - 2uy) \qquad (33)$$

where P_0^m is by definition the rigid-plastic collapse load for a shell with mixed boundary conditions of the type under discussion. Equation (33) shows that the stress field is statically admissible. A kinematically admissible velocity field is given by

$$w/a = \dot{W}_u y/u \quad 0 \leq y \leq u$$
$$w/a = \dot{W}_u(2 - y)/(2 - u) \quad u \leq y \leq 2 \qquad (34)$$

where $\dot{W}_u$, the velocity at $y = u$, is a positive number.

Having the rigid-plastic solution as a guide it now seems reasonable to assume that, at least for short shells, the same regions will be occupied by the elastic-plastic shell. Therefore Equation (12) must be integrated subject to the boundary conditions (30). The general solution of Equation (12) is

$$m = C_1 \cos ky + C_2 \sin ky + (2c^2/k^2)(1 - P) \qquad (35)$$

Upon substitution of boundary conditions (30a), and (30c) into (35) one obtains

$$C_1 = (2c^2/k^2)(P - 1); \quad C_2 = C_1 \tan ku \qquad (36a,b)$$

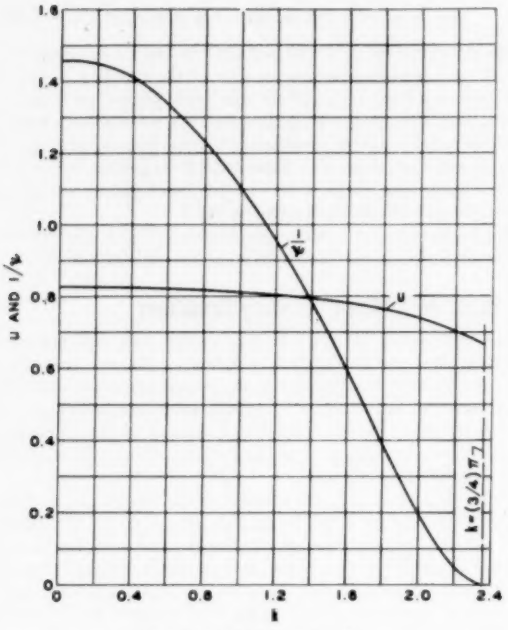

Fig. 9 u and $1/\psi$ versus k

With the aid of Equations (36) the remaining two boundary conditions become

$$(2c^2/k^2)(1 - P)(1 - \sec ku) = 1 - P/2, \tag{37}$$

$$(2c^2/k^2)(1 - P)[1 - \sec ku \cos k(2 - u)] = -1 + P/2 \tag{38}$$

Upon addition of Equations (37) and (38) there appears a transcendental equation, in k and u alone, of the form

$$2 \cos ku = 1 + \cos k(2 - u) \tag{39}$$

Equation (39) can be solved to give u as a function of k, either graphically or analytically. The details of the analytic solution are given in the Appendix, and the results are illustrated in Fig. 9. Equation (37) is now written in the convenient form

$$P = (2 + 2c^2\psi)/(1 + 2c^2\psi) \tag{40}$$

where

$$\psi = (2/k^2)(\sec ku - 1) \tag{41}$$

From the function $u(k)$ it is a simple matter to compute $\psi(k)$. For convenience $1/\psi$ is plotted in Fig. 9. The procedure for finding $P(c^2, b^2)$ can now be systematized as follows: For a fixed value of c^2, Equation (40) and Fig. 9 give $P(k)$, and finally Equation (13) gives the correct b^2 associated with any value of k and its associated $P(k)$. It is shown in the Appendix that, as $E \to \infty$, P approaches the rigid-plastic collapse load P_0^∞ given by Equation (32).

Fig. 10 shows a typical curve of $P(b^2)$ for $c^2 = 3$. It is instructive to compare this curve with similar curves for shells having both ends simply supported or clamped, as discussed in Sections 2 and 3 and shown in Fig. 10 by broken lines.

In order to determine the range of applicability of Equation (40) it should be noted that $1 \leq P \leq 2$ so long as $0 \leq \psi$, or, from Equation (41), so long as

$$0 \leq ku \leq \pi/2 \tag{42}$$

Since $m(y)$ consists of a sinusoidal term plus a constant term, In-

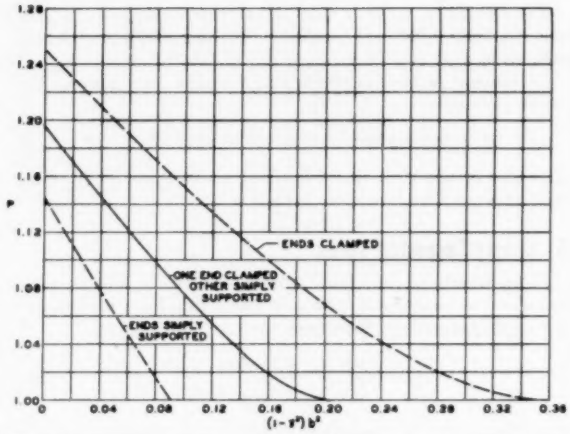

Fig. 10 Carrying capacity for shells with various end conditions and $c^2 = 3$

equality (42) together with the boundary conditions (30a, b, c) is a sufficient condition for static admissibility in the range $0 \leq y \leq u$. This is easily seen by examination of Fig. 11. The moment distribution in the range $u \leq y \leq 2$ is evidently statically admissible provided that $k(2 - u) \leq \pi$. With the use of (42) this latter condition becomes

$$2k \leq \pi + ku < 3\pi/2 \tag{43}$$

Therefore, if all shells having $k \leq 3\pi/4$ are defined as short shells, the foregoing solution is statically admissible for short shells. A kinematically admissible velocity distribution is given by

$$\dot{W} = \dot{W}_u y/u \qquad 0 \leq y \leq u$$

$$\dot{W} = \dot{W}_u \left(\frac{y - 2}{u - 2}\right) \qquad u \leq y \leq 2$$

where $\dot{W}_u$ is the (positive) velocity at $y = u$.

This completes the solution for short shells with mixed boundary conditions. For $k \geq 3\pi/4$ (long shells) the load $P = 1$ can be associated with more than one set of statically and kinematically admissible moment and velocity fields. Figs. 12(a, b) illustrate two typical sets of moment and velocity fields for long shells.

5 Conclusions

A general technique has been established for finding improved upper bounds on the carrying capacities of elastic, perfectly plastic shells, with various end conditions, submersed in a hydrostatic-pressure field.

The solutions obtained satisfy the equations of equilibrium (including the beam-column effect of axial load), the required boundary conditions, and the plastic potential-flow law associated with a linearized singular yield condition. However, the uniqueness of the collapse load is not guaranteed by the theorems of limit analysis, which are based upon the satisfaction of equilibrium in the undeformed state. In fact, a counterexample has been given which shows that the upper-bound theorem of limit analysis is not valid if significant changes in geometry occur.

In any case, the carrying capacities predicted by the present method are always below the rigid-plastic collapse loads predicted by standard techniques of limit analysis. Further it may easily be verified [1] that in many practical cases the carrying capacities found here are well below the lowest known elastic buckling loads. It may be of significance that in many such cases the experimentally determined collapse loads were indeed below

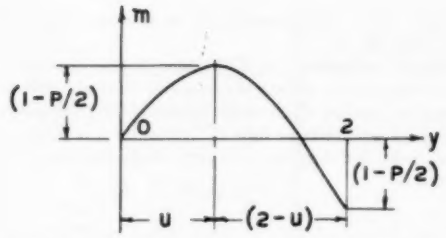

Fig. 11 Moment distribution for short shells with mixed boundary conditions

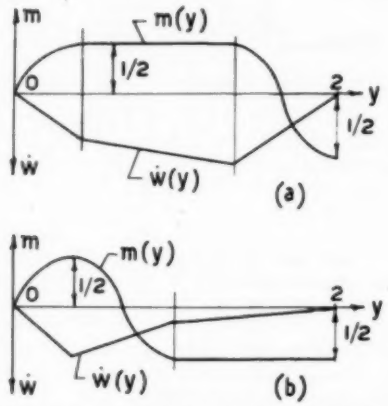

Fig. 12 Alternate sets of admissible moment and velocity fields associated with long shells having mixed boundary conditions

the computed elastic buckling load.[8] Although the disagreement with elastic theory may be due to initial deviations from a truly cylindrical shape [7], it is possible that plasticity effects have been instrumental in causing collapse.

It is of interest that, for the entire range of shell parameters shown in Fig. 8, all short simply supported shells have an elastic-plastic carrying capacity which is lower than the elastic (asymmetric) buckling load. This is shown clearly in Fig. 3 of reference [1]. Furthermore, only an extremely narrow range of long simply supported shells has an elastic-plastic carrying capacity which is lower than the elastic (asymmetric) buckling load. These observations suggest a rule-of-thumb which may prove useful for design purposes; viz, "long shells will tend to buckle elastically; short shells will tend to fail by yielding." The utility of this rule is enhanced by the simple definitions for long shells given in Sections 2, 3, and 4; that is, a shell is long if

$$\gamma^2 = (3/2)(1 - \nu^2)(Y/E)(L/h)^2 > (n\pi/4)^2,$$

where $n = 2, 3, 4$, accordingly as the ends are both simply supported, alternately simply supported and clamped, or both clamped.

The influence of strain-hardening probably would be small (at least for incipient collapse) for most structural metals [8] and would in any case tend to raise the predicted carrying capacity, so that the present results are conservative from this point of view.

Similarly, the linearization of the yield surface by an inscribed polyhedron should lead to a conservative evaluation of carrying capacity.

Finally it should be pointed out that the common carrying capacity $P = 1$ for all long shells indicates that rigid reinforcing rings have very little (if any) utility if spaced farther apart than

$$2L = h\pi[8E/3Y(1 - \nu^2)]^{1/2}$$

in so far as plastic collapse is concerned.

[8] Reference [6], p. 7.

Acknowledgment

The author takes pleasure in acknowledging the guidance of his thesis adviser Prof. P. G. Hodge, Jr., now of the Illinois Institute of Technology.

The contents of this paper and reference [1] have been taken from a dissertation, submitted to the Polytechnic Institute of Brooklyn, in partial fulfillment of the requirements for the degree of PhD in Applied Mechanics. The complete dissertation has been submitted as a report to the Office of Naval Research: PIBAL Report No. 420, Polytechnic Institute of Brooklyn, Department of Applied Mechanics, April, 1958.

References

1 B. Paul and P. G. Hodge, Jr., "Carrying Capacity of Elastic-Plastic Shells Under Hydrostatic Pressure," Proceedings of the Third U. S. National Congress of Applied Mechanics, ASME, 1958, pp. 631–640.

2 J. N. Goodier and P. G. Hodge, Jr., "Elasticity and Plasticity," John Wiley & Sons, Inc., New York, N. Y., 1958.

3 J. Prescott, "Applied Elasticity," Dover Publications, New York, N. Y., 1946.

4 E. T. Onat, "The Plastic Collapse of Cylindrical Shells Under Axially Symmetrical Loading," *Quarterly of Applied Mathematics*, vol. 13, 1955, pp. 63–72.

5 P. G. Hodge, Jr., "Rigid-Plastic Analysis of Symmetrically Loaded Cylindrical Shells," JOURNAL OF APPLIED MECHANICS, vol. 21, TRANS. ASME, vol. 76, 1954, pp. 336–342.

6 S. B. Batdorf, "A Simplified Method of Elastic-Stability Analysis for Thin Cylindrical Shells," NACA Report No. 874, 1947.

7 L. H. Donnell, "A New Theory for the Buckling of Thin Cylinders Under Axial Compression and Bending," TRANS. ASME, vol. 56, 1934, pp. 795–806.

8 P. G. Hodge, Jr., and S. V. Nardo, "Carrying Capacity of an Elastic-Plastic Cylindrical Shell With Linear Strain Hardening," JOURNAL OF APPLIED MECHANICS, vol. 25, TRANS. ASME, vol. 80, 1958, pp. 79–85.

APPENDIX

Solution of Transcendental Equation (39)

Equation (39) can be written in the expanded form

$$2 \cos ku = 1 + \cos 2k \cos ku + \sin 2k \sin ku \qquad (44)$$

It will prove convenient to introduce the new variable ϑ defined by the transformation

$$\begin{aligned} \sin 2k/(5 - 4 \cos 2k)^{1/2} &= \sin \vartheta, \\ (2 - \cos 2k)/(5 - 4 \cos 2k)^{1/2} &= \cos \vartheta \end{aligned} \qquad (45)$$

If Equations (45) are substituted into Equation (44), the following relationship results:

$$\cos \vartheta \cos ku - \sin \vartheta \sin ku = (5 - 4 \cos 2k)^{-1/2}, \qquad (46)$$

or

$$\cos (\vartheta + ku) = (5 - 4 \cos 2k)^{-1/2} \qquad (47)$$

The solution of Equation (47) can be written

$$u = (1/k)(\varphi - \vartheta + 2n\pi), \qquad (48)$$

where $n = 0, \pm 1, \pm 2, \ldots$, and

$$\cos \varphi = (5 - 4 \cos 2k)^{-1/2}, \qquad (49)$$

$$\tan \vartheta = \sin 2k/(2 - \cos 2k) \qquad (50)$$

The inverse trigonometric functions are considered restricted to the ranges

$$-\pi/2 \leq \varphi \leq \pi/2$$
$$-\pi/2 \leq \vartheta \leq \pi/2 \tag{51}$$

It must be remembered that the solution desired is subject to the following two inequalities

$$0 \leq ku \leq \pi/2, \tag{42}$$
$$0 \leq 2k \leq 3\pi/2 \tag{43}$$

It will now be shown that Inequality (42) requires that $n = 0$ in Equation (48). Because of Inequalities (51), Equation (48) can be transformed into the inequality

$$-\pi/2 - \pi/2 + 2n\pi \leq ku \leq \pi/2 + \pi/2 + 2n\pi \tag{52}$$

Now if $n > 0$, the left-hand side of (52) violates Inequality (42). On the other hand if $n < 0$ the right-hand side of (52) will violate Inequality (42). Thus it follows that $n = 0$.

Equation (48) still does not define u uniquely since the function φ is double-valued in the range defined by (51), and it is necessary to choose either the positive or negative value of φ defined by Equation (49). In the range $0 \leq 2k \leq \pi$, it can be seen from Equation (50), or Equations (45), that $\vartheta \geq 0$. Therefore, in order to have $0 \leq ku$, it is necessary to use the positive value of φ in Equation (48). In the range $\pi \leq 2k \leq 3\pi/2$, it may be shown that $1.11 \leq |\varphi| \leq 1.23$ and $-0.46 \leq \vartheta \leq 0$, so that once again it is necessary to choose the positive value of φ in order to have $0 \leq ku$.

In short, the solution may be written

$$u = (1/k)(|\varphi| - \vartheta), \tag{53}$$

where $|\varphi|$ and ϑ are uniquely defined by Equations (49), (50), and Inequalities (51). The function $u(k)$ is shown in Fig. 9 for the range of interest.

It will now be shown that, if the modulus of elasticity E increases without limit so that the material becomes rigid-plastic, the carrying capacity P given by Equation (40) becomes equal to the rigid-plastic collapse load P_0^m given by Equation (32). If E is very large, and therefore k is very small, Equation (41) can be written as

$$\psi = \frac{2}{k^2}\,\frac{1 - \cos ku}{\cos ku} = \frac{2}{k^2}\,\frac{k^2u^2}{2} + \ldots \doteq u^2, \tag{54}$$

and Equation (50) shows that

$$\vartheta \doteq 2k \tag{55}$$

Equation (49) becomes

$$\cos\varphi = [5 - 4(1 - 4k^2/2)]^{-1/2} = [1 + 8k^2]^{-1/2}$$
$$= 1 - 4k^2 + \ldots = 1 - \frac{1}{2}\,(\sqrt{8}\,k)^2 + \ldots$$

or

$$\varphi \doteq \sqrt{8}\,k \tag{56}$$

If Equations (55) and (56) are substituted into Equation (48) there results, for small values of k,

$$u \doteq (1/k)(\sqrt{8}\,k - 2k) = 2(\sqrt{2} - 1) \tag{57}$$

This result agrees completely with Equation (31) as it should.

Upon substitution of Equations (54) and (57) into Equation (40) one obtains

$$P = (2 + 2c^2u^2)/(1 + 2c^2u^2) = P_0^m \tag{58}$$

R. D. MINDLIN

Professor of Civil Engineering, Columbia University, New York, N. Y. Mem. ASME

M. A. MEDICK[2]

Senior Staff Scientist, Avco Research and Advanced Development Division, Avco Manufacturing Company, Lawrence, Mass.

Extensional Vibrations of Elastic Plates[1]

A system of approximate, two-dimensional equations of extensional motion of isotropic, elastic plates is derived. The equations take into account the coupling between extensional, symmetric thickness-stretch and symmetric thickness-shear modes and also include two face-shear modes. The spectrum of frequencies for real, imaginary, and complex wave numbers in an infinite plate is explored in detail and compared with the corresponding solution of the three-dimensional equations.

In a previous paper [1][3] a derivation was given of approximate equations of motion that take into account the coupling between face and thickness modes of extensional vibration of elastic plates. The thickness motion considered was that of the lowest thickness-stretch mode, in which the displacement is normal to the middle plane of the plate and the middle plane is the nodal plane. The frequency of this mode depends on Poisson's ratio (ν); the frequency increasing with increasing ν. When $\nu > 1/3$, the frequency of the lowest thickness-stretch mode is higher than the frequency, independent of ν, of the lowest, symmetric thickness-shear mode. In the latter, the displacement is also unidirectional but it is parallel to the middle plane of the plate and there are two nodal planes symmetrically disposed with respect to the middle plane. In the range of Poisson's ratios commonly encountered, both thickness modes can couple with the face modes and with each other. This circumstance has a marked influence on phase and group velocities of waves and on the frequencies and shapes of high-frequency vibrational modes. In the present paper, a derivation is given of approximate equations of motion which include the effects of both thickness modes.

The approximate, two-dimensional equations are deduced from the three-dimensional equations of elasticity by a procedure based on the series-expansion methods of Poisson [2] and Cauchy [3], and the integral method of Kirchhoff [4]. A detailed exposition of the procedure, using a power series, and its application to approximations of orders zero and one are given elsewhere [5]. In approximations of the second and higher orders, awkward mathematical forms are encountered due to the lack of orthogonality of the terms of a power series. At the suggestion of W. Prager, an expansion in a series of Legendre polynomials was studied. In that case, although similar awkward forms appear as a result of the more complicated formula for the derivative, they do not occur, for the most part, until the terms of the third order are reached. Hence the expansion in a series of Legendre polynomials is a convenient one on which to base the present second-order approximation. The method of derivation and the resulting equations (with the inertia terms omitted) are closely related to E. Reissner's theory [6] of three-dimensional corrections for the equations of generalized plane stress.

The expansion in a series of Legendre polynomials of the thickness co-ordinate, followed by an integration across the thickness, converts the three-dimensional equations of elasticity into an infinite series of two-dimensional equations which then are truncated to produce the approximate equations. The full series expressions of displacement, strain, stress, energies, and equations of motion, in conjunction with an understanding of Rayleigh's [7] exact solution of the problem of vibrations of an infinite plate, are of aid in deciding what to include in various orders of approximation and in understanding the implications of what is discarded and what retained. The series expressions and Rayleigh's exact solution also supply both the motivation and the necessary data for making adjustments, of terms that are left after the truncation, in addition to an adjustment of the type made by Poisson in establishing the zero-order equations.

The adjustment analogous to Poisson's serves to uncouple the modes retained from the higher ones without seriously affecting the behavior of the lower ones. The additional adjustments are made to improve the match between the frequency spectra of an infinite plate as obtained from the approximate and exact equations. This is accomplished by the introduction of coefficients analogous to the shear coefficient in the Timoshenko beam equations [8] and the analogous equations for plates [9]. In the latter paper [9] it was shown how the shear coefficient may be chosen to effect a perfect match in one or another part of the spectrum depending upon the frequency range and mode of greatest interest in a particular application of the approximate equations. In the present case, four such coefficients are introduced and, owing to the complexity of the spectrum, several possible combinations of matching points present themselves. The choice is made here to do all the matching at zero wave number. The range of wave numbers and frequencies over which the match remains good is a measure of both the usefulness of the approximate equations and their range of applicability. In this range, solutions of the approximate equations, in the case of finite plates, may be expected to be reliable inasmuch as these solutions are composed essentially of combinations of the modes and overtones of the infinite plate.

When both the symmetric thickness-shear and thickness-stretch deformations are taken into account, important properties of the frequency spectrum contained in the exact theory are reproduced in the resulting approximate equations of the second order, whereas they do not appear in the previous approximation of the first order [1]. These properties of the exact frequency spectrum include the imaginary loop discovered by Aggarwal and Shaw [10]; the anomalous behavior of the second and third branches

---

[1] This investigation was supported by the Office of Naval Research and the U. S. Army Signal Engineering Laboratories.

[2] Formerly Research Assistant, Department of Civil Engineering and Engineering Mechanics, Columbia University, New York, N. Y.

[3] Numbers in brackets designate References at end of paper.

Presented at the Summer Conference of the Applied Mechanics Division, Troy, N. Y., June 18–20, 1959, of The American Society of Mechanical Engineers.

Discussion of this paper should be addressed to the Secretary, ASME, 29 West 39th Street, New York, N. Y., and will be accepted until January 10, 1960, for publication at a later date. Discussion received after the closing date will be returned.

Note: Statements and opinions advanced in papers are to be understood as individual expressions of their authors and not those of the Society. Manuscript received by ASME Applied Mechanics Division, June 25, 1958. Paper No. 59—APM-4.

with variation of Poisson's ratio [5]; the frequency minimum of the second branch [5] with its associated zero group velocity at a nonzero wave number and phase and group velocities of opposite sign at smaller wave numbers, as described by Tolstoy and Usdin [11]; and, finally, a pair of complex branches which account for edge vibrations observed in experiments.

Expansion in Infinite Series

We refer the plate to rectangular co-ordinates x_i ($i = 1, 2, 3$) with x_1 and x_3 in the middle plane and the faces at $x_2 = \pm b$. The components of displacement u_j ($j = 1, 2, 3$) are expressed as

$$u_j = \sum_{n=0}^{\infty} P_n(\eta) u_j^{(n)}(x_1, x_3, t), \tag{1}$$

where $\eta = x_2/b$, the $P_n(\eta)$ are the Legendre polynomials

$$P_0(\eta) = 1, \quad P_1(\eta) = \eta, \quad P_2(\eta) = (3\eta^2 - 1)/2, \ldots$$

$$\ldots P_n(\eta) = \frac{1}{2^n n!} \frac{d^n(\eta^2 - 1)^n}{d\eta^n}, \ldots$$

and the $u_j^{(n)}$, it is to be noted, are functions of the co-ordinates x_1, x_3, and the time t, only. The $u_j^{(n)}$ are the amplitudes of polynomial distributions of displacements across the thickness of the plate. For convenience, however, they will be referred to as displacements of order n or, simply, as displacements.

Stress Equations of Motion. The series expression for the displacement is substituted in the equation

$$\int_V (\tau_{ij,i} - \rho \ddot{u}_j) \delta u_j dV = 0, \tag{2}$$

which is obtained from the variational equation of motion.[4] In Equation (2) the integration is over the volume V of the plate; the τ_{ij} are the components of stress; and the summation convention for repeated indexes is employed, as are the comma notation for differentiation with respect to the co-ordinates x_i and the dot notation for differentiation with respect to time.

When the integration with respect to η, from -1 to $+1$, is performed in Equation (2), the result is

$$\int_A \sum_{n=0}^{\infty} (b\tau_{ij,i}^{(n)} - \sum_{m=1,3\ldots}^{n} D_{mn}\tau_{2j}^{(n-m)} + F_j^{(n)} - \rho b C_n \ddot{u}_j^{(n)}) \delta u_j^{(n)} dA = 0, \tag{3}$$

where A is the area of the plate and

$$\tau_{ij}^{(n)} = \int_{-1}^{1} P_n(\eta)\tau_{ij} d\eta, \quad F_j^{(n)} = [P_n(\eta)\tau_{2j}]_{-1}^{1},$$
$$D_{mn} = 2(n - m) + 1, \quad C_n = 2/(2n + 1). \tag{4}$$

The $\tau_{ij}^{(n)}$ and $F_j^{(n)}$ are defined as the nth-order components of stress and face traction, respectively; while the constants D_{mn} and C_n arise from the operations

$$\frac{dP_n}{d\eta} = \sum_{m=1,3\ldots}^{n} D_{mn} P_{n-m}, \quad \int_{-1}^{1} P_m P_n d\eta = \begin{cases} 0, & m \neq n, \\ C_n, & m = n. \end{cases} \tag{5}$$

The appearance of $F_j^{(n)}$ and $\tau_{2j}^{(n-m)}$, in Equation (3), follows from an integration, by parts, of the terms in Equation (2) that contain $\partial/\partial x_2$.

Since Equation (3) must hold for all A and arbitrary $\delta u_j^{(n)}$, the quantity in parentheses must vanish and we arrive at the stress equations of motion of order n:

$$b\tau_{ij,i}^{(n)} - \sum_{m=1,3\ldots}^{n} D_{mn}\tau_{2j}^{(n-m)} + F_j^{(n)} = \rho b C_n \ddot{u}_j^{(n)}. \tag{6}$$

In the analogous equations of motion obtained from an expansion in power series,[5] an infinite series appears on the right-hand side and no series appears on the left-hand side. However, the series in Equation (6) contributes more than one term only for $n > 2$.

Strain. In the three-dimensional theory, the components of strain ϵ_{ij} are expressed in terms of the components of displacement by

$$2\epsilon_{ij} = u_{i,j} + u_{j,i}. \tag{7}$$

Inserting the series expansion from Equation (1) and using the formula for the derivative from Equation (5), we find

$$2\epsilon_{ij} = \sum_{n=0}^{\infty} \sum_{m=1,3\ldots}^{n} [(u_{i,j}^{(n)} + u_{j,i}^{(n)})P_n + (\delta_{2j}u_i^{(n)} + \delta_{2i}u_j^{(n)})b^{-1}D_{mn}P_{n-m}], \tag{8}$$

where δ_{2j} is the Kronecker symbol δ_{ij} with $i = 2$.

In order to define components of strain of order n, the summand in Equation (8) must be expressed as the product of P_n and a function independent of x_2. Considering the double sum as a triangular array and interchanging the order of summation of columns and rows, we find

$$\epsilon_{ij} = \sum_{n=0}^{\infty} P_n \epsilon_{ij}^{(n)} \tag{9}$$

where the $\epsilon_{ij}^{(n)}$, defined as the components of strain of order n, are given by

$$2\epsilon_{ij}^{(n)} = u_{i,j}^{(n)} + u_{j,i}^{(n)} + b^{-1}(2n + 1) \sum_{m=1,3\ldots}^{\infty} (\delta_{2j}u_i^{(m+n)} + \delta_{2i}u_j^{(m+n)}). \tag{10}$$

In the analogous expression obtained by a power-series expansion[6] there is no sum over m. However, the additional terms in Equation (10) do not appear until $m = 3$.

Stress-Strain Relations. The relations between the $\tau_{ij}^{(n)}$ and the $\epsilon_{ij}^{(n)}$ may be obtained by inserting the three-dimensional expressions

$$\tau_{ij} = c_{ijkl}\epsilon_{kl} = c_{ijkl} \sum_{n=0}^{\infty} P_n \epsilon_{kl}^{(n)} \tag{11}$$

in the first of Equations (4). After performing the integration, we find

$$\tau_{ij}^{(n)} = C_n c_{ijkl} \epsilon_{kl}^{(n)}. \tag{12}$$

For later use, it is convenient to have Equation (12) expressed in the reduced indicial notation, in which double indexes ranging from 1 to 3 are replaced by single indexes, ranging from 1 to 6, as follows:

$$\tau_1 = \tau_{11}, \quad \tau_4 = \tau_{23}, \quad \epsilon_1 = \epsilon_{11}, \quad \epsilon_4 = 2\epsilon_{23},$$
$$\tau_2 = \tau_{22}, \quad \tau_5 = \tau_{31}, \quad \epsilon_2 = \epsilon_{22}, \quad \epsilon_5 = 2\epsilon_{31},$$
$$\tau_3 = \tau_{33}, \quad \tau_6 = \tau_{12}; \quad \epsilon_3 = \epsilon_{33}, \quad \epsilon_6 = 2\epsilon_{12}.$$

Then Equation (12) becomes

$$\tau_p^{(n)} = C_n c_{pq} \epsilon_q^{(n)}; \quad p, q = 1, 2, \ldots 6, \; c_{pq} = c_{qp}. \tag{13}$$

[4] Reference [12], p. 167.

[5] Reference [5], p. 3.04.

[6] Ibid., p. 3.08.

Energy Densities. Using the strain energy density U given in the three-dimensional theory by

$$2U = c_{ijkl}\epsilon_{ij}\epsilon_{kl} = c_{pq}\epsilon_p\epsilon_q, \tag{14}$$

we define a plate-strain energy density

$$\bar{U} = \int_{-1}^{1} U d\eta \tag{15}$$

and find, with the aid of Equations (14), (9), and the second of (5),

$$2\bar{U} = c_{pq}\sum_{n=0}^{\infty} C_n \epsilon_p^{(n)}\epsilon_q^{(n)}. \tag{16}$$

We also note that

$$2\bar{U} = \sum_{n=0}^{\infty} \tau_p^{(n)}\epsilon_p^{(n)}, \tag{17}$$

$$\tau_p^{(n)} = \partial\bar{U}/\partial\epsilon_p^{(n)}. \tag{18}$$

Similarly, using the kinetic energy density K as given in the three-dimensional theory by

$$2K = \rho\dot{u}_j\dot{u}_j, \tag{19}$$

we define a kinetic energy density of the plate by

$$2\bar{K} = 2\int_{-1}^{1} K d\eta = \rho\sum_{n=0}^{\infty} C_n \dot{u}_j^{(n)}\dot{u}_j^{(n)}. \tag{20}$$

Extensional Vibrations of Isotropic Plates

When the plate is isotropic, motions symmetric (extensional) and antisymmetric (flexural), with respect to the middle plane, may be considered separately. In the case of the former, only those components of displacement $u_j^{(n)}$ are retained for which $j + n$ is odd. As a result, only those components of stress $\tau_{ij}^{(n)}$ and strain $\epsilon_{ij}^{(n)}$ appear for which $i + j + n$ is even.

The stress-equations of motion (6) then are

$$\begin{aligned}
&\frac{\partial\tau_1^{(0)}}{\partial x_1} + \frac{\partial\tau_5^{(0)}}{\partial x_3} + \frac{F_1^{(0)}}{b} = 2\rho\frac{\partial^2 u_1^{(0)}}{\partial t^2}\\
&\frac{\partial\tau_5^{(0)}}{\partial x_1} + \frac{\partial\tau_3^{(0)}}{\partial x_3} + \frac{F_3^{(0)}}{b} = 2\rho\frac{\partial^2 u_3^{(0)}}{\partial t^2}\\
&\frac{\partial\tau_6^{(1)}}{\partial x_1} + \frac{\partial\tau_4^{(1)}}{\partial x_3} - \frac{\tau_2^{(0)}}{b} + \frac{F_2^{(1)}}{b} = \frac{2\rho}{3}\frac{\partial^2 u_2^{(1)}}{\partial t^2}\\
&\frac{\partial\tau_1^{(2)}}{\partial x_1} + \frac{\partial\tau_5^{(2)}}{\partial x_3} - \frac{3\tau_6^{(1)}}{b} + \frac{F_1^{(2)}}{b} = \frac{2\rho}{5}\frac{\partial^2 u_1^{(2)}}{\partial t^2}\\
&\frac{\partial\tau_5^{(2)}}{\partial x_1} + \frac{\partial\tau_3^{(2)}}{\partial x_3} - \frac{3\tau_4^{(1)}}{b} + \frac{F_3^{(2)}}{b} = \frac{2\rho}{5}\frac{\partial^2 u_3^{(2)}}{\partial t^2}\\
&\frac{\partial\tau_6^{(3)}}{\partial x_1} + \frac{\partial\tau_4^{(3)}}{\partial x_3} - \frac{5\tau_2^{(2)}}{b} - \frac{\tau_2^{(0)}}{b} + \frac{F_2^{(3)}}{b} = \frac{2\rho}{7}\frac{\partial^2 u_2^{(3)}}{\partial t^2}\\
&\quad\cdots\qquad\cdots\\
&\quad\cdots\qquad\cdots\\
&\quad\cdots\qquad\cdots
\end{aligned} \tag{21}$$

The components of strain that remain, in Equations (10), are

$$\begin{aligned}
\epsilon_1^{(0)} &= \partial u_1^{(0)}/\partial x_1\\
\epsilon_2^{(0)} &= (u_2^{(1)} + u_2^{(3)} + \ldots)/b\\
\epsilon_3^{(0)} &= \partial u_3^{(0)}/\partial x_3\\
\epsilon_5^{(0)} &= \partial u_3^{(0)}/\partial x_1 + \partial u_1^{(0)}/\partial x_3\\
\epsilon_4^{(1)} &= \partial u_2^{(1)}/\partial x_3 + 3(u_2^{(2)} + u_3^{(4)} + \ldots)/b\\
\epsilon_6^{(1)} &= \partial u_2^{(1)}/\partial x_1 + 3(u_1^{(2)} + u_1^{(4)} + \ldots)/b
\end{aligned}$$

$$\begin{aligned}
\epsilon_1^{(2)} &= \partial u_1^{(2)}/\partial x_1\\
\epsilon_2^{(2)} &= 5(u_2^{(3)} + u_2^{(5)} + \ldots)/b\\
\epsilon_3^{(2)} &= \partial u_3^{(2)}/\partial x_3\\
\epsilon_5^{(2)} &= \partial u_3^{(2)}/\partial x_1 + \partial u_1^{(2)}/\partial x_3\\
\epsilon_4^{(3)} &= \partial u_2^{(3)}/\partial x_3 + 7(u_3^{(4)} + u_3^{(6)} + \ldots)/b\\
\epsilon_6^{(3)} &= \partial u_2^{(3)}/\partial x_1 + 7(u_1^{(4)} + u_1^{(6)} + \ldots)/b\\
&\cdots\qquad\cdots\\
&\cdots\qquad\cdots\\
&\cdots\qquad\cdots
\end{aligned} \tag{22}$$

The stress-strain relations (13) reduce to

$$\begin{aligned}
\tau_1^{(0)} &= 2[(\lambda + 2\mu)\epsilon_1^{(0)} + \lambda(\epsilon_2^{(0)} + \epsilon_3^{(0)})]\\
\tau_2^{(0)} &= 2[(\lambda + 2\mu)\epsilon_2^{(0)} + \lambda(\epsilon_3^{(0)} + \epsilon_1^{(0)})]\\
\tau_3^{(0)} &= 2[(\lambda + 2\mu)\epsilon_3^{(0)} + \lambda(\epsilon_1^{(0)} + \epsilon_2^{(0)})]\\
\tau_5^{(0)} &= 2\mu\epsilon_5^{(0)}\\
\tau_4^{(1)} &= 2\mu\epsilon_4^{(1)}/3\\
\tau_6^{(1)} &= 2\mu\epsilon_6^{(1)}/3\\
\tau_1^{(2)} &= 2[(\lambda + 2\mu)\epsilon_1^{(2)} + \lambda(\epsilon_2^{(2)} + \epsilon_3^{(2)})]/5\\
\tau_2^{(2)} &= 2[(\lambda + 2\mu)\epsilon_2^{(2)} + \lambda(\epsilon_3^{(2)} + \epsilon_1^{(2)})]/5\\
\tau_3^{(2)} &= 2[(\lambda + 2\mu)\epsilon_3^{(2)} + \lambda(\epsilon_1^{(2)} + \epsilon_2^{(2)})]/5\\
\tau_5^{(2)} &= 2\mu\epsilon_5^{(2)}/5\\
\tau_4^{(3)} &= 2\mu\epsilon_4^{(3)}/7\\
\tau_6^{(3)} &= 2\mu\epsilon_6^{(3)}/7\\
&\cdots\qquad\cdots\\
&\cdots\qquad\cdots\\
&\cdots\qquad\cdots
\end{aligned} \tag{23}$$

where λ and μ are Lamé's constants.

The strain energy density, in the form given in Equation (17), becomes

$$\begin{aligned}
2\bar{U} = {}& \tau_1^{(0)}\epsilon_1^{(0)} + \tau_2^{(0)}\epsilon_2^{(0)} + \tau_3^{(0)}\epsilon_3^{(0)}\\
&+ \tau_5^{(0)}\epsilon_5^{(0)} + \tau_4^{(1)}\epsilon_4^{(1)} + \tau_6^{(1)}\epsilon_6^{(1)}\\
&+ \tau_1^{(2)}\epsilon_1^{(2)} + \tau_2^{(2)}\epsilon_2^{(2)} + \tau_3^{(2)}\epsilon_3^{(2)}\\
&+ \tau_5^{(2)}\epsilon_5^{(2)} + \tau_4^{(3)}\epsilon_4^{(3)} + \tau_6^{(3)}\epsilon_6^{(3)}\\
&+ \ldots
\end{aligned} \tag{24}$$

and, finally, the kinetic energy density (20) is

$$\begin{aligned}
\bar{K} = {}& \rho(\dot{u}_1^{(0)}\dot{u}_1^{(0)} + \dot{u}_2^{(0)}\dot{u}_2^{(0)} + {}^1/_3\dot{u}_2^{(1)}\dot{u}_2^{(1)}\\
&+ {}^1/_5\dot{u}_1^{(2)}\dot{u}_1^{(2)} + {}^1/_5\dot{u}_3^{(2)}\dot{u}_3^{(2)} + {}^1/_7\dot{u}_2^{(3)}\dot{u}_2^{(3)} + \ldots).
\end{aligned} \tag{25}$$

Truncation of Series

We begin by setting

$$\begin{aligned}
u_1^{(n)} &= 0, \quad u_3^{(n)} = 0, \quad n > 2,\\
u_2^{(n)} &= 0, \quad n > 3.
\end{aligned} \tag{26}$$

This leaves only the components $u_1^{(0)}$, $u_3^{(0)}$, $u_2^{(1)}$, $u_1^{(2)}$, $u_3^{(2)}$, and $u_2^{(3)}$, as illustrated in Fig. 1. The terms $u_1^{(0)}$ and $u_3^{(0)}$ are the amplitudes of uniform distributions that represent the thickness distributions of displacements which occur in low-frequency extensional and shear motions in the plane of the plate; $u_2^{(1)}$ is the amplitude of a linear distribution of displacement which is

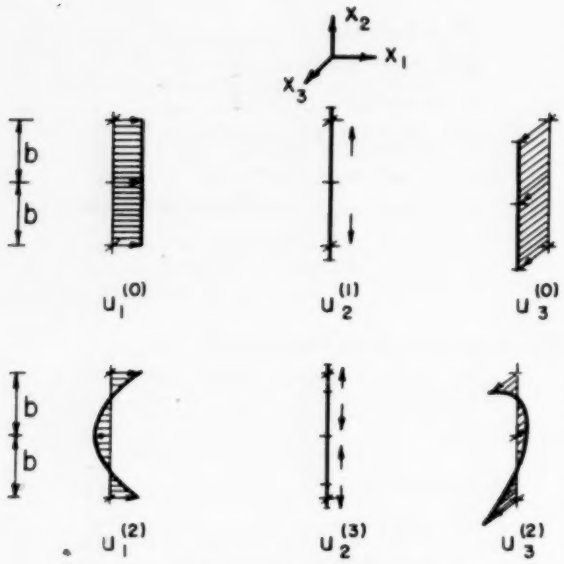

Fig. 1 Components of displacement

an approximation to the exact sinusoidal distribution in the lowest, symmetric, thickness-stretch mode; $u_1^{(2)}$ and $u_3^{(2)}$ are the amplitudes of quadratic distributions of displacements which are approximations to the sinusoidal distributions in the lowest, symmetric, thickness-shear mode, and the face-shear mode of the same order.

The last "displacement" retained ($u_2^{(3)}$) is the amplitude of a cubic distribution which is an approximation to the sinusoidal distribution of displacement in the second, symmetric, thickness-stretch mode. This is a mode of higher order than is to be included in the approximate equations of the second order which we seek. However, $u_2^{(3)}$ produces the second-order strain $\epsilon_2^{(2)}$ [see the eighth of Equations (22)] which, in turn, appears in the second-order stress-strain relations [see the seventh, eighth, and ninth of Equations (23)]. In order to permit the alternating expansion and contraction, through the thickness, which should accompany the stresses $\tau_1^{(2)}$ and $\tau_3^{(2)}$ (by coupling through Poisson's ratio) and at the same time avoid coupling with the undesired higher mode, the thickness stress $\tau_2^{(2)}$ and the velocity $\dot{u}_2^{(3)}$ are set equal to zero. The eighth of Equations (23) is then used to express $\epsilon_2^{(2)}$ in terms of $\epsilon_1^{(2)}$ and $\epsilon_3^{(2)}$:

$$\epsilon_2^{(2)} = -\lambda(\epsilon_2^{(2)} + \epsilon_1^{(2)})/(\lambda + 2\mu) \tag{27}$$

and this result is substituted in the expressions for $\tau_1^{(2)}$ and $\tau_3^{(2)}$ to obtain

$$\begin{aligned} \tau_1^{(2)} &= 2E'(\epsilon_1^{(2)} + \nu\epsilon_3^{(2)})/5, \\ \tau_3^{(2)} &= 2E'(\epsilon_3^{(2)} + \nu\epsilon_1^{(2)})/5, \end{aligned} \tag{28}$$

where $\nu = \lambda/2(\lambda + \mu)$ is Poisson's ratio and

$$E' = 4\mu(\lambda + \mu)/(\lambda + 2\mu) = E/(1 - \nu^2), \tag{29}$$

in which E is Young's modulus. In addition, the contributions of the stresses $\tau_4^{(2)}$ and $\tau_6^{(2)}$ to the strain energy [see Equation (24)] are neglected in order to destroy coupling with the unwanted higher mode when the displacements vary with x_1 and x_3.

At this stage, the stress equations of motion end with the fifth of Equations (21); the strain-displacement relations end with $\epsilon_5^{(2)}$ in Equations (22); the stress-strain relations end with $\tau_5^{(2)}$ in Equations (23), with the expressions for $\tau_1^{(2)}$, $\tau_2^{(2)}$, and $\tau_3^{(2)}$ replaced by Equations (27) and (28); the strain energy density ends with the third line in Equation (24); and the kinetic energy density ends with the fifth term in Equation (25).

Up to this point, the process of truncating the series expressions and adjusting the remaining terms is similar to the one employed by Poisson [2] to obtain the zero-order equations of extensional motions of isotropic plates,[7] the main difference being that here the process is carried on at a level two orders higher. In Poisson's equations only the zero-order displacements $u_1^{(0)}$ and $u_3^{(0)}$ survive. These are the amplitudes of uniform distributions, across the thickness of the plate, which are good approximations to the nearly uniform distributions found in the lowest extensional mode of the exact theory (at long wave lengths) and are exact for the lowest face-shear mode at all wave lengths. The additional terms $u_2^{(1)}$, $u_1^{(2)}$, and $u_3^{(2)}$, which are now included, are the amplitudes of first and second-degree polynomials and these are not good approximations to the distributions in the thickness-stretch and thickness-shear modes of the exact theory. For example, at infinite wave length along the plate, the exact distributions are sinusoidal across the thickness. It is advisable, therefore, to introduce additional adjustments to compensate, as well as possible, for the omission of the polynomials of higher degrees.

The incorrect distributions of displacements affect the frequencies mainly through the thickness strains and velocities. Accordingly, we make the substitutions

$$\begin{aligned} &\kappa_1\epsilon_2^{(0)} \text{ for } \epsilon_2^{(0)}, \qquad &&\kappa_3\dot{u}_2^{(1)} \text{ for } \dot{u}_2^{(1)}, \\ &\kappa_2\epsilon_4^{(1)} \text{ for } \epsilon_4^{(1)}, \qquad &&\kappa_4\dot{u}_1^{(2)} \text{ for } \dot{u}_1^{(2)}, \\ &\kappa_2\epsilon_6^{(1)} \text{ for } \epsilon_6^{(1)}, \qquad &&\kappa_4\dot{u}_3^{(2)} \text{ for } \dot{u}_3^{(2)} \end{aligned}$$

in the strain energy and kinetic energy densities, so that the coefficients κ_r ($r = 1, 2, 3, 4$) will be available for appropriate adjustments of the equations.

Finally, as a matter of expediency, we omit the term $u_2^{(3)}$ from the strain $\epsilon_2^{(0)}$. This term complicates the equations and may be shown to have little influence on the long wave-length end of the spectrum.

Second-Order Approximation

As a result of the truncations and adjustments described in the preceding section, the variables and equations of the second-order approximation are

Kinetic Energy Density:

$$\begin{aligned} \bar{K}^{(2)} = \rho\,[&\dot{u}_1^{(0)}\dot{u}_1^{(0)} + \dot{u}_3^{(0)}\dot{u}_3^{(0)} + {}^1/_3\,\kappa_3^2\dot{u}_2^{(1)}\dot{u}_2^{(1)} \\ &+ {}^1/_5\,\kappa_4^2(\dot{u}_1^{(2)}\dot{u}_1^{(2)} + \dot{u}_3^{(2)}\dot{u}_3^{(2)})] \end{aligned} \tag{30}$$

Strain Energy Density:

$$\begin{aligned} \bar{U}^{(2)} = {}&(\lambda + 2\mu)(\epsilon_1^{(0)}\epsilon_1^{(0)} + \kappa_1^2\epsilon_2^{(0)}\epsilon_2^{(0)} + \epsilon_3^{(0)}\epsilon_3^{(0)}) \\ &+ 2\lambda(\kappa_1\epsilon_2^{(0)}\epsilon_5^{(0)} + \epsilon_5^{(0)}\epsilon_1^{(0)} + \kappa_1\epsilon_1^{(0)}\epsilon_2^{(0)}) \\ &+ \mu\epsilon_5^{(0)}\epsilon_5^{(0)} + \mu\kappa_2^2(\epsilon_4^{(1)}\epsilon_4^{(1)} + \epsilon_6^{(1)}\epsilon_6^{(1)})/3 \\ &+ E'(\epsilon_1^{(2)}\epsilon_1^{(2)} + \epsilon_3^{(2)}\epsilon_3^{(2)} + 2\nu\epsilon_1^{(2)}\epsilon_3^{(2)})/5 + \mu\epsilon_5^{(2)}\epsilon_5^{(2)}/5 \end{aligned} \tag{31}$$

Stress-Strain Relations ($\tau_p^{(n)} = \partial\bar{U}^{(2)}/\partial\epsilon_p^{(n)}$):

$$\begin{aligned} \tau_1^{(0)} &= 2[(\lambda + 2\mu)\epsilon_1^{(0)} + \lambda(\kappa_2\epsilon_2^{(0)} + \epsilon_2^{(0)})] \\ \tau_2^{(0)} &= 2[\kappa_1^2(\lambda + 2\mu)\epsilon_2^{(0)} + \lambda\kappa_1(\epsilon_2^{(0)} + \epsilon_1^{(0)})] \\ \tau_3^{(0)} &= 2[(\lambda + 2\mu)\epsilon_3^{(0)} + \lambda(\epsilon_1^{(0)} + \kappa_1\epsilon_2^{(0)})] \end{aligned}$$

[7] Reference [12], p. 497.

$$
\begin{aligned}
\tau_3^{(0)} &= 2\mu\epsilon_3^{(0)} \\
\tau_4^{(1)} &= 2\mu\kappa_2^2\epsilon_4^{(1)}/3 \\
\tau_6^{(1)} &= 2\mu\kappa_2^2\epsilon_6^{(1)}/3 \\
\tau_1^{(2)} &= 2E'(\epsilon_1^{(2)} + \nu\epsilon_3^{(2)})/5 \\
\tau_2^{(2)} &= 2E'(\epsilon_3^{(2)} + \nu\epsilon_1^{(2)})/5 \\
\tau_5^{(2)} &= 2\mu\epsilon_5^{(2)}/5
\end{aligned} \tag{32}
$$

(The components of stress are illustrated in Fig. 2.)

Strain-Displacement Relations:

$$
\begin{aligned}
\epsilon_1^{(0)} &= \partial u_1^{(0)}/\partial x_1 \\
\epsilon_2^{(0)} &= u_2^{(1)}/b \\
\epsilon_3^{(0)} &= \partial u_3^{(0)}/\partial x_3 \\
\epsilon_5^{(0)} &= \partial u_3^{(0)}/\partial x_1 + \partial u_1^{(0)}/\partial x_3 \\
\epsilon_4^{(1)} &= 3u_3^{(2)}/b + \partial u_2^{(1)}/\partial x_3 \\
\epsilon_6^{(1)} &= \partial u_2^{(1)}/\partial x_1 + 3u_1^{(2)}/b \\
\epsilon_1^{(2)} &= \partial u_1^{(2)}/\partial x_1 \\
\epsilon_3^{(2)} &= \partial u_3^{(2)}/\partial x_3 \\
\epsilon_5^{(2)} &= \partial u_3^{(2)}/\partial x_1 + \partial u_1^{(2)}/\partial x_3
\end{aligned} \tag{33}
$$

(The components of strain are illustrated in Fig. 3.)

Stress Equations of Motion:

$$
\begin{aligned}
&\frac{\partial\tau_1^{(0)}}{\partial x_1} + \frac{\partial\tau_5^{(0)}}{\partial x_3} + \frac{F_1^{(0)}}{b} = 2\rho\frac{\partial^2 u_1^{(0)}}{\partial t^2} \\
&\frac{\partial\tau_5^{(0)}}{\partial x_1} + \frac{\partial\tau_3^{(0)}}{\partial x_3} + \frac{F_3^{(0)}}{b} = 2\rho\frac{\partial^2 u_3^{(0)}}{\partial t^2} \\
&\frac{\partial\tau_6^{(1)}}{\partial x_1} + \frac{\partial\tau_4^{(1)}}{\partial x_3} - \frac{\tau_2^{(0)}}{b} + \frac{F_2^{(1)}}{b} = \frac{2\rho\kappa_2^2}{3}\frac{\partial^2 u_2^{(1)}}{\partial t^2} \\
&\frac{\partial\tau_1^{(2)}}{\partial x_1} + \frac{\partial\tau_5^{(2)}}{\partial x_3} - \frac{3\tau_6^{(1)}}{b} + \frac{F_1^{(2)}}{b} = \frac{2\rho\kappa_4^2}{5}\frac{\partial^2 u_1^{(2)}}{\partial t^2} \\
&\frac{\partial\tau_5^{(2)}}{\partial x_1} + \frac{\partial\tau_3^{(2)}}{\partial x_3} - \frac{3\tau_4^{(1)}}{b} + \frac{F_3^{(2)}}{b} = \frac{2\rho\kappa_4^2}{5}\frac{\partial^2 u_3^{(2)}}{\partial t^2}
\end{aligned} \tag{34}
$$

Displacement Equations of Motion:

[obtained by substituting (33) in (32) and the result in (34)]:

$$
\begin{aligned}
&\mu\nabla^2 u_1^{(0)} + (\lambda+\mu)\frac{\partial e_0}{\partial x_1} + \frac{\lambda\kappa_1}{b}\frac{\partial u_2^{(1)}}{\partial x_1} + \frac{F_1^{(0)}}{2b} = \rho\frac{\partial^2 u_1^{(0)}}{\partial t^2} \\
&\mu\nabla^2 u_3^{(0)} + (\lambda+\mu)\frac{\partial e_0}{\partial x_3} + \frac{\lambda\kappa_1}{b}\frac{\partial u_2^{(1)}}{\partial x_3} + \frac{F_3^{(0)}}{2b} = \rho\frac{\partial^2 u_3^{(0)}}{\partial t^2} \\
&\mu\kappa_2^2\nabla^2 u_2^{(1)} - \frac{3\lambda\kappa_1 e_0}{b} - \frac{3\kappa_1^2(\lambda+2\mu)u_2^{(1)}}{b^2} \\
&\qquad + \frac{3\mu\kappa_2^2 e_2}{b} + \frac{3F_2^{(1)}}{2b} = \rho\kappa_2^2\frac{\partial^2 u_2^{(1)}}{\partial t^2} \\
&\frac{E'}{2}\left[(1-\nu)\nabla^2 u_1^{(2)} + (1+\nu)\frac{\partial e_2}{\partial x_1}\right] \\
&\qquad - \frac{5\mu\kappa_2^2}{b}\left(\frac{\partial u_2^{(1)}}{\partial x_1} + \frac{3u_1^{(2)}}{b}\right) + \frac{5F_1^{(2)}}{2b} = \rho\kappa_4^2\frac{\partial^2 u_1^{(2)}}{\partial t^2} \\
&\frac{E'}{2}\left[(1-\nu)\nabla^2 u_3^{(2)} + (1+\nu)\frac{\partial e_2}{\partial x_3}\right] \\
&\qquad - \frac{5\mu\kappa_2^2}{b}\left(\frac{\partial u_2^{(1)}}{\partial x_3} + \frac{3u_3^{(2)}}{b}\right) + \frac{5F_3^{(2)}}{2b} = \rho\kappa_4^2\frac{\partial^2 u_3^{(2)}}{\partial t^2}
\end{aligned} \tag{35}
$$

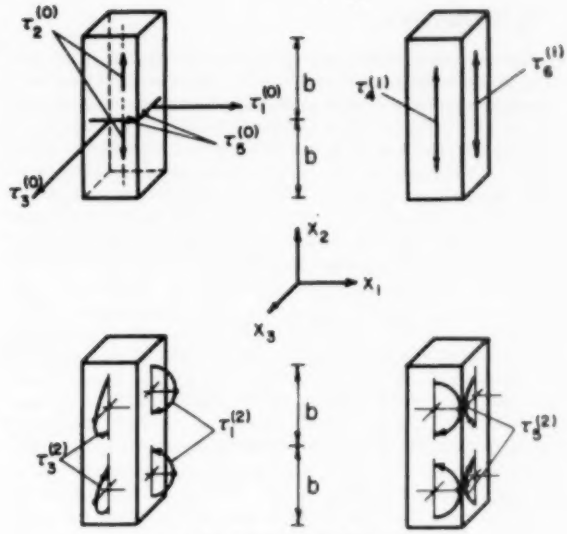

Fig. 2 Components of stress

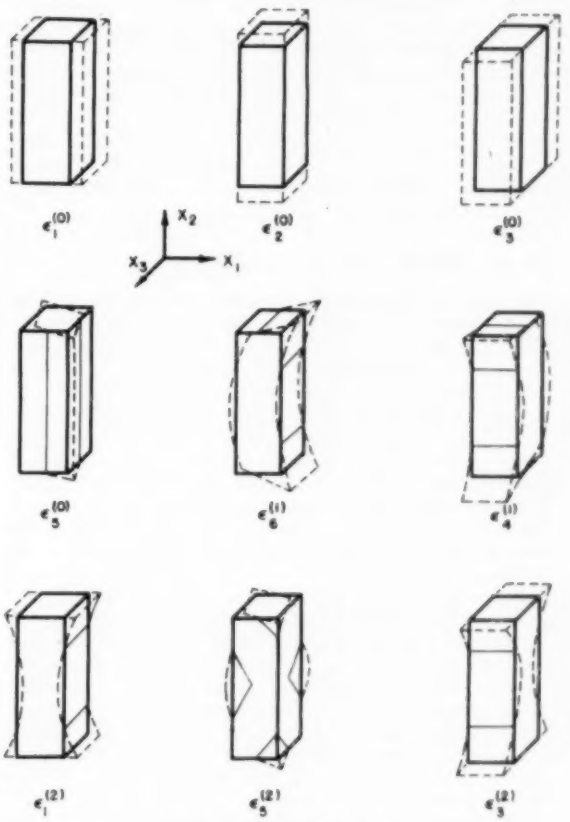

Fig. 3 Components of strain

where

$$
\nabla^2 = \frac{\partial^2}{\partial x_1^2} + \frac{\partial^2}{\partial x_3^2}, \quad e_0 = \frac{\partial u_1^{(0)}}{\partial x_1} + \frac{\partial u_3^{(0)}}{\partial x_3}, \quad e_2 = \frac{\partial u_1^{(2)}}{\partial x_1} + \frac{\partial u_3^{(2)}}{\partial x_3}.
$$

The Coefficients κ_i

The coefficients κ_i are determined from a comparison of properties of the solutions of Equations (35), for the case of straight-crested waves in an infinite plate, with the corresponding properties of the analogous solution of the three-dimensional equations. Taking the wave normal in the direction of x_1, we find that Equations (35) separate into a group of three coupled equations on $u_1^{(0)}$, $u_2^{(1)}$, and $u_1^{(2)}$, and two independent equations: one on $u_3^{(0)}$ and one on $u_3^{(2)}$. The coupled equations govern three "compressional modes" and the remaining two equations govern "face-shear" modes. To consider, first, the group of three, we set $F_j^{(n)} = 0$ and

$$u_1^{(0)} = A \sin \xi x_1 \, e^{i\omega t}, \quad u_3^{(0)} = 0,$$
$$u_2^{(1)} = B \cos \xi x_1 \, e^{i\omega t}, \tag{36}$$
$$u_1^{(2)} = C \sin \xi x_1 \, e^{i\omega t}, \quad u_3^{(2)} = 0$$

in Equations (35) and obtain the secular equation

$$\begin{vmatrix} a_{11} & a_{12} & 0 \\ a_{12} & a_{22} & a_{23} \\ 0 & a_{23} & a_{33} \end{vmatrix} = 0 \tag{37}$$

where

$$a_{11} = k^2 z^2 - \Omega^2$$
$$a_{22} = \kappa_2^2 z^2/3 + 4\kappa_1^2 k^2/\pi^2 - \kappa_2^2 \Omega^2/3$$
$$a_{33} = E' z^2/5\mu + 12\kappa_2^2/\pi^2 - \kappa_4^2 \Omega^2/5$$
$$a_{12} = 2\kappa_1 (k^2 - 2) z/\pi$$
$$a_{23} = -2\kappa_2^2 z/\pi$$

and

$$z = 2\xi b/\pi, \quad \Omega = \omega/\omega_s, \quad \omega_s = \pi(\mu/\rho)^{1/2}/2b,$$
$$k^2 = (\lambda + 2\mu)/\mu = 2(1 - \nu)/(1 - 2\nu). \tag{38}$$

We also obtain the three sets of amplitude ratios

$$A_i : B_i : C_i = 1 : a_i/z_i : a_i/b_i, \quad i = 1, 2, 3 \tag{39}$$

where

$$a_i = \pi(\Omega^2 - k^2 z_i^2)/2\kappa_1 (k^2 - 2)$$
$$b_i = \frac{3}{2\pi}\left(\frac{\pi^2 \kappa_4^2 \Omega^2}{15\kappa_2^2} - 4\right) - \frac{2\pi(k^2 - 1) z_i^2}{5\kappa_2^2 k^2}$$

and the z_i are the roots of Equation (37).

It may be seen that z, which is proportional to the wave number ξ, is the ratio of the thickness of the plate to the real half wave length along the plate; k is the ratio of the velocity of dilatational waves to the velocity of equivoluminal waves in an infinite medium; and Ω is the ratio of the frequency to the frequency of the lowest antisymmetric thickness-shear mode.

The relation between Ω and z, in Equation (37), should match, as closely as possible, the corresponding relation obtained from the three-dimensional equations. The match is improved, within the framework of the present approximation, by choosing appropriate values for the coefficients κ_i; but, since the κ_i are constants, a perfect match can be made only at one value of z for each of them. Now, large enough z corresponds to frequencies high enough to enter the range of modes that have not been included in the approximate equations. In a plate vibrating at such high frequencies under practical (i.e., not mixed) edge conditions, the high modes would, in general, couple with the ones of lower order. Thus the applicability of the approximate equations to bounded plates is limited to frequencies below the lowest frequency of the lowest neglected mode. There is, then, little advantage to be gained in matching the approximate and exact solutions at short wave lengths (large z) at the expense of a good match at long wave lengths. In fact, we go to the extreme and do all of the matching in the neighborhood of $z = 0$ primarily because of the intricate behavior of the exact solution at long wave lengths and also because this choice results in a reasonably good match out to as short wave lengths as the frequency limitation permits.

When $z = 0$, Equation (37) has the three roots

$$\Omega^2 = 0, \quad 12\kappa_1^2 k^2/\pi^2 \kappa_3^2, \quad 60\kappa_2^2/\pi^2 \kappa_4^2 \tag{40}$$

corresponding to the amplitude ratios

$$A : B : C = 1 : 0 : 0, \quad 0 : 1 : 0, \quad 0 : 0 : 1$$

respectively. It may be seen that, at infinite wave length, the three compressional modes uncouple to form an extensional, a thickness-stretch, and a thickness-shear mode. The three limiting frequencies are to be compared with the exact values

$$\Omega^2 = 0, \quad k^2, \quad 4 \tag{41}$$

of the cut-off frequencies of the extensional, first thickness-stretch and first symmetric thickness-shear modes in Rayleigh's exact solution [7]. Hence, we set

$$\kappa_1/\kappa_3 = \pi/\sqrt{12}, \quad \kappa_2/\kappa_4 = \pi/\sqrt{15} \tag{42}$$

and these relations between pairs of κ_i are used in what follows.

We proceed to examine the roots of Equation (37) in the neighborhood of the roots given in Equations (40) or (41) (which are now the same).

First, for $z \ll 1$, $\Omega \ll 1$, we find

$$\Omega^2 = 4z^2(k^2 - 1)/k^2, \tag{43}$$

i.e., phase velocity $[E/\rho(1 - \nu^2)]^{1/2}$. This is exactly the result obtained from the three-dimensional theory for the lowest mode at long wave lengths.

Next, for $z \ll 1$, $\Omega = k + \epsilon$, $\epsilon \ll 1$, Equation (37) gives

$$\frac{d\Omega}{dz} = \frac{z}{k^2 - 4}\left(\frac{\pi^2 k \kappa_2^2}{12\kappa_1^2} + \frac{(k^2 - 2)^2 (k^2 - 4)}{k^3}\right) \tag{44a}$$

and in the limit, as $k \to 2$ and $z \to 0$,

$$\frac{d\Omega}{dz} = \pm \frac{\pi \kappa_2}{4\kappa_1 \sqrt{3}}. \tag{45a}$$

Finally, for $z \ll 1$, $\Omega = 2 + \epsilon$, $\epsilon \ll 1$, we find

$$\frac{d\Omega}{dz} = \frac{\pi^2 z}{6(k^2 - 4)}\left(\frac{4(k^2 - 1)(k^2 - 4)}{5k^2 \kappa_2^2} - \frac{\kappa_2^2}{\kappa_1^2}\right) \tag{46a}$$

and in the limit, as $k \to 2$ and $z \to 0$,

$$\frac{d\Omega}{dz} = \mp \frac{\pi \kappa_2}{4\kappa_1 \sqrt{3}}. \tag{47a}$$

Equations (44a) to (47a) are to be compared with the exact values[8] given in the following correspondingly numbered equations:

$$\frac{d\Omega}{dz} = \frac{4kz}{\pi}\left(\frac{\pi}{4} + \frac{4}{k^3} \cot \frac{\pi k}{2}\right) \tag{44b}$$

$$\frac{d\Omega}{dz} = \pm \frac{2}{\pi} \tag{45b}$$

$$\frac{d\Omega}{dz} = \frac{z}{\pi}\left(\frac{\pi}{2} - \frac{4}{k} \tan \frac{\pi}{k}\right) \tag{46b}$$

[8] Reference [5], p. 2.43.

$$\frac{d\Omega}{dz} = \mp \frac{2}{\pi} \tag{47b}$$

Equating (44a) to (44b) and (46a) to (46b), we find

$$\frac{\kappa_2^2}{\kappa_1^2} = \frac{48(k^2-4)}{\pi^2 k^4}\left[\pi(k^2-1) + 4k\cot\frac{\pi k}{2}\right],$$

$$\frac{1}{\kappa_1^2} = \frac{5k^2\kappa_2^2}{4\kappa_1^2(k^2-1)(k^2-4)} \left[\frac{\kappa_2^2}{\kappa_1^2} + \frac{6(k^2-4)}{\pi^2}\left(\frac{\pi}{2} - \frac{4}{k}\tan\frac{\pi}{k}\right)\right]. \tag{48}$$

We also note, from Equations (48), that

$$\lim_{k\to 2}\frac{\kappa_2^2}{\kappa_1^2} = \frac{192}{\pi^4},$$

$$\lim_{k\to 2}\frac{1}{\kappa_1^2} = \frac{3840(\pi^2-6)}{\pi^6}. \tag{49}$$

Equations (42) and (48) give the values of the four coefficients κ_i in terms of Poisson's ratio. As a result of these relations, all of the ordinates, slopes, and curvatures of the curves Ω versus z, characterizing the frequency spectrum of the compressional modes of the approximate theory, are identical with those of the exact solution at $z = 0$. Equations (48) and, in fact, all of the equations of this second-order approximation should be used only for Poisson's ratios less than about $^7/_{16}$. Above that value, the frequency of the thickness-stretch mode is so high in the spectrum that, in the exact theory, coupling with the second symmetric thickness-shear mode becomes important and that mode is not included in the present approximation.

Turning, now, to the two face-shear modes, we set $F_j^{(n)} = 0$,

$$u_1^{(0)} = u_2^{(1)} = u_1^{(2)} = 0,$$
$$u_2^{(0)} = A_1 \cos \xi x_1 \, e^{i\omega t},$$
$$u_2^{(2)} = A_2 \cos \xi x_1 \, e^{i\omega t}, \tag{50}$$

in Equations (35), and find that $u_3^{(0)}$ and $u_3^{(2)}$ are not coupled and have frequencies given by

$$\Omega^2 = z^2, \quad 4 + z^2/\kappa_4^2 \tag{51}$$

respectively. These are to be compared with the frequencies

$$\Omega^2 = z^2, \quad 4 + z^2 \tag{52}$$

of the face-shear modes of orders zero and two obtained from the exact equations. It may be seen that the zero-order face-shear mode is reproduced exactly, in the approximate equations, for all wave lengths. The second order face-shear mode has the correct ordinate (Ω) and slope ($d\Omega/dz$) at $z = 0$ but it does not have the correct curvature because of the presence of the coefficient κ_4. By choosing $\kappa_4 = 1$, this discrepancy could be eliminated, but only at the expense of incorrect behavior of one of the coupled modes.

Frequency Spectrum

The spectrum of frequencies of the five possible modes of vibration of an infinite plate, which the approximate theory contains, is given by the five independent roots of Equations (37) and (51). We consider, first, the three compressional modes.

Equation (37) relates Ω^2 and z^2 but only real, positive values of Ω have physical significance. For real, positive Ω, the roots z^2 may be three real positive or two real positive and one real negative or one real positive and two conjugate complex. Hence the roots

$$z = x + iy$$

may be three real or two real and one imaginary or one real and two conjugate complex. In addition, the character of the spectrum is different according as Poisson's ratio is less than equal to, or greater than $^1/_3$.

We consider the case $\nu < {}^1/_3$ (i.e., $k < 2$) first. Then, when $\Omega > 2$, the three roots of Equation (37) are real ($y = 0$). They are illustrated in Fig. 4(a) (for $\nu = {}^1/_4$, i.e., $k^2 = 3$) by the three curves (full lines) marked ϕ_1, ϕ_2, ϕ_3 in the plane $y = 0$ and the region $\Omega > 2$. As Ω drops below $\Omega = 2$, the largest root ϕ_1 approaches zero with asymptotic behavior given by Equation (43); the intermediate root ϕ_2 approaches a minimum Ω^*, below which there are no real roots other than ϕ_1; the smallest root ϕ_3 approaches a minimum in the real plane $y = 0$ at $\Omega = 2$, $x = 0$ with asymptotic behavior given by Equation (46a) or (46b) which are the same in view of Equations (48). Continuing with the root ϕ_3, as Ω drops below $\Omega = 2$, the root is imaginary ($x = 0$), again with asymptotic behavior given by Equation (46a) or (46b) in the neighborhood of $\Omega = 2$. As Ω approaches k, from above, the root ϕ_2 forms a loop in the imaginary plane ($x = 0$) and approaches $\Omega = k$, $y = 0$ with asymptotic behavior given by Equation (44a) or (44b). As Ω continues to drop below $\Omega = k$, the root ϕ_2 becomes real, with behavior in the neighborhood of $\Omega = k$, $x = 0$ again given by (44a) but now x is negative. Upon further diminution of Ω, the root ϕ_2 approaches a minimum at $\Omega = \Omega^*$ and negative x. This portion of ϕ_2 (i.e., between $\Omega = k$ and $\Omega = \Omega^*$) is identified in Fig. 4(a) by $[\phi_2]$, where the brackets indicate that it is the reflection in the plane $x = 0$ that is shown. Finally, when $\Omega < \Omega^*$, the roots ϕ_2 and ϕ_3 are conjugate complex ($z = \pm x + iy$). One of them is shown, in Fig. 4(a), as the curve marked ϕ_2; this curve is also $[\phi_2]$, i.e., the reflection of the conjugate root ϕ_3 in the plane $x = 0$.

As Poisson's ratio approaches $^1/_3$ from below, the frequency of the thickness-stretch mode increases, approaching the frequency of the thickness-shear mode; i.e., at $z = 0$ the intercept $\Omega = k$ approaches $\Omega = 2$. Conjointly, the curvature of ϕ_2 at $\Omega = k$, $z = 0$ approaches negative infinity in the plane $y = 0$ and positive infinity in the plane $x = 0$ while both slopes remain zero; all in accordance with Equation (44a) or (44b). At the same time, the curvature of ϕ_3 at $\Omega = 2$, $z = 0$ approaches positive infinity in the plane $y = 0$ and negative infinity in the plane $x = 0$ while the slopes remain zero: all in accordance with Equation (46a) or (46b). Meanwhile, the imaginary loop shrinks toward the point $\Omega = 2$, $y = 0$.

At $\nu = {}^1/_3$, the thickness-stretch and thickness-shear modes have the same frequency and the slopes of the two branches of ϕ_3 become $2/\pi$ in accordance with Equations (45a) and (47a). This situation is illustrated in Fig. 4(b). Here, again, the portions marked $[\phi_3]$ are the reflections, in the plane $x = 0$ of the actual branches.

When $\nu > {}^1/_3$ the thickness-stretch mode has a frequency higher than that of the thickness-shear mode. The spectrum [illustrated in Fig. 4(c) for $\nu = {}^3/_8$] has now undergone an important change in that the imaginary branch loops up, from $\Omega = 2$, instead of down.

Since only powers of z^2 occur in Equation (35), there is another set of physically significant roots given by the reflections of the curves of Fig. 4 in the planes $x = 0$ and $y = 0$.

Turning, now, to the face-shear modes, the first root in Equation (51) yields the straight line marked H_0 in Fig. 4. The second face-shear mode gives the roots marked H_2 in the figures; these roots are real for $\Omega > 2$ and imaginary for $\Omega < 2$. As before, there is an additional set of roots given by the reflections of the curves H_0 and H_2 in the planes $x = 0$ and $y = 0$.

The spectra of the corresponding five modes, as computed from

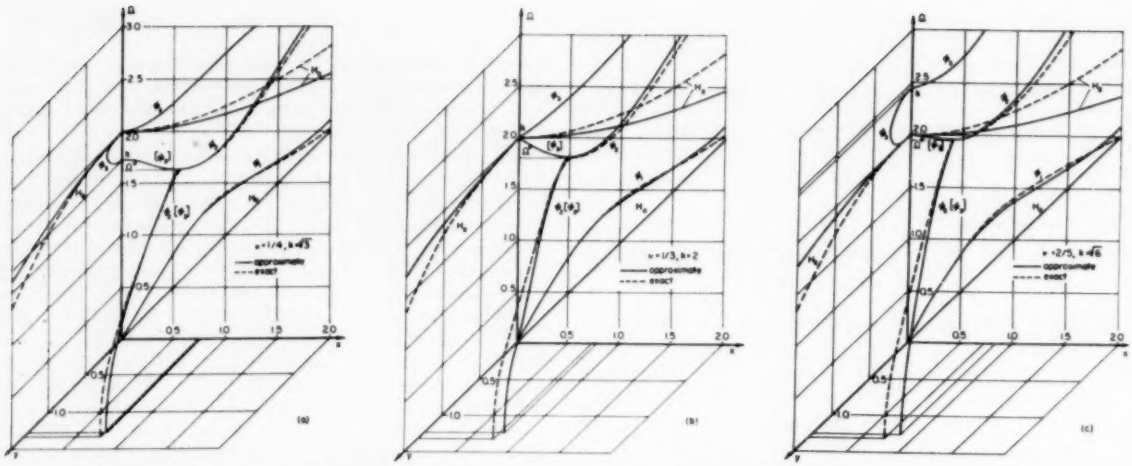

Fig. 4 Frequency spectrum of an infinite plate. Comparison of approximate and exact branches for three values of Poisson's ratio.

Rayleigh's solution of the exact equations, are also shown[9] in Figs. 4(*a*), (*b*), and (*c*) (as dashed lines). The importance of the introduction of the coefficients κ_i and their definitions, in terms of Poisson's ratio, is apparent. Without these coefficients, the extraordinarily complicated behavior of the branches of the exact frequency spectrum at long wave lengths would not be reproduced in the approximate equations. In the whole range of frequencies and wave numbers depicted, the approximate spectrum is reasonably close to the exact one; the poorest representation occurring in portions of the complex branches and the spectrum of the second face-shear mode. On the whole, fair results may be expected from solutions of the approximate equations in the case of finite plates.

The shapes of modes in the various ranges of frequency can be anticipated from the real, imaginary, or complex character of the roots. In rectangular co-ordinates, for example, real roots correspond to trigonometric mode-shapes; imaginary roots to exponential or hyperbolic mode-shapes; and complex roots correspond to modes whose shapes are given by products of trigonometric and exponential or hyperbolic functions. A striking example of the latter is to be found in the experiments with circular disks by Shaw [13].

The phase velocities (v) and group velocities (v_g) can be visualized readily from Fig. 4 inasmuch as

$$v = \frac{\omega}{\xi} = \frac{\Omega}{x}\left(\frac{\mu}{\rho}\right)^{1/2}, \qquad v_g = \frac{d\omega}{d\xi} = \frac{d\Omega}{dx}\left(\frac{\mu}{\rho}\right)^{1/2}. \tag{53}$$

For example, the phenomenon of phase and group velocities of opposite sign, noticed by Tolstoy and Usdin [11] in Rayleigh's solution, is represented by the branch [ϕ_3] in the real plane. Also, the minimum at Ω^* represents zero group velocity and nonzero phase velocity. As the wave length approaches zero ($x \to \infty$) the frequencies rise beyond the range of applicability of the equations and the asymptotic behavior of the velocities of the three compressional modes are

$$v = v_g = \frac{\kappa_2}{\kappa_3}\left(\frac{\mu}{\rho}\right)^{1/2}, \quad \left(\frac{\lambda+2\mu}{\rho}\right)^{1/2}, \quad \frac{1}{\kappa_4}\left[\frac{E}{\rho(1-\nu^2)}\right]^{1/2}. \tag{54}$$

According to the exact theory, the first of these should be the velocity of Rayleigh surface waves and the second and third should be the velocity of equivoluminal waves.

[9] The complex roots were kindly supplied by Dr. Morio Onoe.

Additional Results

(a) The equations of compatibility may be obtained by eliminating the displacements from Equations (33), with the result:

$$\begin{gathered}
\frac{\partial^2\epsilon_1^{(0)}}{\partial x_3^2} + \frac{\partial^2\epsilon_3^{(0)}}{\partial x_1^2} = \frac{\partial^2\epsilon_5^{(0)}}{\partial x_1 \partial x_3} \\
\frac{\partial^2\epsilon_2^{(0)}}{\partial x_1^2} + \frac{3\epsilon_1^{(2)}}{b^2} = \frac{1}{b}\frac{\partial\epsilon_6^{(1)}}{\partial x_1} \\
\frac{3\epsilon_3^{(2)}}{b^2} + \frac{\partial^2\epsilon_2^{(0)}}{\partial x_3^2} = \frac{1}{b}\frac{\partial\epsilon_4^{(1)}}{\partial x_3} \\
\frac{\partial^2\epsilon_1^{(2)}}{\partial x_3^2} + \frac{\partial^2\epsilon_3^{(2)}}{\partial x_1^2} = \frac{\partial^2\epsilon_5^{(2)}}{\partial x_1 \partial x_3} \qquad (55) \\
\frac{3}{b}\frac{\partial\epsilon_1^{(2)}}{\partial x_3} = \frac{1}{2}\frac{\partial}{\partial x_1}\left(-\frac{\partial\epsilon_4^{(1)}}{\partial x_1} + \frac{3\epsilon_5^{(2)}}{b} + \frac{\partial\epsilon_6^{(1)}}{\partial x_3}\right) \\
\frac{\partial^2\epsilon_2^{(0)}}{\partial x_1 \partial x_3} = \frac{1}{2b}\left(-\frac{3\epsilon_5^{(2)}}{b} + \frac{\partial\epsilon_6^{(1)}}{\partial x_3} + \frac{\partial\epsilon_4^{(1)}}{\partial x_1}\right) \\
\frac{3}{b}\frac{\partial\epsilon_3^{(2)}}{\partial x_1} = \frac{1}{2}\frac{\partial}{\partial x_3}\left(-\frac{\partial\epsilon_6^{(1)}}{\partial x_3} + \frac{\partial\epsilon_4^{(1)}}{\partial x_1} + \frac{3\epsilon_5^{(2)}}{b}\right)
\end{gathered}$$

The first of (55) is the usual compatibility equation of generalized plane stress and the remaining six equations correspond to the ordinary six compatibility equations; the main differences being that here the components $\epsilon_p^{(2)}$ have a factor 3 and the operator $\partial/\partial x_2$ is replaced by $1/b$.

(b) It also may be shown that there are nine dislocations when the nine components of strain and their derivatives are continuous. Three of them are the two translational and one rotational dislocations of generalized plane stress. Of the remaining six, three are translational (in the displacements $u_1^{(2)}$, $u_2^{(2)}$, $u_3^{(2)}$) and three are rotational, in the component of rotation

$$\frac{1}{2}\left(\frac{3u_2^{(2)}}{b} - \frac{\partial u_2^{(1)}}{\partial x_3}\right), \quad \frac{1}{2}\left(\frac{\partial u_3^{(2)}}{\partial x_1} - \frac{\partial u_1^{(2)}}{\partial x_3}\right), \quad \frac{1}{2}\left(\frac{\partial u_2^{(1)}}{\partial x_1} - \frac{3u_1^{(2)}}{b}\right). \tag{56}$$

(c) A theorem of uniqueness of solutions of the approximate equations of motion may be established along the lines of Neumann's theorem.[10] This leads to the following conditions sufficient for a unique solution (in the absence of discontinuities and singularities):

(i) Initial values of $u_1^{(0)}$, $u_3^{(0)}$, $u_2^{(1)}$, $u_1^{(2)}$, and $u_3^{(2)}$ throughout the plate.

(ii) Initial values of $\dot{u}_1^{(0)}$, $\dot{u}_3^{(0)}$, $\dot{u}_2^{(1)}$, $\dot{u}_1^{(2)}$, and $\dot{u}_3^{(2)}$ throughout the plate.

(iii) One member of each of the five products $F_1^{(0)}u_1^{(0)}$, $F_3^{(0)}u_3^{(0)}$, $F_2^{(1)}u_2^{(1)}$, $F_1^{(2)}u_1^{(2)}$, $F_3^{(2)}u_3^{(2)}$ at each point of the plate; i.e., five surface conditions.

(iv) At each point on the edge of the plate (normal n tangent s) one member of each of the five products $\tau_{nn}^{(0)}u_n^{(0)}$, $\tau_{ns}^{(0)}u_s^{(0)}$, $\tau_{ns}^{(1)}u_2^{(1)}$, $\tau_{nn}^{(2)}u_n^{(2)}$, $\tau_{ns}^{(2)}u_s^{(2)}$; i.e., five edge conditions.

The requirement that the strain energy-density $\bar{U}^{(2)}$, Equation (31), be positive definite is satisfied by the addition of the requirements $\kappa_1 > 0$, $\kappa_2 > 0$ to the usual requirements $3\lambda + 2\mu > 0$, $\mu > 0$.

(d) In the case of steady vibrations, the displacements may be expressed conveniently in terms of potentials that satisfy Helmholtz equations. Omitting a factor $e^{i\omega t}$ the results are

$$
\begin{aligned}
u_1^{(0)} &= \frac{\partial\phi_1}{\partial x_1} + \frac{\partial\phi_2}{\partial x_1} + \frac{\partial\phi_3}{\partial x_1} - \frac{\partial H_0}{\partial x_3} \\
u_3^{(0)} &= \frac{\partial\phi_1}{\partial x_3} + \frac{\partial\phi_2}{\partial x_3} + \frac{\partial\phi_3}{\partial x_3} + \frac{\partial H_0}{\partial x_1} \\
u_2^{(1)} &= \alpha_1\phi_1 + \alpha_2\phi_2 + \alpha_3\phi_3 \\
u_1^{(2)} &= \beta_1\frac{\partial\phi_1}{\partial x_1} + \beta_2\frac{\partial\phi_2}{\partial x_1} + \beta_3\frac{\partial\phi_3}{\partial x_1} - \frac{\partial H_2}{\partial x_3} \\
u_3^{(2)} &= \beta_1\frac{\partial\phi_1}{\partial x_3} + \beta_2\frac{\partial\phi_2}{\partial x_3} + \beta_3\frac{\partial\phi_3}{\partial x_3} + \frac{\partial H_2}{\partial x_1}
\end{aligned}
\tag{57}
$$

$$
\begin{aligned}
&\mu\nabla^2 H_0 + \rho\omega^2 H_0 = 0 \\
&\mu\nabla^2 H_2 + (\kappa_1^2\rho\omega^2 - 15b^{-2}\kappa_2^2\mu)H_2 = 0 \\
&\nabla^2\phi_i + \xi_i^2\phi_i = 0, \quad i = 1, 2, 3
\end{aligned}
\tag{58}
$$

where

$$
\begin{aligned}
\alpha_i &= b[(\lambda + 2\mu)\xi_i^2 - \rho\omega^2]/\kappa_1\lambda \\
\beta_i &= \alpha_i b \Big/ \left[\frac{3}{4}(\Omega^2 - 4) - \frac{E'b^2\xi_i^2}{5\mu\kappa_2^2}\right]
\end{aligned}
\tag{59}
$$

and the ξ_i^2 are, again, the roots of Equation (37). It may be seen that H_0 and H_2 are the potentials of the two face-shear modes and the ϕ_i are the potentials of the three compressional modes.

(e) The tensor, and hence invariant, characters of the quantities that appear in the second-order equations are, for the most part, apparent. For example, in the displacement equations of motion (35), if the first and second equations are regarded as the rectangular components of a vector and the fourth and fifth equations the rectangular components of another vector, the only differential operators that appear are the gradient, divergence, Laplacian, and $\partial^2/\partial t^2$: all invariants. The dependent variables are the scalar $u_2^{(1)}$ and the two vectors

$$
\begin{aligned}
\mathbf{u}^{(0)} &= u_1^{(0)}\mathbf{k}_1 + u_3^{(0)}\mathbf{k}_3 = u_\alpha^{(0)}\mathbf{k}_\alpha + u_\gamma^{(0)}\mathbf{k}_\gamma, \\
\mathbf{u}^{(2)} &= u_1^{(2)}\mathbf{k}_1 + u_3^{(2)}\mathbf{k}_3 = u_\alpha^{(2)}\mathbf{k}_\alpha + u_\gamma^{(2)}\mathbf{k}_\gamma,
\end{aligned}
\tag{60}
$$

[10] References [11], p. 176, and [9].

while the gradient operator is

$$
\nabla = \mathbf{k}_1\frac{\partial}{\partial x_1} + \mathbf{k}_3\frac{\partial}{\partial x_3} = \mathbf{k}_\alpha\frac{\partial}{\partial s_\alpha} + \mathbf{k}_\gamma\frac{\partial}{\partial s_\gamma} \tag{61}
$$

where $\mathbf{k}_1$, $\mathbf{k}_3$, and $\mathbf{k}_\alpha$, $\mathbf{k}_\gamma$ are unit vectors in the rectangular directions 1, 3, and the orthogonal curvilinear directions α, γ, respectively: all in the plane of the plate.

The appropriate strain tensors and their expression in terms of vector displacements are not quite as apparent. We define another vector displacement

$$
\mathbf{u}' = \mathbf{u}^{(2)} + \mathbf{k}_2 u_2^{(1)} \tag{62}
$$

and a gradient operator

$$
\nabla' = \nabla + \mathbf{k}_2/b \tag{63}
$$

where $\mathbf{k}_2$ is a unit vector normal to the plane of the plate. Then the two tensors

$$
\begin{aligned}
\boldsymbol{\varepsilon}^{(0)} &= {}^1/_2(\nabla\mathbf{u}^{(0)} + \mathbf{u}^{(0)}\nabla), \\
\boldsymbol{\varepsilon}' &= {}^1/_2(\nabla'\mathbf{u}' + \mathbf{u}'\nabla')
\end{aligned}
\tag{64}
$$

constitute the strain. The seven equations of compatibility, for example, become

$$
\begin{aligned}
\nabla \times \boldsymbol{\varepsilon}^{(0)} \times \nabla &= 0, \\
\nabla' \times \boldsymbol{\varepsilon}' \times \nabla' &= 0.
\end{aligned}
\tag{65}
$$

References

1 T. R. Kane and R. D. Mindlin, "High-Frequency Extensional Vibrations of Plates," JOURNAL OF APPLIED MECHANICS, vol. 23, TRANS. ASME, vol. 78, 1956, pp. A-277–283.

2 S. D. Poisson, "Mémoire sur l'Équilibre et le Mouvement des Corps Élastiques," *Mémoires de l'Académie des Sciences*, series 2, vol. 8, Paris, 1829, pp. 357–570.

3 A. L. Cauchy, "Sur l'Équilibre et le Mouvement d'une Plaque Solide," *Exercices de Mathématique*, vol. 3, 1828, pp. 328–355.

4 G. Kirchhoff, "Über das Gleichgewicht und die Bewegung einer Elastichen Scheibe," *Crelles Journal*, vol. 40, 1850, pp. 51–88.

5 R. D. Mindlin, "An Introduction to the Mathematical Theory of Vibrations of Elastic Plates," Signal Corps Engineering Laboratories, Fort Monmouth, N. J., 1955.

6 E. Reissner, "On the Calculation of Three-Dimensional Corrections for the Two-Dimensional Theory of Plane Stress," *Proceedings of the Fifteenth Semi-Annual Eastern Photoelasticity Conference*, Addison-Wesley Press, Cambridge, Mass., 1942.

7 Lord Rayleigh, "On the Free Vibrations of an Infinite Plate of Homogeneous Isotropic Elastic Matter," *Proceedings of The London Mathematical Society*, vol. 20, 1889, pp. 225–234.

8 S. Timoshenko, "On the Correction for Shear of the Differential Equation for Transverse Vibrations of Prismatic Bars," *Philosophical Magazine*, series 6, vol. 41, 1921, pp. 744–746.

9 R. D. Mindlin, "Influence of Rotatory Inertia and Shear on Flexural Vibrations of Isotropic, Elastic Plates," JOURNAL OF APPLIED MECHANICS, vol. 18, TRANS. ASME, vol. 73, 1951, pp. 31–38.

10 R. R. Aggarwal and E. A. G. Shaw, "Axially Symmetrical Vibrations of a Finite Isotropic Disk. IV," *Journal of the Acoustical Society of America*, vol. 26, 1954, pp. 341–342.

11 I. Tolstoy and E. Usdin, "Wave Propagation in Elastic Plates: Low and High Mode Dispersion," *Journal of the Acoustical Society of America*, vol. 29, 1957, pp. 37–42.

12 A. E. H. Love, "A Treatise on the Mathematical Theory of Elasticity," Cambridge University Press, London, 1927.

13 E. A. G. Shaw, "On the Resonant Vibrations of Thick Barium Titanate Disks," *Journal of the Acoustical Society of America*, vol. 28, 1956, pp. 38–50.

Triaxial Tension at the Head of a Rapidly Running Crack in a Plate

J. M. FRANKLAND

Consultant, Mechanics Division, Engineering Mechanics Section, National Bureau of Standards, Washington, D. C.

The conditions near a crack in a plate, whether stationary or growing, are usually considered to be a state of plane stress. In this note, however, it is shown that appreciable normal stress through the thickness can occur when the crack is growing rapidly. This gives rise to a state of triaxial tension in the core of the plate near the head of the crack and can thus contribute to the brittle behavior observed in such cases. The amount of triaxiality is strongly dependent on the extent of the plastically deformed zone at the end of the crack. This fact may be one reason for the greater brittleness shown by thick plates.

At the head of a crack in a plate stressed in tension, the stress concentration produces a localized contraction in thickness. When the crack advances through the plate, this dimpled depression moves with it, thus giving rise to accelerations which produce a tensile stress in a direction normal to the plane of the plate. Cracks have been reported to run as fast as 6000 fps in steel and at such speeds the accelerations might be large. If the thickness stress becomes appreciable, it would give rise to a triaxial tension and thus would contribute to the brittle behavior associated with rapidly growing cracks. Curiously enough, little or no attention has been given to this question in the literature of brittle-fracture mechanics. This paper attempts to estimate the magnitude of the effect.

The available solutions for the stresses near the head of a crack, whether stationary[1] or advancing,[2] are restricted to conditions of generalized plane stress. The three-dimensional problem is quite intractable, especially if plastic flow occurs. Nevertheless, it will be shown that a plausible extrapolation from the two-dimensional solutions can be used for estimation of the triaxial tension in the core of the plate.

Let the faces of the plate be given by $z = \pm h$ in a rectangular co-ordinate system x, y, z. The crack is advancing with constant velocity v along the x-axis. At large distances from the crack the plate is under the constant uniaxial tension σ_y. Consider the instant at which the head of the crack has reached the origin. A plastically deformed zone extends ahead of the crack to small positive values of x. We focus our attention on the intersection of the elastic-plastic interface with the x-axis.

We have the equation of motion

$$\frac{\partial \tau_{xz}}{\partial x} + \frac{\partial \tau_{yz}}{\partial y} + \frac{\partial \sigma_z}{\partial z} = \rho \frac{\partial^2 w}{\partial t^2}$$

where τ_{xz}, τ_{yz}, σ_z are stresses, ρ is the density of the material, w the component of displacement perpendicular to the surface of the plate, and t is time. The boundary conditions at $z = \pm h$ are

$$\tau_{xz} = \tau_{yz} = \sigma_z = 0,$$

which imply

$$\frac{\partial \tau_{xz}}{\partial x} = \frac{\partial \tau_{yz}}{\partial y} = 0 \quad \text{at} \quad z = \pm h$$

Hence

$$\left.\frac{\partial \sigma_z}{\partial z}\right|_{z=h} = \rho \left.\frac{\partial^2 w}{\partial t^2}\right|_{z=h} \tag{1}$$

Now $E(\partial w/\partial z) = \sigma_z - \nu(\sigma_x + \sigma_y)$, where ν is Poisson's ratio. Integrating from $z = 0$ to $z = h$,

$$Ew^* = h[\bar{\sigma}_z - \nu(\bar{\sigma}_x + \bar{\sigma}_y)], \tag{2}$$

where w^* is the normal displacement at the surface and the bars over the stresses signify average values through the thickness of the plate.

For $y = 0$ and for small positive values of x, assume

$$w^* \cong kx^{-n}, \quad n > 0 \tag{3}$$

and therefore

$$\frac{\partial^2 w^*}{\partial t^2} = n(n+1)kx^{-n-2}v^2 = n(n+1)w^*v^2/x^2 \tag{4}$$

Let σ_0 be the maximum value of σ_z,

$$\left.\frac{\partial \sigma_z}{\partial z}\right|_{z=h} = -\alpha\sigma_0/h, \tag{5a}$$

and

$$\bar{\sigma}_z = \beta\sigma_0 \tag{5b}$$

Consider the stresses $\bar{\sigma}_x$ and $\bar{\sigma}_y$. On the x-axis near the head of a stationary crack these are equal. When the crack is growing, according to Yoffe,[2] the two stresses are unequal and the ratio depends on the speed of the crack. We shall define κ as the ratio of the smaller to the larger of these two principal stresses in the plane of the plate. In addition, we shall assume that σ_z is the least principal stress. Taking the maximum-shearing-stress criterion for yield since it is more conservative for our purpose than the von Mises' condition, yield occurs when

$$\sigma_1 = \sigma_0 + \sigma_Y \tag{6}$$

[1] C. E. Inglis, "Stresses in a Plate Due to the Presence of Cracks and Sharp Corners," *Trans. Institution of Naval Architects*, vol. 55, part 1, 1913, p. 219.

[2] E. A. Yoffe, "The Moving Griffith Crack," *Philosophical Magazine*, vol. 42, 1951, p. 739.

Presented at the Summer Conference of the Applied Mechanics Division, Troy, N. Y., June 18–20, 1959, of The American Society of Mechanical Engineers.

Discussion of this paper should be addressed to the Secretary, ASME, 29 West 39th Street, New York, N. Y., and will be accepted until January 10, 1960, for publication at a later date. Discussion received after the closing date will be returned.

Note: Statements and opinions advanced in papers are to be understood as individual expressions of their authors and not those of the Society. Manuscript received by ASME Applied Mechanics Division, June 30, 1958. Paper No. 59—APM-11.

where σ_1 is the greater of σ_x and σ_y, and σ_Y is the yield strength in tension with allowance for strain-rate and temperature effects.

At the elastic-plastic interface, equation (2) becomes

$$Ew^* = h[\beta\sigma_0 - \nu(1 + \kappa)(\sigma_0 + \sigma_Y)] \tag{7}$$

Substituting equations (4), (5), and (7) in (1) and solving for σ_0,

$$\frac{\sigma_0}{\sigma_Y} = \frac{A}{B\dfrac{c^2x^2}{v^2h^2} + C} \tag{8}$$

where

$$A = \nu(1 + \kappa),$$

$$B = \frac{2\alpha(1 + \nu)}{n(n + 1)},$$

and

$$C = \beta - \nu(1 + \kappa)$$

Here c represents the velocity of waves of rotation; viz.:

$$c = (G/\rho)^{1/2} = \{E/[2\rho(1 + \nu)]\}^{1/2},$$

and x is the distance from the head of the crack to the elastic-plastic interface.

The only *ad hoc* hypothesis introduced in the foregoing derivation is the assumption of equation (3). In support of this, the static[1] and dynamic[2] elastic solutions agree in finding $n = 1/2$. Equation (8) seems, therefore, to be well justified.

To draw useful conclusions from equation (8), we must give reasonable values of A, B, and C, as well as of x, the extent of the plastic zone. The available information is sufficient for fair estimates of A, B, and C; but knowledge of the extent of the plastic zone is sketchy. About all that can be said from examinations of fractures accompanying rapidly running cracks is that, in steel plates of thickness around $^3/_4$ in., obvious plastic deformation extends no further than a few hundredths of an inch.

As stated previously, the dynamic and static elastic solutions assign the same kind of singularity to the head of the crack, and this is characterized by $n = {}^1/_2$. This value will be assumed in the calculations. The values of κ will be taken from Yoffe's dynamic solution and are given in Table 1.

Table 1 Values of κ

v/c	0	0.4	0.5	0.6
κ	1.00	0.86	0.77	0.62

in which a Poisson's ratio of 0.3 has been assumed.

The parameters α and β depend on the distribution of σ_x through the thickness of the plate. For a rapidly running crack, the crack front is approximately parabolic and fractures seem to initiate at the mid-thickness.[3] Accordingly we assume

$$\sigma_x = \sigma_0(1 - |z/h|^m), \tag{9}$$

and it is plausible that m is in the neighborhood of 2. Since larger values of m lead to smaller values of σ_0, calculations will be made for both $m = 2$ and $m = 3$. From equation (9), using (5*a*) and (5*b*),

$$\alpha = m \quad \text{and} \quad \beta = \frac{m}{m + 1}$$

It should be noted that the assumed distribution of σ_x is suitable only for a running crack, since equation (1) demands that $\alpha = 0$ for a stationary crack.

Putting these estimates in equation (8), one obtains

$$\frac{\sigma_0}{\sigma_Y} = \frac{\nu(1 + \kappa)}{\dfrac{8}{3}\, m(1 + \nu)\dfrac{c^2x^2}{v^2h^2} + \dfrac{m}{m + 1} - \nu(1 + \kappa)} \tag{10}$$

For a material with a Poisson's ratio $\nu = 0.3$, the estimates from equation (10) are plotted against the extent of the plastic zone in Fig. 1 and Fig. 2 for $m = 2$ and $m = 3$, respectively. Crack speeds of 40 to 60 per cent of the speed of rotational waves are assumed in accordance with experimental observations on high-speed cracks; e.g., 4000 to 6000 fps for steel.

An upper bound for σ_0 can be found by setting $w^* = 0$ in equation (7), which gives

$$\frac{\sigma_0}{\sigma_Y} < \frac{\nu(1 + \kappa)}{\dfrac{m}{m + 1} - \nu(1 + \kappa)} \tag{11}$$

Actual values of σ_0 can be expected to be considerably less than

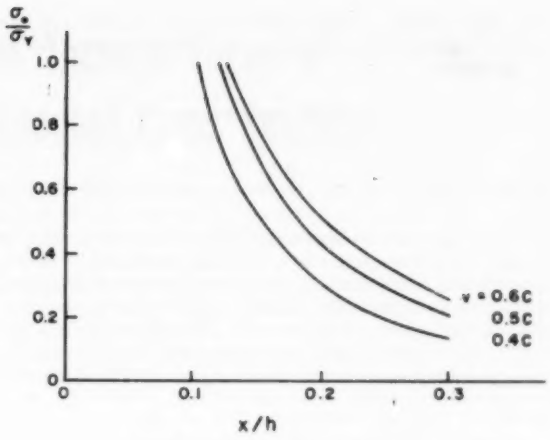

POSITION OF PLASTIC FRONT

Fig. 1 Maximum values of σ_x for $m = 2$

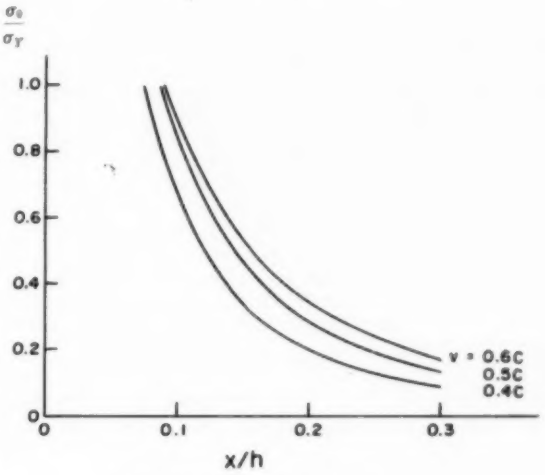

POSITION OF PLASTIC FRONT

Fig. 2 Maximum values of σ_x for $m = 3$

[3] G. M. Boyd, "The Propagation of Fractures in Mild-Steel Plates," *Engineering*, vol. 175, 1953, pp. 65, 100.

this upper bound. Values calculated from equation (11) are given in Table 2. These bounds are well above the values plotted in the figures.

Table 2 Upper bounds

	m = 2			m = 3		
v/c =	0.4	0.5	0.6	0.4	0.5	0.6
σ_0/σ_Y =	5.14	3.19	2.69	2.91	2.42	1.84

Observations of contractions in thickness at brittle fractures in $^3/_4$-in. steel plate suggest that x/h is of the order of 0.1, but it is possible that this criterion is insensitive and may underestimate the extent of the plastically deformed region. Calculations therefore have been extended to $x/h = 0.3$. The figures indicate that appreciable triaxial tensions may exist at the core of the plate in the case of high-speed cracks and that this condition is strongly dependent on the extent of the plastic zone at the head of the crack.

Dr. G. R. Irwin has suggested that with increase of plate thickness the ratio of the extent of the plastic region to the plate thickness might be expected to decrease. This would contribute to a size effect in which thicker plates would show a more brittle behavior.

The real test of the foregoing speculations must be experimental. It is urged that those observing the behavior of rapidly growing cracks pay more attention to the factors brought out in this analysis, and, in particular, to the extent of the plastically deformed region.

Acknowledgment

The author is grateful for helpful discussions with Dr. G. R. Irwin and Mr. J. A. Kies of the Naval Research Laboratory.

Viscous Flow Through Tubes of Multiply Connected Cross Sections

F. A. GAYDON
Senior Lecturer
in Theoretical Mechanics,
University of Bristol,
Bristol, England

H. NUTTALL
Lecturer in Theoretical Mechanics,
University of Bristol,
Bristol, England

A new method is proposed for estimating the volume flow of a viscous incompressible fluid through a cylindrical tube of multiply connected cross section. The method brackets the magnitude of the volume flow between upper and lower bounds. The essential feature of the method is that the calculation of both upper and lower bounds is based upon the same approximating function for the velocity distribution, thus avoiding the usual approach to a lower bound via the Rayleigh-Ritz method. For multiply connected cross sections of the form discussed, a Rayleigh-Ritz solution of sufficient accuracy becomes extremely laborious. Efforts to solve the problem by relaxation methods are also rendered difficult by the presence of high-velocity gradients in the vicinity of an internal boundary, particularly when this is a small circle. In contrast to these methods the one presented achieves the result with considerably less labor; moreover, the method is directly applicable to simply connected cross sections with many-sided boundaries.

The Schwarz inequality can be used to deduce upper and lower bounds to the volume flow of a viscous incompressible fluid through a cylindrical tube. The inequality has been used by Diaz and Weinstein [1][1] to establish the procedures generally known as the Rayleigh-Ritz and Trefftz methods. Papers by Diaz and Weinstein [2], Polya and Weinstein [3] and Diaz [4] give methods for bounding the torsional rigidity of uniform rods having simply and multiply connected cross sections. Likewise the continued inequality given by Hill [5] when applied to such problems reduces to the Rayleigh-Ritz and Trefftz bounds.

It is well known that, for simply connected cross sections, the torsion problem and the flow problem under discussion are identical. For multiply connected cross sections, however, they differ because of the requirement that the displacements in the elastic material shall be single-valued. This introduces boundary conditions which are not identical with those of the flow problem. Essentially, the flow problem is the easier, but for multiply connected cross sections, indeed for many-sided simply connected cross sections, the Rayleigh-Ritz approach is extremely cumbersome.

It is the purpose of this paper to establish upper and lower bounds to the volume flow by using the same function in the calculation of both bounds. In the method to be discussed the work involved in obtaining the two bounds is little more than is involved in obtaining the upper bound alone.

As illustrations of the method, bounds for a square cross section with a central circular hole and for an hexagonal cross section with central circular hole have been obtained for various diameters of hole.

Upper and Lower Bounds to Rate of Volume Flow

The outer boundary of the cross section is taken as C_0, the internal boundaries as C_1, C_2, and so on. The contour C_0 taken in the anticlockwise direction, together with C_1, C_2, and so on, taken in the clockwise direction is denoted by C. The total cross-sectional area is S. If the z-axis is taken parallel to the generators of the cylinder, it may be shown that the velocity distribution for the flow of a viscous incompressible fluid is independent of z and is governed by the differential equation

$$\nabla^2 w = -P/\mu,$$

where w is the velocity parallel to the generators of the cylinder, μ is the coefficient of viscosity, and P the pressure gradient which is constant along the axis of the cylinder.

The boundary conditions on w are that

$$w = 0 \quad \text{on} \quad C$$

Make a change of variable

$$\chi = 2w\mu/P \tag{1}$$

Then

$$\nabla^2\chi = -2 \tag{2}$$

and

$$\chi = 0 \quad \text{on} \quad C \tag{3}$$

By Green's theorem

$$\iint_S (\chi_x^2 + \chi_y^2)dx\,dy = 2\iint_S \chi\,dx\,dy = Q, \quad \text{say.}$$

Let ϕ be a continuous function in and on C with continuous first and second derivatives and suppose

$$\nabla^2\phi = -2 \tag{4}$$

From the Schwarz inequality it follows that

$$a^2 - b^2 \geqslant 2b(a - b),$$

with equality if, and only if, $a = b$. Therefore

$$\iint_S (\phi_x^2 + \phi_y^2)dx\,dy - \iint_S (\chi_x^2 + \chi_y^2)dx\,dy$$

$$\geqslant 2\iint_S \{\chi_x(\phi_x - \chi_x) + \chi_y(\phi_y - \chi_y)\}dx\,dy$$

[1] Numbers in brackets designate References at end of paper.

Presented at the Summer Conference of the Applied Mechanics Division, Troy, N. Y., June 18–20, 1959, of THE AMERICAN SOCIETY OF MECHANICAL ENGINEERS.

Discussion of this paper should be addressed to the Secretary, ASME, 29 West 39th Street, New York, N. Y., and will be accepted until January 10, 1960, for publication at a later date. Discussion received after the closing date will be returned.

NOTE: Statements and opinions advanced in papers are to be understood as individual expressions of their authors and not those of the Society. Manuscript received by ASME Applied Mechanics Division, June 26, 1958. Paper No. 59—APM-28.

$$= 2\int_C \chi\left(\frac{\partial\phi}{\partial n} - \frac{\partial\chi}{\partial n}\right) ds + 2\iint_S \chi(\nabla^2\chi - \nabla^2\phi)dx\,dy$$

$$= 0$$

from equations (2), (3) and (4), where $\vec{n}$ is the outward normal to an element of arc ds of C. Therefore

$$\iint_S (\chi_x^2 + \chi_y^2)dx\,dy \leqslant \iint_S (\phi_x^2 + \phi_y^2)dx\,dy$$

that is, $Q \leqslant E$, say.

The upper bound for the volume rate of flow is then given by

$$\iint_S w\,dx\,dy \leqslant \frac{PE}{4\mu} \tag{5}$$

Now consider the line integral

$$\int_C \left\{\phi\frac{\partial\chi}{\partial n} - \chi\frac{\partial\phi}{\partial n}\right\} ds = \iint_S \{\phi\nabla^2\chi - \chi\nabla^2\phi\}dx\,dy,$$

$$= 2\iint_S (\chi - \phi)dx\,dy,$$

that is

$$\int_C \phi\frac{\partial\chi}{\partial n}\,ds = 2\iint_S (\chi - \phi)dx\,dy,$$

from equations (2), (3), (4).

If ϕ is chosen so that

$$\int_C \phi\frac{\partial\chi}{\partial n}\,ds$$

is positive, then

$$\iint_S \chi\,dx\,dy > \iint_S \phi\,dx\,dy$$

The lower bound for the volume rate of flow is then given by

$$\iint_S w\,dx\,dy = \frac{P}{2\mu}\iint_S \chi\,dx\,dy > \frac{P}{2\mu}\iint_S \phi\,dx\,dy \tag{6}$$

provided that ϕ satisfies equation (4) and that

$$\int_C \phi\frac{\partial\chi}{\partial n}\,ds$$

is positive.

The fact that $\partial\chi/\partial n$ is negative or zero on C follows since it can be shown that χ is positive at all points interior to C. For $\nabla^2\chi < 0$ in S and χ is zero on C. If there is an interior point at which $\chi < 0$ there is also an interior point at which χ is a true minimum, since χ is bounded and continuous. Application of Gauss's theorem to a neighborhood containing this minimum point shows that $\nabla^2\chi > 0$ which is a contradiction. Therefore $\chi > 0$ at all interior points. The integral

$$\int_C \phi\frac{\partial\chi}{\partial n}\,ds$$

can therefore be made positive by insuring that ϕ is negative on C. This condition assumes the minimum of knowledge as to the behavior of χ. In particular cases of symmetry the condition could be relaxed.

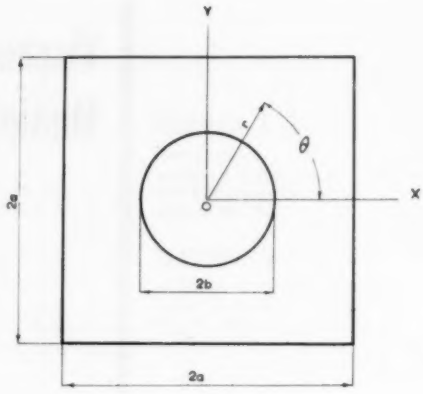

Fig. 1

Square Cross Section With a Central Circular Hole

Let the origin O of (x, y) co-ordinates in the plane of a cross section be the center of the circle of radius b and the sides of the square have equations $x = \pm a$, $y = \pm a$. Polar co-ordinates (r, θ) with O as pole and Ox as initial line are also used. Fig. 1. Let

$$\phi/a^2 = -\tfrac{1}{2}\left(\frac{r^2}{a^2} - 1\right) + \alpha\ln(r/a) + \beta\left(\frac{r^4}{a^4}\cos 4\theta - 1\right) + \gamma\left(\frac{r^8}{a^8}\cos 8\theta - 1\right) + \delta \tag{7}$$

α, β, γ, δ are constants, δ being chosen to make $\phi \leqslant 0$ on C. Then

$$\nabla^2\phi = -2$$

and

$$E = \iint_S \left\{\phi_r^2 + \frac{1}{r^2}\phi_\theta^2\right\} r\,dr\,d\theta$$

E is now evaluated and is given by

$$E/a^4 = \{2.6\dot{6} + \alpha^2(2\pi\ln\lambda + 0.691304) + 43.8856\beta^2 + 605.965\gamma^2 - 6.13584\alpha\beta + 13.9800\alpha\gamma - 215.145\beta\gamma - 8\alpha + 8.5\dot{3}\beta - 22.7560\gamma - \pi(1/2\lambda^4 + 4\beta^2/\lambda^8 + 8\gamma^2/\lambda^{16} - 2\alpha/\lambda^2)\} \tag{8}$$

where $\lambda = a/b$.

The value obtained for $PE/4\mu$ is always an upper bound to the rate of volume flow, and the best upper bound is that obtained by minimizing (8) with respect to α, β, γ. The lower bound is

$$\frac{P}{2\mu}\iint_S \phi\,dx\,dy$$

and is given by

$$\frac{P}{2\mu}\iint_S \phi dx\,dy = \frac{Pa^4}{2\mu}\left\{0.6\dot{6} + \alpha\left[\frac{\pi\ln\lambda}{\lambda^2} + (\pi/2\lambda^2) - 1.47211\right] + \beta[\pi/\lambda^2 - 5.0\dot{6}] + \gamma[\pi/\lambda^2 - 2.57775] + \pi/4\lambda^4 - \pi/2\lambda^2 + \delta[4 - \pi/\lambda^2]\right\} \tag{9}$$

This is valid as a lower bound provided

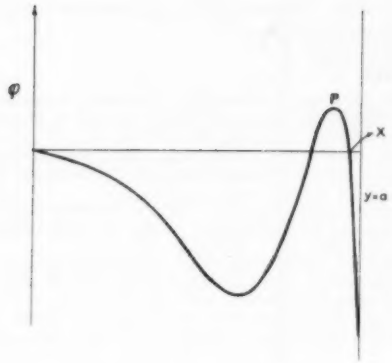

Fig. 2

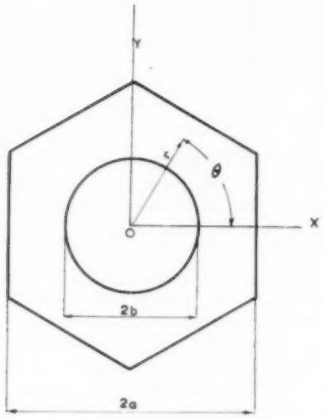

Fig. 3

$$\int_C \phi \frac{\partial \chi}{\partial n}\, ds$$

is positive. It has been established that $\partial\chi/\partial n$ is negative on C so that it is sufficient for ϕ to be negative or zero on $x = a$ and $r = b$.

With $\delta = 0$ it is found that $\phi < 0$ on $r = b$. The graph in Fig. 2 depicts the general form of ϕ along the outer boundary $x = a$. It will be apparent that the line integral will be positive if δ is chosen to be the negative of the value of ϕ at the maximum point P. Clearly $|\delta|$ can be decreased by taking more terms in the expression for ϕ. In particular cases it may be possible to insure that the line integral is positive without insisting that ϕ should be negative along the entire outer boundary. For instance, in the case of a solid square cross section, for which it is physically plain that $\left|\frac{\partial \chi}{\partial n}\right|$ decreases along $x = a$ as $|y|$ increases, it would be sufficient to insure that the area between the ϕ-curve and the y-axis up to the point X of Fig. 2 is negative.

Table 1 lists the values of the upper and lower bounds to the rate of volume flow for a section in which the ratio a/b is denoted by λ. The result is given in the form

$$Q = kPa^4/\mu$$

It is apparent from the analysis that as the ratio λ tends to ∞ the upper and lower bounds tend to those for a simply connected square cross section. If the bounds calculated are plotted against

Table 1

λ	k lower bound	k upper bound	Max error from mean, per cent
2	0.0942	0.0974	1.7
3	0.1729	0.1764	1.0
6	0.2797	0.2835	0.7
10	0.3328	0.3368	0.6
20	0.3815	0.3855	0.5
∞ (Simply connected)	0.5583	0.5624	0.36

λ, the resulting curve approaches the simply connected solution asymptotically. The convergence is, however, extremely slow as will be shown more clearly in the solution for the hexagon, which follows. It is of interest to note that the value of the upper bound for the simply connected section is indistinguishable from the exact solution. In fact, the values of the function over the entire cross section are very close indeed to those obtained from the exact series solution.

Hexagonal Cross Section With a Central Circular Hole

Let the origin O of (x, y) and (r, θ) co-ordinates be the center of a circle of radius b as before. The radius of the inscribed circle of the hexagon is a. Fig 3. Let

$$\frac{\phi}{a^2} = -\tfrac{1}{2}\left(\frac{r^2}{a^2} - 1\right) + \alpha \ln (r/a) + \beta\left(\frac{r^6}{a^6}\cos 6\theta - 1\right) + \gamma\left(\frac{r^{12}}{a^{12}}\cos 12\theta - 1\right) + \delta \quad (10)$$

$\alpha, \beta, \gamma, \delta$ are constants as before.

Then following the method given for the square cross section

$$\frac{E}{a^4} = \{1.92450 + \alpha^2(2\pi \ln \lambda + 0.295402) + 38.2004\beta^2 + 207.991\gamma^2 - 3.09906\alpha\beta + 4.17684\alpha\gamma - 85.4199\beta\gamma - 6.92820\alpha + 3.51908\beta - 5.13325\gamma - \pi[(6\beta^2/\lambda^{12}) + (12\gamma^2/\lambda^{24}) - (2\alpha/\lambda^2) + (1/2\lambda^4)]\} \quad (11)$$

The lower bound is

$$\frac{P}{2\mu}\iint \phi\, dx\, dy$$

and is given by

$$\frac{P}{2\mu}\iint \phi\, dx\, dy = \frac{Pa^4}{2\mu}\left\{0.769801 + \alpha\left[\frac{\pi \ln \lambda}{\lambda^2} + (\pi/2\lambda^2) - 1.55627\right] + \beta[(\pi/\lambda^2) - 3.75736] + \gamma[(\pi/\lambda^2) - 3.25022] + (\pi/4\lambda^4) - (\pi/2\lambda^2) + \delta[2\sqrt{3} - (\pi/\lambda^2)]\right\}$$

Table 2 lists the upper and lower bounds to the rate of volume flow using the same notation as for the square cross section

Table 2

λ	k lower bound	k upper bound	Max error from mean, per cent
2	0.0634	0.0656	1.7
3	0.1282	0.1311	1.1
6	0.2189	0.2225	0.8
10	0.2645	0.2683	0.7
20	0.3062	0.3101	0.7
10^3	0.3902	0.3944	0.5
10^6	0.4229	0.4273	0.5
∞ (Simply connected)	0.4555	0.4603	0.5

$$Q = kPa^4/\mu$$

As indicated earlier, the convergence of the solution as λ tends to infinity is extremely slow. This is shown in Table 2 by the calculations for $\lambda = 10^3$ and $\lambda = 10^6$.

The function values ϕ for the simply connected hexagonal cross section were compared with the χ-values by means of a relaxation calculation using a triangular lattice of side $a/4\sqrt{3}$. The agreement was within 1 per cent.

Validity of Method

The validity of the results and of the method is limited by the necessity for laminar flow and the assumption that $u = v = 0$, as in the classical theory for slow viscous flow through simply connected tubes. In practice the tube must be sufficiently long for end effects to be ignored.

References

1 J. B. Diaz and A. Weinstein, "Schwarz's Inequality and the Methods of Rayleigh-Ritz and Treffts," *Journal of Mathematics and Physics*, vol. 26, 1947, pp. 133–136.

2 J. B. Diaz and A. Weinstein, "The Torsional Rigidity and Variational Methods," *American Journal of Mathematics*, vol. 70, 1948 pp. 107–116.

3 G. Polya and A. Weinstein, "On the Torsional Rigidity of Multiply Connected Cross-Sections," *Annals of Mathematics*, vol. 52, 1950, pp. 154–163.

4 J. B. Diaz, "On the Estimation of Torsional Rigidity and Other Physical Quantities," Proceedings of the First U. S. National Congress of Applied Mathematics, 1951, pp. 259–263.

5 R. Hill, "New Horizons in the Mechanics of Solids," *Journal of the Mechanics and Physics of Solids*, vol. 5, 1956–1957, pp. 66–74

On the Accuracy of Some Shell Solutions

G. D. GALLETLY
Shell Development Company,
Emeryville, Calif.
Assoc. Mem. ASME

J. R. M. RADOK[1]
Shell Development Company,
Emeryville, Calif.

R. B. Dingle's method [1][2] for finding asymptotic solutions of ordinary differential equations of a type such as occur in the bending theory of thin shells of revolution is presented in outline. This method leads to the same results as R. E. Langer's method [2], recently used for problems of this kind, and permits a simple analytical and less formal interpretation of the asymptotic treatment of such equations. A comparison is given of edge influence coefficients due to bending loads, obtained by use of these asymptotic solutions and numerical integration of the equilibrium equations, respectively. The particular shells investigated are of the open-crown, ellipsoidal, and negative-curvature toroidal types. The results indicate that the agreement between these solutions is satisfactory. In the presence of uniform pressure, the use of the membrane solutions for the determination of the particular integrals appears to lead to acceptable results in the case of ellipsoidal shells. However, in the case of toroidal shells, the membrane and the numerical solutions disagree significantly.

THEORETICAL studies of the bending deformation of thin uniform shells such as ellipsoids, toroids, and paraboloids have encountered some basic analytical difficulties until quite recently, when various authors began to employ R. E. Langer's method for finding asymptotic solutions of differential equations involving large parameters. These authors applied this method to single, complex, second-order differential equations which they obtained by combining the pairs of coupled ordinary differential equations governing the behavior of various types of shells of revolution in bending. The asymptotic solutions of these complex equations were then used to obtain expressions for the bending stresses in the corresponding shells which are valid for all practical values of the colatitude angle ϕ, including the apex where often singularities occur in the basic differential equations.

The foregoing reduction of the differential equations to single complex equations necessitates, especially in the case of ellipsoidal and paraboloidal shells, the introduction of various approximations. Nevertheless, little effort seems to have been made to compare the approximate Langer-type solutions with those of the more exact equations. The present paper makes an effort to fill this gap by presenting:

(*a*) Edge influence coefficients due to bending loads for an open-crown ellipsoidal shell and for a toroidal shell of negative Gaussian curvature, using the Langer-type solutions of Naghdi-de Silva [3] and Clark [4].

(*b*) Edge influence coefficients for the same shells as under (*a*), obtained by numerical integration of the classical small-deflection equations by use of a high-speed computer.

(*c*) An investigation of the particular integrals for both types of shells, since previous work on toroidal shells of positive curvature had demonstrated the inaccuracy of the commonly used membrane solutions.

Before presenting this information, the Langer-type solutions for toroidal, ellipsoidal, and paraboloidal shells will be deduced by use of the "generalized WKB method" of Dingle [1], since it was found that this approach, which contains the method of Langer as a special case, offers a clear and systematic alternative for obtaining asymptotic solutions.

Determination of Asymptotic Solutions

It is not the purpose of this paper to give a rigorous statement of the generalized WKB method, which is readily available in the work by Dingle [1], but rather a heuristic description and interpretation of the process of finding asymptotic solutions for ordinary differential equations of the type which occur in shell theory. With this object in mind, it will be convenient to base the present discussion on a particular case, for example, on that of paraboloidal shells, since it represents one of the most complicated problems for which asymptotic solutions have been obtained by other workers in the field.

It will be assumed that the relevant differential equation has been reduced to its standard form

$$\frac{d^2w}{d\phi^2} = \gamma(\phi)w(\phi) \tag{1}$$

For the case of paraboloidal shells, one thus has [5]

$$\gamma(\phi) = -i^3\mu^2 \sin^{\bar{b}-1}\phi \sec^{\bar{b}+4}\phi + \frac{4\bar{b}^2-1}{4}\operatorname{cosec}^2\phi \sec^2\phi + \frac{9}{4}\tan^2\phi - \left(\frac{5}{2} - \frac{\bar{b}}{2}\right)\sec^2\phi + \frac{6(1+\nu)}{5}\bar{b}\sec^4\phi, \tag{2}$$

where

$$0 < \bar{b} = \frac{b}{1-b},\ \mu \text{ a large parameter} \tag{3}$$

Expanding $\gamma(\phi)$ in powers of ϕ, one finds the expression

$$\gamma(\phi) = -i^3\mu^2\phi^{\bar{b}-1} + \frac{4\bar{b}^2-1}{4\phi^2} + \text{const} + O(\phi^2) \tag{4}$$

[1] Now, Associate Professor of Applied Mechanics, Polytechnic Institute of Brooklyn, Brooklyn, N. Y.

[2] Numbers in brackets designate References at end of paper.

Presented at the Summer Conference of the Applied Mechanics Division, Troy, N. Y., June 18–20, 1959, of THE AMERICAN SOCIETY OF MECHANICAL ENGINEERS.

Discussion of this paper should be addressed to the Secretary, ASME, 29 West 39th Street, New York, N. Y., and will be accepted until January 10, 1960, for publication at a later date. Discussion received after the closing date will be returned.

NOTE: Statements and opinions advanced in papers are to be understood as individual expressions of their authors and not those of the Society. Manuscript received by ASME Applied Mechanics Division, June 27, 1958. Paper No. 59—APM-30.

which characterizes the behavior of $\gamma(\phi)$ for small values of ϕ.

In order to find solutions to Equation (1) which are asymptotic in the large parameter μ, one has now to find a comparison equation

$$\frac{d^2W(\sigma)}{d\sigma^2} = \Gamma(\sigma)W(\sigma) \tag{5}$$

for which analytic solutions in terms of tabulated special functions are known. In Dingle's paper [1], a large table of comparison functions $\Gamma(\sigma)$ and their corresponding solutions are given. In the case of paraboloidal shells, the form of the comparison function $\Gamma(\sigma)$ is indicated by Equation (4):

$$\Gamma(\sigma) = -\nu^2\sigma^{2\nu-2} + \frac{4p^2\nu^2 - 1}{4\sigma^2} \tag{6}$$

with

$$\nu = \frac{b+1}{2} = \frac{1}{2(1-b)}, \quad p = 2k \tag{7}$$

and the corresponding solutions of Equation (5) are

$$W_1, W_2 = \sigma^{1/2}J_{\pm p} = \sigma^{1/2}J_{\pm 2k}(\sigma^\nu), \tag{8}$$

where J_ν are Bessel functions.

It is now clear that the solutions (8) have near $\sigma = 0$ the same analytic features as the solutions of Equation (1) with $\gamma(\phi)$ given by Equation (2). However, for larger values of the independent variable ϕ, the term involving the large parameter μ becomes dominant.

The next step is concerned with the determination of the independent variable σ in terms of ϕ. Writing the solution $w(\phi)$ in the form

$$w(\phi) = \left(\frac{d\sigma}{d\phi}\right)^{-1/2} W(\sigma) \tag{9}$$

one finds

$$\gamma(\phi) = \left(\frac{d\sigma}{d\phi}\right)^2 \Gamma(\sigma) + \left(\frac{d\sigma}{d\phi}\right)^{1/2} \frac{d^2}{d\phi^2}\left(\frac{d\sigma}{d\phi}\right)^{-1/2}, \tag{10}$$

where the last term in this exact equation is called the correction term. There are various conditions under which this correction term will be negligible; in particular, this is the case when $\gamma(\phi)$ and the comparison function $\Gamma(\sigma)$ have almost the same analytic behavior. For more details, the reader may consult the paper by Dingle [1].

Omitting in Equation (10) the correction term, one finds for the equation

$$\int_0^\sigma (\Gamma(\sigma))^{1/2}d\sigma = \int_0^\phi (\gamma(\phi))^{1/2}d\phi \tag{11}$$

Having assured the correct analytic behavior of the comparison function and, hence, by the Relation (9), of the solution $w(\phi)$ in the neighborhood of the point $\phi = 0$, Equation (11) may now be evaluated by taking only the dominant term in $\gamma(\phi)$ and its corresponding term in $\Gamma(\sigma)$ into account. One thus finds from Equations (2) and (6)

$$\int_0^\sigma \frac{\sigma^{\frac{b-1}{2}}}{2(1-b)}\,d\sigma = \sigma^{\frac{b+1}{2}} = i^{3/2}\mu\int_0^\phi \sin^{\frac{b-1}{2}}\phi \sec^{\frac{b+4}{2}}\phi\, d\phi, \tag{12}$$

and hence the asymptotic solutions of the original equation by use of Equations (8) and (9). It is readily verified that these solutions agree with those found by de Silva [5] on the basis of Langer's method, as given by Naghdi [6]. It should be noted here that Dingle's paper gives a simple method for assessing the effect of the omission of the correction term.

In Table 1, the various stages of the foregoing procedure for toroidal, ellipsoidal, and paraboloidal shells are given in a convenient form for comparison with the results obtained by Clark, Naghdi and de Silva.

Edge Coefficients as Given by Langer-Type Solutions

(a) Ellipsoidal Shell. The geometric characteristics of the open-crown ellipsoidal shell used in this investigation were, Fig. 1:

$$a/h = 100; \; c/a = 1/2; \text{ central opening} = 2\alpha = 60 \text{ deg},$$

where

a = semimajor axis
c = semiminor axis
h = shell thickness

The solution given by Naghdi and de Silva for the ellipsoidal shell involves Kelvin functions of the first order. These functions are tabulated for arguments less than 10, while for larger arguments their asymptotic expansions can be used. The argument of the Kelvin functions involves the following integral

$$\Phi = \int_0^t \frac{dt}{(1-t^2)^{1/2}[1+\rho^2(1-2t^2)^2]^{5/4}} \tag{13}$$

where

$$t = \sin\phi/2,$$
$$\rho^2 = c^2/a^2 - 1, \tag{14}$$
$$\phi = \text{colatitude angle}$$

As, to the authors' knowledge, the foregoing integral has not been tabulated, it was evaluated numerically using the method of Gauss [7].

The edge coefficients were found in the usual manner by applying suitable edge moments and horizontal shears. Using the equations given by Naghdi and de Silva and satisfying the boundary conditions, the rotation V and the horizontal displacement δ may be found.[3] The calculation turned out to be some-

[3] Naghdi-de Silva and Clark use the notation $-\beta$ instead of V. The positive sign of the horizontal shear force H_φ, used by these authors, is also opposite to the sense in which it is used herein.

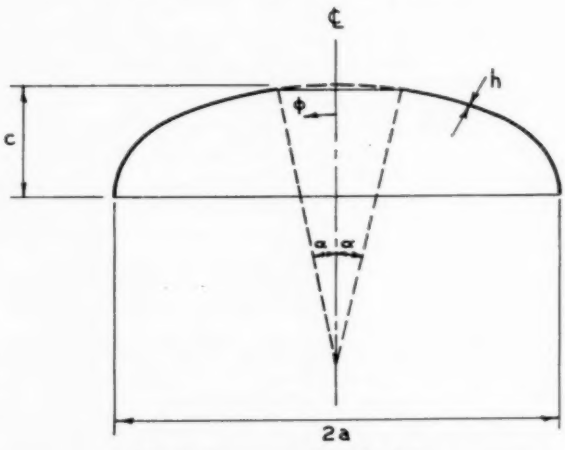

Fig. 1 Open-crown ellipsoidal shell

Table 1 Asymptotic solutions for various shells of revolution

Type of shell	$\gamma(\phi)$	$\Gamma(\sigma)$	$W(\sigma)$	ϖ
Toroidal	$\dfrac{iu\sin\phi}{1+\lambda\sin\phi}+{}^{3}/_{4}\left(\dfrac{\lambda\cos\phi}{1+\lambda\sin\phi}\right)$, $\lambda = b/a$,	σ	$\sigma^{1/2}J_{\pm 1/5}({}^{2}/_{3}\sigma^{3/2})$	$i^{1/2}\mu^{1/5}({}^{3}/_{5}\omega)^{2/5}$, $\omega = \int_0^{\phi}\left(\dfrac{\sin\phi}{1+\lambda\sin\phi}\right)^{1/2}d\phi$
Ellipsoidal	$\dfrac{-2i^{3}\mu^{2}}{\Omega^{5/2}}+{}^{3}/_{4}(1+\rho^{2})^{2}\left(\dfrac{\cot\phi}{\Omega}\right)^{2}$ $-{}^{3}/_{16}\left(\dfrac{\rho^{2}\sin 2\phi}{\Omega}\right)^{2}-{}^{3}/_{2}\dfrac{\rho^{2}\cos 2\phi}{\Omega}$ $-{}^{1}/_{2}(1+\rho^{2})\dfrac{\sin^{2}\phi+\rho^{2}\cos^{2}\phi}{\Omega^{2}}$, where $\Omega = 1+\rho^{2}\cos^{2}\phi$, $\rho^{2} = \dfrac{c^{2}}{a^{2}}-1$,	$-1+\dfrac{3}{4\sigma^{2}}$	$\sigma^{1/2}J_{\pm 1}(\sigma)$	$(2i^{3}\mu^{2})^{1/2}\Phi$, $\Phi = \int_0^{\phi}\Omega^{-5/4}d\phi$,
Paraboloidal	$-i^{3}\mu^{2}\sin^{\bar{b}-1}\phi\sec^{4+\bar{b}}\phi$ $+\dfrac{4\bar{b}^{2}-1}{\sin^{2}\phi\cos^{2}\phi}+{}^{9}/_{4}\tan^{2}\phi$ $-\left({}^{5}/_{2}-\dfrac{\bar{b}}{2}\right)\sec^{2}\phi+\dfrac{6(1+\nu)}{5}\bar{b}\sec^{4}\phi$, $\bar{b} = \dfrac{b}{1-b}$, ν Poisson's ratio,	$\dfrac{-\sigma^{\bar{b}-1}}{4(1-b)^{2}}+\dfrac{4\bar{b}^{2}-1}{4\sigma^{2}}$	$\sigma^{1/2}J_{\pm 2/(1-b)}\left(\sigma^{\frac{1}{2(1-b)}}\right)$	$i^{\frac{3}{\bar{b}+1}}\mu^{\frac{2}{\bar{b}+1}}\Lambda^{\frac{2}{\bar{b}+1}}$, $\Lambda = \int_0^{\phi}\sin\phi^{\frac{\bar{b}-1}{2}}\sec\phi^{\frac{\bar{b}+4}{2}}d\phi$

Table 2 Edge coefficients for ellipsoidal shell—Naghdi-de Silva solution

	V_{90}	δ_{90}/h	V_{20}	δ_{20}/h
$H_{90} = Eh$.....	329.77	−2567.6	...	...
$M_{90} = Eh^{2}$.....	−84.879	329.75	...	...
$H_{20} = Eh$.....	...	...	238.22	+1232.4
$M_{20} = Eh^{2}$.....	...	...	+99.869	238.19

Table 3 Edge coefficients for toroidal shell—Clark's solution

	V_{-90}	δ_{-90}/b	V_{-20}	δ_{-20}/b
$H_{-90} = Eb$.....	−11947	+3396.1	290.86	−193.54
$M_{-90} = Eb^{2}$.....	+84136.3	−11944.7	−7489.6	−147.15
$H_{-20} = Eb$.....	165.41	+217.87	−11921.3	−2874.2
$M_{-20} = Eb^{2}$.....	+8429	−327.06	−109744	−11921.2

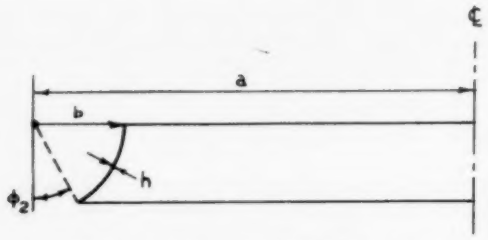

Fig. 2 Negative-curvature toroidal shell

what tedious, owing to the complicated functional dependence between the primary dependent variables and the independent variable.

It was found that an edge effect exists for the particular shell under consideration. As a result, it was possible to deal with two equations at a time, instead of having to solve all four equations simultaneously.

The resulting edge influence coefficients for this case are given in Table 2.

(b) Toroidal Shell of Negative Gaussian Curvature. The use of Clark's method for toroidal shells of positive curvature has been discussed previously [8]. However, negative-curvature toroidal shells, which are often used as transition elements between cylinders and cones or spheres, do not appear to have been treated previously. They will be considered in this section.

The toroidal shell shown in Fig. 2 was chosen as a specific example, its geometric characteristics being

$$\lambda = b/a = 0.2;\ b/h = 30;\ \phi_2 = -30 \text{ deg},$$

where

b = meridional radius of curvature
a = distance of center of generating circle of the shell from the axis of revolution
h = shell thickness
ϕ_2 = colatitude angle of lower edge of shell

Clark's solution is in terms of modified Hankel functions of order one third. These functions are tabulated in the Harvard Tables [9]. The argument of the Hankel functions involves the integral

$$\omega(\phi, \lambda) = \int_0^{\phi} \left(\frac{\sin \phi}{1 + \lambda \sin \phi}\right)^{1/2} d\phi \tag{15}$$

The shell under consideration has negative values of ϕ, as far as Clark's solution is concerned. This means that the integral ω will have a purely imaginary value, as is readily seen by letting $-\phi = \theta$.

The integral then becomes

$$\omega(-\phi, \lambda) = \int_0^{-\phi} \left(\frac{\sin \phi}{1 + \lambda \sin \phi}\right)^{1/2} d\phi = -i \int_0^{\phi} \left(\frac{\sin \theta}{1 - \lambda \sin \theta}\right)^{1/2} d\theta \tag{16}$$

For positive ϕ, the values of ω were tabulated by Clark. For negative ϕ one has, at the present time, to use numerical integration. For this purpose, Gauss' method was found adequate.

Another point which for negative values of ϕ requires some care is the evaluation of the modified Hankel functions of order one third. It is known that

$$h_1(z) = [h_2(z^*)]^*, \tag{17}$$

where the asterisks represent complex conjugates. Hence

$$h_1(-iy) = [h_2(iy)]^* \tag{18}$$

Writing $h_2(iy)$, which is tabulated in the Harvard Tables, in the form

$$h_2(iy) = A + iB, \tag{19}$$

one has

$$h_1(-iy) = A - iB \tag{20}$$

A similar relation holds for $h_2(-iy)$.

Apart from these aspects, the application of Clark's method to shells with negative angles of ϕ is the same as for positive angles. Hence, applying suitable edge moments and shears, one obtains the edge influence coefficients listed in Table 3.

It is also of interest to note that for toroidal shells which involve small angles of ϕ, and for which an edge effect may be expected, Clark gives some even more approximate formulas. These formulas have the advantage over the others given by Clark that they are relatively simple. For negative angles of ϕ, these simple formulas have to be modified. They should read:

$$\begin{aligned} \beta &= Ch_{2,r} - Dh_{2,i}, \\ \psi &= Dh_{2,r} + Ch_{2,i}, \\ \beta' &= -\mu^{1/3}[Dh_{2',r} + Ch_{2',i}], \\ \psi' &= \mu^{1/3}[Ch'_{2,r} - Dh_{2',i}]. \end{aligned} \tag{21}$$

The argument of the foregoing modified Hankel functions of order one third is $i\mu^{1/3}\phi$. The subscripts r and i denote the real and imaginary parts. The other parameters are

β = negative of the change in the angle of rotation
ψ = is proportional to transverse shearing force
$\mu = [12(1 - \nu^2)]^{1/2} b^2/ah$
ν = Poisson's ratio

(22)

while the primes denote differentiation with respect to ϕ.

Utilizing the foregoing approximate formulas for the toroidal shell under discussion at $\phi = -30$ deg, one finds:

Due to $M_{-30} = Eh^2$: $\beta_{-30} = 110{,}820$; $\delta_{-30}/b = -11{,}720$;
Due to $H_{-30} = Eh$: $\beta_{-30} = +11{,}725$; $\delta_{-30}/b = -2821$

These values are in good agreement with those given in Table 3.

Edge Coefficients Found by Numerical Integration

The differential equations governing the behavior of constant-thickness shells of revolution subjected to edge bending loads and uniform radial pressure can be obtained by extending the analysis given in Timoshenko [10] to include pressure effects. One obtains

$$\begin{aligned} L(U) + \nu U' - Ehr_1 V &= pG(\phi), \\ L(V) - \nu V' + r_1 U/D &= 0, \end{aligned} \tag{23}$$

where

$$L(\ldots) = \frac{r_2}{r_1}(\ldots)'' + \left[\left(\frac{r_2}{r_1}\right)' + \frac{r_2}{r_1}\cot\phi\right](\ldots)' - \frac{r_1}{r_2}\cot^2\phi(\ldots) \tag{24}$$

and the primes denote differentiation with respect to ϕ. The notation used is similar to that of Timoshenko:

Table 4 Edge coefficients for ellipsoidal shell—Numerical integration

	V_{90}	δ_{90}/h	V_{30}	δ_{30}/h
$H_{90} = Eh$	334.37	−2580.8	−10.418	−33.181
$M_{90} = Eh^2$	−85.349	334.37	0.91900	6.6027
$H_{30} = Eh$	−4.9803	25.043	238.46	1232.1
$M_{30} = Eh^2$	−0.69157	7.8585	99.879	238.46

Table 5 Edge coefficients for toroidal shell—Numerical integration

	V_{-90}	δ_{-90}/b	V_{-30}	δ_{-30}/b
$H_{-90} = Eb$	−12021	3410.2	293.36	−195.64
$M_{-90} = Eb^2$	84575	−12021	−7571.5	−145.53
$H_{-30} = Eb$	163.61	220.10	−11954	−2879.6
$M_{-30} = Eb^2$	8517.2	−329.93	−110145	−11954

U = r_2Q_ϕ
Q_ϕ = transverse shearing force
V = angle of rotation of a meridional tangent
h = shell thickness
r_1 = meridional radius of curvature
r_2 = radius of curvature in normal plane perpendicular to a meridian
p = uniform, internal pressure
E = modulus of elasticity
D = flexural rigidity of shell = $Eh^3/[12(1-\nu^2)]$
ν = Poisson's ratio
ϕ = colatitude angle (25)

The right-hand side of Equation (23) is given by

$$G(\phi) = \frac{r_1 r_2 \cot\phi}{2}\left(\frac{r_2}{r_1} - 1\right)\left(\frac{r_2}{r_1} - 3\right) - \frac{r_2^2}{2}\left(\frac{r_2}{r_1}\right)' \quad (26)$$

For the types of shell under discussion the quantities r_1 and r_2 are given by

1 Ellipsoidal Shell

$$r_1 = ka\zeta^3, \quad r_2 = ka\zeta \quad (27)$$

where

$$\zeta = [1 + (k^2 - 1)\sin^2\phi]^{-1/2}, \qquad k = a/c, \qquad a = \text{semimajor axis}, \qquad c = \text{semiminor axis}. \quad (28)$$

2 Toroidal Shell

$$r_1 = b, \quad r_2 = b\left(1 + \frac{1}{\lambda \sin\phi}\right), \quad (29)$$

where

$\lambda = b/a$
a = distance of center of generating circle of shell from axis of revolution

In order to obtain the edge influence coefficients due to edge bending loads, the function $G(\phi)$ was set equal to zero and the relevant values of r_1 and r_2 were substituted into the differential equations. These equations were then integrated on a high-speed digital computer, using the Runge-Kutta integration scheme with a step length of $^1/_2$ deg. Linear independence of the numerical solutions was assured by using the unit matrix for the initial values of U, U', V, and V'. The resulting edge influence coefficients are given in Tables 4 and 5.

Particular Integrals for Ellipsoidal and Toroidal Shells

An accepted approximate procedure for evaluating particular integrals for shells is based on the membrane solution. This solution, while satisfying equilibrium requirements, is known to violate the compatibility conditions. For some types of shell, the approximation gives good results. However, it was shown recently [11] that the approximation is not very good for toroidal shells of positive Gaussian curvature. It is thus of some interest to investigate the edge coefficients for the ellipsoidal and negative-curvature toroidal shells subject to uniform internal pressure. The membrane solution gives the following results:

1 Ellipsoidal Shell

$$EV = -p\frac{k}{2}\left(\frac{a}{h}\right)\frac{(\zeta^2-1)(3\zeta^2+1)}{\zeta^2}\cot\phi,$$
$$E\delta = k\left(\frac{a}{h}\right)\zeta\sin\phi(N_\theta - \nu N_\phi),$$
$$N_\theta = \frac{pka}{2\zeta}(2\zeta^2 - 1),$$
$$N_\phi = \frac{pk\zeta a}{2} \quad (30)$$

2 Toroidal Shell of Negative Curvature[4] ($\phi \geq 0$)

$$EV = \frac{p}{2}\left(\frac{b}{h}\right)\frac{\cot\phi}{\lambda^2\sin^2\phi}(\lambda\sin\phi - 1)(\lambda\sin\phi + 2),$$
$$E\delta = \left(\frac{b}{h}\right)\left(\frac{1 - \lambda\sin\phi}{\lambda}\right)(N_\theta - \nu N_\phi),$$
$$N_\theta = \frac{pb}{2\lambda^2\sin^2\phi}(\lambda^2\sin^2\phi - 1),$$
$$N_\phi = \frac{pb}{2\lambda\sin\phi}(\lambda\sin\phi - 1) \quad (31)$$

The edge deformations due to uniform internal pressure were also obtained by integrating the nonhomogeneous differential

Table 6 Ellipsoidal shell-edge coefficients due to uniform internal pressure

	—Membrane solution—		Numerical integration	
ϕ, deg	$EV \div p$	$E\frac{\delta}{h} \div p$	$EV \div p$	$E\frac{\delta}{h} \div p$
90	0	−11500	28.932	−12372
30	466.45	−285.74	528.96	−195.05

Table 7 Toroidal shell-edge coefficients due to uniform internal pressure

	—Membrane solution—		—Numerical integration—	
ϕ, deg	$EV \div p$	$E\frac{\delta}{b} \div p$	$EV \div p$	$E\frac{\delta}{b} \div p$
−90	0	−1368.0	−1705.1	−978.24
−30	−49105	−6500.3	−7914.0	−4613.1

[4] In using these formulas φ should be considered positive.

Equation (23) on a high-speed computer. The step length used was again $^1/_2$ deg.

The results obtained by the two methods are given in Tables 6 and 7.

Discussion of Results

1 Edge Influence Coefficients Due to Edge Bending Loads. Before comparing Table 2 with Table 4 it should be noted that the coefficients at one edge due to a load applied at a distant edge are zero in Table 2. This is because it was assumed that there was no interaction between the two edges.

Taking the foregoing into account, it can be seen that, for the specific shells investigated, the Langer-type solutions agree very well with the results obtained by means of numerical integration.

2 Edge Coefficients Due to Uniform Internal Pressure. It can be seen from Tables 6 and 7 that:

(*a*) For ellipsoidal shells, the membrane solution gives an acceptable particular integral of the differential equations. The rotation at $\phi = 30$ deg and the horizontal displacement at $\phi = 90$ deg differ only by about 10 per cent. For the other two quantities, the discrepancy is larger. However, the magnitudes of these are smaller than the others. Their effect on the final stress distribution remains to be investigated.

(*b*) For the toroidal shell of negative curvature, the horizontal displacements obtained by numerical integration are only about 70 per cent of those found by the membrane solution. The discrepancy for the edge rotations is much larger, with the numerical integration method giving a more uniform distribution over the shell. These results are similar to those obtained for toroidal shells of positive Gaussian curvature [11].

The stress resultants for the ellipsoidal and toroidal shells, obtained from the numerical integration results and the membrane solutions, are given in Figs. 3 and 4. For the ellipsoidal shell, the direct stress resultants N_ϕ and N_θ obtained by the two methods agree quite closely. This is also the case for N_ϕ in the torus. However, the numerical integration results for N_θ in the torus differ considerably from the membrane results, especially at $\phi = -30$ deg. This, in part, explains why the rotation for the ellipsoid agrees better with the membrane solution than the torus, since the rotation can be written as

$$V = (\epsilon_\phi - \epsilon_\theta) \cot \phi - \frac{r_2}{r_1} \frac{d}{d\phi} (\epsilon_\theta) \qquad (32)$$

Comparing the maximum transverse shears Q_ϕ and the maximum meridional bending moments M_ϕ due to pressure with their corresponding maximum meridional direct stress resultants N_ϕ, one finds (using the notation $\sigma_\phi{}^b$ and $\sigma_\phi{}^d$ to denote meridional bending and direct stresses, respectively):

	Ellipsoid	Toroid
Q_ϕ/N_ϕ	0.0018	0.03
$\sigma_\phi{}^b/\sigma_\phi{}^d$	0.095	1.56

For both types of shell the transverse shears due to pressure are quite small. The maximum meridional bending stress in the torus is seen to be 50 per cent greater than the corresponding direct stress. However, it is only 20 per cent of the maximum circumferential direct stress.

Final Comment

While the Langer-type solutions have been shown to give good results, their application to practical cases is time-consuming and tedious. If a computer is available, the authors of this paper recommend the use of direct methods of integration of the equations. This is because it is possible to code a program for general shells of revolution which will give both edge and interior influence coefficients in a relatively short time. Shells with varying wall thickness also can be analyzed readily by similar numerical methods.

References

1 R. B. Dingle, "The Method of Comparison Equations in the Solution of Linear Second-Order Differential Equations (Generalized-WKB Method)," *Applied Scientific Research*, vol. 5, section B, 1956, pp. 345–367.

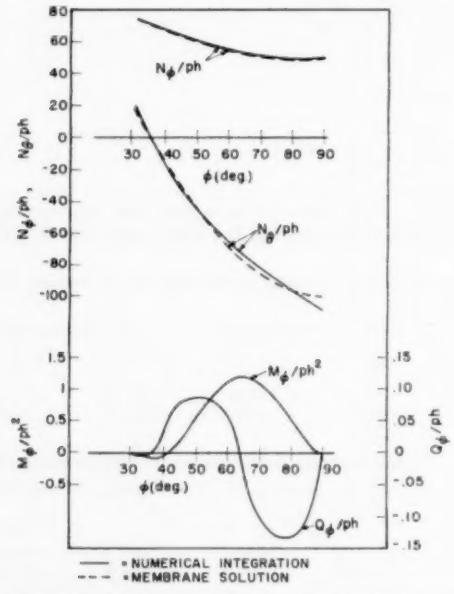

Fig. 3 Ellipsoidal shell—stress resultants resulting from uniform pressure

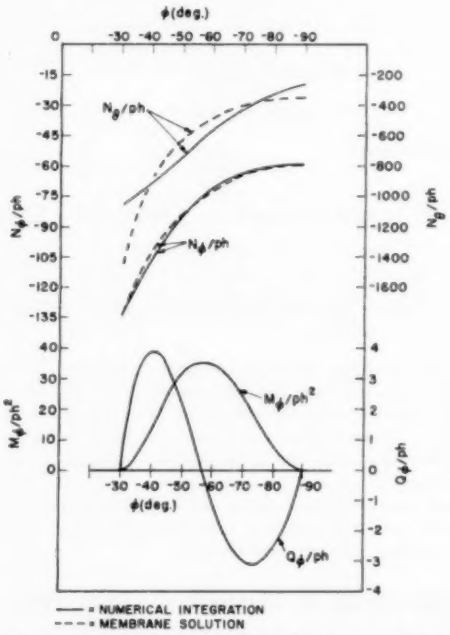

Fig. 4 Toroidal shell—stress resultants resulting from uniform pressure

2 R. E. Langer, "On the Asymptotic Solution of Ordinary Differential Equations, With Reference to the Stokes' Phenomenon About a Singular Point," *Transactions American Mathematical Society*, vol. 37, 1935, pp. 397–416.

3 P. M. Naghdi and C. N. de Silva, "Deformation of Elastic Ellipsoidal Shells of Revolution," Proceedings of the 2nd U. S. National Congress of Applied Mechanics, ASME, 1955, pp. 333–343.

4 R. A. Clark, "On the Theory of Thin Elastic Toroidal Shells," *Journal of Mathematics and Physics*, vol. 29, 1950, pp. 146–178.

5 C. N. de Silva, "Deformation of Elastic Paraboloidal Shells of Revolution," JOURNAL OF APPLIED MECHANICS, vol. 24, TRANS. ASME, vol. 79, 1957, pp. 397–404.

6 P. M. Naghdi, "The Effect of Transverse Shear Deformation on the Bending of Elastic Shells of Revolution," *Quarterly of Applied Mathematics*, vol. 15, 1957, pp. 41–52.

7 F. B. Hildebrand, "Introduction to Numerical Analysis," McGraw-Hill Book Company, Inc., New York, N. Y., 1956, pp. 323–325.

8 G. D. Galletly, "A Comparison of Methods for Analyzing Bending Effects in Toroidal Shells," JOURNAL OF APPLIED MECHANICS, vol. 25, TRANS. ASME, vol. 80, 1958, p. 413.

9 "Modified Hankel Functions of Order One-Third," Annals of the Harvard Computation Laboratory, vol. 2, 1945.

10 S. Timoshenko, "Theory of Plates and Shells," McGraw-Hill Book Company, Inc., New York, N. Y., 1940, pp. 450–457.

11 G. D. Galletly, "On Particular Integrals for Toroidal Shells Subjected to Uniform Internal Pressure," JOURNAL OF APPLIED MECHANICS, vol. 25, TRANS. ASME, vol. 80, 1958, p. 412.

The Drag on Spheres and Cylinders in a Stream of Dust-Laden Air

THOMAS GILLESPIE

The Dow Chemical Company, Physical Research Laboratory, Midland, Mich.

A. W. GUNTER

Defence Research Board, Suffield Experimental Station, Ralston, Alberta, Canada

A system has been developed for measuring the drag on small spheres and cylinders in a stream of dust-laden air. The drag was found to be proportional to the kinetic energy of the air plus the kinetic energy of the dust, and to be independent of particle size for particles having diameters in the range of 50 to 400μ. The well-known drag-coefficient versus Reynolds-number plots are the same for dust-free and dust-laden air provided the drag coefficient is calculated using the density of the two-phase system and the Reynolds numbers are calculated using the density of air alone. This suggests that the dust has little effect on the flow pattern. The results indicate that an instrument utilizing the drag principle to measure dust concentration could be developed.

EXTENSIVE studies have been made of the drag exerted on cylinders and spheres by moving air [1, 2],[1] but no previous attempt has been made to determine the effect of introducing dust into the air stream. In a number of practical cases, dust is present and, in consequence, we have carried out some experiments to determine its effect.

In recent years, there has been considerable interest in dust streams as fluidized-particle systems for catalysis and for possible heat control in nuclear reactors. Previous work [3, 4] would indicate that a new technique for measuring the mass transfer in such systems would be useful. Hence, apart from determining the effect of dust on drag, we also have been interested in assessing the possibility of estimating this quantity utilizing the drag principle.

Experimental

It has been established [1, 2] that the drag exerted by a moving fluid on a sphere or a cylinder placed at right angles to the stream direction is given by

$$F = {}^1/_2\rho V^2 C_d A \qquad (1)$$

where F is the drag, ρ is the density of the fluid which is moving at velocity V, and A is the cross-sectional area of the sphere or cylinder. C_d is the drag coefficient which is a function of the Reynolds number, **R**.

Introducing dust into an air stream might have two possible effects. In the first place, one would expect that the value of ρ to be used in Equation (1) would be increased from ρ_a the density of air, to ρ^* where

$$\rho^* = \rho_a + \text{mass of dust per unit volume of stream} \qquad (2)$$

In addition, there is some doubt as to the appropriate value of C_d. Whether it is determined by Reynolds number, calculated using the kinematic viscosity of the air alone, or by taking the dust into account is an important question, which, at this stage, is best answered by experiment.

Fig. 1 is a schematic diagram of the apparatus. The air flow originated from a compressor and was controlled at a relative humidity of 30 per cent. The dust was fed into the air stream continuously by means of an auger system. As Pinkus [4] has pointed out, it was necessary to use a venturi orifice at the dust entrance. The pipes through which the dust was blown were copper tubes (inside diameter, 2.5 cm).

The dust concentration was varied by controlling the speed of the auger. The rate at which dust was being transported through the tubes was assessed by inserting a trap between the cyclone separator and the graduated cylinder, Fig. 1. The trap was an 8-cm length of $^1/_8$-in. tube with the bottom end covered by a piece of Whatman No. 1 filter paper. By measuring the rate of fall of the level of the dust in the graduated column, the dust concentration was easily calculated.

The dust consisted of sized fractions of glass spheres procured from Minnesota Mining and Manufacturing Company. The apparent density of each of the powders needed to calculate dust concentration was determined in each case by weighing known volumes of the powders.

The air velocities used in the present experiments were below 1000 cm per sec. The dust concentration varied from zero to 5.1 kg per cu m. In most of the experiments, a rotameter was placed in the system as illustrated in Fig. 1. Owing to the fact that air was sucked into the tubes through the auger bearings by the action of the venturi nozzle, the rotameter did not record the correct flow rate. This was remedied by a subsidiary calibration using a rotameter placed between the sensing unit and the cyclone separator.

The air used to force the dust through the system was humidified, as mentioned previously, to avoid electrostatic effects. It was found that when these were present two effects were observable: (*a*) The glass beads tended to stick to the sides of the tubes; and (*b*) the pressure drop across a given section of the system increased with time. The following data were obtained in experiments where these effects were not present.

The sensing unit for measuring the drag exerted on a sphere is illustrated in Fig. 2. It consisted of a steel or aluminum ball hanging from a quartz or tungsten cantilever fiber. The fiber diameters were of the order of 1 to 2 mm. The ball was situated centrally in the "dust tube." It was connected to the cantilever by another thin fiber. The deflection of the horizontal fiber was measured by means of a traveling microscope sighted through a

[1] Numbers in brackets designate References at end of paper.

Presented at the Summer Conference of the Applied Mechanics Division, Troy, N. Y., June 18–20, 1959, of THE AMERICAN SOCIETY OF MECHANICAL ENGINEERS.

Discussion of this paper should be addressed to the Secretary, ASME, 29 West 39th Street, New York, N. Y., and will be accepted until January 10, 1960, for publication at a later date. Discussion received after the closing date will be returned.

NOTE: Statements and opinions advanced in papers are to be understood as individual expressions of their authors and not those of the Society. Manuscript received by ASME Applied Mechanics Division, July 8, 1958. Paper No. 59—APM-14.

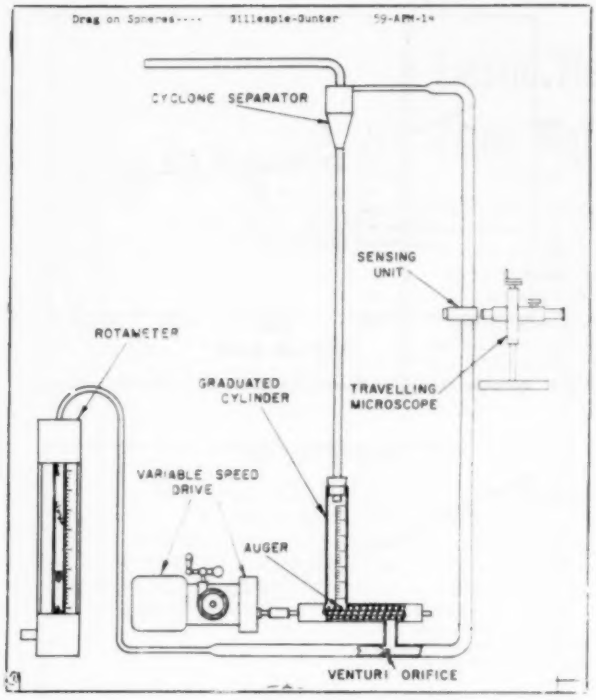

Fig. 1 Schematic diagram of apparatus

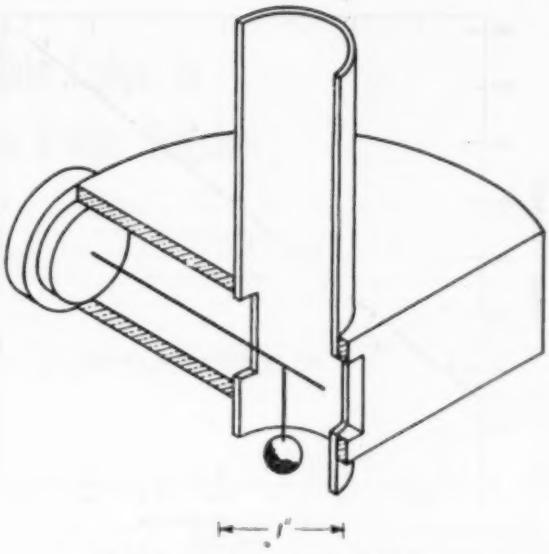

Fig. 2 Sensing unit for measuring drag

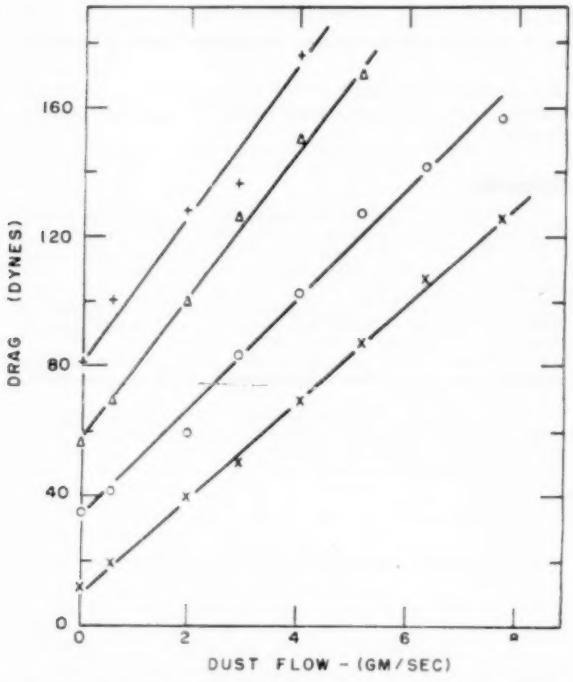

Fig. 3 Illustration of linear relation between dust flow and drag on a unit such as illustrated in Fig. 2. Symbols X, Δ, and + refer to data obtained at air velocities of 272, 435, 560, and 700 cm per sec, respectively.

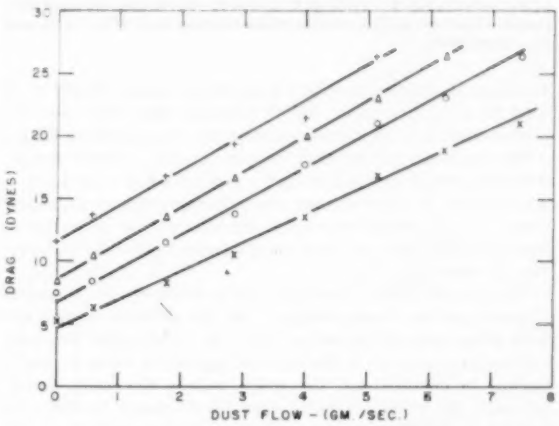

Fig. 4 Illustration of linearity between dust flow and drag on a cylinder. Symbols X, 0, Δ, and + refer to data obtained at air velocities of 294, 435, 560, and 700 cm per sec, respectively.

small plastic window in the side of the copper tube. The unit was calibrated by hanging small pieces of wire of known weight on the cantilever directly above the sphere.

For measuring the drag on cylinders, the horizontal fiber was used without the sphere and its connecting fiber. To determine the drag on a sphere alone, the drag on the horizontal fiber was subtracted from the total drag on a unit such as illustrated in Fig. 2. By attaching the connecting fiber behind the sphere, interference effects were minimized.

To correct for wall effects, the Ladenburg correction [2, 5] was used. Each value of the drag on the sphere was divided by $(1 + 2.4\ a/R)$ where a and R are the sphere radius and tube radius, respectively.

Experimental Results and Discussion

Figs. 3 and 4 illustrate the variation in drag with the amount of dust passing the sphere or cylinder per unit time at various constant air velocities. The linearity of these plots indicate that

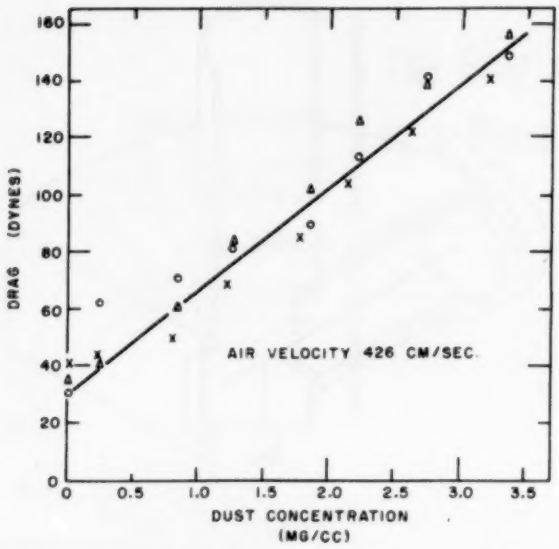

Fig. 5 Illustration of effect of dust-particle size on drag on a unit such as illustrated in Fig. 2. Symbols 0, Δ, and × refer to data obtained with screened fractions having number median diameters of 470μ, 155μ, and 55μ, respectively.

Equation (1) applies, provided that the two-phase density ρ^* is used for ρ. In addition, Fig. 5 indicates that there were no particle-size effects in the particle-diameter range of 50 to 400 μ.

The results are correlated in the same manner as previous work with dust-free air by plotting log C_D versus log **R** in Figs. 6 and 7. The full line in each case was drawn from previously published data [1]. The Reynolds number for each point in these figures was calculated from the drag measurements by means of Equation (1) and using ρ^* for ρ.

The present study has been limited to relatively low Reynolds numbers and the results indicate that the presence of dust has little effect upon the pattern of flow. At much higher Reynolds numbers, particularly in the region of separation where C_D drops sharply in dust-free air, this might not be the case. Unfortunately, the present type of experiment cannot be extended easily to study effects in this region.

Conclusion

It was found in these experiments that the drag on a fiber could only be assessed at dust concentrations below 5 kg per cu m owing to the fact that it was not possible to see the end of the fiber at higher dust concentrations. Our results show that up to this limit the drag phenomenon might be used to assess mass concentration in a moving fluidized-particle system. It is possible

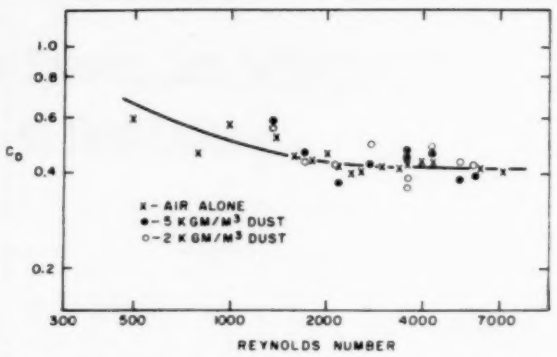

Fig. 6 Variation of drag coefficient with Reynolds number for spheres

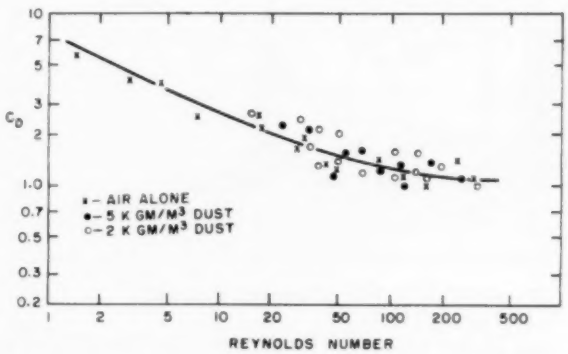

Fig. 7 Variation of drag coefficient with Reynolds number for cylinders

that the applicable range of dust concentration could be extended by using some nonvisual method of assessing fiber deflection.

References

1 S. Goldstein, "Modern Developments in Fluid Dynamics," vol. 2, Oxford University Press, first edition, 1938, p. 491.

2 J. M. Dalla Valle, "Micromeritics, The Technology of Fine Particles," Pitman Publishing Corporation, New York, N. Y., first edition, 1943, pp. 18–19.

3 O. H. Hariu and M. C. Molstad, "Pressure Drop in Vertical Tubes in Transport of Solids by Gases," *Industrial and Engineering Chemistry*, vol. 41, 1949, pp. 1148–1160.

4 O. Pinkus, "Pressure Drops in the Pneumatic Conveyance of, Solids," JOURNAL OF APPLIED MECHANICS, vol. 19, TRANS. ASME vol. 74, 1952, pp. 425–431.

5 R. Ladenburg, "Uber den Einfluss von Wänden auf die Bewegung einer Kügel in einer reibenden Flüssigkeit," *Annalen der Physik und Chemie*, vol. 23. 1907, pp. 447–458.

Elastic Flexible Cable in Plane Motion Under Tension

WEN-HSIUNG LI
Associate Professor of Civil Engineering, The Johns Hopkins University, Baltimore, Md.

The motion and stresses of a non-Hookian elastic flexible cable in plane motion under tension are described with four simultaneous quasilinear, partial differential equations which are totally hyperbolic. The propagation of the longitudinal elastic waves and the transverse waves are described by the four characteristics. From the characteristic equations, solutions for simple longitudinal waves and simple transverse waves are obtained for uniform Hookian cables. The problem of an infinite string moved at one point with a constant velocity can be solved. Solutions also have been obtained for the interaction of transverse and longitudinal waves with sharp fronts.

General Equations

In deriving the following equations, two assumptions are made: The cable is assumed to be perfectly flexible and of negligible weight such that the motion is governed solely by the tension in the cable. The longitudinal stress in the cable is assumed to be a single-valued function of the strain, such that the tensile force T in the cable can be expressed as

$$T = k \text{ (longitudinal strain)} \tag{1}$$

For a nonuniform non-Hookian cable, k is a function of s and T.

Let the x-y plane be the plane of motion and s-axis be a rest position of the cable under tension T_0 as shown in Fig. 1. The cable elements are identified with their position s along the s-axis. During motion, the positions of the elements are $x(s, t)$ and $y(s, t)$. Thus the equations of motion:

$$x_{tt} = \frac{1}{m}(T \cos \theta)_s \tag{2}$$

$$y_{tt} = \frac{1}{m}(T \sin \theta)_s \tag{3}$$

Let dl be the length under zero stress of the element which is ds in length under T_0. Then according to the second assumption,

$$T_0 = k_0 \frac{ds - dl}{dl}$$

or

$$ds = \frac{dl}{k_0}(k_0 + T_0)$$

Similarly,

$$dL = \frac{dl}{k}(k + T)$$

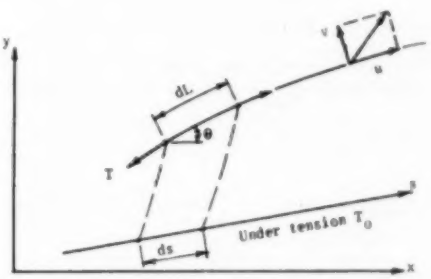

Fig. 1 Velocity and stress of cable

Contributed by the Applied Mechanics Division and presented at the Annual Meeting, Atlantic City, N. J., November 29–December 4, 1959, of The American Society of Mechanical Engineers.

Discussion of this paper should be addressed to the Secretary, ASME, 29 West 39th Street, New York, N. Y., and will be accepted until January 10, 1960, for publication at a later date. Discussion received after the closing date will be returned.

Note: Statements and opinions advanced in papers are to be understood as individual expressions of their authors and not those of the Society. Manuscript received by ASME Applied Mechanics Division, July 8, 1958. Paper No. 59—A-6.

Nomenclature

- c = wave speed of longitudinal wave; see Equations (16) and (24)
- $\bar{c}$ = wave speed of transverse wave; see Equations (17) and (25)
- F = function of α
- f = function of β
- K = function of cable properties as defined in Equations (18) and (26)
- k = elastic coefficient of cable as defined in Equation (1)
- k_0 = value of k when $T = T_0$
- m = mass per unit length of cable under tension T_0
- s = co-ordinate along cable in a rest position under tension T_0
- t = time
- T = tensile force in cable
- T_0 = a reference value of T; e.g., initial tension
- u = tangential velocity of cable element as defined in Equation (6)
- v = normal velocity of cable element as defined in Equation (7)
- x, y = rectangular co-ordinates in plane of motion
- α = variable identifying curves with $(dt)/(ds) = 1/c$
- β = variable identifying curves with $(dt)/(ds) = -1/c$
- γ = variable identifying curves with $(dt)/(ds) = 1/\bar{c}$
- δ = variable identifying curves with $(dt)/(ds) = -1/\bar{c}$
- θ = angle between cable element and x-axis
- τ = function of cable properties as defined in Equations (19) and (27)
- ϕ = function of γ
- ψ = function of δ

Subscripts s, t, and T indicate partial derivatives.

The angle θ can then be shown to be

$$\cos\theta = \frac{dx}{dL} = \frac{x_s ds}{dL} = \frac{k_0 + T_0}{k_0}\frac{k}{k+T}x_s$$

$$\sin\theta = \frac{dy}{dL} = \frac{y_s ds}{dL} = \frac{k_0 + T_0}{k_0}\frac{k}{k+T}y_s$$

which, upon differentiation, yield

$$x_{st} = \frac{k_0}{k_0 + T_0}\left(\frac{k - k_T T}{k^2}\cos\theta\, T_t - \frac{k+T}{k}\sin\theta\theta_t\right) \quad (4)$$

$$y_{st} = \frac{k_0}{k_0 + T_0}\left(\frac{k - k_T T}{k^2}\sin\theta\, T_t + \frac{k+T}{k}\cos\theta\theta_t\right) \quad (5)$$

Equations (2) to (5) can be reduced to a set of quasilinear equations.

Let variables $u(s, t)$ and $v(s, t)$ be defined as

$$u = x_t\cos\theta + y_t\sin\theta \quad (6)$$

$$v = y_t\cos\theta - x_t\sin\theta \quad (7)$$

They are the tangential and normal components of the velocity of a cable element. Equations (2) to (5) can be reduced to four equations with dependent variables u, v, θ, and T:

$$u_t - v\theta_t - \frac{1}{m}T_s = 0 \quad (8)$$

$$v_t - v\theta_s - \frac{k_0}{k_0 + T_0}\frac{k - k_T T}{k^2}T_t = 0 \quad (9)$$

$$v_t + u\theta_t - \frac{T}{m}\theta_s = 0 \quad (10)$$

$$v_s - \frac{k_0}{k_0 + T_0}\frac{k+T}{k}\theta_t + u\theta_s = 0 \quad (11)$$

These four equations are totally hyperbolic with four characteristics. Four characteristic equations can be obtained:[1]

$$\sigma \text{ along } \frac{dt}{ds} = +\frac{1}{c}, \quad \frac{du}{d\sigma} - v\frac{d\theta}{d\sigma} - K\frac{dT}{d\sigma} = 0 \quad (12)$$

$$\sigma \text{ along } \frac{dt}{ds} = -\frac{1}{c}, \quad \frac{du}{d\sigma} - v\frac{d\theta}{d\sigma} + K\frac{dT}{d\sigma} = 0 \quad (13)$$

$$\sigma \text{ along } \frac{dt}{ds} = +\frac{1}{\tilde{c}}, \quad \frac{dv}{d\sigma} - (\tau - u)\frac{d\theta}{d\sigma} = 0 \quad (14)$$

$$\sigma \text{ along } \frac{dt}{ds} = -\frac{1}{\tilde{c}}, \quad \frac{dv}{d\sigma} + (\tau + u)\frac{d\theta}{d\sigma} = 0 \quad (15)$$

where

$$c(s, T) = +\left(\frac{k}{m}\frac{k}{k - k_T T}\frac{k_0 + T_0}{k_0}\right)^{1/2} \quad (16)$$

$$\tilde{c}(s, T) = +\left(\frac{T}{m}\frac{k}{k+T}\frac{k_0 + T_0}{k_0}\right)^{1/2} \quad (17)$$

$$K(s, T) = +\left(\frac{1}{mk}\frac{k - k_T T}{k}\frac{k_0}{k_0 + T_0}\right)^{1/2} \quad (18)$$

$$\tau(s, T) = +\left(\frac{T}{m}\frac{k+T}{k}\frac{k_0}{k_0 + T_0}\right)^{1/2} \quad (19)$$

[1] R. Courant and K. O. Friedrichs, "Supersonic Flow and Shock Waves," Interscience Publishers, Inc., New York, N. Y., 1948, chapter 2.

Let each curve of the families defined by $(dt)/(ds) = 1/c$, $-1/c$, $1/\tilde{c}$, and $-1/\tilde{c}$ in the s-t plane be identified with a constant value of α, β, γ, and δ, respectively. Then

$$u - \int v d\theta - \int K dT = 2F(\alpha) \quad (20)$$

$$u - \int v d\theta + \int K dT = 2f(\beta) \quad (21)$$

$$v - \int(\tau - u)d\theta = 2\phi(\gamma) \quad (22)$$

$$v + \int(\tau + u)d\theta = 2\psi(\delta) \quad (23)$$

In these equations, the integration is performed along a curve of constant α, β, γ, and δ, respectively.

Simple Waves in a Uniform Hookian Cable

For a uniform Hookian cable, k and m are constants. The values of c and K are therefore constant while $\tilde{c}$ and τ are functions of the cable tension T only:

$$c = +\left(\frac{k + T_0}{m}\right)^{1/2} \quad (24)$$

$$\tilde{c}(T) = +\left(\frac{T}{m}\frac{k + T_0}{k + T}\right)^{1/2} < c \quad (25)$$

$$K = +[m(k + T_0)]^{-1/2} \quad (26)$$

$$\tau(T) = +\left(\frac{T}{m}\frac{k + T}{k + T_0}\right)^{1/2} \quad (27)$$

Since c is constant, the lines of constant α (or F) and the lines of constant β (or f) are straight lines in the s-t plane.

A trivial solution of the problem is that of a constant state with constant u, v, θ, and T, and therefore constant F, f, ϕ, and ψ. The solutions next in simplicity are those of simple waves propagated along one of the characteristics. Such a wave is described by a solution with three of F, f, ϕ, and ψ being constants.

1 Longitudinal wave propagated along $(dt)/(ds) = 1/c$:

The solution for this wave is obtained with f, ϕ, and ψ being constants. From Equations (20) to (23), we have θ = const, v = const, $u = f + F(\alpha)$, and KT = const $f - F(\alpha)$. The lines of constant α are therefore lines of constant u and T. Throughout the wave, u and T are related by:

$$u + KT = \text{const} \quad (28)$$

2 Longitudinal wave propagated along $(dt)/(ds) = -1/c$:

With F, ϕ, and ψ being constants, the solutions are: θ = const, v = const, u = const $F + f(\beta)$, and $KT = f(\beta)$ − const F. The lines of constant β are lines of constant u and T. Throughout the wave, u and T are related by:

$$u - KT = \text{const} \quad (29)$$

3 Transverse wave with constant strain, propagated along $(dt)/(ds) = 1/\tilde{c}$:

Let F, f, and ψ be constants. For any point P in the s-t plane, choose four points, one on each of the characteristics through P, as shown in Fig. 2. For u, v, θ, and T at P:

$$u - KT - \int_{\theta_1}^{\theta} v d\theta = 2F = \text{const}$$

$$u + KT - \int_{\theta_2}^{\theta} v d\theta = 2f = \text{const}$$

$$v - \int_{\theta_3}^{\theta}(\tau - u)d\theta = 2\phi(\gamma)$$

$$v + \int_{\theta_4}^{\theta}(\tau + u)d\theta = 2\psi = \text{const}$$

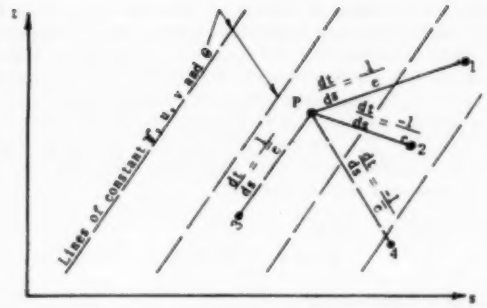

Fig. 2 Transverse wave with constant strain propagated at $(dt)/(ds) = 1/c$

These equations give u, v, θ, and T as functions of $\phi(\gamma)$. Let points 1 and 2 be located on an arbitrary line of constant γ. With $\theta_1 = \theta_2$, we have from the first two equations:

$$T = \text{const} \tag{30}$$

and

$$\frac{du}{d\theta} - v = 0$$

From the last of the four equations,

$$\frac{dv}{d\theta} + u = -\tau(T) = \text{const}$$

The two foregoing equations yield the relationship among u, v, and θ throughout the wave:

$$u = A \sin\theta + B \cos\theta - \tau \tag{31}$$

$$v = A \cos\theta - B \sin\theta \tag{32}$$

where A and B are constants:

$$A = u' \sin\theta' + v' \cos\theta' + \tau \sin\theta' \tag{33}$$

$$B = u' \cos\theta' - v' \sin\theta' + \tau \cos\theta' \tag{34}$$

The prime indicates values at an arbitrary point in the wave.

4 Transverse wave with constant strain, propagated along $(dt)/(ds) = -1/c$:

The solution is obtained with F, f, and ϕ being constants. Lines of constant δ are lines of constant u, v, and θ. Throughout the wave, T is constant, and u, v, and θ are related by:

$$u = C \sin\theta + D \cos\theta + \tau \tag{35}$$

$$v = C \cos\theta - D \sin\theta \tag{36}$$

where C and D are constants:

$$C = u' \sin\theta' + v' \cos\theta' - \tau \sin\theta' \tag{37}$$

$$D = u' \cos\theta' - v' \sin\theta' - \tau \cos\theta' \tag{38}$$

The prime indicates values at an arbitrary point in the wave.

Waves With Sharp Fronts

Several problems are to be studied by using the solutions of simple waves:

Semi-Infinite Cable Moved at One End in a Constant State. Let a cable, initially parallel to the x-axis under tension T_0, be moved at $s = L$ such that T_1 and θ_1 at $s = L$ are const. In each of the three regions in the s-t plane shown in Fig. 3, four characteristics can be drawn from any point to intersect the $t = 0$ line where $u = 0, v = 0, \theta = 0$, and $T = T_0$, or the $s = L$ line where $\theta = \theta_1$ and $T = T_1$. It can be shown by using Equations (20) to (23)

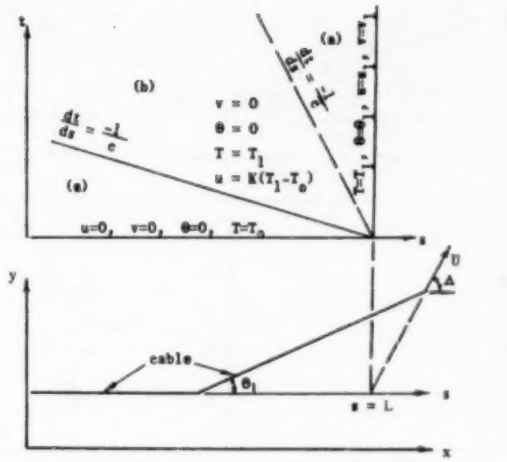

Fig. 3 Cable moved at one point with constant velocity

that these three regions are regions of constant state separated by two characteristics which are simple waves with a sharp front. Since there is no change of v and θ across the longitudinal wave we have, for region (b), $v = 0$, and $\theta = 0$. Since there is no change of T across the simple transverse wave, we have $T = T_1$ for region (b). The value of u in this region is given by Equation (29): $u - KT_1 = -KT_0$. The values of u_1 and v_1 in region (a) can be expressed in terms of T_0, T_1, and θ_1 by using Equations (35) and (36):

$$u_1 = [K(T_1 - T_0) - \tau_1] \cos\theta_1 + \tau_1$$

$$v_1 = -[K(T_1 - T_0) - \tau_1] \sin\theta_1$$

Since u_1, v_1, and θ_1 are constant along $s = L$, this point must be moved at a constant velocity U at a constant angle Δ with the x-axis:

$$u_1 = U \cos(\Delta - \theta_1)$$

$$v_1 = U \sin(\Delta - \theta_1)$$

Thus we have

$$U \cos(\Delta - \theta_1) = [K(T_1 - T_0) - \tau_1] \cos\theta_1 + \tau_1 \tag{39}$$

$$U \sin(\Delta - \theta_1) = -[K(T_1 - T_0) - \tau_1] \sin\theta_1 \tag{40}$$

From these equations, T_1 and θ_1 can be computed for given U and Δ, and vice versa. For the case with $\Delta = \pi/2$, Equations (39) and (40) yield

$$\sin\theta_1 = U/\tau_1 \tag{41}$$

and

$$\cos\theta_1 = 1 - K(T_1 - T_0)/\tau_1$$

Squaring both sides of these equations, adding and simplifying, we have

$$\left(\frac{U}{c}\right)^2 = 2\,\frac{T_1 - T_0}{k + T_0}\left(\frac{T_1}{k + T_0}\,\frac{k + T_1}{k + T_0}\right)^{1/2} - \left(\frac{T_1 - T_0}{k + T_0}\right)^2 \tag{42}$$

Equations (41) and (42) give the relation among θ_1, T_1, and U in normal impact. This problem has been studied by Ringleb[2] and Cole, Dougherty, and Huth[3] with other methods.

[2] F. O. Ringleb, "Motion and Stress of an Elastic Cable Due to Impact," JOURNAL OF APPLIED MECHANICS, vol. 24, TRANS. ASME, vol. 79, 1957, pp. 417–425.

[3] J. D. Cole, C. B. Dougherty, and J. H. Huth, "Constant-Strain Waves in Strings," JOURNAL OF APPLIED MECHANICS, vol. 20, TRANS. ASME, vol. 75, 1953, pp. 519–522.

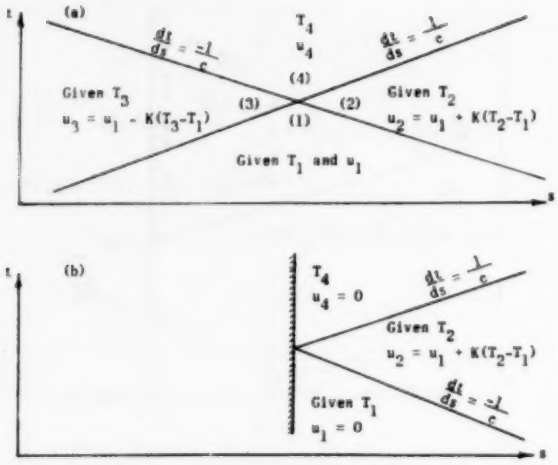

Fig. 4 Transmission and reflection of longitudinal waves with sharp front

Meeting of Two Longitudinal Waves. Two longitudinal waves with a sharp front are shown in Fig. 4(*a*). The values of T_1, u_1, T_2, and T_3 being given, u_2 and u_3 can be computed from Equations (29) and (28), respectively. Equation (28) also relates T_4 and u_4 to T_2 and u_2, and Equation (29) relates T_4 and u_4 to T_3 and u_3, giving

$$u_4 = u_1 + K(T_2 - T_3) \tag{43}$$

$$T_4 - T_2 = T_3 - T_1 \tag{44}$$

These two waves are seen to be completely transmitted.

When a longitudinal wave meets a fixed end where $u = 0$, we have, by comparing Figs. 4(*a*) and 4(*b*) and setting $u_4 = 0$ and eliminating T_3 in Equations (43) and (44),

$$T_4 - T_2 = T_2 - T_1$$

In other words, the stress is completely reflected.

Meeting of a Longitudinal Wave and a Transverse Wave. A longitudinal wave and a transverse wave with a sharp front are shown to meet in Fig. 5. The initial conditions in region 1 are given. With θ_2 given across the oncoming transverse wave, u_2 and v_2 can be computed according to Equations (35) and (36). With T_2 given across the oncoming longitudinal wave, u_3 can be computed according to Equation (28). Of the twelve values of u, v, θ, and T in regions 4, 5, and 6, we have $v_4 = v_2$, $\theta_4 = \theta_2$, $v_5 = v_3$, and $\theta_5 = \theta_3$ across the transmitted and reflected longitudinal waves. Also, across the reflected and transmitted transverse waves, we have $T_5 = T_6 = T_4$. Six additional equations are obtained according to Equations (28), (29), (31), (32), (35), and (36) as follows: According to Equation (28),

$$u_4 = u_2 + K(T_2 - T_4) =$$
$$C_1 \sin\theta_2 + D_1 \cos\theta_2 + \tau_1 + K(T_1 - T_6)$$

According to Equation (29),

$$u_5 = u_3 - K(T_3 - T_5) = u_1 - K(T_2 - T_1) - K(T_3 - T_4)$$

According to Equations (31) and (32),

$$u_6 = A_4 \sin\theta_6 + B_4 \cos\theta_6 - \tau_6 \tag{45}$$

$$v_6 = A_4 \cos\theta_6 - B_4 \sin\theta_6 \tag{46}$$

where

$$A_4 = u_4 \sin\theta_4 + v_4 \cos\theta_4 + \tau_4 \sin\theta_4$$
$$= [C_1 \sin\theta_2 + D_1 \cos\theta_2 + \tau_1 + K(T_1 - T_6)] \sin\theta_2$$
$$+ [C_1 \cos\theta_2 - D_1 \sin\theta_2] \cos\theta_2 + \tau_6 \sin\theta_2$$
$$= C_1 + [\tau_1 + K(T_1 - T_6) + \tau_6] \sin\theta_2 \tag{47}$$

and

$$B_4 = u_4 \cos\theta_4 - v_4 \sin\theta_4 + \tau_4 \cos\theta_4$$
$$= D_1 + [\tau_1 + K(T_1 - T_6) + \tau_6] \cos\theta_2 \tag{48}$$

Finally, according to Equations (35) and (36),

$$u_6 = C_5 \sin\theta_6 + D_5 \cos\theta_6 + \tau_6 \tag{49}$$

$$v_6 = C_5 \cos\theta_6 - D_5 \sin\theta_6 \tag{50}$$

where

$$C_5 = u_5 \sin\theta_5 + v_5 \cos\theta_5 - \tau_5 \sin\theta_5$$
$$= [u_1 - K(T_4 - T_1) - K(T_3 - T_6) - \tau_6] \sin\theta_1$$
$$+ v_1 \cos\theta_1 \tag{51}$$

and

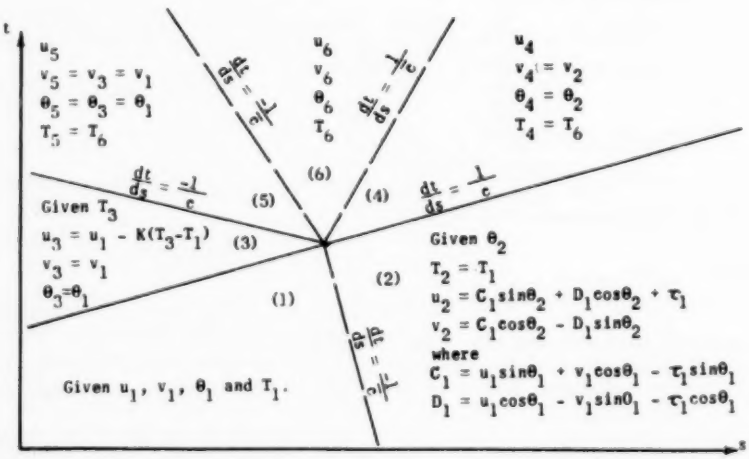

Fig. 5 Meeting of longitudinal wave and transverse wave with sharp front

$$D_5 = u_5 \cos\theta_5 - v_5 \sin\theta_5 - \tau_5 \cos\theta_5$$
$$= [u_1 - K(T_2 - T_1) - K(T_3 - T_5) - \tau_6] \cos\theta_1 - v_1 \sin\theta_1 \quad (52)$$

Noting that A_4, B_4, C_5, and D_5 involve one unknown only, namely, T_6 (τ_6 being a function of T_6), we have, by equating u_6 and v_6 in Equations (45), (46), (49), and (50), two equations for the two unknowns T_6 and θ_6:

$$A_4 \sin\theta_6 + B_4 \cos\theta_6 - \tau_6 = C_5 \sin\theta_6 + D_5 \cos\theta_6 + \tau_6$$
$$A_4 \cos\theta_6 - B_4 \sin\theta_6 = C_5 \cos\theta_6 - D_5 \sin\theta_6$$

From these two equations, we have

$$\theta_6 = \sin^{-1}\frac{1}{2\tau_6}(A_4 - C_5) = \cos^{-1}\frac{1}{2\tau_6}(B_4 - D_5) \quad (53)$$

$$(A_4 - C_5)^2 + (B_4 - D_5)^2 = 4\tau_6^2 \quad (54)$$

Substituting Equations (47), (48), (51), and (52) into Equation (54), and making use of Equation (27), we have

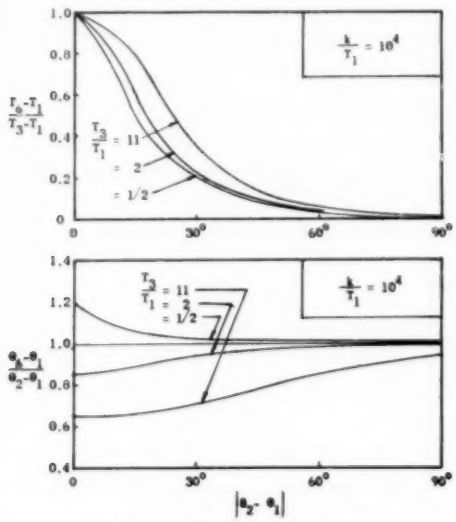

Fig. 6 Sample solutions of cases shown in Fig. 5

$$2\frac{T_6}{T_1}\left(\frac{k}{T_1} + \frac{T_6}{T_1}\right) - 2\frac{T_3}{T_1}[1 + \cos(\theta_2 - \theta_1)]$$
$$\left\{\left[\frac{T_6}{T_1}\left(\frac{k}{T_1} + \frac{T_6}{T_1}\right)\right]^{1/2} - \frac{T_6}{T_1}\right\}$$
$$- [1 + \cos(\theta_2 - \theta_1)]\left\{\left[\frac{T_6}{T_1}\left(\frac{k}{T_1} + \frac{T_6}{T_1}\right)\right]^{1/2} - \frac{T_6}{T_1}\right\}^2$$
$$= \left[\frac{k}{T_1} + 1 - 2\left(\frac{k}{T_1} + 1\right)^{1/2}\left(\frac{T_3}{T_1} - 1\right)\right]$$
$$[1 - \cos(\theta_2 - \theta_1)] + \left(\frac{2T_3}{T_1} - 1\right)[1 + \cos(\theta_2 - \theta_1)]$$
$$+ 2\left(\frac{T_3}{T_1} - 1\right)^2 \quad (55)$$

from which T_6 can be determined. From Equation (53), we have

$$2\tau_6 \sin(\theta_6 - \theta_1) = (A_4 - C_5)\cos\theta_1 - (B_4 - D_5)\sin\theta_1$$

or

$$\sin(\theta_6 - \theta_1) = \frac{\sin(\theta_2 - \theta_1)}{2\left[\frac{T_6}{T_1}\left(\frac{k}{T_1} + \frac{T_6}{T_1}\right)\right]^{1/2}}\left\{\left[\frac{T_6}{T_1}\left(\frac{k}{T_1} + \frac{T_6}{T_1}\right)\right]^{1/2} - \frac{T_6}{T_1} + 1 + \left(\frac{k}{T_1} + 1\right)^{1/2}\right\} \quad (56)$$

from which θ_6 can be determined. Solutions for several cases with given k/T_1, T_3/T_1, and $|\theta_2 - \theta_1|$ have been obtained according to Equations (55) and (56). The fractions of transmission of stress $(T_6 - T_1)/(T_2 - T_1)$, and of angle $(\theta_6 - \theta_1)/(\theta_2 - \theta_1)$ are shown in Fig. 6.

A Longitudinal Wave Overtaking a Transverse Wave. A longitudinal wave is shown overtaking a transverse wave in Fig. 7. It can be shown that the unknowns T_6 and θ_6 are given by:

$$2\frac{T_6}{T_1}\left(\frac{k}{T_1} + \frac{T_6}{T_1}\right) - 2\frac{T_3}{T_1}[1 + \cos(\theta_2 - \theta_1)]$$
$$\left\{\left[\frac{T_6}{T_1}\left(\frac{k}{T_1} + \frac{T_6}{T_1}\right)\right]^{1/2} - \frac{T_6}{T_1}\right\}$$

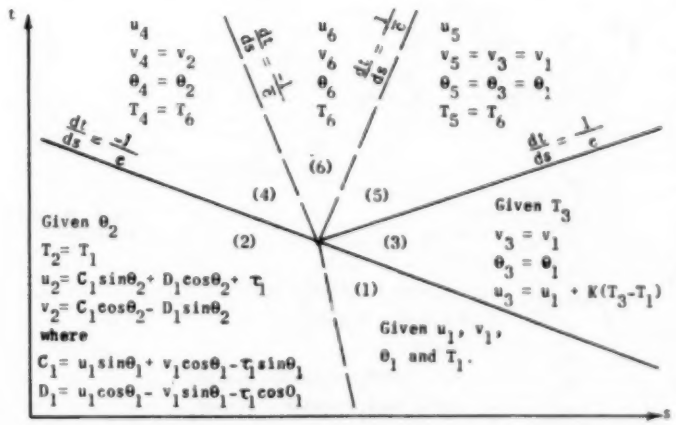

Fig. 7 Longitudinal wave overtaking transverse wave with sharp front

$$- [1 + \cos(\theta_2 - \theta_1)] \left\{ \left[\frac{T_6}{T_1} \left(\frac{k}{T_1} + \frac{T_6}{T_1} \right) \right]^{1/2} - \frac{T_6}{T_1} \right\}$$
$$= \left[\frac{k}{T_1} + 1 + 2 \left(\frac{k}{T_1} + 1 \right)^{1/2} \left(\frac{T_2}{T_1} - 1 \right) \right]$$
$$[1 - \cos(\theta_2 - \theta_3)] + \left(2 \frac{T_3}{T_1} - 1 \right) [1 + \cos(\theta_2 - \theta_1) + 2 \left(\frac{T_3}{T_1} - 1 \right)^2 \quad (57)$$

and

$$\sin(\theta_6 - \theta_2) = \frac{\sin(\theta_1 - \theta_2)}{2 \left[\frac{T_6}{T_1} \left(\frac{k}{T_1} + \frac{T_6}{T_1} \right) \right]^{1/2}} \left\{ \left[\frac{T_6}{T_1} \left(\frac{k}{T_1} + \frac{T_6}{T_1} \right) \right]^{1/2} - \frac{T_6}{T_1} - 1 + 2 \frac{T_2}{T_1} + \left(\frac{k}{T_1} + 1 \right)^{1/2} \right\} \quad (58)$$

Sample solutions are shown in Fig. 8.

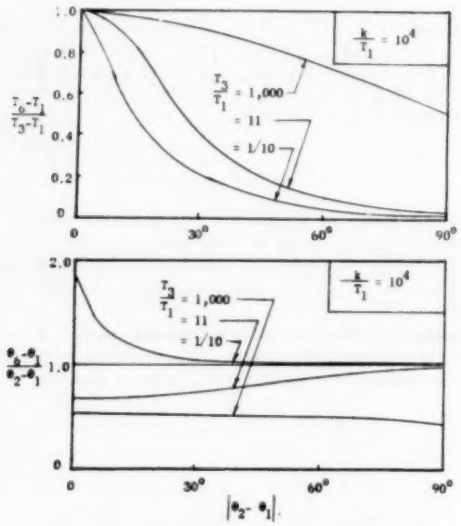

Fig. 8 Sample solutions of cases shown in Fig. 7

Meeting of Two Transverse Waves. Two transverse waves with a sharp front are shown to meet in Fig. 9. It can be shown that the two unknowns T_6 and θ_6 are given by:

$$2 \frac{T_6}{T_1} \left(\frac{k}{T_1} + \frac{T_6}{T_1} \right) - 2 \left\{ \left(\frac{k}{T_1} + 1 \right)^{1/2} [1 + \cos(\theta_2 - \theta_3) - \cos(\theta_2 - \theta_1) - \cos(\theta_3 - \theta_1)] + 1 + \cos(\theta_2 - \theta_3) \right\} \left\{ \left[\frac{T_6}{T_1} \left(\frac{k}{T_1} + \frac{T_6}{T_1} \right) \right]^{1/2} - \frac{T_6}{T_1} \right\} - [1 + \cos(\theta_2 - \theta_3)] \left\{ \left[\frac{T_6}{T_1} \left(\frac{k}{T_1} + \frac{T_6}{T_1} \right) \right]^{1/2} - \frac{T_6}{T_1} \right\}^2 = \left(\frac{k}{T_1} + 1 \right) [3 + \cos(\theta_2 - \theta_3) - 2 \cos(\theta_2 - \theta_1)]$$

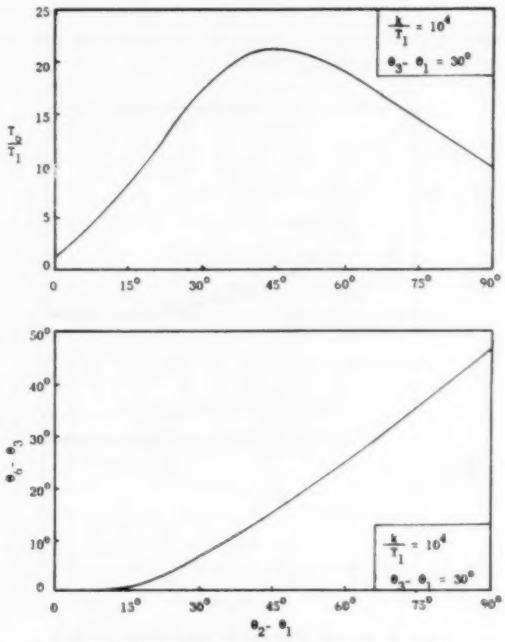

Fig. 10 Sample solutions of cases shown in Fig. 9

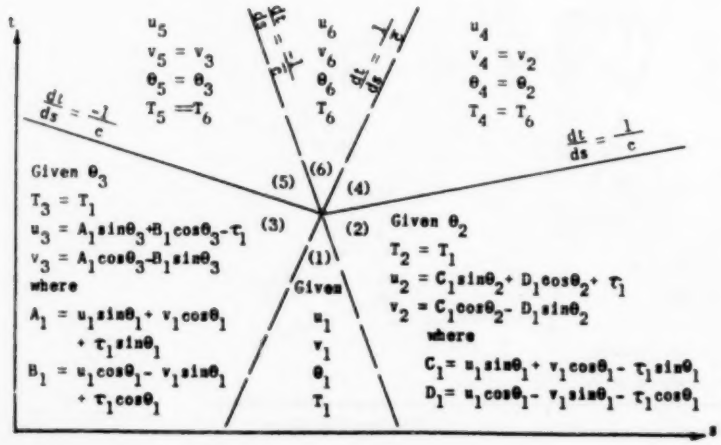

Fig. 9 Meeting of two transverse waves with sharp front

$$- 2 \cos (\theta_1 - \theta_3)] + 2\left(\frac{k}{T_1} + 1\right)^{1/2} [1 + \cos (\theta_2 - \theta_3)$$

$$- \cos (\theta_2 - \theta_1) - \cos (\theta_1 - \theta_3)] + 1 + \cos (\theta_2 - \theta_3) \quad (59)$$

and

$$2\left[\frac{T_6}{T_1}\left(\frac{k}{T_1} + \frac{T_6}{T_1}\right)\right]^{1/2} \sin (\theta_6 - \theta_3)$$

$$= \left\{\left(\frac{k}{T_1} + 1\right)^{1/2} + 1 - \frac{T_6}{T_1}\right.$$

$$\left. + \left[\frac{T_6}{T_1}\left(\frac{k}{T_1} + \frac{T_6}{T_1}\right)\right]^{1/2}\right\} \sin (\theta_2 - \theta_3)$$

$$- 2\left(\frac{k}{T_1} + 1\right)^{1/2} \sin (\theta_1 - \theta_3) \quad (60)$$

Sample solutions are shown in Fig. 10. In the derivation of these two equations, it has been assumed that T_6 is positive. In cases with $(\theta_2 - \theta_1)$ and $(\theta_3 - \theta_1)$ of opposite signs, T_6 may become negative. For such cases, these equations are not applicable.

It can be verified that, when $u_1 = 0$, $v_1 = 0$, and $\theta_2 = \theta_3$, T_6 and θ_6 must assume such values that $u_6 = 0$ and $v_6 = 0$. This is the solution for the reflection of a transverse wave with a sharp front at a fixed end. The value of T_6 can be computed from Equation (59) with $\theta_2 = \theta_3$. From Equation (60),

$$\sin (\theta_6 - \theta_2) = \left[\frac{T_1(k + T_1)}{T_6(k + T_6)}\right]^{1/2} \sin (\theta_3 - \theta_1) \quad (61)$$

Because of the difference between T_1 and T_6, the reflected wave $(\theta_6 - \theta_2)$ is different from the incident wave $(\theta_3 - \theta_1)$.

Acknowledgments

This investigation is part of a research project at The Johns Hopkins University under the sponsorship of U.S. Navy, Bureau of Aeronautics, Ships Installations Division. Dr. Robert S. Ayre is the Director of the project. The curves in Figs. 6 and 8 were computed and constructed by Mr. Fang-An Lee, Research Assistant in Civil Engineering.

Incremental Stress-Strain Law Applied to Work-Hardening Plastic Materials

CHINTSUN HWANG
Head, Commercial Systems,
The National Cash Register Company,
Electronics Division,
Hawthorne, Calif.
Mem. ASME

For problems involving work-hardening plastic materials, the incremental stress-strain law is considered to be a more rational approach than the conventional total stress-strain law. Up to the present the incremental stress-strain law was not subject to widespread use because it is mathematically inconvenient to handle. In this paper a method is developed in which the incremental law is applied to a work-hardening material in plane stress corresponding to the yield condition of von Mises. The method is illustrated by an analysis of the plastic bending of a simply supported work-hardening circular plate under uniformly distributed transverse load. The resulting difference-differential equations are solved by the NCR 304 digital computer.

THE incremental stress-strain law, which states that the principal axes of stress deviation coincide with the principal axes of the increments of the plastic strains, has been favored from the theoretical point of view, and has been verified to a certain degree by experiments [1, 2].[1] The ratio of the strain increments to the stress deviation is a function of the amount of work-hardening of the material. For practical problems the incremental stress-strain law introduces a relation between the stresses, the stress increments, and the strain increments to be used in the compatibility equations. The compatibility equations are then solved together with the equilibrium equations. Usually this combination of equations is inconvenient to work with and has hampered the application of the incremental stress-strain law to problems involving work-hardening plastic material.

To overcome the inconvenience of the incremental stress-strain law, and at the same time to retain its sound physical features, Prager [3] developed a method in which segmentwise linear yield conditions are used in conjunction with the appropriate flow rules. In his method, the linear yield conditions are assigned to the various parts of the work-hardening plastic material so that each part of the material follows a flow rule corresponding to the yield condition. Continuity conditions between the various parts are used to determine the transition points of the linear yield conditions and the velocity fields of the material. Several plate problems [3, 4, 5] have been solved by this method.

In the present paper the work-hardening plastic material is assumed to follow the yield condition of von Mises. The work-hardening process is isotropic so that the Mises' yield surface expands uniformly during the loading process. Incremental flow rules are used for each stepwise increase in external load. A process incorporating the von Mises' yield condition and the incremental flow rule into workable form is presented. The difference-differential equations thus obtained are solved by a high-speed digital computer. As is true in the numerical method, the desired degree of accuracy of the results can be achieved by using sufficiently fine steps in integration; at the same time there is no limitation to the type of external loads applied. The method is also adaptable to problems where unloading occurs in some parts of the plastic material.

Yield Condition and Incremental Flow Rule

In plane stress, the yield condition of von Mises is:

$$\sigma_1^2 - \sigma_1\sigma_2 + \sigma_2^2 = \sigma_0^2 \tag{1}$$

where σ_1 and σ_2 are the principal stresses, σ_0 is the yield stress in simple tension. For a rigid-plastic material with work-hardening characteristics, no strain is developed in the material until the yield condition is reached. After the yield condition has been reached, we can rewrite the stress condition in the following form replacing σ_0 by the parameter $\bar{\sigma}$; $\bar{\sigma}$ is called the equivalent stress:

$$f(\sigma_1, \sigma_2) = \sigma_1^2 - \sigma_1\sigma_2 + \sigma_2^2 - \bar{\sigma}^2 = 0 \tag{2}$$

Now that the material is in the work-hardening range, the incremental flow rule applies. In its most general form, the hypothesis that the equivalent stress depends only on the plastic work done leads to the flow rule [2]:

$$de_i = \frac{3\sigma_i' \, d\bar{\sigma}}{2\bar{\sigma}H'}, \quad i = 1, 2, 3 \tag{3}$$

where e_i are the plastic strains along the principal axes, σ_i' are the components of the stress deviation (the principal stresses minus the mean stress); $\bar{\sigma}$ is defined by the expression:

$$\bar{\sigma} = \left[\frac{3}{2}\sum(\sigma_i')^2\right]^{1/2}, \quad i = 1, 2, 3 \tag{4}$$

and is seen to be identical to the equivalent stress as given in (2) for the particular case of plane stress. H' is the slope of the curve of the equivalent stress $\bar{\sigma}$ versus the equivalent plastic strain $\bar{e}$. $\bar{e}$ is defined by

$$\bar{e} = \int\left[\frac{2}{3}\sum(de_i)^2\right]^{1/2}, \quad i = 1, 2, 3 \tag{5}$$

In this paper, H' is assumed to be a constant in the stress range under consideration. Applying equation (3) in the case of plane stress, and using equation (2) to eliminate $\bar{\sigma}$, we obtain the following expressions for the plastic-strain increments:

$$de_1 = \frac{(2\sigma_1 - \sigma_2)\bar{\sigma}d\bar{\sigma}}{2H'\bar{\sigma}^2} = \frac{1}{4H'}\frac{\dfrac{\partial f}{\partial\sigma_1}\left(\dfrac{\partial f}{\partial\sigma_1}d\sigma_1 + \dfrac{\partial f}{\partial\sigma_2}d\sigma_2\right)}{\sigma_1^2 - \sigma_1\sigma_2 + \sigma_2^2} \tag{6}$$

[1] Numbers in brackets designate References at end of paper.

Presented at the Summer Conference of the Applied Mechanics Division, Troy, N. Y., June 18–20, 1959, of THE AMERICAN SOCIETY OF MECHANICAL ENGINEERS.

Discussion of this paper should be addressed to the Secretary, ASME, 29 West 39th Street, New York, N. Y., and will be accepted until January 10, 1960, for publication at a later date. Discussion received after the closing date will be returned.

NOTE: Statements and opinions advanced in papers are to be understood as individual expressions of their authors and not those of the Society. Manuscript received by ASME Applied Mechanics Division, July 11, 1958. Paper No. 59—APM-15.

$$de_2 = \frac{(-\sigma_1 + 2\sigma_2)\partial d\partial}{2H'\partial^2} = \frac{1}{4H'}\frac{\frac{\partial f}{\partial \sigma_2}\left(\frac{\partial f}{\partial \sigma_1}d\sigma_1 + \frac{\partial f}{\partial \sigma_2}d\sigma_2\right)}{\sigma_1^2 - \sigma_1\sigma_2 + \sigma_2^2} \quad (6)\ (cont.)$$

A geometrical representation of equations (6) can be given as follows: In plane stress, if the co-ordinates of the plastic strains coincide with the co-ordinates of the principal stresses, then for a certain stress increment, the corresponding incremental strain vector is in a direction normal to the stress ellipse as defined by equation (2). The length of the incremental strain vector is proportional to the projection of the stress increment vector on the normal of the stress ellipse, to be modified by a factor

$$\frac{\left(\frac{\partial f}{\partial \sigma_1}\right)^2 + \left(\frac{\partial f}{\partial \sigma_2}\right)^2}{2\partial^2}$$

Using equation (2), it is seen that this factor is equal to

$$\frac{5\sigma_1^2 - 8\sigma_1\sigma_2 + 5\sigma_2^2}{2(\sigma_1^2 - \sigma_1\sigma_2 + \sigma_2^2)}$$

As can be seen by substitution, and through the end results given later, this factor tends to minimize the degree of work-hardening in a region where one of the two principal stresses approaches zero, and where the two principal stresses have opposite signs.

While there is some resemblance between the foregoing geometrical representation and the kinematic model given by Prager [3] for a rigid, work-hardening solid in plane stress, their major difference lies in the manner the yield curve is treated. In this paper the material is assumed to harden isotropically. The yield ellipse expands uniformly in the loading process. In Prager's kinematic model, the yield curve retains its size and shape, but translates on the stress co-ordinate plane as the stresses change. The latter model has the feature of simulating the Bauschinger effect during unloading. On the other hand, the general principle of the method presented in this paper can be used to simulate Prager's kinematic models to solve work-hardening problems.

The application of equations (6) to practical problems is illustrated by an example.

Example

Consider a circular plate made of rigid-plastic material. The radius of the plate is R, its half thickness is h. The plate is simply supported along the circumference and is under uniformly distributed load p per unit area of its horizontal middle surface. Let the bending moments along the radial and circumferential directions be denoted by M_r and M_φ. The bending moments satisfy the equilibrium equation:

$$\frac{dM_r}{dr} + \frac{1}{r}(M_r - M_\varphi) = -\frac{1}{2}pr \quad (7)$$

where r is the radial axis.

When the uniform load p reaches a certain value p_0, a state of incipient plastic flow exists. At this state yield conditions are fulfilled all over the plate. We are interested in the moment distribution in this state and when the load further increases. For a rigid-plastic plate, Hopkins and Prager [6] have shown that the yield curve for plane stress can be used for the yield curve of the bending moments of the plate with appropriate scaling of the co-ordinates. Thus the von Mises yield condition can be rewritten as:

$$M_r^2 - M_rM_\varphi + M_\varphi^2 = M_0^2 \quad (8)$$

where M_0 is the yield moment of the plate and is equal to σ_0h^2. Equations (7) and (8) can be combined to form:

$$\frac{dM_r}{dr} = \frac{1}{r}\left[-\frac{1}{2}M_r + \left(M_0^2 - \frac{3}{4}M_r^2\right)^{1/2}\right] - \frac{1}{2}pr \quad (9)$$

which, together with the boundary condition $M_r = 0$ at $r = R$, was used by Hopkins and Wang [7] to obtain the load-carrying capacity of the circular plate. To solve equation (9) by a digital computer, the Runge-Kutta method of integration [8] is used. The load p_0 corresponding to the incipient plastic flow is found to be $6.516366M_0/R^2$. The bending-moment distribution is tabulated in Table 1 and plotted in Figs. 1–3. The radial moment is equal to M_0 at the center and decreases steadily to zero toward the outer circumference of the plate. The moment along the circumferential direction increases from M_0 at the center to a maximum of $^2/_3(\sqrt{3}\,M_0)$ in the neighborhood of $r = 0.7R$. From there on the bending moment decreases until it reaches the value of M_0 at the outer circumference.

With further increase in the uniformly distributed transverse load p the plate enters the work-hardening range. For a stepwise increase in load Δp, the corresponding changes in bending moments are ΔM_r and ΔM_φ. The equilibrium condition yields the relations:

$$\frac{d\Delta M_r}{dr} = \frac{1}{r}(-\Delta M_r + \Delta M_\varphi) - \frac{1}{2}\Delta pr \quad (10)$$

For a rigid-plastic plate in the work-hardening range, deflections $w(r)$ are developed along the originally horizontal middle surface. If the radial and circumferential curvatures of the deflected middle surface are denoted by k_r and k_φ, then we have:

Table 1 Radial and circumferential moments of a simply supported circular plate of rigid, work-hardening material under uniform transverse load

p/p_0	$r/R = 0$	0.2	0.4	0.6	0.8	1.0
			(a) Radial bending moment M_r/M_0			
1.00	1.0000	0.9668	0.8624	0.6751	0.3921	0.0000
1.10	1.2091	1.1576	1.0116	0.7777	0.4462	0.0000
1.20	1.3971	1.3343	1.1562	0.8791	0.5000	0.0000
1.30	1.5732	1.5019	1.2972	0.9795	0.5535	0.0000
1.40	1.7417	1.6631	1.4350	1.0792	0.6068	0.0000
1.50	1.9050	1.8197	1.5703	1.1781	0.6599	0.0000
			(b) Circumferential bending moment M_φ/M_0			
1.00	1.0000	1.0302	1.0962	1.1488	1.1366	1.0000
1.10	1.2091	1.1998	1.2059	1.2274	1.1973	1.0332
1.20	1.3971	1.3670	1.3231	1.3092	1.2596	1.0679
1.30	1.5732	1.5302	1.4459	1.3938	1.3230	1.1035
1.40	1.7417	1.6895	1.5723	1.4811	1.3873	1.1398
1.50	1.9050	1.8456	1.7009	1.5709	1.4524	1.1767

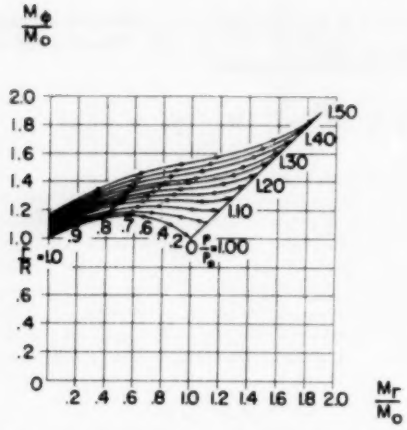

Fig. 1 Radial and circumferential bending-moment distribution of a simply supported circular plate of rigid, work-hardening material under uniformly distributed transverse load

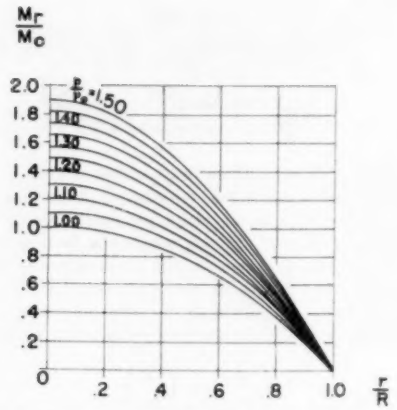

Fig. 2 Radial bending-moment distribution of the rigid, work-hardening plate

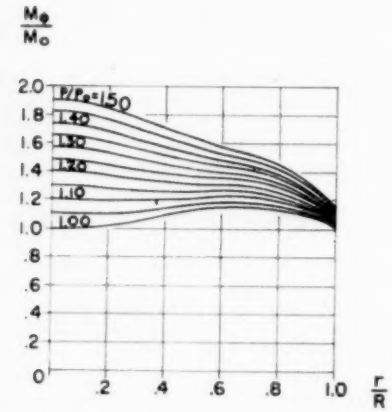

Fig. 3 Circumferential bending-moment distribution of the rigid, work-hardening plate

$$k_r = -\frac{d^2w}{dr^2}$$
$$k_\varphi = -\frac{1}{r}\frac{dw}{dr} \tag{11}$$

so that

$$\frac{dk_\varphi}{dr} = \frac{1}{r}(k_r - k_\varphi) \tag{12}$$

Now let us consider the plate with the uniformly distributed transverse load p, corresponding to an increase in load Δp, the middle surface of the plate goes through a deflection change Δw. If we assume that the change in deflection does not change the radial position of the plate material to any appreciable extent, then we have the following equation for the curvature changes Δk_r, Δk_φ of the plate:

$$\frac{d\Delta k_\varphi}{dr} = \frac{1}{r}(\Delta k_r - \Delta k_\varphi) \tag{13}$$

To establish a relation between the changes in bending moments and the changes in curvatures of the work-hardening plate, the incremental flow rules are used as follows: To represent the moment distribution at any location in the plate, we have, similar to equation (2), the equation of a moment ellipse:

$$F(M_r, M_\varphi) = M_r^2 - M_rM_\varphi + M_\varphi^2 - \bar{M}^2 = 0 \tag{14}$$

where $\bar{M}$ is equal to $\bar{\sigma}h^2$. Similar to the strain equations (6), we have the curvature equations based on the flow rules:

$$\Delta k_r = \frac{1}{4C}\frac{\dfrac{\partial F}{\partial M_r}\left(\dfrac{\partial F}{\partial M_r}\Delta M_r + \dfrac{\partial F}{\partial M_\varphi}\Delta M_\varphi\right)}{M_r^2 - M_rM_\varphi + M_\varphi^2}$$
$$\Delta k_\varphi = \frac{1}{4C}\frac{\dfrac{\partial F}{\partial M_\varphi}\left(\dfrac{\partial F}{\partial M_r}\Delta M_r + \dfrac{\partial F}{\partial M_\varphi}\Delta M_\varphi\right)}{M_r^2 - M_rM_\varphi + M_\varphi^2} \tag{15}$$

where C is a constant of the plate and can be interpreted as the slope of the curve of the equivalent moment $\bar{M}$ versus the equivalent curvature

$$\left\{\sqrt{2/3}\int[(dk_r)^2 + (dk_\varphi)^2]^{1/2}\right\}$$

Equations (15) are substituted into the compatibility equation (13) using equations (10), (14). After some rearranging we obtain

$$\begin{aligned}(M_r^2 - 4M_rM_\varphi + 4M_\varphi^2)\frac{d\Delta M_\varphi}{dr} &= \frac{1}{r}[(4M_r^2 - 4M_rM_\varphi + M_\varphi^2)\Delta M_r \\ &\quad + (-M_r^2 + 4M_rM_\varphi - 4M_\varphi^2)\Delta M_\varphi] \\ &\quad - \left[(-4M_r + 5M_\varphi)\frac{dM_r}{dr} + (5M_r - 4M_\varphi)\frac{dM_\varphi}{dr}\right]\Delta M_r \\ &\quad - 2(M_r - 2M_\varphi)\left(\frac{dM_r}{dr} - 2\frac{dM_\varphi}{dr}\right)\Delta M_\varphi \\ &\quad + [(-2M_r^2 + 5M_rM_\varphi - 2M_\varphi^2)\Delta M_r \\ &\quad + (M_r^2 - 4M_rM_\varphi + 4M_\varphi^2)\Delta M_\varphi] \\ &\quad \times \frac{(2M_r - M_\varphi)\dfrac{dM_r}{dr} - (M_r - 2M_\varphi)\dfrac{dM_\varphi}{dr}}{M_r^2 - M_rM_\varphi + M_\varphi^2} \\ &\quad - \frac{1}{2}(2M_r^2 - 5M_rM_\varphi + 2M_\varphi^2)\Delta p\end{aligned} \tag{16}$$

Equations (10) and (16) are solved simultaneously to obtain the

Table 2 Radial and circumferential curvatures of a simply supported circular plate of rigid, work-hardening material under uniform transverse load

p/p_0	$r/R = 0$	0.2	0.4	0.6	0.8	1.0
			(a) Radial curvature Ck_r/M_0			
1.10	0.1046	0.0821	0.0396	0.0086	−0.0080	−0.0166
1.20	0.1986	0.1637	0.0868	0.0216	−0.0150	−0.0339
1.30	0.2866	0.2435	0.1388	0.0386	−0.0208	−0.0517
1.40	0.3709	0.3215	0.1937	0.0590	−0.0256	−0.0699
1.50	0.4525	0.3978	0.2505	0.0823	−0.0292	−0.0883
			(b) Circumferential curvature Ck_φ/M_0			
1.10	0.1046	0.0968	0.0789	0.0601	0.0448	0.0332
1.20	0.1986	0.1868	0.1568	0.1217	0.0914	0.0678
1.30	0.2866	0.2722	0.2333	0.1840	0.1392	0.1035
1.40	0.3709	0.3545	0.3085	0.2468	0.1878	0.1398
1.50	0.4525	0.4344	0.3825	0.3097	0.2370	0.1767

moment distribution in the work-hardening range. Before the addition of the transverse load Δp, the radial and circumferential moments M_r, M_φ are known. Also known are the slopes of the moments with respect to r, dM_r/dr, and dM_φ/dr. With a relatively small increase in the load Δp, the bending moment changes ΔM_r and ΔM_φ are the dependent variables of the simultaneous differential equations (10) and (16). First, we assume a certain value for the moment changes $\Delta M_r = \Delta M_\varphi$ at $r = 0$. Equations (10) and (16) are integrated by the digital computer [9] to obtain a set of ΔM_r, ΔM_φ values at various positions of r. For a simply supported plate it is required that $\Delta M_r = 0$ at $r = R$. When the integration process yields a value of ΔM_r at $r = R$ which is not equal to zero, the assumed value of ΔM_r at $r = 0$ is adjusted and the integration process is repeated. After several repetitions of the process, the boundary condition at $r = R$ is satisfied. The final set of ΔM_r and ΔM_φ are the solutions of equations (10) and (16). The radial and circumferential moments in the plate after the addition of load Δp are then $M_r + \Delta M_r$, $M_\varphi + \Delta M_\varphi$. The corresponding slopes of the moments with respect to r are

$$\frac{dM_r}{dr} + \frac{d\Delta M_r}{dr}, \quad \frac{dM_\varphi}{dr} + \frac{d\Delta M_\varphi}{dr}$$

These new values of the bending moments and their slopes are used to solve equations (10) and (16) for further increase in the transverse load p. In the working example a value of $\Delta p = 0.05p_0$ is used. Integration corresponding to the stepwise increase in load is carried out ten times so that the load reaches $1.50p_0$ in the final stage. The moment distribution thus obtained is given in Table 1 and plotted in Figs. 1–3.

With each set of solutions of ΔM_r, ΔM_φ for equations (10), (16), equations (15) can be used to obtain the corresponding increase in the radial and circumferential curvatures of the plate middle surface. The curvature changes for the plate under the transverse loads are tabulated in Table 2 and plotted in Fig. 4. Based on the second equation of (11), the plate deflection w is calculated by integrating rk_φ with respect to r. The results thus obtained are plotted in Fig. 5.

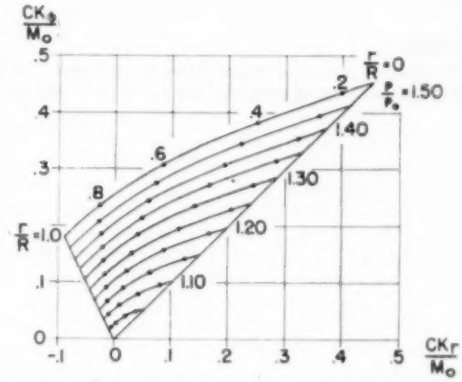

Fig. 4 Radial and circumferential curvature distribution of a simply supported circular plate of rigid, work-hardening material under uniformly distributed transverse load

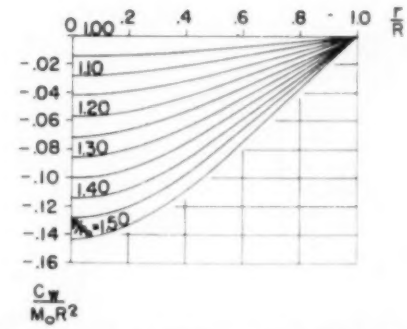

Fig. 5 Deflection curves of the simply supported circular plate of rigid, work-hardening material under uniformly distributed load

Conclusion

The underlying principle of the incremental flow rule for a work-hardening material is that the change in plastic strain is dependent on both the stress change and the stress distribution at the time of the stress change. The plastic strain of the material is thus dependent on the loading history of the material. In this paper the loading history of a plate is traced by the digital computer in a stepwise fashion so that the strain (curvature) changes for each loading step can be established.

Equations (10) and (16) can be considered as an exact representation of the flow rule if the load increment Δp approaches zero. For practical purposes a finite load increment has to be used. The finite load increment gives rise to finite moment and curvature changes which are determined by the moment distribution at the beginning of the load step, while in an exact sense the "immediate" moment distribution should be used. In this respect, the method described in the paper is an approximate method. To solve equations (10) and (16) on the computer, 21 equidistant stations are used along the radius of the plate so that $\Delta r = 0.05\,R$. Eight significant figures are used for all the variables. For each stepwise integration along the radius r, an iteration process is used [9]. The process continues in one step until an accuracy of six significant figures is reached.

In Figs. 1 and 4 the bending-moment changes and the corresponding curvature changes of the plate are plotted. Marked

down on the curves are several radial positions of the plate. If we follow the moment and curvature changes for a certain radial position, it is apparent that no direct relationship can be deduced between the curvature change and the moment distribution or between the curvature change and the corresponding moment change.

In Fig. 1 it is seen that the moment increments near the simply supported edge ($r = R$) of the plate are relatively small in magnitude as compared with the center part of the plate, while in Fig. 4 the corresponding curvature increments near the simply supported edge are not quite as small on a proportion basis. This phenomenon indicates a relatively small amount of work-hardening in a region where one of the principal stresses approaches zero, as was explained earlier in connection with equations (6).

References

1 W. Prager, "Theory of Plastic Flow Versus Theory of Plastic Deformation," *Journal of Applied Physics*, vol. 19, 1948, pp. 540–543.

2 R. Hill, "The Mathematical Theory of Plasticity," Oxford University Press, London, 1950, pp. 14–49.

3 W. Prager, "A New Method of Analyzing Stresses and Strains in Work-Hardening Plastic Solids," JOURNAL OF APPLIED MECHANICS, vol. 23, TRANS. ASME, vol. 78, 1956, pp. 493–496.

4 W. Boyce, "The Bending of a Work-Hardening Circular Plate by a Uniform Transverse Load," *Quarterly of Applied Mathematics*, vol. 14, 1956, pp. 277–288.

5 P. G. Hodge, Jr., "Plastic Bending of an Annular Plate," *Journal of Mathematics and Physics*, vol. 36, 1957, pp. 130–137.

6 H. G. Hopkins and W. Prager, "The Load-Carrying Capacities of Circular Plates," *Journal of the Mechanics and Physics of Solids*, vol. 2, 1953, pp. 1–13.

7 H. G. Hopkins and A. J. Wang, "Load-Carrying Capacities for Circular Plates of Perfectly-Plastic Material With Arbitrary Yield Condition," *Journal of the Mechanics and Physics of Solids*, vol. 3, 1955, pp. 117–129.

8 S. Gill, "A Process for the Step-by-Step Integration of Differential Equations in an Automatic Digital Computing Machine," *Proceedings*, The Cambridge Philosophical Society, vol. 47, 1950, pp. 96–108.

9 K. L. Nielsen, "Methods in Numerical Analysis," The Macmillan Company, New York, N. Y.,1956, p. 224.

A. W. JENIKE
Director, Flow of Bulk Solids Project,
University of Utah,
Salt Lake City, Utah.
Mem. ASME

R. T. SHIELD
Associate Professor,
Division of Applied Mathematics,
Brown University,
Providence, R. I.

On the Plastic Flow of Coulomb Solids Beyond Original Failure[1]

Principles developed for rigid-plastic solids exhibiting Coulomb's properties are adapted to the analysis of flow beyond original failure. A variable yield function is proposed to account for the changes of cohesion during flow and equations are evolved for the stress field in two dimensions. It is shown that, while in the stress field an effective angle of friction larger than the actual angle of friction is mandatory for these materials, in the velocity field the materials can be assumed incompressible.

The Yield Function

An unconsolidated Coulomb solid is quite loose and evidences no cohesion. As consolidation proceeds, cohesion increases. The relation is of the type shown in Fig. 1, where c is the Coulomb cohesion, ϕ the angle of internal friction, and σ the consolidating hydrostatic pressure. The time of consolidation t is also important, so that the yield function is of the general form

$$f(\sigma_1, \sigma_2, \sigma_3) = F(\sigma, t). \tag{1}$$

σ_1, σ_2, and σ_3 are assumed positive for pressure and negative for tension. For the sake of simplicity of argument, the time of consolidation will be considered constant in the following discussion. A relation exists also between mass density γ and σ, Fig. 2. Eliminating σ between the relations of Figs. 1 and 2, we obtain a relation between $c \cot \phi$ and γ of the type shown in Fig. 3. These relations can be determined experimentally for any particular material.

Following Drucker [1],[2] the pyramid yield surface proposed by Shield [2] can be adapted to the solids under study by closing it off with a base

$$^1/_3(\sigma_1 + \sigma_2 + \sigma_3) = \sigma.$$

This is shown in Fig. 4 in principal stress space. The abscissa $\sigma_1\sqrt{2} = \sigma_2\sqrt{2}$ is in the σ_1, σ_2 plane and bisects the angle between the σ_1, σ_2-axes. The evolution of the yield surface can be visualized as follows: In its uncompacted state, the material is under zero pressure. In accordance with Fig. 1, $c \cot \phi$ is also zero and the yield surface is a point at the origin O, Fig. 5. As pressures are applied the material consolidates, provided that the stress vector lies within some cone or pyramid centered at the hydrostatic axis with apex at O. Fig. 5 shows the outlines of three yield surfaces as they develop due to progressively increasing hydrostatic pressure σ.

At any stage of consolidation the solid is rigid (or elastic) for states of stress within the yield surface appropriate for the consolidating pressure σ. Yield can only occur when the stress point lies on the yield surface. During the process of consolidation, the plastic strain-rate vector ϵ is normal to the base of the pyramid which expands in size as the density and consolidating pressure increase. For a stress state represented by a point on the side of the pyramid, the plastic strain-rate vector is again normal to the side and the flow involves expansion which is opposite to consolidation. From Fig. 3, expansion implies reduction in $c \cot \phi$ and the yield surface diminishes in size as the flow progresses. Thus the intensity of the stress must fall as expansion occurs (in the sense that successive stress points will lie on yield surfaces each of which is enclosed by the preceding one).

At the edge of the base, the plastic strain-rate vector lies within

Fig. 1 Relation $c \cot \phi = a(\sigma + \sigma_0)$

Fig. 2 Relation between mass density γ and the consolidating hydrostatic pressure σ

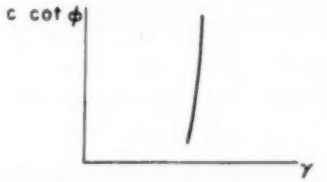

Fig. 3 Relation between $c \cot \phi$ and mass density γ

[1] This study was made in the course of the "Flow of Bulk Solids Project" in an attempt to provide a basis for the application of the theory of plasticity to problems of bulk-solids flow. The project is sponsored by: Utah Engineering Experiment Station, University of Utah; Engineering Foundation, United Engineering Trustees; American Iron and Steel Institute; Kaiser Engineers, Division of Henry J. Kaiser Company.

[2] Numbers in brackets designate References at end of paper.

Contributed by the Applied Mechanics Division and presented at the Annual Meeting, Atlantic City, N. J., November 29–December 4, 1959, of The American Society of Mechanical Engineers.

Discussion of this paper should be addressed to the Secretary, ASME, 29 West 39th Street, New York, N. Y., and will be accepted until January 10, 1960, for publication at a later date. Discussion received after the closing date will be returned.

Note: Statements and opinions advanced in papers are to be understood as individual expressions of their authors and not those of the Society. Manuscript received by ASME Applied Mechanics Division, July 23, 1958. Paper No. 59—A-7.

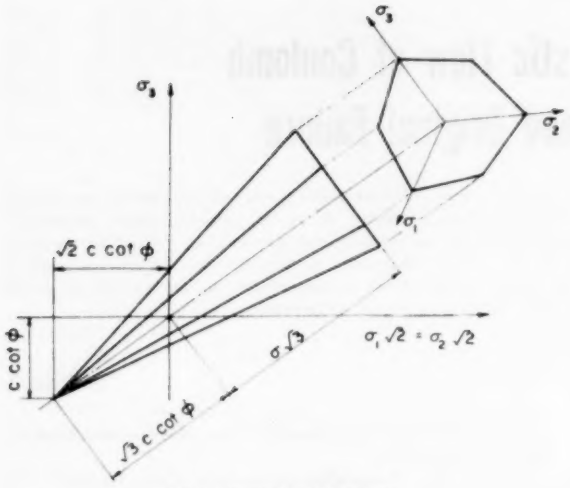

Fig. 4 Pyramid yield surface

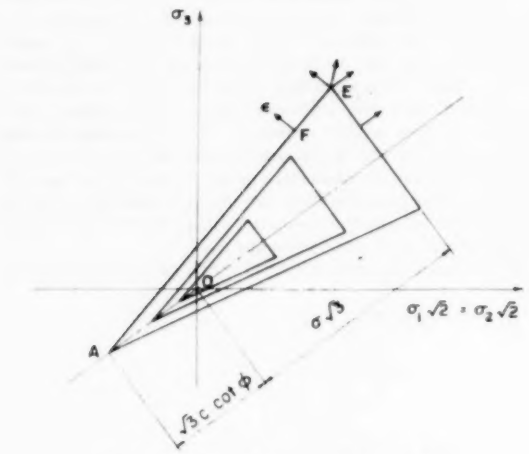

Fig. 5 Evolution of the pyramid yield surface

the directions of the normals to the adjacent surfaces. Depending on whether the flow involves expansion or consolidation the stress must fall or rise. Only when no change in volume occurs and the flow is one of pure shear can flow occur at constant stress. In this case the strain-rate vector is parallel to the base of the pyramid. The actual direction of the strain-rate vector wi be estimated, in the text which follows, for continued flow.

For two-dimensional problems an open pyramid is represented by the Coulomb yield function which is expressed as follows:

$$-\tfrac{1}{2}(\sigma_x + \sigma_y) + \frac{[\tfrac{1}{4}(\sigma_x - \sigma_y)^2 + \tau^2_{xy}]^{1/2}}{\sin\phi} - c\cot\phi = 0. \quad (2)$$

In order to adapt this function to describe the variable closed pyramid, let us assume that the hydrostatic pressure is given by

$$\sigma_c = \tfrac{1}{2}(\sigma_x + \sigma_y)$$

and that the function of Fig. 1 can be approximated by

$$c\cot\phi = a(\sigma + \sigma_0) \quad (3)$$

where a and σ_0 are material constants. The yield function can now be written as

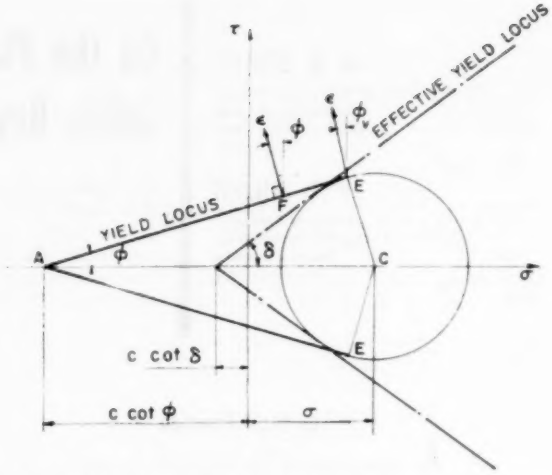

Fig. 6 Yield locus and effective yield locus in the (σ, τ) co-ordinates

$$-\sigma_c + \frac{[\tfrac{1}{4}(\sigma_x - \sigma_y)^2 + \tau_{xy}{}^2]^{1/2}}{\sin\phi} - a(\sigma + \sigma_0) = 0 \quad (4)$$

$$\sigma_c \leqslant \sigma$$

The inequality provides the closing base of the pyramid. This yield locus is shown in Fig. 6 in the (σ, τ) system of co-ordinates. Lines A-E correspond to the sides of the pyramid, the Mohr circle through points E to the edge of the base of the pyramid and smaller circles (not shown in the figure), with a common center at C, to points on the base of the pyramid.

Velocity-Field Characteristics

Consider now an element of material under a state of stress represented by the point E in Fig. 6 and suppose that during flow of the element the plastic strain-rate vector ϵ is inclined at an angle ϕ_v to the τ-axis. We will show that the value of ϕ_v is a function of the degree of convergence or divergence of flow and of the rate of consolidation or expansion of the solid during flow. Convergent flow occurs when one of the principal components of the strain rate, say ϵ_1, in the direction of flow, is positive while the lateral principal components of the strain rate are negative. For this condition we have from [2]

$$\epsilon_1 = (\lambda + \mu)(1 + \sin\phi_v), \qquad \epsilon_2 = -\lambda(1 - \sin\phi_v), \qquad \epsilon_3 = -\mu(1 - \sin\phi_v) \quad (5)$$

from which

$$\sin\phi_v = \frac{\epsilon_1 + \epsilon_2 + \epsilon_3}{\epsilon_1 - \epsilon_2 - \epsilon_3} \quad (6)$$

Divergent flow takes place when component ϵ_1 of the plastic strain rate is negative and the other two components are positive. We then have

$$\epsilon_1 = -(\lambda + \mu)(1 - \sin\phi_v), \qquad \epsilon_2 = \lambda(1 + \sin\phi_v), \qquad \epsilon_3 = \mu(1 + \sin\phi_v) \quad (7)$$

from which

$$\sin\phi_v = \frac{\epsilon_1 + \epsilon_2 + \epsilon_3}{-\epsilon_1 + \epsilon_2 + \epsilon_3} \quad (8)$$

Evidently the denominators in (6) and (8) are positive and ϕ_v assumes the sign of $\epsilon_1 + \epsilon_2 + \epsilon_3$ which is positive for expansion and negative for consolidation.

Let our element of material be dR, $R\,d\theta_1$, $(R + R_0)d\theta_2$, Fig. 7. The degree of convergence or divergence is expressed by $1/R$ and $1/(R + R_0)$, the reciprocals of the instantaneous distances from the element to the vertices of flow in the planes ϵ_1, ϵ_2 and ϵ_1, ϵ_3, respectively. The sum of the principal lateral strain rates is

$$\epsilon_2 + \epsilon_3 = \frac{1}{R}\frac{dR}{dt} + \frac{1}{R + R_0}\frac{dR}{dt} = \frac{1}{R}\frac{2R + R_0}{R + R_0}\frac{dR}{dt} \tag{9}$$

For plane strain $R_0 = \infty$, for axially symmetric strain $R_0 = 0$.

Consolidation or expansion involves a change in density

$$\epsilon_1 + \epsilon_2 + \epsilon_3 = -\frac{1}{\gamma}\frac{d\gamma}{dt} = -\frac{1}{\gamma}\frac{d\gamma}{dR}\frac{dR}{dt}. \tag{10}$$

Eliminating the principal strain rates in (6) by means of (9) and (10), we obtain for convergent flow

$$\sin\phi_v = \frac{1}{2\dfrac{2R + R_0}{R + R_0}\dfrac{\gamma}{R}\dfrac{dR}{d\gamma} + 1} \tag{11}$$

For divergent flow the sign of $\sin\phi_v$ should be reversed.

In the case of flow of bulk solids, the range of likely values of ϕ_v for convergent flow can be estimated from experimental data obtained at the Bulk Solids Flow Laboratory, Utah Engineering Experiment Station, University of Utah [3, 4]. Assume that the relation of Fig. 2 can be expressed by

$$\gamma = \alpha(1 + \sigma)^\beta \tag{12}$$

then

$$\frac{\gamma}{R}\frac{dR}{d\gamma} = \frac{1}{\beta}\frac{1 + \sigma}{R}\frac{dR}{d\sigma} \tag{13}$$

In conformance with experimental data, let us assume

$$\frac{\sigma}{R} > \frac{d\sigma}{dR} \tag{14}$$

so that

$$\left|\frac{\gamma}{R}\frac{dR}{d\gamma}\right| > \frac{1}{\beta}\left(1 + \frac{1}{\sigma}\right). \tag{15}$$

For σ measured in lb per sq ft, $1/\sigma$ can be neglected, and

$$\left|\frac{\gamma}{R}\frac{dR}{d\gamma}\right| > \frac{1}{\beta} \tag{16}$$

Equation (11) now transforms into

$$\frac{1}{-\dfrac{2}{\beta}\dfrac{2R + R_0}{R + R_0} + 1} < \sin\phi_v < \frac{1}{\dfrac{2}{\beta}\dfrac{2R + R_0}{R + R_0} + 1} \tag{17}$$

From [4] β is estimated at not more than 0.075 and the following bounds are found for ϕ_v:

$-2°\ 14' < \phi_v < 2°\ 4'$ for plane strain and

$-1°\ 6' < \phi_v < 1°\ 3'$ for axially symmetric strain.

These angles are so small that they seem to justify the assumption of $\phi_v = 0$ in the calculation of the velocity field. This assumption would imply that, in so far as the velocity field is concerned, the solid is incompressible during flow. For two-dimensional flow the characteristics of the velocity field would then form angles $\pi/4$ with the principal strain directions and, with the assumption of isotropy, also with the directions of principal stress.

Fig. 7 Flow of an element of material

It should be noted that, in the case of incipient flow, the problem is one of instability, and the foregoing conclusions do not apply. In determining incipient flow, equations (6) and (8) with $\phi_v = \phi$ may apply in regions of the mass of material. The conclusions of this section apply only to continued deformations when a value of ϕ_v which is not small would require excessively large changes of density.

Stress-Field Characteristics

As the angle ϕ_v is uniquely determined by normality at all points of the yield surface except points E (and A, but the last is outside the considered range of stress), Figs. 5 and 6, it follows that during the expansion stage the stresses are continuously at one of points E; i.e., at the edge of the base of the pyramid. Should stresses in a rigid, moving particle approach the yield surface at some other point F, normality would force $\phi_v = \phi$ with resulting rapid expansion and reduction of $c\cot\phi$ in accordance with the relation of Fig. 3; this would shrink the pyramid so that point E would join point F. Thus during the expansion stage, the stresses are always represented by the Mohr circle through points E.

Placing in (4)

$$\sigma_c = \sigma \qquad \sin\delta = (1 + a)\sin\phi \qquad C\cot\delta = \frac{a\sigma_c}{1 + a}, \tag{18}$$

we obtain

$$-\sigma + \frac{[1/4(\sigma_x - \sigma_y)^2 + \tau_{xy}^2]^{1/2}}{\sin\delta} - C\cot\delta = 0 \tag{19}$$

which is the equation of the *effective yield locus* shown in Fig. 6. It should be noted that, during rapid expansions which occur at a point F, the strain-rate vector ϵ is normal to the yield locus and not normal to the effective yield locus.

The equations of equilibrium for the two-dimensional case are

$$\frac{\partial\sigma_x}{\partial x} + \frac{\partial\tau_{xy}}{\partial y} = 0 \qquad \frac{\partial\sigma_y}{\partial y} + \frac{\partial\tau_{xy}}{\partial x} = -\gamma g \tag{20}$$

the y-axis being chosen in the upward vertical direction. Equations (19), (20) are hyperbolic, and the two characteristic directions are inclined at an angle $(\pi/4) - (\delta/2)$ to the direction of the major pressure σ_1 (see [5], for example). Calling

$$q = +\frac{[1/4(\sigma_x - \sigma_y)^2 + \tau_{xy}^2]^{1/2}}{\sin \delta} \tag{21}$$

it follows from (19) that

$$\begin{aligned} \sigma_x &= q[1 + \sin \delta \sin (2\theta + \delta)] - C \cot \delta \\ \sigma_y &= q[1 - \sin \delta \sin (2\theta + \delta)] - C \cot \delta \\ \tau_{xy} &= q \sin \delta \cos (2\theta + \delta) \end{aligned} \tag{22}$$

where θ denotes the angle of inclination of the first characteristic line with the x-axis, Fig. 8. The equations of equilibrium (20) can now be replaced by the equations

$$\begin{aligned} dq + 2q \tan \delta \, d\theta &= -\gamma g(\tan \delta \, dx + dy) \\ dq - 2q \tan \delta \, d\theta &= +\gamma g(\tan \delta \, dx - dy) \end{aligned} \tag{23}$$

along the first and second characteristic, respectively.

Steady and Pulsating Gravity Flow

During the steady flow of a solid in a gravitational field the rate of work of the external forces is equal to the rate of plastic work. When the rate of work of the external forces is less than the required rate of plastic work, the solid stops flowing. On the other hand, when the supplied energy exceeds the energy dissipated by steady flow, pulsating flow develops. This is so because all energy supplied by the external forces must be dissipated. When flow velocities are small and inertia and viscous terms insignificant, the only way material can dissipate the excess energy is by successive over-expansions and over-consolidations. The angle ϕ_w defined in the foregoing, oscillates about a value required for steady flow. Pulsating flow is observed quite commonly in the flow of bulk solids through smooth, steep channels.

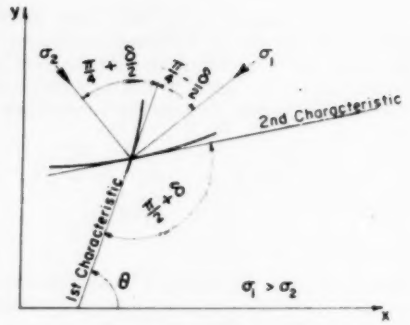

Fig. 8 Principal stresses and characteristics of the stress field in two dimensions

References

1 D. C. Drucker, "Stress-Strain Relations in Plastic and Frictional Soils," DA-3703/1, Brown University, Providence, R. I., March, 1956. See also: D. C. Drucker, R. E. Gibson, and D. J. Henkel, "Soil Mechanics and Work-Hardening Theories of Plasticity," *Transactions of the ASCE*, vol. 122, 1957, pp. 338–346.

2 R. T. Shield, "On Coulomb's Law of Failure in Soils," *Journal of the Mechanics and Physics of Solids*," vol. 4, 1955, pp. 10–16.

3 A. W. Jenike, "Flow of Bulk Solids," Bulletin No. 64, Utah Engineering Experiment Station, University of Utah, Salt Lake City, Utah, March, 1954.

4 A. W. Jenike, P. J. Elsey, and R. H. Woolley, "Flow Properties of Bulk Solids," Bulletin No. 95, Utah Engineering Experiment Station, University of Utah, Salt Lake City, Utah, December, 1958.

5 V. V. Sokolovski, "Statics of Earthy Media," State Publishing House of Technical and Theoretical Literature, Moscow, Russia, 1954.

J. P. ELLINGTON
United Kingdom Atomic Energy Authority,
Industrial Group Headquarters,
Risley, Warrington, England

H. McCALLION
Department of Mechanical Engineering,
University of Nottingham,
Nottingham, England

The Free Vibrations of Grillages

Frequency equations and modal shapes are derived for the transverse vibrations of beam grillages consisting of two sets of equally spaced uniform beams, the mass of the beams and associated plating being taken as lumped at the nodes.

In a previous paper [1][1] the authors discussed the static bending moments and deflections of a simply supported beam grillage subjected to concentrated loads applied at the nodes, a solution being found through the calculus of finite differences. Now, in a similar manner, the frequency equations and modal shapes of such a grillage are found for various boundary conditions.

Although several studies have been made of static loading of grillages, apart from the method of replacing the grillage by an equivalent anisotropic plate, the only work on the vibrations of such systems seems to be that of Cox and Denke [2], who have shown how to cast the problem into matrix form suitable for use with a digital computer.

The system to be considered is made up of two orthogonal sets of beams attached at the nodes so that no moments, bending or torsional, are transmitted from one set to the other. The mass of the beams and associated plating or covering is taken as lumped at the nodes, so that there is an equal point load at each node. Taking the bending moments and deflections under each load as unknowns the equations of continuity and equilibrium taken with appropriate boundary conditions furnish the required frequency equations.

[1] Numbers in brackets designate References at end of paper.

Presented at the West Coast Conference of the Applied Mechanics Division, Stanford, Calif., September 9–11, 1959, of THE AMERICAN SOCIETY OF MECHANICAL ENGINEERS.

Discussion of this paper should be addressed to the Secretary, ASME, 29 West 39th Street, New York, N. Y., and will be accepted until January 10, 1960, for publication at a later date. Discussion received after the closing date will be returned.

NOTE: Statements and opinions advanced in papers are to be understood as individual expressions of their authors and not those of the Society. Manuscript received at ASME Applied Mechanics Division, July 25, 1958. Paper No. 59—APMW-12.

The Difference Equations

Consider now a rectangular grillage of uniform beams. The beams in the r-direction are of modulus of elasticity E and second moment of area I_r and are spaced at equal distances apart L_s. These beams are crossed by beams in the s-direction, at right angles to them, the cross beams having a second moment of area I_s and being spaced L_r apart.

The deflection at a point where the beams cross (r, s) is $y_{r,s}$, it being assumed that the two sets of beams are simply attached to each other without any torsional or bending restraints. The bending moment in the r-beams at the intersection (r, s) is $M_{r,s}$ and the moment in the s-beams is $m_{r,s}$. Then, if masses are carried only at the nodes of the grillage, Clapeyron's three-moments equation [3] may be written for two adjacent spans of a beam in the r-direction as

$$M_{r+2,s} + 4M_{r+1,s} + M_{r,s} = (6EI_r/L_r^2)(y_{r+2,s} - 2y_{r+1,s} + y_{r,s})$$

Similarly, in the s-direction

$$m_{r,s+2} + 4m_{r,s+1} + m_{r,s} = (6EI_s/L_s^2)(y_{r,s+2} - 2y_{r,s+1} + y_{r,s})$$

Then, when the grillage is vibrating at a natural circular frequency ω, an equilibrium equation can be written for the shear forces and inertia loading at a node $(r + 1, s + 1)$,

$$\frac{M_{r+2,s+1} - 2M_{r+1,s+1} + M_{r,s+1}}{L_r} + \frac{m_{r+1,s+2} - 2m_{r+1,s+1} + m_{r+1,s}}{L_s} = \frac{W}{g}\omega^2 y_{r+1,s+1}$$

W being the concentrated load at each node.

These equations constitute a set of homogeneous linear partial difference equations [4] in the unknown deflections and bending moments and, using the partial finite-difference "shifting" opera-

Nomenclature

(r, s) = nodal point of orthogonal sets of beams in r and s-directions
R, S = total number of r-beams is $(R - 1)$ and s-beams is $(S - 1)$
Z = in some cases number of s-beams is $(2Z + 1)$
I_r, I_s = second moments of area of r and s-beams
L_r, L_s = spacing of beams in s and r-directions
E = Young's modulus
$y_{r,s}$ = nodal deflection
$M_{r,s}$ = nodal bending moment in r-beams
$m_{r,s}$ = nodal bending moment in s-beams
W = nodal concentrated load
ω = natural circular frequency
p, q = integers
$\mathbf{E}_r, \mathbf{E}_s$ = finite-difference "shifting" operators, defined by $\mathbf{E}_r^x \mathbf{E}_s^t y_{r,s} = y_{r+x,s+t}$
ζ = finite difference operator, $(\mathbf{E} - 1)^2/\mathbf{E}$
k = flexural stiffness, $12EI/L^3$
2λ = $(W\omega^2/gk_s) - (k_r/k_s)$ $[\cos(p\pi/R) - 1]^2/[\cos(p\pi/R) + 2]$
A, B, F, G, etc. = disposable constants in general solutions of difference equations
σ, ρ = characteristic exponents
α, β = characteristic exponents, $\sigma_{1,2} = \alpha, i\beta$; $\rho_{1,2} = \phi, i\psi$
ϕ, ψ = characteristic exponents, $\sigma_{1,2} = \alpha, i\beta$; $\rho_{1,2} = \phi, i\psi$
μ, ν = characteristic constants, $\mu_1 = (\cosh \sigma_1 - 1)/(\cosh \sigma_1 + 2)$, etc.

tors $\mathbf{E}_r$ and $\mathbf{E}_s$ defined by $\mathbf{E}_r^a y_{r,s} = y_{r+a,s}$ and $\mathbf{E}_s^a y_{r,s} = y_{r,s+a}$ they may be written in operational form as

$$\frac{L_r^2}{6EI_r}(\mathbf{E}_r - 1)^2 M_{r,s} + \frac{L_r^3}{EI_r}\mathbf{E}_r M_{r,s} - (\mathbf{E}_r - 1)^2 y_{r,s} = 0 \quad (1)$$

$$\frac{L_s^2}{6EI_s}(\mathbf{E}_s - 1)^2 m_{r,s} + \frac{L_s^3}{EI_s}\mathbf{E}_s m_{r,s} - (\mathbf{E}_s - 1)^2 y_{r,s} = 0 \quad (2)$$

and

$$\frac{1}{L_r}(\mathbf{E}_r - 1)^2\mathbf{E}_s M_{r,s} + \frac{1}{L_s}(\mathbf{E}_s - 1)^2\mathbf{E}_r m_{r,s} = \frac{W}{g}\omega^2\mathbf{E}_r\mathbf{E}_s y_{r,s} \quad (3)$$

Since there is no danger of ambiguity, the suffixes r, s will be dropped from the symbols for deflections and moments.

Equations (1) and (2) can then be written as

$$M = \frac{6EI_r}{L_r^2}\left\{\frac{(\mathbf{E}_r - 1)^2}{(\mathbf{E}_r - 1)^2 + 6\mathbf{E}_r}\right\} y \quad (4)$$

and

$$m = \frac{6EI_s}{L_s^2}\left\{\frac{(\mathbf{E}_s - 1)^2}{(\mathbf{E}_s - 1)^2 + 6\mathbf{E}_s}\right\} y \quad (5)$$

Substituting equations (4) and (5) in equation (3) gives

$$\left\{\frac{6EI_r}{L_r^3}\left[\frac{(\mathbf{E}_r - 1)^4\mathbf{E}_s}{(\mathbf{E}_r - 1)^2 + 6\mathbf{E}_r}\right] + \frac{6EI_s}{L_s^3}\left[\frac{(\mathbf{E}_s - 1)^4\mathbf{E}_r}{(\mathbf{E}_s - 1)^2 + 6\mathbf{E}_s}\right]\right\} y = \frac{W}{g}\omega^2\mathbf{E}_r\mathbf{E}_s y$$

or

$$\left\{\frac{k_r}{2}\left(\frac{\zeta_r^2}{\zeta_r + 6}\right) + \frac{k_s}{2}\left(\frac{\zeta_s^2}{\zeta_s + 6}\right) - \frac{W}{g}\omega^2\right\} y = 0 \quad (6)$$

in which

$$k = \frac{12EI}{L^3} \quad \text{and} \quad \zeta = \frac{(\mathbf{E} - 1)^2}{\mathbf{E}} \quad (7)$$

A solution for the free vibrations of a grillage simply supported on all four sides is readily found by taking a suitable deflected shape for the load points. In this case, with the origin $(r, s) = (0, 0)$ at one corner it is assumed that

$$y = A \sin(p\pi r/R) \sin(q\pi s/S) \quad (8)$$

Here $(R - 1)$ is the number of beams in the s-direction, $(S - 1)$ is the number of beams in the r-direction, while p and q are integers.

In substituting this expression for the deflections in equations (4) to (6) use is made of the property of the partial $\mathbf{E}$ operator that for the functions encountered here $f(\mathbf{E}_r)a^r b^s = a^r b^s f(a)$, so that

$$\begin{aligned}\zeta_r \sin(p\pi r/R) \sin(q\pi s/S) &= \sin(q\pi s/S)\mathcal{S}\zeta_r \exp(ip\pi r/R) \\ &= \sin(q\pi s/S)\mathcal{S}\frac{[\exp(ip\pi/R) - 1]^2}{\exp(ip\pi/R)}\exp(ip\pi r/R) \\ &= 2[\cos(p\pi/R) - 1]\sin(q\pi s/S)\sin(p\pi r/R)\end{aligned}$$

Thus the bending moments in the r and s-beams are, from equations (4) and (5),

$$M = \frac{6EI_r}{L_r^2}\frac{[\cos(p\pi/R) - 1]}{[\cos(p\pi/R) + 2]} A \sin(p\pi r/R) \sin(q\pi s/S) \quad (9)$$

and

$$m = \frac{6EI_s}{L_s^2}\frac{[\cos(q\pi/S) - 1]}{[\cos(q\pi/S) + 2]} A \sin(p\pi r/R) \sin(q\pi s/S) \quad (10)$$

The assumed deflected shape thus satisfies the boundary conditions of zero deflection and zero bending moment along the edges, $r = 0$ and R, and $s = 0$ and S, and finally, substitution in equation (6) gives the frequency equation

$$\frac{W}{g}\omega^2 = k_r\frac{[\cos(p\pi/R) - 1]^2}{[\cos(p\pi/R) + 2]} + k_s\frac{[\cos(q\pi/S) - 1]^2}{[\cos(q\pi/S) + 2]} \quad (11)$$

Permissible values of p and q are $1, 2, \ldots\ldots\ldots (R - 1)$, and $1, 2, \ldots\ldots\ldots (S - 1)$. If say $p = R$ then $\sin(p\pi r/R)$ is always zero, while the values $p = (R + 1), (R + 2), \ldots\ldots$ merely repeated the values of ω given by $p = (R - 1), (R - 2), \ldots\ldots$

Exactly as in the case of the vibration of membranes, equation (11) may have multiple roots, in which case the model shape is not determined solely by the frequency. For instance, if the grillage is square and composed of beams of equal stiffnesses and equal lengths so that $k_r = k_s$ and $R = S$, then the frequencies are given by

$$\frac{W\omega^2}{gk_r} = \frac{[\cos(p\pi/R) - 1]^2}{[\cos(p\pi/R) + 2]} + \frac{[\cos(q\pi/R) - 1]^2}{[\cos(q\pi/R) + 2]}$$

so that interchanging p and q yields the same value of the frequency. Some discussion of the resulting deflected shapes is given by Rayleigh [5].

Grillage With Simple Supports at Two Opposite Edges

Taking a grillage with the r-beams simply supported at the ends $r = 0$ and $r = R$ then the deflected shape may be assumed as

$$y = A \sin(p\pi r/R) \exp(\sigma s) \quad (12)$$

where, again, A is a disposable constant and σ is to be determined.

Substitution in equation (6) gives,

$$k_r\frac{[\cos(p\pi/R) - 1]^2}{[\cos(p\pi/R) + 2]} + k_s\frac{[\cosh\sigma - 1]^2}{[\cosh\sigma + 2]} - \frac{W\omega^2}{g} = 0 \quad (13)$$

and since the first and third terms of this equation are real it follows that $\cosh\sigma$ must be real, so that σ may be real or imaginary, but not complex.

Writing

$$2\lambda = \frac{W\omega^2}{gk_s} - \frac{k_r}{k_s}\frac{[\cos(p\pi/R) - 1]^2}{[\cos(p\pi/R) + 2]}$$

where λ is a positive quantity, then equation (13) becomes

$$\cosh^2\sigma - 2(1 + \lambda)\cosh\sigma + (1 - 4\lambda) = 0$$

or

$$\cosh\sigma_{1,2} = (1 + \lambda) \pm (\lambda^2 + 6\lambda)^{1/2} \quad (14)$$

This is the characteristic equation giving a total of four roots, there being a positive and a negative value of σ associated with each $\cosh\sigma$.

Taking the positive sign in equation (14) the corresponding value, $\cosh\sigma_1$, is always greater than unity and so the corresponding roots are real, say $\pm\alpha$. However, on taking the negative sign, difficulties arise and it is necessary to examine the expected range of values of λ.

The minimum value of λ is zero giving the roots $\sigma_2 = 0$. The maximum value of λ occurs when the grillage is vibrating at its highest frequency, in which case each mass will vibrate in antiphase with its neighbors, the frequency reaching a value given by

$$\frac{W}{g}\omega^2 = 48\left(\frac{EI_r}{L_r^3} + \frac{EI_s}{L_s^3}\right)$$

$$= 4(k_r + k_s)$$

At the same time p and R will be commensurate so that

$$2\lambda = 4[(k_r/k_s) + 1] - 4(k_r/k_s)$$

the maximum value of λ thus being 2.

Values of cosh σ_s then lie between $+1$ and -1 and the corresponding roots must be imaginary, say $\pm i\beta$.

Fig. 1 shows the variation of α and β with λ and it can be seen that, over a large range of values, α and β are equal. Thus with values of λ less than 1, as will be the case for grillages in their gravest modes, the frequency equations to be derived can be simplified by taking α and β as equal.

The general solution for the deflection under a load point becomes then,

$$y = \sin(p\pi r/R)(A\cosh\alpha s + B\sinh\alpha s + C\cos\beta s + D\sin\beta s) \quad (15)$$

From equations (4) and (5) the corresponding bending moments are

$$M = \frac{L_r k_r}{2}\frac{[\cos(p\pi/R) - 1]}{[\cos(p\pi/R) + 2]}y \quad (16)$$

and

$$m = (L_s k_s/2)\sin(p\pi r/R)[\mu_1(A\cosh\alpha s + B\sinh\alpha s) + \mu_2(C\cos\beta s + D\sin\beta s)] \quad (17)$$

where

$$\mu_1 = \frac{\cosh\alpha - 1}{\cosh\alpha + 2}, \quad \text{and} \quad \mu_2 = \frac{\cos\beta - 1}{\cos\beta + 2} \quad (18)$$

These expressions for the deflection and bending moments show that the boundary conditions of simple supports are satisfied at $r = 0$ and R and so the constants $A - D$ must be chosen to satisfy the boundary conditions at the end of the s-beams.

All Edges Simply Supported

The simplest example of the use of the foregoing equations is again the application to the grillage with all edges simply supported. The boundary conditions to be satisfied are that the bending moments in the s-beams, and the deflections, are zero at $s = 0$ and S.

From equations (15) and (17) at $s = 0$, $0 = A + C$ and $0 = \mu_1 A + \mu_2 C$ and as $\mu_1 \neq \mu_2$ then $A = C = 0$.

Similarly at $s = S$, $0 = B\sinh\alpha S + D\sin\beta S$, and $0 = \mu_1 B\sinh\alpha S + \mu_2 D\sin\beta S$. These equations are satisfied if $B = 0$ and $\sin\beta S = 0$ or $\beta = q\pi/S$.

The corresponding value of σ is $iq\pi/S$ ($i \equiv \sqrt{-1}$), and from equation (13) the frequencies are given as before, by

$$\frac{W}{g}\omega^2 = k_r\frac{[\cos(p\pi/R) - 1]^2}{[\cos(p\pi/R) + 2]} + k_s\frac{[\cos(q\pi/S) - 1]^2}{[\cos(q\pi/S) + 2]} \quad (19)$$

Symmetric and Asymmetric Modes

When the s-beams are free at the ends, or alternatively clamped, it is convenient to study a grillage with an odd number of s-beams; the origin of s is then taken at the center and symmetric and asymmetric modes may be considered separately.

(a) Symmetric Modes. In a symmetric mode the deflections and bending moments on either side of the origin of s are equal, or

$$y_{r,1} = y_{r,-1} \quad \text{and} \quad m_{r,1} = m_{r,-1}$$

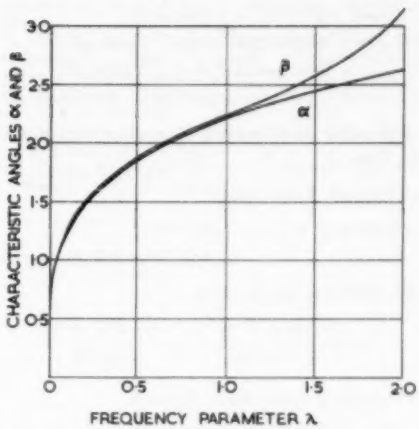

Fig. 1 Variation of characteristic angles α, β from Equation (14)

Therefore $B\sinh\alpha + D\sin\beta = 0$, and $\mu_1 B\sinh\alpha + \mu_2 D\sin\beta = 0$. Then as $\mu_1 \neq \mu_2$

$$B = D = 0 \quad (20)$$

(b) Asymmetric Modes. In an asymmetric mode the center of the grillage is a node and the deflection and bending moment at the origin are zero, and $y_{r,0} = 0$ and $m_{r,0} = 0$, or $A + C = 0$ and $\mu_1 A + \mu_2 C = 0$. Thus,

$$A = C = 0 \quad (21)$$

Two Opposite Edges Free

When two opposite edges of the grillage are free, there being an odd number of s-beams ($2Z + 1$), there is no bending moment at the edges and from equation (17)

$$0 = m_{r,s} = \mu_1(A\cosh\alpha Z + B\sinh\alpha Z) + \mu_2(C\cos\beta Z + D\sin\beta Z) \quad (22)$$

Also, for equilibrium of the shear forces and inertia force at the end of a beam

$$\frac{(M_{r+1,s} - 2M_{r,s} + M_{r-1,s})}{L_r} + \frac{m_{r,s-1}}{L_s} = \frac{W}{g}\omega^2 y_{r,s}$$

or

$$0 = \frac{1}{L_r}\frac{(\mathsf{E}_r - 1)^2}{\mathsf{E}_r}M_{r,s} + \frac{m_{r,s-1}}{L_s} - \frac{W}{g}\omega^2 y_{r,s}$$

On using equation (16) this becomes

$$0 = \left\{k_r\frac{[\cos(p\pi/R) - 1]^2}{[\cos(p\pi/R) + 2]} - \frac{W}{g}\omega^2\right\}y_{r,s} + \frac{m_{r,s-1}}{L_s} \quad (23)$$

Now from equation (13),

$$\left\{k_r\frac{[\cos(p\pi/R) - 1]^2}{[\cos(p\pi/R) + 2]} - \frac{W}{g}\omega^2\right\} = -k_s\frac{(\cosh\alpha - 1)^2}{(\cosh\alpha + 2)} = -k_s\frac{(\cos\beta - 1)^2}{(\cos\beta + 2)}$$

Thus noting $\mu_1 = (\cosh\alpha - 1)/(\cosh\alpha + 2)$, and so on, and using equations (15) and (17) for the deflection and bending moment, the equilibrium equation (23) becomes after reduction

$$0 = \mu_1[A[\cosh \alpha(Z+1) - 2\cosh \alpha Z] + B[\sinh \alpha(Z+1) - 2\sinh \alpha Z]] + \mu_2[C[\cos \beta(Z+1) - 2\cos \beta Z] + D[\sin \beta(Z+1) - 2\sin \beta Z]] \quad (24)$$

In a symmetric mode putting $B = D = 0$ in equations (22) and (24), then,

$$0 = \mu_1 A \cosh \alpha Z + \mu_2 C \cos \beta Z$$

$$0 = \mu_1 A[\cosh \alpha(Z+1) - 2\cosh \alpha Z] + \mu_2 C[\cos \beta(Z+1) - 2\cos \beta Z]$$

giving the characteristic equation

$$0 = \frac{\cosh \alpha(Z+1)}{\cosh \alpha Z} - \frac{\cos \beta(Z+1)}{\cos \beta Z} \quad (25)$$

The corresponding modal shape becomes

$$y = A \sin (p\pi r/R) \left\{ \frac{(\cosh \alpha + 2)}{(\cosh \alpha - 1)} \frac{\cosh \alpha s}{\cosh \alpha Z} - \frac{(\cos \beta + 2)}{(\cos \beta - 1)} \frac{\cos \beta s}{\cos \beta Z} \right\} \quad (26)$$

In a similar manner, for the asymmetric modes, $A = C = 0$, the characteristic equation is

$$0 = \frac{\sinh \alpha(Z+1)}{\sinh \alpha Z} - \frac{\sin \beta(Z+1)}{\sin \beta Z} \quad (27)$$

the deflected shape being

$$y = B \sin (p\pi r/R) \left\{ \frac{(\cosh \alpha + 2)}{(\cosh \alpha - 1)} \frac{\sinh \alpha s}{\sinh \alpha Z} - \frac{(\cos \beta + 2)}{(\cos \beta - 1)} \frac{\sin \beta s}{\sin \beta Z} \right\} \quad (28)$$

For a grillage with Z greater than 10 say, then in the lower modes the values of α and β will be approximately equal and also sufficiently small to put $\sinh \alpha \simeq \sin \beta$. The characteristic equation (25) then reduces to

$$\tanh \alpha Z + \tan \alpha Z = 0$$

This will be recognized as being similar to the equation governing the vibrations of a uniform continuous beam free at one end and sliding at the other end, the roots of the equation being $\alpha Z = 2.365, 5.498$, and so on.

The asymptotic form of the characteristic equation for the asymmetric modes is

$$\tanh \alpha Z - \tan \alpha Z = 0$$

and has roots $\alpha Z = 3.927, 7.069$, and so on.

Two Opposite Edges Clamped

Again taking a grillage with an odd number of s-beams, clamped at edges $\pm(Z+1)$, then since there is no deflection at the edges,

$$0 = y_{r,s+1} = A \cosh \alpha(Z+1) + B \sinh \alpha(Z+1) + C \cos \beta(Z+1) + D \sin \beta(Z+1) \quad (29)$$

The condition for zero slope at the clamped edges is given by the static equations of bending as,

$$0 = -(y_{r,s}/L_s) + (L_s/6EI_s)(2m_{r,s+1} + m_{r,s})$$

or on substitution from equations (15), (17), and (18),

$$0 = A\{-\cosh \alpha Z + \mu_1[2\cosh \alpha(Z+1) + \cosh \alpha Z]\} + B\{-\sinh \alpha Z + \mu_1[2\sinh \alpha(Z+1) + \sinh \alpha Z]\} + \text{similar terms in } \beta \text{ and } \mu_2$$

$$= [A/(\cosh \alpha + 2)][-3\cosh \alpha Z + 2(\cosh \alpha - 1)\cosh \alpha(Z+1)] + [B/(\cosh \alpha + 2)][-3\sinh \alpha Z + 2(\cosh \alpha - 1)\sinh \alpha(Z+1)] + \text{similar terms in } \beta \text{ and } \mu_2 \quad (30)$$

In a symmetric mode $B = D = 0$ so the elimination of A and C from equations (29) and (30) gives the characteristic equation

$$0 = \frac{\sinh \alpha \tanh \alpha(Z+1)}{(\cosh \alpha + 2)} + \frac{\sin \beta \tan \beta(Z+1)}{(\cos \beta + 2)} \quad (31)$$

From equation (29) the modal shape is

$$y = A \sin (p\pi r/R) \left\{ \frac{\cosh \alpha s}{\cosh \alpha(Z+1)} - \frac{\cos \beta s}{\cos \beta(Z+1)} \right\} \quad (32)$$

For the asymmetric modes, $A = C = 0$, and

$$0 = \frac{\sinh \alpha \coth \alpha(Z+1)}{(\cosh \alpha + 2)} - \frac{\sin \beta \cot \beta(Z+1)}{(\cos \beta + 2)} \quad (33)$$

and

$$y = B \sin (p\pi r/R) \left\{ \frac{\sinh \alpha s}{\sinh \alpha(Z+1)} - \frac{\sin \beta s}{\sin \beta(Z+1)} \right\} \quad (34)$$

The General Case

The solution for the case of a grillage with any specified boundary conditions is readily found from the foregoing results.

Taking a solution of the form,

$$y = A \exp(\rho r) \exp(\sigma s) \quad (35)$$

from equation (6) the frequency equation is

$$k_r \frac{(\cosh \rho - 1)^2}{(\cosh \rho + 2)} + k_s \frac{(\cosh \sigma - 1)^2}{(\cosh \alpha + 2)} - \frac{W\omega^2}{g} = 0$$

This equation is a quadratic in either $\cosh \rho$ or $\cosh \sigma$ and following the discussion of the section, "Grillage with Simple Supports. . .," the values of ρ may be taken as $\pm\phi$ and $\pm i\psi$, the values of σ being $\pm\alpha$ and $\pm i\beta$.

The expression for the deflections of the nodal points then becomes

$$y = (F \cosh \phi r + G \sinh \phi r + H \cos \psi r + J \sin \psi r)(A \cosh \alpha s + B \sinh \alpha s + C \cos \beta s + D \sin \beta s) \quad (36)$$

The corresponding expressions for the bending moments in the r-beams and s-beams are

$$M = (L_r k_r/2)[\nu_1(F \cosh \phi r + G \sinh \phi r) + \nu_2(H \cos \psi r + J \sin \psi r)](A \cosh \alpha s + B \sinh \alpha s + C \cos \beta s + D \sin \beta s) \quad (37)$$

and

$$m = (L_s k_s/2)(F \cosh \phi r + G \sinh \phi r + H \cos \psi r + J \sin \psi r)[\mu_1(A \cosh \alpha s + B \sinh \alpha s) + \mu_2(C \cos \beta s + D \sin \beta s)] \quad (38)$$

where

$$\nu_1 = \frac{\cosh \phi - 1}{\cosh \phi + 2}, \quad \mu_1 = \frac{\cosh \alpha - 1}{\cosh \alpha + 2}, \text{ etc.} \quad (39)$$

These equations thus allow the results previously derived to be

used immediately. For instance, for a grillage with all four edges free, the two characteristic equations for the determination of ϕ, ψ and α, β are as the equations given in the section, "Two Opposite Edges Free," as are also the modal shapes. The expressions for the bending moments are as given in the foregoing.

References

1 J. P. Ellington and H. McCallion, "Moments and Deflections of a Simply-Supported Beam Grillage," *Aeronautical Quarterly*, vol. 8, 1957, p. 360.

2 H. L. Cox and P. H. Denke, "Stress Distribution, Instability and Free Vibrations of Beam Gridworks on Elastic Foundations," *Journal of the Aeronautical Sciences*, vol. 23, 1956, p. 173.

3 R. V. Southwell, "Theory of Elasticity," Oxford University Press, New York, N. Y., 1941.

4 L. M. Milne-Thomson, "The Calculus of Finite Differences," Macmillan, London, England, 1951.

5 Third Baron Rayleigh, "Theory of Sound," The Macmillan Company, New York, N. Y., 1926.

Piping Flexibility Analysis by Stiffness Matrix

L. H. CHEN
Head, Applied Mechanics Section,
Electric Boat Division,
General Dynamics Corporation,
Groton, Conn.
Mem. ASME

A method of analysis is formalized for the solution of thermal-expansion stress problems in piping systems. The method is particularly suited for a complex system involving many anchors, closed loops within loops and/or interconnecting branch lines but without intermediate partial constraints. A summary of formulas and procedures necessary for practical application is included in the Appendix. Emphasis has been placed on the simplicity of the procedures which are well suited for automatic computation in digital computers.

Several analytical methods for calculating thermal-expansion stresses in high-temperature piping have been available in the literature. Although all methods of analysis are essentially based on the same fundamental structure theory, their adaptability and limitations differ considerably in application. One would find a method of analysis adapts particularly well to one type of piping design or configuration but is unsuitable to handle another. This paper attempts to formalize a method of analysis which proves to be distinctly advantageous in the solution of a complex piping system involving many anchors, closed loops within loops, and/or interconnecting branch lines. The analysis makes use of the stiffness matrix which is defined as the inverse of the matrix of influence coefficients. The result of the analysis is particularly well suited for digital-computer application. It should be pointed out, however, that the advantages of the method will be nullified quickly in the case of a piping system involving a great number of partial constraints at intermediate points.

An analytical method in piping flexibility analysis, as distinguished from the graphical, semigraphical, or numerical methods, will lead eventually to the solution of a set of simultaneous algebraic equations. In general, these equations may be written in the following form:

$$[\Delta][F] = [D]$$

in which $[\Delta]$ represents the matrix of influence coefficients[1] or shape coefficients.[2] These coefficients denote deflections and rotations due to unit forces and moments and are functions of the geometrical configuration of the piping system. $[F]$ represents the unknown redundant forces and moments to be solved and $[D]$ is the known displacement from thermal expansion.

The fact that all known methods of piping flexibility analysis are concerned with the solution of the redundant $[F]$ is indeed not surprising since the problem is basically a statically indeterminate structure. From elementary structure theory, the number of equations of elasticity required to specify a statically indeterminate structure corresponds exactly to the degree of redundancy of the system. In practice, however, the number of equations required to solve a particular piping system differs with the various methods of analysis and, essentially, it depends on the manner in which the influence coefficients $[\Delta]$ are obtained and manipulated. For example, the number of equations may be reduced to half by the method of elastic center as exemplified by its application to two-anchor problems,[3] and to three-anchor problems.[4] In this method the influence coefficients and therefore the redundant forces are obtained with reference to the elastic center of the system. This method of approach has its definite merits in "hand" computations of relatively simple piping systems. However, the extra labor required in determining the elastic center for a complex system will not justify its use, particularly in the case of digital computation. It is also possible to "cut" down the size of a complex piping system, by means of a series of matrix-inversion processes, eventually to a two-anchor problem if desired. This approach is essentially mathematical in nature since the number of algebraic equations in the expression $[\Delta][F] = [D]$ and therefore the amount of arithmetic operations involved basically remains unchanged.

For a piping system involving many anchors, interconnecting branches or closed loops within loops, there is not only the problem of the size of the equations, which often imposes a limitation on practical application even in the case of digital computation, but also the problem of how the equations may be set up readily for solution. The present paper formulates a method of analysis by which these difficulties may be overcome. It should be pointed out that the idea of using a stiffness matrix for structural analysis is not new. Notably in recent years, it has been applied to airframe analysis in the aircraft industry. In so far as the author is aware, the present method is based on a different approach. This paper also makes use of Brock's matrices of linear transformation.[1] A tabulation of generalized formulas for the computation of influence coefficients is included in the Appendix. This would be helpful for those who are interested in the practical solution of a problem.

Theory

We introduce the following matrix notations:

$[F] = \{F_x F_y F_z M_x M_y M_z\}$ be a 6×1 column matrix giving the 3 component forces and 3 component moments with reference to a co-ordinate system (xyz). (For brevity, called 6 forces.)

[1] J. E. Brock, "A Matrix Method for Flexibility Analysis of Piping Systems," Journal of Applied Mechanics, vol. 19, Trans. ASME, vol. 74, 1952, pp. 501–516.

[2] "Design of Piping Systems," The M. W. Kellogg Company, New York, N. Y., first edition, 1941; second edition, 1956.

Presented at the Summer Conference of the Applied Mechanics Division, Troy, N. Y., June 18–20, 1959, of The American Society of Mechanical Engineers.

Discussion of this paper should be addressed to the Secretary, ASME, 29 West 39th Street, New York, N. Y., and will be accepted until January 10, 1960, for publication at a later date. Discussion received after the closing date will be returned

Note: Statements and opinions advanced in papers are to be understood as individual expressions of their authors and not those of the Society. Manuscript received by ASME Applied Mechanics Division, August 4, 1958. Paper No. 59—APM-24.

[3] S. W. Spielvogel, "Piping Stress Calculations Simplified," McGraw-Hill Book Company, Inc., New York, N. Y., 1943.

[4] B. Lochak, "Simplified Method of Analysis of Reactions Developed by Expansion in a Three-Anchor Piping System," Trans. ASME, vol. 66, 1944, pp. 311–318.

$[D] = \{\delta_x \delta_y \delta_z \phi_x \phi_y \phi_z\}$ be a 6 × 1 column matrix giving the 3 component deflections and 3 component rotations (called 6 deflections).

$[\Delta] = [C_{ij}]$ be a 6 × 6 matrix of influence coefficients. (For brevity, called flexibility matrix.) For example, the elements in the first row of the matrix ($i = 1, j = 1 \ldots\ldots 6$) denote the 6 deflections due to a unit F_x.

$$[b_{PQ}] = \begin{bmatrix} 0 & (z_p - z_Q) & -(y_p - y_Q) \\ -(z_p - z_Q) & 0 & (x_p - x_Q) \\ (y_p - y_Q) & -(x_p - x_Q) & 0 \end{bmatrix}$$

be a 3 × 3 matrix of co-ordinates of points P-$(x_p y_p z_p)$ and $Q(x_Q y_Q z_Q)$ referring to the same co-ordinate system (xyz).

$$[B_{PQ}] = \begin{bmatrix} I & 0 \\ [b_{PQ}] & I \end{bmatrix}$$ be a 6 × 6 matrix in which I is a unit matrix and 0 is a null matrix, both of order 3.

$[S] = [\Delta]^{-1}$ be the inverse of the flexibility matrix $[\Delta]$. (For brevity, called stiffness matrix.)

$$[N_{PQ}] = H_0(\Delta T) \begin{vmatrix} x_P - x_Q \\ y_P - y_Q \\ z_P - z_Q \\ 0 \\ 0 \\ 0 \end{vmatrix}$$

be a 6 × 1 column matrix of thermal expansion between points P and Q. H_0 is the mean coefficient of thermal expansion in. per in. deg F. ΔT is the difference of maximum and minimum operating temperatures (deg F).

We denote the operation of transposition by a tilde (~) over the matrix; e.g., $[\tilde{B}_{PQ}]$ is a transposed matrix of $[B_{PQ}]$.

Consider the free-body diagram of a flexible element in space, Fig. 1. This element represents a pipeline between two branch points and consists of a number of pipe pieces (straight lengths and bends). $[\Delta_j]$ is the flexibility matrix of the element referred to point O, the origin of a chosen co-ordinate system (xyz). The pipe pieces may be arbitrarily oriented (skew) with respect to the co-ordinate axes. Formulas and procedures for obtaining $[\Delta_j]$ are given in the Appendix. It may be noted that the determination of $[\Delta_j]$ is an entirely separate and independent problem. It may be determined by experiment, if desired. The main text of this paper is concerned with the method of analysis or, more specifically, how the necessary equations may be set up readily for solution.

The forces and deflections at the two ends of the element may be transferred to a common point by the following equations:

$$\left.\begin{aligned} [F_i^0] &= [B_{0i}][F_i] \\ [F_j^0] &= [B_{0j}][F_j] \\ [D_i^0] &= [\tilde{B}_{i0}][D_i] \\ [D_j^0] &= [\tilde{B}_{j0}][D_j] \end{aligned}\right\} \quad (1)$$

in which the superscript denotes the origin of the co-ordinate system as the common point selected. This method of linear transformation in matrix notation as applied to elastic structures has been treated most rigorously and elegantly by Brock.[1]

The equation of elasticity describing the flexible element, Fig. 1, may be written in two alternative forms:

$$[\Delta_j][F_i^0] = [D_i^0] - [D_j^0] - [N_{ij}] \quad (2)$$

or

$$[\Delta_j][F_j^0] = [D_j^0] - [D_i^0] - [N_{ji}] \quad (3)$$

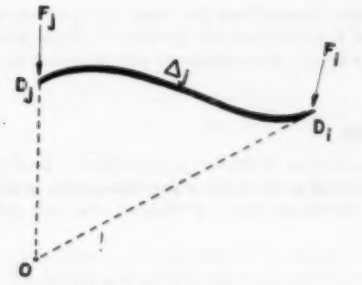

Fig. 1 A flexible element in space

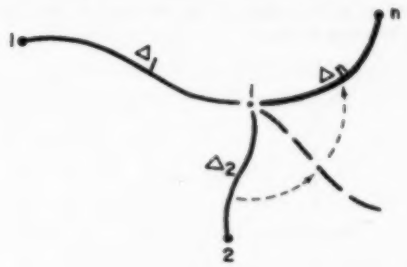

j = 1 ----- n

Fig. 2 n-pipe branches joining to a common branch point

Note that the premultiplication of the thermal expansion matrix $[N]$ by the transformation matrix $[\tilde{B}]$ leaves $[N]$ unaltered as is readily verified. From equations (2) and (3), it follows

$$[F_i^0] = -[F_j^0] \quad (4)$$

Equation (4) is essentially a statement of the condition of static equilibrium. However, it formalizes a procedure in which only one force matrix when transferred to a common point may be used to represent the forces at the two ends (or any internal points) of the elastic element. The difference in signs depends on the interpretation of the nature of the forces; i.e., internal or external. It can be taken care of easily as we shall see later.

Now consider n elastic elements (pipe branches) joining to a common branch point i, Fig. 2. From equations (2) and (4), we may write

$$[F_i^0] = -[F_j^0] = [S_j]([D_i^0] - [D_j^0] - [N_{ij}]) \quad (5)$$

in which $[S_j]$ is the stiffness matrix. Since the flexibility matrix of a piping element can be obtained easily by analytical means, it is most convenient to determine the stiffness matrix from the flexibility matrix by the process of matrix inversion.

The condition of static equilibrium at branch point i gives

$$\sum_{j=1}^{n} [F_j^0] = 0 \quad (6)$$

or, from equation (5),

$$\sum_{j=1}^{n} [S_j]([D_i^0] - [D_j^0] - [N_{ij}]) = 0 \quad (7)$$

Equation (7) serves as a basic equation from which equations necessary for the solution of a complete piping system may be set up conveniently. It is seen that, for a complex piping system in-

volving many branch lines but relatively few branch points, the solution of the deflections at the branch points provides a most convenient approach as compared with the solution of redundant forces.

Application

The application of the foregoing theory is best illustrated by an example. Fig. 3 shows a complex piping system having 5 anchors, 13 branch lines, 4 closed loops, and only 5 branch points.

Let $[M_j]$ be a 6×1 column matrix, the elements of which are known components of anchor extraneous movement at anchor A_j. We transfer $[M_j]$ to the origin of the co-ordinate system; i.e., $[M_j{}^0] = [B_{j0}][M_j]$. A total of thirteen matrix equations of elasticity similar to equations (2) or (3) may be written for the thirteen branches in Fig. 3

$$\left.\begin{aligned} [\Delta_1][F_1{}^0] &= [D_a{}^0] - [M_0] - [N_{aA0}] \\ [\Delta_2][F_2{}^0] &= [D_a{}^0] - [D_b{}^0] - [N_{ab}] \\ &\vdots \\ [\Delta_{13}][F_{13}{}^0] &= [D_d{}^0] - [M_4{}^0] - [N_{dA4}] \end{aligned}\right\} \quad (8)$$

The equation of static equilibrium at branch point a, for example, is

$$[F_1{}^0] + [F_2{}^0] + [F_3{}^0] + [F_4{}^0] = 0 \quad (9)$$

Substitution of equation (8) in equation (9) gives

$$\begin{aligned} [S_1]\{[D_a{}^0] - [M_0] - [N_{aA0}]\} + [S_2]\{[D_a{}^0] - [D_b{}^0] - [N_{ab}]\} \\ + [S_3]\{[D_a{}^0] - [D_c{}^0] - [N_{ac}]\} \\ + [S_4]\{[D_a{}^0] - [D_d{}^0] - [N_{ad}]\} = 0 \end{aligned} \quad (10)$$

Similar equations may be written for other branch points. The complete system of equations for the solution of the unknowns $[D_a{}^0] \ldots . [D_e{}^0]$ is given in Table 1. It may be noted that the signs of the forces in equations of equilibrium should be taken into account. For example, when $[F_2{}^0]$ is used in the equation of equilibrium for branch point a, a negative $[F_2{}^0]$ should be used in the equation of equilibrium for branch point b, equation (4).

An examination of the system of equations in Table 1 indicates two formal simplicities:

1 The matrix of coefficients is a symmetrical matrix. As in the case of other known methods of piping flexibility analysis in which the redundant forces are to be solved, the mathematical advantage of symmetry is retained.

2 The coefficients and the constant terms follow a simple and definite pattern such that a formal procedure can be established to set up the equations (Table 1) directly from the sketch of piping configuration, Fig. 3. For any given problem, the process

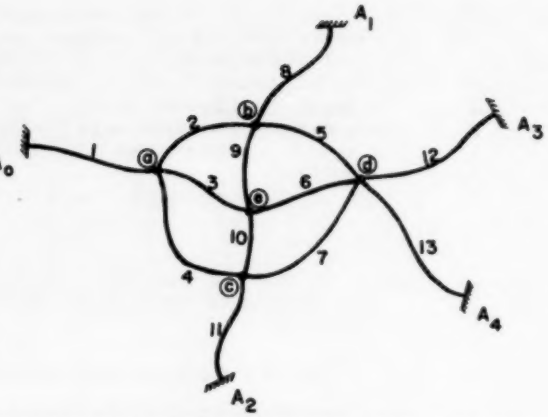

Fig. 3 Example of a complex 5-anchor problem. Anchor A_0 is selected as the origin of the co-ordinate system

of writing down the equations of elasticity and equilibrium such as involved in equations (8), (9), and (10) is not necessary. The practical value of this simplicity is obvious. It not only represents a saving in time of analysis but also provides a simple and straightforward procedure well suited for digital computation. Take, for example, the first matrix equation in Table 1. This equation actually describes the condition of static equilibrium at branch point a, Fig. 3. The coefficient associated with $[D_a{}^0]$ in this equation is the sum of the stiffness matrices of branches 1, 2, 3, and 4 which are all the branches joining to point a. The coefficient associated with $[D_b{}^0]$ is a negative stiffness matrix of branch 2 which connects points b and a. This formal pattern prevails throughout the entire system of equations and permits automatic computation in digital computers by means of a simple coding scheme.

The system of equations may be solved by any standard method. In fact, it may be reduced eventually to six linear algebraic equations by partitioning the matrices and by a series of matrix-inversion processes. This is, of course, a pure mathematical procedure and is not concerned with the method of analysis. Once the unknown deflections at the branch points are solved, the "branch" forces $[F_i{}^0]$ are readily obtained in accordance with equation (5). The actual forces (and therefore stresses) at any point k in the branch i may be obtained by the formula of linear transformations,

$$[F_k] = [B_{k0}][F_i{}^0]$$

For the case of a piping system involving partial constraints (spring or rigid hangers, and so on), the application of the present method is complicated by the introduction of redundant constraint forces. Two possible approaches may be considered: (*a*) The point of constraint attachment to the piping may be con-

Table 1 System of equations for solution of problem in Fig. 3. All symbols *D*, *S*, *M*, and *N* are matrix quantities as defined in text

$D_a{}^0$	$D_b{}^0$	$D_c{}^0$	$D_d{}^0$	$D_e{}^0$	Constants
$S_1 + S_2 + S_3 + S_4$	$-S_2$	$-S_4$		$-S_3$	$S_1(M_0 + N_{aA_0}) + S_2N_{ab} + S_3N_{ac} + S_4N_{ad}$
$-S_2$	$S_2 + S_5 + S_8 + S_9$		$-S_5$	$-S_9$	$S_2N_{ba} + S_5N_{bd} + S_8(M_1{}^0 + N_{bA_1}) + S_9N_{be}$
$-S_4$		$S_4 + S_7 + S_{10} + S_{11}$	$-S_7$	$-S_{10}$	$S_4N_{ca} + S_7N_{cd} + S_{10}N_{ce} + S_{11}(M_2{}^0 + N_{cA_2})$
	$-S_5$	$-S_7$	$S_5 + S_6 + S_7 + S_{12} + S_{13}$	$-S_6$	$S_5N_{db} + S_6N_{dc} + S_7N_{dc} + S_{12}(M_3{}^0 + N_{dA_3}) + S_{13}(M_4{}^0 + N_{dA_4})$
$-S_3$	$-S_9$	$-S_{10}$	$-S_6$	$S_3 + S_6 + S_9 + S_{10}$	$S_3N_{ea} + S_6N_{ed} + S_9N_{eb} + S_{10}N_{ec}$

sidered as a branch point with six-component unknown deflections. One additional equation is required to specify the known displacement in the direction of the constraint. In this approach, a total of seven algebraic equations is required for one constraint at a point. The formal simplicity of the entire system of equations is retained which permits a simple coding scheme for automatic digital computation. However, the size of the equations will be increased quickly for a piping system involving a great number of partial constraints at intermediate points. (*b*) It is possible to eliminate the six-component unknown deflections at the constraint point in terms of the redundant constraint force by matrix manipulation. The resulting system of equations, involving the solution of deflections in the "regular" branch points and the redundant constraint forces, would require a rather complex coding scheme for a generalized computer program.

An advanced pipe-stress program which was developed by the author's company has been in operation in an IBM 704 digital computer for over a year. The program was based on the method of Brock[1] with essential modifications. Brock's approach of solving all the redundant forces both at anchors and at constraints is particularly well suited for problems involving a great number of partial constraints. A fruitful extension of the present method to this type of problems will depend on the success of the second approach as mentioned in the preceding paragraph. It is hoped that a simplified logical scheme may be developed in the near future. In this event, the special situation of a piping system involving many loops and many partial constraints may be handled in a routine and generalized manner.

APPENDIX

As mentioned in the text of the paper, the determination of influence coefficients is an entirely independent and separate problem. They may be obtained by experiment or by analytical means. For a practical piping system consisting of straight lengths (tangents) and circular bends, the influence coefficients are obtained readily by the application of Castigliano's theorem. The flexibility matrix $[\Delta_i]$ of a branch i is the sum of the flexibility matrices of each individual pipe piece (tangents or bends) in the branch. Let us denote the latter by $[\Delta_p]$. It may be noted that one of the factors which contribute to the formal simplicity achieved in the setup of the equations is the fact that $[\Delta_i]$ of all the branches were defined as the flexibility matrices referred to an arbitrarily chosen common co-ordinate system[5] and transferred to the origin of that system. Therefore $[\Delta_p]$ should follow the same definition. A summary of formulas and procedure for the computation of $[\Delta_p]$ is given in the following.

(I) Flexibility Matrix for Skew Tangents. (*a*) For a tangent oriented arbitrarily in space, the nonvanishing elements of the 6×6 flexibility matrix $[C_{ij}]$ with reference to the mid-point of the tangent, are:

$$
\left.
\begin{aligned}
C_{11} &= (1 - a_1^2)f_1 + (2.6 - 2.1a_1^2)f_2 \\
C_{12} &= C_{21} = -a_1a_2f_1 - 2.1a_1a_2f_2 \\
C_{13} &= C_{31} = -a_1a_3f_1 - 2.1a_1a_3f_2 \\
C_{22} &= (1 - a_2^2)f_1 + (2.6 - 2.1a_2^2)f_2 \\
C_{23} &= C_{32} = -a_2a_3f_1 - 2.1a_2a_3f_2 \\
C_{33} &= (1 - a_3^2)f_1 + (2.6 - 2.1a_3^2)f_2 \\
C_{44} &= (1 + \mu a_1^2)f_2 \\
C_{45} &= C_{54} = a_1a_2\mu f_2 \\
C_{46} &= C_{64} = a_1a_3\mu f_2 \\
C_{55} &= (1 + \mu a_2^2)f_2 \\
C_{56} &= C_{65} = a_2a_3\mu f_2 \\
C_{66} &= (1 + \mu a_3^2)f_2
\end{aligned}
\right\} \qquad (11)
$$

where

$f_1 = L^3/12EI$
$f_2 = L/EI$
$f_3 = r^2L/EI$
E = modulus of elasticity
I = flexural moment of inertia
μ = Poisson's ratio
L = length of tangent
r = mean radius of (nominal) pipe cross section
(a_1, a_2, a_3) = direction cosines of tangent with reference to common co-ordinate system (xyz)

Those terms in equation (11) involving f_3 represent the effect of normal force and shears. Since this is a minor effect in most piping systems consisting of long and slender elements, the Poisson ratio of 0.3 and a shear-distribution factor of 2 were assumed. Note that the latter depends on the shape of the cross section and equals 2 for thin-walled cylinders. For solid cylinder, its value is unity.

(*b*) The desired flexibility matrix $[\Delta_p]$, which is referred to the origin O, may be obtained by the following formula of linear transformation:

$$[\Delta_p] = [\tilde{B}_{pi}][C_{ij}][B_{pi}] \qquad (12)$$

in which the B-matrix is a function of the co-ordinates of the mid-point of the tangent (see the definition of the B-matrix in the text).

(II) Flexibility Matrix for Elementary Case of a Bend. The most elementary case of a bend is the one which lies in the co-ordinate plane $(x - y)$ as shown in Fig. 4. The nonvanishing elements of the 6×6 flexibility matrix $[C_{ij}]$, with reference to the center of the circle described by the pipe center line, are:

$$
\left.
\begin{aligned}
C_{11} &= k(2\psi - \sin 2\psi)f_6 + (1.55\psi + 0.525 \sin 2\psi)f_7 \\
C_{12} &= C_{21} = -k(1 - \cos 2\psi)f_6 + 0.525(1 - \cos 2\psi)f_7 \\
C_{16} &= C_{61} = k(1 - \cos \psi)f_5 \\
C_{22} &= k(2\psi + \sin 2\psi)f_6 + (1.55\psi - 0.525 \sin 2\psi)f_7 \\
C_{26} &= C_{62} = -k(\sin \psi)f_5 \\
C_{33} &= 4(1 + \mu)\psi f_6 + 2.6\psi f_7 \\
C_{34} &= C_{43} = -(1 + \mu)(1 - \cos \psi)f_5 \\
C_{35} &= C_{53} = (1 + \mu)(\sin \psi)f_5 \\
C_{44} &= [2(1 + \mu + k)\psi - (1 + \mu - k) \sin 2\psi]f_4 \\
C_{45} &= C_{54} = -(1 + \mu - k)(1 - \cos 2\psi)f_4 \\
C_{55} &= [2(1 + \mu + k)\psi + (1 + \mu - k) \sin 2\psi]f_4 \\
C_{66} &= 4k\psi f_4
\end{aligned}
\right\} \qquad (13)
$$

[5] Hereafter called "common" co-ordinate system.

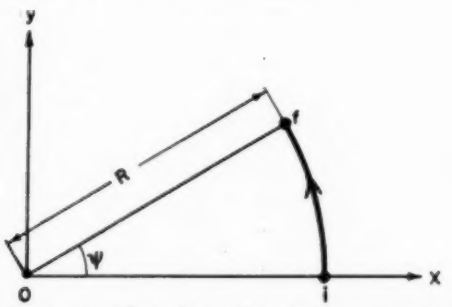

Fig. 4 The elementary case of a bend lying in the x-y co-ordinate plane

where

$f_4 = R/4EI$
$f_5 = R^2/EI$
$f_6 = R^3/4EI$
$f_7 = r^2R/EI$
R = radius of bend
ψ = bend subtended angle
k = flexibility factor for in-plane and out-of-plane bending (see ASA B31.1 Code for Pressure Piping, 1955)

Other symbols remain the same as those used in equation (11).

The terms involving f_7 represent the effect of normal force and shears. The same assumptions concerning the Poisson ratio and the shear-distribution factor were used as in the case of skew tangents. The formulas in equation (13) are applicable only to bends as specified in Fig. 4. However, for bends (say, lying in the $y - z$ plane) corresponding formulas are readily obtainable by the rule of cyclic permutation in (xyz) co-ordinates. Also, if neither of the two end points of the bend lies in the co-ordinate axes, equation (13) can be modified easily to take care of this situation. These would appear to be most expedient in the case of hand computation. However, in the case of automatic computation in digital computers, this type of approach is no longer necessary. A generalized scheme is possible to compute, directly from the formulas in equation (13), the influence coefficients of a bend oriented arbitrarily in space. A bend lying in plane parallel to any one of the co-ordinate planes is now nothing but a special case of a skew bend.

(III) Determination of Flexibility Matrix of a Skew Bend. The influence coefficients at the bend center point of a skew bend may be obtained by the following scheme:

1 Select a co-ordinate system, say $(x_2y_2z_2)$, such that both x_2 and y_2-axes lie in the plane of the bend with the x_2-axis passing through the "initial" point i[6] in exactly the same manner as shown in Fig. 4. The z_2-axis will be perpendicular to the plane of the bend and is so chosen that $(x_2y_2z_2)$ forms a right-handed co-ordinate system. (The original common co-ordinate system is also assumed as a right-handed one.) The influence coefficients of the skew bend referring to system $(x_2y_2z_2)$ may now be obtained from the formulas in equation (13).

2 Apply the process of linear transformation to transform these influence coefficients from the $(x_2y_2z_2)$ system to the original (xyz) system.

By means of vector analysis, equations suitable for routine computation may be set up to represent the necessary procedures involved in the foregoing scheme. For notation purpose, we denote the original (xyz) system as the 1-system $(x_1y_1z_1)$. We further introduce the following notations:

Let $(a_1a_2a_3)$ and $(b_1b_2b_3)$ be the direction cosines, with reference to system $(x_1y_1z_1)$, of the bend radii at the initial and the final points, respectively.

$[K_{21}]$ be a 3×3 matrix relating the two co-ordinate systems $(x_1y_1z_1)$ and $(x_2y_2z_2)$. Its elements are the direction cosines of $(x_2y_2z_2)$-axes with respect to the $(x_1y_1z_1)$-axes. By simple analyses, $[K_{21}]$ can be expressed in terms of $(a_1a_2a_3)$, $(b_1b_2b_3)$, and the bend subtended angle ψ

$$[K_{21}] = \frac{1}{\sin \psi} \begin{bmatrix} a_1 \sin \psi & a_2 \sin \psi & a_3 \sin \psi \\ (b_1 - a_1 \cos \psi) & (b_2 - a_2 \cos \psi) & (b_3 - a_3 \cos \psi) \\ (a_2b_3 - a_3b_2) & (a_3b_1 - a_1b_3) & (a_1b_2 - a_2b_1) \end{bmatrix}$$

$[L_{21}] = \begin{bmatrix} K_{21} & 0 \\ 0 & K_{21} \end{bmatrix}$ be a 6×6 matrix in which 0 is 3×3 null matrix.

By process of linear transformation,[1] we have

$$[C_1] = [\tilde{L}_{21}][C_2][L_{21}] \tag{14}$$

in which

$[C_1]$ = flexibility matrix for the skew bend at bend center point referring to system $(x_1y_1z_1)$
$[C_2]$ = flexibility matrix referring to system $(x_2y_2z_2)$ as computed by the formulas given in equation (13)

Note that the only required data to obtain the matrices $[L_{21}]$ and $[\tilde{L}_{21}]$ are: The co-ordinates of the bend center, the initial and the final points with respect to the originally chosen co-ordinate system (xyz) and the bend subtended angle ψ. For reason of proper orientation, the angle ψ should be less than 180 deg. In practice, bends of angle greater than 180 deg may be treated as two or more bends.

Finally, the desired $[\Delta_p]$ matrix of a skew bend is obtained by the same type of transformation as in equation (12)

$$[\Delta_p] = [\tilde{B}_{p0}][C_1][B_{p0}]$$

where the B-matrix is a function of the co-ordinates of the bend center point.

[6] To account correctly for the orientation of the system, the end of a bend first encountered in tracing through the pipe system in the direction away from the origin of the common co-ordinate system (such as anchor A_0 in Fig. 3) is called the initial point. The other end is the "final" point.

A Photoelastic Approach to Transient Stress Problems Employing Low-Modulus Materials[1]

J. W. DALLY[2]
Senior Research Engineer,
Stress Analysis Section,
Mechanical Engineering Research Department,
Armour Research Foundation,
Chicago, Ill.
Assoc. Mem. ASME

W. F. RILEY
Research Engineer,
Stress Analysis Section,
Mechanical Engineering Research Department,
Armour Research Foundation

A. J. DURELLI[3]
Supervisor, Stress Analysis Section,
Mechanical Engineering Research Department,
Armour Research Foundation
Assoc. Mem. ASME

The objective of the program discussed in this paper was to develop a method, using photoelasticity and low-modulus materials, for studying dynamic stress distributions. Early in the program a number of low-modulus materials were studied and Hysol 8705 (a urethane-rubber compound) was selected as the most promising. A complete study of its mechanical and optical properties was made under static and dynamic loadings. It was established that Poisson's ratio ν is independent of rate of loading, the stress fringe value f_σ is independent of rate of loading for strain rates greater than 8 in/in/sec, and both the modulus of elasticity E and the strain fringe value f_ϵ were dependent on the rate of loading. The specific energy loss for the material was about 10 per cent for the stress ranges associated with photoelastic determinations. Experimental observations of photoelastic fringe patterns in a rectangular strut subjected to axial impact were made to illustrate the potential of the method. Three different end conditions were imposed on the unloaded end of the strut: (a) A free end normal to the axis; (b) a fixed end normal to the axis; and (c) a free end inclined 45 deg to the axis. For the cases where the ends were normal to the axis it was found that the fringes followed the same law of reflection as the law for stresses given by elementary wave theory.

In recent years a large number of investigators have applied photoelastic methods to the transient-stress problem. As a consequence, many different experimental approaches have been developed. Most of the investigators have employed conventional two-dimensional photoelastic materials such as Columbia Resin CR-39 or Castolite; however, the means of recording the fringe patterns have varied appreciably, at least four different recording systems having been used.

Christie [1],[4] Sutton [2], and Feder and others [3] have employed very high-speed full-field cameras operating at more than 200,000 frames per sec. Streak cameras which provide a continuous record of the fringe pattern along a line on the model have been employed by Tuzi and Nisida [4], Frocht and Flynn [5], and Betser and Frocht [6]. Single photographs of the fringe patterns recorded with ordinary cameras and a flash-type light source (about 2 microsec duration) have been obtained by Senior and Wells [7], and more recently by Goldsmith and Norris [8]. Clark [9] and Marshall [10] have used a photomultiplier in conjunction with a dynamic polariscope to record fringe-order changes electronically.

A second approach to the problem is to use low-modulus photoelastic materials ($E < 800$ psi) in place of the more rigid materials. This method has been investigated by Perkins [11] and Durelli and Riley [12]. In low-modulus materials the velocity of propagation of the stress wave is decreased (by an order of magnitude) over the velocity of propagation in conventional photoelastic materials, and it is possible to record clearly the dynamic fringe patterns using a Fastax camera operating at about 13,000 frames per sec.

This paper describes a further investigation of this low-modulus-material approach. A simple dynamic polariscope is described. A comprehensive study of the behavior of certain photoelastic materials under varying rates of loading is presented, and some results from experiments on struts subjected to axial impact are shown.

Throughout the investigation, the photoelastic method is employed in such a way as to provide a whole field representation of the stresses, since it is believed that the primary advantage of photoelasticity over strain gages is the whole field potentialities of the former. Also, emphasis has been placed primarily on the development of the experimental methods, and the applications to specific problems are presented primarily as illustrations of these methods.

Photoelastic Equipment

A diffused-light polariscope was used throughout the investigation. Groups of flash bulbs (Sylvania Type 2A or GE Type 31) were used as the light source and provided light of sufficient intensity and duration to record the fringe patterns on Tri-X film in an 8-mm Fastax camera operating at 14,000 frames per sec. Wratten 77A and Corning 4303 filters were used with the Tri-X film which was developed in DK-50 developer.

Low-Modulus Model Materials

Preliminary studies with Keystone gelatine, Interchemical

[1] Sponsored by the Mechanics Division, Air Force Office of Scientific Research ARDC, Washington, D. C., under Contract No. AF18-(603)-144, File No. 17500-721.

[2] Presently, Assistant Professor, Department of Mechanics and Materials, Cornell University, Ithaca, N. Y.

[3] Also, Professor at Illinois Institute of Technology, Chicago, Ill.

[4] Numbers in brackets designate References at end of paper.

Contributed by the Applied Mechanics Division and presented at the Annual Meeting, Atlantic City, N. J., November 29–December 4, 1959, of The American Society of Mechanical Engineers.

Discussion of this paper should be addressed to the Secretary, ASME, 29 West 39th Street, New York, N. Y., and will be accepted until January 10, 1960, for publication at a later date. Discussion received after the closing date will be returned.

Note: Statements and opinions advanced in papers are to be understood as individual expressions of their authors and not those of the Society. Manuscript received by ASME Applied Mechanics Division, July 28, 1958. Paper No. 59—A-10.

Company's flexible Polyester 401, a modified epoxy resin, Mobay Chemical Company's Vulkollan, and Houghton Laboratories urethane-rubber compounds indicated that the urethane-rubber compounds were the most satisfactory of all of these low-modulus materials. A compound known commercially as Hysol 8705 was selected for a more comprehensive study. Before interpreting the dynamic photoelastic fringe patterns, information regarding the dynamic stress-strain curves, modulus of elasticity E, Poisson's ratio ν, and the material fringe value in terms of stress and strain f_σ and f_ϵ, respectively, had to be established.

In order to determine the stress-strain curves of the low-modulus materials under different rates of loading, an adaptation of the method employed by Volterra and Barton [13] was used. This method consists of loading a small specimen in dynamic compression between two pendulums and measuring the acceleration of one of the pendulums during impact. If the specimen can be considered to be loaded in uniaxial compression, the acceleration record provides sufficient information to give both the stress and the strain in the specimen as a function of time. The method used in this investigation differed from the original method in only a few respects. Specimen contractions as a function of time were recorded in three different ways; namely, (*a*) by means of a linear differential transformer mounted between the pendulums, (*b*) by a double integration of the accelerometer data, and (*c*) by measurements from the Fastax motion pictures of the impacted specimen. In addition, photoelastic fringe patterns produced in the specimen during impact were recorded by a Fastax camera operating at about 13,000 frames per sec. The mechanical loading system, electronic equipment, polariscope, Fastax camera, and camera control unit are shown schematically in Fig. 1. Although some difficulty was encountered in establishing the exact time of impact on the linear differential transformer record, the three determinations of specimen contraction (double integration of the acceleration, linear differential transformer, and film measurements) were in good agreement.

The stress and strain in the specimen at any time were determined from the following relationships:

$$\sigma(t) = \frac{Ma[L_0 - \delta(t)]}{V_0} \tag{1}$$

$$\epsilon(t) = \log_e \frac{L_0}{L_0 - \delta(t)} \tag{2}$$

where $\sigma(t)$, $\epsilon(t)$, and $\delta(t)$ are the axial stress, axial strain, and contraction, respectively, at any time t; M and a are the mass and acceleration of the impacted pendulum; and L_0 and V_0 are the initial length and volume of the specimen.

The stress-strain curves for Hysol 8705 at a number of different strain rates are shown in Fig. 2. Examination shows that the curves are essentially linear over their initial portions. Since the

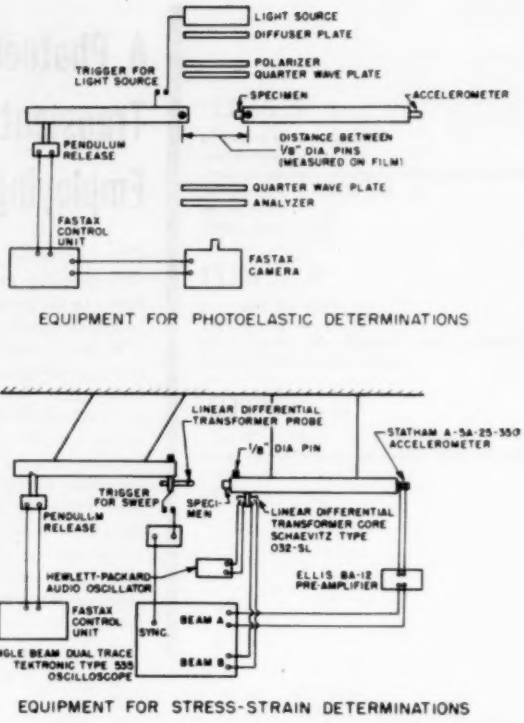

Fig. 1 Schematic diagrams showing equipment employed in determining dynamic properties of low-modulus photoelastic materials

photoelastic determinations are made at a relatively low stress level, these results indicate that the modulus of elasticity can be considered constant over the stress range encountered in the photoelastic tests. A plot of the initial modulus of elasticity as a function of strain rate is shown in Fig. 3.

Although not shown in Fig. 2, the determination of the stress-strain curve was continued to zero load and the entire hysteresis loop was established at each of the loading rates. The area enclosed in this loop is proportional to the energy loss in the specimen due to internal friction and gives a measure of the viscoelastic character of the material. The energy loss per unit volume ΔW at each strain rate is given in Table 1. It is evident that ΔW increased as the loading rate increased; however, with the double-pendulum loading system the maximum stress applied to the specimen also increases with the loading rate. Since one of the most

Table 1 Properties of Hysol 8705 as a function of strain rate

Strain rate, in/in/sec	Stress amplitude, psi	ΔW in-lb/in.[a]	$\frac{\Delta W}{\sigma^3} \times 10^{-6}$	$\frac{\Delta W}{\sigma^{3.5}} \times 10^{-4}$	$\frac{\Delta W}{\sigma^4} \times 10^{-4}$	E, psi	$f_\epsilon \times 10^{-3}$, in/in-in. fringe	f_σ, psi-in. fringe	ΔW^a, in-lb per cu in.	W^a, in-lb per cu in.	$\frac{\Delta W^a}{W}$
0	...	...	...	...	...	444	1.50	0.455	...	...	...
4.4	14.9	0.02	5.86	0.236	0.83	550	1.28	0.50	0.03	0.36	0.08
8.5	28.7	0.08	3.27	0.182	0.97	595	1.24	0.52	0.03	0.34	0.09
16.8	56.1	0.57	1.07	0.242	1.81	660	1.18	0.52	0.03	0.30	0.10
25.5	85.9	0.96	1.51	0.142	1.31	700	1.12	0.52	0.03	0.29	0.10
34.1	116.9	1.40	0.87	0.095	1.03	730	1.07	0.52	0.03	0.27	0.11
42.6	143.4	2.32	0.79	0.095	1.13	750	1.01	0.52	0.03	0.27	0.11
51.2	171.3	7.18	1.43	0.187	2.44	770	0.95	0.52	0.03	0.26	0.12
63.6	214.0	10.50	1.07	0.157	2.30	805	0.88	0.52	0.03	0.25	0.12

Average value $= \frac{\Delta W}{\sigma^{3.5}} = 0.167$

[a] Based on a stress amplitude of 20 psi. For curves of E versus strain rate see Fig. 3. For curves of f_σ and f_ϵ versus strain rate see Fig. 5. For dynamic stress-strain curves see Figs. 2(*a*) and (*b*).

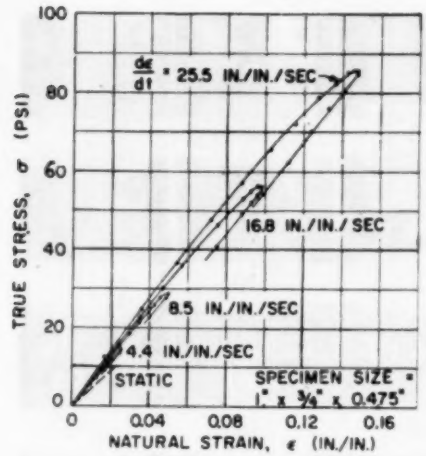

(a)

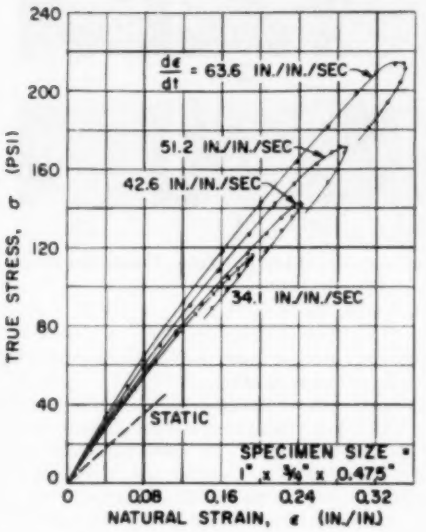

(b)

Fig. 2 Dynamic stress-strain curves for Hysol 8705

important variables affecting internal friction in solids is the stress amplitude, this factor must be taken into consideration before drawing any conclusions regarding ΔW. Some disagreement exists between investigators regarding the power law governing this stress dependency. Robertson and Yorgiadis [14] found that ΔW is nearly independent of the frequency and is proportional to a power of the stress amplitude which they estimated to be the third power. Kimball and Lovell [15] found that ΔW varied as the second power of the stress amplitude.

In Table 1, ratios $(\Delta W)/\sigma^n$, where σ is the stress amplitude, have been computed for $n = 2$, 2.5, and 3. Although some scatter in the data exists, it is apparent that the value of $n = 2.5$ fits the Robertson and Yorgiadis power law more closely than either $n = 2$ or $n = 3$. Since photoelastic studies are made at stress levels which seldom exceed 20 psi, the evaluation of ΔW was made using the relationship

$$\Delta W = C\sigma^{2.5}$$

where C is the average value $\Delta W/\sigma^{2.5}$ taken from Table 1, and σ is the stress amplitude taken as 20 psi.

The average energy loss ΔW based on a stress amplitude of 20 psi is then 0.03 in-lb/in.^{3} The total energy W was computed from the well-known relationship:

$$W = 1/2\,\frac{\sigma^2}{E}$$

Results for W and $\Delta W/W$ based on the stress amplitude of 20 psi are listed in Table 1. Undoubtedly, internal friction produces energy losses in the material; however, it can be concluded from the foregoing that if the stress range is limited to a value lower than 20 psi then the specific loss is only about 8 to 12 per cent for the loading rates considered here. In a photoelastic model 0.5 in. thick, 20 psi will produce ten fringes; hence it is practical to limit the stress to this level. The 8 to 12 per cent specific loss represents energy which will be removed from the stress waves as they propagate through the material.

The fringe order as a function of the time after impact was obtained by counting the fringes as they formed in the specimen during the impact period. The specimens were photographed in a field of circularly polarized light, and a typical example of the records obtained is given in Fig. 4. It is noted that the 0.5-fringe order requires about 4 frames to propagate across the specimen. The fringe order at the central section of the specimen increased as the stress wave propagated back and forth across the specimen. By starting at frame 4 in Fig. 4 and observing the build-up in the fringe order as a function of time it was possible to establish that the fringe order varied linearly with time. It was also possible to

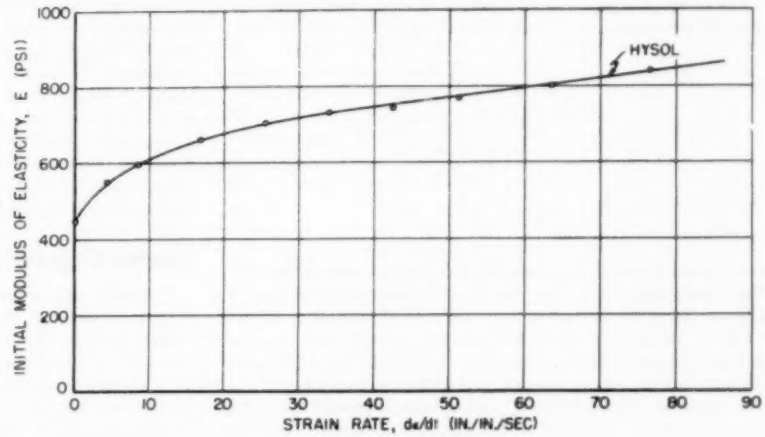

Fig. 3 Initial modulus of elasticity of Hysol 8705 as a function of strain rate

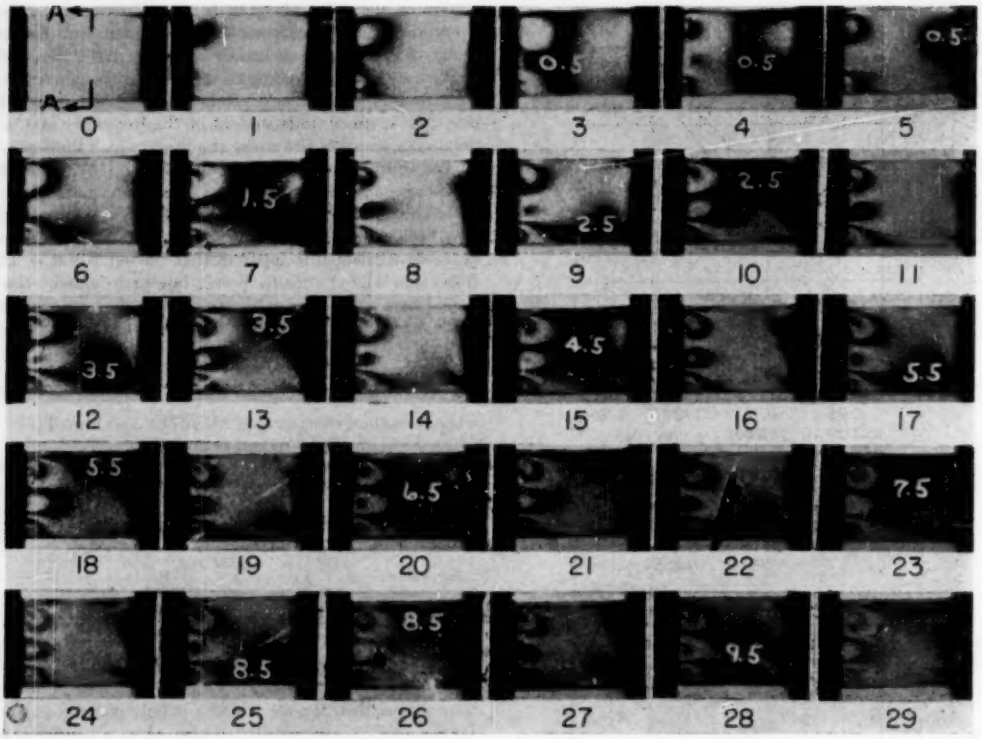

Fig. 4 Isochromatic fringe pattern produced in a Hysol 8705 specimen at a strain rate of 16.8 in/in/sec. Photographs were taken with a Fastax camera operating at 13,440 frames per sec.

establish the slope of the fringe order versus time curve, which is used in later calculations.

Except for very low impact velocities, the fringe patterns were discernible only over the initial portion of the impact period; for this reason the acceleration determinations were repeated and emphasis was placed on obtaining oscilloscope records of the acceleration-time trace over only the initial portion of the impact period. In this manner it was possible to employ a higher amplification of signal and obtain greater accuracy. Examination of the records indicated that the acceleration and hence stress varied linearly as a function of time over the interval of time considered.

The material fringe values in terms of stress and strain were obtained by employing the following relations:

$$f_\sigma = \frac{h\dfrac{d\sigma}{dt}}{2\dfrac{dn}{dt}} = \frac{hM\dfrac{da}{dt}}{2\dfrac{dn}{dt}}\frac{L_0}{V_0} \tag{3}$$

$$f_\epsilon = \frac{1+\nu}{E} f_\sigma \tag{4}$$

where f_σ and f_ϵ are the material fringe values in terms of maximum shear stress and strain, respectively, h is the model thickness, M is the mass of the impacted pendulum, da/dt and dn/dt are the slopes of the acceleration and fringe order versus time curves, ν is Poisson's ratio (0.46), and E is the modulus of elasticity evaluated at the rate of loading used in each determination.

In equation (3) the term δ_i/V_0 has been neglected since it is very small when compared to 1. This is true only for the relatively low values of stress where the fringe-order and acceleration curves are linear functions of time.

The use of the rates da/dt and dn/dt in Equation (3) eliminates any error which would result from a slight mismatch in the initial time for the two sets of data. The static value of Poisson's ratio was used in the calculation; however, later work [16] with a dynamic application of the grid method established the fact that the static and dynamic values of Poisson's ratio are the same.

By employing Equations (3) and (4) it was possible to determine the values of f_σ and f_ϵ as a function of strain rate as shown in Fig. 5. All of the values shown in Fig. 5 were obtained using the methods just described except for the last two points corresponding to a strain rate of 65 in/in/sec. These values were obtained by employing the grid method in conjunction with photoelasticity on the problem of a simple strut subjected to axial impact. This method is the subject of another paper [16]; however, it can be stated here that the grid method was employed successfully to determine dynamic values of f_σ, f_ϵ, and Poisson's ratio. It will be noted from Fig. 5 that the results obtained using the grid method are consistent with the results obtained using the double-pendulum method.

Dynamic Fringe Patterns

A simple strut subjected to axial impact was selected to illustrate the application of the methods discussed. A strut 0.36 by 1.25 by 7.5 in. was machined from a sheet of Hysol 8705 and loaded axially by impacting one of its ends with a 216-gram flat-bottom weight traveling at a velocity of about 63 in. per sec. The contact was effected over the entire upper surface of the strut. Owing to frictional constraint at the interface of the weight and

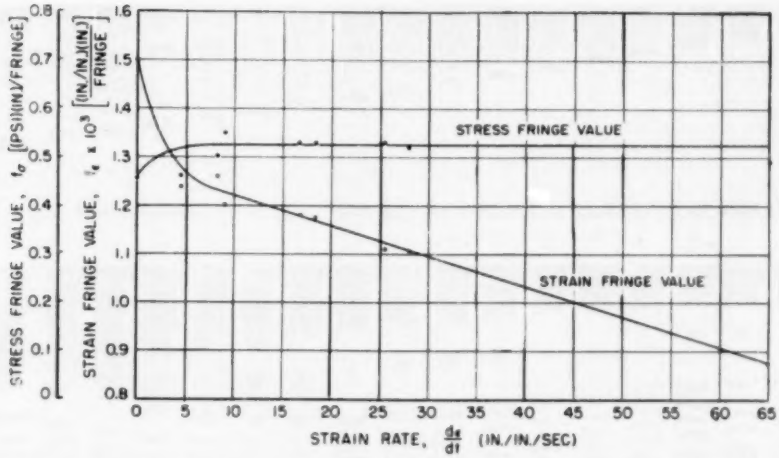
STRESS FRINGE VALUE, f_σ [(PSI/IN)/FRINGE]
STRAIN FRINGE VALUE, $f_\epsilon \times 10^3$ [(IN./IN.)/IN./FRINGE]
STRESS FRINGE VALUE
STRAIN FRINGE VALUE
STRAIN RATE, $\frac{d\epsilon}{dt}$ (IN./IN./SEC)

Fig. 5 Material fringe values in terms of stress and strain as a function of strain rate for Hysol 8705

the strut, the stress distribution was not uniform at the impacted end. Three different boundary conditions were imposed on the other end of the strut; namely, (*a*) free end normal to the axis of the strut, (*b*) fixed end normal to the axis of the strut, and (*c*) free end inclined 45 deg to the axis of the strut. High-speed motion pictures were taken with a Fastax camera operating at about 13,000 frames per sec to record the photoelastic fringe patterns formed during impact. The photoelastic fringe patterns obtained for two of the end conditions are shown in Figs. 6 and 7.

The Free-End Strut. An examination of the 68 photographs shown in Fig. 6 indicates that the fringes produced by the impact propagated down the strut, reflected from the free end, and then propagated back up the strut. As the fringes propagated down the strut, the maximum fringe order increased during the interval between photographs 1 and 10, then the maximum fringe order began to decrease. This decrease in fringe order continued as the fringes propagated down the strut until the reflection phenomenon occurred and prevented its direct observation. Also, as the fringes propagated down the strut, the slope of the wave front became less sharp and the spacing between the fringes increased. Finally, certain fringes exhibited curvature, indicating a nonuniform distribution of stress across sections of the strut.

The positions of the fringes were determined at a number of different frames during the impact period, Fig. 8. At position $x/D = 0.7$ the maximum fringe order was 6.75; however, by the time the wave propagated to the position $x/D = 4$ the maximum fringe order decreased two orders to 4.75. The degree of dispersion is indicated by the form of the curve which gives maximum fringe order as a function of position in Fig. 8. This dispersion presumably results from the combined influence of two factors: (*a*) Elastic dispersion due to Poisson's effect; and (*b*) attenuation due to the viscoelastic behavior of the material.

From the data presented in Fig. 6 it was possible to compute the velocity of fringe propagation. It was found that each fringe propagates down the strut with a constant velocity. As the fringes approach the free end, their velocities decrease, going to zero for a short time, then the fringes assume a negative velocity and propagate up the strut.

Although a fringe of a given order propagates down the strut at a constant velocity, the fringes of other orders travel with different velocities. This fact is illustrated in Table 2 where the fringe velocities are shown as a function of fringe orders.

The difference in the fringe velocities presumably can be attributed to the dispersion effects which change the shape of the wave front as it propagates down the bar.

Table 2 Fringe velocities down the strut

Fringe order	Fringe velocity, ips
0.5	3420
1.5	2970
2.5	2750
3.5	2560
4.5	2340
5.5	2150

It can be shown from elementary wave theory that when a stress wave strikes a free surface at normal incidence, it reflects opposite in sign and begins to cancel the remaining portion of the pulse. To determine whether the fringes follow this same reflection law the following analysis was conducted: The locations of the fringes corresponding to frame 26 were established together with the line of maximum fringe order by reference to Fig. 8. The line of maximum fringe order was extrapolated beyond the free boundary of the strut as if the boundary did not exist. Next, the positions of the fringes for frames 30 to 58 were constructed using the velocities of each fringe order and neglecting the existence of the free boundary. These curves, showing fringe order versus position beyond the free boundary, were reflected by reversing their sign and position. These reflected fringes were then subtracted from the fringes still existing at each position along the strut, and a resultant fringe order equivalent to this difference was obtained. The subtraction process was repeated along the strut for a number of different frames. A comparison between the constructed fringes and the actual fringes obtained after reflection is given in Fig. 9. This figure shows close agreement between the two curves even with the large amount of extrapolation necessary in the graphical construction process. This indicates that the reflection of a fringe very nearly follows the reflection law for stress pulses obtained from the elementary theory.

The Fixed-End and Oblique-End Strut. Similar observations can be made with the fixed-end strut except for the differences in the reflection due to the fixed-end condition. Again it can be shown that the fringes follow the same law of reflection as the stresses.

With the oblique-end strut the law of reflection is much more complex since the impinging dilatational wave produces both a

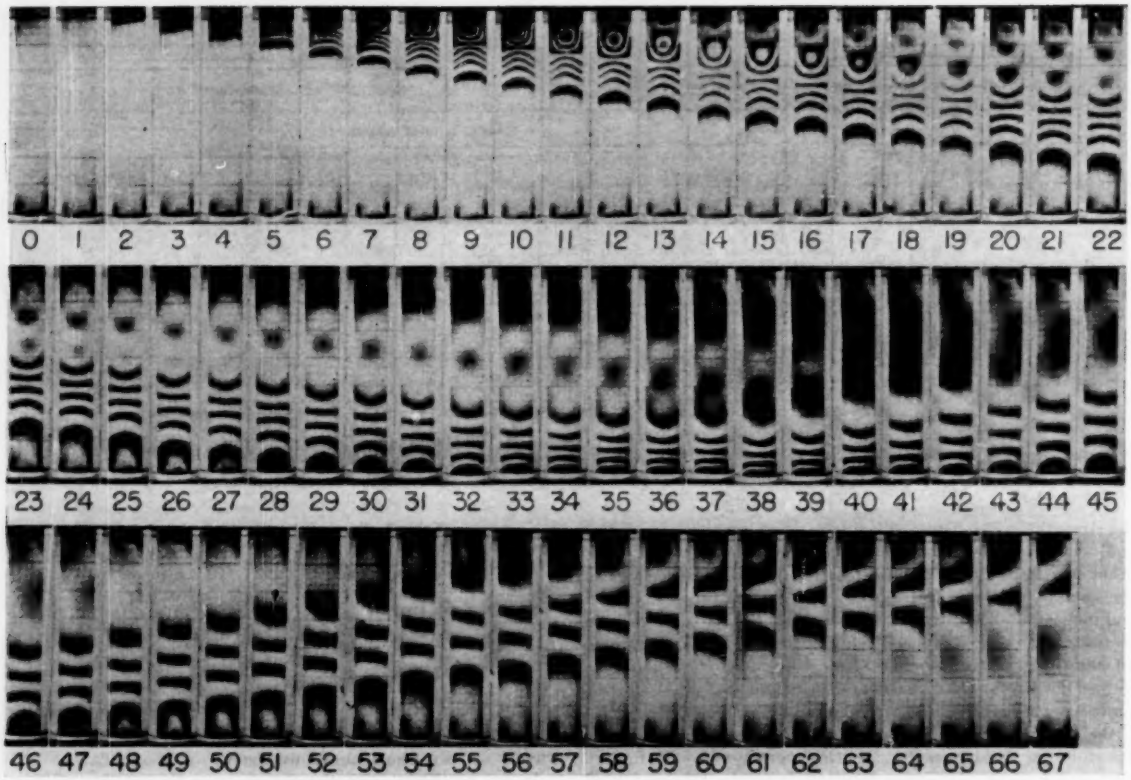

Fig. 6 Dynamic fringe patterns associated with propagation of stress wave in a strut of Hysol 8705

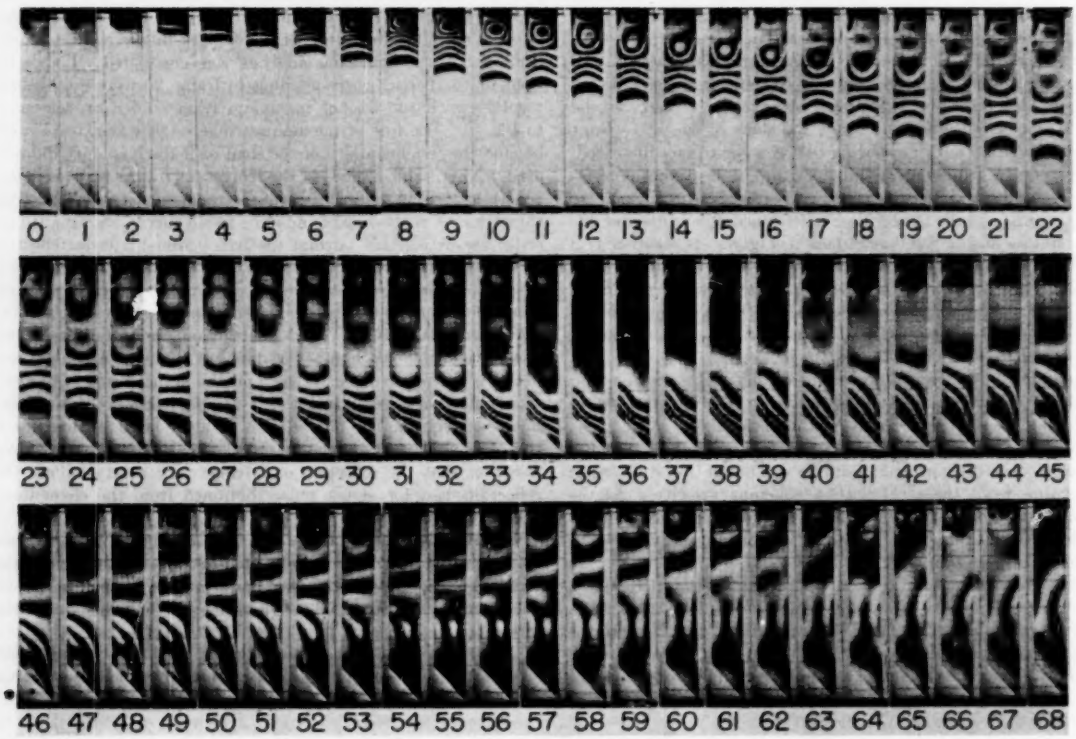

Fig. 7 Dynamic fringe patterns associated with propagation of a stress wave in a strut of Hysol 8705. (Free end at oblique incidence, Fastax camera at 13,440 frames/sec.)

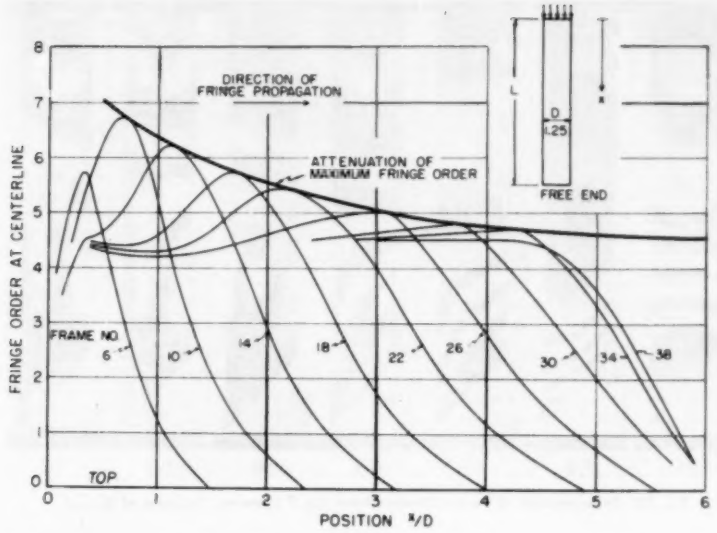

Fig. 8 Fringe order as a function of position with frame number as a parameter. (1 frame = 76.5 microsec)

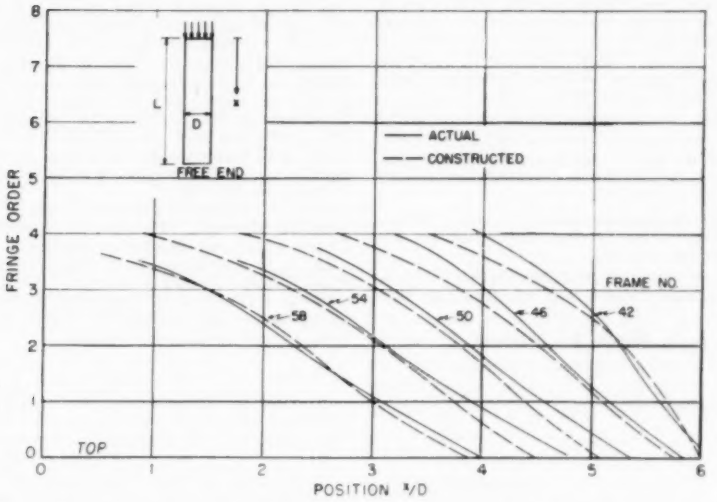

Fig. 9 Comparison of actual positions of fringes with constructed positions of fringes after reflection from free end

reflected dilatational and distortional wave. This reflection can be observed readily by noting the fringe patterns shown in Fig. 7. The fringe propagation down the strut, as expected, is not influenced by the presence of the oblique boundary until the 1/2-order fringe reaches the boundary as shown in frame 24. At this time the 1/2-order fringe begins to rotate about the left-hand corner of the oblique boundary. Fig. 10 shows enlargements of some of the frames from Fig. 7.

The fringes of higher order also rotate until at frame 37 they are all nearly parallel to the oblique boundary. The fringe order at the oblique free end in frame 34 warrants a remark. The very tip shows a fringe order less than 1/2, probably zero, but at no other portion of the entire free boundary is the fringe order zero. In fact, at the center portion the fringe order is about 1, indicating that a stress parallel to the free boundary is present.

The 1/2-order fringe begins to take a complicated shape after frame 43, and in frame 60 the 1/2-order fringes are parallel to the longitudinal axis of the strut. The 1/2-order fringe propagates back up the strut three different times in the frames shown here.

Acknowledgments

This research was supported in part by the United States Air Force under Contract No. AF18(603)-144 with the Air Force Office of Scientific Research of the Air Research and Development Command. The authors wish to express their appreciation to Dr. L. H. Donnell for his helpful suggestions on the work dealing with material properties.

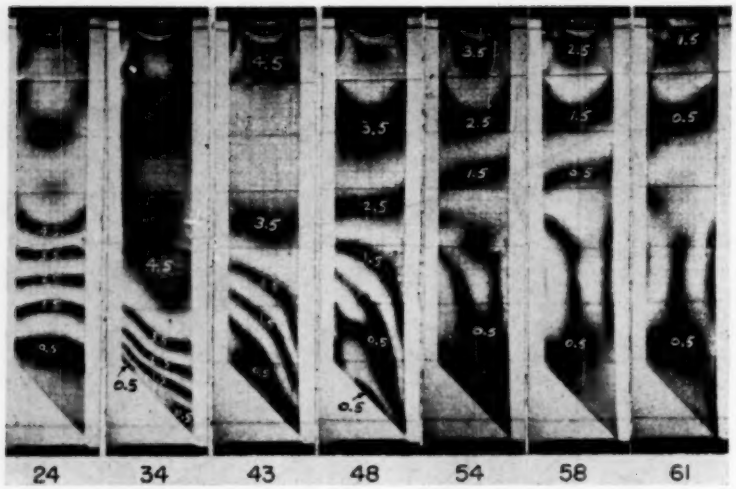

Fig. 10 Enlargements of various frames from Fig. 7 showing the order of fringes

References

1 D. G. Christie, "An Investigation of Cracks and Stress Waves in Glass and Plastics by High-Speed Photography," *Transactions of the Society for Glass Technology*, vol. 36, 1952, pp. 74–89.

2 G. W. Sutton, "A Photoelastic Study of Strain Waves Caused by Cavitation," JOURNAL OF APPLIED MECHANICS, vol. 24, TRANS. ASME, vol. 79, 1957, pp. 340–348.

3 J. C. Feder, R. A. Gibbons, J. T. Gilbert, and E. L. Offenbacher, "The Study of the Propagation of Stress Waves by Photoelasticity," *Proceedings of SESA*, vol. 14, 1956, p. 109.

4 Z. Tuzi and M. Nisida, "Photoelastic Study of Stresses Due to Impact," *Philosophical Magazine*, series 7, vol. 21, 1936, pp. 448–473.

5 M. M. Frocht and P. D. Flynn, "Studies in Dynamic Photoelasticity," JOURNAL OF APPLIED MECHANICS, vol. 23, TRANS. ASME, vol. 78, 1956, p. 116.

6 A. A. Betser and M. M. Frocht, "Stresses in Short Beams Under Central Impact," JOURNAL OF APPLIED MECHANICS, vol. 24, TRANS. ASME, vol. 79, 1957, pp. 509–514.

7 D. A. Senior and A. A. Wells, "A Photoelastic Study of Stress Waves," *Philosophical Magazine*, series 7, vol. 37, 1946, pp. 463–469.

8 W. Goldsmith and G. W. Norris, Jr., "Stresses in Curved Beams Due to Transverse Impact," Proceedings, Third U. S. National Congress of Applied Mechanics, ASME, 1958, p. 153.

9 A. B. J. Clark, "Static and Dynamic Calibration of a Photoelastic Model Material CR-39," *Proceedings of SESA*, vol. 14, 1956, p. 1956.

10 D. F. Marshall, "The Dynamic Stress Optic Coefficient of Perspex," *Physical Society Proceedings*, section B, 1957, p. 1033.

11 H. C. Perkins, "Movies of Stress Waves in Photoelastic Rubber," JOURNAL OF APPLIED MECHANICS, vol 20, TRANS. ASME, vol. 75, 1953, pp. 140–141.

12 A. J. Durelli and W. F. Riley, "Experiments on Transient Two-Dimensional Stress-Strain Distributions," JOURNAL OF APPLIED MECHANICS, vol. 24, TRANS. ASME, vol. 79, 1957, p. 69.

13 E. G. Volterra and C. S. Barton, "An Impact Testing Machine for Plastics and Rubber-Like Materials," *Proceedings of SESA*, vol. 16, 1958, pp. 157–170.

14 J. M. Robertson and A. J. Yorgiadis, "Internal Friction in Engineering Materials," JOURNAL OF APPLIED MECHANICS, vol. 13, TRANS. ASME, vol. 68, 1946, p. A-173.

15 A. L. Kimball and D. E. Lovell, "Internal Friction in Solids," *Physical Review*, second series, vol. 30, 1927, pp. 948–959.

16 A. J. Durelli, J. W. Dally, and W. F. Riley, "Developments in the Application of the Grid Method to Dynamic Problems," this issue of the JOURNAL, pp. 629–634.

Rupture Characteristics of Safety Diaphragms

N. A. WEIL

The M. W. Kellogg Company, New York, N. Y.
Now Director, Mechanical Research Division, Armour Research Foundation, Chicago, Ill.

Instability (maximum pressure) criteria for materials obeying a parabolic stress-strain law are investigated. Two special solutions are formulated, accompanied by the instability condition obtained from the author's approximate theory. Bursting pressure is most accurately predicted by the approximate theory. In turn, the polar deflection and strain at instability are more closely predicted by special solution II. It is shown that neither the "pureness" nor the annealed condition of a metal gives adequate assurance of reliability in frangible disk service. The way to insure this requirement is to confirm experimentally that, in the uniaxial test, fracture will not occur before the logarithmic strain exceeds roughly (0.36 + 0.73 m), or that in a bulge test the applied hydrostatic pressure passes through a maximum prior to bursting.

THE CHEMICAL, power, and transportation industries frequently employ equipment which operates at high pressures and elevated temperatures. To protect the safety of operating personnel and minimize potential damage, proper means must be provided to safeguard against distress resulting from malfunctioning of the equipment. On pressure vessels this is usually afforded by supplying the vessel with frangible diaphragms. Attention will be restricted here to the "bulge-type" safety disks; the "shear-type" disk has been the subject of less intensive study [10],[1] due to its poorer service performance.

In the design of safety diaphragms it is necessary to predict the pressure at which a frangible membrane will burst. The experimental approach [1, 3, 4, 5] provides information only on the actual size and material of disk used; predictions for different conditions are of dubious value. Theories, on the other hand, were either too approximate [2, 6, 7] or required extremely lengthy calculations [11] to provide an answer.

For a simple and reliable formulation of the maximum pressure, it will be assumed that the true stress-logarithmic strain characteristics of materials in uniaxial tension can be represented by the relationship

$$\sigma = A\epsilon^m \tag{1}$$

[1] Numbers in brackets designate References at end of paper.

Presented at the West Coast Conference of the Applied Mechanics Division, Stanford, Calif., September 9–11, 1959, of THE AMERICAN SOCIETY OF MECHANICAL ENGINEERS.

Discussion of this paper should be addressed to the Secretary, ASME, 29 West 39th Street, New York, N. Y., and will be accepted until January 10, 1960, for publication at a later date. Discussion received after the closing date will be returned.

NOTE: Statements and opinions advanced in papers are to be understood as individual expressions of their authors and not those of the Society. Manuscript received by ASME Applied Mechanics Division, July 30, 1958. Paper No. 59—APMW-3.

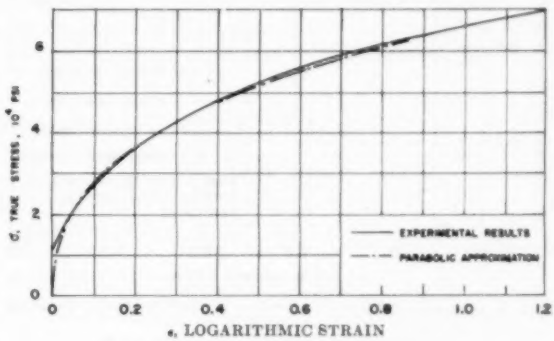

Fig. 1 Stress-strain curve for annealed copper

The degree of approximation of Equation (1) for annealed copper is shown in Fig. 1. With this assumption two approaches are open for an investigation of instability. In one type of solution a stipulation is made regarding the deflected shape, regardless of whether this satisfies the boundary conditions or strain-displacement laws. These are called "special solutions." The other approach is to base the instability investigation on some known solution [12].

Special Solution I

Special solution I is based upon the stipulations that under lateral pressure the plate (*a*) deforms into a spherical cap; (*b*) thins down uniformly at all points. These assumptions, implying that stresses and strains will be constant throughout the bulge at any pressure level, are too crude to lead to satisfactory results

Nomenclature

a = radius of diaphragm, in.
$\bar{h}$ = initial thickness of diaphragm, in.
h = thickness of deformed diaphragm, in.
σ = true stress, psi
ϵ = logarithmic strain
P = hydrostatic pressure, psi
p = $Pa/\bar{h}$ = relative pressure, psi
w = vertical deflection, in.
ω = w/a = dimensionless vertical deflection
m = strain-hardening exponent
A = hardness factor, psi
R = radial radius of curvature, in.
r = radial distance from pole, in.
ρ = r/a = dimensionless radial distance

Subscripts r, θ, z represent quantities acting in the meridional, circumferential, and normal directions, respectively. The subscript 0 denotes entities at the pole; asterisks designate variables at instability. Primes indicate differentiation with respect to ρ.

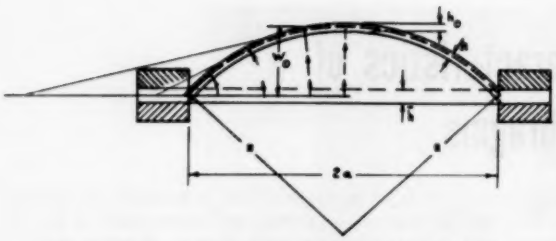

Fig. 2 Assumed deflection profile in special solution II

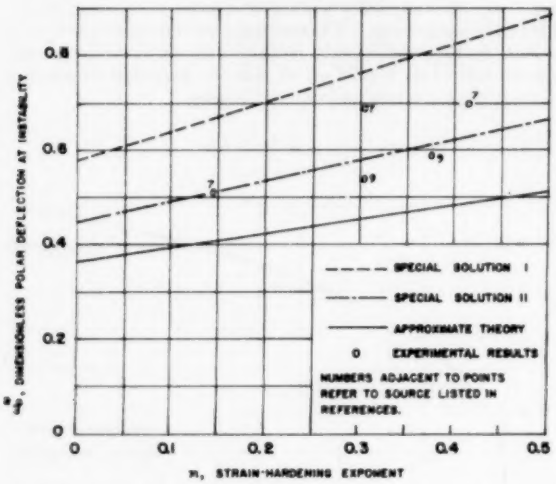

Fig. 3 Instability deflection as function of strain-hardening exponent

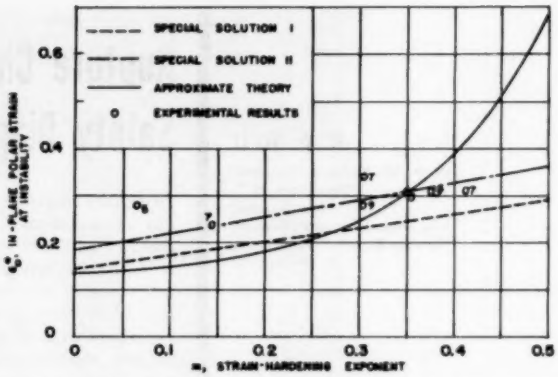

Fig. 4 Instability strain as function of strain-hardening exponent

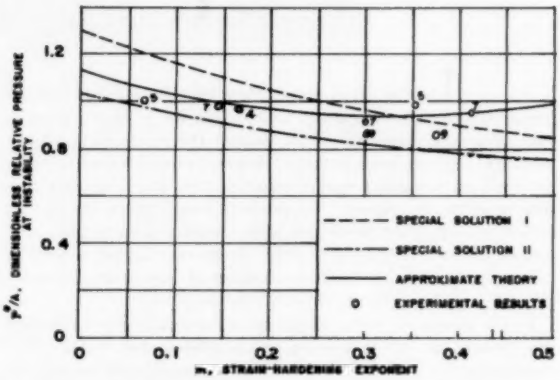

Fig. 5 Instability pressure as function of strain-hardening exponent

Special Solution II

Assume now that the distortion of the plate under lateral pressure is subject to the following conditions:

(*a*) The shape of the bulge is again a spherical cap.

(*b*) During deformation the particles travel along paths which are arcs of a set of coaxial circles. The center of each circle is located by the intersection of the base plane with the tangent to the deformed profile, as shown in Fig. 2.

It has been shown [9] that these conditions will again lead to a state of balanced biaxiality throughout the diaphragm. However, in this case stress as well as strain will vary from a minimum at the clamping edge to a maximum at the crown.

The following relationships can now be written:

From geometry of the spherical cap

$$R/a = (1 + \omega_0^2)/2\omega_0 \tag{2}$$

From static equilibrium

$$p = \frac{2\sigma_\theta h_0/\bar{h}}{R/a} \tag{3}$$

The thickness variation through the bulge will be given by [9]

$$\bar{h}/h_0 = (1 + \omega_0^2)^2 \tag{4}$$

Accepting the Hencky-Mises stress-strain laws of plasticity, for balanced biaxial tension, Equation (1) becomes

$$\sigma_r = \sigma_\theta = \sigma = A(-\epsilon_z)^m \tag{5}$$

By definition $\epsilon_z = \log (h/\bar{h})$, so that from Equation (4)

$$-\epsilon_z|_{r=0} = 2 \log (1 + \omega_0^2) \tag{6}$$

With this result, polar in-plane strain, polar stress and pressure become (noting that $\epsilon_r = \epsilon_\theta = -\epsilon_z/2$ at the pole)

$$\epsilon_r|_{r=0} = \epsilon_0 = \log (1 + \omega_0^2) \tag{7}$$

$$\sigma_r|_{r=0} = \sigma_0 = 2^m A \, [\log (1 + \omega_0^2)]^m \tag{8}$$

$$p/A = \frac{2^{2+m} \, [\log (1 + \omega_0^2)]^m \omega_0}{(1 + \omega_0^2)^2} \tag{9}$$

A pressure maximum (instability) will occur when $dp/d\omega_0 = 0$. This condition is satisfied, according to Equation (9), at

$$m = {}^1/_2 \left[5 - \frac{1}{(\omega_0^*)^2} \right] \log [1 + (\omega_0^*)^2] \tag{10}$$

Equation (10) can be solved inversely for ω_0^* in terms of m. One can then successively obtain ϵ_0^* (in-plane polar strain at instability) and p^*/A (dimensionless instability pressure) as functions of m from Equations (7) and (9). The resulting curves are plotted in Figs. 3, 4, and 5.

Equations (10) and (7) can be expanded in infinite-series form to

$$m = -{}^1/_2 + \sum_{n=1}^{\infty} (-1)^{n+1} \frac{5 + 6n}{4 \sum_{n=1}^{\infty} n} (\omega_0^*)^{2n}$$

$$\epsilon_0^* = \sum_{n=1}^{\infty} \frac{(-1)^{n+1}}{n} (\omega_0^*)^{2n}$$

Omitting now all terms past the first in the series expansions leads to the approximate relationships for the significant quantities at instability:

$$\omega_0^* = [2(1 + 2m)/11]^{1/2} \tag{11}$$

$$\epsilon_0^* = 2(1 + 2m)/11 \tag{12}$$

The maximum error involved in Equation (11) is 9.2 per cent (on the low side).

Equation (12) is identical with the result obtained by Hill [9]. Although this result corresponds to a severe curtailment of two infinite series, a favorable mutual cancellation of errors makes the approximate instability strain very accurate. Within the limits considered in this work ($0 \leq m \leq 0.5$), Equation (12) deviates not more than 0.6 per cent (on the low side) from the exact results of special solution II.

Instability Condition Based on Approximate Theory

The salient results of the approximate theory were given in a previous paper [12]. From Equation (22) of this reference it can be shown that

$$\omega_0' = 0$$

$$\omega_0'' = -(2 - 0.6111m + 0.1312m^2)\omega_0 + (1 + 0.4444m - 0.4992m^2)\omega_0^3 + (3.722 - 1.400m + 5.035m^2)\omega_0^5 \tag{13}$$

The dimensionless radial radius of curvature is given by

$$R/a = -[1 + (\omega')^2]^{3/2}(\omega'')^{-1} \tag{14}$$

and, by substitution of Equations (13), the polar radius of curvature can be given, to this approximation, as

$$R_0/a = (0.5 + 0.1528m + 0.0139m^2)/\omega_0 + (0.25 + 0.2639\,m - 0.0897m^2)\omega_0 + (1.056 + 0.3299\,m + 0.8399m^2)\omega_0^3 \tag{15}$$

In this case, the expression governing instability becomes

$$\frac{d\sigma_0}{d\omega_0} = 2\sigma_0 \frac{d\epsilon_0}{d\omega_0} + \frac{\sigma_0}{R_0/a} \frac{dR_0/a}{d\omega_0} \tag{16}$$

Expressions for σ_0 and ϵ_0 were given in Equations (30) and (31) of reference [12], while R_0/a is expressed by Equation (15). Performing now the indicated operations and inserting the results into Equation (16) leads to

$$(19.94 + 1.76m - 12.68m^2)(\omega_0^*)^4 + (5 - 2.917m - 2.664m^2)(\omega_0^*)^2 - (1 + 2m) = 0 \tag{17}$$

Then, from Equation (17), the polar deflection at instability will be given by

$$\omega_0^* = [(104.8 + 137.4m - 54.78m^2 - 85.92m^3 + 7.097m^4)^{1/2} - 5 + 2.917m + 2.664m^2]^{1/2}(39.82 + 3.52m - 25.36m^2)^{-1/2} \tag{18}$$

This equation enables one to evaluate ω_0^* for various values of n.; the relationship is almost linear over $0 \leq m \leq 0.5$, as plotted in Fig. 3. Inserting the resulting values of ω_0^* into Equations (31) and (21) of reference [12], one can obtain the instability strain and instability pressure as shown graphically in Figs. 4 and 5, respectively.

Comparison of Theories With Experiments

In carrying out this comparison, attention was restricted to bulge tests on materials whose uniaxial stress-strain properties were reported or could be secured readily. Furthermore, the listing was confined to disks which passed through instability prior to bursting. The test data are assembled in Table 1 as well as in Figs. 3 to 5.

The experimental values for deflection and strain at instability are closest to the results of special solution II. The predictions of the approximate theory for instability deflection are consistently low. The reason for this lies in the fact that the approximate theory [11] underestimates deflections near the maximum pressure.

Table 1 Data from comparison of theories and experiments

			Stress-strain properties		Diaphragm dimensions		Significant quantities at instability				
Ref. no.	Authors	Material	Hardness factor, A, 10^3 psi	Strain-Hardening exponent m	Radius, a, in.	Initial thickness $\bar{h}$, in.	Actual pressure, P^*, psi	Relative pressure, $p^* = \frac{P^* a}{\bar{h}}$, 10^3 psi	Dimensionless relative pressure, p^*/A	Dimensionless polar deflection, ω_0^*	In-plane polar strain, ϵ_0^*
[5][a]	Sachs, Espey, Kasik	Aluminum 24-T, clad	100.0	0.168	3.2	0.040	1200	96.0	0.960	...	...
[6]	Brown, Sachs	Annealed copper	60.0	0.352	3.2	0.040	740	59.2	0.987	...	~0.30
		Hard-rolled copper	60.0	0.066	3.2	0.040	750	60.0	1.000	...	~0.28
[8]	Brown, Thompson	Aluminum 75S-O, bare	54.5	0.145	3.2	0.041	680	53.1	0.974	~0.51	~0.24
		Annealed low-carbon steel	100.0	0.301	3.2	0.041	1160	90.5	0.905	~0.69	~0.34
		Annealed stainless steel	190.0	0.415	3.2	0.036	2050	182.5	0.961	~0.70	~0.31
[11]	Weil, Newmark	Annealed copper	65.5	0.375	5.75	0.0209	205	55.8	0.853	~0.59	~0.31
		5–7 pct rolled copper	65.5	0.303	5.75	0.1313	1289	56.4	0.861	~0.54	~0.28

[a] Attainment of instability not stated.

The reasons for the good agreement of special solution II with experiments, in so far as strains and deflections at instability are concerned, are found in the fact that this approach postulates only that the bulge be deformed into a spherical cap and that the particles travel along prescribed paths. Beyond these conditions (and allowing for the correctness of the parabolic stress-strain curve), the derivation for the instability condition can be regarded as being exact. Investigators repeatedly report [6, 8] that near instability the bulge does assume a shape closely resembling a spherical cap.

The second assumption, dealing with particle travel, is also in reasonable accord with the true physical behavior. However, one may mention that neither is it easy to determine accurately the instability strain or deflection (due to the flatness of the strain-pressure or deflection-pressure curve at their respective maxima), nor are these quantities important from the viewpoint of design.

The significant design quantity, and one that can be ascertained reliably in the bulge test, is the bursting pressure. This quantity is a function of stress, strain, and polar radius of curvature; therefore the assumptions of the special solutions do not insure its close prediction. As Fig. 5 shows, the results of special solution II are consistently low for the instability pressure, while the approximate theory is in good agreement with the experimental points.

Instability deflections and strains are functions of the strain-hardening exponent m only, according to all three theories described. The instability pressure, however, is a linear function of "hardness factor" A, and is hardly influenced by the magnitude of m. As seen in Fig. 5, the instability pressure can be represented over the range $0 \leq m \leq 0.5$ likely to be encountered in metals by the rough approximation:

$$p^* = A \tag{19}$$

The relative insensitivity of the bursting pressure to variations of m is confirmed by test results. Over the experimental range of $0.066 \leq m \leq 0.415$, the pressure at instability remained within $0.853 \leq p^*/A \leq 1.0$.

Conclusions and Design Considerations

The following conclusions can be drawn on the basis of evidence assembled in Figs. 3 to 5.

If large deflection prior to bursting is desired, safety diaphragms should be constructed of materials with high values of m. On the other hand, if a high bursting pressure is to be attained, a material with a high A-value should be chosen regardless of its strain-hardening exponent.

Concerning the correct selection of materials, it has been recommended [3, 4] that, for consistent and reliable performance, only "pure" metals in the annealed condition should be employed for the manufacture of safety diaphragms. This reasoning appears to be in error.

The fact is that the reproducibility of bursting pressures depends only on the ability of the metal to stretch until the bulge passes through instability. This requires that in the uniaxial test the logarithmic strain at failure should exceed $(4 + 8m)/11$; in the bulge test the recorded pressure should pass through a maximum prior to bursting. Many pure metals, specifically certain grades of aluminum alloys, do not possess this ability.

A further word of caution is in order. Regardless of the straining capacity of materials, premature fractures are greatly enhanced if the material is very thin (say, $\bar{h} < 0.020$ in.). Therefore, if reliability of safety diaphragms is to be insured, this should not be obtained at the expense of material thickness, but rather by increasing the diameter of the disk.

References

1 M. E. Bonyun, "Frangible Disks as Protection for Pressure Vessels," *Transactions of the American Institute of Chemical Engineers*, vol. 31, 1935, pp. 256–277.

2 R. Bestehorn, "Rupture Disks and Safety Membranes," *Die Technik*, vol. 2, 1947, pp. 93–95.

3 G. F. Lake and N. P. Inglis, "The Design and Manufacture of Bursting Disks," *Proceedings of The Institution of Mechanical Engineers*, vol. 142, 1939, pp. 365–379.

4 T. S. Murphy, Jr., "Rupture Diaphragms," *Chemical and Metallurgical Engineering*, vol. 51, November, 1944, pp. 108–112, and December, 1944, pp. 99–103.

5 G. Sachs, G. Espey, and G. B. Kasik, "Circular Bulging of Aluminum-Alloy Sheet at Room and Elevated Temperatures," TRANS. ASME, vol. 68, 1946, pp. 161–173.

6 W. F. Brown, Jr., and G. Sachs, "Strength and Failure Characteristics of Thin Circular Membranes," TRANS. ASME, vol. 70, 1948, pp. 241–251.

7 A. N. Gleysal, "Plastic Deformation of a Circular Diaphragm Under Pressure," JOURNAL OF APPLIED MECHANICS, vol. 15, TRANS. ASME, vol. 70, 1948, pp. 288–296.

8 W. F. Brown, Jr., and F. C. Thompson, "Strength and Failure Characteristics of Metal Membranes in Circular Bulging," TRANS. ASME, vol. 71, 1949, pp. 575–586.

9 R. Hill, "A Theory of the Plastic Bulging of a Metal Diaphragm by Lateral Pressure," *Philosophical Magazine*, vol. 41, 1950, pp. 1133–1142.

10 G. R. Prescott, "Rupture-Disk Design Evaluation and Bursting Tests," TRANS. ASME, vol. 75, 1953, pp. 355–359.

11 N. A. Weil and N. M. Newmark, "Large Plastic Deformations of Circular Membranes," JOURNAL OF APPLIED MECHANICS, vol. 22, TRANS. ASME, vol. 77, 1955, pp. 533-538.

12 N. A. Weil, "Approximation to Plastic Behavior of Circular Membranes," *Proceedings of The American Society of Civil Engineers*," vol. 83, paper no. 1139, 1957.

Bending of Isosceles Right Triangular Plates[1]

H. J. FLETCHER
Chairman,
Department of Mathematics,
Brigham Young University,
Provo, Utah

Two methods are presented for the solutions of problems of an isosceles right triangular plate bent by arbitrary transverse loads. One method makes use of a concentrated diagonal load on a square plate. The other uses an antisymmetric load on a square plate. A numerical solution is given for the case of clamped hypotenuse and simply supported legs. A table is given indicating how to solve fifteen of the possible eighteen problems in which an edge is free, clamped, or supported.

SEVERAL problems of the bending of thin isotropic triangular plates have been solved in closed form. S. Timoshenko[2] solved the right triangular plate bent by moments on the edge. S. Woinowsky, A. Nadai, and B. G. Galerkin[3] solved the equilateral plate and right isosceles triangular plate simply supported on all sides and subject to arbitrary transverse loads. It is the purpose of this paper to treat additional problems of an isosceles right triangular plate subject to a transverse load, and different boundary conditions.

Problem

Deflections and moments of the shaded area of the plate in Fig. 1 are sought, using the assumptions of thin-plate theory. The equation to be solved is

$$\frac{\partial^4 w}{\partial x^4} + 2\frac{\partial^4 w}{\partial x^2 \partial y^2} + \frac{\partial^4 w}{\partial y^4} = \frac{q(x, y)}{D} \tag{1}$$

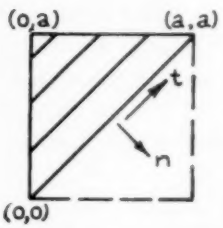

Fig. 1 Isosceles right triangular plate

subject to boundary conditions of a free, clamped or simply supported edge, where

$w(x, y)$ = deflection of plate at co-ordinates (x, y)
$q(x, y)$ = force per unit area normal to plate
D = modulus of rigidity
ν = Poisson's ratio
M_n = moment in direction n in Fig. 1
M_t = moment in direction t in Fig. 1
a = length of a leg of triangle

Solution

The solutions can be obtained from those of a square plate as given by Fletcher and Thorne.[4]

If the load on a square plate is chosen so that

$$q(x, y) = -q(y, x) \tag{2}$$

and if the boundary conditions have a similar symmetry then

$$w(x, y) = -w(y, x) \tag{3}$$

It follows that

$$w(x, x) = w_{nn}(x, x) = w_{tt}(x, x) = 0 \tag{4}$$

where the subscripts indicate partial derivatives. These are the conditions for a simply supported edge along the diagonal.

If the load on a square plate is chosen so that

$$q(x, y) = -q(a - y, a - x)$$

and if the boundary conditions have a similar symmetry then we have the condition of a simply supported edge along the diagonal $x + y = a$.

If the load $q(x, y)$ is chosen symmetrically so that

$$q(x, y) = q(y, x) \tag{5}$$

and if the boundary conditions are symmetric, then the slope along the diagonal is zero. If one superimposes a concentrated load $P(x)$ along the diagonal, the slope is still zero. $P(x)$ can be chosen so that the deflection, $w(x, x)$, along the diagonal is also zero. These are the two conditions for a clamped edge. Combinations of clamped and supported edges are indicated in Fig. 2. The three problems that cannot be solved by these two methods are those which have both a free leg and a free hypotenuse.

In Fig. 2, S represents a simply supported edge; C represents a clamped edge; F represents a free edge; + represents a load sym-

[1] This work was supported by the Army Ordnance Department, Contract No. DA-04-495-ORD-560.

[2] S. Timoshenko, "Theory of Plates and Shells," McGraw-Hill Book Company, Inc., New York, N. Y., 1940, pp. 102, 293–295.

[3] S. Woinowsky-Kreiger, "Berechnung der ringsum frei aufliegendn glichseitiger Dreiecksplatte," *Ingenieur-Archiv*, vol. 4, 1933, p. 254, and Bulletin Polytechnic Institute, vol. 28, St. Petersburg, 1919, p. 1; A. Nadai, "Die Elastischen Platten," Springer, Berlin, 1925, p. 178; B. G. Galerkin, "Investigation on Triangular Plates," Bulletin Academy de Russie, vol. 13, 1919, pp. 223–238 (in Russian).

Presented at the West Coast Conference of the Applied Mechanics Division, Stanford, Calif., September 9–11, 1959, of THE AMERICAN SOCIETY OF MECHANICAL ENGINEERS.

Discussion of this paper should be addressed to the Secretary, ASME, 29 West 39th Street, New York, N. Y., and will be accepted until January 10, 1960, for publication at a later date. Discussion received after the closing date will be returned.

NOTE: Statements and opinions advanced in papers are to be understood as individual expressions of their authors and not those of the Society. Manuscript received by ASME Applied Mechanics Division, August 5, 1958. Paper No. 59—APMW-19.

[4] H. J. Fletcher and C. J. Thorne, "Bending of Thin Rectangular Plates," Proceedings of the Second U. S. National Congress of Applied Mechanics, ASME, 1954, p. 389.

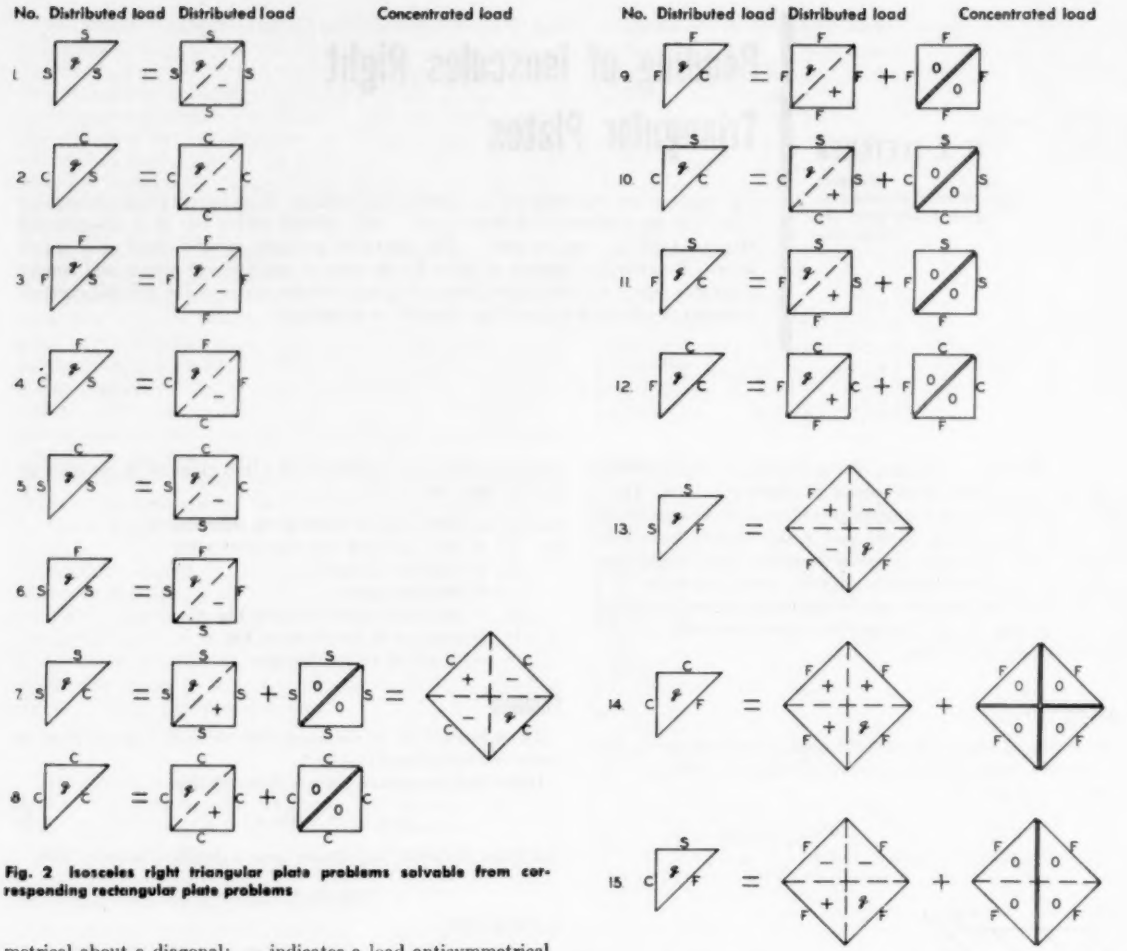

Fig. 2 Isosceles right triangular plate problems solvable from corresponding rectangular plate problems

metrical about a diagonal; − indicates a load antisymmetrical about a diagonal; 0 indicates zero load. Heavy diagonals indicate concentrated loads.

In problems 3 and 9, $q(x, y)$ and a concentrated load at the free corner must be in equilibrium. In problems 1 to 6, $q(x, y)$ is chosen so that

$$q(y, x) = -q(x, y) \qquad 0 \leq x \leq y \leq a \tag{6}$$

In problems 7 to 12, $q(x, y)$ is chosen so that

$$q(y, x) = q(x, y) \qquad 0 \leq x \leq y \leq a \tag{7}$$

In problem 13, $q(x, y)$ is chosen antisymmetric to both diagonals. Problem 7 also can be treated this way. In problem 14, $q(x, y)$ is chosen symmetric to both diagonals. In problem 15, $q(x, y)$ is symmetric with respect to one diagonal and antisymmetric with respect to the other diagonal. In problems 7 to 12 and 15, a concentrated load is superimposed along the diagonal. In problem 14, a concentrated load is superimposed along both diagonals. In problems 7, 13, 14, 15, the co-ordinate system is rotated 45 deg.

Clamped Diagonal—Supported Legs

As an illustration of both methods let us consider problem 7, which is that of an isosceles right triangular plate clamped on the hypotenuse and simply supported on the legs. The solution for the square plate clamped on all edges, given by Fletcher and Thorne in dimensionless units is

$$\left.\begin{aligned} &w(x, y) = w_1(x, y) + w_2(x, y) \\ &\text{where} \\ &w_1(x, y) = \frac{4}{\pi^2} \sum_{m=1}^{\infty} \sum_{n=1}^{\infty} \lambda_{mn}\, q_{mn}\, s_x s_y \\ &\text{and} \\ &w_2(x, y) = \frac{-8}{\pi^2} \sum_{m=1}^{\infty} \sum_{n=1}^{\infty} \lambda_{mn}(n e_m - m e_n) s_x s_y \\ &s_x = \sin n\pi x \\ &s_y = \sin m\pi y \\ &\lambda_{mn} = (m^2 + n^2)^{-2} \\ &q_{mn} = \frac{1}{D} \int_0^1 \int_0^1 q(x, y) s_x s_y \, dx dy \end{aligned}\right\} \tag{8}$$

and e_m is the set of coefficients given by

$$w_{xx}(0, y) = 2 \sum_{m=1}^{\infty} e_m s_y \tag{9}$$

$w_{ss}(0, y)$ is not known, but e_m can be found by using the conditions for a clamped edge. This gives rise to the infinite set of equations:

$$\left.\begin{aligned} &\frac{-e_n}{4nS^2}(s + n\pi)(c - 1) + \frac{2n}{\pi}\sum_{m=1}^{\infty} m\lambda_{mn}e_m \\ &\qquad - \frac{1}{\pi^2}\sum_{m=1}^{\infty} m\lambda_{mn}q_{mn} = 0 \qquad n = 1, 3, 5, \ldots \end{aligned}\right\} \quad (10)$$

where

$$e_{2m} = 0, \qquad s = \sinh n\pi, \quad c = \cosh n\pi$$

In particular, if $q(x, y)$ is a constant load q in Problem 1 of Fig. 2, then

$$q_{mn} = -\frac{q}{D}\frac{4}{\pi^2 mn(m^2 - n^2)}\left(m^2 + n^2 - 2mn\sin\frac{m\pi}{2}\sin\frac{n\pi}{2}\right) \quad (11)$$

if both m and n are odd and $m \neq n$; $q_{mn} = 0$ otherwise. $w_1(x, y)$ is the same as the deflection of a simply supported isosceles right triangular plate. Numerical values are given in Table 1.

A corner load at $(0, a)$ is given by

$$R = 0.02679\, qa^2 \quad (12)$$

The values of e_m are given in Table 2.

Values of the deflection and moments on the perpendicular bisector of the hypotenuse in Fig. 1 are given in Table 3.

Diagonal Load

The second method superimposes a constant load q, on a diagonal load $P(x)$. The deflections and moments of a simply supported plate under a constant load are given in Table 4.

The deflection of a plate due to a diagonal load $P(x)$ is

$$w_a(x, y) = \frac{1}{\pi^4 D}\sum_{m=1}^{\infty}\sum_{n=1}^{\infty}\lambda_{mn}(a_{|m-n|} - a_{m+n})s_x s_y \quad (13)$$

where a_m are the coefficients

$$a_m = \int_0^1 P(x)\cos m\,\pi x dx$$

$m = 0, 1, 2, \ldots$

If $P(x)$ is symmetric about the center of the diagonal, $w(x, y)$ can be summed to

$$\begin{aligned} w_a(x, y) = {} & \frac{a_0}{48D}x(y - 1)(x^2 + y^2 - 2y) + \frac{1}{16\pi^3 D}\sum_{l=1}^{\infty}\frac{a_{2l}}{l^3\sinh^2 l\pi} \\ & \{\cos\pi l(x + y)[\sinh l\pi\cosh l\pi(1 + x - y) + \pi l\cosh l\pi \\ & \cosh l\pi(1 + x - y) - \pi l(1 + x - y)\sinh l\pi\sinh l\pi(1 + \\ & x - y)] \\ & - \cos\pi l(y - x)[\sinh l\pi\cosh l\pi(1 - x - y) + \pi l\cosh l\pi \\ & \cosh l\pi(1 - x - y) - \pi l(1 - x - y)\sinh l\pi \\ & \sinh l\pi(1 - x - y)]\} \end{aligned} \quad (14)$$

Table 1 Deflections and moments of right triangular plate simply supported on all edges under constant load q

x/a	y/a	$w(qa^4/D)$	$w_{xx}(qa^2/D)$	$w_{xy}(qa^2/D)$	$M_n(qa^2)$	$M_t(qa^2)$
0.00	1.00	0	0	−0.019135	−0.013395	0.013395
0.05	0.95	0.000046	−0.00189	−0.017284	−0.009645	0.014553
0.10	0.90	0.000167	−0.00514	−0.013109	−0.002491	0.015862
0.15	0.85	0.000327	−0.00864	−0.008478	0.005296	0.017165
0.20	0.80	0.000486	−0.01175	−0.003827	0.012601	0.017960
0.25	0.75	0.000607	−0.01385	0.000192	0.018126	0.017875
0.30	0.70	0.000658	−0.01478	0.003394	0.021595	0.016844
0.35	0.65	0.000619	−0.01404	0.005216	0.021900	0.014598
0.40	0.60	0.000486	−0.01152	0.005500	0.018824	0.011123
0.45	0.55	0.000269	−0.00692	0.003868	0.011702	0.006287
0.50	0.50	0	0	0	0	0

Table 2 Values of e_m (units of q/D)

m	e_m
1	0.0665417
3	−0.0014623
5	−0.0001646
7	−0.0000498
9	−0.0000213
11	−0.0000110
13	−0.0000063

Table 4 Simply supported plate (square)

x/a	$w_{xx}(x, a - x)$ qa^2/D	$w_{xy}(x, a - x)$ qa^2/D	$M_n(qa^2)$	$M_t(qa^2)$
0.00	0	−0.0464	−0.0323	0.0323
0.05	−0.0021	−0.0440	−0.0280	0.0336
0.10	−0.0065	−0.0390	−0.0188	0.0358
0.15	−0.0118	−0.0327	−0.0075	0.0382
0.20	−0.0173	−0.0259	0.0042	0.0406
0.25	−0.0226	−0.0191	0.0161	0.0428
0.30	−0.0274	−0.0128	0.0267	0.0446
0.35	−0.0314	−0.0075	0.0356	0.0460
0.40	−0.0344	−0.0034	0.0423	0.0471
0.45	−0.0362	−0.0009	0.0465	0.0477
0.50	−0.0368	0	0.0479	0.0479

Table 3 Isosceles right triangular plate clamped along diagonal and supported on edges

x/a	$w(x, a - x)(qa^4/D)$	$w_{nn}(x, a - x)(qa^2/D)$	$w_{tt}(qa^2/D)$	$M_n(qa^2)$	$M_t(qa^2)$
0	0	0.0142	−0.0142	−0.00991	0.00991
0.05	0.0000336	0.0107	−0.0142	−0.00644	0.01098
0.10	0.0001186	0.0041	−0.0133	−0.00013	0.01204
0.15	0.0002240	−0.0026	−0.0121	0.00625	0.01293
0.20	0.0003167	−0.0084	−0.0106	0.01156	0.01315
0.25	0.0003686	−0.0119	−0.0088	0.01450	0.01234
0.30	0.0003622	−0.0126	−0.0067	0.01465	0.01047
0.35	0.0002943	−0.0094	−0.0045	0.01082	0.00731
0.40	0.0001080	−0.0018	−0.0023	0.00255	0.00291
0.45	0.0000604	0.0114	−0.0007	−0.01120	−0.00273
0.50	0	0.0316	0	−0.03156	−0.00947

Table 5 Values of a_{2n}

n	a_{2n}
0	−1.097
1	0.434
2	0.034
3	0.016
4	0.009
5	0.005

$$a_{2n} + 1 = 0$$

Table 6 Isosceles right triangular plate clamped along the diagonal and supported on edges, (concentrated diagonal load method)

x/a	$M_x(qa^2)$	$M_t(qa^2)$
0.00	−0.00991	0.00991
0.05	−0.00643	0.01070
0.10	−0.00014	0.01204
0.15	0.00630	0.01294
0.20	0.01152	0.01313
0.25	0.01456	0.01236
0.30	0.01459	0.01045
0.35	0.01085	0.00732
0.40	0.00255	0.00291
0.45	−0.01119	−0.00270
0.50	−0.03151	−0.00945

The first term represents the deflection of a simply supported plate due to a constant diagonal load a_0. If we superimpose the deflection of a simply supported plate given by

$$W_b(x, y) = \frac{16}{\pi^4}\frac{q}{D}\sum_{\substack{m=1\\ \text{odd}\\ m,n}}^{\infty}\sum_{n=1}^{\infty}\frac{\lambda_{mn}}{mn}\varepsilon_x\varepsilon_y \tag{15}$$

and impose the condition that

$$w_a(x, x) + w_b(x, x) = 0 \tag{16}$$

we obtain the infinite set of equations given by

$$0 = \sum_{m=1}^{\infty}\sum_{n=1}^{\infty}\lambda_{mn}(\delta^k_{|m-n|} - \delta^k_{m+n})[a_{|m-n|} - a_{m+n}$$

$$+ \frac{4q}{\pi^2 mn}[1-(-1)^m][1-(-1)^n]] \quad \text{where } \delta_m{}^n = 0 \quad \text{if } m \neq n$$

$$\delta_m{}^m = 1 \tag{17}$$

This can be reduced to a single series. The solution for the unknown coefficient a_m is given in Table 5.

The deflections and moments are given in Table 6. They compare well with those in Table 3.

A. J. DURELLI
Professor
Illinois Institute of Technology;
Supervisor, Stress Analysis Section,
Mechanical Engineering Research Department,
Armour Research Foundation,
Chicago, Ill.

J. W. DALLY[1]
Senior Research Engineer,
Mechanical Engineering Research Department
Armour Research Foundation,
Illinois Institute of Technology.
Assoc. Mem. ASME

W. F. RILEY
Research Engineer,
Mechanical Engineering Research Department,
Armour Research Foundation,
Illinois Institute of Technology.

Developments in the Application of the Grid Method to Dynamic Problems

The objective of the research reported in this paper was to develop the grid method further for use in dynamic-stress studies. A rubber-thread grid network in a low-modulus model material (a urethane rubber known as Hysol 8705) was used in conjunction with a microflash light source to record grid distortions and photoelastic fringe patterns in a model subjected to dynamic-loading conditions. By considering a strut subjected to axial impact it was possible to establish that the static and dynamic values of Poisson's ratio were identical, and the strain-fringe value of the material varied with strain rate. In addition, stresses in the axial and transverse directions were determined along the center line of the strut. Finally, the methods established were applied to the problem of a circular disk subjected to diametrical impact and both principal stresses were determined along a vertical diameter at one instant during impact.

THE GRID METHOD of experimental stress analysis is perhaps the simplest and oldest of the experimental methods used in determining stresses. However, to the authors' knowledge, no attempt has been made previously to employ the grid method in a dynamic stress analysis. It is the purpose of this paper to introduce the dynamic grid method and to show its application to two example problems.

A publication by two of the authors[2] presents recent developments in the static application of the grid method. The static application consists essentially of the following:

(*a*) A network of lines (rubber threads) is embedded in the model material.

(*b*) A no-load photograph is taken of the model to record the undeformed state of the grid.

(*c*) A photograph is taken under load to record the deformed state of the grid.

(*d*) The grid-line positions are measured on both load and no-load photographs (to within ± 0.0003 in.).

(*e*) Differences are made between the two sets of measurements to obtain the displacement fields.

(*f*) The displacement fields are differentiated to obtain the strain fields.

(*g*) The strain fields are converted to stress fields by using Hooke's law and suitable values for the elastic constants E (modulus of elasticity) and ν (Poisson's ratio).

The dynamic grid method differs from the static grid method only in steps (*c*) and (*g*). In the dynamic case a photograph is taken over a very short interval of time, i.e., short exposure time, and at a number of different times after the application of the time-dependent load. Also, the variations in the elastic constants E and ν with the rate of load application must be taken into consideration in converting the strain field to the stress field.

In this investigation a low-modulus model material was employed, since the use of a low-modulus model material has two advantages: (*a*) The stresses propagate in the material relatively slowly (about 300 fps); hence the exposure times which were of the order of 2 microsec were for all practical purposes instantaneous. (*b*) The material exhibits relatively large displacements under small loads which is advantageous, since a strain level of at least 1 per cent over a 0.25-in. base is necessary for accurate displacement determinations.

The grid method and the photoelastic method were used together in this investigation with data from one method supplementing data from the other. However, if desired it is possible to employ the grid method as an independent method. The investigation described herein covers the following four phases: (*a*) Experimental procedure; (*b*) material properties; (*c*) application of the method to the determination of the stress distribution in a strut subjected to axial impact; (*d*) application of the method to the determination of the stress distribution in a circular disk subjected to diametrical compression.

Experimental Procedure

To use the grid method, a network of rubber threads is strung upon a frame and the model material, which is transparent, is cast about these threads to produce an embedded grid. The rubber threads which are about 0.004 in. diam when stretched provide clear, well-defined lines on photographs which can be measured accurately. The spacing of the grid depends upon the particular application and can vary up to about 64 per in. In this investigation Hysol 8705, a castable urethane rubber compound, was used as a model material. This material was selected because an earlier investigation[3] showed that it exhibited desirable photoelastic

[1] At present, Assistant Professor, Department of Mechanics and Materials, Cornell University, Ithaca, N. Y.

[2] A. J. Durelli and W. F. Riley, "Developments in the Grid Method of Experimental Stress Analysis," *Proceedings of The Society for Experimental Stress Analysis*, vol. 14, no. 2, 1957, pp. 91–100.

Presented at the West Coast Conference of the Applied Mechanics Division, Stanford, Calif., September 9–11, 1959, of THE AMERICAN SOCIETY OF MECHANICAL ENGINEERS.

Discussion of this paper should be addressed to the Secretary, ASME, 29 West 39th Street, New York, N. Y., and will be accepted until January 10, 1960, for publication at a later date. Discussion received after the closing date will be returned.

Note: Statements and opinions advanced in papers are to be understood as individual expressions of their authors and not those of the Society. Manuscript received by ASME Applied Mechanics Division, August 6, 1958. Paper No. 59—APMW-1.

[3] J. W. Dally, W. F. Riley, and A. J. Durelli, "A Photoelastic Approach to Transient Stress Problems Employing Low-Modulus Materials," this issue of the JOURNAL, pp. 613–620.

properties, had a relatively low modulus, and exhibited a relatively low specific energy loss for the stress ranges under consideration. Also, a great deal of information regarding its material properties under dynamic loading conditions had been established.

In the first attempts to employ the grid method dynamically, the photographs of the grid before and after loading were taken with an 8-mm Fastax camera operating at about 13,000 frames per sec. Measurements on the film indicated that consistent results were not obtainable even when large numbers of measurements and statistical methods were employed. The largest source of error in this evaluation was the poor definition of the grid line under the high magnification of the film (×35) which was necessary to make the measurements. A fine-grain, film-and-developer combination was used but the resolution of the negative was not sufficient.

In order to avoid these high magnifications, a system for recording a much larger image was developed. This system utilized a flash-type light source and an ordinary still camera. The light source employed is commercially known as the "Microflash" and is produced by General Radio Company. The Microflash produces a brilliant blue flash of light which is somewhat less than 2 microsec in duration. This exposure time was short enough in comparison to the velocity of wave propagation to stop the motion of the stress wave effectively; i.e., the stress wave moves approximately 0.007 in. during the exposure time. The image of the model was recorded on a 4 × 5-in. film. This method of photography is limited to a single flash; however, a number of single photographs obtained from reproducible loadings can be time-sequenced to provide information over the entire event. Kodak's Royal-X Pan was the only film suitable for use with the microflash light source, and in general it was slightly underexposed. This conclusion is based on the use of a Cooke Apochromatic Process Lens (30-in. focal length) operated at a maximum aperture of f:16. If a lens with a shorter focal length and a larger aperture had been employed more light would have been available and better exposures would have been obtained.

Since both photoelastic fringe patterns and grid deformations were recorded together in this investigation, it was necessary to pass the microflash light through the elements of the polariscope and a Wratten 77A filter. These elements reduced the amount of light considerably and required the use of the fastest film available. If the grid method had been employed independently, the optical elements could have been removed from the assembly and a slower finer-grain film could have been employed.

The image recorded in the manner described was magnified 20 times and the positions of the grid lines were measured using an optical comparator. In most cases the positions of the grid lines could be measured to within ± 0.0003 in. Measurements were repeated three times and the results were averaged in order to reduce measuring errors. Standards placed in the field with the model were measured to establish the scale of the photograph and to check for film shrinkage and magnification errors between the two films being compared. The limiting factor in the accuracy of the measurements was the grain size of the negative.

Material Properties

In order to employ the grid and photoelastic methods the properties of the model materials had to be determined under various loading rates. A number of these determinations had been made previously by the authors[3] by employing Volterra's and Barton's[4] double-pendulum method of loading to establish modulus of elasticity E, stress fringe value f_σ, and strain fringe value f_ϵ as a function of strain rate. The results of this previous work are shown in Figs. 1 to 3. It is important to note in Figs. 2 and 3 that the solid curves were established using the method of Barton and Volterra mentioned; however, the dashed curves were established using the grid on a strut subjected to axial impact. This problem will be considered in the next section.

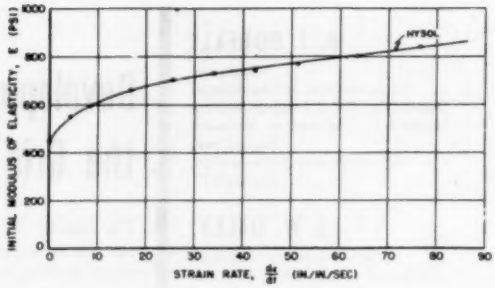

Fig. 1 Initial modulus of elasticity for Hysol 8705 as a function of strain rate

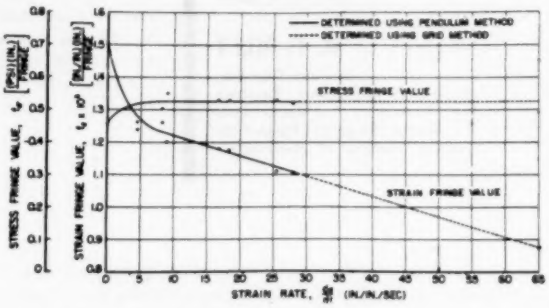

Fig. 2 Material fringe values in terms of stress and strain for Hysol 8705 as a function of strain rate

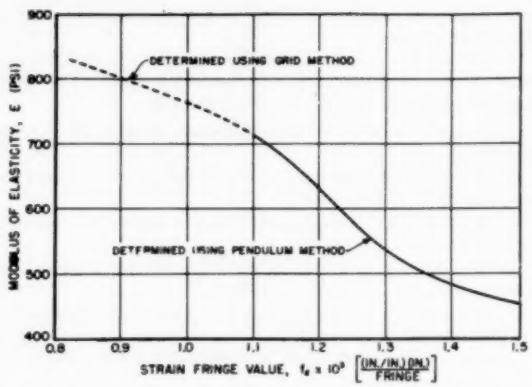
DETERMINED USING GRID METHOD
DETERMINED USING PENDULUM METHOD
MODULUS OF ELASTICITY, E (PSI)
STRAIN FRINGE VALUE, $f_\epsilon \times 10^3$ $\left[\frac{(IN./IN.)(IN.)}{FRINGE}\right]$

Fig. 3 Initial modulus of elasticity as a function of strain fringe value

Material Properties Determined From a Strut Subjected to Axial Impact

A simple strut 0.385 in. thick, 1.25 in. wide, and 7.375 in. long was machined from a sheet of Hysol 8705 with a $^1/_8$-in-square embedded grid. The strut was loaded dynamically by dropping a 216-g weight through a distance of 16 in. on its end. Photographs of the resulting grid deformations and photoelastic fringe patterns were recorded using the microflash light source. Four

[4] E. G. Volterra and C. S. Barton, "An Impact Testing Machine for Plastics and Rubber-Like Materials," *Proceedings of The Society for Experimental Stress Analysis*, vol. 16, no. 1, 1958, pp. 157–166.

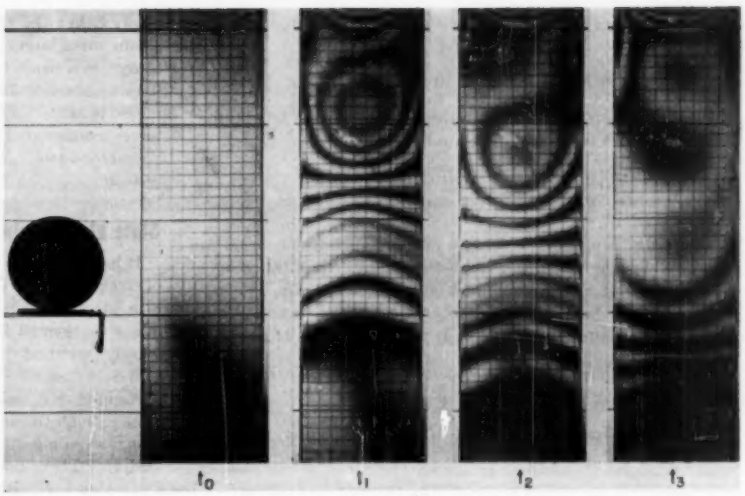

Fig. 4 Microflash photographs taken before impact and 3 times during impact, illustrating combined grid and photoelastic approach to dynamic-stress problem

photographs were taken, one before impact and three others at various times after impact, Fig. 4. It was necessary to repeat the load to obtain the three different photographs after impact.

The positions of the grid lines on the photographs corresponding to times t_0 and t_1 were measured along five vertical lines and a few horizontal lines. The differences between the readings were computed and the values of the displacement along the lines symmetrical in respect to the center line were averaged. The displacement u_x along the three vertical lines A, B, and C is shown in Fig. 5(a). It is noted that the three curves are not identical, contrary to results indicated by elementary theory. Since the differences are too large to be attributed to experimental error, they show the inadequacies of the elementary theory.

The displacement-versus-position curve of Fig. 5(a) were differentiated graphically to obtain the axial strain ϵ_x as shown in Fig. 5(b). An examination of this figure indicates that the strain is uniform across the width of the strut only at a position 2.4 in. from the fixed reference line. At approximately this location transverse displacement measurements were made, Fig. 5(c). Although some scatter of the points occurs, it is evident that a straight line fits most of the points closely. The state of stress here is therefore uniaxial. The slope of the line gives a value for ϵ_y of 0.00978. Reference to Fig 5(b) shows an average value for ϵ_x of -0.0216 at position $x = 2.32$. The dynamic value of Poisson's ratio is therefore given by:

$$\nu = -\epsilon_y/\epsilon_x \tag{1}$$
$$= 0.00978/0.0216 = 0.45$$

The value for ν obtained under static loading conditions was 0.46. The difference between the static and dynamic values of ν is very small and probably can be attributed to experimental error rather than to the rate of loading.

The positions of the fringes shown in Fig. 4 corresponding to a time t_1 approximately 850 microsec after impact are plotted in Fig. 6. The fringe order is not uniform over the cross section of the strut; however, at the afore-mentioned position (2.32 in. from the fixed reference line) the fringe order is nearly constant. By using an average fringe order n of 6.9 and the values previously used for ϵ_x and ϵ_y at this position, it is possible to compute the model and material strain fringe values F_ϵ and f_ϵ, respectively, in the following manner:

$$F_\epsilon = \frac{\epsilon_1 - \epsilon_2}{2n} = -\frac{\epsilon_x - \epsilon_y}{2n} = \frac{0.0216 + 0.00978}{13.8} \tag{2}$$
$$= 2.275 \times 10^{-3} \text{ in/in/fringe}$$

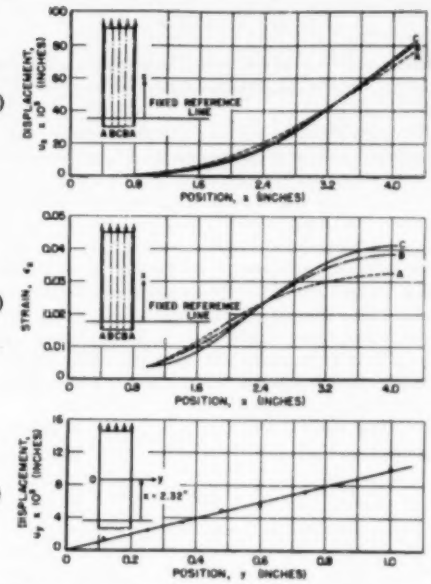

Fig. 5 Axial displacement u_x, axial strain ϵ_x, and transverse displacement u_y as a function of position

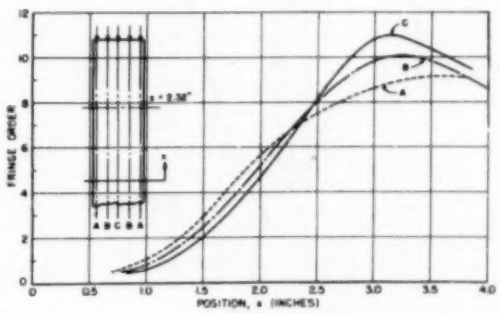

Fig. 6 Position of fringes along vertical lines A, B, and C in strut subjected to axial impact

Since the model thickness h was 0.385 in., the material fringe value f_ϵ is

$$f_\epsilon = F_\epsilon h = 0.875 \times 10^{-3} \text{ in/in-in/fringe} \quad (3)$$

The material fringe value in terms of stress f_σ can be obtained from f_ϵ by use of the following relationship:

$$f_\sigma = \frac{E}{1+\nu} f_\epsilon \quad (4)$$

To employ Equation (4) it is necessary to determine the strain rate at which the value of f_ϵ was established because the value of E used in this expression is a function of the strain rate. In order to determine the strain rate the following method was employed. Substituting Equations (1) and (3) into Equation (2) gives

$$\epsilon_1 = \frac{2}{1+\nu} \frac{f_\epsilon}{h} n \quad (5)$$

Differentiating Equation (5) with respect to time gives an expression for the strain rate:

$$\frac{d\epsilon}{dt} = \frac{2}{1+\nu} \frac{f_\epsilon}{h} \frac{dn}{dt} \quad (6)$$

The strain rate $(d\epsilon)/(dt)$ depends therefore upon the fringe rate $(dn)/(dt)$ at the point and the time at which the determination of f_ϵ was made.

To determine the quantity $(dn)/(dt)$ at the position $x = 2.32$ in., an experiment was conducted using the Fastax camera to record the propagation of the fringe pattern in a similar strut. The loading was identical to that used in the grid experiments. From the film record of the fringe motion a graph of fringe order versus time at the particular position was constructed as is illus rated in Fig. 7. The slope of this curve at the position $x = 2.32$ where the 6.9 fringe order occurs provides a value of $(dn)/(dt) = 20{,}850$ fringes per sec. Substitution of this value of $(dn)/(dt)$ together with previously listed values of ν, h, and f_ϵ into Equation (6) gives a value of 65 in/in/sec for $(d\epsilon)/(dt)$. To obtain E fo use in Equation (4) reference is made to Fig. 1 which shows that E is about 810 psi for this strain rate.

Substituting this value of E into Equation (4) gave a value of 0.49 psi-in/fringe for f_σ. This value when plotted in Fig. 2 showed that the change in f_σ with strain rate was negligible for strain rates larger than about 8 in/in/sec. From a strain rate of zero to a strain rate of 8 in/in/sec the value of f_σ increases from 0.45 to about 0.52 psi-in/fringe (about 15 per cent). This increase is somewhat larger than the experimental error which may have accumulated in the determinations of f_σ, and is substantiated by seven different determinations of f_σ in the neighborhood of 0.50.

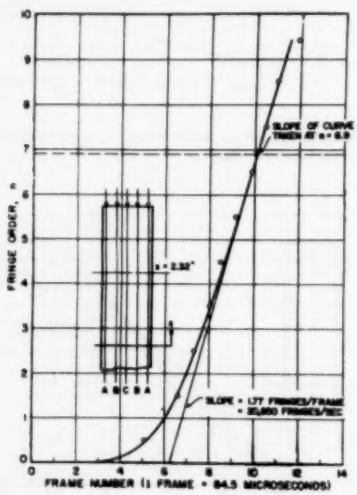

Fig. 7 Fringe order as a function of time at position $x = 2.32$ in. on strut subjected to axial impact. Fastax camera operating at 11,820 frames per sec.

State of Stress in Strut

It has been shown that for Hysol 8705, ν is totally independent of strain rate, f_σ is essentially independent of strain rate if $d\epsilon/dt > 8$ in/in/sec, and both E and f_ϵ are dependent upon strain rate. These facts must be kept in mind, in the following development where a method for separating the stresses in a strut subjected to axial impact is established.

Assume that the outermost vertical grid line A in the strut is close enough to the free boundary so that the stresses and strains along this line are identical to the boundary stresses and strains. Then, the following relations hold:

$$\sigma_y = 0$$
$$\sigma_x = 2nF_\sigma \quad (7)$$

where n is measured along line A.

The values obtained for σ_x are given in Fig. 8. The axial strain

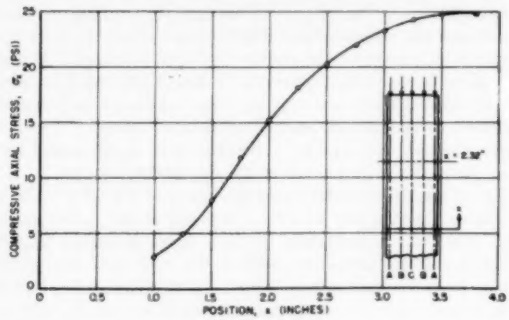

Fig. 8 Compressive axial stress as a function of position along line A approximately 850 microsec after impact

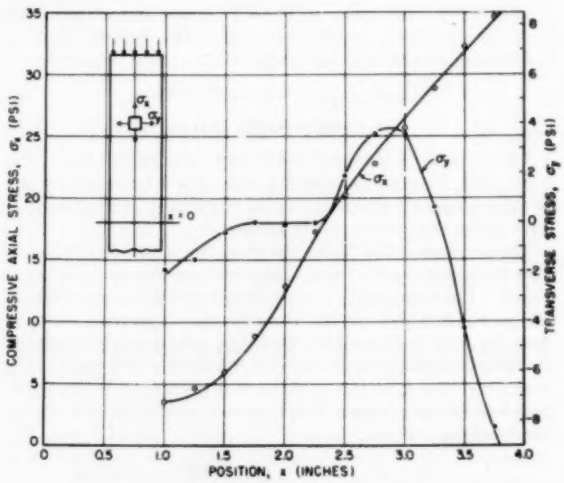

Fig. 9 Axial and transverse stresses σ_x and σ_y as a function of position along center line of strut approximately 850 microsec after impact

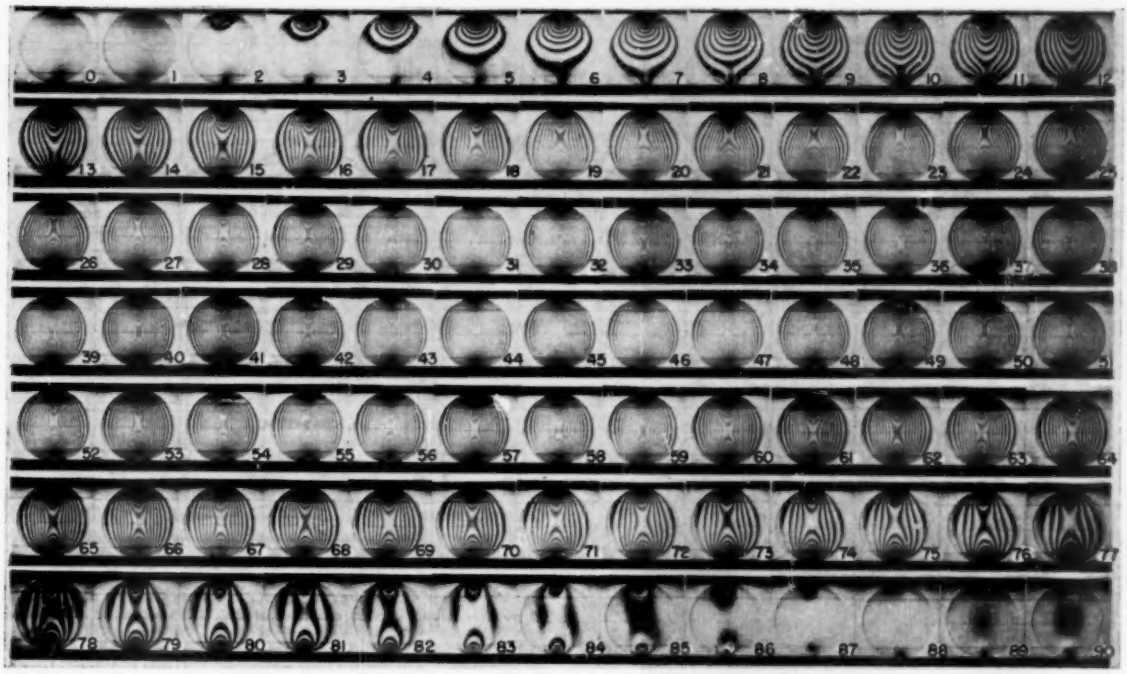

Fig. 10 Complete set of photoelastic fringe patterns produced by dropping a 216-g weight from height of 3 in. on a 3-in-diam disk of Hysol 8705. Photographs were taken with a Fastax camera operating at 6720 frames per sec.

ϵ_x along this line has been established previously, Fig. 5(*b*). Since the stress is uniaxial along this line the transverse strain ϵ_y is given by Equation (1).

Attention was then turned to the center line of the strut where ϵ_x had previously been determined, Fig. 5(*b*). The transverse strain ϵ_y was computed from the strain optic law Equations (2) and (3) as indicated in the following:

$$\epsilon_y = \epsilon_x + \frac{2nf_\epsilon}{h} \tag{8}$$

where ϵ_x and n were determined along the center line, and f_ϵ was determined along the free boundary from Equation (5).

Using a value of f_ϵ from the boundary implies that the strain rate was uniform across a section of the strut. This assumption is justified because slight changes in strain rate which probably occur produce very small changes in f_ϵ.

The transverse stress σ_y was computed using Hooke's law

$$\sigma_y = \frac{E}{1 - \nu^2}[\epsilon_y + \nu\epsilon_x] \tag{9}$$

where ϵ_x was obtained by direct grid measurements, ϵ_y was computed from Equation (8), and E was assumed to be uniform across the strut and was determined at the free boundary from f_ϵ and the results of Fig. 3.

The use of E as described, again assumes that the influence of strain-rate changes across the section on the value of E will be small. For instance, if the strain rate varies from 20 to 30 in/in/sec, E will vary from 680 to 720 psi, a change of only 6 per cent.

It would have been possible to solve this problem without making assumptions regarding the uniformity of E and f_ϵ across a section of the strut if a series of strain determinations were made at different times after impact. From these determinations it would have been possible to compute the strain rate by finite differences. The work involved in this approach would have been prohibitively long for the slight increases in accuracy which would be gained from the more exact approach.

The axial stress σ_x was computed by using the stress optic law

$$\sigma_x = \sigma_y - \frac{2nf_\sigma}{h} \tag{10}$$

Both σ_x and σ_y are shown as a function of position in Fig. 9. It is clear from an examination of this figure that a uniaxial state of stress does not exist at each point along the center line of the strut. Between positions x equal 1 and 1.5 the transverse stress σ_y was negative. This negative stress is believed to be due to the transverse inertia effects produced by dynamic loading of the strut. Between positions x equal 1.5 and 2.4 the transverse stress is negligible and essentially a uniaxial state of stress exists in this region. (It is here that the determination of ν and f_ϵ was made.) From position x equal 2.4 to 3.8 the behavior of σ_y is difficult to explain. Perhaps the large values of σ_y noted were due to the influence of shearing tractions at the interface between the model and the impacting weight. This traction would result from the frictional constraint at the interface due to the transverse displacement produced by the impact.

Although the grid method as applied in this case permitted the accurate determination of the axial strain ϵ_x, it could give only average values of the transverse strain ϵ_y. In order to obtain ϵ_y at each point, Equation (8) was used. If the grid network had been finer and if the transverse strain had been somewhat larger in magnitude, the grid measurements would have been sufficiently accurate to indicate the changes in ϵ_y across the section of the strut.

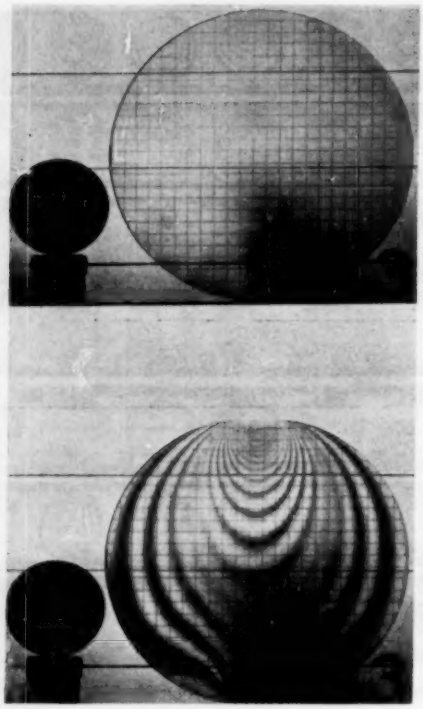

Fig. 11 Microflash photographs of Hysol 8705 circular disk before loading and at 1635 microsec after impact

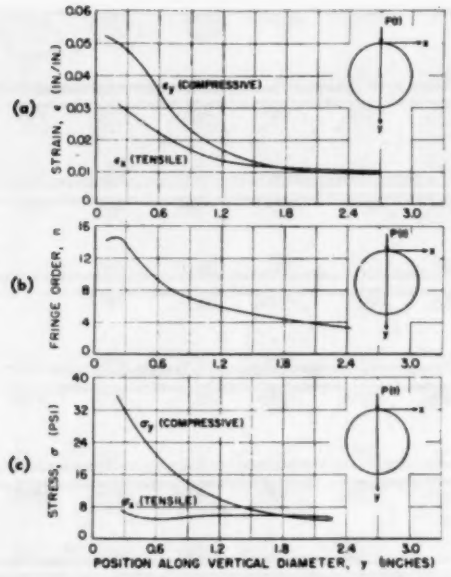

Fig. 12 Strains ϵ_x, ϵ_y; stresses σ_x, σ_y; and fringe order n as a function of position along vertical diameter of disk 1635 microsec after impact

Application of the Grid Method to Problem of Stress Distribution in a Circular Disk Subjected to Diametrical Impact

Experimental Procedure. A circular disk 3 in. diam was machined from a 0.385-in-thick sheet of Hysol 8705 which had an embedded grid with $^1/_8$-in. spacing. The disk was subjected to diametrical impact by dropping a 216-g weight a height of 3 in. on the model. A complete record of the resulting fringe pattern was obtained with a 16-mm Fastax camera as is illustrated in Fig. 10. In addition, the loading was repeated and a number of microflash photographs were taken at various intervals during the initial period when the fringe pattern propagated across the disk. Two of these photographs are shown in Fig. 11.

Analysis. Grid measurements were made along the vertical diameter and along nine horizontal grid lines passing through the vertical diameter. Displacement curves were plotted from these grid measurements and graphically differentiated to obtain the strain ϵ_x and ϵ_y along the vertical diameter. These results are shown in Fig. 12(*a*). The position of the fringes along the vertical diameter were measured and recorded in Fig. 12(*b*).

From the values of the fringe order and strains it was possible to determine f_σ at each point along the vertical diameter by employing Equations (2) and (3). The value of E at each point was then taken from the curve in Fig. 3 where E is plotted as a function of f_σ. The values of E, ν, ϵ_x, and ϵ_y were then substituted into Equation (9) to obtain results for σ_x and σ_y given in Fig. 12(*c*). If necessary, it would be possible to duplicate each of the 90 Fastax photographs shown in Fig. 10 with a microflash photograph and determine stresses and strains as a function of time as well as position.

In order to shorten the time required for the strain determinations to a reasonable limit, an attempt should be made to apply the Moire method[5] to the dynamic problem. This method differs from the grid method in that the field of the model is covered with thin closely spaced lines (several hundred lines per inch) and when the model is deformed fringes are produced related directly to the displacement field. This eliminates the time-consuming operation of measuring each grid line before and after application of the load.

Acknowledgment

This research was supported in part by the United States Air Force under Contract No. AF18(603)-144, monitored by the AF Office of Scientific Research of the Air Research and Development Command.

[5] P. Dantu, "Utilisation des Reseaux pour l'Etude des Deformations," Publication No. 57-6, Laboratoire Central des Ponts et Chaussées, Paris, France, 1957.

J. H. SHIELDS
Project Engineer,
Engineering Service Division,
Computer Engineering Associates, Inc.,
Pasadena, Calif.

R. H. MacNEAL
Manager,
Engineering Service Division,
Computer Engineering Associates, Inc.,
Pasadena, Calif.

The Solution of Elastic Stability Problems With the Electric Analog Computer

An application of electric analog computing methods to the analysis of elastic stability problems is described. An electrical circuit is first devised which satisfies a general differential equation that is frequently encountered in the literature of elastic stability. This circuit, composed of inductors, capacitors, transformers, and current generators, is then used to obtain solutions for several classical column, framework, and plate-stability problems.

PROBLEMS which involve the lateral deflections of beams can be analyzed successfully by using electrical circuits as analogies. Thus, in recent years, various electrical beam analogies have been devised and have been widely used in the static and dynamic analysis of airframes, missiles, and ships. These analogies arise from a similarity in form between the equations which describe the behavior of elastic structures and the equations which relate currents and voltages in electrical networks.

In the present paper, an electrical analogy that can be used in the analysis of classical elastic stability problems is obtained by modifying conventional electrical beam analogies [1, 2, 3][1] to allow inclusion of axial load effects. The resulting electrical circuit, composed of inductors, capacitors, transformers, and current generators, is then used to obtain buckling loads for several types of elastic structures including columns, frames, and rectangular plates. It is believed that the techniques described in this paper can be readily extended to obtain solutions to many other elastic stability problems.

Derivation of the General Electrical Analogy

Many problems in the classical theory of elastic stability satisfy differential equations which have the following general form:

$$(Aw'')'' - [(a - bN_x)w']' + (c - dN_x)w = q \qquad (1)$$

where w is a lateral displacement, q is a lateral load, N_x is an axial load, and the coefficients A, a, b, c, and d are normally positive. Equation (1) is a linear, inhomogeneous differential equation of fourth order, for which an electrical circuit analogy is desired. It is convenient to write this fourth-order differential equation as four first-order differential equations and then to devise an electrical circuit which will approximately satisfy each of the four first-order differential equations. One way to accomplish this is to define slopes and moments as follows:

$$\theta = w' = \frac{dw}{dx} \qquad (2a)$$

$$M = Aw'' = A\theta' = A\frac{d\theta}{dx} \qquad (2b)$$

If one further defines the "shear" as

$$V = -[M' - (a - bN_x)\theta] \qquad (2c)$$

then Equations (1) and (2c) combine to give the fourth required first-order equation

$$\frac{dV}{dx} = (c - dN_x)w - q \qquad (2d)$$

The four first-order differential equations, (2*a*), (2*b*), (2*c*), and (2*d*), which can be recombined readily to give Equation (1), are replaced by a set of four finite-difference equations. It is convenient to use the technique used in [1] and to define quantities at equally spaced intervals as shown in Fig. 1(*a*). Thus, angular rotations and shears are defined at half-integer points, while lateral deflections and moments are defined at integer points. The four finite-difference equations can then be written in central difference form as

$$\theta_{n+1/2} = \frac{w_{n+1} - w_n}{\Delta x} \qquad (3a)$$

$$M_n = A\left(\frac{\theta_{n+1/2} - \theta_{n-1/2}}{\Delta x}\right) \qquad (3b)$$

$$V_{n+1/2} = (a - bN_x)\theta_{n+1/2} - \left(\frac{M_{n+1} - M_n}{\Delta x}\right) \qquad (3c)$$

$$\left(\frac{V_{n+1/2} - V_{n-1/2}}{\Delta x}\right) = (c - dN_x)w_n - q \qquad (3d)$$

An electrical circuit which satisfies the four first-order finite-difference differential equations (3*a*), (3*b*), (3*c*), and (3*d*), is shown in Fig. 1(*b*). The current-voltage relationships involved in this circuit can be summarized as follows:

$$E_{\theta_{n+1/2}} = \frac{E_{w_{n+1}} - E_{w_n}}{\Delta x} \qquad (4a)$$

$$i_{M_n} = \frac{1}{j\omega L_3}(E_{\theta_{n+1/2}} - E_{\theta_{n-1/2}}) \qquad (4b)$$

$$(i_{V_{n+1/2}})(\Delta x) = \left(\frac{1}{j\omega L_1} + j\omega C_1\right)E_{\theta_{n+1/2}} - (i_{M_{n+1}} - i_{M_n}) \qquad (4c)$$

$$i_{V_{n+1/2}} - i_{V_{n-1/2}} = \left(\frac{1}{j\omega L_2} + j\omega C_2\right)E_{w_n} - i_n \qquad (4d)$$

Thus Equation (4*a*) merely expresses the voltage relationship

[1] Numbers in brackets designate References at end of paper.

Presented at the West Coast Conference of the Applied Mechanics Division, Stanford, Calif., September 9–11, 1959, of THE AMERICAN SOCIETY OF MECHANICAL ENGINEERS.

Discussion of this paper should be addressed to the Secretary, ASME, 29 West 39th Street, New York, N. Y., and will be accepted until January 10, 1960, for publication at a later date. Discussion received after the closing date will be returned.

NOTE: Statements and opinions advanced in papers are to be understood as individual expressions of their authors and not those of the Society. Manuscript received by ASME Applied Mechanics Division, August 15, 1958. Paper No. 59—APMW-20.

existing across the primary and secondary windings of an ideal transformer. Equation (4*b*) expresses the voltage-current relationship existing across an inductive-circuit element. Equations (4*c*) and (4*d*) are statements of Kirchhoff's current law for currents into nodes $E_{\theta_{n+1/2}}$ and E_{w_n}, respectively. If voltages and currents are identified in the electrical circuit with deflections and forces in the mechanical system as follows:

$$\theta_i = \frac{1}{j\omega} E_{\theta_i}$$

$$w_i = \frac{1}{j\omega} E_{w_i}$$

$$V_i = i_{V_i}$$

$$M_i = i_{M_i}$$

$$q\Delta x_i = i_i$$

then

$$\theta_{n+1/2} = \frac{w_{n+1} - w_n}{\Delta x} \tag{5a}$$

$$M_n = \frac{1}{L_3} (\theta_{n+1/2} - \theta_{n-1/2}) \tag{5b}$$

$$V_{n+1/2} = \left(\frac{1}{L_1 \Delta x} - \frac{\omega^2 C_1}{\Delta x}\right) \theta_{n+1/2} - \left(\frac{M_{n+1} - M_n}{\Delta x}\right) \tag{5c}$$

$$\frac{V_{n+1/2} - V_{n-1/2}}{\Delta x} = \left(\frac{1}{L_2 \Delta x} - \frac{\omega^2 C_2}{\Delta x}\right) w_n - q \tag{5d}$$

Equations (5*a*) through (5*d*) are identical to Equations (3*a*) through (3*d*) if electrical inductors and capacitors are chosen as follows:

$$L_1 = \frac{1}{a\Delta x} \qquad C_1 = \frac{bN_x \Delta x}{\omega^2}$$

$$L_2 = \frac{1}{c\Delta x} \qquad C_2 = \frac{dN_x \Delta x}{\omega^2}$$

$$L_3 = \frac{\Delta x}{A}$$

Details of the Electrical Analogy

Having obtained an electrical circuit which is analogous to a simple structural element, one can connect several such circuits together to form an analogy for a complete structure. However, before using the electrical circuit to solve any specific problem, it is important to point out a few of the techniques which are commonly used in connection with the direct analog computer and their relationships to the physical systems analyzed:

1 Lumping. In order to represent a continuous elastic system as an electrical circuit, it is necessary to lump the continuous elastic properties of the structure into discrete units. Thus, for example, the magnitude of the electrical circuit element L_3 of Fig. 1(*b*) is made equal to $\Delta x/A$. The inductor L_3 is therefore used to represent, as a single entity, the bending flexibility of a finite segment of beam.

2 Symmetry. If a structure is symmetrical, advantage can be taken of its symmetry properties in order to minimize the number of computer elements required to represent the structure. Symmetry conditions are replaced by boundary conditions for one half of the structure in the plane of symmetry.

3 Boundary Conditions. The three principal boundary conditions which arise in solving the buckling problems that follow are:

(*a*) The structure is hinged (the deflection w and the bending moment M are zero at the boundary).

(*b*) The structure is clamped (the deflection w and the slope θ are zero at the boundary).

(*c*) The structure is free (the shear V and the bending moment M are zero at the boundary).[2]

In the electrical analogy, to set a co-ordinate such as θ_i or w_i to zero, the point which corresponds to that θ_i or w_i is grounded; to set a shear V_i or moment M_i to zero, the element which corresponds to that specific V_i or M_i is open-circuited.

The boundary conditions which apply at a plane of symmetry will be discussed as the need arises.

4 Eigenvalues. As is well known, the determination of a buckling or crippling load is an eigenvalue problem. There are several critical loads N_x, which give nontrivial solutions of Equa-

[2] These conditions are not correct for the free edge of a buckled plate, as is explained later in this paper.

(*a*) BEAM SEGMENT

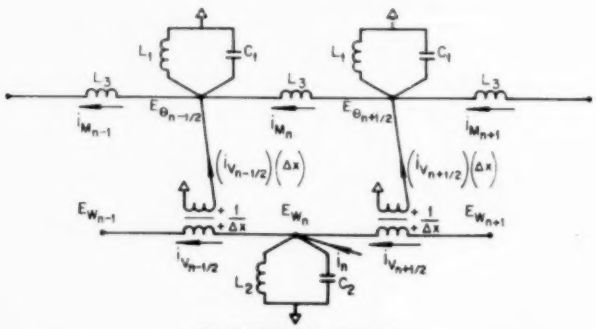

(*b*) ELECTRICAL ANALOG

Fig. 1 Finite-difference beam analogy

tion (1) with $q = 0$ and which satisfy the specified boundary conditions. However, in general, only the first critical buckling, or crippling, load is of interest since at this load the physical structure fails. Since the analogous electrical circuit has been shown to satisfy the same differential equation as its mechanical counterpart, the electrical circuit will have resonant frequencies that correspond to the eigenvalues of the elastic system. To obtain the buckling loads for a given structure with the aid of the electrical analogy introduced in this paper, the analogous electrical circuit is driven with a variable-frequency voltage source, attached to the circuit at a point where the expected amplitude of motion is large. As the frequency of this driving voltage is varied, frequencies will be found at which the current inserted into the circuit by the voltage source is zero. With the electrical frequencies and appropriate capacitor values (C_1 or C_2) known, the critical load is obtained from the following relationship:

$$N_x = \frac{\omega^2 C_1}{b\,\Delta x} = \frac{\omega^2 C_2}{d\,\Delta x} \tag{6}$$

Higher eigenvalues as well as the lowest, or critical, eigenvalue can be obtained in this way.

Specific Applications of the Electrical Analogy

1 Buckling of a Column With Hinged Ends. In all cases considered in this paper, the weight of the column will be considered negligible in comparison with the load it supports. In addition, the column will be assumed to be of homogeneous material, of uniform cross section, and subjected to axial loads only. Under these assumptions, the differential equation of the column deflection is simply

$$\frac{d}{dx}\left(EI\,\frac{d^2w}{dx^2}\right) + N_x\,\frac{dw}{dx} = \text{const}$$

or

$$(EIw'')'' + (N_x w')' = 0$$

This equation is identical to Equation (1) with

$$A = EI$$

$$a = c = d = q = 0$$

$$b = 1$$

A column under axial load can therefore be represented by an electrical analog of the specific form shown in Fig. 2(*b*). Only half of an 11-cell column representation has been used in the analogy since the column will buckle first in a manner which is symmetric about a plane drawn perpendicular to the x-axis at $x = l/2$. The boundary conditions at the plane of symmetry are simply that the slope θ is zero and that the shear V is zero. Since the column is hinged at each end, the point in the electrical circuit corresponding in the w-deflection at $x = 0$ is grounded, and the inductor corresponding to the bending flexibility of the segment closest to the hinge is open-circuited. Note that the transformers are superfluous in this circuit since no current can flow in them; i.e., the primaries of the transformers are open-circuited at $x = l/2$. To verify the electrical circuit the critical load N_x was calculated from the following equation, assuming $EI = 15 \times 10^6$ and $l = 110$ in.:

$$N_x\ (\text{critical}) = \frac{\pi^2 EI}{l^2} = 1.22 \times 10^4\ \text{lb}$$

The critical load obtained from the computer by varying the frequency of the exciting force was found from Equation (6) to be

$$N_x(\text{critical}) = 1.21 \times 10^4\ \text{lb}$$

2 Buckling of a Column With Clamped Ends. This problem is identical with that involving a hinged column except for different boundary conditions at the ends. Thus, in the electrical analogy, Fig. 2(*b*), the point in the electrical circuit corresponding to θ at $x = 0$ is grounded. The critical load was calculated from the following equation, assuming $EI = 15 \times 10^6$ and $l = 110$ in.:

$$N_x\ (\text{critical}) = \frac{4\pi^2 EI}{l^2} = 4.89 \times 10^4\ \text{lb}$$

The critical load obtained from the computer by varying the frequency of the exciting force was calculated from Equation (6) as

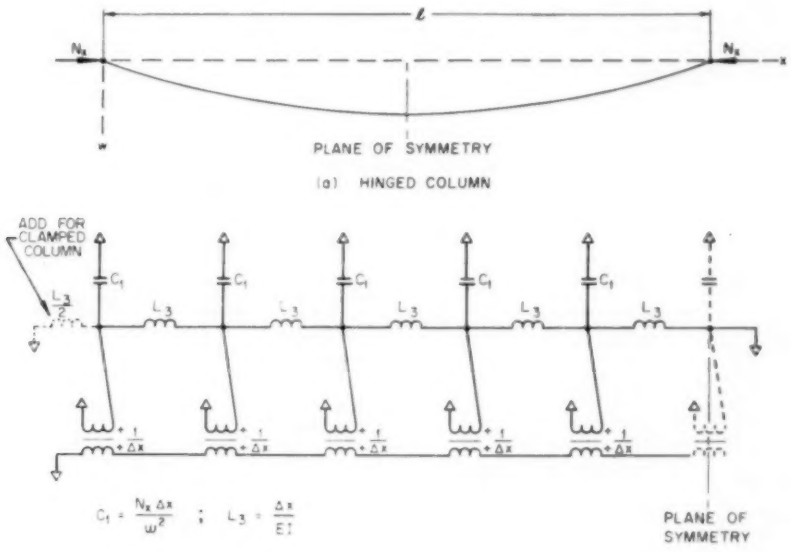

Fig. 2 Circuit used to represent hinged column

$$N_x(\text{critical}) = 4.82 \times 10^4 \text{ lb}$$

3 Buckling of a Simple Frame. The analysis of a three-member frame structure was next performed. In Fig. 3(*a*), a sketch has been drawn showing the first buckling shape assumed by the three-member frame under the action of compressive forces applied to a hinged member *AB* and a clamped member *CD* which are elastically coupled by means of a third member *BC*. The differential equation which describes the bending of *AB* or *CD* is identical with that used under items 1 and 2 and, therefore, the circuit representation of each column, Fig. 3(*b*), is the same as that previously used, Fig. 2(*b*). Note that the transformers are not superfluous in this circuit since a closed path exists in which the currents, corresponding to shear in the vertical members, can flow.

Elastic coupling between the two upright columns is provided by a simple beam which is not subjected to axial load. The electrical analogy for this beam is derived in references [3] and [4]. Since in small-deflection theory the lateral deflection of the horizontal member at the end of the two uprights must be zero, the primary of one of the transformers representing the cross member *BC* is grounded at both ends. This means that in Fig. 3(*b*) the transformer shown in dashed lines need not appear.

Several variations were made in this problem, the results of which are listed in Table 1. For all cases the members labeled *AB* and *CD* in Fig. 3(*a*) were considered to have identical physical properties although allowed different boundary conditions. The effects of variations in the bending stiffness of the coupling member, *BC*, were studied and the results are presented graphically in Fig. 4. It is interesting to note that the effectiveness of the transverse member increases rapidly for small *EI*. The deflection shape shown in Fig. 3(*a*) was obtained from the computer and corresponds to the case where all three members have equal stiffness.

4 Buckling of a Beam on an Elastic Foundation. The next problem considered was the buckling of a uniform beam with hinged ends, supported along its entire length by a uniform elastic foundation, Fig. 5(*a*). The differential equation governing the deflection of this beam is

$$(EIw'')'' + (N_x w')' + \beta w = 0$$

where βw is the magnitude of the reaction of the foundation per unit length. This differential equation is identical to Equation (1) with

$$A = EI$$
$$a = d = q = 0$$
$$b = 1$$
$$c = \beta$$

By reason of symmetry only half of an 11-cell beam representation, Fig. 5(*b*), has been used to study the buckling loads of the

Table 1 Buckling loads for three-member frame. l = 50 in.

Boundary Conditions	$(EI)_{AB} = (EI)_{CD}$, lb-in^2	$(EI)_{BC}$, lb-in^2	Critical Load, 10^4 lb	
			Theoretical	Computer
Columns AB and CD Hinged	10×10^6	∞	.987	.986
	10×10^6	10×10^6	.728	.725
Columns AB and CD Built-in	10×10^6	∞	3.95	3.79
	10×10^6	0	.987	.986
Column AB Hinged Column CD Built-in	10×10^6	0	- - -	.545
	10×10^6	1.0×10^6	- - -	.842
	10×10^6	2.5×10^6	- - -	1.14
	10×10^6	5.0×10^6	- - -	1.43
	10×10^6	$10. \times 10^6$	- - -	1.71
	10×10^6	$20. \times 10^6$	- - -	1.94
	10×10^6	∞	- - -	2.33

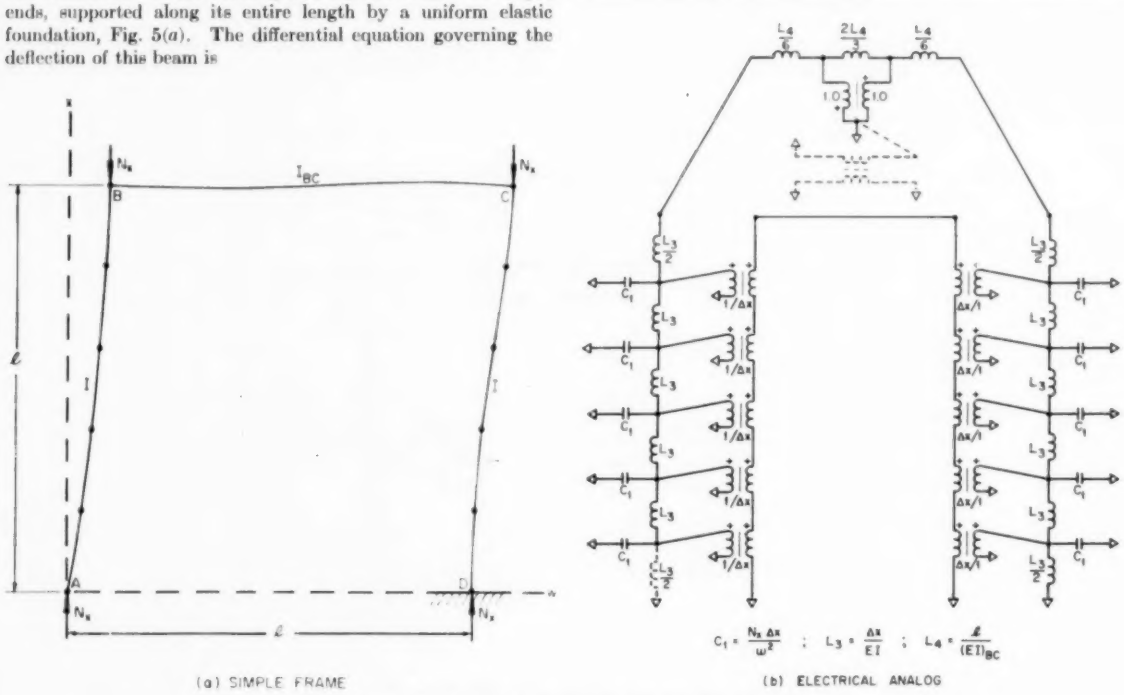

(a) SIMPLE FRAME (b) ELECTRICAL ANALOG

Fig. 3 Circuit used to represent three-member frame

Table 2 Buckling loads for a hinged beam on electric foundation

β, lb/in^2	L/ℓ	Critical Load N_x, 10^4 lb	
		Theoretical	Computer
0	1.00	1.22	1.21
4.92	.819	1.82	1.82
8.20	.741	2.23	2.19
16.39	.615	3.23	3.21

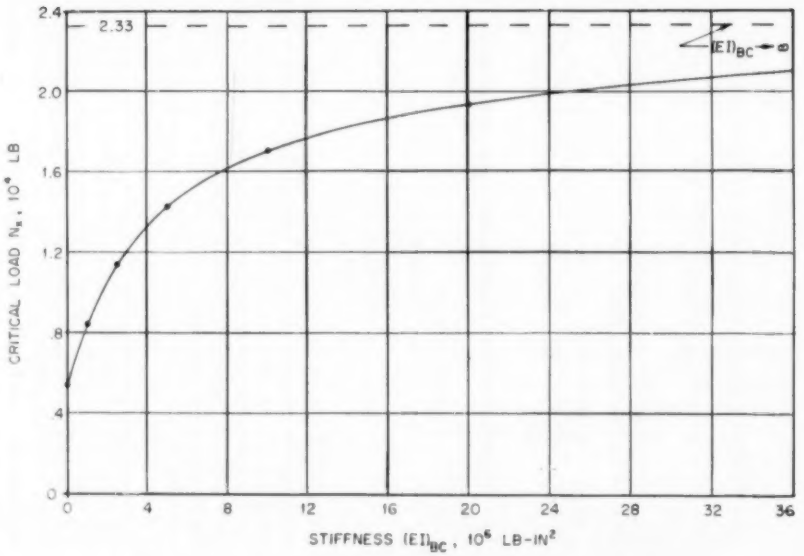

Fig. 4 Critical load versus stiffness of beam BC in three-member frame

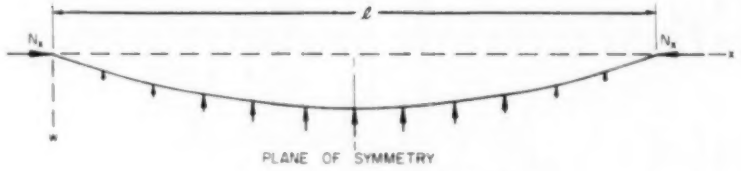

(a) HINGED COLUMN ON AN ELASTIC FOUNDATION

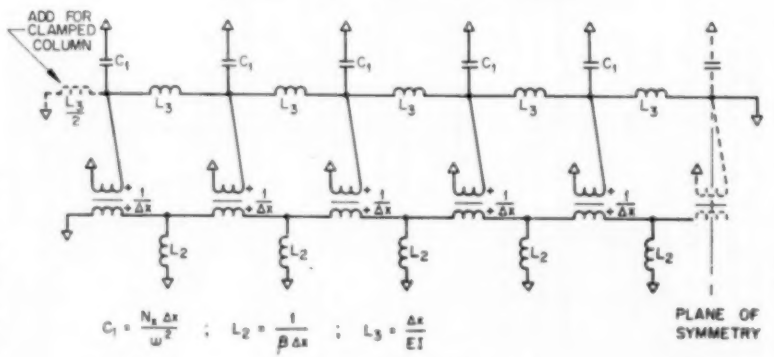

(b) ELECTRICAL ANALOG

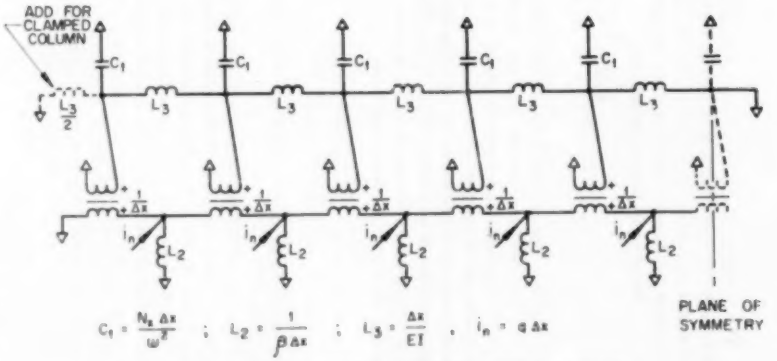
ADD FOR CLAMPED COLUMN
C_1
L_3
$\frac{L_3}{2}$
$\frac{1}{\Delta x}$
i_n
L_2
PLANE OF SYMMETRY
$C_1 = \frac{N_x \Delta x}{\omega^2}$; $L_2 = \frac{1}{\beta \Delta x}$; $L_3 = \frac{\Delta x}{EI}$, $i_n = q \Delta x$

(c) ELECTRICAL ANALOG INCLUDING LATERAL LOADING

Fig. 5 Circuit used to represent hinged column on elastic foundation

system. The buckling of a uniform beam resting upon an elastic foundation under the action of a compressive load has been fully discussed elsewhere,[3] where it is shown that the buckling load is dependent upon a reduced length L instead of the actual length l of the beam. In terms of this reduced length L,

$$N_x \text{ (critical)} = \frac{\pi^2 EI}{L^2} \tag{7}$$

Table 2 shows a comparison between the buckling loads obtained from the electrical circuit and the theoretical results obtained from Equation (7) for several values of β.

For problems in which the beam is laterally loaded, the deflections and internal forces below the buckling limit are obtained by using the circuit shown in Fig. 5(*c*). Thus lateral loads are inserted as currents into the circuit at the w-nodes, while capacitors placed in the slope circuit are defined as

$$C_1 = \frac{N_x \Delta x}{\omega^2} \tag{8}$$

where N_x is now merely the value of the axial load and need not be an eigenvalue.

A small number of representative analog-computer results for the bending of a beam on an elastic foundation under lateral loads alone are shown in Table 3. Also presented are some analog-computer results for the bending of a beam subjected to both lateral and compressional loads with β equal to zero. Thus, the electrical circuit used to obtain buckling loads can be adapted quite readily to obtain the deflections and internal forces existing in an elastic structure subjected to compressional as well as lateral loads. The physical constants assumed for each system were $EI = 15 \times 10^6$ psi, $q = 10$ lb per in., $l = 110$ in., and N_x (where applicable) = 6000 lb.

5 Buckling of a Flat Plate. The next problem considered was that of a uniformly compressed rectangular plate, simply supported along two opposite sides perpendicular to the direction of compression, but having various edge conditions along the other two sides, Fig. 6. The differential equation that describes the deflection of this uniform plate is

$$\frac{\partial^4 w}{\partial x^4} + 2\frac{\partial^4 w}{dx^2 dy^2} + \frac{\partial^4 w}{dy^4} = -\frac{N_x}{D}\frac{\partial^2 w}{dx^2} \tag{9}$$

If it is assumed that, under the action of compressive forces N_x the plate buckles into m sinusoidal half-waves and that the fourth-order differential equation is satisfied by a solution of the form

$$w = f(y) \sin \frac{m\pi x}{p} \tag{10}$$

$f(y)$ is a function of y alone, the following differential equation is obtained for determining $f(y)$:

$$D\frac{d^4 f(y)}{dy^4} - \frac{2m^2\pi^2 D}{p^2}\frac{d^2 f(y)}{dy^2} + \left[\frac{m^4\pi^4 D}{p^4} - N_x\frac{m^2\pi^2}{p^2}\right] f(y) = 0 \tag{11}$$

This differential equation is of the same form as Equation (1) with

$$\begin{aligned} A &= D \\ a &= 2m^2\pi^2 D/p^2 \\ b &= q = 0 \\ c &= m^4\pi^4 D/p^4 \\ d &= m^2\pi^2/p^2 \end{aligned}$$

It is therefore possible to find the buckling loads of such a rectangular plate by using the general electrical analogy derived in this paper. If one considers the specific case where both sides $y = 0$ and $y = k$ are built in, then the first buckling mode is symmetrical about $y = k/2$. Critical loads were obtained with these boundary conditions for several ratios of p/k assuming $D = 333.3$ in-lb, $\nu = 0.25$, and $p = 28$ in. The circuit used to represent the plate is shown in Fig. 6(*b*). The critical loads obtained from the computer have been plotted against the ratio of p/k in Fig. 7, for the case where $m = 1$; i.e., for the case where the plate buckles into only one half-wave. As the value of p increases (for a given k), the critical load decreases, reaches a minimum, and then increases. At $p/k = 1.0$, the critical load for $m = 1$ is larger than the critical load for $m = 2$ and for this ratio of p/k the plate will, therefore, not buckle into one half-wave but into two half-waves.

6 Buckling of a Simple Angle. The last problem that was investigated is an extension of the previous one. In the case of a simple angle, the free longitudinal edges of the angle buckle while the side AB, Fig. 8, remains straight. The edge conditions along AB are that the deflection is zero (in all directions) and that the bending moment is continuous. The circuit used to represent the angle is therefore quite similar to that used to simulate a single rectangular plate. The representation chosen was a finite-difference circuit having a maximum of 6 cells per side. The electrical circuit shown in Fig. 8 illustrates the electrical representation for the case in which the width of one side of the angle was double the width of the other side. It was assumed that $D =$

[3] Reference [5], p. 108.

Table 3 Results of computer analysis of beams subjected to lateral and compressional loading

Descriptive Title	Boundary Conditions	Quantity Measured	Results	
			Theoretical	Experimental
Uniform Beam on Elastic Foundation Subjected to Lateral Loading: β = 18.5 lb/in./in.	Hinged At x = 0, ℓ: w = 0 M = 0	Deflection at x = 55 in.	.126 in.	.132 in.
		Deflection at x = 30 in.	.311 in.	.330 in.
		Bending Moment at x = 55 in.	4,240 in-lb	4,330 in-lb
Uniform Beam Subjected to Lateral and Compressional Loading: β = 0	Hinged At x = 0, ℓ: w = 0 M = 0	Deflection at x = 55 in.	2.50 in.	2.45 in.
		Deflection at x = 30 in.	1.99 in.	1.97 in.
		Bending Moment at x = 55 in.	30,100 in-lb	29,200 in-lb
Uniform Beam Subjected to Compressional Loading with Equal Bending Moments Applied at the Two Ends: β = 0	At x = 0, ℓ: w = 0 M = 11,000 in-lb	Deflection at x = 55 in.	2.10 in.	2.10 in.
		Deflection at x = 30 in.	1.71 in.	1.65 in.
		Bending Moment at x = 55 in.	24,200 in-lb	23,000 in-lb

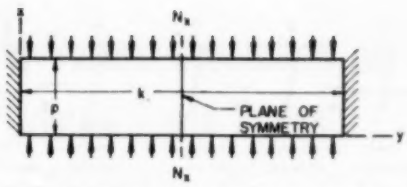

(a) RECTANGULAR PLATE: SIMPLY SUPPORTED AT x = 0 AND x = p, BUILT-IN AT y = 0 AND y = k

Fig. 6 Circuit used to represent rectangular plate

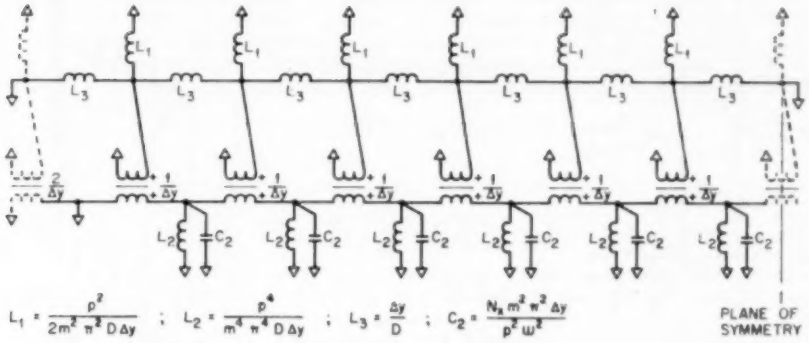

(b) ELECTRICAL ANALOG

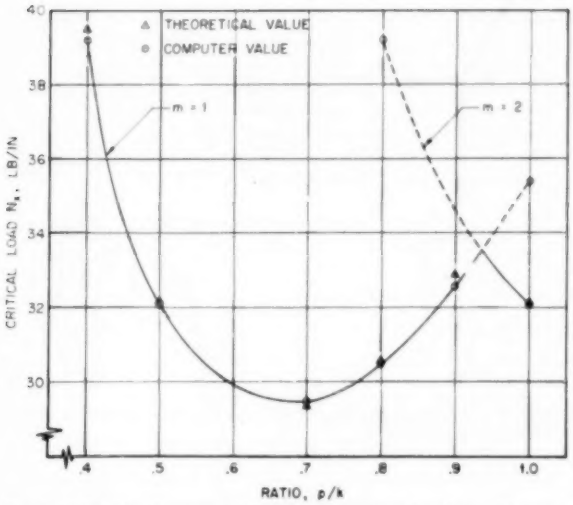

Fig. 7 Critical load versus ratio of p/k for rectangular plate with two clamped edges and two simply supported edges

576 in-lb, $\nu = 0.25$, and $k = 6$ in. The side labeled k' in Fig. 8 was allowed to vary from zero to 6 in. for each of two ratios of p/k. Results of this study are shown in Fig. 9 as a plot of buckling load N_x versus the length of side k'.

As has been noted previously, the boundary conditions at the free edge of a plate are not as simple as the boundary conditions at the free end of a column. The boundary conditions which apply at a free edge can be written as follows:[4]

$$\frac{\partial^2 w}{\partial y^2} + \nu \frac{\partial^2 w}{\partial x^2} = 0 \tag{12}$$

and

$$\frac{\partial^3 w}{\partial y^3} + (2 - \nu) \frac{\partial^3 w}{\partial x^2 \partial y} = 0 \tag{13}$$

[4] See for example, reference [5], p. 338.

If the assumed solution for w, Equation (10), and the definition of "shear" from Equation (2c) are substituted into these differential equations, the following matrix relationship is obtained:

$$\begin{bmatrix} M \\ V \end{bmatrix}_{y=k} = \begin{bmatrix} 0 & \frac{Dvm^2\pi^2}{p^2} \\ \frac{Dvm^2\pi^2}{p^2} & 0 \end{bmatrix} \begin{bmatrix} \theta \\ w \end{bmatrix}_{y=k} \tag{14}$$

Thus the "bending moment" at the free edge of the plate is not zero as in the case of a free-ended column, but is a function of the lateral deflection of the free edge. Likewise, the "shear" at the free edge of the plate is not zero but, instead, is a function of the angular rotation at the free edge. Since, in the finite-difference beam analogy, the angular and lateral deflections are not defined at the same point, it was necessary to terminate each side of the angle with one cell of the beam analogy derived in [3] in order to obtain the angular rotation θ and the lateral deflection w existing at the edge.

With both θ and w defined at $y = k$ it was possible to derive an electrical network satisfying the given boundary conditions. Thus in the simple electrical circuit shown in Fig. 10:

$$\begin{bmatrix} i_1 \\ i_2 \end{bmatrix} = \begin{bmatrix} -(Y_{11} + Y_{12}) & +Y_{12} \\ +Y_{12} & -(Y_{22} + Y_{12}) \end{bmatrix} \begin{bmatrix} E_1 \\ E_2 \end{bmatrix} \tag{15}$$

But this is of the same form as Equation (14) provided $(Y_{11} + Y_{12})$ and $(Y_{22} + Y_{12})$ are both equal to zero. If the impedance elements are chosen as follows:

$$C_{11} = C_{22} = \frac{Y_{11}}{j\omega} = \frac{Y_{22}}{j\omega} = \frac{Dvm^2\pi^2}{p^2\omega^2}$$

and

$$L_{12} = \frac{1}{j\omega Y_{12}} = \frac{p^2}{Dvm^2\pi^2}$$

then the diagonal terms in the electrical matrix, Equation (15), are zero and the identification is complete.

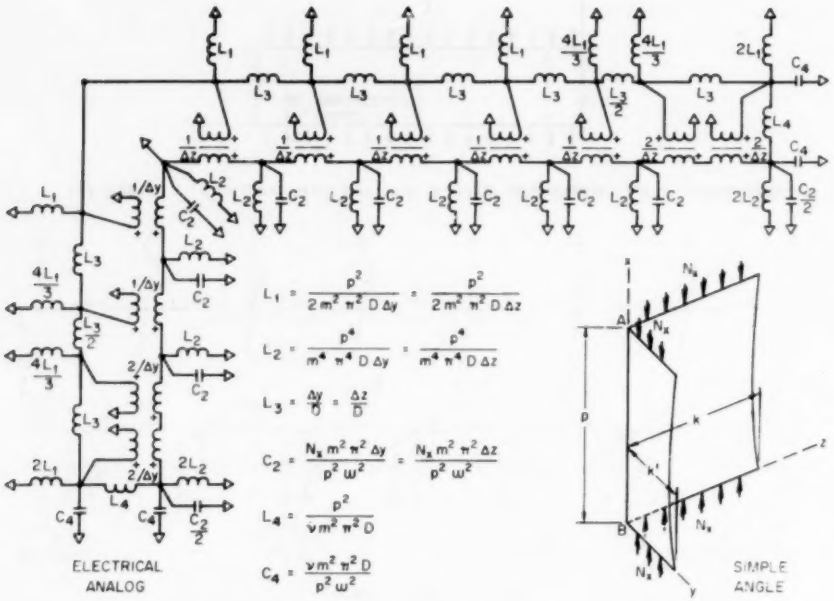

Fig. 8 Circuit used to represent simple angle

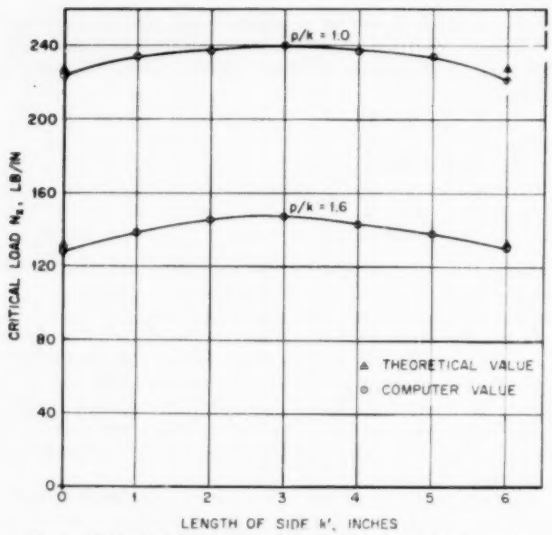

Fig. 9 Critical load versus length of side k' for simple angle

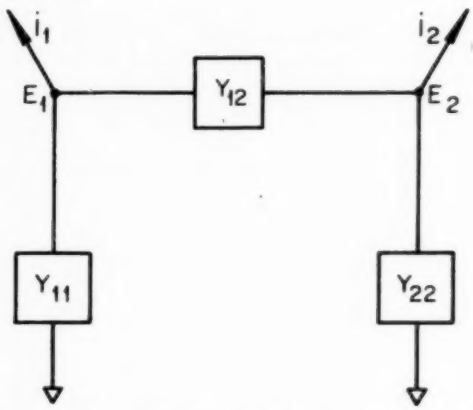

Fig. 10 Electrical circuit used to simulate boundary conditions at free edge of rectangular plate

Throughout the analysis, the angle between the two edges was represented as rigid for a distance of one half a cell along each side.

Conclusion

An electrical analogy has been obtained for a general type of differential equation that describes the lateral motion of axially loaded beams and edge-loaded plates. This analogy has been used to obtain classical buckling solutions for several types of structures. It should be emphasized that the relatively simple problems actually solved in this paper are merely examples of the types of problems which can be solved by the electrical analogy method. Thus, for example, no fundamental changes are necessary in the electrical circuit used to represent the three-member frame if the vertical columns are continuously loaded or if they do not possess uniform stiffness. The only changes required are in the values of the circuit elements. The number of structural elements that can be considered simultaneously is only limited by the number of electrical elements in the analog computer that is available.

References

1 G. D. McCann and R. H. MacNeal, "Beam Vibration Analysis With the Electric Analog Computer," JOURNAL OF APPLIED MECHANICS, vol. 17, TRANS. ASME, vol. 72, 1950, p. 13.

2 H. M. Trent, "An Equivalent Circuit for a Vibrating Beam Which Includes Shear Motions," *Journal of The Acoustical Society of America*, vol. 22, 1950, p. 355.

3 W. T. Russell and R. H. MacNeal, "An Improved Electrical Analogy for the Analysis of Beams in Bending," JOURNAL OF APPLIED MECHANICS, vol. 20, TRANS. ASME, vol. 75, 1953, p. 349.

4 F. Ryder, "Electrical Analogs of Statically Loaded Structures," *Proceedings of The American Society of Civil Engineers*, vol. 79, 1953, p. 376.

5 S. Timoshenko, "Theory of Elastic Stability," McGraw-Hill Book Company, Inc., New York, N. Y., first edition, 1936.

Symmetric Vortex Separation on Circular Cylinders and Cones

A. E. BRYSON
Associate Professor,
Division of Engineering and Applied Physics,
Harvard University, Cambridge, Mass.

The symmetric vortex separation that is observed on the leeward side of slender bodies of revolution at high angle of attack in the subsonic to moderately supersonic-velocity range is analyzed by means of the "lumped-vorticity" approximation suggested by Edwards and Hill. The equivalent unsteady two-dimensional problem of indicial motion of a cylinder in an incompressible fluid with symmetric vortex wake is also considered. Body vortex position and normal force per unit length are presented for a cylinder and a slender cone at high angle of attack and compared with available experimental information.

Two-Dimensional Unsteady Wake Development Behind a Cylinder

When a circular cylinder is suddenly accelerated from rest to a speed V in a fluid (Mach number small compared to unity), it is observed that the initial flow field is closely irrotational, but very soon after starting, the boundary layer separates at the rearward stagnation point and two separation points propagate symmetrically away from this point around the sides of the cylinder. When these boundary-layer separation points reach a certain angular distance from the rearward point, two regions of vorticity break away from the boundary layer and move downstream, beginning the formation of a wake, Fig. 1. Excellent pictures of this process were taken by Rubach and are reproduced in [1].[1] This description applies for Reynolds number, $\mathrm{Re} = Ud/\nu$, greater than about 5. At lower Re no wake is formed as the flow is governed primarily by viscous forces (Stokes' flow). Further development of the wake depends on Re; for $50 < R < 100$ an antisymmetry builds up quickly and regular eddy shedding (von Karman vortex street) begins. For $\mathrm{Re} > 10^6$, the alternate eddy shedding begins but is quickly superseded by a completely turbulent flow in the wake. This paper is concerned only with the initial symmetric wake development.

Fig. 1 Symmetric vortex separation on a circular cylinder shortly after beginning of cylinder motion

Three-Dimensional Steady Flow Past Slender Bodies of Revolution at High Angle of Attack

Symmetric vortex separation is also observed on the leeward side of slender bodies of revolution at high angle of attack in the subsonic to moderately supersonic range, Fig. 2. If we imagine a fixed plane in the fluid, perpendicular to the axis of the body, Fig. 2, then as the body pierces this plane its trace moves laterally in this plane with velocity $U \sin \alpha$ and time is related to distance x along the body by $t = x/(U \cos \alpha)$; if we approximate the fluid flow in this plane as two-dimensional, then the picture is almost identical to the one we have just been considering if we replace V by $U \sin \alpha$. The main difference is the "expanding circle" as the

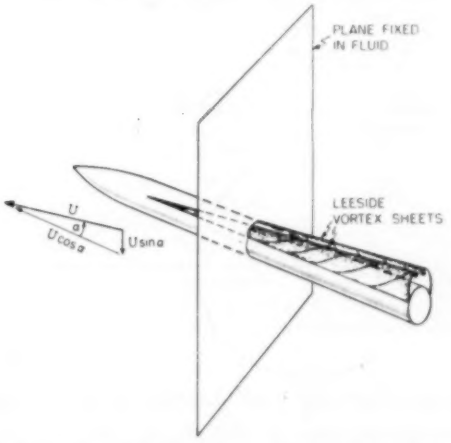

Fig. 2 Symmetric vortex separation on a slender body of revolution at high angle of attack

[1] Numbers in brackets designate References at end of paper.

Presented at the Summer Conference of the Applied Mechanics Division, Troy, N. Y., June 18–20, 1959, of THE AMERICAN SOCIETY OF MECHANICAL ENGINEERS.

Discussion of this paper should be addressed to the Secretary, ASME, 29 West 39th Street, New York, N. Y., and will be accepted until January 10, 1960, for publication at a later date. Discussion received after the closing date will be returned

NOTE: Statements and opinions advanced in papers are to be understood as individual expressions of their authors and not those of the Society. Manuscript received by ASME Applied Mechanics Division, July 15, 1958. Paper No. 59—APM-13.

nose pierces the fixed plane. In many instances vortex separation occurs behind the nose-cylindrical body juncture, hence the previous model is applicable.

Lumped Vorticity Approximation of Early Phase of Wake Formation

In terms of the two-dimensional unsteady problem, the regions of vorticity that separate from the boundary layer and move downstream are quite thin, justifying a description of them as vortex sheets. Furthermore these sheets roll up, concentrating most of the vorticity toward the downstream end of the sheet. If we approximate the sheet by a single concentrated line vortex at the center of gravity of the vorticity but maintain, conceptually, a connecting sheet of vanishingly small vorticity to the body, we can formulate a relation for motion of this vortex that gives no net force on the vortex and its connecting sheet (Appendix A):

$$\dot{\bar{\zeta}}_1 + (\zeta_1 - \zeta_0)\frac{\dot{\Gamma}}{\Gamma} = W_1 \tag{1}$$

where

ζ_1 = complex co-ordinate = $y_1 + iz_1$ of vortex
ζ_0 = complex co-ordinate of point on body where sheet is being "fed"
Γ = circulation of vortex
W_1 = $v_1 + iw_1$ = complex velocity vector at ζ_1 leaving out infinite rotational velocity induced by vortex itself
$(\dot{})$ indicates time differentiation = $d(\ )/dt$

Note that if $\dot{\Gamma} = 0$, this relation indicates that the vortex moves with the local fluid velocity. Also, even though the net force on the vortex and connecting sheet is zero, a moment acts on the combination, Fig. 3, an inherent inaccuracy in this type of approximation. Another objection is that this model of the phenomenon implies a discontinuous drop in pressure on the body going across the "feeding point" of amount $\Delta p = \rho\dot{\Gamma}$. It is true, however, that the high suction on the rear end of the cylinder accounts for most of the drag experienced by the cylinder.

Another relationship is needed to determine completely the motion of the two symmetrically disposed "lumped" vortexes in the wake, and it is related to the choice of location for the feeding points $\zeta = \zeta_0$ and $\zeta = -\bar{\zeta}_0$. For the cases considered previously (e.g., references [2, 3]) this additional relationship is a Kutta condition at the sharp edge where the sheet is fed; it simply states

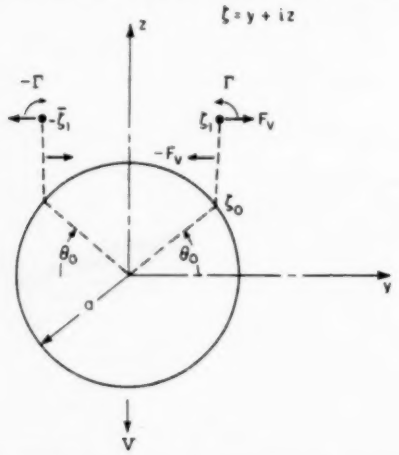

Fig. 3 Simplified theoretical model of symmetric vortex separation on a circular cylinder

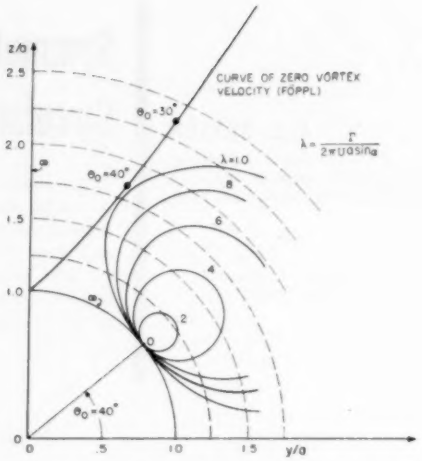

Fig. 4 Contours of constant vortex strength for feeding points at θ_0 = 4 deg and 140 deg

that the fluid velocity at the edge is finite. In the present problem the condition used is that:

> The feeding points are stagnation points; that is, the fluid velocity relative to the cylinder vanishes at these points. (2)

This still leaves open the choice of where these points are to be located. Observation indicates they are located about 50 deg from the rear point (θ_0 = 40 deg) when the boundary layer is turbulent, and somewhat farther away when the boundary layer is laminar ($\theta_0 < 40$ deg).

Fig. 4 shows a downstream quadrant of the flow field with lines of constant vortex strength determined by condition (2) [see Equation (6)] for the case θ_0 = 40 deg. It also shows the "Föppl curve" which is the locus of points where a vortex pair can be at rest with respect to a cylinder in a steady flow (see, for example, Reference [5]). The points on the Föppl curve for θ_0 = 30 and 40 deg are shown. These may be regarded as equilibrium points for the vortexes, but they are unstable to an antisymmetric disturbance [1].

Computation of Vortex Motion

The fluid motion is governed by Laplace's equation, hence we use the complex variable $\zeta = y + iz$ where the y and z-axes are body axes with origin at the center of the cylinder, Fig. 3, and a complex conjugate velocity vector $v - iw = dF/d\zeta$, where F is the complex velocity potential. F is made up of the potentials due to (a) the free-stream flow, (b) a doublet at the origin to simulate the cylinder, (c) the two vortexes in the wake, and (d) the "reflection" of the two vortexes in the cylinder

$$F = -iV\left(\zeta - \frac{a^2}{\zeta}\right) - \frac{i\Gamma}{2\pi}\log\frac{\zeta - \zeta_1}{\zeta - \frac{a^2}{\bar{\zeta}_1}}\frac{\zeta + \frac{a^2}{\zeta_1}}{\zeta + \bar{\zeta}_1} \tag{3}$$

The velocity is thus:

$$\frac{v - iw}{V} = -i\left(1 + \frac{a^2}{\zeta^2}\right) - i\lambda a\left[\frac{1}{\zeta - \zeta_1} + \frac{1}{\zeta + \frac{a^2}{\zeta_1}} - \frac{1}{\zeta - \frac{a^2}{\bar{\zeta}_1}} - \frac{1}{\zeta + \bar{\zeta}_1}\right] \tag{4}$$

where $\lambda = \Gamma/(2\pi aV)$. The velocity at vortex 1, which we earlier called W_1, is thus given by:

$$W_1 = v_1 - iw_1 = -iV\left[1 + \frac{a^2}{\zeta_1^2} + \lambda a\left(\frac{1}{\zeta_1 + \frac{a^2}{\zeta_1}} - \frac{1}{\zeta_1 - \frac{a^2}{\bar{\zeta}_1}} - \frac{1}{\zeta_1 + \bar{\zeta}_1}\right)\right] \quad (5)$$

Also, to obtain the relation that satisfies condition (2) and that is plotted in Fig. 4, we put $v - iw = 0$ at $\zeta = \zeta_0 = ae^{i\theta_0}$ into (4) and, after some algebra, we find:

$$\lambda = \frac{(\zeta_1 - \zeta_0)(\bar{\zeta}_1 - \bar{\zeta}_0)(\zeta_1 + \bar{\zeta}_0)(\bar{\zeta}_1 + \zeta_0)}{(\zeta_1\bar{\zeta}_1 - a^2)(\zeta_1 + \bar{\zeta}_1)} \quad (6)$$

which is always real and positive.

Equation (1) can be written as

$$\dot{\bar{\zeta}}_1 + (\zeta_1 - \zeta_0)\frac{\dot{\lambda}}{\lambda} = W_1 \quad (7)$$

and, with equations (5) and (6), represents a rather involved nonlinear first-order ordinary differential equation for the complex co-ordinate of vortex 1, $\zeta_1(t)$. This was integrated numerically, by finite-difference approximation, on an IBM 704 for the case $\theta_0 = 40$ deg with time increments equal to $(1/20)(a/V)$. Fig. 5 shows the result of this calculation (every 20th computation point plotted) as the solid curve. (Note $\Delta s = V\Delta t$ = distance traveled laterally by the cylinder in time Δt, so $\Delta s/a$ is the number of cylinder radii traveled in time Δt.)

It can be seen that the symmetric vortexes begin to move very slowly downstream relative to the cylinder, accelerate to a maximum velocity, then decelerate as they approach the Föppl curve. However, instead of heading for the equilibrium points on the Föppl curve that correspond to $\theta_0 = 40$ deg, the vortexes went outside these points and curved back toward them; in so doing $\dot{\Gamma}$ became negative; i.e., circulation was "fed back" into the body boundary layer. This seems unlikely and hence we discard the computation for times after $\dot{\Gamma}$ went through zero. Possibly, what really happens here is that the feeding sheet is cut and a new vortex sheet starts out from the feeding point while the old vortex, now of constant strength, drifts further downstream, starting a von Karman vortex street.

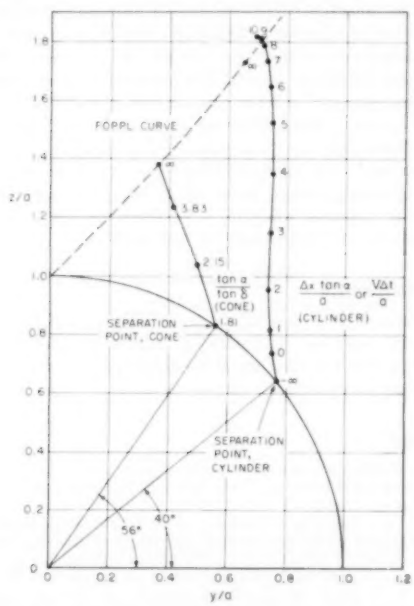

Fig. 5 Theoretical vortex trajectory for a cylinder ($\theta_0 = 40$ deg) and vortex location on a cone as a function of angle of attack ($\theta_0 = 56$ deg)

A difficulty arises in starting the problem because the feeding points, which are also the starting points of the vortexes, are unstable equilibrium points for the vortexes in the mathematical problem (see later text). Furthermore, the vortexes can start out from these feeding points in only one preferred direction: namely, 30 deg to the downstream tangent to cylinder. Thus, to start the problem, the vortexes were placed on this preferred line a short distance from the feeding point (5 per cent of cylinder radius).

Feeding Points as Unstable Equilibrium Points

Splitting Equation (7) into its real and imaginary parts we can write it, for fixed ζ_0, as two simultaneous first-order nonlinear differential equations of the form:

$$\dot{y}_1 = f(y_1, z_1)$$

$$\dot{z}_1 = g(y_1, z_1)$$

where $y_1 = y_1(t)$ and $z_1 = z_1(t)$. The points where $\dot{y}_1$ and $\dot{z}_1$ vanish are called equilibrium points. For a given value of ζ_0 there are two such points for these equations: (*a*) the feeding point, and (*b*) the Föppl point. To investigate the stability of an equilibrium point, f and g must be expanded in Taylor series about this point to see if a small motion away from it will cause the vortex to continue moving away (unstable) or will cause it to return toward the point (stable) [6]. This is done for the feeding point $\zeta_0 = ae^{i\theta_0}$ in Appendix B, and it is found that this point is unstable for $\theta_0 > 0$. Furthermore, it is shown in Appendix B that the feeding point is a "saddle point" in that only one integral curve passes through it; this integral curve starts out of the feeding point at an angle of 30 deg to the downstream tangent to the cylinder.

Drag Force on Cylinder

A drag force is predicted by this calculation because of the lack of fore-and-aft symmetry. The total impulse imparted to a unit length of the cylinder can be deduced from the instantaneous position of the wake vortexes (see Appendix C):

$$I = i\rho\Gamma\left(\zeta_1 - \frac{a^2}{\bar{\zeta}_1} + \bar{\zeta}_1 - \frac{a^2}{\zeta_1}\right)$$

The instantaneous drag force is the time derivative of the impulse. This is often expressed in terms of an instantaneous crossflow drag coefficient C_{D_c} defined as

$$C_{D_c} = \frac{D}{\frac{1}{2}\rho V^2(2a)}$$

where D = drag force per unit length of cylinder. This relation is plotted for the case $\theta_0 = 40$ deg in Fig. 6. Note that C_{D_c} first increases, then reaches a maximum, then decreases as the vortexes approach the Föppl curve.

Normal Force on an Inclined Cylinder With Vortex Separation

Normal force per unit length dN/dx on the three-dimensional inclined cylinder is the same as the crossflow drag per unit length on the two-dimensional cylinder. Total normal force up to a

certain axial station x on the body is proportional to the total impulse I in the two-dimensional unsteady problem, since

$$I = \int_0^t \frac{dN}{dx}\, dt$$

and in the analogy $t = x/(U \cos \alpha)$ so

$$N = \int_0^x \frac{dN}{dx}\, dx = IU \cos \alpha$$

$$= \rho \Gamma U \cos \alpha \left(\zeta_1 - \frac{a^2}{\bar{\zeta}_1} + \bar{\zeta}_1 - \frac{a^2}{\zeta_1} \right)$$

If we define normal force coefficient as

$$C_N = \frac{N}{\frac{1}{2} \rho U^2 \pi a^2}$$

then

$$C_N = 2\lambda \sin 2\alpha \left(\frac{\zeta_1}{a} - \frac{a}{\bar{\zeta}_1} + \frac{\bar{\zeta}_1}{a} - \frac{a}{\zeta_1} \right)$$

where

$$\lambda = \frac{\Gamma}{2\pi a U \sin \alpha}$$

Normal Force on a Slender Cone With Vortex Separation

Here the flow field is assumed conical; i.e., velocity components and pressure are assumed constant on rays through the cone apex. At each axial station then the crossflow picture is the same, only increased in scale, Fig. 7. The crossflow velocity field is slightly different from that of the cylinder since a "source" term must be added to the velocity of Equation (4) to represent the expanding circle; namely, $+\epsilon \dot{a}/\zeta$. Replacing t by $x/U \cos \alpha$ and V by $U \sin \alpha$ in Equation (4) we also take advantage of the conical nature of the flow by putting

$$\frac{d\zeta_1}{dx} = \frac{\zeta_1}{a} \frac{da}{dx} = \frac{\zeta_1}{a} \tan \delta$$

where δ = semiapex angle of the cone. It follows that the circulation strength of the separated vortexes must increase linearly with x; hence:

$$\frac{1}{\lambda} \frac{d\lambda}{dx} = \frac{1}{x} = \frac{\tan \delta}{a}$$

Making these additions and substitutions in Equation (7) it becomes a complex algebraic equation for the location of the vortexes (ζ_1 and $-\bar{\zeta}_1$) with a parameter $\beta = \tan \alpha / \tan \delta$ (Appendix D). This equation has been solved for the case $\theta_0 = 56$ deg and the results are shown as the left-hand curve in Fig. 5 and the corresponding normal force is shown in Fig. 7.

One interesting feature of this analysis is that vortex separation does not occur until $\beta = 1.5 \csc \theta_0$. Moore in [7] has shown that laminar boundary-layer separation on a cone does not occur until $\beta = 0.8$ and he speculates that turbulent boundary-layer separation is delayed until even higher values of β.

Comparison With Experiment

Observations and measurements of this phenomenon are given in [4] and [8] through [13]. In particular [13] shows measurements of vortex trajectories and lift per unit length on slender inclined ogive-cylinder bodies summarized from several sources. It was on the basis of these observations that we chose $\theta_0 = 40$ deg as the feeding point. Fig. 6 shows the experimental data of Schwabe [8]. The time origin of the theoretical curve (which is

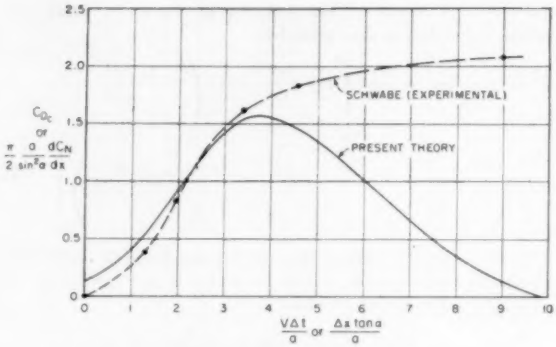

Fig. 6 Crossflow drag on a cylinder as a function of time

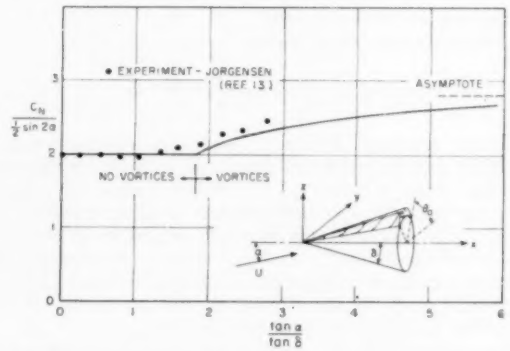

Fig. 7 Normal force on a cone with vortex separation as a function of angle of attack

not predicted by the theory) has been shifted to fit the experimental data for small time. For $V\Delta t/a > 5$ the theory shows a drop-off in crossflow drag whereas Schwabe's experiments do not. However, other experiments do show a drop-off in C_{D_c} to about 1.2 for laminar flow and 0.35 for turbulent flow [11].

Jorgensen [14] gives data on lift, drag, and vortex position for a circular cone with $\delta = 7.8$ deg at Mach number 1.97 up to 21 deg angle of attack. These data are plotted on Fig. 7 and show a reasonable agreement with the theory if θ_0 is put equal to 56 deg. With this value of θ_0 the position of the vortexes also checks well with Jorgensen's observations. The theory predicts the appearance of vortexes when $\alpha = 13.9$ deg and the experiments show them appearing between 10 and 15 deg.

Acknowledgments

The author is indebted to a paper of J. A. F. Hill [4] for much preliminary work on this problem and to Harold Soule and Barbara Casa of the Raytheon Missile Systems Division for their interest and computational assistance.

References

1 S. Goldstein, editor, "Modern Developments in Fluid Dynamics," Oxford University Press, London, England, 1938, pp. 39–41, 62–65, plates 7 and 8.

2 R. H. Edwards, "Leading Edge Separation From Delta Wings," *Journal of the Aeronautical Sciences*, vol. 21, 1954, p. 134.

3 N. Rott, "Diffraction of a Weak Shock With Vortex Generation," *Journal of Fluid Mechanics*, vol. 1, 1956, pp. 111–128.

4 J. A. F. Hill, "A Non-Linear Theory of the Lift on Slender Bodies of Revolution," NavOrd Report 5338, Proceedings U. S. Navy Symposium on Aeroballistics, 1954.

5 L. M. Milne-Thompson, "Theoretical Hydrodynamics," The

Macmillan Company, New York, N. Y., second edition, 1950, pp. 331–333.

6 T. von Karman and M. A. Biot, "Mathematical Methods in Engineering," McGraw-Hill Book Company, Inc., New York, N. Y., 1940, pp. 150–158.

7 F. K. Moore, "Laminar Boundary Layer on a Cone in Supersonic Flow at Large Angle of Attack," NACA Technical Report 1132, 1953.

8 M. Schwabe, "Pressure Distribution in Non-Uniform Two Dimensional Flow," NACA TM 1039, 1943.

9 H. R. Kelley, "The Estimation of Normal Force, Drag, and Pitching Moment Coefficients for Blunt-Based Bodies of Revolution at Large Angles of Attack," *Journal of the Aeronautical Sciences*, vol. 21, 1954, pp. 549–555.

10 F. E. Gowen and E. W. Perkins, "A Study of the Effects of Body Shape on the Vortex Wakes of Inclined Bodies at a Mach Number of Two," NACA Research Memo, A53117, 1953.

11 R. L. Maltby and D. H. Peckham, "Low Speed Flow Studies on the Vortex Patterns Above Inclined Slender Bodies Using a New Smoke Technique," Royal Aircraft Establishment Technical Note No. Aero. 2482, 1956.

12 E. W. Perkins and L. H. Jorgensen, "Comparison of Experiments and Theoretical Normal Force Distributions (Including Reynolds Number Effects) on an Ogive-Cylinder Body at M = 1.98," NACA TN 3716, 1956.

13 J. N. Nielsen and G. E. Kaatari, "The Effects of Vortex and Shock-Expansion Fields on Pitch and Yaw Instabilities of Supersonic Airplanes," Institute of The Aeronautical Sciences Preprint No. 743, 1957.

14 L. H. Jorgensen, "Elliptic Cones Alone and With Wings at Supersonic Speeds," NACA TN 4045, 1957.

APPENDIX A

Approximating a Vortex Sheet of Growing Strength by a Single Concentrated Vortex[2]

In Fig. 3, consider the vortex sheet on the right which we approximate by the concentrated vortex of circulation Γ at ζ_1 and a connecting sheet of vanishingly small circulation connecting ζ_1 to the feeding point ζ_0 on the body. Mathematically, there is a branch line between ζ_1 and ζ_0 and the velocity potential ϕ is discontinuous across this branch line, the discontinuity in ϕ being Γ, the circulation of the vortex. There is therefore a discontinuity in pressure across this branch line (alias vortex sheet) of amount $\rho\dot{\Gamma}$, the total (complex vector) force acting on this vortex sheet is therefore $i\rho\dot{\Gamma}(\zeta_1 - \zeta_0)$. The force acting on the concentrated vortex is $-i\rho\Gamma(W_1 - \dot{\zeta}_1)$ where W_1 is the local fluid-velocity vector at the vortex and $\dot{\zeta}_1$ is the velocity vector of the vortex. Thus to make the net force on the concentrated vortex and its feeding vortex sheet vanish we must have

$$i\rho\dot{\Gamma}(\zeta_1 - \zeta_0) - i\rho\Gamma(W_1 - \dot{\zeta}_1) = 0 \tag{8}$$

or, rearranging, we obtain Equation (1) in the text.

APPENDIX B

Feeding Points as Unstable Saddle Points

Let $\zeta_1 - \zeta_0 = a\rho\, e^{i\phi}$ and $\zeta_0 = ae^{i\theta_0}$ and consider $\rho \ll 1$. From Equation (6) we find that:

$$\lambda \cong \rho \cos\theta_0 \sec(\phi - \theta_0) \quad \text{as} \quad \rho \to 0 \tag{9}$$

Hence the second term on the left side of Equation (7) becomes:

$$(\zeta_1 - \zeta_0)\frac{\dot{\lambda}}{\lambda} = a\rho e^{i\phi}\frac{\dot{\rho}}{\rho} \cong \dot{\zeta}_1 \quad \text{as} \quad \rho \to 0 \tag{10}$$

since we assume $\rho\dot{\phi}$ is of second order as $\rho \to 0$. Thus Equation (7) for $\rho \ll 1$ becomes:

$$\dot{\zeta}_1 = \frac{W_1}{2} \tag{11}$$

[2] After references [2] and [3].

Expanding W_1 in a power series in ρ for fixed, but as yet unknown ϕ, we find:

$$W_1 = W_{10}(\phi) + \rho W_{11}(\phi) + \cdots\cdots \tag{12}$$

$$W_{10}(\phi) = \frac{1}{2}\, ie^{i\theta_0}\cos\theta_0[4 - \sec^2(\phi - \theta_0)] \tag{13}$$

and we have nondimensionalized W_1 by $U \sin\alpha$. Since we wish to have W_1 vanish as $\rho \to 0$, it follows that $W_{10}(\phi)$ must be zero, which implies that:

$$\phi = \theta_0 + \frac{\pi}{3} \quad \text{as} \quad \rho \to 0 \tag{14}$$

This establishes the direction the vortex takes as it leaves the feeding point; namely, 30 deg from the downstream tangent to the cylinder.

To investigate stability of the feeding point we let

$$\phi = \theta_0 + \frac{\pi}{3} + \alpha,$$

where $\alpha \ll 1$, and expand W_{10} in a Taylor series in α and evaluate W_{11} at $\alpha = 0$:

$$\begin{aligned} W_{10} &= -(4\sqrt{3}\, ie^{i\theta_0})\alpha + \cdots\cdots \\ W_{11} &= 2e^{i\phi}\left[\sin\left(\frac{\pi}{3} - \theta_0\right) + i\cos\left(\frac{\pi}{3} + \theta_0\right)\right] \end{aligned} \tag{15}$$

Substituting (15) into (12) and in turn into (11) yields:

$$\rho' e^{i\phi} = -(4\sqrt{3}\, ie^{i\theta_0})\alpha + 2e^{i\phi}\left[\sin\left(\frac{\pi}{3} - \theta_0\right) + i\cos\left(\frac{\pi}{3} + \theta_0\right)\right]\rho + \cdots\cdots \tag{16}$$

where

$$(\,)' = \frac{a}{U\sin\alpha}\frac{d}{dt}(\,)$$

Now multiply (16) by $e^{-i\phi}$ and then split it into real and imaginary parts:

$$\rho' = -(3\cos\theta_0)\alpha + \rho\sin\left(\frac{\pi}{3} - \theta_0\right) + \cdots\cdots \tag{17}$$

$$0 = -(\sqrt{3}\cos\theta_0)\alpha + \rho\cos\left(\frac{\pi}{3} + \theta_0\right) + \cdots\cdots \tag{18}$$

Equation (18) gives a linear relation between α and ρ which, when substituted into (17), gives:

$$\rho' = \rho\sin\theta_0 + \cdots\cdots \tag{19}$$

Thus the point ζ_0 is an unstable saddle point for $0 < \theta_0 < \pi/2$, and the integral curve through ζ_0 is given by:

$$\phi = \frac{\pi}{3} + \theta_0 + \frac{\cos\left(\frac{\pi}{3} + \theta_0\right)}{\sqrt{3}\cos\theta_0}\rho + \cdots\cdots \tag{20}$$

APPENDIX C

Impulse and Force per Unit Length on Cylinder

The impulse of a pair of vortexes of equal and opposite strength Γ, which are a (complex) distance $\Delta\zeta$ apart, is:

$$i\rho\Gamma(\Delta\zeta)$$

Since, in our problem, we have arranged to have no net force on the vortex and connecting sheet, the total impulse acting on the cylinder is the sum of the impulses of the two vortex pairs, one at ζ_1 and $-\bar{\zeta}_1$ the other at $a^2/\bar{\zeta}_1$ and $-a^2/\zeta_1$. Since at the beginning $\Gamma = 0$, the total impulse is then:

$$I = i\rho\Gamma\left(\zeta_1 + \bar{\zeta}_1 - \frac{a^2}{\bar{\zeta}_1} - \frac{a^2}{\zeta_1}\right) \tag{21}$$

The drag force per unit length acting on the cylinder is the time rate of change of the impulse

$$D = \frac{dI}{dt} \tag{22}$$

APPENDIX D

Normal Force on a Slender Cone at High Angle of Attack

Making the substitutions and additions mentioned in the text, Equation (7) becomes:

$$\frac{1}{\beta}\left[\frac{\zeta_1}{a} + \frac{a}{\bar{\zeta}_1} + \frac{\bar{\zeta}_1}{a} - \frac{\zeta_0}{a}\right] = \frac{W_1}{U\sin\alpha} \tag{23}$$

where W_1 is the same as Equation (5) and the λ that occurs in W_1 is the same as in Equation (6). Now let:

$$\begin{aligned}\zeta_1 &= ar_1e^{i\theta_1}\\ \zeta_0 &= ae^{i\theta_0}\end{aligned} \tag{24}$$

and separate (23) into its real and imaginary parts. After some manipulation this gives:

$$\frac{1}{\beta}\sin(\theta_1 - \theta_0) = \left(1 + \frac{1}{r_1^2}\right)\cos\theta_1 + \lambda\left[\frac{\frac{1}{8r_1}\left(r_1^2 - \frac{1}{r_1^2}\right)}{\frac{1}{4}\left(r_1 - \frac{1}{r_1}\right)^2 + \cos^2\theta_1} - \frac{1}{r_1 - \frac{1}{r_1}}\right] \tag{25}$$

$$\frac{1}{\beta}\left[\left(1 - \frac{1}{r_1}\right)(2r_1 + 1) + 2\sin^2\frac{\theta_1 - \theta_0}{2}\right] = \left(1 - \frac{1}{r_1^2}\right)\sin\theta_1 - \frac{\lambda}{2r_1}\frac{\frac{1}{4}\left(r_1 - \frac{1}{r_1}\right)^2\tan\theta_1}{\frac{1}{4}\left(r_1 - \frac{1}{r_1}\right)^2 + \cos^2\theta_1} \tag{26}$$

where

$$\lambda = \frac{8}{\left(r_1 - \frac{1}{r_1}\right)\cos\theta_1}\left[\frac{\left(\sqrt{r_1} - \frac{1}{\sqrt{r_1}}\right)^2}{4} + \sin^2\frac{\theta_1 - \theta_0}{2}\right]\left[\frac{\left(\sqrt{r_1} - \frac{1}{\sqrt{r_1}}\right)^2}{4} + \cos^2\frac{\theta_1 + \theta_0}{2}\right] \tag{27}$$

These last three relations determine the location of the right-hand vortex (r_1, θ_1) as a function of the parameter $\beta = \tan\alpha/\tan\delta$. They were solved by assuming a value of r_1, then varying θ_1 until both (25) and (26) gave the same values of $1/\beta$.

When the vortexes are very close to the feeding points we can linearize Equation (23) by letting

$$\zeta_1 - \zeta_0 = a\rho e^{i\phi}, \quad \phi = \theta_0 + \frac{\pi}{3} + \alpha$$

and expanding both sides up to linear terms in ρ and α (as in the second section of Appendix B):

$$\frac{1}{\beta}\rho e^{i\phi}\left(1 + e^{-i\frac{\pi}{3}}\right) = -(4\sqrt{3}\,ie^{i\theta_0}\cos\theta_0)\alpha + 2\rho e^{i\phi}\left[\sin\left(\frac{\pi}{3} - \theta_0\right) + i\cos\left(\frac{\pi}{3} + \theta_0\right)\right] \tag{28}$$

and, upon multiplying through by $e^{-i\phi}$ and splitting into real and imaginary parts, we obtain:

$$\begin{aligned}\left[\frac{3}{2}\frac{1}{\beta} - 2\sin\left(\frac{\pi}{3} - \theta_0\right)\right]\rho + (6\cos\theta_0)\alpha &= 0\\ \left[-\frac{\sqrt{3}}{2}\frac{1}{\beta} - 2\cos\left(\frac{\pi}{3} + \theta_0\right)\right]\rho + (2\sqrt{3}\cos\theta_0)\alpha &= 0\end{aligned} \tag{29}$$

For consistency the determinant of these equations must vanish, yielding the eigenvalue:

$$\beta = \frac{3}{2}\csc\theta_0 \tag{30}$$

and the equation of the vortex path as

$$\alpha = \frac{1}{3}\left(\frac{\sqrt{3}}{2} - \tan\theta_0\right)\rho + \cdots\cdots \tag{31}$$

The normal force on the cone is made up of two parts, the usual linear theory (slender-body) value, plus the nonlinear contribution due to the vortexes:

$$\frac{C_N}{\frac{1}{2}\sin 2\alpha} = 2 + 8\lambda\left(r_1 - \frac{1}{r_1}\right)\cos\theta_1 \tag{32}$$

This relation is plotted in Fig. 7 for $\theta_0 = 56$ deg.

Note on a Thermoelastic Problem for a Transversely Isotropic Hollow Sphere Embedded in an Elastic Medium[1]

J. NOWINSKI
Professor,
Army Mathematics Research Center,
University of Wisconsin, Madison, Wis.
Formerly of
Mechanical Engineering Department,
The Johns Hopkins University,
Baltimore, Md.

This note concerns a hollow sphere composed of two different transversely isotropic layers and subjected to an internal pressure and a steady-state, spherically symmetrical temperature field. The sphere is surrounded by an elastic medium treated as a Winkler material or transversely isotropic medium, respectively.

THE problem of an isotropic thick-walled tube embedded in an elastic medium of the Winkler type, under internal pressure and a uniform temperature increase has been studied by B. G. Galerkin.[2] In a recent paper, the Galerkin problem has been generalized to an orthotropic cylinder subjected to any axisymmetric temperature field.[3] The present note is confined to a further generalization of the Galerkin problem, in connection with the anisotropic bodies, using the results of a previous paper by the author.[4] In this paper a thermal steady-state polar symmetrical temperature field in a thick-walled transversely isotropic vessel has been studied. Thus the present paper deals with the Galerkin problem for such a two-layer anisotropic vessel. It seems that the problem considered may be of practical interest in some instances, such as that of a reinforced-concrete container, with a special inner coating, surrounded by a rocky ground and subjected to an internal pressure and a temperature field.

General Equations

Let us consider a thick-walled hollow sphere of transversely isotropic material the center of the sphere coinciding both with the center of the spherical anisotropy and the origin of a polar coordinate system ρ, θ, φ, in which θ and φ represent the angles of longitude and latitude, respectively. The sphere is composed of two different transversely isotropic concentric layers; an inner layer $a' \leqslant \rho \leqslant a$, and an outer layer $a \leqslant \rho \leqslant a''$. In what follows, the quantities connected with the inner layer will be denoted by a prime. The sphere is embedded in an elastic medium, for the time being, of the Winkler type, and subjected to an internal pressure p and a spherically symmetrical steady-state temperature field $T = T(\rho)$.

Denote by u the radial displacement and by E' and E the Young's moduli in the radial directions and in the directions perpendicular to the radii, respectively. The Poisson coefficients will be denoted by ν' and ν, the first quantity representing the lateral contractions (in the planes tangent to the concentric spheres of isotropy) provoked by a radial elongation, and the second quantity the lateral contractions, in the same planes, provoked by the elongations in these planes.

The relations between the components of the strain and the stress fields in a spherically transversely isotropic material have the known form

$$\epsilon_\rho = \frac{\sigma_\rho}{E'} - \frac{2\nu'\sigma_t}{E'} + \alpha_\rho T, \quad \epsilon_t = -\frac{\nu'\sigma_\rho}{E'} + \frac{(1-\nu)\sigma_t}{E} + \alpha_t T, \tag{1}$$

[1] This research was supported in whole by the United States Air Force under Contract No. AF 49 (638)-377, monitored by the AF Office of Scientific Research.

[2] B. G. Galerkin, "State of Stress in a Circular Tube Surrounded by an Elastic Medium" (in Russian), Sobr. Soch., vol. 1, 1952.

[3] J. Nowinski, "Thermoelastic States in a Thick-Walled Orthotropic Cylinder Surrounded by an Elastic Medium," *Bulletin de l'Academie Polonaise des Sciences*, vol. 5, 1957.

[4] J. Nowinski, "Thermal Stresses in a Thick-Walled Spherical Vessel of Transversely Isotropic Material," *Arch. Appl. Mech.*, Warsaw, vol. 7, 1955.

Presented at the Summer Conference of the Applied Mechanics Division, Troy, N. Y., June 18–20, 1959, of THE AMERICAN SOCIETY OF MECHANICAL ENGINEERS.

Discussion of this paper should be addressed to the Secretary, ASME, 29 West 39th Street, New York, N. Y., and will be accepted until January 10, 1960, for publication at a later date. Discussion received after the closing date will be returned.

NOTE: Statements and opinions advanced in papers are to be understood as individual expressions of their authors and not those of the Society. Manuscript received by ASME Applied Mechanics Division, September 16, 1958. Paper No. 59—APM-27.

Nomenclature

ρ, θ, φ	= polar co-ordinates	A_{11}, A_{12}	= coefficients defined by Equations (3)	Δ_1, γ_1	= coefficients defined by Equations (9)
a', a, a''	= radii corresponding to inner and outer layer, respectively	A_{22}, A_{23}		γ_1', γ_3	
		Δ, D_1, D_2		γ_2'	
p	= pressure	α_1, α_2		F_1, F_2	
T	= temperature	β_1, β_2	= coefficients defined by Equations (5)	α, α'	
u	= radial displacement	β_3, μ		ω', β, β'	
E', E	= Young's moduli	m, d_1, d_2		*	= star, denoting case of a transversely isotropic medium
ν', ν	= Poisson coefficients	$\varphi(\rho), \psi(\rho)$	= functions of ρ defined by Equations (5)	′	= prime, denoting quantities connected with inner layer
α_ρ, α_t	= coefficients of thermal linear expansion	K, L	= constants of integration		
$\epsilon_\rho, \epsilon_t$	= unit elongations	$\delta = 1/A_{11}$	= a coefficient		
σ_ρ, σ_t	= normal stresses	κ	= Winkler's coefficient of medium		

where $\sigma_t \equiv \sigma_\varphi = \sigma_\theta$, and α_ρ and α_t are the coefficients of the thermal linear expansion in the radial directions and in the surfaces of isotropy, respectively. We assume that all elastic and thermal coefficients do not depend on temperature in the range of the changes of the temperature field considered.

By solving Equations (1) with respect to stresses we obtain

$$\begin{aligned} \sigma_\rho &= A_{11}\epsilon_\rho + 2A_{12}\epsilon_t - D_1 T, \\ \sigma_t &= A_{12}\epsilon_\rho + (A_{22} + A_{23})\epsilon_t - D_2 T, \end{aligned} \tag{2}$$

where the following notations were used:

$$A_{11} = (1 - \nu)\frac{E'}{E}\Delta, \quad A_{12} = \nu'\Delta, \quad A_{22} + A_{23} = \Delta,$$

$$\Delta = E:\left[1 - \nu - 2(\nu')^2\frac{E}{E'}\right], \tag{3}$$

$$D_1 = \left[(1 - \nu)\frac{E'}{E}\alpha_\rho + 2\nu'\alpha_t\right]\Delta, \quad D_2 = (\nu'\alpha_\rho + \alpha_t)\Delta.$$

The solution of the given thermoelastic problem for a transversely isotropic sphere yields the following components of the stress field:[4]

$$\begin{aligned} \sigma_\rho &= \alpha_1[\varphi(\rho) + K]\rho^{\frac{\mu-3}{2}} + \alpha_2[\psi(\rho) - L]\rho^{\frac{-\mu-3}{2}}, \\ \sigma_t &= \beta_1[\varphi(\rho) + K]\rho^{\frac{\mu-3}{2}} + \beta_2[\psi(\rho) - L]\rho^{\frac{-\mu-3}{2}} + \beta_3 T, \end{aligned} \tag{4}$$

in which

$$\begin{aligned} \alpha_1 &= \frac{\mu - 1}{2} + \frac{2A_{12}}{A_{11}}, \quad \alpha_2 = \frac{\mu + 1}{2} - \frac{2A_{12}}{A_{11}}, \\ \beta_1 &= \frac{\mu - 1}{2}\frac{A_{12}}{A_{11}} + \frac{A_{22} + A_{23}}{A_{11}}, \quad \beta_2 = \frac{\mu + 1}{2}\frac{A_{12}}{A_{11}} + \frac{A_{22} + A_{23}}{A_{11}}, \\ \beta_3 &= \frac{A_{12}}{A_{11}}D_1 - D_2, \quad \mu = (1 + 8m^2)^{1/2}, \\ m^2 &= \frac{A_{22} + A_{23} - A_{12}}{A_{11}} = \frac{E(1 - \nu')}{E'(1 - \nu)}, \\ \varphi(\rho) &= \frac{d_1}{\mu}\int_a^\rho T\rho^{\frac{1-\mu}{2}}\,d\rho, \quad \psi(\rho) = \frac{d_2}{\mu}\int_a^\rho T\rho^{\frac{1+\mu}{2}}\,d\rho, \\ d_1 &= \frac{1 + \mu}{2}D_1 - 2D_2, \quad d_2 = \frac{1 - \mu}{2}D_1 - 2D_2. \end{aligned} \tag{5}$$

K and L are the constants of integration and a the inner radius of the sphere. For the radial displacement one obtains

$$u = \delta\left\{[\varphi(\rho) + K]\rho^{\frac{\mu-1}{2}} - [\psi(\rho) - L]\rho^{\frac{-\mu-1}{2}}\right\}, \tag{6}$$

where a notation $\delta = 1/A_{11}$ is used. Denote the Winkler coefficient of the elastic medium surrounding the two-layer sphere by κ. We have the obvious boundary conditions in the instance considered:

$$\begin{aligned} \sigma_\rho'(a') &= -\rho, \quad \sigma_\rho'(a) = \sigma_\rho(a), \quad u'(a) = u(a), \\ \sigma_\rho(a'') &= -\kappa u(a''), \end{aligned} \tag{7}$$

which, after some elementary computations, yield the following values of the constants of integration:

$$\begin{aligned} K &= \frac{1}{\Delta_1}(\gamma_2'F_1 - \gamma_1'F_2), \quad K' = \frac{1}{\Delta_1}(\gamma_2 F_1 - \gamma_1 F_2), \\ L &= \alpha + \beta(a'')^\mu K, \quad L' = \alpha' + \beta'(a')^{\mu'}K', \end{aligned} \tag{8}$$

where

$$\begin{aligned} \Delta_1 &= \gamma_1'\gamma_2 - \gamma_2'\gamma_1, \\ \gamma_1' &= \delta' a^{\mu'/2}[1 + \beta' a^{-\mu'}(a')^{\mu'}], \\ \gamma_1 &= \delta a^{\mu/2}[1 + \beta a^{-\mu}(a'')^\mu], \\ \gamma_2' &= \alpha_1' a^{\mu'/2}[1 + a^{-\mu'}(a')^{\mu'}], \\ \gamma_2 &= a^{\mu/2}[\alpha_1 - \alpha_2\beta a^{-\mu}(a'')^\mu], \\ F_1 &= \delta a^{-\mu/2}\alpha - \delta' a^{\mu'/2}[\varphi'(a) + \omega'], \\ F_2 &= -\alpha_2 a^{-\mu/2}\alpha - \alpha_2' a^{\mu'/2}[\beta'\varphi'(a) - \omega'], \\ \alpha &= \beta(a'')^\mu\varphi(a'') + \psi(a''), \quad \alpha' = \frac{p}{\alpha_2'}(a')^{\frac{\mu'+3}{2}} \\ \omega' &= a^{-\mu'}[\alpha' - \psi'(a)], \quad \beta = \frac{\alpha_1 + \kappa\delta a''}{\alpha_2 - \kappa\delta a''}, \quad \beta' = \frac{\alpha_1'}{\alpha_2'}. \end{aligned} \tag{9}$$

Limit Cases

Clearly, for $\kappa = 0$, and no difference between the basic quantities (5) with and without primes, one obtains the known solution for a unilayer transversely isotropic sphere.[4, 5]

For $\kappa = \infty$, a case of a two-layer sphere surrounded by an ideally rigid medium is obtained. In this instance $\beta = 1$.

Assume now that the surrounding medium is transversely isotropic, and denote the respective elastic constants by a star. Then it is easy to find the respective value of the Winkler coefficient by using the results of the foregoing discussion. To this end we attribute primes to all basic quantities (5), and substitute, in the final equations a'' and, say, b for a' and a'', respectively. Again we put $\kappa = 0$ and substitute for p the value κ. The last quantity will now be obtained from the obvious condition

$$u'(a') = 1 \tag{10}$$

(before a'' being substituted for a'). A lengthy calculation yields finally

$$\kappa = \frac{\alpha_1^*\alpha_2^*[b^{\mu^*} - (a'')^{\mu^*}]}{\delta^* a''[\alpha_1^* b^{\mu^*} - \alpha_2^*(a'')^{\mu^*}]}. \tag{11}$$

For a limit case, $b \to \infty$, we obtain for a transversely isotropic surrounding medium

$$\kappa = \frac{(\mu^* + 1)A_{11}^* - 4A_{12}^*}{2a''}, \tag{12}$$

or, for an isotropic medium

$$\kappa = \frac{2E^*}{a''(1 + \nu^*)}. \tag{13}$$

By substituting the values (12) or (13) for κ into the formula (9) for β we obtain, clearly, the solution for a transversely isotropic two-layer sphere surrounded by a classical transversely isotropic or isotropic medium, respectively.

[5] S. G. Lekhnitsky, "The Theory of Elasticity of an Anisotropic Body" (in Russian), Gos. Izd. Tekhn. Teor. Lit., Moscow-Leningrad, 1950, p. 287.

Transient Analysis of Stress-Wave Penetration in Plates[1]

NORMAN DAVIDS
Professor,
Department of Engineering Mechanics,
The Pennsylvania State University,
University Park, Pa.

This paper carries out an analysis of the propagation of a transient stress pulse concentrated at a point on the boundary of a plate whose thickness is of the order of a wave length. It is based on an expansion method used by Caignard in geophysical-layer problems which obviates the contour-integration difficulties and whose terms represent successively reflected waves of increasing time delay. From the general formulas obtained in this paper for an arbitrary forcing function, the stress versus time distribution along the axis of a 1-in-thick aluminum plate is obtained for a 5-microsec exponentially decaying pressure pulse. Inside the plate it is found there is a compressed zone which is relieved by a negative front traveling with the distortional wave velocity. When this interferes with a certain reflected negative front, the stress reverses in sign. A comparison of the location of this reversal is made with those based on plane-wave assumptions. Limiting cases are discussed.

THIS work is a continuation of an analysis of stress waves penetrating axially into plates, caused by a concentrated impact on the boundary. This is described in [1][2] and in [2]. One purpose of this analysis is to furnish basic theoretical information for determining scabbing effects in plates. Since this type of damage is caused by changeover of the initial compression wave into a tensile wave at a free boundary of the specimen, it is necessary for the analysis not only to follow the wave across the plate, particularly along the axis, but to study up to a certain point the superposed effect caused by multiple reflection at these free surfaces.

In principle, the steady-state analysis of stress waves is made equivalent mathematically to the transient-pulse problem by means of the Fourier integral theorem. However, it is another matter to actually carry through the synthesis expressed by this theorem. This has been done in a few seismological wave-propagation problems, which are somewhat related to our present problem; e.g., Pekeris [3] for the buried line source. Nevertheless, there are some significant differences between earth-layer analyses and the type of information desired for metal plates: (*a*) The time duration of the pulse in plates is of the order of the time required for it to propagate across the specimen. (*b*) The behavior of the wave through the plate is of primary interest, rather than surface displacements or stresses.

Pursey [4] has obtained propagation data for harmonic inputs, including briefly the case of thicknesses of the order of a wave length. In this paper we consider the transient problem, which is, in certain respects, more difficult than the steady-state one. For one thing, the time variation can no longer be eliminated from the analysis through its replacement by a single constant, the frequency. One cannot infer the location of stress-reversal points from the steady-state solution or from nodal points, as the successive modes do not superpose in a simple way. Essentially another integration would have to be performed over the frequency variable, which enters into the expressions in a complicated way.

Mencher [5] has made an analysis of a problem of waves in a stratified layer emanating from a point source in the center. Garvin [6] has worked out the exact transient solution for the buried line source in closed form. These have been based on the pioneering work of Caignard [7]. The present paper, by starting from the representation of the desired stresses as Laplace transforms, works out the normal stress distribution along the axis of the plate. This is done by an expansion method originally em-

[1] This research was performed at the Pennsylvania State University, and was sponsored by the Office of Ordnance Research, U. S. Army, under Contract No. TB2-0001(1253), entitled "Scabbing and Fracture of Materials by Stress Waves." The support is gratefully acknowledged.

[2] Numbers in brackets designate References at end of paper.

Contributed by the Applied Mechanics Division and presented at the Annual Meeting, Atlantic City, N. J., November 29–December 4, 1959, of THE AMERICAN SOCIETY OF MECHANICAL ENGINEERS.

Discussion on this paper should be addressed to the Secretary, ASME, 29 West 39th Street, New York, N. Y., and will be accepted until January 10, 1960, for publication at a later date. Discussion received after the closing date will be returned.

NOTE: Statements and opinions advanced in papers are to be understood as individual expressions of their authors and not those of the Society. Manuscript received by ASME Applied Mechanics Division, September 22, 1958. Paper No. 59—A-16.

Nomenclature

r, z = cylindrical co-ordinates in plate
t = time
d = thickness of plate
a = half-thickness = $d/2$
$P(t)$ = forcing function
P_m = maximum force
$\bar{\xi}$ = displacement vector
u_r, u_θ, u_z = displacement components
ρ = density
λ, μ = Lamé constants
σ_{zz}, σ_{rr} = stress components
$\gamma_1 = [\rho p^2/(\lambda + 2\mu)]^{1/2}$, $\gamma_2 = [\rho p^2/\mu]^{1/2}$
γ, h, k = wave-number parameters; $h = [\gamma_1^2 + \gamma^2]^{1/2}$, $k = [\gamma_2^2 + \gamma^2]^{1/2}$
$\tilde{h} = h/p$, $\tilde{k} = k/p$, $\tilde{\gamma} = \gamma/p$
A, B, C, D = coefficients
p = frequency parameter
$\delta(r)$ = singularity (Dirac delta) function
$x = e - p\tilde{\lambda}d$, $y = e - p\tilde{k}d$
b = fall-off rate of input pulse
m, n = summation indices
$d, \beta, p, q, \Delta, g, \varphi_{mn}, \psi_{mn}, f_{mn}, \tau_{ij}$, functional abbreviations defined in text
$L[\ldots]$ = Laplace transform
H = unit step function

ployed by Caignard which obviates the need for having to invert the Laplace transform directly.[3]

Basic Mathematical Solution

Fig. 1 shows a plate which is assumed to be infinite in extent, of given thickness d, together with the appropriate cylindrical coordinate system. The impact is represented by a concentrated force acting at the point O of the boundary, with prescribed time-variation $P(t)$. Tension is taken as positive.

The front and back faces of the plate are supposed free of stress except at the impact point, where the normal stress is infinite. This is expressed by the following conditions:

$$\sigma_{zz}(r, 0) = \delta(r), \qquad \sigma_{rz}(r, 0) = 0 \tag{1}$$

$$\sigma_{zz}(r, d) = 0, \qquad \sigma_{rz}(r, d) = 0 \tag{2}$$

$$\sigma_{\theta z} \equiv 0 \quad \text{by radial symmetry} \tag{3}$$

where $\delta(r, t)$ is a "Dirac delta function"; i.e., such that

$$\delta(0, t) = \infty, \qquad \delta(r, t) = 0 \quad \text{for} \quad r \neq 0 \tag{4}$$

and

$$\int_0^{2\pi}\int_0^{\infty} \delta(r, t) r dr d\theta = P(t) \tag{4a}$$

The equations of motion, in vector form, are given by

$$\rho \ddot{\mathbf{s}} = (\lambda + 2\mu) \operatorname{grad} \operatorname{div} \mathbf{s} - \mu \operatorname{curl} \operatorname{curl} \mathbf{s} \tag{5}$$

where $\mathbf{s} = (u_r, u_\theta, u_z)$ is the displacement vector, λ, μ are the Lamé constants, and ρ the density of the material. These are the classical Pochhammer-Chree equations [8]. Their basic radially symmetric solution, as can be verified, is given by

$$u_r = \int_C (Ae^{hz} + Be^{kz} + Ce^{-hz} + De^{-kz}) Z_1(\gamma r) e^{\pm pt} d\gamma \tag{6}$$

$$u_z = \int_C \left(-\frac{Ah}{\gamma} e^{hz} - \frac{B\gamma}{k} e^{kz} + \frac{Ch}{\gamma} e^{-hz} + \frac{D\gamma}{k} e^{-kz} \right) Z_0(\gamma r) e^{\pm pt} d\gamma \tag{7}$$

where A, B, C, D, are functions of the wave-number parameter γ to be determined, h and k wave numbers, given by

$$h = [\gamma_1^2 + \gamma^2]^{1/2} \qquad k = [\gamma_2^2 + \gamma^2]^{1/2} \tag{8}$$

$$\gamma_1^2 = \rho p^2/(\lambda + 2\mu) \qquad \gamma_2^2 = \rho p^2/\mu \tag{9}$$

Z_0, Z_1 functions of Bessel type, and C some path of integration or contour. When the parameter p is real, as shall be taken hereafter, the solution is referred to as of exponential type. The stresses are calculated from the relations

$$\sigma_{zz} = \lambda \frac{\partial u_r}{\partial r} + \lambda \frac{u_r}{r} + (\lambda + 2\mu) \frac{\partial u_z}{\partial z} \tag{10}$$

$$\sigma_{zr} = \mu \left(\frac{\partial u_r}{\partial z} + \frac{\partial u_z}{\partial r} \right) \tag{11}$$

Working out, starting from (6) and (7),

$$\sigma_{zz} = \int_C \left\{ \left[\lambda\gamma - (\lambda + 2\mu) \frac{h^2}{\gamma} \right] (Ae^{hz} + Ce^{-hz}) - 2\mu\gamma(Be^{kz} + De^{-kz}) \right\} Z_0(\gamma r) e^{pt} d\gamma \tag{12}$$

$$\sigma_{zr} = \int_C \left\{ 2\mu h(Ae^{hz} - Ce^{-hz}) + \mu\left(k + \frac{\gamma^2}{k}\right)(Be^{kz} - De^{-kz}) \right\} Z_1(\gamma r) e^{pt} d\gamma \tag{13}$$

[3] Broberg, in a paper to be published (Transactions of the Royal Institute of Technology, Stockholm), has also approached the problem starting from this standpoint and has done some interesting experiments measuring the displacement opposite the point of impact.

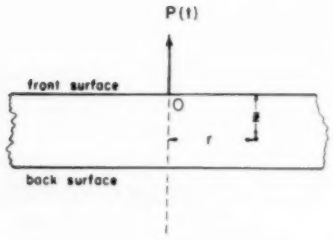

Fig. 1 Plate specimen, normal impact

The quantities A to D are functions of γ to be determined next from the boundary conditions.

Completion of the Boundary-Value Problem

In this section we shall work out the values of the coefficients A to D from the boundary conditions.

First, we represent the concentrated load function (4) as an integral of Bessel a function, as follows:

$$\delta(r) = \frac{1}{2\pi} \int_0^{\infty} \gamma J_0(\gamma r) d\gamma \tag{14}$$

This may be verified by starting from the known definite integral [9],

$$f(\rho, r) = \int_0^{\infty} e^{-\gamma\rho} J_0(\gamma r) d\gamma = [\rho^2 + r^2]^{-1/2}, \tag{15}$$

differentiating with respect to ρ, and letting $\rho \to 0$, giving

$$\delta(r) = 0, \qquad r \neq 0, \qquad \delta(0) = \infty$$

and

$$\int_0^{2\pi}\int_0^{\infty} \delta(r) r dr d\theta = 1$$

Also, in order to be able to cancel a common time factor in the boundary equations below, we assume the basic load time-variation to be in the form

$$P(t) = e^{pt} \tag{16}$$

to be extended later by the Laplace transform.

Starting from the operations (10), (11), and applying the boundary conditions (1)–(3), choosing the Bessel function J_0 for Z_0 and the positive real axis for path C, as required by (14), we obtain

$$\sigma_{zz}\Big|_{z=0} = \int_0^{\infty} \left\{ \alpha(A + C) - 2\mu\gamma(B + D) \right\} J_0(\gamma r) d\gamma e^{pt} = \frac{1}{2\pi} \int_0^{\infty} \gamma J_0(\gamma r) d\gamma e^{pt} \tag{17a}$$

$$\sigma_{zr}\Big|_{z=0} = \int_0^{\infty} \{2\mu h(A - C) + \mu\beta(B - D)\} J_1(\gamma r) e^{pt} d\gamma = 0 \tag{17b}$$

$$\sigma_{zz}\Big|_{z=d} = \int_0^{\infty} \{\alpha(Ae^{hd} + Ce^{-hd}) - 2\mu\gamma(Be^{kd} + De^{-kd})\} J_0(\gamma r) e^{pt} d\gamma = 0 \tag{17c}$$

$$\sigma_{zr}\Big|_{z=d} = \int_0^{\infty} \{2\mu h(Ae^{hd} - Ce^{-hd}) + \mu\beta(Be^{kd} - De^{-kd})\} J_1(\gamma r) e^{pt} d\gamma = 0 \tag{17d}$$

$$\alpha = \lambda\gamma - (\lambda + 2\mu)\frac{h^2}{\gamma} = -\frac{\mu}{\gamma}(\gamma_2^2 + 2\gamma^2)$$

$$\beta = k + \frac{\gamma^2}{k} = (\gamma_2^2 + 2\gamma^2)/k \tag{18}$$

Since these equations must hold for all values of r,

$$\begin{aligned}
&\alpha(A + C) - 2\mu\gamma(B + D) = \gamma/2\pi \\
&2h(A - C) + \beta(B - D) = 0 \\
&\alpha(Ae^{hd} + Ce^{-hd}) - 2\mu\gamma(Be^{hd} + De^{-hd}) = 0 \\
&2h(Ae^{hd} - Ce^{-hd}) + \beta(Be^{hd} - De^{-hd}) = 0
\end{aligned} \tag{19}$$

The solution to this set of linear equations is

$$\left.\begin{aligned}
A &= \frac{\gamma\beta}{2\pi\Delta}[8\mu\gamma h - pe^{-(h+k)d} - qe^{-(h-k)d}] \\
&= \frac{\gamma\beta}{4\pi}e^{-hd}\left(-\frac{\cosh ka}{\Delta_1} + \frac{\sinh ka}{\Delta_2}\right) \\
B &= \frac{\gamma h}{\pi\Delta}[-2\alpha\beta + pe^{-(h+k)d} - qe^{(h-k)d}] \\
&= \frac{\gamma h}{2\pi}e^{-hd}\left(\frac{\cosh ha}{\Delta_1} - \frac{\sinh ha}{\Delta_2}\right) \\
C &= \frac{\gamma\beta}{2\pi\Delta}[8\mu\gamma h - qe^{(h-k)d} - pe^{(h+k)d}] \\
&= \frac{\gamma\beta}{4\pi}e^{hd}\left(\frac{\cosh ka}{\Delta_1} + \frac{\sinh ka}{\Delta_2}\right) \\
D &= \frac{\gamma h}{\pi\Delta}[-2\alpha\beta + pe^{(h+k)d} - qe^{-(h-k)d}] \\
&= \frac{\gamma h}{2\pi}e^{hd}\left(-\frac{\cosh ha}{\Delta_1} - \frac{\sinh ha}{\Delta_2}\right)
\end{aligned}\right\} \tag{20}$$

where

$$\begin{aligned}
p &= 4\mu\gamma h + \alpha\beta = \frac{\mu}{\gamma k}[4\gamma^2 hk - (\gamma_2^2 + 2\gamma^2)^2] \\
q &= 4\mu\gamma h - \alpha\beta = \frac{\mu}{\gamma k}[4\gamma^2 hk + (\gamma_2^2 + 2\gamma^2)^2] \\
a &= d/2
\end{aligned} \tag{21}$$

and Δ is the determinant, given by

$$\begin{aligned}
\Delta &= 2(p^2 - q^2) - p^2e^{-(h+k)d} - p^2e^{(h+k)d} \\
&\qquad + q^2e^{-(h-k)d} + q^2e^{(h-k)d} \\
&= -4\Delta_1\Delta_2
\end{aligned} \tag{22}$$

where

$$\begin{aligned}
\Delta_1 &= p\sinh(h + k)a - q\sinh(h - k)a \\
\Delta_2 &= p\sinh(h + k)a + q\sinh(h - k)a
\end{aligned} \tag{23}$$

The Axial Normal Stress

When the expressions (20) are substituted into the stress expressions (10) and (11), the exact mathematical solution to the plate problem is obtained. We shall exhibit the result explicitly here for the normal stress:

$$\sigma_{zz} = -\frac{e^{pt}}{4\pi}\int_0^\infty \frac{\begin{matrix}\sinh h(z-a)\cosh ka \\ -\,g(\gamma)\sinh k(z-a)\cosh ha\end{matrix}}{\begin{matrix}\sinh ha\cosh ka \\ -\,g(\gamma)\sinh ka\cosh ha\end{matrix}}\gamma J_0(\gamma r)d\gamma +$$

$$\frac{e^{pt}}{4\pi}\int_0^\infty \frac{\begin{matrix}\cosh h(z-a)\sinh ka \\ -\,g(\gamma)\cosh k(z-a)\sinh ha\end{matrix}}{\begin{matrix}\cosh ka\sinh ka \\ -\,g(\gamma)\cosh ka\sinh ha\end{matrix}}\gamma J_0(\gamma r)d\gamma \tag{24}$$

in which we also have introduced the notation

$$g(\gamma) = -\frac{4\mu\gamma h}{\alpha\beta} = \frac{4\gamma^2 hk}{(\gamma_2^2 + 2\gamma^2)^2} \tag{25}$$

From the physical point of view the most important direction of propagation from the source is that along the axis $r = 0$, where the shearing stress is zero, and where the factor $J_0(\gamma r)$, being equal to unity, may be dropped. We shall continue the explicit analysis on this basis.

At this point the classical mathematical analysis would proceed to a solution for arbitrary time variation of the load, by integrating (24) with respect to the frequency variable p. The difficulty of carrying this out is increased by the presence of p implicitly under the integrals in (24), since it enters through (9). We shall use a procedure in the remainder of this paper which avoids having to integrate either with respect to p or γ.

The first step is to rewrite our expression (24) for the stress in a form where p enters explicitly. To this end, introduce the following reduced variables:

$$\begin{aligned}
\tilde{\gamma} &= \gamma/p; \qquad d\tilde{\gamma} = d\gamma/p \\
\tilde{h} &= h/p; \qquad \tilde{k} = k/p
\end{aligned}$$

Then $g(\gamma) = g(\tilde{\gamma})$, since p cancels. We then have, for the normal stress,

$$\begin{aligned}
\sigma_{zz} = \frac{p^2}{4\pi}e^{pt}\Bigg\{ &-\int_0^\infty \frac{\sinh p\tilde{h}(z-a)\tilde{\gamma}d\tilde{\gamma}}{\left(1 - g\dfrac{\tanh p\tilde{k}a}{\tanh p\tilde{h}a}\right)\sinh p\tilde{h}a} \\
&+\int_0^\infty \frac{g\sinh p\tilde{k}(z-a)\cosh p\tilde{h}a\,\tilde{\gamma}\,d\tilde{\gamma}}{\left(1 - g\dfrac{\tanh p\tilde{k}a}{\tanh p\tilde{h}a}\right)\sinh p\tilde{h}a\cosh p\tilde{k}a} \\
&+\int_0^\infty \frac{\cosh p\tilde{h}(z-a)\tilde{\gamma}\,d\tilde{\gamma}}{\left(1 - g\dfrac{\tanh p\tilde{h}a}{\tanh p\tilde{k}a}\right)\cosh p\tilde{h}a} \\
&-\int_0^\infty \frac{g\cosh p\tilde{k}(z-a)\sinh p\tilde{h}a\,\tilde{\gamma}\,d\tilde{\gamma}}{\left(1 - g\dfrac{\tanh p\tilde{h}a}{\tanh p\tilde{k}a}\right)\cosh p\tilde{h}a\sinh p\tilde{k}a}\Bigg\}
\end{aligned} \tag{26}$$

This breakdown into four terms corresponds physically to wave components of different delay, as will be seen later.

Next we note, since $g(\gamma)$ is independent of p, that the integrands in (26) are rational function of

$$x = e^{-p\tilde{h}d}; \qquad y = e^{-p\tilde{k}d} \tag{27}$$

as follows:

$$\sigma_{zz} = \frac{p^2}{4\pi}e^{pt}\int_0^\infty \Bigg\{\frac{e^{-p\tilde{h}z} - e^{-p\tilde{h}(d-z)}}{(1 - gR)(1 - x)} - gR\frac{e^{-p\tilde{k}z} - e^{-p\tilde{k}(d-z)}}{(1 - gR)(1 - y)}$$

$$+\frac{e^{-p\tilde{h}(d-z)} + e^{-p\tilde{h}z}}{(1 - g/R)(1 + x)} - \frac{e^{-p\tilde{k}z} + e^{-p\tilde{k}(d-z)}}{(1 - g/R)(1 + y)}\frac{g}{R}\Bigg\}\tilde{\gamma}\,d\tilde{\gamma}$$

where

$$R = (1 + x)(1 - y)/(1 - x)(1 + y)$$

The parts containing g, R, x, and y may now be expanded formally in a power series in x and y. We need not consider whether it converges nor justify rearranging or regrouping of terms as the

final solution is justified directly. We obtain, again formally,

$$\sigma_{zz} = \frac{p^2 e^{pt}}{2\pi} \sum_{m,n=0}^{\infty} \left\{ \left[\frac{1 + (-1)^{m+n}}{2} \right] \int_0^\infty e^{-p\bar{h}z} \varphi_{mn}(g) x^m y^n \tilde{\gamma}\, d\tilde{\gamma} \right.$$
$$+ \left[\frac{1 - (-1)^{m+n}}{2} \right] \int_0^\infty e^{-p\bar{h}(d-z)} \varphi_{mn}(g) x^m y^n \tilde{\gamma}\, d\tilde{\gamma}$$
$$+ \left[\frac{1 + (-1)^{m+n}}{2} \right] \int_0^\infty e^{-p\bar{k}z} \psi_{mn}(g) x^m y^n \tilde{\gamma}\, d\tilde{\gamma}$$
$$\left. + \left[\frac{1 - (-1)^{m+n}}{2} \right] \int_0^\infty e^{-p\bar{k}(d-z)} \psi_{mn}(g) x^m y^n \tilde{\gamma}\, d\tilde{\gamma} \right\} \quad (28)$$

It will be seen later that the terms represented by the indexes m, n are successively reflected waves. The functions φ_{mn}, ψ_{mn} are weight factors. Their first few values are

$$\varphi_{00} = 1/(1-g) \qquad \psi_{00} = -g/(1-g)$$
$$\varphi_{10} = -(1+g)/(1-g)^2 \qquad \psi_{10} = 2g/(1-g)^2$$
$$\varphi_{01} = 2g/(1-g)^2 \qquad \psi_{01} = -g(1+g)/(1-g)^2$$
$$\varphi_{20} = (1+g)^2/(1-g)^3 \qquad \psi_{20} = -2g(1+g)/(1-g)^3 \quad (29)$$
$$\varphi_{11} = -2g(3+g)/(1-g)^3 \qquad \psi_{11} = 2g(3g+1)/(1-g)^3$$
$$\varphi_{02} = 2g(1+g)/(1-g)^3 \qquad \psi_{02} = -g(1+g)^2/(1-g)^3$$
$$\varphi_{30} = -(1+g)^3/(1-g)^4$$

When the values (27) for x and y are substituted in (28),

$$\sigma_{zz} = \frac{p^2 e^{pt}}{2\pi} \sum_{m,n=0}^{\infty} \left\{ \frac{1 + (-1)^{m+n}}{2} \int_0^\infty e^{-p(\bar{h}z + m\bar{h}d + n\bar{k}d)} \varphi_{mn} \tilde{\gamma}\, d\tilde{\gamma} \right.$$
$$+ \frac{1 - (-1)^{m+n}}{2} \int_0^\infty e^{-p(\bar{h}(d-z) + m\bar{h}d + n\bar{k}d)} \varphi_{mn} \tilde{\gamma}\, d\tilde{\gamma}$$
$$+ \frac{1 + (-1)^{m+n}}{2} \int_0^\infty e^{-p(\bar{k}z + m\bar{h}d + n\bar{k}d)} \psi_{mn} \tilde{\gamma}\, d\tilde{\gamma}$$
$$\left. + \frac{1 - (-1)^{m+n}}{2} \int_0^\infty e^{-p(\bar{k}(d-z) + m\bar{h}d + n\bar{k}d)} \psi_{mn}\, \tilde{\gamma}\, d\tilde{\gamma} \right\} \quad (30)$$

These represent, respectively, downgoing dilatation, upgoing dilatation, downgoing distortion, and upgoing-distortion-type waves.

Figs. 2 and 3 interpret in physical terms how the successive terms in the series are generated. Thus a φ_{ij}-term refers to a dilatation-wave operator generated from i previous dilatation waves and j previous distortion waves by successive $i + j$ reflections. When either type wave is incident at a free surface it generates the pair of reflections with modifying factors as follows:

$$\varphi_{i+1,j} = \varphi_{ij}[-(1+g)/(1-g)]; \qquad \varphi_{i,j+1} = \psi_{ij}(1+g)/(1-g) \quad (30a)$$
$$\psi_{i+1,j} = \varphi_{ij} 2g/(1-g); \qquad \psi_{i,j+1} = \psi_{ij}[-2/(1-g)]$$

Fig. 3 diagrams the successive reflections up to the second order.

Expressing the fact that each wave is generated by reflection from incident waves of both types, we have the following recurrence relations:

$$\varphi_{ij} = \varphi_{i-1,j}\left(-\frac{1+g}{1-g}\right) + \psi_{i,j-1}\left(-\frac{2}{1-g}\right)$$
$$\psi_{ij} = \psi_{i,j-1}\left(\frac{1+g}{1-g}\right) + \varphi_{i-1,j}\left(\frac{2g}{1-g}\right) \quad (31)$$

starting from

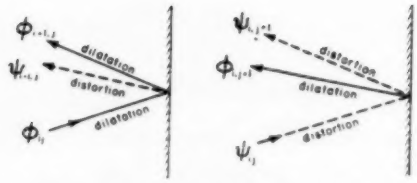

Fig. 2 Reflection operators at free surface of plate

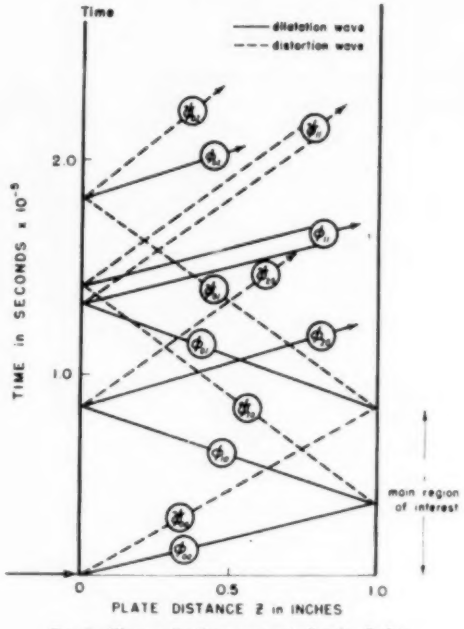

Fig. 3 Wave reflections on central axis of plate

$$\varphi_{00} = 1/(1-g), \qquad \psi_{00} = -g/(1-g) \quad (32)$$

(If an index is negative, the corresponding function is zero.)

The identical procedures given in this section for the axial normal stress can be carried through for any of the other stresses, or for any location in the plate.

Arbitrary Forcing Function

The work of the previous section has been to put the expression for the required stress in a form where the parameter p in addition to $p^2 e^{pt}$ appears explicitly as part of a negative exponential, as in (30). This is essential for carrying through the remainder of the procedure, since it forms the kernel of the Laplace-transform operation.

To put our expressions in the desired form, a change of variable must be made affecting the functions in parentheses which multiply p in each of the integrals of (30). These functions are individually replaced by new independent variables τ_i, as follows:

$$\sigma_{zz} = \frac{p^2 e^{pt}}{2\pi} \sum_{m,n=0}^{\infty} \left(\sum_{i=1,2,3,4} \int_0^\infty e^{-p\tau_i} f_{mn}{}^{i}(\tau_i) d\tau_i \right) \quad (33)$$

$$\tau_1 = \bar{h}z + m\bar{h}d + n\bar{k}d$$
$$\tau_2 = \bar{h}(d-z) + m\bar{h}d + n\bar{k}d \quad (34)$$
$$\tau_3 = \bar{k}z + m\bar{h}d + n\bar{k}d \quad (cont.)$$

$$\tau_4 = \tilde{k}(d - z) + m\tilde{h}d + n\tilde{k}d \tag{34}$$

and

$$\begin{aligned}
f_{mn}^{1} &= \frac{1 + (-1)^{m+n}}{2}\,\varphi_{mn}(\tilde{\gamma})\tilde{\gamma}\,\frac{d\tilde{\gamma}}{d\tau_1}\,H(\tau_1 - \tau_1(0)) \\
f_{mn}^{2} &= \frac{1 - (-1)^{m+n}}{2}\,\varphi_{mn}(\tilde{\gamma})\tilde{\gamma}\,\frac{d\tilde{\gamma}}{d\tau_2}\,H(\tau_2 - \tau_2(0)) \\
f_{mn}^{3} &= \frac{1 + (-1)^{m+n}}{2}\,\psi_{mn}(\tilde{\gamma})\tilde{\gamma}\,\frac{d\tilde{\gamma}}{d\tau_3}\,H(\tau_3 - \tau_3(0)) \\
f_{mn}^{4} &= \frac{1 - (-1)^{m+n}}{2}\,\psi_{mn}(\tilde{\gamma})\tilde{\gamma}\,\frac{d\tilde{\gamma}}{d\tau_4}\,H(\tau_4 - \tau_4(0))
\end{aligned} \tag{35}$$

in which H is the unit step function and $\tau_i(0) = \tau_i(\tilde{\gamma} = 0)$. In order to make each f_{mn} a function of the corresponding τ_i, it is necessary to solve each of the relations (34) for $\tilde{\gamma}$ and substitute for it in the corresponding expression of (35).

The purpose of introducing the step functions in (35) is purely formal in that it permits writing the lower limit of the integrals as zero, instead of $\tau_i(0)$. When $\tilde{\gamma} = 0$, this value represents physically the arrival time of the corresponding wave, before which the disturbance must be zero. There is of course a discontinuity in the function at this time.

It is to be noted that the quantity in parenthesis in (33) is in the form of a Laplace transform. If we multiply (33) by any function of p it still remains a solution to the wave equations (5) and continues to satisfy the boundary conditions (1–3). We shall now choose this function as the Laplace transform of the prescribed load function $P(t)$:

$$L[P(t)] = \int_0^\infty e^{-pt}P(t)dt \tag{36}$$

Thus each term of (33) now takes the form (we shall suppose the subscripts i and m, n to be understood on each symbol f up to equation (48))

$$2\pi\sigma_{zz} = L[P(t)]f(p, z)e^{pt} \tag{37}$$

Since the inverse Laplace transform of this expression involves only a further integration with respect to p, the result of this transformation remains a solution to the wave equations:

$$2\pi\sigma_{zz}(z, t) = L^{-1}\{L[P(t)]f(p, z)\} \tag{38}$$

The factor e^{pt} no longer appears explicitly as it is part of the operator L^{-1}. This result now satisfies the time condition (4a) also. For, on the front boundary of the plate $z = 0$,

$$2\pi\sigma_{zz}(0, t) = L^{-1}\{L[P(t)]f(p, 0)\} \tag{39}$$

But $f(p, 0) = \delta(r)$ as may be seen by putting $z = 0$ in (24). Hence (38) becomes

$$2\pi\sigma_{zz}(0, t) = L^{-1}\{L[P(t)]\delta(r)\} = \delta(r)L^{-1}L[P(t)] = \delta(r)P(t) \tag{40}$$

as was to be shown.

From (33) and (38) we have

$$2\pi\sigma_{zz} = L^{-1}\{p^2L[P(t)]L[f]\} \tag{41}$$

Next, by employing the convolution theorem[4] we may write

$$L[P(t)]L[f] = L\int_0^t P(t - \tau)f(\tau)d\tau \tag{42}$$

Its use is legitimate since $f(\tau)$ is piecewise continuous, as is required. We next apply the identity[5]

$$L[F''(t)] = p^2L[F(t)] - pF(0) - F'(0)$$

to $F(t) = \int_0^t P(t - \tau)f(\tau)d\tau$. In this expression $F(0) = 0$, and from

$$F'(t) = \int_0^t P'(t - \tau)f(\tau)d\tau + P(0)f(t) \tag{43}$$

follows that $F'(0) = P(0)f(0) = 0$, since the arrival time of any of the waves in the interior is always positive. At these times, however, discontinuities occur in $f(\tau)$ which introduce additional terms in the foregoing differentiations. For the sake of carrying on the main argument we shall suppose, for the moment, that all jumps have been smoothed off by gradual transitions. With this in mind,

$$p^2L\int_0^t P(t - \tau)f(\tau)d\tau = L\frac{d^2}{dt^2}\int_0^t P(t - \tau)f(\tau)d\tau \tag{44}$$

By differentiation once under the integral sign and integrating by parts, noting that $f(0) = 0$, this becomes

$$L\left[\frac{d}{dt}\int_0^t P(t - \tau)f'(\tau)d\tau\right] \tag{45}$$

Hence when this is substituted into (41), the L and L^{-1} operations cancel, leaving the expression

$$2\pi\sigma_{zz} = \frac{d}{dt}\int_0^t P(t - \tau)f'(\tau)d\tau \tag{46}$$

It is not advantageous for practical purposes to carry out the differentiation indicated here.

We can now easily take care of the discontinuities. Each function $f(\tau)$ has a step at $\tau(0) = \tau(\gamma = 0)$ where it jumps from zero to $f^+(\tau(0))$ signaling the arrival of the wave. Differentiation of the step function $H(\tau - \tau(0))$ is formally handled by inserting a δ-function, so that, from (35),

$$f'(\tau)\Big|_{\tau = \tau(0)} = f'(\tau)\Big|_{\tau = \tau^+(0)} + f(\tau(0))\delta(\tau - \tau(0)) \tag{47}$$

The first term on the right refers to the derivative from the right-hand side. When this is substituted into the integral (46), the first term changes the lower limit to $t^+(0)$, while the δ-function integrates out, giving

$$2\pi\sigma_{zz} = \frac{d}{dt}\int_{t(0)^+}^t P(t - \tau)f'(\tau)d\tau + f(t(0))P'(t - \tau(0))$$

Summarizing, the complete expression for the normal stress is

$$\sigma_{zz} = \frac{1}{2\pi}\sum_{m,n=0}^{\infty}\sum_{i=1}^{4}\frac{d}{dt}\int_{\tau_i(0)}^t P(t - \tau_i)\frac{d}{d\tau_i}f_{mn}^{i}(\tau_i)d\tau_i + f_{mn}^{i}(\tau_i(0))P'(t - \tau_i(0)) \tag{48}$$

Thus we have expressed the stress explicitly in terms of the forcing function, with the Laplace-transform operation eliminated.

Questions of convergence of the series appearing in (48) do not actually arise since only a finite number of terms differs from zero. Given a value of t, only those terms contribute whose indexes m, n are such as to make the values of τ_i in (34), for $\tilde{\gamma} = 0$, less than t. This of course corresponds physically, because of the increasing delay, to the fact that only a finite number of waves has been generated up to the time t. That (48) satisfies the boundary conditions may be verified directly, with the help of the relations (30a) and that the wave equation is also satisfied, from the fact that each term is traceable to the terms of (30), which is in the elementary form of solution when the radial factor $J_0(\gamma r)$ is reinserted.

[4] Reference [10], p. 36.
[5] Ibid., p. 8.

Particular Cases—Exponential Pulse, Step Pulse

We shall consider the case of an input pulse which rises suddenly to unit amplitude then declines more gradually at an exponential rate, as shown in Fig. 4(*a*). This type of pulse when reversed in sign is a good approximation to the pressure variation caused by explosives. The step pulse is shown in Fig. 4(*b*).

For pulse (*a*), we have

$$\begin{aligned} P(t) &= 0 \qquad t < 0 \\ &= e^{-bt} \quad t > 0 \end{aligned} \tag{49}$$

Each term of the stress in (48) becomes

$$2\pi\sigma_{zz} = \frac{d}{dt}\int_0^t e^{-b(t-\tau)}f'(\tau)d\tau - bf(t(0))e^{-b(t-t(0))} \tag{50}$$

When the differentiation with respect to t is carried out, this becomes

$$2\pi\sigma_{zz} = -b[e^{-bt}\int_{t_0}^t e^{b\tau}f'(\tau)d\tau + f(t(0))e^{-b(t-t(0))}] + f'(t)$$

The complete expression is obtained by summation on m, n, i, as previously.

The corresponding expression for the step pulse is obtained by letting $b \to 0$, giving

$$2\pi\sigma_{zz} = f'(t). \tag{51}$$

The Aluminum Plate

In actual physical problems the waves decrease in amplitude rapidly enough so that only the first few reflections need be considered. We shall use this fact in considering here an aluminum plate with $d = 1$ in. having the following constants:

$$\begin{aligned} \tilde{\gamma}_1 &= 0.4105 \times 10^{-5} \text{ sec/in.} \\ \tilde{\gamma}_2 &= 0.823 \times 10^{-5} \text{ sec/in.} \end{aligned}$$

The dilatation velocity happens to be just twice the distortional. On the diagram in Fig. 3, the region of practical interest lies between $t = 0$ and $t = \tilde{\gamma}_2$ sec, which is the time when the incident distortion wave ψ_{00} reaches the back surface. If failure should not have occurred by this time, the material will probably be safe from further destruction, as we shall see. Thus the only waves with which we have to deal, referring to (35) and Fig. 3, are:

f_{00}^1 = incident dilatation

f_{00}^2 = incident distortion

f_{10}^2 = first reflected dilatation

f_{10}^4 = first reflected distortion

The remaining waves in the series get started too late to be of any practical importance for this problem.

For the pulse, we must select a value for the constant b. Now if b is large compared with $\tilde{\gamma}_1$, the pulse is practically over by the time required for the leading wave to reach the back face, so that it behaves essentially as though it were in an infinite medium. On the other hand, if b is small compared with $\tilde{\gamma}_1$, it acts as in a thin plate. The in-between case we are interested in studying thus occurs when $b\tilde{\gamma}_1$ is of the order of unity. We shall here actually make this unity, so that

$$b = 1/\tilde{\gamma}_1 = 2.435 \times 10^5 \text{ sec}^{-1} \tag{52}$$

(*a*) *The 0, 0 Wave.* Starting from (34) and (32), $\tau_1 = \tilde{h}z$, $\tau_1(0) = \tilde{\gamma}_1 z$, and $\varphi_{00} = 1/(1-g)$. Also

$$\tilde{\gamma}\, d\tilde{\gamma} = \frac{\tau d\tau}{z^2} \text{ so}$$

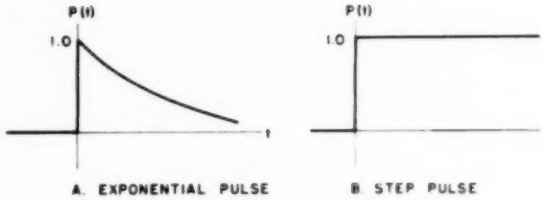

Fig. 4 Pulse inputs

$$\begin{aligned} f_{00}^1(t, z) &= 0 \qquad t < \tilde{\gamma}_1 z \\ &= \varphi_{00}\frac{t}{z^2} \quad t > \tilde{\gamma}_1 z \end{aligned} \tag{52a}$$

This is not completely explicit in t as it also enters into φ_{00} via the variables g and $\tilde{\gamma}$. It does not pay to carry out its elimination, however.

The form of the function shows that a wave front advances with velocity $z/t = \tilde{\gamma}_1$, decreases in amplitude as the square of the penetration distance, but is subject to a shape modification factor φ_{00}. For the stress, noting that $\varphi_{00} = 1$ when $\tilde{\gamma} = 0$, from (50),

$$\sigma_{zz} = 0 \qquad t < \tilde{\gamma}_1 z$$

$$\sigma_{zz} = \frac{1}{2\pi z^2}\frac{d}{dt}\left\{e^{-bt}\int_{\tilde{\gamma}_1 z}^t e^{b\tau}f'(\tau)d\tau\right\} - \frac{b\tilde{\gamma}_1}{z}e^{-b(t-\tilde{\gamma}_1 z)} \tag{53}$$

$$t > \tilde{\gamma}_1 z$$

To evaluate this it is convenient to introduce the function

$$F(t) = e^{-bt}\int_{\tilde{\gamma}_1 z}^t e^{b\tau}f'(\tau)d\tau + \tilde{\gamma}_1 z e^{-b(t-\tilde{\gamma}_1 z)} \tag{54}$$

We then have simply

$$\sigma_{zz} = \frac{1}{2\pi z^2}F'(t) \tag{55}$$

and note that the following differential equation is satisfied

$$F'(t) = -bF(t) + f'(t) \tag{56}$$

Numerical Evaluation

The job of calculating from an expression such as (53) a set of stress curves from given numerical data is still far from straightforward. Hence an indication of the techniques used may be helpful.

First a general table was calculated with $\tilde{\gamma}$ as the independent variable ranging at steps of 0.1 from 0 to 1; summarized in Table 1.

From the relation

$$\frac{d\varphi}{dt} = \frac{d\varphi}{dg}\frac{dg}{d\tilde{\gamma}}\frac{d\tilde{\gamma}}{dt}$$

we get

$$\frac{d\varphi}{dt} = \frac{g}{(1-g)^2}\left(\frac{2}{\tilde{\gamma}^2} + \frac{1}{\tilde{h}^2} + \frac{1}{\tilde{k}^2} - \frac{8}{\tilde{\gamma}_2^2 + 2\tilde{\gamma}^2}\right)\frac{t}{z^2} \tag{57}$$

which is a convenient formula for calculating $\varphi'(t)$, and then

$f'(t) = t\varphi'(t) + \varphi$. For $\tilde{\gamma} = 0$, $d\varphi/dt = 8\tilde{\gamma}_1^2/z\tilde{\gamma}_2^3$.

Next we decide on a series of positions inside the plate where the time variations of the waves are to be determined and plotted. For each such value of z we calculate the values of t,

Table 1 Wave functions for aluminum plate

$\tilde{\gamma}$ $\times 10^{-6}$	$\tilde{k} = [\tilde{\gamma}_1^2 + \tilde{\gamma}^2]^{1/2}$ $\times 10^{-6}$	$\tilde{k} = [\gamma_2^2 + \tilde{\gamma}^2]^{1/2}$ $\times 10^{-6}$	$g(\tilde{\gamma})$	$\varphi_{10} = 1/(1-g)$	ψ_{00}	φ_{10}	ψ_{10}
0.0	0.4109	0.8230	0.0000	1.000	−0.000	−1.000	0.0000
0.1	0.4229	0.8290	0.0288	1.030	−0.0297	−1.092	0.0612
0.2	0.4570	0.8469	0.1081	1.121	−0.1214	−1.392	0.2722
0.3	0.5088	0.8759	0.2182	1.279	−0.279	−1.993	0.7136
0.4	0.5734	0.9150	0.337	1.508	−0.508	−3.040	1.532
0.5	0.6472	0.9629	0.450	1.818	−0.818	−4.792	2.974
0.6	0.7272	1.018	0.543	2.188	−1.188	−7.387	5.198
0.7	0.8116	1.080	0.626	2.67	−1.672	−11.60	8.935
0.8	0.8994	1.148	0.690	3.23	−2.23	−17.64	14.41
0.9	0.9894	1.219	0.7408	3.89	−2.89	−26.37	22.48
1.0	1.081	1.295	0.7813	4.57	−3.57	−37.23	32.66

$\tilde{\gamma}_1 = 0.4105 \times 10^{-6}$ sec/in.
$\tilde{\gamma}_2 = 0.823 \times 10^{-6}$ sec/in.

Table 2 Typical Stress Calculation $z = 0.9$

$\tilde{\gamma}$ $\times 10^{-6}$	$t_1 = \tilde{h}z$ $\times 10^{-6}$	$f'(t)$	$F(t)$	$-bF(t)$	$F'(t)$	$2\pi\sigma_{zz} = F'/z^2$
0.00	0.370	2.000	0.370	−0.900	1.100	1.36
0.1	0.381	2.099	0.382	−0.928	1.171	1.45
0.2	0.411	2.415	0.418	−1.016	1.399	1.73
0.3	0.458	2.948	0.483	−1.178	1.770	2.19
0.4	0.516	3.699	0.586	−1.428	2.271	2.81
0.5	0.583	4.724	0.737	−1.795	2.929	3.62
0.6	0.645	5.879	0.948	−2.307	3.572	4.41
0.7	0.730	7.455	1.219	−2.965	4.490	5.54
0.8	0.810	9.242	1.574	−3.830	5.412	6.68
0.9	0.891	11.37	2.012	−4.900	6.47	7.99
1.0	0.973	13.42	2.545	−6.19	7.23	8.92
1.1	1.057	15.89	3.150	−7.69	8.22	10.13

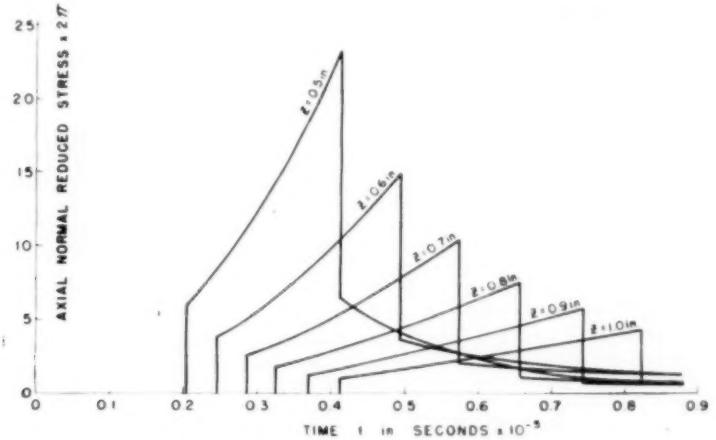

Fig. 5 Stress wave amplitudes versus time at 6 locations in plate (incident waves only)

then via φ, φ', the values of $f'(t)$, using (57). Next, in order to obviate the necessity of calculating the integral in (53), an iterative numerical procedure based on the differential equation (56) was used. Table 2 shows an example of this work as carried out for the position $z = 0.9$.

In constructing this table, first the values of t and $f'(t)$ were calculated. Then $F(t) = \tilde{\gamma}_1 z$ was entered for the value of t on the top line, then $-bF(t)$, then $F'(t)$ from (56), across the line. Then the value of F for the next entry $t + \Delta t$ was obtained simply from

$$F(t + \Delta t) = F(t) + \Delta t F'(t)$$

The remaining waves were calculated in the same manner as the foregoing. The progress of the stress wave through the plate is shown in the series of figures mentioned in the following text. The two incident waves φ_{00} and ψ_{00} alone are shown in Fig. 5 so that we can see how they would propagate through a semi-infinite medium. When ϕ_{00} reaches the back face of the plate it reflects two waves ϕ_{10} and ψ_{10} which are shown in Fig. 6. The combined effect of all the waves at each of the positions is shown in the series of curves of Fig. 7. Finally, the series of profiles was just enough to sketch a contour plot as shown in Fig. 8 of the stress as function of time and distance over the region $0 \leq t < 0.823 \times 10^{-6}$ sec, 0.5 in. $\leq z \leq 1$ in., respectively. From this diagram we also can take horizontal cross sections which show the appearance of the wave in the plate at any given moment.

For the unit-step pulse, where the stress is given by (50), the stress variation (considering only the two incident waves) is quite similar to the curves in Fig. 5. The only difference is that the tail of the pulse tends asymptotically to a constant value greater than zero. From (52a), at a constant position z,

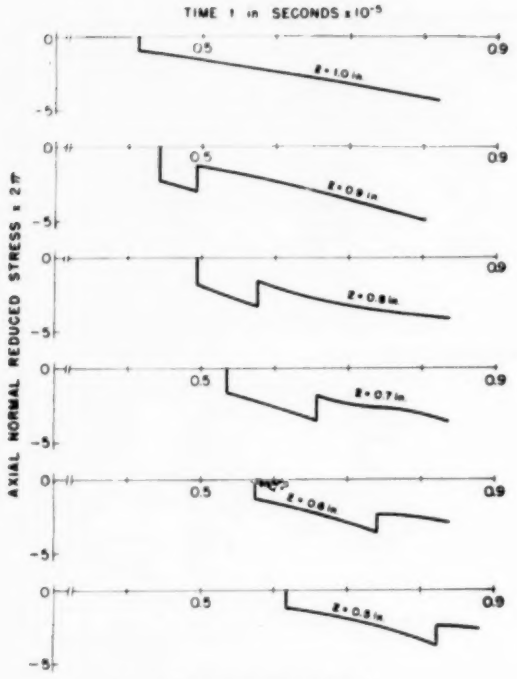

Fig. 6 First reflection from back face

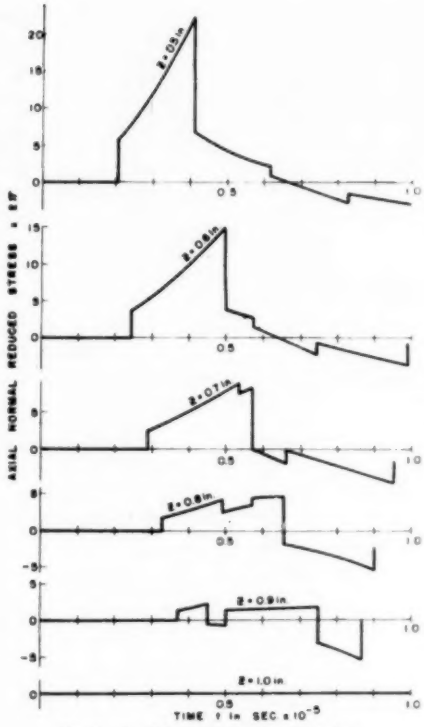

Fig. 7 Combined wave system in plate

$$2\pi\sigma_{zz} = f'(t) = \frac{1}{z^2}\,(\varphi_{00} + \psi_{00}) + t(\varphi_{00}' + \psi_{00}')$$

To evaluate the limit of this as $t \to \infty$, it is necessary to express the function φ and ψ explicitly in terms of t and expand in descending powers of t. When this is accomplished we obtain (for $z = 1$):

$$\varphi_{00} \cong \frac{2t^2}{\tilde{\gamma}_2^2 - \tilde{\gamma}_1^2} + \frac{\tilde{\gamma}_2^4 - 6\tilde{\gamma}_2^2\tilde{\gamma}_1^2 + 3\tilde{\gamma}_1^4}{2(\tilde{\gamma}_2^2 - \tilde{\gamma}_1^2)^2} - \frac{(\tilde{\gamma}_2^2 - 2\tilde{\gamma}_1^2)\,(2\tilde{\gamma}_2^4 - 3\tilde{\gamma}_2^2\tilde{\gamma}_1^2 + 3\tilde{\gamma}_1^4)}{2t^2} + \cdots$$

$$\psi_{00} \cong -\frac{2t^2}{\tilde{\gamma}_2^2 - \tilde{\gamma}_1^2} - \frac{-5\tilde{\gamma}_2^4 + 6\tilde{\gamma}_2^2\tilde{\gamma}_1^2 - 3\tilde{\gamma}_1^4}{2(\tilde{\gamma}_2^2 - \tilde{\gamma}_1^2)^2} + \frac{\tilde{\gamma}_1^2\tilde{\gamma}_2^2(\tilde{\gamma}_1^2 + \tilde{\gamma}_2^2)}{2(\tilde{\gamma}_2^2 - \tilde{\gamma}_1^2)^2 2t^2} + \cdots$$

It is seen that the ascending power terms cancel, and we have

$$\lim_{t\to\infty} \varphi_{00} + \psi_{00} = 3$$

$$\varphi_{00}' + \psi_{00}' = 0$$

Our limiting stress is therefore

$$\sigma_{zz} = \frac{3}{2\pi z^2}$$

This checks with the classical static value for a unit load on a semi-infinite body, as it should.[6]

Propagation Features—Limiting Cases

We consider first the question of pulse-shape preservation

[6] Timoshenko and Goodier [11], p. 364.

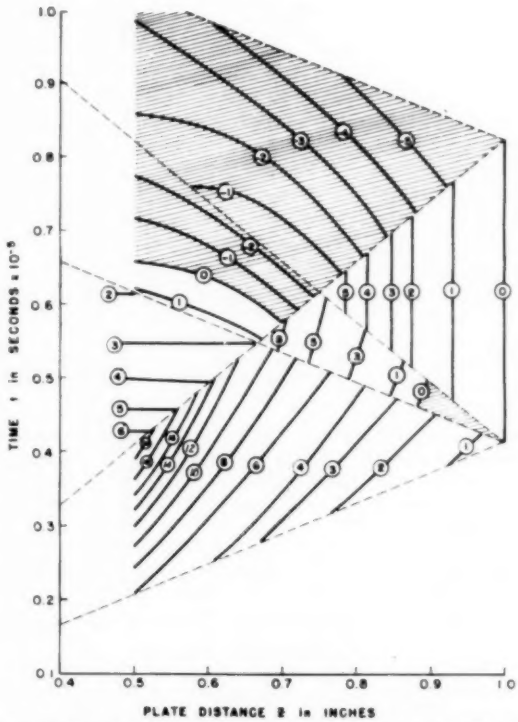

Fig. 8 Stress-contours showing distance-time propagation of pulse; numbers = stress × 2π

during propagation through the plate. From Fig. 5 we note that the sudden initial rise propagates with the dilatation velocity and signals the arrival of the pulse at each position. However, after this front has passed the intensity continues to rise until a negative front arrives with the distortion velocity. This cancels out most of the wave, leaving only a small residual tail which decreases further at an exponential rate. Unlike the input pulse, the peak intensity is reached just ahead of the second front, rather than at the primary one. Its magnitude however, diminishes as the square of the distance into the plate, as is to be expected from the spreading of the wave.

Thus wave shape is preserved only after a time long relative to that required for the zone of high stress to pass by.

The fact that there exists (a) the front moving with distortion velocity, and (b) the zone of high stress, is not predicted by steady-state analysis or by plane-wave theory. The generation of the distortion front is, however, well understood physically—its source is the interference or reflection of the spreading wave at the front surface. Sauter [12] and Goodier and Bishop [13] have discussed the formation of this second wave in plates from considerations of Snell's law of refraction at glancing incidence. Christie [14] and Schardin [15] also have studied this question and observed it experimentally. Fig. 9 shows this, together with the spreading stressed zone (here compression) in the plate. Satisfying the boundary conditions at A, A' requires the two shear waves AB and $A'B'$. At C, by symmetry, these must result in an axial stress moving with the distortion velocity.

While the foregoing ray analysis does predict the secondary wave at the front surface, and thus would apply in a semi-infinite medium, it does not predict the first distortion wave (ψ_{10}) reflected off the back surface, since an axial ray is normally incident there. The reason is that one cannot here assume the wave front to be plane until it is at least several wave lengths away from the source.

If we consider pulses of other shape than the exponential one, the same essential features of the propagation are present. Thus it has been pointed out that the step pulse also propagates a high-stress zone quite similar in shape. Here static equilibrium with the load left on is attained shortly after the unloading distortion front passes—certainly by the time required for the loading front to go about three times the distance from the source to the observing point.

When the first wave front is reflected from the back face of the plate, we have seen that two additional discontinuity fronts of opposite sign are reflected, interfering in a rather complicated manner with the oncoming waves. The contour map of Fig. 8 gives a better physical picture of the state of stress in the plate than do the profiles. The figure being drawn for a compression pulse, the regions of reversed stress (tension) are demarcated by shading. The triangular region near the boundary is of low intensity, and probably of little significance. The main tensile region begins at $z = 0.7$, 5.35×10^{-4} sec after the initial pulse, and soon builds up in intensity while spreading over a large part of the plate. If a tensile crack should start at this point it further weakens the material nearby to the extent that a full scab develops. There may possibly be enough tensile stresses still trapped in the remaining material to repeat the process, resulting in multiple scabs.

It is interesting to compare the foregoing results with what the more elementary plane-wave theory would give. Here, of course, there is no loss allowed for due to spreading of the wave. Also, the input pulse must here be considered as being spread over the entire front surface of the plate, instead of being concentrated at one point. On this basis, if we suppose an input stress pulse of the standard form

$$\sigma_{zz} = -P_m e^{-bt}$$

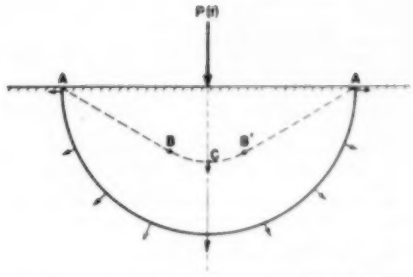

Fig. 9 Formation of distortion front by glancing incidence at front surface of plate

and suppose it transmitted through the plate without loss of shape, it will have the form

$$\sigma_{zz} = -P_m e^{-b(t-\tilde{\gamma}_1 z)} + P_m e^{-b[t-\tilde{\gamma}_1(2d-z)]}$$

where we have included the reflection off the back face. If σ_m denotes the critical fracture stress (or any critical stress), we can find the corresponding critical point in the plate as the intersection of the locus $\sigma_{zz} = \sigma_m$ with the equation $t - \tilde{\gamma}_1(2d - z) = 0$ of the reflected wave front. This gives the relation

$$\sigma_m = -P_m e^{-b[\tilde{\gamma}_1(2d-z)-\tilde{\gamma}_1 z]} + P_m$$

or

$$z = d + \frac{1}{2\tilde{\gamma}_1 b} \log\left(1 - \frac{\sigma_m}{P_m}\right)$$

If we assume arbitrarily that

$$\sigma_m = {}^1/_2 P_m$$

under the same numerical conditions used in the example of this paper, we obtain $z = 0.653$.

A comparison with the value $z = 0.71$ obtained from Fig. 8 would seem to show that the plane-wave result is not too far off—at least in this instance. However, we must be careful to note that the stress is reversed for different reasons. The analysis presented here shows that it occurs because the unloading distortion front meets the negative reflected dilatation front. The unloading due to the decreasing amplitude of the pulse itself plays a very small role. As an extreme case, the step pulse would never cause a reversed stress at all if it were analyzed on the plane-wave basis.

The effect of plate thickness d depends on its relation to the pulse length, measured, for example, by the value $1/b\tilde{\gamma}_1$ in equation (49). If d is increased by a factor of about 3 or more, the reflected stress waves are weakened as the square of this factor and we have essentially an infinite medium. At the opposite limit where $d \ll 1/(b\tilde{\gamma}_1)$ we can take $b \sim 0$ which makes the pulse effectively a step pulse, discussed already. However, from the point of view of practical situations, it may be that the actual rise time of the pulse becomes appreciable. Under these new input conditions, the corresponding propagation problem can be worked by essentially the same method as the foregoing.

Impacts with prescribed displacement boundary conditions instead of stress, or shear stresses, will, of course, lead to different expressions for the coefficients $A - D$ (20); but after these have been found from the boundary conditions, the same method of procedure can be carried all the way through.

References

1 N. Davids, "Stress Waves of Penetration in Plates," Interim Technical Report No. 12, OOR Project TB2-0001(1253), Pennsylvania State University.

2 N. Davids, same title as [1] to appear in *Proceedings of the Third Conference on Theoretical and Applied Mechanics*, Bangalore, India, December, 1957, pp. 35–48.

3 C. L. Pekeris, "The Seismic Surface Pulse," *Proceedings of the National Academy of Science*, vol. 41, 1955, pp. 469–480.

4 H. Pursey, "The Launching and Propagation of Elastic Waves in Plates," *Quarterly Journal of Mechanics and Applied Mathematics* (Oxford), vol. 10, 1957, pp. 45–62.

5 A. G. Mencher, "Epicentral Displacement Caused by Elastic Waves in an Infinite Slab," *Journal of Applied Physics*, vol. 24, 1953, pp. 1240–1246.

6 W. W. Garvin, "Exact Transient Solution of the Buried Line Source Problem," *Proceedings of The Royal Society of London*, England, series A, vol. 234, 1956, pp. 528–541.

7 L. Cagniard, "Reflexion et Refraction des Ondes Seismiques Progressives," Gauthier-Villars, Paris, 1939.

8 A. H. Love, "The Mathematic Theory of Elasticity," Cambridge University Press, 1927, fourth edition, Chapter 13.

9 G. N. Watson, "Theory of Bessel Functions," Cambridge University Press, 1922.

10 R. V. Churchill, "Modern Operational Mathematics in Engineering," McGraw-Hill Book Company, Inc., New York, N. Y., 1944.

11 S. Timoshenko and J. N. Goodier, "Theory of Elasticity," McGraw-Hill Book Company, Inc., New York, N. Y., 1951.

12 F. Sauter, "Der elastische Halbraum bei einer mechanischen Beeinflussung seiner Oberflache (Zweidimensionales Problem)," *"Zeitschrift für angewandte Mathematik und Physik*, 1950, pp. 203–215.

13 J. N. Goodier and R. E. D. Bishop, "A Note on Critical Reflections of Elastic Waves at Free Surfaces," *Journal of Applied Physics*, vol. 23, 1952, pp. 124–126.

14 D. G. Christie, "Reflections of Elastic Waves From a Free Boundary," *Philosophical Magazine*, series 7, vol. 46, 1955, pp. 527–541.

15 H. Schardin, "Uber das Bruchkriterium bei kurzzeitiger Beanspruchung," *Glastechnische Berichte*, vol. 23, 1950, pp. 189–193.

Transverse Flexure of a Semi-Infinite Thin Plate Containing an Infinite Row of Circular Holes

O. TAMATE
Professor of Mechanical Engineering,
Tohoku University,
Sendai, Japan

The problem of finding stress resultants in a semi-infinite plate under plain bending and containing an infinite row of equal and equally spaced circular holes is discussed on the basis of the Poisson-Kirchhoff theory of thin plates. A method of perturbation is adopted for the determination of parametric coefficients included in the solution. The maximum bending moments occurring on the rim of the hole across the minimum section are calculated for several cases and shown in graphs, from which the mutual interference of adjacent boundaries will be informed.

THE problem of determining the deflection and stresses in a plate under transverse bending and containing one or more holes has long attracted the attention of the elastician as well as the engineer. When the plate may be considered infinite, the influence of a single hole of various shapes has been solved by several investigators. Such names as J. N. Goodier [1],[1] H. Neuber [2], S. Holgate [3], G. N. Sawin [4], Yi-Yuan Yu [5], E. Reissner [6], and P. M. Naghdi [7] may be mentioned in this connection. Further, the presence of adjacent boundaries greatly influences the maximum stress and introduces some complications. For instance, the solution for a semi-infinite plate with a circular hole, subject to plain bending along the direction of the straight boundary [8] indicates a considerable stress concentration at the rim of the hole on the minimum section. On the other hand, an infinite row of circular holes in a thin plate, transmitting the constant bending moment about the cross axis to the line of centers [9], shows the shielding effect which reduces the maximum stress. Thus the mutual interference of adjacent boundaries in a bent plate may be considered to be a problem of both theoretical interest and practical importance.

The present paper concerns the problem mentioned. The plate is supposed to be semi-infinite, bounded by a straight line, and to contain an infinite row of equal and equally spaced circular holes. A solution of the plain bending problem is sought by use of the Poisson-Kirchhoff theory of thin plates [10]. A method of perturbation is adopted for the determination of parametric coefficients involved in the solution. Numerical examples of the solution also are worked out in several cases and compared with the results available.

Method of Analysis

Consider a semi-infinite plate with an infinite row of circular holes and take its middle plane, before bending occurs, as the x, y-plane. Let the plate occupy the region $x > -d$ in the x, y-plane. The holes will be supposed to have the same radius a ($<b/2$) and to have their centers at the points $(0, \pm mb)$, m being any integer or zero, Fig. 1. At the center O_m $(0, mb)$ of each hole, a subsidiary co-ordinate system is taken parallel to the x, y-axes. Referred to these axes, complex co-ordinates z and z_m may be defined as

$$z = x + iy = re^{i\theta}, \quad z_m = x_m + iy_m = r_m e^{i\theta_m}, \qquad (1)$$

both co-ordinate system being connected by

$$z_m = z - imb \qquad (2)$$

It is convenient to introduce nondimensional quantities measured in a unit d as follows:

$$\zeta = z/d, \quad \xi = x/d, \quad \eta = y/d, \quad \rho = r/d$$
$$\zeta_m = z_m/d, \quad \xi_m = x_m/d, \quad \eta_m = y_m/d \quad \rho_m = r_m/d, \qquad (3)$$

and

[1] Numbers in brackets designate References at end of paper.

Presented at the West Coast Conference of the Applied Mechanics Division, Stanford, Calif., September 9–11, 1959, of THE AMERICAN SOCIETY OF MECHANICAL ENGINEERS.

Discussion of this paper should be addressed to the Secretary, ASME, 29 West 39th Street, New York, N. Y., and will be accepted until January 10, 1960, for publication at a later date. Discussion received after the closing date will be returned.

NOTE: Statements and opinions advanced in papers are to be understood as individual expressions of their authors and not those of the Society. Manuscript received at ASME Applied Mechanics Division, October 8, 1958. Paper No. 59—APMW-15.

Nomenclature

x, y = rectangular co-ordinates
r, θ = polar co-ordinates
$z = x + iy = re^{i\theta}$ = middle plane of plate
D = flexural rigidity of plate
ν = Poisson's ratio
$\epsilon = (1 - \nu)/(3 + \nu)$
a = radius of circular hole
b = center distance of holes
d = distance between straight boundary and line of centers of holes
w = deflection of plate
$\xi = x/d$, $\eta = y/d$ = dimensionless rectangular co-ordinates
$\rho = r/d$ = dimensionless radial co-ordinate
$\zeta = \xi + i\eta$
$\lambda = a/d$ = dimensionless hole radius
$\mu = b/d$ = dimensionless center distance
M_0 = applied bending moment
$^k\alpha_n, {}^k\beta_n, {}^k\gamma_n, {}^k\delta_n$ = coefficients of transformation
M_r, M_θ, $H_{r\theta}$ = bending and twisting moments per unit length with reference to (r, θ)-direction
d_n, e_n, l_n, m_n = parametric coefficients involved in solution
Ω = conjugate function of $\nabla^2 w$
∇^2 = Laplacian operator

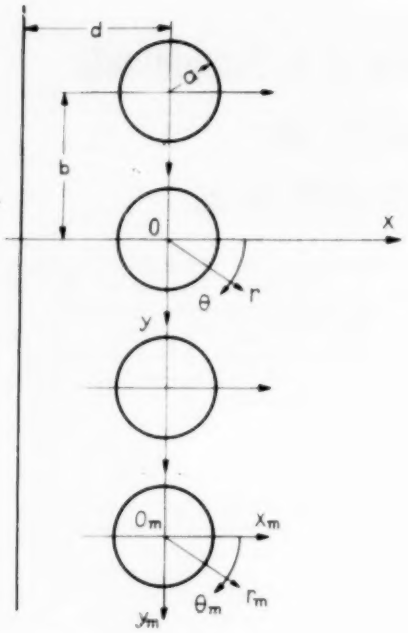

Fig. 1

$$\lambda = a/d, \quad \mu = b/d \tag{4}$$

Now we shall seek the solution for the case where the plate is bent about the x-axis and all the rims of the holes as well as the straight boundary are supposed to be stress-free. The plate will be considered subject to the limitation of the Poisson-Kirchhoff theory of thin plates. Then the transverse deflection of the plate, free from lateral loads, can be expressed by a biharmonic function of x and y.

If no hole is present, the deflection of the plate under the plain bending about x-axis is given by

$$w_{00} = -\frac{M_0 d^2}{2D(1-\nu^2)}(\eta^2 - \nu\xi^2) = -\frac{M_0 d^2}{2D(1-\nu^2)}\rho^2\left[\frac{2\epsilon}{1+\epsilon} - \frac{1-\epsilon}{1+\epsilon}\cos 2\theta\right] \tag{5}$$

where D is the flexural rigidity of the plate and ν is Poisson's ratio of the plate material and

$$\epsilon = (1-\nu)/(3+\nu) \tag{6}$$

M_0 means the intensity of the uniformly distributed moment M_y. It is clear that w_{00} leaves stress resultants of the same amount on all the holes. To satisfy the stress-free conditions at the rims of these holes, we shall introduce series of biharmonic functions. These functions are to give no stresses at infinity, no tractions on the straight boundary and the same stress resultants on each hole. With these functions added to w_{00}, the boundary conditions at the rim of one of the holes are satisfied by adjusting the parametric coefficients attached to the functions. Then the conditions on the other holes of the set will be automatically satisfied and all the requirements of the solution will be fulfilled.

To derive the biharmonic functions having the characteristics just alluded to, we first construct a fundamental set of biharmonic functions which have singularities at the center O_m and leave no stress at infinity and satisfy the stress-free condition on the straight boundary. Of these, the following are required for our present purpose:

$$(U_n)_m = \begin{cases} -\log \rho_m \\ \rho_m^{-n}\cos n\theta_m \end{cases} + (-1)^n \frac{\epsilon}{(n-1)!}\int_0^\infty \{u^{n-1}e^{-2u}[(1+2u)e^{-u\xi_m} + 2u\xi_m e^{-u\xi_m}]\cos u\eta_m - u^{-1}e^{-u}\delta_{0,n}\}du, \tag{7}$$

$$(V_n)_m = \rho_m^{-(n-2)}\cos n\theta_m + (-1)^n \frac{\epsilon}{(n-2)!}\int_0^\infty \{u^{n-3}e^{-2u}[(\epsilon^{-2} - n + 1 - 2nu + 4u + 4u^2)e^{-u\xi_m} - 2(n-1-2u)u\xi_m e^{-u\xi_m}] \cos u\eta_m - u^{-1}e^{-u}(\epsilon^{-2}-1)\delta_{2,n}\}du, \quad (n \geqq 2) \tag{8}$$

where $\delta_{m,n}$ is the Kronecker delta and $n!$ is interpreted as unity when $n = 0$ and -1.

Summing up these functions, we obtain the biharmonic functions having the requisite properties, which are then expressed in terms of the polar co-ordinates (ρ, θ) by using Equations (1), (2), and (3) as follows:

$$U_n = \sum_{m=-\infty}^{\infty}(U_n)_m = \begin{cases} -\log \rho \\ \rho^{-n}\cos n\theta \end{cases} + {}^0\beta_n\rho^2 + {}^1\beta_n\rho^3\cos\theta + \sum_{k=2}^{\infty}({}^k\alpha_n + {}^k\beta_n\rho^2)\rho^k\cos k\theta, \tag{9}$$

$$V_n = \sum_{m=-\infty}^{\infty}(V_n)_m = \rho^{-(n-2)}\cos n\theta + {}^0\delta_n\rho^2 + {}^1\delta_n\rho^3\cos\theta + \sum_{k=2}^{\infty}({}^k\gamma_n + {}^k\delta_n\rho^2)\rho^k\cos k\theta, \tag{10}$$

where some of the constant terms are omitted as they contribute nothing to the stress resultants and the plate can be placed at any level since the boundary conditions are given by stresses. The coefficients in Equations (9) and (10) are designated by

$$\begin{aligned} {}^k\alpha_n &= {}^k\alpha_n^{(0)} + \epsilon^k\alpha_n^{(1)}, & {}^k\beta_n &= \epsilon^k\beta_n^{(1)} \\ {}^k\gamma_n &= \epsilon^{-1k}\gamma_n^{(-1)} + {}^k\gamma_n^{(0)} + \epsilon^k\gamma_n^{(1)}, & {}^k\delta_n &= {}^k\delta_n^{(0)} + \epsilon^k\delta_n^{(1)}, \end{aligned} \tag{11}$$

where

$$\left.\begin{aligned} {}^{2k}\alpha_0^{(0)} &= (-1)^k\frac{1}{k}\sigma_{2k}\mu^{-2k}, \\ {}^{2k}\alpha_{2n}^{(0)} &= (-1)^{k+n}2\binom{2k+2n-1}{2k}\sigma_{2k+2n}\mu^{-(2k+2n)}, \quad (n \geqq 1) \\ {}^{2k+1}\alpha_{2n+1}^{(0)} &= (-1)^{k+n}2\binom{2k+2n+1}{2k+1}\sigma_{2k+2n+2}\mu^{-(2k+2n+2)}, \quad (n \geqq 0) \end{aligned}\right\} (k \geqq 1)$$

$$\left.\begin{aligned} {}^{2k}\gamma_{2n}^{(0)} &= (-1)^{k+n}2\binom{2k+2n-2}{2k}\sigma_{2k+2n-2}\mu^{-(2k+2n-2)}, \\ {}^{2k+1}\gamma_{2n+1}^{(0)} &= (-1)^{k+n}2\binom{2k+2n}{2k+1}\sigma_{2k+2n}\mu^{-(2k+2n)}, \end{aligned}\right\} (k \geqq 1, n \geqq 1)$$

$$
\left.
\begin{aligned}
{}^{2k}\delta_{2n}^{(0)} &= (-1)^{k+n+1}\,2\binom{2k+2n-1}{2k+1}\sigma_{2k+2n}\mu^{-(2k+2n)},\\
{}^{2k+1}\delta_{2n+1}^{(0)} &= (-1)^{k+n+1}\,2\binom{2k+2n+1}{2k+2}\sigma_{2k+2n+2}\mu^{-(2k+2n+2)},
\end{aligned}
\right\}\quad (k \geqq 0,\ n \geqq 1)
$$

$${}^{k}\alpha_n^{(0)} = {}^{k}\gamma_n^{(0)} = {}^{k}\delta_n^{(0)} = 0, \quad \text{if} \quad k+n = \text{odd},$$

$${}^{k}\alpha_n^{(1)} = (-1)^{k+n+1}\frac{1}{k!(n-1)!}\,[(k-1)\sigma_{k+n-1,\mu} - 2\sigma_{k+n,\mu}],\ (k \geqq 2,\ n \geqq 0)$$

$${}^{k}\beta_n^{(1)} = (-1)^{k+n+1}\frac{1}{(k+1)!(n-1)!}\,\sigma_{k+n+1,\mu},\quad (k \geqq 0,\ n \geqq 0)$$

$${}^{k}\gamma_n^{(-1)} = (-1)^{k+n}\frac{1}{k!(n-2)!}\,\sigma_{k+n-2,\mu},\ (k \geqq 2,\ n \geqq 2)$$

$${}^{k}\gamma_n^{(1)} = (-1)^{k+n}\frac{1}{k!(n-2)!}\,\{(n-1)[(k-1)\sigma_{k+n-2,\mu} - 2\sigma_{k+n-2,\mu}] - 2[(k-1)\sigma_{k+n-2,\mu} - 2\sigma_{k+n-1,\mu}]\},\ (k \geqq 2,\ n \geqq 2)$$

$${}^{k}\delta_n^{(1)} = (-1)^{k+n}\frac{1}{(k+1)!(n-2)!}\,[(n-1)\sigma_{k+n-1,\mu} - 2\sigma_{k+n,\mu}],\quad (k \geqq 0,\ n \geqq 2)$$

σ_n and $\sigma_{n,\mu}$ are defined as follows:

$$\sigma_n = \sum_{m=1}^{\infty} m^{-n},\quad \sigma_{n,\mu} = \left(\frac{2\pi}{\mu}\right)^{n+1}\sum_{m=1}^{\infty} m^n \exp\left\{-2m\left(\frac{2\pi}{\mu}\right)\right\} \tag{12}$$

Now, the required function which expresses the deflection of the plate is constructed in the form

$$w = w_{00} - \frac{M_0 d^2}{2D(1-\nu)}\sum_{n=2}^{\infty}(d_{n-2}U_{n-2} + e_n V_n) \tag{13}$$

where d_n and e_n are parametric coefficients to be determined from the boundary conditions. The corresponding bending moments M_r, M_θ, and twisting moment $H_{r\theta}$ are

$$\begin{aligned}
M_r &= -\frac{D}{d^2}\left[\frac{\partial^2}{\partial\rho^2} + \nu\left(\frac{\partial}{\rho\partial\rho} + \frac{\partial^2}{\rho^2\partial\theta^2}\right)\right]w\\
&= (M_0/2)\left\{1 - \cos 2\theta + d_0\rho^{-2} + d_1 2\rho^{-3}\cos\theta\right.\\
&+ \sum_{n=2}^{\infty}[d_n n(n+1) + e_n(n-1)(n+1-\epsilon^{-1})\rho^2]\rho^{-(n+2)}\cos n\theta\\
&+ m_0(-1+\epsilon^{-1}) + m_1 2\epsilon^{-1}\rho\cos\theta + \sum_{n=2}^{\infty}[l_n n(n-1)\\
&\left.+ m_n(n+1)(n-1+\epsilon^{-1})\rho^2]\rho^{n-2}\cos n\theta\right\},
\end{aligned} \tag{14}$$

$$\begin{aligned}
M_\theta &= -\frac{D}{d^2}\left[\frac{\partial}{\rho\partial\rho} + \frac{\partial^2}{\rho^2\partial\theta^2} + \nu\frac{\partial^2}{\partial\rho^2}\right]w\\
&= (M_0/2)\left\{1 + \cos 2\theta - d_0\rho^{-2} - d_1 2\rho^{-3}\cos\theta\right.\\
&- \sum_{n=2}^{\infty}[d_n n(n+1) + e_n(n-1)(n-1+\epsilon^{-1})\rho^2]\rho^{-(n+2)}\cos n\theta\\
&- m_0(1-\epsilon^{-1}) - m_1 2(2-\epsilon^{-1})\rho\cos\theta - \sum_{n=2}^{\infty}[l_n n(n-1)\\
&\left.+ m_n(n+1)(n+1-\epsilon^{-1})\rho^2]\rho^{n-2}\cos n\theta\right\},
\end{aligned} \tag{15}$$

$$\begin{aligned}
H_{r\theta} &= \frac{D}{d^2}(1-\nu)\frac{\partial}{\partial\rho}\left(\frac{\partial}{\rho\partial\theta}\right)w\\
&= (M_0/2)\left\{-\sin 2\theta - d_1 2\rho^{-2}\sin\theta\right.\\
&- \sum_{n=2}^{\infty}[d_n n(n+1) + e_n(n-1)n\rho^2]\rho^{-(n+2)}\sin n\theta + m_1 2\rho\sin\theta\\
&\left.+ \sum_{n=2}^{\infty}[l_n n(n-1) + m_n n(n+1)\rho^2]\rho^{n-2}\sin n\theta\right\},
\end{aligned} \tag{16}$$

where

$$\left.
\begin{aligned}
l_n &= d_0{}^n\alpha_0 + d_1{}^n\alpha_1 + \sum_{k=2}^{\infty}(d_k{}^n\alpha_k + e_k{}^n\gamma_k),\\
m_n &= d_0{}^n\beta_0 + d_1{}^n\beta_1 + \sum_{k=2}^{\infty}(d_k{}^n\beta_k + e_k{}^n\delta_k)
\end{aligned}
\right\} \tag{17}$$

The boundary conditions at the rims of the holes are satisfied when

$$M_r = 0,\quad D\Omega + H_{r\theta} = \text{const},$$

on the circle $r = a$, where Ω is a conjugate function of $\nabla^2 w$, ∇^2 being the Laplacian operator referred to x, y; that is

$$1 + \lambda^{-2}d_0 + (-1+\epsilon^{-1})m_0 = 0,\quad 2\lambda^{-3}d_1 + 2\epsilon^{-1}\lambda m_1 = 0,$$

$$\left.
\begin{aligned}
&(-1)\delta_{2,n} + n(n+1)\lambda^{-(n+2)}d_n\\
&+ (n-1)(n+1-\epsilon^{-1})\lambda^{-n}e_n + n(n-1)\lambda^{n-2}l_n\\
&+ (n+1)(n-1+\epsilon^{-1})\lambda^n m_n = 0,\\
&(-1)\delta_{2,n} - n(n+1)\lambda^{-(n+2)}d_n\\
&- (n-1)(n+1+\epsilon^{-1})\lambda^{-n}e_n + n(n-1)\lambda^{n-2}l_n\\
&+ (n+1)(n-1-\epsilon^{-1})\lambda\, m_n = 0
\end{aligned}
\right\}\quad (n \geqq 2)$$

These are equivalent to

$$\left.
\begin{aligned}
d_0 &= -\lambda^2 - (-1+\epsilon^{-1})\lambda^2 m_0,\qquad d_1 = -\epsilon^{-1}\lambda^4 m_1,\\
d_n &= 2^{-1}\epsilon\lambda^4\delta_{2,n} - (n-1)\epsilon\lambda^{2n}l_n\\
&\quad - [(n-n^{-1})\epsilon + (n\epsilon)^{-1}]\lambda^{2n+2}m_n,\\
e_n &= -\epsilon\lambda^2\delta_{2,n} + n\epsilon\lambda^{2n-2}l_n\\
&\quad + (n+1)\epsilon\lambda^{2n}m_n
\end{aligned}
\right\}\quad (n \geqq 2) \tag{18}$$

The set of Equations (17) and (18) solves completely the problem of determining the parametric coefficients included in w.

Determination of Coefficients d_n and e_n

To solve the infinite set of Equations (17) and (18), it is rather convenient to use a method of perturbation in which λ and ϵ are

the perturbation parameters. Now, we shall seek a solution in the form

$$\left.\begin{aligned} d_0 &= {}^{(0)}d_0{}^{(0)}\lambda^2 + \sum_{p=1}^{\infty}\sum_{q=0}^{2p} {}^{(q)}d_0{}^{(p)}\epsilon^q\lambda^{2p+2}, \\ d_n &= {}^{(1)}d_2{}^{(0)}\epsilon\lambda^4\delta_{2,n} + \sum_{p=1}^{\infty}\sum_{q=0}^{2p+1} {}^{(q)}d_n{}^{(p)}\epsilon^q\lambda^{2p+2n}, \\ e_n &= {}^{(1)}e_2{}^{(0)}\epsilon\lambda^2\delta_{2,n} + \sum_{p=1}^{\infty}\sum_{q=1}^{2p+1} {}^{(q)}e_n{}^{(p)}\epsilon^q\lambda^{2p+2n-2}, \\ l_n &= \sum_{p=1}^{\infty}\sum_{q=0}^{2p} {}^{(q)}l_n{}^{(p)}\epsilon^q\lambda^{2p}, \quad m_n = \sum_{p=1}^{\infty}\sum_{q=1}^{2p} {}^{(q)}m_n{}^{(p)}\epsilon^q\lambda^{2p} \end{aligned}\right\} \tag{19}$$

Substituting these expansions and Equations (11) into Equations (17) and (18) and then equating the coefficients of the same powers of λ and ϵ on both sides, we obtain

$${}^{(0)}d_0{}^{(0)} = -1, \quad {}^{(1)}d_2{}^{(0)} = 1/2, \quad {}^{(1)}e_2{}^{(0)} = -1, \tag{20}$$

and for $p > 0$,

$$\left.\begin{aligned} {}^{(q)}l_n{}^{(p)} &= {}^{n}\alpha_0{}^{(0)(q)}d_0{}^{(p-1)} + {}^{n}\alpha_0{}^{(1)(q-1)}d_0{}^{(p-1)} \\ &\quad + \sum_{k=1}^{t}\left({}^{n}\alpha_k{}^{(0)(q)}d_k{}^{(p-k)} + {}^{n}\gamma_{k+1}{}^{(0)(q)}e_{k+1}{}^{(p-k)}\right) \\ &\quad + \sum_{k=1}^{t'}\left({}^{n}\alpha_k{}^{(1)(q-1)}d_k{}^{(p-k)} + {}^{n}\gamma_{k+1}{}^{(1)(q-1)}e_{k+1}{}^{(p-k)}\right) \\ &\quad + \sum_{k=1}^{t''}{}^{n}\gamma_{k+1}{}^{(-1)(q+1)}e_{k+1}{}^{(p-k)}, \\ {}^{(q)}m_n{}^{(p)} &= {}^{n}\beta_0{}^{(1)(q-1)}d_0{}^{(p-1)} \\ &\quad + \sum_{k=1}^{t'}\left({}^{n}\beta_k{}^{(1)(q-1)}d_k{}^{(p-k)} + {}^{n}\delta_{k+1}{}^{(1)(q-1)}e_{k+1}{}^{(p-k)}\right) \\ &\quad + \sum_{k=1}^{t}{}^{n}\delta_{k+1}{}^{(0)(q)}e_{k+1}{}^{(p-k)}, \end{aligned}\right\} \tag{21}$$

where

$$t = \begin{cases} p - (q/2) \\ p - [(q-1)/2] \end{cases}, \quad t' = \begin{cases} t+1 \\ t \end{cases}, \quad t'' = \begin{cases} t \\ t-1 \end{cases}, \quad \text{if } q = \begin{cases} \text{even} \\ \text{odd} \end{cases}$$

and

$$\left.\begin{aligned} {}^{(q)}d_1{}^{(p)} &= -{}^{(q+1)}m_0{}^{(p)} + {}^{(q)}m_0{}^{(p)}, \\ {}^{(q)}d_1{}^{(p)} &= -{}^{(q+1)}m_1{}^{(p-1)}, \\ {}^{(q)}d_n{}^{(p)} &= -(n-1)^{(q-1)}l_n{}^{(p)} \\ &\quad - n^{-1(q+1)}m_n{}^{(p-1)} - (n-n^{-1})^{(q-1)}m_n{}^{(p-1)}, \\ {}^{(q)}e_n{}^{(p)} &= n^{(q-1)}l_n{}^{(p)} + (n+1)^{(q-1)}m_n{}^{(p-1)} \end{aligned}\right\} (n \geqq 2) \tag{22}$$

In the foregoing expressions, all the coefficients which are not included in the Series (19) are to be zero. With these formulas the coefficients ${}^{(q)}d_n{}^{(p)}$, ${}^{(q)}e_n{}^{(p)}$, ${}^{(q)}l_n{}^{(p)}$, and ${}^{(q)}m_n{}^{(p)}$ in the Series (19) can be determined successively for $p = 1, 2, \ldots$.

The foregoing method of solution is valid in so far as the series in Equation (19) are convergent. No proof of convergence is pursued here, for brevity, but numerical computations carried out show that the Series (19) truncated after $p = 7$ gives practically satisfactory results for $\lambda < 0.35$ when $\mu = 1$ and for $\lambda < 0.65$ when $\mu = 2$ and 2.5.

Numerical Examples

The foregoing solution was worked out for the cases $b/d = 1, 2$ and 2.5. The calculation of ${}^{(q)}d_n{}^{(p)}$, ${}^{(q)}e_n{}^{(p)}$, ... is carried out until $p = 7$ and corresponding values of q, but their values are not shown here for brevity.

It is now rather straightforward to compute the deflection and stress resultants in the neighborhood of the holes. The most interesting, however, is the maximum value of bending moment occurring at the rim of the hole across the minimum section where $(\rho, \theta) = (\lambda, \pi)$. Since $M_r = 0$ on the same rim, the maximum bending moment is given by

$$M_{\max}/M_0 = [-D(1+\tilde{\nu})\nabla^2 w]_{\lambda,\pi} = 1 - (\epsilon^{-1} - 1)\sum_{n=2}^{\infty}(-1)^n(n-1)(e_n\lambda^{-n} - m_{n-2}\lambda^{n-2}) \tag{23}$$

Substituting in this equation for e_n and m_n from Equation (19), we obtain

$$M_{\max}/M_0 = (2-\epsilon) + (1-\epsilon)\sum_{p=2}^{\infty}\sum_{q=0}^{t} M_{p,q}\lambda^p\epsilon^q, \tag{24}$$

where

$$t = \begin{cases} p \\ p-1 \end{cases}, \quad \text{if} \quad p = \begin{cases} \text{even} \\ \text{odd} \end{cases}$$

and

$$\left.\begin{aligned} M_{2p,q} &= -\sum_{n=1}^{s}(2n-1)^{(q+1)}e_{2n}{}^{(p-n+1)} \\ &\quad + \sum_{n=1}^{s'}(2n-1)^{(q+1)}m_{2n-2}{}^{(p-n+1)}, \\ M_{2p+1,q} &= \sum_{n=1}^{s}2n^{(q+1)}e_{2n+1}{}^{(p-n+1)} \\ &\quad - \sum_{n=1}^{s'}2n^{(q+1)}m_{2n-1}{}^{(p-n+1)} \end{aligned}\right\} \tag{25}$$

Here upper limits of the summations take the following values

$$s = \begin{cases} p+1-(q/2) \\ p-[(q-1)/2] \end{cases}, \quad s' = \begin{cases} s-1 \\ s \end{cases}, \quad \text{if} \quad q = \begin{cases} \text{even} \\ \text{odd} \end{cases}$$

except $q = 0$, for which $s = s' = p$.

The value in the limiting case $a/d \to 0$ is $2 - \epsilon = (5 + 3\nu)/(3 + \nu)$ which coincides with the one obtained for an isolated hole

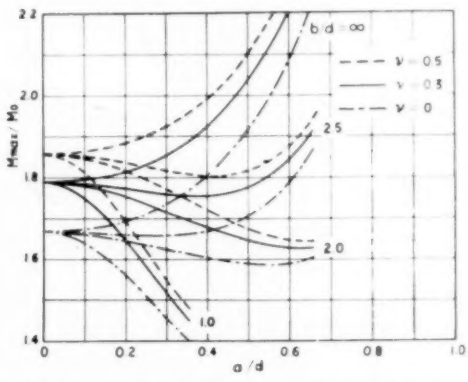

Fig. 2 Maximum bending moment versus a/d for various ν and b/d values

in an infinite plate [1, 2]. Fig. 2 shows the results graphically. In this figure, the maximum moments are plotted versus a/d for the cases of $\nu = 0$, 0.3, 0.5 and $b/d = 1$, 2, 2.5. The values for the limiting case $b/d \to \infty$ [8] are also shown for comparison. When the distance between adjacent holes is small, e.g., $b/d = 1$, the shielding effect is predominant and the maximum moment decreases with increasing value of a/d. But when the adjacent holes are somewhat apart, e.g., $b/d = 2$ and 2.5, the shielding effects are weakened by the effect of the straight boundary, and the maximum moment decreases slowly up to a certain value of a/d and then increases rapidly. Thus, for this range of b/d, the maximum moment attains its least value at some values of a/d. It is known from the figure that the corresponding values of a/d becomes smaller when b/d is large and ν small. If the maximum moment has its least value at $a/d = 0$, and it increases with a/d, it may be said that the effect of the straight boundary becomes stronger. As is easily seen from Equation (24), this situation occurs when

$$M_2(\mu, \epsilon) = M_{2,0}(\mu) + M_{2,1}(\mu)\epsilon + M_{2,2}(\mu)\epsilon^2 > 0 \qquad (26)$$

Table 1

$\nu = 0$	0.3	0.5
$b/d > 3.33$	3.76	4.08

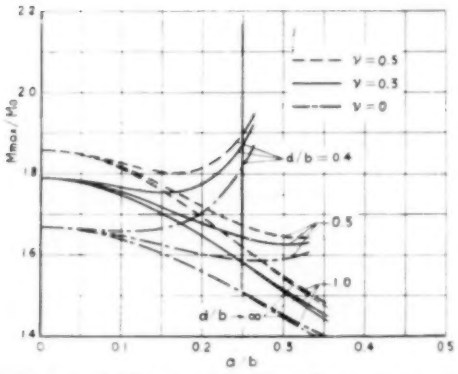

Fig. 3 Maximum bending moment versus a/b for various ν and d/b values

The values of $\mu(= b/d)$ that satisfy the foregoing relation are shown in Table 1.

Fig. 3 shows the maximum bending moment plotted versus a/b, d/b, and ν being parameters. The limiting case $d/b \to \infty$, i.e., the case of the infinite plate containing an infinite row of holes [9], is also plotted. It is shown that the values of the limiting case give a good approximation for the case where the distance between the straight boundary and the line of centers is larger than the center distance of the holes.

Acknowledgment

The author wishes to express his hearty thanks to Seiichi Higuchi, Professor Emeritus of Tohoku University, for his kind advice and encouragement throughout the progress of the present investigation.

References

1 J. N. Goodier, "The Influence of Circular and Elliptical Holes on the Transverse Flexure of Elastic Plates," *Philosophical Magazine*, series 7, vol. 22, 1936, pp. 68–80.

2 H. Neuber, "Über das Kerbproblem in der Plattentheorie," *Zeitschrift für angewandte Mathematik und Mechanik*, vol. 20, 1940, pp. 199–209.

3 S. Holgate, "The Transverse Flexure of Perforated Isotropic Plates," *Proceedings of the Royal Society of London*, England, series A, vol. 185, 1946, pp. 35–49.

4 G. N. Sawin, "Spannungserhöhung am Rande von Löchern," VEB Verlag Technik, Berlin, 1956, chapter 6 (German translation from the Russian by H. Neuber and O. Everling).

5 Yi-Yuan Yu, "The Influence of a Small Hole or Rigid Inclusion on the Transverse Flexure of Thin Plates," Proceedings of the Second U. S. National Congress of Applied Mechanics, 1954, pp. 381–387.

6 E. Reissner, "The Effect of Transverse Shear Deformation on the Bending of Elastic Plates," JOURNAL OF APPLIED MECHANICS, vol. 12, TRANS. ASME, vol. 67, 1945, p. A-69.

7 P. M. Naghdi, "The Effect of Elliptic Holes on the Bending of Thick Plates," JOURNAL OF APPLIED MECHANICS, vol. 22, TRANS. ASME, vol. 77, 1955, pp. 89–94.

8 O. Tamate, "Einfluss eines Kreisloches auf die Durchbiegung einer dünnen Halbebene," *Ingenieur-Archiv*, vol. 26, 1958, pp. 181–186.

9 O. Tamate, "Einfluss einer unendlichen Reihe gleicher Kreislöcher auf die Durchbiegung einer dünnen Platte," *Zeitschrift für angewandte Mathematik und Mechanik*, vol. 37, 1957, pp. 431–441.

10 S. Timoshenko, "Theory of Plates and Shells," McGraw-Hill Book Company, Inc., New York, N. Y., 1940, chapter 4.

The Fundamental Frequency of a Thin, Flat, Circular Plate Simply Supported Along a Circle of Arbitrary Radius[1]

R. Y. BODINE
Department of Mechanics, University of Wisconsin, Madison, Wis.

The fundamental transverse frequency is determined for a thin, flat, circular plate simply supported along a circle of arbitrary radius. It is shown that there are three support locations which coincide with "classical" plate solutions. The dimensionless frequency is plotted against the ratio of the support radius and outer-edge radius, showing the frequency variation with support location. The maximum frequency occurs when the support is located at the diameter of the first nodal circle of a free-edge plate.

THE differential equation describing the transverse oscillation, in vacuo, of a thin, flat, circular plate of homogeneous, isotropic material is [1][2]

$$\Delta^2 w = -\frac{mh}{D}\frac{\partial^2 w}{\partial t^2} \tag{1}$$

where

$$\Delta = \frac{\partial^2}{\partial r^2} + \frac{1}{r}\frac{\partial}{\partial r} + \frac{1}{r^2}\frac{\partial^2}{\partial \psi^2}$$

The solution for the fundamental, or umbrella, mode, with time implicit, is

$$w(r) = a_1 J_0(kr) + a_2 Y_0(kr) + a_3 I_0(kr) + a_4 K_0(kr) \tag{2}$$

The frequency is given by

$$\omega = \left(\frac{\rho^2}{b^2}\right)\left(\frac{D}{mh}\right)^{1/2} \tag{3}$$

where $kb = \rho$, zero root of the frequency-criteria equations developed in the following sections.

The plate, Fig. 1, is considered composed of two elements, an inner panel and an outer web, joined at the support by reasons of equal slope and radial bending moment, and hence curvature.

It is noted that there are three locations of the support which produce solutions corresponding to "classical" solutions:

1 When $a/b = 0$, the support at the center, the plate has zero deflection at the center. Since the slope at the center is always zero for reasons of symmetry, the center has the same conditions as if it were fixed, a problem previously discussed by Southwell [2].

2 When $a/b = 0.680$, the support radius coincides with the radius of the first nodal circle on a free-edge plate, a problem discussed by several authors [3, 4].

3 When $a/b = 1.0$, the support at the outer edge, the plate becomes "simply supported," a problem solved by Poisson in an early paper to the French Academy [5].

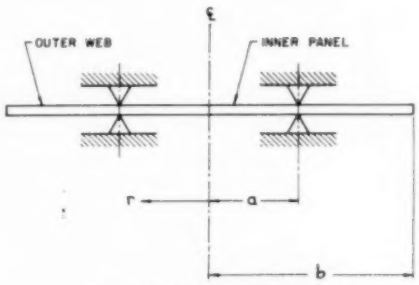

Fig. 1 Typical diametral section

Since the calculations in this paper were performed using a Poisson's ratio of 1/3, the special problems of $a/b = 0$ and 1.0 are solved using this value. Reference [6] was employed as the source of the tabulated Bessel functions, and the form of the functions and their derivatives used in this paper are those defined therein.

Solution

The boundary conditions for the inner panel, $0 \leq r \leq a$ are as follows:

(i) $w(0) \neq \infty$
(ii) $V(0) \neq \infty$
(iii) $w(a) = 0$
(iv) $\theta(a) = \theta_0$
(v) $P(a) = P_0$

Equation (2) represents the deflection curve, with time implicit and, by applying boundary conditions (i), (ii), and (iii), the deflection of the inner panel can be written as

$$w(r) = a_3\left[I_0(kr) - \frac{I_0(ka)}{J_0(ka)}J_0(kr)\right] \tag{4}$$

Differentiating Equation (4) once for the slope and twice for the curvature results in the following equations, respectively:

$$\theta(a) = \theta_0 = a_3 k\left[I_1(ka) + \frac{I_0(ka)}{J_0(ka)}J_1(ka)\right] \tag{5}$$

[1] From a thesis submitted to the School of Engineering and Architecture and the Faculty of the Graduate School of the University of Kansas in partial fulfillment of the requirements for the degree of Master of Science.

[2] Numbers in brackets designate References at end of paper.

Presented at the West Coast Conference of the Applied Mechanics Division, Stanford, Calif., September 9–11, 1959, of THE AMERICAN SOCIETY OF MECHANICAL ENGINEERS.

Discussion of this paper should be addressed to the Secretary, ASME, 29 West 39th Street, New York, N. Y., and will be accepted until January 10, 1960, for publication at a later date. Discussion received after the closing date will be returned.

NOTE: Statements and opinions advanced in papers are to be understood as individual expressions of their authors and not those of the Society. Manuscript received at ASME Applied Mechanics Division, November 3, 1958. Paper No. 59—APMW-10.

$$P(a) = P_0 = a_3 k^2 \left\{ \left[I_0(ka) - \frac{1}{ka} I_1(ka) \right] + \frac{I_0(ka)}{J_0(ka)} \left[J_0(ka) - \frac{1}{ka} J_1(ka) \right] \right\} \quad (6)$$

The boundary conditions for the outer web, $a \leq r \leq b$ are:

(i) $w(a) = 0$
(ii) $\theta(a) = \theta_0$
(iii) $P(a) = P_0$
(iv) $M(b) = 0$
(v) $V(b) = 0$

A different set of constants is used in the equation defining the elastic plane of the outer web,

$$w(r) = b_1 J_0(kr) + b_2 Y_0(kr) + b_3 I_0(kr) + b_4 K_0(kr) \quad (7)$$

When this equation is differentiated appropriately [7] the boundary conditions at the outer edge can be expressed as in the following equations:

$$M(b) = 0 = k^2 \left\{ b_1 \left[J_0(kb) - \frac{1-\mu}{kb} J_1(kb) \right] + b_2 \left[Y_0(kb) - \frac{1-\mu}{kb} Y_1(kb) \right] - b_3 \left[I_0(kb) - \frac{1-\mu}{kb} I_1(kb) \right] - b_4 \left[K_0(kb) + \frac{1-\mu}{kb} K_1(kb) \right] \right\} \quad (8)$$

$$V(b) = 0 = k^3 [b_1 J_1(kb) + b_2 Y_1(kb) + b_3 I_1(kb) - b_4 K_1(kb)] \quad (9)$$

It was noted at the beginning of the paper that there are three locations of the support which will produce known solutions to the vibrating plate. From these solutions the range of ka, the Bessel function argument at the support, could be anticipated. Rather than forming a 4×4 matrix of the coefficients of b_1, b_2, b_3, and b_4, which could be accomplished by solving for a_3 in terms of b_1, b_2, b_3, and b_4 by equating support slope and curvature equations, the constant a_3 was assumed equal to unity. Inspection of equation (4) will show a_3 is only a scale factor for the amplitude, the separation constant k being the only term that reflects the existence of the outer web. With a_3 equal to unity, the support slope and curvature can be numerically computed for any presumed value of ka. Since the range of ka could be anticipated from the classical plate solutions, quite reasonable values of ka could be presumed. The complete solution can best be illustrated by a numerical example, using a typical value of ka.

When $ka = 1.500$, θ_0 and P_0 are equal to $2.7737k$ and $1.4428k^2$, respectively, from equations (5) and (6). From the outer-web slope and curvature equations at the support, found by differentiating equation (7) once for θ and twice for P, the constants b_3 and b_4 are found in terms of b_1 and b_2 as

$$b_3 = -83.4416 - 14.4604 b_1 + 36.9626 b_2 \quad (10)$$

$$b_4 = -134.6492 - 23.6304 b_1 + 58.6999 b_2 \quad (11)$$

From equation (7) at the support, where $r = a$, b_2, b_3, and b_4 can be expressed in terms of b_1. Equation (7) becomes

$$w(r) = b_1 [J_0(kr) - 0.2577 Y_0(kr) + 0.3554 I_0(kr) - 2.7685 K_0(kr)] - 2.1743 Y_0(kr) + 2.1424 I_0(kr) - 8.8805 K_0(kr) \quad (12)$$

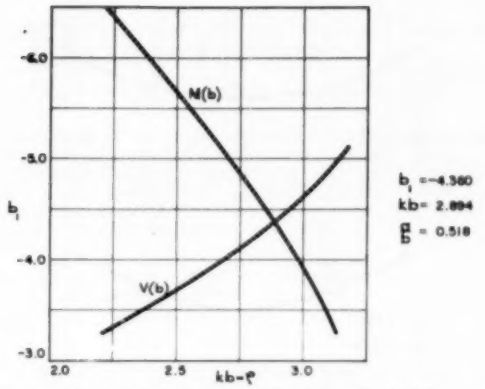

Fig. 2 Graphic representation of solution of Equation (12) for gravest root

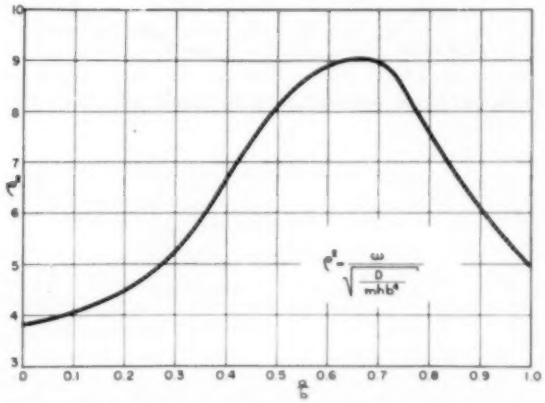

Fig. 3 Dimensionless frequency ρ^2, versus radius ratio a/b, for fundamental mode

By applying to equation (12) the boundary conditions of zero edge moment and vertical shear force, two equations are obtained with two unknowns, b_1 and kb. The gravest kb is then found by trial and error as shown in Fig. 2. The radius ratio, a/b, and the dimensionless frequency are then established for the presumed support location.

The support locations where $a/b = 0$ and 1.0 have, as it was noted, known solutions. The present analysis produces the solution for $a/b = 0$ if a new boundary condition for the center panel is added, $V(0) \to \infty$, since the central support is essentially a concentrated load. The solution for $a/b = 1.0$ was found by using a ka slightly less and slightly greater than Poisson's root, 2.204 [5], and interpolating for $a/b = 1.0$. Using $\mu = 1/3$ this produced a kb equal to 2.228.

The numerical computations outlined for $ka = 1.5$ were performed for several other values, producing Fig. 4, showing the effect of support location on the dimensionless plate frequency. All computations were performed on a 10-place Marchant desk calculator, but the accuracy was limited to five significant figures by the tabulated Bessel functions.

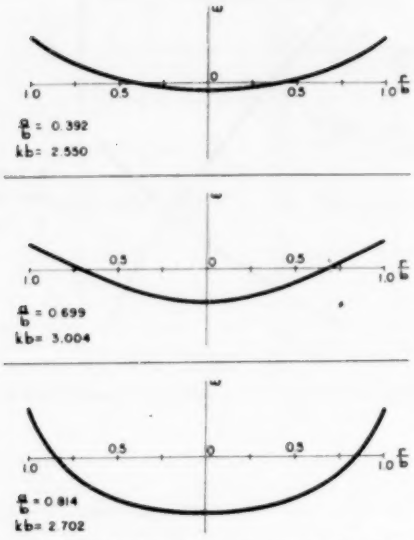

Fig. 4 Typical deflection curves for several a/b ratios

Acknowledgment

The author wishes to acknowledge the able counsel offered during the course of the investigation by Dr. E. J. McBride, Head of the Mechanical Engineering Department, University of Kansas, Lawrence, Kan.

References

1 N. W. McLachlan, "Theory of Vibrations," Dover Publications, New York, N. Y., 1951, pp. 139–140.

2 R. V. Southwell, "On the Free Transverse Vibrations of a Uniform Circular Disk Clamped at its Center, and on the Effects of Rotation," *Proceedings of the Royal Society of London*, series A, vol. 101, 1922, p. 133.

3 J. R. Airey, "The Vibrations of Circular Plates and Their Relation to Bessel Functions," *Proceedings of the Physical Society of London*, vol. 23, 1911, p. 225.

4 Lord Rayleigh, "The Theory of Sound," Dover Publications New York, N. Y., vol. 1, 1945, p. 362.

5 S. D. Poisson, "L'Equilibre et le Mouvement des Corps Elastiques," *Mémoires de l'Academie Royale des Sciences de l'Institut de France*, series 2, vol. 8, 1829, p. 357.

6 N. W. McLachlan, "Bessel Functions for Engineers," second edition, Oxford at the Clarendon Press, England, 1955, pp. 190–221.

7 J. P. Den Hartog, "Advanced Strength of Materials," McGraw-Hill Book Company, Inc., New York, N. Y., 1952, p. 100.

Journal of APPLIED MECHANICS

Brief Notes

On the recommendation of the Executive Committee of the ASME Applied Mechanics Division, it was decided to initiate a section devoted to brief notes on technical matters in mechanics. These notes must not be longer than 750 words (about 2½ double-spaced typewritten pages, including figures) and will be subject to the usual review procedure prior to publication. After approval such notes will be published as soon as possible, normally in the next issue of the Journal. The notes should be submitted to the Technical Editors of the Journal of Applied Mechanics.

Flexure of Nonhomogeneous Cylindrically Aeolotropic Plate

R. L. THORKILDSEN[1] **and W. H. HOPPMANN, II**[2]

A method is presented for determining the deflection of a circular plate in which the elastic constants are cylindrically aeolotropic but vary along the radius.

Nomenclature

D = bending stiffness of the core

$D^* = \dfrac{S_{22}h^3}{12S^*}$ = radial bending stiffness of the ring

$Q = \displaystyle\int_{-\frac{h}{2}}^{\frac{h}{2}} \tau dz$ = vertical shearing force

$(M_r,\ M_\theta) = \displaystyle\int_{-\frac{h}{2}}^{\frac{h}{2}} (\sigma_r,\ \sigma_\theta) z dz$ = radial and tangential bending moments

$R = \dfrac{-h^3}{12S^*}\left(S_{22}J'' - \dfrac{S_{12}}{r}J'\right)$

$S = \dfrac{-h^3}{12S^*}\left(S_{22}K'' - \dfrac{S_{12}}{r}K'\right)$

S_{ij} = elastic compliances

$S^* = \begin{vmatrix} S_{11} & S_{12} \\ S_{21} & S_{22} \end{vmatrix}$

h = thickness of the plate

$p(r)$ = transverse load per unit area, acting in the $+z$-direction

r_1 = inner radius of the ring-type plate or outer radius of the isotropic core

r_2 = outer radius of the plate

$r,\ \theta$ = radial and tangential co-ordinates

w = deflection, in the $+z$-direction, of the middle surface of the equivalent plate

z = co-ordinate perpendicular to the plane of the plate

ϵ_i = extensional strains

$\lambda^2 = \dfrac{S_{11}}{S_{22}}$

$\rho = \dfrac{r}{r_2}$

σ_i = extensional stress

τ = vertical shearing stress

$\varphi = w'$

Primes indicate differentiation with respect to r. Single subscripts 1, or 2 (on J, K, R, S, T, U) indicate that the function is evaluated at the inner, or outer radius, respectively.

Analysis

In the analysis, the circular plate is treated as a uniformly thick ring, with cylindrically aeolotropic properties, and an isotropic core.

The three-dimensional stress equations of equilibrium with central symmetry are[3]

$$\frac{\partial \sigma_r}{\partial r} + \frac{\partial \tau}{\partial z} + \frac{1}{r}(\sigma_r - \sigma_\theta) = 0$$

$$\frac{\partial \tau}{\partial r} + \frac{\partial \sigma_z}{\partial z} + \frac{1}{r}\tau = 0 \qquad (1\text{–}2)$$

where body forces are neglected, and τ_{rz} is written simply as τ.

Using the surface conditions

$$[\tau]_{\pm\frac{h}{2}} = 0$$

$$[\sigma_z]_{\pm\frac{h}{2}} = 0,\ -p(r) \qquad (3\text{–}4)$$

and neglecting stretch of the middle surface, (1), (2) can be integrated over the thickness h of a uniformly thick plate to obtain

$$Q' + \frac{1}{r}Q + p(r) = 0 \qquad (5)$$

$$M_r' + \frac{1}{r}(M_r - M_\theta) - Q = 0 \qquad (6)$$

The stress-strain relations for a cylindrically aeolotropic material may be written in terms of the compliances S_{ij} as

$$\epsilon_r = S_{11}\sigma_r + S_{12}\sigma_\theta$$

$$\epsilon_\theta = S_{21}\sigma_r + S_{22}\sigma_\theta \qquad (7\text{–}8)$$

where

$$S_{12} = S_{21}$$

The strains are defined as usual

$$(\epsilon_r,\ \epsilon_\theta) = \left(u',\ \frac{u}{r}\right) \qquad (9)$$

---

[1] General Electric Company, Schenectady, N. Y. Assoc. Mem. ASME.

[2] Professor of Mechanics, Rensselaer Polytechnic Institute, Troy, N. Y.

Discussion of papers in Brief Notes should be addressed to the Secretary, ASME, 29 West 39th Street, New York, N. Y., and will be accepted until January 10, 1960, for publication at a later date. Discussion received after the closing date will be returned.

Note: Statements and opinions advanced in papers are to be understood as individual expressions of their authors and not those of the Society. Manuscript received by Applied Mechanics Division, February 27, 1959.

[3] S. Timoshenko and J. N. Goodier, "Theory of Elasticity," McGraw-Hill Book Company, Inc., New York, N. Y., 1951, p. 343.

where $u = -w'z$

so that, combining (7) to (9), the stresses may be expressed as

$$\sigma_r = \frac{1}{S^*}\left(-S_{22}w'' + S_{12}\frac{w'}{r}\right)z$$
$$\sigma_\theta = \frac{1}{S^*}\left(S_{21}w'' - S_{11}\frac{w'}{r}\right)z \qquad (10\text{–}11)$$

Integrating over the thickness of the plate, the resulting bending moments are

$$M_r = -\frac{h^3}{12S^*}\left(S_{22}w'' - S_{12}\frac{w'}{r}\right)$$
$$M_\theta = -\frac{h^3}{12S^*}\left(-S_{21}w'' + S_{11}\frac{w'}{r}\right) \qquad (12\text{–}13)$$

Now, substituting Q from (6) into (5), introducing the moments from (12–13), the resulting differential equation is

$$w^{IV} + H_1w''' + H_2w'' + H_3w' = \frac{p(r)}{D^*} \qquad (14)$$

where

$$H_1 = 2\left(\frac{1}{r} + \frac{S_{22}'}{S_{22}} - \frac{S^{*\prime}}{S^*}\right)$$

$$H_2 = \frac{1}{S_{22}}\left\{S_{22}'' + \frac{1}{r}\left(2S_{22}' - S_{12}' - \frac{S_{11}}{r}\right) + \frac{1}{S^*}\left[S_{22}\left(2S^{*\prime}\left[\frac{S^{*\prime}}{S^*} - \frac{1}{r}\right] - S^{*\prime\prime}\right) + S^{*\prime}\left(\frac{S_{12}}{r} - 2S_{22}'\right)\right]\right\}$$

$$H_3 = \frac{1}{rS_{22}}\left\{\frac{1}{r}\left(\frac{S_{11}}{r} - S_{11}'\right) - S_{12}'' + \frac{1}{S^*} \times \left[S^{*\prime}\left(2\left[S_{12}' - \frac{S^{*\prime}S_{12}}{S^*}\right] - \frac{S_{11}}{r}\right) + S_{12}S^{*\prime\prime}\right]\right\}$$

$$D^* = \frac{S_{22}h^3}{12S^*} \qquad (15\text{–}18)$$

By first integrating equation (5), substituting $Q(r)$ thus obtained into equation (6), and then using the values of M_r, M_θ from (12), (13), the equation of equilibrium can be written as follows:

$$w''' + \left(\frac{1}{r} + \frac{S_{22}'}{S_{22}} - \frac{S^{*\prime}}{S^*}\right)w'' - \frac{1}{rS_{22}} \times \left(\frac{S_{11}}{r} + S_{12}' - \frac{S_{12}S^{*\prime}}{S^*}\right)w' = -\frac{Q(r)}{D^*} \qquad (19)$$

where, from (5),

$$Q(r) = -\frac{1}{r}\int_0^r p(r)r\,dr \qquad (20)$$

Solution of the Differential Equation

The homogeneous part of (19) may be rewritten

$$\varphi'' + A_1\varphi' + A_2\varphi = 0 \qquad (21)$$

where

$$A_1 = \frac{1}{\rho}\left\{\frac{1}{r_2} + \rho\left(\frac{S_{22}'}{S_{22}} - \frac{S^{*\prime}}{S^*}\right)\right\}$$
$$A_2 = \frac{-1}{\rho^2}\left\{\frac{1}{r_2S_{22}}\left[\frac{S_{11}}{r} + \rho\left(S_{12}' - \frac{S_{12}S^{*\prime}}{S^*}\right)\right]\right\} \qquad (22\text{–}23)$$

It is now assumed that the expressions in braces in (22–23) can be expressed as convergent infinite power series so that

$$A_m = \frac{1}{\rho^m}\sum_{k=0}^{\infty} a_{mk}\rho^k, \qquad m = 1, 2 \qquad (24)$$

and that the solutions of (21) are in the form

$$\varphi(\rho) = \sum_{l=0}^{\infty} b_l\rho^{l+c}, \qquad b_0 \neq 0 \qquad (25)$$

The deflection w can be found by integrating (25). This introduces another independent constant B which must be evaluated to satisfy the boundary conditions. Then,

$$w(\rho) = B + \sum_{l=0}^{\infty} b_l\frac{\rho^{l+c+1}}{l+c+1} \qquad (26)$$

Substituting (25) into (21),

$$\sum_{l=0}^{\infty} b_l\rho^{l+c-2}\left\{(l+c)(l+c-1) + \sum_{k=0}^{\infty}\rho^k[(l+c)a_{1k} + a_{2k}]\right\} = 0 \qquad (27)$$

The indicial equation for c, and the recurrence equations for the b_l are obtained by equating to zero the coefficients of the lowest power, and successively higher powers, of ρ in (27).

The indicial equation is

$$c^2 + (a_{10} - 1)c + a_{20} = 0 \qquad (28)$$

If the roots of (28) are distinct and do not differ by an integer, then there are two linearly distinct solutions of (21) of type (25). If the roots are equal or do differ by an integer, then only one solution of type (25) exists; the other solution will contain logarithmic terms.

In terms of the series (24–25) then, the deflection, slope, and moments can be expressed as

$$w = B + \sum_{l=0}^{\infty} b_l\frac{\rho^{l+c+1}}{l+c+1}$$
$$w' = \sum_{l=0}^{\infty} b_l\rho^{l+c}$$
$$M_r = \frac{-h^3}{12S^*}\sum_{l=0}^{\infty} b_l\rho^{l+c-1}[(l+c)S_{22} - S_{12}]$$
$$M_\theta = \frac{-h^3}{12S^*}\sum_{l=0}^{\infty} b_l\rho^{l+c-1}[-(l+c)S_{21} + S_{11}] \qquad (29\text{–}32)$$

Now, the recurrence relations reduce all b_l to expressions in b_0 and b_1, so that (29–32) can be rewritten

$$w = B + Jb_0 + Kb_1$$
$$\varphi = J'b_0 + K'b_1$$
$$M_r = Rb_0 + Sb_1$$
$$M_\theta = Tb_0 + Ub_1 \qquad (33\text{–}36)$$

The functions J, K, R, S, T, and U are obtained directly from (29–32) after the S_{ij} and c have been specified.

Particular solutions of the nonhomogeneous equation (19)

$$\varphi'' + A_1\varphi' + A_2\varphi = -\frac{Q(\rho)}{D^*} \qquad (37)$$

are only indicated here, since J and K are left as unspecified functions of ρ. If the method of variation of parameters is used, a particular solution is given by

$$\Phi = \alpha J' + \beta K' \tag{38}$$

where the coefficients α, β are computed from

$$(\alpha, \beta) = \int \frac{(K', -J')Q(\rho)}{(J'K'' - K'J'')D^*}\, d\rho \tag{39}$$

The complete solution of (37) is then

$$\varphi = J'b_0 + K'b_1 + \Phi \tag{40}$$

Discussion

If the S_{ij} are independent of radius, equations (14) and (19) reduce to the usual equations for a cylindrically aeolotropic plate,[4] viz.,

$$w^{IV} + \frac{2}{r}w''' - \left(\frac{\lambda}{r}\right)^2\left(w'' - \frac{1}{r}w'\right) = \frac{p(r)}{D^*}$$

$$w''' + \frac{1}{r}w'' - \left(\frac{\lambda}{r}\right)^2 w' = -\frac{Q(r)}{D^*} \tag{41–42}$$

Complementary solutions of (41) are

$$w(\lambda \neq 0 \text{ or } \pm 1) = a_1 r^{1+\lambda} + a_2 r^{1-\lambda} + a_3 r^2 + a_4$$

$$w(\lambda = 0) = a_1 + a_2 r^2 + a_3 r + a_4 r \ln r \tag{43–45}$$

$$w(\lambda = \pm 1) = a_1 + a_2 r^2 + a_3 \ln r + a_4 r^2 \ln r$$

For $\lambda = 1$ (isotropic), the constant a_4 can be eliminated by requiring that there not be a cusp in the deflection curve at $r = 0$. For $\lambda \neq 0$ or ± 1, the constant a_3 must vanish to insure that the radial and tangential moments are identical at $r = 0$. These conditions reduce (43–45) to the solutions obtained from equation (42). The remaining three constants are evaluated from two boundary conditions at the outer edge and a single condition either at the inner edge or at the center of the plate. The center condition is that the slope must be zero.

Typical Problems

1 Ring With Uniform Moments on Both Edges. Simply Supported Outer Edge, and Free on the Inner Edge.

Boundary conditions are

$$M_r(r_2) = M_2$$

$$M_r(r_1) = M_1 \tag{46–48}$$

$$w(r_2) = M_0$$

From (48) and (33),

$$B = -J_2 b_0 - K_2 b_1 \tag{49}$$

and from (46–47) and (35),

$$b_0 = V(M_2 S_1 - M_1 S_2)$$

$$b_1 = V(M_1 R_2 - M_2 R_1) \tag{50–51}$$

where

$$V = (R_2 S_1 - R_1 S_2)^{-1} \tag{52}$$

Thus, from (33–36),

$$w = V\{M_1[-S_2(J - J_2) + R_2(K - K_2)] + M_2[S_1(J - J_2) - R_1(K - K_2)]\}$$

$$w' = V[M_1(K'R_2 - J'S_2) + M_2(J'S_1 - K'R_1)]$$

$$M_r = V[M_1(R_2 S - S_2 R) + M_2(S_1 R - R_1 S)]$$

$$M_\theta = V[M_1(R_2 U - S_2 T) + M_2(S_1 T - R_1 U)] \tag{53–56}$$

where T and U are:

$$T = \frac{-h^3}{12S^*}\left(-S_{22}J'' + \frac{S_{11}}{r}J'\right)$$

$$U = \frac{-h^3}{12S^*}\left(-S_{22}K'' + \frac{S_{11}}{r}K'\right) \tag{57–58}$$

2 Plate With Solid Elastic Core and Uniform Moment M_0 Applied on the Outer Edge of the Plate.

The equations which apply to an isotropic core with uniform edge moment M_0 are

$$w = \frac{M_0 r_1^2}{2D(1+\mu)}\left[1 - \left(\frac{r}{r_1}\right)^2\right]$$

$$w' = -\frac{M_0 r}{D(1+\mu)} \tag{59–60}$$

Equations for the ring are (53–56).

Matching conditions at the ring-core interface are

$$w_{Ring}'(r_1) = w_{Core}'(r_1)$$

$$M_1 = M_0 \tag{61–62}$$

Thus, substituting (62) into (60), and equating (60) at r_1 to (5)4 at r_1,

$$N = \left[\frac{K_1'R_1 - J_1'S}{\frac{r_1}{D(1+\mu)} + V(K_1'R_2 - J_1'S_2)}\right] \tag{63}$$

The equations for deflection are obtained by subetituting $M_1 = NM_2$ into (53) and (59). The results are

$$w(r_1 \leq r \leq r_2) = M_2 V[(J - J_2)(S_1 - NS_2) - (K - K_2)(R_1 - NR_2)] \tag{64}$$

$$w(0 \leq r \leq r_1) = \frac{M_2 N r_1^2}{2D(1+\mu)}\left[1 - \left(\frac{r}{r_1}\right)^2\right] \tag{65}$$

3 Ring With Clamped Outer Edge and Uniform Moment on the Inner Edge.

The boundary conditions

$$M_r(r_1) = M_1$$

$$w(r_2) = 0 \tag{66–68}$$

$$w'(r_2) = 0$$

lead to the values

$$B = -J_2 b_0 - K_2 b_1$$

$$b_0 = -V^* K_2' M_1 \tag{69–71}$$

$$b_1 = V^* J_2' M_1$$

where

$$V^* = (J_2'S_1 - K_2'R_1)^{-1} \tag{72}$$

[4] G. F. Carrier, "The Bending of the Cylindrically Aeolotropic Plate," JOURNAL OF APPLIED MECHANICS, vol. 11, TRANS. ASME, vol. 66, 1944, pp. A-129-A-133.

so that

$$w = M_1V^*[(K - K_2)J_2' - (J - J_2)K_2']$$
$$w' = M_1V^*(K'J_2' - J'K_2')$$
$$M_r = M_1V^*(SJ_2' - RK_2') \qquad (73\text{–}76)$$
$$M_\theta = M_1V^*(UJ_2' - TK_2')$$

Heat Transfer From a Nonisothermal Disk Rotating in Still Air

J. P. HARTNETT[1]

THE LAMINAR velocity distribution occurring in the vicinity of a large disk rotating in a fluid of infinite extent, with the main fluid at rest, has been given by Karman [1][2] and Cochran [2]. Assuming the disk to be at a constant temperature different from that of the isothermal surroundings, the heat-transfer performance of such a surface has been determined by Wagner [3] and Millsaps and Pohlhausen [4]. Ostrach and Thornton [5] have recently treated this same isothermal rotating-disk problem, extending the results to include the influence of variable physical properties for gases with a Prandtl number of 0.72. The present note examines the influence of a variation in the surface temperature on the heat transfer from a disk rotating in still air, allowing the temperature difference between the disk surface and the fluid at rest to vary as a power function of the radius.

Nomenclature

- c_p = specific heat at constant pressure
- F = dimensionless radial velocity defined by Equation (3)
- H = dimensionless axial velocity defined by Equation (3)
- h_r = local heat-transfer coefficient for rotating disk, $q_r/(T_w - T_\infty)$
- h_x = local heat-transfer coefficient for flat plate geometry, $q_x/(T_w - T_\infty)$
- k = thermal conductivity of the fluid
- m = exponent in the assumed power function wall temperature distribution, Equation (5)
- Nu_r = local Nusselt number for rotating disk, $(h_r/k)(\nu/\omega)^{1/2}$
- Nu_x = local Nusselt number for flat plate geometry, $h_x x/k$
- Pr = Prandtl number of the fluid, $\mu c_p/k$
- q_r = local heat transfer from rotating disk per unit area per unit time
- q_x = local heat transfer from flat plate per unit area per unit time
- r = radial distance from center of disk
- T = temperature
- u = radial velocity
- w = axial velocity
- x = distance from leading edge of flat plate geometry
- z = axial distance from rotating disk surface
- ω = rotational speed of disk
- μ = dynamic viscosity of the fluid
- ν = kinematic viscosity of the fluid
- ρ = fluid density
- θ = dimensionless temperature, Equation (4)
- η = dimensionless distance from disk, Equation (2)

Subscripts

- w = conditions at the solid surface
- ∞ = conditions in the main fluid region outside the boundary layer
- iso = isothermal conditions ($m = 0$)

Analysis

Employing the usual boundary-layer assumptions, the equation describing the conservation of energy in the fluid surrounding a large rotating disk with the main body of the fluid at rest, may be written

$$\rho c_p u \frac{\partial T}{\partial r} + \rho c_p w \frac{\partial T}{\partial z} = k \frac{\partial^2 T}{\partial z^2} \qquad (1)$$

This partial differential equation may be transformed into an ordinary one if the following substitutions originally proposed by Karman and Cochran are introduced:

$$\eta = z\sqrt{\omega/\nu} \qquad (2)$$

$$u = r\omega F(\eta),\ w = \sqrt{\nu\omega}\, H(\eta) \qquad (3)$$

We next introduce a dimensionless temperature θ, which is a function only of the new variable η:

$$\theta(\eta) = \frac{T - T_\infty}{T_w - T_\infty} \qquad (4)$$

At this point, we depart from the isothermal analysis by allowing the wall temperature to vary in the following manner:

$$T_w - T_\infty = Ar^m \qquad (5)$$

When Equations (2) through (5) are substituted into Equation (1) there results:

$$mF\theta + H\frac{d\theta}{d\eta} = \frac{1}{\mathrm{Pr}}\frac{d^2\theta}{d\eta^2} \qquad (6)$$

Boundary conditions:

$$\theta = 1 \text{ at } \eta = 0$$
$$\theta = 0 \text{ at } \eta \to \infty \qquad (7)$$

Using the velocity functions F and H previously reported elsewhere [2, 5], the solution to this equation was obtained for a Prandtl number of 0.72 (i.e., air) for values of m ranging from 0 to 10. The resulting dimensionless temperature profiles θ are shown in Fig. 1.

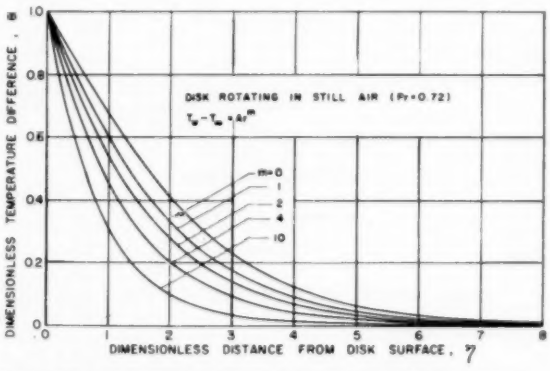

Fig. 1 Effect of power-function wall-temperature variation on temperature distribution

[1] Professor of Mechanical Engineering, Heat Transfer Laboratory, University of Minnesota, Minneapolis, Minn.; also, Consultant, The RAND Corporation, Santa Monica, Calif.

[2] Numbers in brackets indicate References at end of Note.

Manuscript received by ASME Applied Mechanics Division, June 4, 1959.

Heat-Transfer Results

The local heat transfer per unit area, q_r, is of major interest and is generally given in the form of a local Nusselt number. To accomplish this we define the local heat-transfer coefficient, h_r:

$$q_r = h_r (T_w - T_\infty) \tag{8}$$

where q_r is determined from

$$q_r = -k \left(\frac{\partial T}{\partial z} \right)_{z=0} \tag{9}$$

Equating (8) and (9) and transforming to the new variables

$$h_r = -k \left(\frac{\omega}{\nu} \right)^{1/2} \left(\frac{d\theta}{d\eta} \right)_{\eta=0} \tag{10}$$

we obtain the desired result, the local Nusselt number:

$$\mathrm{Nu}_r = \frac{h_r (\nu/\omega)^{1/2}}{k} = -\left(\frac{d\theta}{d\eta} \right)_{\eta=0} \tag{11}$$

The local Nusselt number is, therefore, directly obtainable as the slope of the dimensionless temperature distribution shown on Fig. 1, evaluated at the disk surface. The results are given in Table 1.

Table 1

m	Nu_r	$(\mathrm{Nu}_r)/(\mathrm{Nu}_r)_{\mathrm{iso}}$
0	0.330	1.00
1	0.437	1.33
2	0.524	1.59
4	0.661	2.00
10	0.935	2.83

Fig. 2 presents these results as the ratio of the local Nusselt value for a power-function wall-temperature variation to the isothermal Nusselt value, $(\mathrm{Nu}_r)/(\mathrm{Nu}_r)_{\mathrm{iso}}$. Similar results are available for (*a*) the flat plate, placed in a laminar air stream [6], and (*b*) the vertical flat plate in laminar free convection [7], in both cases allowing the temperature difference between the wall and free stream to vary as a power function, i.e., $(T_w - T_\infty) = Ax^m$. These results referred to the isothermal Nusselt values are also shown in Fig. 2. It is seen that the influence of the wall-temperature variation is somewhat less for the rotating disk than for the other two convection situations; however, the effect is still appreciable and considerable error would result from using isothermal relations in the presence of nonisothermal temperature variations.

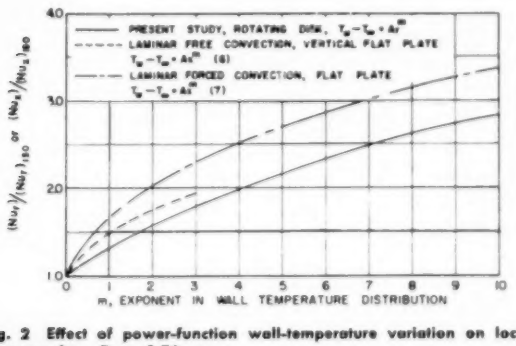

Fig. 2 Effect of power-function wall-temperature variation on local heat transfer. Pr = 0.72.

At the present time, no comparable nonisothermal analysis is available for the rotating disk when the flow is turbulent. However, a semiempirical analysis by Seban [8], recently substantiated by experiment [9, 10], is available for the nonisothermal flat plate in turbulent flow. From the present laminar results it would appear that such a flat-plate prediction should serve as an upper limit for turbulent flow over nonisothermal disks rotating in air.

Acknowledgment

The author is indeed indebted to Mr. E. C. Deland of The RAND Corporation for his efforts in programming and obtaining the machine calculations reported in this paper.

References

1 Th. von Karman, "Ueber laminare und turbulent Reibung," *Zeitschrift für Angewandte Mathematik und Mechanik*, vol. 4, 1921, p. 233.

2 W. G. Cochran, "The Flow Due to a Rotating Disc," Proceedings of the Cambridge Philosophical Society, vol. 30, 1934, p. 365.

3 C. Wagner, "Heat Transfer From a Heated Disk to Ambient Air," *Journal of Applied Physics*, vol. 19, 1948, p. 837.

4 Knox Millsaps and Karl Pohlhausen, "Heat Transfer by Laminar Flow From a Rotating Plate," *Journal of the Aeronautical Sciences*, vol. 19, 1952, p. 120.

5 Simon Ostrach and Phillip R. Thornton, "Compressible Laminar Flow and Heat Transfer About a Rotating Isothermal Disk," NACA Technical Note 4320, 1958.

6 D. R. Chapman and M. W. Rubesin, "Temperature and Velocity Profiles in the Compressible Laminar Boundary Layer With Arbitrary Distribution of Surface Temperature," *Journal of the Aeronautical Sciences*, vol. 16, 1949, p. 341.

7 E. M. Sparrow and J. L. Gregg, "Similar Solutions for Free Convection From a Nonisothermal Vertical Plate," TRANS. ASME, vol. 80, 1958, p. 379.

8 S. Scesa, "Experimental Investigation of Convective Heat Transfer to Air From a Flat Plate With a Stepwise Discontinuous Surface Temperature," MS thesis, University of California, Berkeley, Calif., 1949.

9 W. C. Reynolds, W. M. Kays, and S. J. Kline, "Heat Transfer in Turbulent Incompressible Boundary Layers," Parts 1–4, Final Report, Contract NAW-6494, Stanford University, Palo Alto, Calif., July, 1957.

10 R. Eichhorn, E. R. G. Eckert, and A. D. Anderson, "An Experimental Study of the Effects of Nonuniform Wall Temperature on Heat Transfer in Laminar and Turbulent Axisymmetric Flow Along a Cylinder," WADC Technical Report 58-33, July, 1958.

Harmonic Analysis of Crank-and-Rocker Mechanisms With Application

F. FREUDENSTEIN[1]

Introduction

THE increasing use of mechanisms for high-speed applications requires knowledge of inertia forces which in turn requires a harmonic analysis of the motion involved. Such analyses have been developed for the slider-crank mechanism [1, 2],[2] for the connecting-rod drives in high-speed engines [2], and more recently to link work involving sliding pairs [3, 4, 5]. The following represents an analysis of the general crank-and-rocker linkage with turning pairs, yielding the previously developed analyses as special cases. The results are applied to determine crank-and-rocker proportions minimizing the higher harmonics and optimiz-

[1] Chairman, Department of Mechanical Engineering, Columbia University, New York, N. Y.

[2] Numbers in brackets indicate References at end of Note.

Manuscript received by ASME Applied Mechanics Division, March 10, 1959.

ing the transmission angle [6]. The methods can be applied also to problems of kinematic synthesis, to the harmonic analysis of other types of four-bar mechanisms, and to coupler motions.

Harmonic Analysis of Crank-and-Rocker Mechanisms

We begin by mentioning two well-known series expansions [7]:

$$\frac{\cos\psi + k}{1 + 2k\cos\psi + k^2} = \sum_{m=1}^{\infty} (-k)^{m-1}\cos m\psi \quad (k^2 < 1) \quad (1)$$

$$\frac{\sin\psi}{1 + 2k\cos\psi + k^2} = \sum_{m=1}^{\infty} (-k)^{m-1}\sin m\psi \quad (k^2 < 1) \quad (2)$$

and note that in the crank-and-rocker mechanism in Fig. 1,

$$\psi = \psi_1 + \psi_2 = \tan^{-1}\left(\frac{\lambda\sin\phi}{1 + \lambda\cos\phi}\right) + \tan^{-1}\left(\frac{\delta\sin\beta}{1 + \delta\cos\beta}\right) \quad (3)$$

where

$$\lambda = \frac{b}{a}, \quad \delta = \frac{c}{d}, \quad \cos\beta = \mu_1 + \mu_2\cos\phi,$$

$$\mu_1 = \frac{a^2 + b^2 - c^2 + d^2}{2cd}, \quad \mu_2 = \frac{ab}{cd} \quad (4)$$

Equation (3) will be expanded in a Fourier series in ϕ. Let

$$\psi_1 = \sum_{m=1}^{\infty} a_m \sin m\phi$$

where

$$a_m = \frac{1}{\pi}\int_{-\pi}^{\pi} \psi_1 \sin m\phi d\phi$$

Integrating by parts,

$$a_m = \frac{1}{m\pi}\int_{-\pi}^{\pi} \frac{d\psi_1}{d\phi}\cos m\phi d\phi$$

$$= \frac{\lambda}{m}\left[\frac{1}{\pi}\int_{-\pi}^{\pi} \frac{\lambda + \cos\phi}{1 + 2\lambda\cos\phi + \lambda^2}\cos m\phi d\phi\right]$$

$$\therefore \psi_1 = \sum_{m=1}^{\infty} \frac{(-\lambda)^m}{(-m)}\sin m\phi \text{ using equation (1)} \quad (5)$$

Since ψ_2 is an even function of ϕ,

$$\psi_2 = \sum_{m=0}^{\infty} b_m \cos m\phi$$

where

$$b_m\,(m \neq 0) = \frac{1}{\pi}\int_{-\pi}^{\pi} \psi_2 \cos m\phi d\phi$$

$$= -\frac{1}{m\pi}\int_{-\pi}^{\pi} \frac{d\psi_2}{d\phi}\sin m\phi d\phi$$

and

$$b_0 = \frac{1}{2\pi}\int_{-\pi}^{\pi} \psi_2 d\phi.$$

Solving for the derivative $d\psi_2/d\phi$, we have

$$b_m(m \neq 0) = -\frac{1}{m}\left[\frac{1}{\pi}\int_{-\pi}^{\pi} fg\sin m\phi d\phi\right] \quad (6)$$

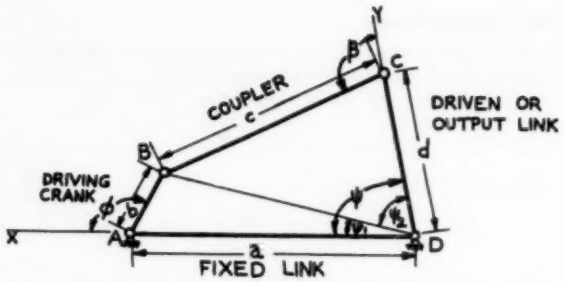

Fig. 1 Four-link mechanism with crank AB = b, coupler BC = c, driven link CD = d, fixed link AD = a. Input angle ϕ = angle XAB, output angle $\psi = \psi_1 + \psi_2$ = angle ADC; angle BCY = β; angles in radians, length units arbitrary.

where

$$f = \frac{1}{2}\mu_2\sin\phi + \lambda\left(\frac{\delta^2 - 1}{2\delta}\right)\left(\frac{\sin\phi}{1 + 2\lambda\cos\phi + \lambda^2}\right) \quad (7)$$

$$g = \frac{1}{\{1 - [\mu_1 + \mu_2\cos\phi]^2\}^{1/2}} \quad (8)$$

It follows from equation (6), that $(-mb_m)$ is equal to the coefficient f_m of the Fourier sine series for $F = fg = \sum_{m=1}^{\infty} f_m \sin m\phi$. Thus we can obtain b_m from the product of the series for f and g, each of which can readily be obtained separately.

From equation (2), we can deduce at once that

$$f = \frac{1}{2}\mu_2\sin\phi + \left(\frac{1 - \delta^2}{2\delta}\right)\sum_{m=1}^{\infty} (\sin m\phi)(-\lambda)^m \quad (9)$$

With the MacLaurin series for $(1 - x^2)^{-1/2}$, $x = \mu_1 + \mu_2\cos\phi$, and the formulas expressing $\cos^m\phi$ as a series of $\cos p\phi$ ($p = 0, 1, 2 \ldots m$), g can be expressed as a Fourier series in ϕ. Thus, in the special case $\mu_1 = 0$, we have

$$g(\phi) = C_0 + C_2\cos 2\phi + C_4\cos 4\phi + C_6\cos 6\phi + C_8\cos 8\phi + \ldots\ldots \quad (10)$$

where

$$\left.\begin{aligned} C_0 &= 1 + \frac{1}{4}\mu_2^2 + \frac{9}{64}\mu_2^4 + \frac{25}{256}\mu_2^6 + \left(\frac{35}{128}\right)^2 \mu_2^8 + \ldots. \\ C_2 &= \frac{1}{4}\mu_2^2 + \frac{3}{16}\mu_2^4 + \frac{75}{512}\mu_2^6 + \frac{(35)(56)}{(128)^2}\mu_2^8 + \ldots \\ C_4 &= \frac{3}{64}\mu_2^4 + \frac{15}{256}\mu_2^6 + \frac{(35)(28)}{(128)^2}\mu_2^8 + \ldots\ldots \\ C_6 &= \frac{5}{512}\mu_2^6 + \frac{35}{(16)(128)}\mu_2^8 + \ldots. \\ C_8 &= \frac{35}{(128)^2}\mu_2^8 + \ldots \end{aligned}\right\} \quad (11)$$

In general,

$$g(\phi) = \sum_{k=0}^{\infty} C_k\cos k\phi \quad (12)$$

Thus

$$\psi = b_0 + \sum_{m=1}^{\infty} \frac{(-\lambda)^m}{(-m)} \sin m\phi - \frac{1}{m} \sum_{m=1}^{\infty} f_m \cos m\phi \quad (13)$$

where

$$\sum_{m=1}^{\infty} f_m \sin m\phi = fg = \left\{ \frac{1}{2} \mu_2 \sin \phi + \left(\frac{1 - \delta^2}{2\delta} \right) \times \sum_{m=1}^{\infty} (-\lambda)^m \sin m\phi \right\} \left[\sum_{k=0}^{\infty} C_k \cos k\phi \right] \quad (14)$$

Equating coefficients in equation (14), and using the formula $2 \sin A \cos B = \sin (A + B) + \sin (A - B)$, we obtain finally

$$\psi = b_0 + \sum_{m=1}^{\infty} \frac{(-\lambda)^m}{(-m)} \sin m\phi - \frac{1}{4} \mu_2 C_0 \cos \phi - \sum_{m=1}^{\infty} \left\{ \frac{\mu_2}{4} (C_{m-1} + C_{m+1}) + \left(\frac{1 - \delta^2}{2\delta} \right) [C_0(-\lambda)^m + E_m + D_m] \frac{\cos m\phi}{m} \right\} \quad (15)$$

where

$$\left. \begin{aligned} D_m &= \sum_{a=1}^{m-1} (\tfrac{1}{2})(-\lambda)^a C_{m-a} \; (m \geq 2); \; D_1 = 0 \\ E_m &= \sum_{a=1}^{\infty} [(-\tfrac{1}{2})(-\lambda)^a C_{m+a} + (\tfrac{1}{2})(-\lambda)^{m+a} C_a] \end{aligned} \right\} \quad (16)$$

Equation (15) is the required expansion and can be used to calculate the harmonics of the output link motion.

Proportions of Crank-and-Rocker Linkages for High-Speed Operation

An examination of equation (15) reveals the desirability of the following proportions:

(i) $c/d = 1$; this eliminates a portion of the cosine series.

(ii) $\mu_1 = 0$; this eliminates another portion of that series [equation (8)].

(iii) (b/a) to be as small as possible; this attenuates the sine series and corresponds to good slider-crank proportions.

Crank-and-rocker linkages satisfying these proportions are defined as follows: Let $a = 1$; $b = \tan \frac{1}{2}u$; $c = d = 1/(\sqrt{2} \cos \frac{1}{2}u)$, where $\sin u = \mu_2$. Geometrically, the angle u is the maximum pressure angle of the linkage, where by pressure angle is meant the complement of the transmission angle, angle BCD in Fig. 1. Thus the requirements of good transmission and minimum "overtones" coincide in this case. While equation (15) is generally valid (except possibly when $\lambda = 1$, $\delta = 1$), the convergence of the series, especially for g in equation (11), is quite rapid for crank-and-rocker proportions suitable for high-speed operations, as can be seen by examining the magnitude of C_8 in that equation.

Example: When the maximum desired pressure angle is $u = 30$ deg, $\mu_2 = \frac{1}{2}$, $a = 1$, $b = 0.2680$, $c = d = 0.7320$,

$$\psi = b_0 - \sum_{m=1}^{\infty} \frac{(-0.268)^m}{m} \sin m\phi - \frac{1}{8} C_0 \cos \phi - \sum_{m=1}^{\infty} (C_{m-1} + C_{m+1}) \frac{\cos m\phi}{8m}$$

where

$C_0 = 1.073107$, $C_2 = 0.076975$, $C_4 = 0.004079$, $C_6 = 0.000221$, $C_8 = 0.000008$

from equation (11). The amplitudes a_m, b_m of the first six sine and cosine terms are as follows:

m	a_m	b_m	$[(a_m^2 + b_m^2)]^{1/2}$
1	0.268	−0.277899	0.386078
2	−0.035912	0	0.035912
3	0.006416	−0.003377	0.007250
4	−0.001290	0	0.001290
5	0.000277	−0.000108	0.000297
6	−0.000062	0	0.000062

Conclusions

The derivations enable a designer to determine whether a given mechanism possesses sizable overtones. Charts can be constructed based upon the recommended crank-and-rocker proportions and tables computed for the coefficients C_k in equation (11). The approach to ideal harmonic transformer behavior is asymptotic and can be realized to any required degree of accuracy at the expense of range.

References

1 R. E. Root, Jr., "Dynamics of Engine and Shaft," John Wiley & Sons, New York, N. Y., 1932.

2 C. B. Biezeno and R. Grammel, "Engineering Dynamics, vol. 4," Blackie and Son, Ltd., London, England, 1954.

3 W. Meyer zur Capellen, "Harmonische Analysis bei der Kurbelschleife," *Zeitschrift für angewandte Mathematik und Mechanik*, vol. 36, March/April, 1956.

4 W. Meyer zur Capellen, "Die Kurbelschleife zweiter Art," *Werkstatt und Betrieb*, 1957, no. 5, pp. 306–308.

5 W. Meyer zur Capellen, "Kinematik und Dynamik der Kurbelschleife," *Werkstatt und Betrieb*, 1956, part 1, no. 10, pp. 581–548; part 2, no. 12, pp. 677–683.

6 K. Hain, "How to Apply Drag Links in the Synthesis of Mechanisms," *Machine Design*, June 26, 1958, pp. 104–113.

7 R. V. Churchill, "Complex Variables," McGraw-Hill Book Co., Inc., New York, N. Y., first edition, 1948, p. 114.

Deflection Curve of a Simply Supported Beam[1]

D. GOSPODNETIC[2]

A THIN elastic beam, of a constant cross section and flexural rigidity EI, is forced to deflect by three symmetrically arranged knife-edged supports which, in the absence of friction, exert forces normal to the deflected beam.

The differential equation of the deflected beam is

$$d\varphi/ds = -M/EI \quad (1)$$

By introducing $\beta = [P/EI]^{1/2}$ and integrating once, we obtain

$$\frac{1}{2} \left(\frac{d\varphi}{ds} \right)^2 = -\beta^2 \sin \varphi + \beta^2 \tan \varphi_0 \cos \varphi + C \quad (2)$$

The integration constant C is equal to zero because of $d\varphi/ds = 0$ for $\varphi = \varphi_0$. Hence

$$d\varphi/ds = -\beta \sqrt{2} \, [\tan \varphi_0 \cos \varphi - \sin \varphi_0]^{1/2} \quad (3)$$

The negative sign of the root is chosen to satisfy $d\varphi/ds < 0$. Because of $d\varphi/ds = \sin \varphi d\varphi/dy = \cos \varphi d\varphi/dx$, we can separate the variables and integrate. We obtain

$$\frac{y}{l} = \frac{\sqrt{2} \sin \varphi_0 \cos \theta + \cos \varphi_0 \Phi(\theta)}{\sqrt{2} \cos \varphi_0 \cos \theta_0 - \sin \varphi_0 \Phi(\theta_0)} \quad (4)$$

[1] Written during a visit to the Electrical Engineering Department, University of Birmingham, Birmingham, England, which was made possible by the British Council.

[2] Physics Department, Faculty of Electrical Engineering, The University, Zagreb, Yugoslavia.

Manuscript received by ASME Applied Mechanics Division, Dec. 5, 1958; revised draft received June 17, 1959.

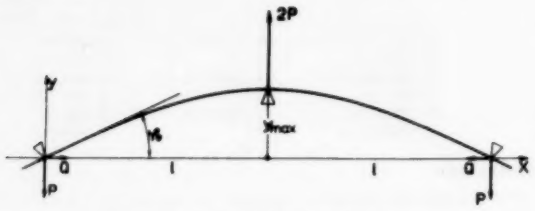

Fig. 1 Geometry of the beam

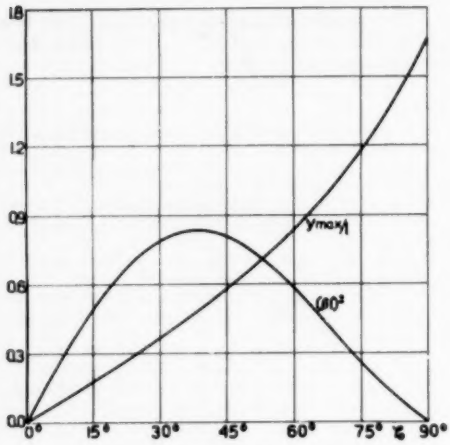

Fig. 2 Forces and deflections

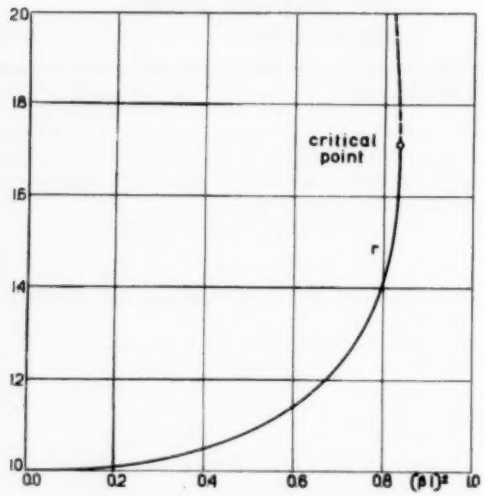

Fig. 3 Comparison diagram

$$\frac{x}{l} = \frac{\sqrt{2}\cos\varphi_0\cos\theta - \sin\varphi_0\Phi(\theta)}{\sqrt{2}\cos\varphi_0\cos\theta_0 - \sin\varphi_0\Phi(\theta_0)} \qquad (5)$$

where

$$\cos\theta = [\sin(\varphi_0 - \varphi)]^{1/2} \quad \cos\theta_0 = [\sin\varphi_0]^{1/2}$$

$$\Phi(\theta) = F(k, 90°) - F(k, \theta) - 2E(k, 90°) + 2E(k, \theta)$$

$$= -0.8472 - F(k, \theta) + 2E(k, \theta) \qquad k = \sqrt{2}/2$$

F and E are the elliptic integrals of the first and second kind, respectively. There is also

$$\beta l = \sqrt{\cos\varphi_0}\,[\sqrt{2}\cos\varphi_0\cos\theta_0 - \sin\varphi_0\Phi(\theta_0)] \qquad (6)$$

Two special cases merit a closer inspection. One is the case where $\varphi_0 = 90°$, and the other is the case for which the reaction force $2P$ at the center support reaches its maximum value.

Consider the case $\varphi_0 = 90°$ first. From (4) and (5), it follows that

$$y/l = -\sqrt{\cos\varphi}\cdot\sqrt{2}/\Phi(0) = 1.6693\sqrt{\cos\varphi} \qquad (7)$$

$$x/l = \Phi(\theta)/\Phi(0) = -1.1803\Phi(\theta) \qquad (8)$$

Vertical forces at the supports vanish because of $\beta l = 0$. Horizontal forces at the end supports are found from (1).

We obtain

$$\gamma l = \frac{\sqrt{2}}{y_{max}/l} = -\Phi(0) = 0.8472 \quad \gamma = \sqrt{Q/EI}$$

The second particular case involves the analysis of $\beta^2 l^2$ and y_{max}/l as functions of φ_0, the result of which is shown in Fig. 2. There is

$$(\beta l)_{max}^2 = 0.8340 \quad \text{for } \varphi_0 = 38.301°$$

The corresponding deflection is $y_{max}/l = 0.4764$.

Our results can now be used to solve the problem of large deflection of a centrally loaded simply supported beam. We have only to remove the central support and apply a force which now causes the deflection. Note that, if $(\beta l)^2 > (\beta l)_{max}^2 = 0.8340$, the beam becomes unstable, begins to move, and finally, in the absence of friction, slips off the supports. This critical point gives us either the largest force which can be applied to the beam, if it is used as a carrying element, or the largest restoring force achieved, if the beam is used as a spring element.

It is interesting to compare this exact solution with the elementary one, which gives as the maximum deflection

$$y_{max}'/l = (\beta l)^2/3$$

Let us introduce $r = y_{max}/y_{max}'$ as a coefficient which compares the exact with the elementary solution. This is plotted on the diagram in Fig. 3. This diagram is not in agreement with the analogous diagram given by Conway.[3]

On Plane-Stress Solution of a Compressible Wedge With the Use of Mises' Yield Condition[1]

A. KALNINS[2]

THE complete plane-strain solution for an acute, elastic, perfectly plastic wedge of incompressible material under uniform pressure on one face (valid for both Mises' and Tresca's yield

[3] H. D. Conway, "The Large Deflection of a Simply Supported Beam," *Philosophical Magazine*, series 7, vol. 38, 1947, pp. 905–911.

[1] The results presented here were obtained in the course of research sponsored by the Office of Naval Research under Contract Nonr-222-(69), Project NR-064-436, with the University of California, Berkeley, Calif.

[2] Institute of Engineering Research, University of California, Berkeley, Calif.

Manuscript received by ASME Applied Mechanics Division, April 13, 1959.

conditions) was given by Naghdi [1],[2] and was subsequently extended for a compressible material by Bland and Naghdi [2] employing Tresca's yield condition. The corresponding plane-stress solution of the acute wedge for a compressible material, again employing Tresca's yield condition, has also been given by Naghdi [3]. The general plane problem of the elastic, perfectly plastic wedge under uniform surface tractions has been examined and discussed by Murch and Naghdi [4]. The stress field of a wedge subjected to uniform pressure on one face has also been discussed in the state of plane strain by Sokolovskii [5] and Shapiro [6]. More recently, the corresponding problem in the state of plane stress has been investigated by Kachanov [7], where, after presentation of the form of the expressions characterizing the stress field, which is statically determinate, the determination of displacements was done by means of a simple total strain (deformation) theory.

The purpose of this note is to present a complete solution for an acute, compressible, elastic, perfectly plastic wedge in the state of plane stress subjected to uniform pressure on one face employing Mises' yield condition and its associated flow rules, and thereby to offer a comparison with the solution given previously in [3].

Analysis

Consider an acute wedge in the state of plane stress having an included angle β, occupying the region $0 \leq \theta \leq \beta$, where θ denotes the polar angle, and subjected to a uniform pressure p on $\theta = 0$. Then, with reference to the fully elastic solution for stresses as given in [1], it can be easily shown that, according to the Mises' yield condition, yielding originates on $\theta = \beta$ when the pressure p assumes the value $p^* = \sqrt{3}\, k(\tan \beta - \beta)/\tan \beta$, where k denotes the yield limit in simple shear. For values of $p > p^*$ an elastic-plastic boundary in the form of the ray $\theta = \phi_1$ will move away from $\theta = \beta$, and a plastic zone will form in the region P_1: $\phi_1 \leq \theta \leq \beta$. At a definite pressure $p = \bar{p}$ and the corresponding position of the elastic-plastic boundary $\phi_1 = \bar{\phi}$ the Mises' yield condition is also satisfied on $\theta = 0$, and subsequently for values of $p > \bar{p}$ a second elastic-plastic boundary $\theta = \phi_2$ and a plastic zone P_2, defined by $0 \leq \theta \leq \phi_2$, will be formed. At this stage, that is for values of $p > \bar{p}$, the wedge will consist of an elastic zone, given by $\phi_2 \leq \theta \leq \phi_1$, with nonsymmetric plastic zones on each side. The limiting plastic state of the wedge will be achieved at the pressure $p = p^{**}$, when both elastic-plastic boundaries coincide on $\theta = \phi^{**}$. It may be of interest to recall that in [3], where Tresca's yield condition was employed, yielding was found to begin simultaneously on $\theta = 0$ and $\theta = \beta$ when the pressure reached the value $p^* = 2k\,(\tan \beta - \beta)/\tan \beta$, and the subsequent locations of the two elastic-plastic boundaries possessed symmetry about $\theta = \beta/2$.

The expressions for the stresses σ_r, σ_θ, $\sigma_{r\theta}$ and displacements u_r, u_θ in the elastic zone with reference to cylindrical co-ordinates (r, θ, z) may be found in [3] where they may be seen to depend on four arbitrary functions of time a, b, c, and d, Poisson's ratio ν, and shear modulus G.

The stress field in the plastic zones, which is statically determinate and has been given previously in [7], may be written in the form

$$\left.\begin{matrix}\sigma_r \\ \sigma_\theta\end{matrix}\right\} = T \pm M \cos 2(\theta - \gamma)$$
$$\sigma_{r\theta} = -M \sin 2(\theta - \gamma) \tag{1}$$

where $T^2 = 3(k^2 - M^2)$, and M and γ are arbitrary functions of time.

According to the flow rules associated with the Mises' yield condition, the plastic strain-rate components are expressed in terms of the stress components by relations of the type $\dot{\epsilon}_r^{\,p} = {}^1/_3\lambda(2\sigma_r - \sigma_\theta)$, $\dot{\epsilon}_{r\theta}^{\,p} = \lambda\sigma_{r\theta}$, and so on, where dot denotes differentiation with respect to time and λ is a function of θ and time only, which is determined from the compatibility equation in a fashion similar to that in [2, 4]. The arbitrary functions of time a, b, c, d, M, and γ as well as the arbitrary functions of integration arising from the computation of displacements are determined from the usual continuity requirements. This procedure may be followed the same way as given in [3], and therefore only the final results will be recorded here.

For values of pressure $p^* \leq p \leq \bar{p}$:
The arbitrary functions in the elastic zone are

$$a = -\frac{1}{4}\sqrt{3}\,k\,\frac{\cos 2(\phi_1 - \beta) - \cos 2\beta}{1 - \cos 2\phi_1}$$
$$b = -\frac{1}{4}\sqrt{3}\,k\,\frac{1 - \cos 2\phi_1 - 2\phi_1 \sin 2\beta}{1 - \cos 2\phi_1} \tag{2}$$
$$c = -\frac{1}{2}\,d = \frac{1}{4}\sqrt{3}\,k\,\frac{\sin 2\beta}{1 - \cos 2\phi_1}$$

In the plastic zone P_1 the stresses are given by (1) and the displacements are

$$u_r = \frac{1}{2(1+\nu)}\,\frac{r}{G}\left\{\int_{t_1}^{t_2}\frac{2\,d}{N}\log\frac{z(\theta, t)}{z(t_2, t)}\,[T + 3M\cos 2(\theta - \gamma)]dt + [(1-\nu)T + (1+\nu)M\cos 2(\theta - \gamma)]\right\}$$
$$u_\theta = -\frac{r}{G}\left\{\frac{6}{1+\nu}\int_{t_2}^{\theta}\int_{t_1}^{t_2}\frac{\dot{d}}{N}\log\frac{z(\xi, t)}{z(t_2, t)}\,M\cos 2(\xi - \gamma)dtd\xi + \frac{1}{2}\,M\sin 2(\theta - \gamma) - \frac{1}{2}\,d + \frac{2d}{1+\nu}\log r\right\} \tag{3}$$

where

$$z(\xi, t) = \frac{3M + T\cos 2(\xi - \gamma) + N\sin 2(\xi - \gamma)}{T + 3M\cos 2(\xi - \gamma)};$$
$$N = [9M^2 - T^2]^{1/2}$$

Here

$$t_1 = \beta,\ t_2 = \phi_1;\quad T = M = -\frac{1}{2}\sqrt{3}\,k;\quad \gamma = \beta. \tag{4}$$

The relation between pressure and the elastic-plastic boundary ϕ_1 is given by

$$p = \frac{1}{2}\sqrt{3}\,k\,\frac{1 - \cos 2\phi_1 - 2\phi_1\sin 2\beta - \cos 2\beta + \cos 2(\phi_1 - \beta)}{1 - \cos 2\phi_1} \tag{5}$$

and $\bar{\phi}$ may be found from

$$6\sin 2\beta\,[\sin 2\bar{\phi}\cos 2(\bar{\phi} - \beta) + \sin 2(\beta - \bar{\phi}) - \sin 2\beta] + 4\bar{\phi}^2\sin^2 2\beta - 4\bar{\phi}\sin 2\beta(1 - \cos 2\bar{\phi}) = 0 \tag{6}$$

Pressure $\bar{p}$ may be calculated from (5) after $\bar{\phi}$ is known.

For values of pressure $\bar{p} \leq p \leq p^{**}$:
In the elastic zone the arbitrary functions are

$$a = -\frac{\sqrt{3}\,k\cos 2(\phi_1 - \beta)\sin 2\phi_2 + 2M\cos 2\phi_2\sin 2\phi_1}{4\sin 2(\phi_1 - \phi_2)}$$

[2] Numbers in brackets indicate References at end of Note.

$$b + \frac{1}{4}\sqrt{3}\,k = -d\phi_1 = \frac{1}{2}\,\phi_1\,\frac{-p + M + \frac{1}{2}\sqrt{3}\,k}{\phi_1 - \phi_2} \quad (7)$$

$$c = \frac{\sqrt{3}\,k\cos 2(\phi_1 - \beta)\cos 2\phi_2 + 2M\cos 2\phi_2 \cos 2\phi_1}{4\sin 2(\phi_1 - \phi_2)}$$

where M will be specified by (8). In the plastic zone P_1 the solution is identical to that given before and is specified by (1), (4), and (3), except that now the coefficient d in (3) must be taken from (7). In the plastic zone P_2 the stresses and displacements are given by (1) and (3) where

$$t_1 = 0, \quad t_2 = \phi_2; \quad M = \frac{1}{4}(p + [12k^2 - 3p^2]^{1/2}); \quad \gamma = 0 \quad (8)$$

The positions of the two elastic-plastic boundaries as a function of pressure may be found from the system of equations

$$\sin(\phi_1 - \phi_2)\left(-p + M + \frac{1}{2}\sqrt{3}\,k\right) = (\phi_1 - \phi_2)F \quad (9a)$$

$$F\sin(\phi_1 + \phi_2) = \frac{1}{2}\sqrt{3}\,k\sin 2\beta$$

$$\text{where} \quad F = \left[\frac{3}{4}k^2 + M^2 + \sqrt{3}\,kM\cos 2\beta\right]^{1/2} \quad (9b)$$

The limiting pressure p^{**} can be easily evaluated from (9a) by setting $\phi_1 = \phi_2$; ϕ^{**} can be then found from (9b) after p^{**} is known.

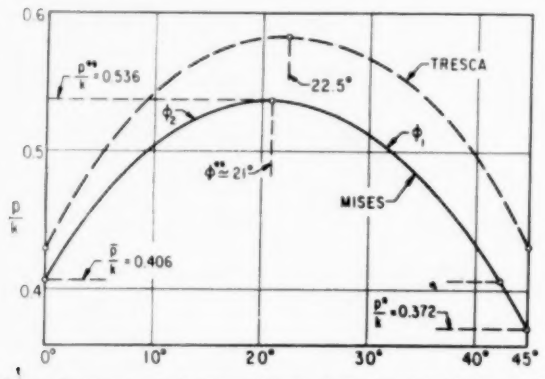

Fig. 1 Pressure versus location of elastic-plastic boundaries for $\beta = \pi/4$

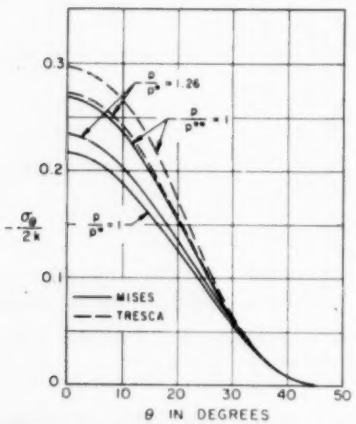

Fig. 2 Distribution of circumferential stress for $\beta = \pi/4$

Discussion

It may be noted that in the plastic zone P_2 the derivatives of Mises' yield condition with respect to the stresses are functions of time and not constants as in [3]. This fact prohibits the direct integration of the displacements in P_2 with respect to time, which was possible in [3], but here necessitates numerical integration which, however, may be performed along the same lines as in [4] and therefore will not be repeated here. To bring out the differences between the solution obtained here with the use of Mises' yield condition, and that obtained in [3] with Tresca's yield condition, the curves showing the dependence of elastic-plastic boundaries on pressure are plotted in Fig. 1, and the circumferential stress distribution for various values of p/p^* is shown in Fig. 2. It may be observed that the difference in circumferential stress between the two solutions varies from 0 to about 15 per cent which is reminiscent of a similar variation for the yield limit in simple tension as predicted by Tresca's and Mises' yield conditions.

Acknowledgment

The author is indebted to Professor P. M. Naghdi for suggesting this problem and the helpful criticism extended during its solution.

References

1 P. M. Naghdi, "Stresses and Displacements in an Elastic-Plastic Wedge," JOURNAL OF APPLIED MECHANICS, vol. 24, TRANS. ASME, vol. 79, 1957, pp. 98–104.

2 D. R. Bland and P. M. Naghdi, "A Compressible Elastic, Perfectly Plastic Wedge," JOURNAL OF APPLIED MECHANICS, vol. 25, TRANS. ASME, vol. 80, 1958, pp. 239–242.

3 P. M. Naghdi, "On Plane Stress Solution of Elastic, Perfectly Plastic Wedge," JOURNAL OF APPLIED MECHANICS, vol. 25, TRANS. ASME, vol. 80, 1958, pp. 407–410.

4 S. A. Murch and P. M. Naghdi, "On the Infinite Elastic, Perfectly Plastic Wedge Under Uniform Surface Tractions," Proceedings of the 3rd U. S. National Congress of Applied Mechanics, ASME, 1958, pp. 611–624.

5 V. V. Sokolovskii, "Theorie der Plastizität," VEB, Verlag Technik, Berlin, Germany, 1955, pp. 342–351.

6 G. S. Shapiro, "Elastic-Plastic Equilibrium of a Wedge and Discontinuous Solutions in the Theory of Plasticity," *Prikladnaia Matematika i Mekhanika*, vol. 16, 1952, pp. 101–106.

7 L. M. Kachanov, "Elastic-Plastic Equilibrium of a Wedge in Plane Stress State," *Prikladnaia Matematika i Mekhanika*, vol. 21, 1957, pp. 413–418.

An Application of a Dynamic Reciprocal Theorem

F. L. DiMAGGIO[1] and H. H. BLEICH[2]

ALTHOUGH the Betti-Maxwell reciprocal theorem of statics is familiar and often used, the existence of a similar theorem in dynamics does not appear to be as well known. In this note, the theorem is stated and an application to a wave propagation problem is discussed.

Let a concentrated force $\vec{f}_1\,g(t)$ applied at a point P_1 in an elastic body initially at rest produce a displacement $\vec{U}_1(P_2,t)$ at a point P_2. Similarly, a concentrated force $\vec{f}_2\,g(t)$ applied at a

[1] Assistant Professor of Civil Engineering, Columbia University, New York, N. Y.

[2] Director, Institute of Flight Structures, Columbia University, New York, N. Y.

Manuscript received by ASME Applied Mechanics Division, April 22, 1959.

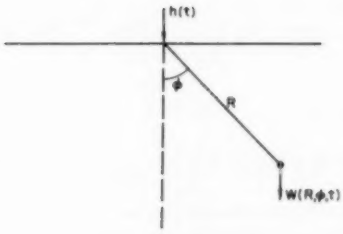

Fig. 1

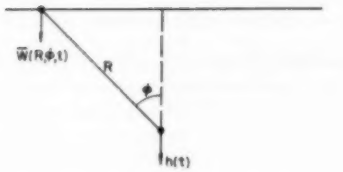

Fig. 2

point P_2 produces a displacement $U_2(P_1,t)$ at P_1. Graffi [1][3] has shown that

$$\vec{f}_1 \cdot \vec{U}_1(P_1,t) = \vec{f}_2 \cdot \vec{U}_1(P_2,t) \tag{1}$$

and that under the same restrictions on forces and initial conditions a relation analogous to Betti's also is valid. These are special cases of a general reciprocal relation for elasticity [2]. Rayleigh [3] had previously given a reciprocal theorem from which the above can be inferred, and Lamb [4] presented a general reciprocal theorem for a wide class of dynamical systems.

An interesting application of Equation (1) occurs in the problem of finding the vertical displacements $W(R,\phi,t)$ in the interior of an elastic half space produced by a concentrated vertical surface force varying with time like the Heaviside step function $h(t)$, Fig. 1.

Pekeris and Lifson [5] have determined curves for the vertical displacements $\overline{W}(R,\phi,t)$ at the surface of an elastic half space produced by a buried pulse $h(t)$, Fig. 2. It follows from Equation (1) that

$$\overline{W}(R,\phi,t) = W(R,\phi,t) \tag{2}$$

In a similar manner, using the work of Chao [6], the horizontal interior displacements due to a vertical force on the surface could be obtained by finding vertical surface displacements due to a horizontal buried pulse.

References

1 D. Graffi, "Sui Teoremi di Reciprocità nei Fenomeni Dipendenti dal Tempo," *Annali di Mathematica*, series 4, vol. 18, 1939, pp. 173–200.

2 D. Graffi, "Sul Teorema di Reciprocità nella Dinamica dei Corpi Elastici," *Memorie della Accademia delle Scienze*, Bologna, series 10, vol. 4, 1946/1947, pp. 103–111.

3 Lord Rayleigh, "Some General Theorems Relating to Vibration," Proceedings of the London Mathematical Society, vol. 4, 1873, pp. 366–368.

4 H. Lamb, "On Reciprocal Theorems in Dynamics," Proceedings of the London Mathematical Society, vol. 19, 1888, pp. 144-151.

5 C. L. Pekeris and H. Lifson, "Motion of the Surface of a Uniform Elastic Half Space Produced by a Buried Pulse," *Journal of the Acoustical Society of America*, vol. 29, 1957, pp. 1233–1238.

6 C. Chao, "Dynamical Response of an Elastic Half Space to Tangential Surface Loading," ONR Project Nr064-401, Institute of Flight Structures, Columbia University, New York, N. Y.

[3] Numbers in brackets indicate References at end of Note.

Simple Thickness-Shear Modes of Vibration of Infinite Sandwich Plates[1]

YI-YUAN YU[2]

THE simple thickness modes of free vibrations of a plate are those in which the faces of the plate are traction-free and the displacements are independent of the co-ordinates in the plane of the plate. The simple thickness-shear modes are further characterized by displacements parallel to the faces of the plate. In the case of infinite homogeneous plates, such modes were discussed by Mindlin[3] on the basis of both the exact elasticity theory and the plate theory that includes the effects of transverse shear deformation and rotatory inertia. The discrepancy between the lowest frequency values obtained from the elasticity and plate theories, respectively, was removed by introducing in the latter a correction factor, namely, a shear coefficient of the constant value of $\pi^2/12$. In this note the simple thickness-shear modes of infinite sandwich plates are similarly investigated on the basis of both the elasticity theory and the new sandwich-plate theory presented in the companion paper,[4] the latter also involving a shear coefficient. By matching frequencies as in the homogeneous case, the shear coefficient may likewise be determined directly for sandwich plates.

Notations used in this note are identical with those in the companion paper.[4]

Solution Based on Elasticity Theory

For our purpose here, the displacement components may be chosen to be

$$u_i = u_i(z,t), \qquad v_i = w_i = 0$$

and the only nonzero stresses are then

$$\tau_{zxi} = \mu_i \frac{\partial u_i}{\partial z} \tag{1}$$

By virtue of Equations (1) and the fact that all quantities are independent of x and y, the stress equations of motion in the elasticity theory reduce to

$$\mu_i \frac{\partial^2 u_i}{\partial z^2} = \rho_i \frac{\partial^2 u_i}{\partial t^2}$$

The general solutions of these equations are, with a factor $e^{i\omega t}$ neglected in writing in the sequel,

$$u_i = A_i \sin \beta_i z + B_i \cos \beta_i z$$

from which

$$\tau_{zxi} = \mu_i \beta_i (A_i \cos \beta_i z - B_i \sin \beta_i z)$$

where

$$\beta_i^2 = \frac{\rho_i}{\mu_i} \omega^2 \tag{2}$$

[1] This research was supported by the Air Force Office of Scientific Research of the Air Research and Development Command under Contract AF49(638)-453.

[2] Professor, Department of Mechanical Engineering, Polytechnic Institute of Brooklyn, Brooklyn, N. Y. Assoc. Mem. ASME.

[3] R. D. Mindlin, "Influence of Rotatory Inertia and Shear on Flexural Motions of Isotropic, Elastic Plates," JOURNAL OF APPLIED MECHANICS, vol. 18, TRANS. ASME, vol. 73, 1951, pp. 31–38; also R. D. Mindlin, "An Introduction to the Mathematical Theory of Vibrations of Elastic Plates," U. S. Army Signal Corps Engineering Laboratories, Fort Monmouth, N. J., 1956.

[4] Yi-Yuan Yu, "A New Theory of Elastic Sandwich Plates—One-Dimensional Case," JOURNAL OF APPLIED MECHANICS, vol. 26, TRANS. ASME, vol. 81, series E, 1959, pp. 415–421.

Manuscript received by ASME Applied Mechanics Division, September 16, 1958; final draft received June 5, 1959.

By satisfying the boundary conditions

$$\tau_{xz2} = 0 \qquad (z = -h)$$
$$\tau_{xz3} = 0 \qquad (z = h)$$
$$\tau_{xz1} = \tau_{xz2}, \qquad u_1 = u_2 \qquad (z = -h_1)$$
$$\tau_{xz1} = \tau_{xz3}, \qquad u_1 = u_3 \qquad (z = h_1)$$

the solution for the antisymmetric mode may readily be deduced. The frequency equation is found to be

$$\tan \beta_1 h_1 \tan \beta_2 h_2 = \frac{\mu_1 \beta_1}{\mu_2 \beta_2} \tag{3}$$

and the mode is given by

$$\left.\begin{aligned} u_1 &= A_1 \sin \beta_1 z \\ \begin{matrix} u_2 \\ u_3 \end{matrix} &= \mp A_1 \frac{\sin \beta_1 h_1}{\cos \beta_2 h_2} \cos \beta_2 (h \pm z) \end{aligned}\right\} \tag{4}$$

By making use of the definition of β_i as given in Equation (2) and the notations

$$\left.\begin{aligned} f &= \frac{\sqrt{\Omega}}{1 + r_h}, \qquad \Omega = \frac{\rho_1}{\mu_1} \omega^2 h^2 \\ r_h &= \frac{h_2}{h_1}, \qquad r_\rho = \frac{\rho_2}{\rho_1}, \qquad r_\mu = \frac{\mu_2}{\mu_1} \end{aligned}\right\} \tag{5}$$

Equations (3) and (4) may be rewritten as

$$\tan f \tan \left(f \sqrt{\frac{r_\rho r_h^2}{r_\mu}} \right) = \frac{1}{\sqrt{r_\rho r_\mu}} \tag{6}$$

$$\left.\begin{aligned} u_1 &= A_1 \sin \left(f \frac{z}{h_1} \right) \\ \begin{matrix} u_2 \\ u_3 \end{matrix} &= \mp A_1 \sin f \frac{\cos \left(f \sqrt{\frac{r_\rho r_h^2}{r_\mu}} \frac{h \pm z}{h_2} \right)}{\cos \left(f \sqrt{\frac{r_\rho r_h^2}{r_\mu}} \right)} \end{aligned}\right\} \tag{7}$$

Solution Based on Sandwich-Plate Theory

The lowest antisymmetric simple thickness-shear mode is also contained in the assumed form of the displacements in the sandwich-plate theory in the companion paper.[4] For this mode, the first two of Equations (30) in the previous paper[4] reduce to

$$\begin{aligned} -G_1 \psi_1 - 2G_2 \psi_2 &= \rho_1 I_{11} \ddot{\bar{\psi}}_1 + \rho_2 I_{22} \ddot{\bar{\psi}}_2 + \rho_2 I_{12} (\ddot{\bar{\psi}}_1 - \ddot{\bar{\psi}}_2) \\ -G_1 \psi_1 &= \rho_1 I_{11} \ddot{\bar{\psi}}_1 + \rho_2 I_{12} \ddot{\bar{\psi}}_2 + \rho_2 I_{21} (\ddot{\bar{\psi}}_1 - \ddot{\bar{\psi}}_2) \end{aligned} \tag{8}$$

By substituting in Equations (8)

$$\psi_1 = \Psi_1 e^{i\omega t}, \qquad \psi_2 = \Psi_2 e^{i\omega t}$$

the frequency equation is found to be

$$\begin{aligned} &[\rho_1 I_{11} \rho_2 (I_{22} - 2I_{12} + I_{21}) + \rho_2^2 (I_{22} I_{21} - I_{12}^2)] \omega^4 \\ &- [G_1 \rho_2 (I_{22} - 2I_{12} + I_{21}) + 2G_2 (\rho_1 I_{11} + \rho_2 I_{21})] \omega^2 + 2G_1 G_2 = 0 \end{aligned} \tag{9}$$

and, with a factor $e^{i\omega t}$ neglected in writing as before, the displacements may be shown to be of the form

$$\left.\begin{aligned} u_1 &= \Psi_1 z \\ \begin{matrix} u_2 \\ u_3 \end{matrix} &= \Psi_1 \left[\mp h_1 + \frac{G_1 - (\rho_1 I_{11} + \rho_2 I_{21}) \omega^2}{(\rho_2 I_{12} - \rho_2 I_{21}) \omega^2} (z \pm h_1) \right] \end{aligned}\right\} \tag{10}$$

Making use of the notations given in Equations (5), we further write Equations (9) and (10) in the following form:

$$\frac{r_\rho r_h^2}{r_\mu} (3 r_\rho r_h + 4) f^4 - 12\kappa \left(3 r_\rho r_h + 1 + \frac{r_\rho r_h^2}{r_\mu} \right) f^2 + 36\kappa^2 = 0 \tag{11}$$

$$\left.\begin{aligned} u_1 &= \Psi_1 z \\ \begin{matrix} u_2 \\ u_3 \end{matrix} &= \Psi_1 \left[\mp h_1 + 2 \frac{\kappa - (r_\rho r_h + {}^1/_3) f^2}{r_\rho r_h^2 f^2} (z \pm h_1) \right] \end{aligned}\right\} \tag{12}$$

In each specific case the value of κ is determined so as to make the lower root of f calculated from Equation (11) equal to the lowest root of f given by Equation (6). The value of κ is constant for a given sandwich plate but differs for sandwich plates with different values of the plate parameters, in contrast to the case of homogeneous plates in which we always have $\kappa = \pi^2/12$.

Ordinary Sandwich Plates

For ordinary sandwich plates the ratio r_h is usually rather small, r_ρ large, and r_μ very large, as compared to one. The fraction $r_\rho r_h^2 / r_\mu$ should therefore be much smaller than one for such plates, for which Equation (6) thus reduces approximately to

$$f \tan f = 1/r_\rho r_h \tag{13}$$

provided that f or $\sqrt{\Omega}$ is sufficiently small. Similarly, the frequency equation (11) of the plate theory yields approximately, by omitting the first term,

$$\kappa = (r_\rho r_h + {}^1/_3) f^2 \tag{14}$$

The shear coefficient κ for ordinary sandwich plates may now be determined from Equation (14) when f is first solved from Equation (13). It is interesting to note that κ depends entirely on $r_\rho r_h$ for such plates.

It is also interesting to examine the limiting values of κ for the case $r_\rho r_h^2 / r_\mu \ll 1$. For $r_\rho r_h$ equal to zero, the right side of Equation (13) becomes infinite, and the lowest root is seen to be $f = \pi/2$. Equation (14) in turn yields $\kappa = \pi^2/12$, which is the value for homogeneous plates. On the other hand, for sufficiently large values of $r_\rho r_h$, Equation (13) becomes approximately

$$f^2 = 1/r_\rho r_h \tag{15}$$

and Equation (14) yields in the limit

$$\kappa = 1$$

The limiting value of $\kappa = 1$ is approached very rapidly as $r_\rho r_h$ increases. For example, for $r_\rho r_h = 1$ and 2, the corresponding values of κ are 0.988 and 0.996, respectively. For $r_\rho r_h > 2$, κ may be taken equal to 1 without appreciable error.

The value $\kappa = 1$ implies that perfect match of the frequency of the simple thickness-shear mode is attained between the elasticity and sandwich-plate theories even when no correction factor is used in the latter. That this can be very nearly so, may be explained by examining the corresponding mode shapes for such cases. For Equation (15) to be valid, f and $f[r_\rho r_h^2 / r_\mu]^{1/2}$ in Equation (6) must both be small so that they may replace their tangents. It follows that Equations (7) reduce to

$$u_1 = A_1 f \frac{z}{h_1}$$

$$\begin{matrix} u_2 \\ u_3 \end{matrix} = \mp A_1 f \tag{16}$$

which represent the approximate mode shape given by the elasticity solution. On the other hand, according to the sandwich-plate theory, the mode shape is given by Equations (12). For ordinary sandwich plates the approximate Equation (14) is

valid and r_h is not zero; Equations (12) thus reduce to, also approximately,

$$u_1 = \Psi_1 z \qquad u_2 = u_3 = \mp \Psi_1 h_1 \tag{17}$$

The approximate mode shapes given by Equations (16) and (17) are obviously the same, which explains why the frequencies given by the two theories are also very nearly the same in those cases in which $r_\rho r_h^2 / r_\mu \ll 1$ and $r_\rho r_h > 2$, even when no correction factor is used in the sandwich-plate theory.

The Nonlinear Conical Spring

R. SCHMIDT[1] and G. A. WEMPNER[1]

THE large symmetric deformations of shallow conical shells are of interest in the design of nonlinear conical disk springs. In most applications a uniformly distributed axial load acts at the inner and outer edges; these edges are otherwise free. Several approximations have been proposed to describe the behavior of these springs. A first approximation [1][2] is based on the assumption that meridional strains are negligible. This requires that the shell remain conical after deformation and also that the extensional strain of meridional lines on the middle surface vanish. Another approximation [2] retains only the assumption that the shell remains conical. The first assumption satisfies neither of the two boundary conditions at the free edges; the latter violates the condition of vanishing moment at the free edges. Recently the authors presented a series solution [3] for a special case, namely, the case of an annular plate under similar loading. Numerical solutions for the shallow conical shell under these conditions of load have also been obtained [4]. An examination of these results indicates that the meridional bending stresses are of much smaller magnitude than the circumferential bending stresses. Hence the present analysis is based on the neglect of the meridional bending moment.

Nomenclature

r, θ = polar co-ordinates of the middle surface
a, b = radii to the inner and outer edges, respectively
ϕ = initial slope of the cone
h = thickness of the shell
E = modulus of elasticity
ν = Poisson's ratio
P = total axial edge load
β = rotation of the meridian of the middle surface
bu, bw = radial and axial displacement components, respectively
$\overline{N}_r, \overline{N}_\theta$ = meridional and circumferential tensions per unit length
$\overline{M}_r, \overline{M}_\theta$ = meridional and circumferential moments per unit length
$\epsilon_r, \epsilon_\theta$ = meridional and circumferential extensional strains

For convenience, the following dimensionless quantities are introduced:

$$\alpha = \frac{r}{b}, \qquad \alpha_0 = \frac{a}{b}, \quad \gamma = \frac{h}{b}, \qquad p = \frac{(1-\nu^2)P}{2\pi E h b},$$

$$N_r = \epsilon_r + \nu\epsilon_\theta = \frac{(1-\nu^2)}{Eh}\overline{N}_r, \qquad N_\theta = \epsilon_\theta + \nu\epsilon_r = \frac{(1-\nu^2)}{Eh}\overline{N}_\theta$$

$$M_r = \frac{12(1-\nu^2)}{Eh^2\gamma}\overline{M}_r, \qquad M_\theta = \frac{12(1-\nu^2)}{Eh^2\gamma}\overline{M}_\theta.$$

Differential Equations and Potential Energy

For finite (but small) deflections the behavior of the shell is described by differential equations of the von Karman type [5]. In the absence of surface tractions the differential equations, in dimensionless form (see Nomenclature), are [2]

$$\frac{d}{d\alpha}\left[\frac{1}{\alpha}\frac{d}{d\alpha}(\alpha^2 N_r)\right] = -(1-\nu^2)\left(\frac{\beta}{2} - \phi\right)\frac{\beta}{\alpha} \tag{1a}$$

$$\frac{d}{d\alpha}\left[\frac{1}{\alpha}\frac{d}{d\alpha}(\alpha\beta)\right] = \frac{12}{\gamma^2}\left[N_r(\beta - \phi) - \frac{p}{\alpha}\right] \tag{1b}$$

The displacements u, w are given by the equations

$$u = \frac{\alpha}{1-\nu^2}\left[(1-\nu)N_r + \alpha\frac{dN_r}{d\alpha}\right], \qquad \frac{dw}{d\alpha} = \beta \tag{2a, b}$$

and the tensions N_r, N_θ and moments M_r, M_θ by

$$N_\theta = \frac{d}{d\alpha}(\alpha N_r) \tag{3a}$$

$$M_r = \frac{d\beta}{d\alpha} + \nu\frac{\beta}{\alpha}, \qquad M_\theta = \frac{\beta}{\alpha} + \nu\frac{d\beta}{d\alpha} \tag{3b, c}$$

The total potential energy V of the system is given by the integral (in dimensionless form),

$$V = \int_{\alpha_0}^{1}\left\{-p\beta + \frac{\alpha}{2(1-\nu^2)}[N_r^2 + N_\theta^2 - 2\nu N_r N_\theta] + \frac{\gamma^2\alpha}{24(1-\nu^2)}[M_r^2 + M_\theta^2 - 2\nu M_r M_\theta]\right\}d\alpha. \tag{4}$$

Method of Solution

The exact solution of the stated problem requires the solution of the nonlinear differential equations (1*a*, *b*) subject to the boundary conditions

$$N_r(\alpha_0) = N_r(1) = 0, \qquad M_r(\alpha_0) = M_r(1) = 0 \tag{5a, b}$$

If we exclude the case of a very small inner radius, previous studies[3] [3], [4] indicate that the meridional moment M_r is small throughout the shell. Consequently a good approximation is obtained by setting $M_r = 0$. Then Equations (3*b*, *c*) yield

$$\beta = \frac{C}{\alpha^\nu}, \qquad M_\theta = (1-\nu^2)\frac{C}{\alpha^{1+\nu}} \tag{6, 7}$$

where C is a constant, as yet undetermined.

By means of Equation (2*b*) the constant C is expressed in terms of the axial edge displacement w_0,

$$w_0 = \int_{\alpha_0}^{1}\beta d\alpha = \frac{C}{1-\nu}(1 - \alpha_0^{1-\nu}) \tag{8}$$

Also, from Equation (1*a*) and the boundary conditions (5*a*), we have

$$N_r = \frac{1-\nu^2}{\nu}\left[\frac{C^2}{8(1-\nu)}(\alpha^{-2\nu} - K_1 + K_2\alpha^{-2}) - \frac{\phi C}{2-\nu}(\alpha^{-\nu} - K_3 + K_4\alpha^{-2})\right] \tag{9}$$

---

[1] Associate Professor, Department of Civil Engineering, University of Arizona, Tucson, Ariz.

[2] Numbers in brackets indicate References at end of Note.

Manuscript received by ASME Applied Mechanics Division, March 10, 1959.

where $K_1 = \dfrac{1 - \alpha_0^{2-2\nu}}{1 - \alpha_0^2}$, $K_3 = \dfrac{1 - \alpha_0^{2-\nu}}{1 - \alpha_0^2}$,

$K_2 = \dfrac{\alpha_0^2(1 - \alpha_0^{-2\nu})}{1 - \alpha_0^2}$, $K_4 = \dfrac{\alpha_0^2(1 - \alpha_0^{-\nu})}{1 - \alpha_0^2}$.

By means of Equation (3*a*) the circumferential tension N_θ is expressed in terms of the constant C. Thus all of the quantities appearing in the potential energy expression are expressed as functions of the independent variable α and the constant C; or, equivalently, in terms of the edge displacement w_0 according to Equation (8). The desired relation between applied load p and displacement w_0 is obtained from the condition that the potential energy V, Equation (4), is to be stationary. That is,

$$\frac{\partial V}{\partial w_0} = \frac{\partial V}{\partial C} = 0.$$

The foregoing equation expresses the load p as a polynomial of third degree in C

$$p = B(A_1C + A_2C^2 + A_3C^3), \tag{10}$$

where

$$A_1 = -\frac{\nu\gamma^2 K_2}{12\alpha_0^2} + \frac{2\phi^2}{(2-\nu)^2}\left[\frac{2 - 4\nu + 3\nu^2}{2(1-\nu)} K_1 - (1-\nu)K_3^2 - \frac{1+\nu}{\alpha_0^2} K_4^2\right],$$

$$A_2 = -\frac{3\phi}{4(1-\nu)(2-\nu)}\left[\frac{2 - 5\nu + 5\nu^2}{2 - 3\nu}\frac{1 - \alpha_0^{2-3\nu}}{1 - \alpha_0^2} - (1-\nu)K_1K_2 - \frac{1+\nu}{\alpha_0^2} K_2K_4\right],$$

$$A_3 = \frac{1}{16(1-\nu)^2}\left[\frac{1 - 3\nu + 4\nu^2}{1 - 2\nu}\frac{1 - \alpha_0^{2-4\nu}}{1 - \alpha_0^2} - (1-\nu)K_1^2 - \frac{1+\nu}{\alpha_0^2} K_2^2\right],$$

$$B = (1-\nu)(1-\nu^2)(1 - \alpha_0^2)/2\nu^2(1 - \alpha_0^{1-\nu})$$

By means of Equations (3), (7), (8), and (9) the tensions N_r, N_θ, and moments M_r, M_θ may be expressed in terms of the displacement w_0.

Discussion of Results

A graphical comparison of Equation (10) with the load-deflection relations of previous analyses [1], [2], [4] is shown in Fig. 1. It is noted that the present results are in very good agreement with previous numerical results [4].

An indication of the accuracy is obtained by a comparison with the series solution [3] for a flat plate. It is apparent from Table 1 that the accuracy is very good for the parameters chosen. However, it should be noted that the present approximation is invalid if the inner (hole) radius is small. This is not a serious limitation, since the inner radius is relatively large in most practical applications.

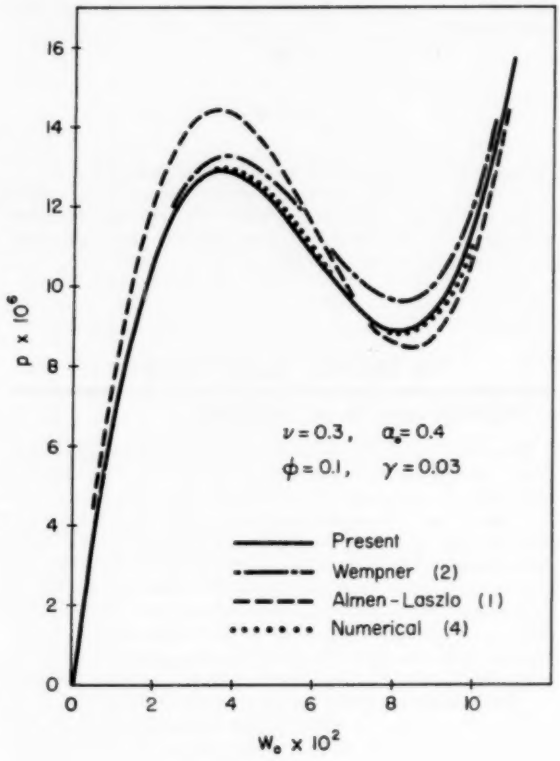

Fig. 1

References

1 J. O. Almen and A. Laszlo, "The Uniform-Section Disk Spring," Trans. ASME, vol. 58, 1936, pp. 305–314.

2 G. A. Wempner, "The Conical Disk Spring," Proceedings of the Third U. S. National Congress of Applied Mechanics, ASME, 1958, pp. 473–478.

3 G. A. Wempner and R. Schmidt, "Large Deflections of Annular Plates," Journal of Applied Mechanics, vol. 25, Trans. ASME, vol. 80, 1958, pp. 449–452.

4 G. A. Wempner, "Axially Symmetric Deformation of a Shallow Conical Shell," Doctoral thesis, University of Illinois, Urbana, Ill., 1957.

5 Th. von Karman, "Festigkeitsprobleme im Maschinenbau," Encyklopaedie der mathematischen Wissenschaften, vol. 4, 1910, Teubner, Leipzig, pp. 348–352.

Table 1

	$p = 0.000, 041, 325$	$\nu = 0.3$			$\gamma = 0.05$,		$\alpha_0 = 0.5$
	α	0.5	0.6	0.7	0.8	0.9	1.0
M_r	Approximate	0	0	0	0	0	0
	Series sol'n	0	+0.00505	+0.0105	+0.0121	+0.00862	0
M_θ	Approximate	+0.209	+0.165	+0.135	+0.114	+0.0975	+0.0850
	Series sol'n	+0.207	+0.165	+0.138	+0.118	+0.102	+0.0870
$10^3 \times N_r$	Approximate	0	+0.251	+0.282	+0.220	+0.118	0
	Series sol'n	0	+0.249	+0.282	+0.221	+0.119	0
$10^3 \times N_\theta$	Approximate	+2.20	+0.911	+0.086	−0.483	−0.896	−1.21
	Series sol'n	+2.18	+0.913	+0.099	−0.473	−0.901	−1.23
β	Approximate	+0.115	+0.109	+0.104	+0.100	+0.0964	+0.0934
	Series sol'n	+0.114	+0.108	+0.104	+0.101	+0.0982	+0.0956
$10^2 \times w$	Approximate	+5.13	+4.01	+2.95	+1.93	+0.949	0
	Series sol'n	+5.14	+4.04	+2.98	+1.96	+0.969	0

A Note on the Calculation of Shallow Shells

W. FLÜGGE[1] and D. A. CONRAD[2]

In 1947, S. A. Ambartsumyan[3] presented a method for the calculation of shallow shells. The method depends on the separation of the Fourier series solution into a portion recognizable as that of a flat plate under the same loading, and the remainder due to the small curvatures of the shell. In 1956 the present authors,[4] unaware of the Russian work, using the same method, computed some solutions for shallow spherical, cylindrical, and hyperboloidal shells under concentrated loading. The purpose of this note is to present these solutions and to point out the substantial computational simplification which results from the method.

Fig. 1 illustrates a shallow shell described by the distance $z(x, y)$ of its middle surface from the x-y plane. The differential equations of the problem, including the effects of load and temperature are:

$$\nabla_*^4 w - \frac{1}{Da}\nabla_\lambda^2 \varphi = \frac{Z}{D} + \frac{1+\nu}{t}\alpha\nabla_*^2(\Delta T)$$
$$\nabla_*^4 \varphi + \frac{Et}{a}\nabla_\lambda^2 w = -Et\alpha\nabla_*^2 \bar{T} \tag{1}$$

where the various symbols are defined as follows:

w = normal deflection of shell
φ = Airy stress function
D = bending rigidity = $Et^3/12(1-\nu^2)$
E = Young's modulus
t = shell thickness
ν = Poisson's ratio
α = coefficient of thermal expansion
$\bar{T}$ = average temperature through shell thickness
ΔT = temperature difference between shell surfaces
a = radius of curvature in y-direction
b = radius of curvature in x-direction
$\lambda = a/b$

$$\nabla_*^2 = \frac{\partial^2}{\partial x^2} + \frac{\partial^2}{\partial y^2}; \quad \nabla_\lambda^2 = \frac{\partial^2}{\partial x^2} + \lambda\frac{\partial^2}{\partial y^2}$$

It has been assumed that the x and y-axes are projections of the lines of principal curvature and that these curvatures are constant. Note, however, that λ can be negative.

The stress resultants are obtained from the Airy stress function by

$$N_x = \frac{\partial^2\varphi}{\partial y^2}; \quad N_{xy} = -\frac{\partial^2\varphi}{\partial x\partial y}; \quad N_y = \frac{\partial^2\varphi}{\partial x^2}, \tag{2}$$

and the moment resultants and tangential displacements result from the stress-displacement relations, which can be written in the form

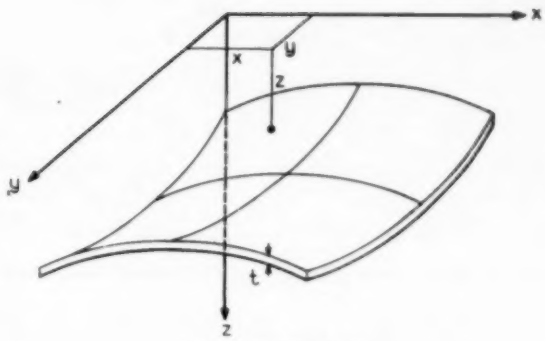

Fig. 1 Shallow shell

$$\frac{\partial u}{\partial x} = \frac{1}{Et}(N_x - \nu N_y) + \frac{w}{b} + \alpha\bar{T}$$
$$\frac{\partial v}{\partial y} = \frac{1}{Et}(N_y - \nu N_x) + \frac{w}{a} + \alpha\bar{T}$$
$$M_x = -D\left[\frac{\partial^2 w}{\partial x^2} + \nu\frac{\partial^2 w}{\partial y^2} - \frac{1+\nu}{t}\alpha(\Delta T)\right]$$
$$M_y = -D\left[\frac{\partial^2 w}{\partial y^2} + \nu\frac{\partial^2 w}{\partial x^2} - \frac{1+\nu}{t}\alpha(\Delta T)\right] \tag{3}$$
$$M_{xy} = -D(1-\nu)\frac{\partial^2 w}{\partial x\partial y}; \quad N_{xy} = \frac{Et}{2(1+\nu)}\left[\frac{\partial u}{\partial y} + \frac{\partial v}{\partial x}\right]$$

The load and temperature terms are then expanded in double Fourier series and the solution taken in the same form. For simplicity, only the even portion will be considered here, so we expand the right-hand sides of equations (1) as follows:

$$\frac{Z}{D} + \frac{1+\nu}{t}\alpha\nabla_*^2(\Delta T) = \sum_{m,n} A_{mn}\cos mx\cos ny$$
$$-\alpha\nabla_*^2\bar{T} = \sum_{m,n} B_{mn}\cos mx\cos ny \tag{4}$$

where

$$m = \frac{m'\pi}{l_1}, \quad n = \frac{n'\pi}{l_2} \tag{5}$$

with m' and n' integers and l_1 and l_2 the extent of the shell in the x and y-directions.

The stress function and displacements then assume the forms

$$\varphi = \sum_{m,n}\Phi_{mn}\cos mx\cos ny$$
$$w = \sum_{m,n} W_{mn}\cos mx\cos ny$$
$$u = \sum_{m,n} U_{mn}\sin mx\cos ny \tag{6}$$
$$v = \sum_{m,n} V_{mn}\cos mx\sin ny$$

By substituting the expansions into the differential equations (1) we find for Φ_{mn} and W_{mn}

[1] Professor of Engineering Mechanics, Stanford University, Stanford, Calif. Mem. ASME.

[2] Member of the Technical Staff, Hughes Aircraft Company, Tucson, Ariz. Formerly with Bell Telephone Laboratories, Inc., Murray Hill, N. J. Assoc. Mem. ASME.

[3] S. A. Ambartsumyan, "On the Calculation of Shallow Shells" (in Russian), Prikladnaia Matematika i Mekhanika, vol. 11, 1947, pp. 527–532. Translated as NACA TM 1425, December, 1956.

[4] D. A. Conrad, "Singular Solutions in the Theory of Shallow Shells," dissertation, Stanford University, September, 1956. Also by W. Flügge and D. A. Conrad, Stanford University, Division of Engineering Mechanics, Technical Report No. 101.

Manuscript received by ASME Applied Mechanics Division, May 25, 1959.

$$\Phi_{mn} = Et\,\frac{B_{mn} + \mu\beta A_{mn}}{(m^2 + n^2)^2(1 + \beta^2)}$$

$$W_{mn} = \frac{A_{mn} - \dfrac{\beta}{\mu} B_{mn}}{(m^2 + n^2)^2(1 + \beta^2)} \tag{7}$$

where

$$\mu = \frac{l}{[12(1 - \nu^2)]^{1/4}}\,; \quad \beta = \beta_{mn} = \frac{m^2 + \lambda n^2}{\mu a (m^2 + n^2)^2} \tag{8}$$

The corresponding values for the plate result when $a \to \infty$, leaving

$$\Phi_{mn}^{(p)} = \frac{EtB_{mn}}{(m^2 + n^2)^2}\,; \quad W_{mn}^{(p)} = \frac{A_{mn}}{(m^2 + n^2)^2} \tag{9}$$

By separating the plate portion from the remainder, equation (7) becomes

$$\Phi_{mn} = \Phi_{mn}^{(p)} - Et\,\frac{\beta^2 B_{mn} - \mu\beta A_{mn}}{(m^2 + n^2)^2(1 + \beta^2)}$$

$$W_{mn} = W_{mn}^{(p)} - \frac{\beta^2 A_{mn} + \dfrac{\beta}{\mu} B_{mn}}{(m^2 + n^2)^2(1 + \beta^2)} \tag{10}$$

The advantage that this form has over equation (7) is its superior convergence. The slowly converging parts now appear in the plate portion and the remainder is improved by the factor β^2 which goes like $1/m^2$ and $1/n^2$. So if the plate solution is readily available, or can be obtained by other means, the separation indicated in equation (10) is of substantial benefit to the computation of shallow shells.

The corresponding tangential displacement coefficients, which result from equations (3) by using equations (4), (6), and (7), are:

$$U_{mn} = U_{mn}^{(p)} - \frac{(n^2 - \nu m^2)\mu\beta - \dfrac{\lambda}{a}}{m(m^2 + n^2)^2(1 + \beta^2)}\left[A_{mn} - \frac{\beta}{\mu} B_{mn}\right]$$

$$V_{mn} = V_{mn}^{(p)} - \frac{(m^2 - \nu n^2)\mu\beta - \dfrac{1}{a}}{n(m^2 + n^2)^2(1 + \beta^2)}\left[A_{mn} - \frac{\beta}{\mu} B_{mn}\right] \tag{11}$$

The plate portions are given by[5]

$$U_{mn}^{(p)} = \frac{m(1 + \nu)}{m^2 + n^2} B_{mn}\,; \quad V_{mn}^{(p)} = \frac{n(1 + \nu)}{m^2 + n^2} B_{mn} \tag{12}$$

It should be noted that the solutions developed here are complete only in the case of freely supported boundaries, i.e.

$$x = \pm\, l_1/2\text{: } w = 0,\ M_x = 0,\ N_x = 0$$

$$y = \pm\, l_2/2\text{: } w = 0,\ M_y = 0,\ N_y = 0 \tag{13}$$

In this case there are shears N_{xy}, M_{xy} remaining on the boundaries. Other boundary conditions can be obtained by superposition of appropriate edge load solutions.

To illustrate the application of the method, several examples have been computed, namely, the shallow sphere ($\lambda = 1$), cylinder ($\lambda = 0$), and hyperboloid ($\lambda = -1$), acted upon by a single concentrated force P at their center. For this loading, and for $l_1 = l_2 = l$, the coefficients

$$A_{mn} = \frac{4P}{l^2 D}\,; \quad B_{mn} = 0 \tag{14}$$

[5] The authors' earlier equations[4] corresponding to (11) and (12) specialized to the hyperboloid ($\lambda = -1$) appear to be in error.

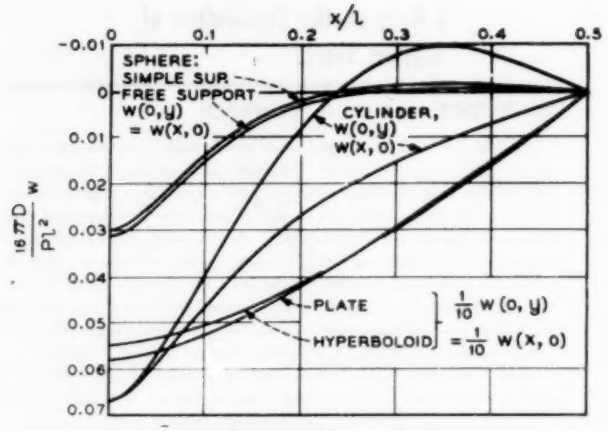

Fig. 2 Normal deflection along lines of symmetry

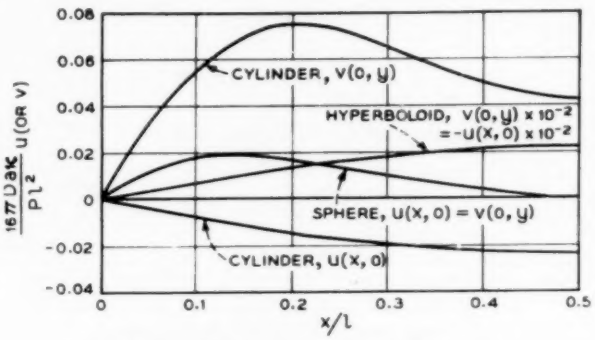

Fig. 3 Tangential deflection along lines of symmetry

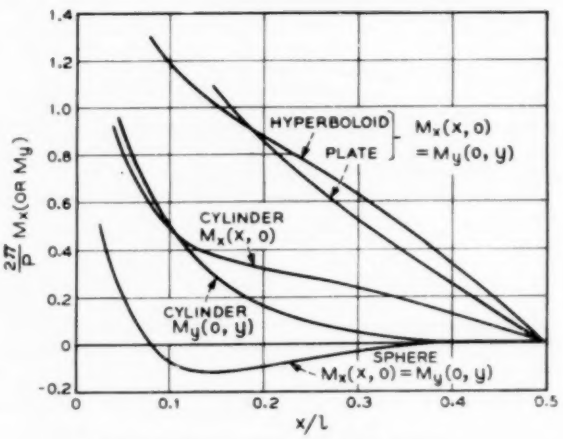

Fig. 4 Bending moment along lines of symmetry

are independent of m and n. In fact, the series representation of the load does not even converge; however, its integrals do converge, and the solutions obtained from (10) and (11) yield the correct result. Figs. 2 to 5 show the results of the computations, which used only three terms of the series. The only constants specified are $l/\sqrt{\mu a} = 10\sqrt{2}$ and $\nu = 0.3$. For comparison, the

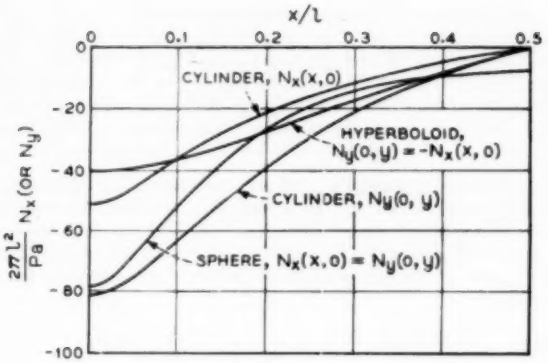

Fig. 5 Tangential stress along lines of symmetry

plate solution is also shown, and a solution for the simply supported sphere taken from Conrad.[4] The condition for simple support is that $u, v, w = 0$ on all boundaries, $M_x = 0$ on $x = \pm l/2$, and $M_y = 0$ on $y = \pm l/2$.

The results show that for the sphere not much stiffness is gained by restraining u and v at the edges, and that the stiffness of the hyperboloid is roughly equal to that of the flat plate.

Acknowledgment

This Note is a result of research sponsored by the Office of Naval Research under contract no. Nonr 225(16), and assisted by the National Science Foundation under their Fellowship program. As a result of the error mentioned in footnote 5, some of the computations were repeated on the IBM 704 computing machine at Bell Telephone Laboratories.

A Solution of the Steady Linear Heat-Flow Equation With Heat Generation and Conductivity Arbitrary Functions of Temperature

R. P. STEIN[1]

A REMARKABLY simple, direct, and general integration of the steady-state linear heat-conduction equation can be obtained for the case when both internal heat generation and thermal conductivity are arbitrary functions of temperature. So far as the writer knows, this form of solution has not been reported elsewhere in the literature.

Consider the homogeneous isotropic solid bounded by the plane $x = 0$, and $x = x$. At $x = 0$ the heat flux density into the solid is q_0 and the temperature is t_0. For $x > 0$ the heat flux density is $q(x)$ and the temperature is $t(x)$. Heat is generated within the solid at a local volumetric heat-generation rate equal to q_v. The familiar steady-state heat-conduction equation for this situation is

$$\frac{d}{dx}\left(k\,\frac{dt}{dx}\right) + q_v = 0 \tag{1}$$

For the case to be considered, both the thermal conductivity, k, and q_v are arbitrary functions of t. Equation (1) is actually a combination of Fourier's heat-conduction law,

$$q = -k\,\frac{dt}{dx}, \tag{2}$$

and a simple heat balance over a differential element of solid thickness,

$$dq = q_v dx. \tag{3}$$

Now multiply both sides of equation (3) by equation (2) and simplify as follows:

$$q dq = -k\,\frac{dt}{dx}\,q_v\,dx \tag{4}$$

$$d(q^2) = -2kq_v dt \tag{5}$$

Equation (5) can be directly integrated to give q^2 as a function of t. The square root is taken to obtain q with its sign chosen consistent with the direction of heat flow for the problem. Equation (2) is then used to eliminate q, and a second integration gives t as a function of x. Thus a complete solution can be obtained with q_v and k any known functions of temperature. (These functions may have finite discontinuities.)

For example, let q_0 and t_0 be the known boundary conditions. The integrations proceed as follows:

$$q^2 - q_0^2 = 2\int_{t_0}^{t} k\,q_v\,dt \tag{6}$$

$$= 2\phi(t_0, t) \tag{7}$$

$$q = [q_0^2 + 2\phi(t_0, t)]^{1/2} \tag{8}$$

$$= -k\,\frac{dt}{dx} \tag{9}$$

and finally

$$x = \int_{t}^{t_0} \frac{k(\lambda)\,d\lambda}{[q_0^2 + 2\phi(t_0, \lambda)]^{1/2}} \tag{10}$$

where λ is a dummy variable of integration.

As a specific example, consider the case when $q_0 = 0$, $k = k_0[1 + \alpha(t_0 - t)]$, and $q_v = q_{v0}[1 + \beta(t_0 - t)]$. For convenience, let $\theta = t_0 - t$. The first integration gives

$$\phi(t_0, t) = k_0 q_{v0}\left[1 + \tfrac{1}{2}(\alpha + \beta)\theta + \frac{\alpha\beta}{3}\,\theta^2\right]\theta \tag{11}$$

and the second integration results in

$$x = \left(\frac{k_0}{2q_{v0}}\right)^{1/2}\int_0^{\theta} \frac{(1 + \alpha\lambda)\,d\lambda}{\lambda^{1/2}\left[1 + \tfrac{1}{2}(\alpha + \beta)\lambda + \dfrac{\alpha\beta}{3}\lambda^2\right]^{1/2}} \tag{12}$$

Although it does not appear possible to evaluate equation (12) in terms of known functions, graphical or numerical integration should not be too difficult. An interesting form of equation (12) is obtained when the following dimensionless parameters are introduced. Let

$$\eta^2 = \theta/\theta_0$$

$$a = \alpha\theta_0$$

$$b = \beta\theta_0$$

where

$$\theta_0 = \frac{q_{v0}\,x^2}{2k_0}$$

Note that θ_0 is the temperature distribution for the case of $\alpha = \beta = 0$, i.e., negligible temperature dependence of q_v and k.

With an appropriate change of the variable of integration, equation (12) becomes

[1] Scientific Staff, Engineering Research Laboratory, Columbia University, New York, N. Y.

Manuscript received by ASME Applied Mechanics Division, May 4, 1959.

$$\int_0^{\eta} \frac{(1 + a\,\lambda^2)\,d\lambda}{\left[1 + \frac{1}{2}(a+b)\,\lambda^2 + \frac{1}{3}\,ab\,\lambda^4\right]^{1/2}} = 1 \qquad (13)$$

Equation (13) is a convenient form for numerical, graphical, or power-series evaluation of η as a function of a and b.

As another example, which leads to an interesting result, consider the case of an electrical current flowing through a metallic plate such that the volumetric heat-generation rate is approximated by

$$q_v \simeq \gamma \epsilon^2 \qquad (14)$$

where γ is the electrical conductivity and ϵ is the voltage gradient normal to the heat flow. As with the previous example, take $q_0 = 0$ (i.e. let the plate be insulated at $x = 0$). Let T_0 be the absolute temperature at $x = 0$, and T be the absolute temperature at any $x > 0$. Now, for most metals, the thermal conductivity temperature dependence can be satisfactorily represented by equations of the form

$$k = k_0 \left(\frac{T_0}{T}\right)^n \qquad (15)$$

where n is a constant usually, but not always, larger than zero. For relatively pure metals at temperatures less than 0 C, equation (15) with $n = 1$ is known as Eucken's relation and is quite accurate. At higher temperatures appropriate values of n satisfactory over moderate temperature ranges are usually less than unity. At very high temperatures, n may become negative. Almost always $-1 \lesssim n \lesssim 1$. Lorenz's equation predicts that the ratio of the thermal conductivity to the electrical conductivity is proportional to the absolute temperature. When combined with equation (15) this results in

$$\gamma = \gamma_0 \left(\frac{T_0}{T}\right)^{1+n} \qquad (16)$$

Use of these thermal and electrical conductivity temperature dependences with equations (7) and (10) results in the following dimensionless integral expression:

$$\left(\frac{2\theta_0}{T_0}\right)^{1/2} = \sqrt{n} \int_{\frac{T}{T_0}}^{1} \frac{d\lambda}{(1 - \lambda^{2n})^{1/2}} \qquad (17)$$

where

$$\theta_0 = \frac{\gamma_0\,\epsilon^2\,x^2}{2k_0}$$

Equation (17) is readily integrated for certain values of n. The following results have been obtained:

(A) For $n = 1$ (metals at low temperatures)

$$\theta = T_0 \left[1 - \cos\left(\frac{2\theta_0}{T_0}\right)^{1/2}\right]$$

$$\simeq \theta_0 \left[1 - \frac{1}{6}\left(\frac{\theta_0}{T_0}\right) + \ldots\right]$$

where

$$\theta = T_0 - T$$

(B) For $n = 1/2$ (metals at moderate temperatures?)

$$\theta = \theta_0$$

(For this case the effects of thermal and electrical conductivity temperature dependence on the temperature distribution evidently completely counteract each other.)

(C) For $n = -1$ (metals at high temperatures?)

$$\theta = T_0 \left[1 - \left(1 - \frac{2\theta_0}{T_0}\right)^{1/2}\right]$$

$$\simeq \theta_0 \left[1 + \frac{1}{2}\left(\frac{\theta_0}{T_0}\right) + \ldots\right]$$

These results suggest the following generalization. With electrical heat generation in a metal plate, if temperature distributions are computed assuming thermal and electrical conductivities independent of temperature, the fractional error will be less than the ratio of the temperature difference to the absolute temperature.

Bending of Thin Rectangular Plates With Edge Beams

M. N. KESHAVA RAO[1]

Nomenclature

ω = deflection of plate at (x, y)
q = load per unit area on plate at (x, y)
a, b = dimensions of plate in x and y-directions, respectively
D = flexural rigidity of plate
ν = Poisson's ratio
$B_{\xi k}$ = flexural ridigity of beam on edge $\xi = k$
$T_{\xi k}$ = torsional rigidity of beam on edge $\xi = k$
$\alpha = n\pi/a$
$\beta = m\pi/b$
S = Sinh βa
$\bar{\mathrm{S}}$ = Sinh $\alpha\, b$
C = Cosh βa
$\bar{\mathrm{C}}$ = Cosh αb
$\lambda_{\xi k}$ = elastic restraint factor of plate at edge $\xi = k$
$\mu_{\xi k}$ = spring constant of elastic support at edge $\xi = k$

THOUGH a number of problems occur in practice, where a plate has beams on all or some of the edges, usually such elastic restraints are replaced by one of the ideal conditions such as a fully fixed or a simply supported or a free edge. In this Note, equations are given leading to the solution of the general problem of a plate with edge beams of different flexural and torsional rigidities. The same equations contain the solution for the ideal conditions also, as special cases, for the limiting values of the rigidities. Solution for plates partially fixed or elastically supported can also be easily included.

The form of the solution and the notation adopted is that developed by Fletcher and Thorne[2] using finite Fourier transforms. The flexural and torsional rigidities of the edge beams are given by B and T, the subscripts referring to the edges. The loading is given by a function $q(x, y)$ expressible as a multiple Fourier series as in [1]. Expression for the deflection ω is taken in three parts as $\omega = \omega_1 + \omega_2 + \omega_3$. ω_1 is the deflection of the loaded plate simply supported on all edges. ω_2 is

[1] Senior Scientific Assistant, Central Building Research Institute, Roorkee (U. P.), India. Formerly with Civil and Hydraulic Engineering Section, Indian Institute of Science, Bangalore, India.

[2] H. J. Fletcher and C. J. Thorne, "Bending of Thin Rectangular Plates," Proceedings of Second U. S. National Congress of Applied Mechanics, ASME, 1954, pp. 389–406.

Manuscript received by ASME Applied Mechanics Division, June 18, 1958; revised draft received April 14, 1959.

the deflection of the plate with no load, such that deflections and moments on all edges are arbitrary except at the corners where the deflections are zero. This function contains eight sets of infinite number of unknown coefficients, B_m to i_n as in a paper by Fletcher and Thorne.[2] ω_b represents the deflection of a free plate bent by concentrated loads at the corners.

The boundary conditions are written down as

$$\omega_{xx}(a, y) + \nu\omega_{yy}(a, y) = -\frac{T_{xa}}{D}\,\omega_{xyy}(a, y) \tag{1a}$$

$$\omega_{xx}(0, y) + \nu\omega_{yy}(0, y) = -\frac{T_{x0}}{D}\,\omega_{xyy}(0, y) \tag{1b}$$

$$\omega_{yy}(x, b) + \nu\omega_{xx}(x, b) = -\frac{T_{yb}}{D}\,\omega_{yxx}(x, b) \tag{1c}$$

$$\omega_{yy}(x, 0) + \nu\omega_{xx}(x, 0) = -\frac{T_{y0}}{D}\,\omega_{yxx}(x, 0) \tag{1d}$$

$$\omega_{xxx}(a, y) + \overline{2-\nu}\,\omega_{xyy}(a, y) = \frac{B_{xa}}{D}\,\omega_{yyyy}(a, y) \tag{1e}$$

$$\omega_{xxx}(0, y) + \overline{2-\nu}\,\omega_{xyy}(0, y) = \frac{B_{x0}}{D}\,\omega_{yyyy}(0, y) \tag{1f}$$

$$\omega_{yyy}(x, b) + \overline{2-\nu}\,\omega_{yxx}(x, b) = \frac{B_{yb}}{D}\,\omega_{xxxx}(x, b) \tag{1g}$$

$$\omega_{yyy}(x, 0) + \overline{2-\nu}\,\omega_{yxx}(x, 0) = \frac{B_{y0}}{D}\,\omega_{xxxx}(x, 0) \tag{1h}$$

where the subscripts to ω denote partial differentiation.

These eight conditions give eight sets of equations for the unknown coefficients, B_m to i_n, and can be put into simpler forms using formulas due to Estanave, given in footnote 2.

Using the notation

$\mathrm{S} = \sinh \beta a$; $\mathrm{C} = \cosh \beta a$,

$\bar{\mathrm{S}} = \sinh \alpha b$, $\bar{\mathrm{C}} = \cosh \alpha b$,

$$2d_m - 2\nu\beta^2a^2B_m = \frac{T_{xa}}{D}\left[\frac{\beta^2a^2}{\mathrm{S}^2}\,B_m\{\mathrm{SC} + \beta a\}\right.$$

$$\frac{-\beta^2a^2C_m}{\mathrm{S}^2}\{\mathrm{S} + \beta a\mathrm{C}\} - \frac{\beta d_m}{\mathrm{S}^2}\{\beta a - \mathrm{SC}\} + \frac{\beta e_m}{\mathrm{S}^2}\{\beta a\mathrm{C} - \mathrm{S}\}$$

$$+ 4\beta^2a(-1)^m\sum_n\frac{\alpha(2\alpha^2+\beta^2)(-1)^n}{(\alpha^2+\beta^2)^2}\,F_n$$

$$- 4\beta^2a\sum_n\frac{\alpha(2\alpha^2+\beta^2)}{(\alpha^2+\beta^2)^2}(-1)^n\,G_n$$

$$+ \frac{4\beta^2(-1)^m}{a}\sum_n\frac{\alpha(-1)^n h_n}{(\alpha^2+\beta^2)^2} - \frac{4\beta^2}{a}\sum_n\frac{\alpha(-)^n i_n}{(\alpha^2+\beta^2)^2}$$

$$\left.+ \frac{4\beta^2}{a^2}\sum_n\frac{\alpha(-1)^n q_{mn}}{(\alpha^2+\beta^2)^2}\right] \tag{2a}$$

$$2e_m - 2\nu\beta^2a^2C_m = \frac{T_{xa}}{D}\left[\frac{\beta^2a^2}{\mathrm{S}^2}\,B_m\{\mathrm{S} + \beta a\mathrm{C}\}\right.$$

$$-\frac{\beta^2a^2}{\mathrm{S}^2}\,C_m\{\mathrm{SC} + \beta a\} - \beta\,\frac{d_m}{\mathrm{S}^2}\{\beta a\mathrm{C} - \mathrm{S}\}$$

$$+ \frac{\beta e_m}{\mathrm{S}^2}\{\beta a - \mathrm{SC}\} + 4\beta^2a\sum_n\frac{\alpha(2\alpha^2+\beta^2)}{(\alpha^2+\beta^2)^2}\{(-1)^m F_n - G_n\}$$

$$+ \frac{4\beta^2}{a}\sum_n\frac{\alpha}{(\alpha^2+\beta^2)^2}\{(-1)^m h_n - i_n\}$$

$$\left.+ \frac{4\beta^2}{a^2}\sum_n\frac{\alpha q_{mn}}{(\alpha^2+\beta^2)^2}\right] \tag{2b}$$

$$\frac{2h_n}{a} - 2\nu\alpha^2aF_n = \frac{T_{yb}}{D}\left[\frac{4\alpha^2a}{b}\sum_m\frac{\beta(2\beta^2+\alpha^2)}{(\alpha^2+\beta^2)^2}(-1)^m\right.$$

$$\{(-1)^nB_m - C_m\} + \frac{4\alpha^2}{ab}\sum_m\frac{\beta(-1)^m}{(\alpha^2+\beta^2)^2}\{(-1)^n d_m - e_m\}$$

$$+ \frac{2\alpha^2a}{\bar{\mathrm{S}}^2}\,F_n\{\bar{\mathrm{S}}\bar{\mathrm{C}} + \alpha b\} - \frac{2\alpha^2a}{\bar{\mathrm{S}}^2}\,G_n\{\bar{\mathrm{S}} + \alpha b\bar{\mathrm{C}}\}$$

$$- \frac{\alpha h_n}{a\bar{\mathrm{S}}^2}\{\alpha b - \bar{\mathrm{S}}\bar{\mathrm{C}}\} + \frac{\alpha i_n}{a\bar{\mathrm{S}}^2}\{\alpha b\bar{\mathrm{C}} - \bar{\mathrm{S}}\}$$

$$\left.+ \frac{4\alpha^2}{a^2b}\sum_m\frac{\beta(-1)^m q_{mn}}{(\alpha^2+\beta^2)^2}\right] \tag{2c}$$

$$\frac{2i_n}{a} - 2\nu\alpha^2aG_n = \frac{T_{yb}}{D}\left[\frac{4\alpha^2a}{b}\sum_m\frac{\beta(2\beta^2+\alpha^2)}{(\alpha^2+\beta^2)^2}\right.$$

$$\{B_m(-1)^n - C_m\} + \frac{4\alpha^2}{ab}\sum_m\frac{\beta}{(\alpha^2+\beta^2)^2}\{(-1)^n d_m - e_m\}$$

$$+ \frac{2\alpha^2a}{\bar{\mathrm{S}}^2}\,F_n\{\bar{\mathrm{S}} + \alpha b\bar{\mathrm{C}}\} - \frac{2\alpha^2aG_n}{\bar{\mathrm{S}}^2}\{\bar{\mathrm{S}}\bar{\mathrm{C}} + \alpha b\}$$

$$- \frac{\alpha h_n}{a\bar{\mathrm{S}}^2}\{\alpha b\,\bar{\mathrm{C}} - \bar{\mathrm{S}}\} + \frac{\alpha i_n}{a\bar{\mathrm{S}}^2}\{\alpha b - \bar{\mathrm{S}}\bar{\mathrm{C}}\}$$

$$\left.+ \frac{4\alpha^2}{a^2b}\sum_m\frac{\beta q_{mn}}{(\alpha^2+\beta^2)^2}\right] \tag{2d}$$

$$\frac{2B_{xa}}{D}\,\beta^4a^2B_m = -\frac{\beta^2a^2B_m}{\mathrm{S}^2}\{\overline{1-\nu}(2\mathrm{SC} + \beta a) + \overline{1+\nu}\,\mathrm{SC}\}$$

$$+ \frac{\beta^2a^2C_m}{\mathrm{S}^2}\{\overline{1-\nu}(2\mathrm{S} + \beta a\mathrm{C}) + \overline{1+\nu}\mathrm{S}\} + \frac{\beta d_m}{\mathrm{S}^2}\{\overline{1-\nu}\beta a$$

$$+ \overline{1+\nu}\mathrm{SC}\} - \beta\frac{e_m}{\mathrm{S}^2}\{\overline{1-\nu}\beta a\mathrm{C} + \overline{1+\nu}\mathrm{S}\}$$

$$+ 4\beta^2a\sum_n\frac{\alpha(\overline{2\nu+1}\alpha^2+\nu\beta^2)}{(\alpha^2+\beta^2)^2}\{(-1)^m F_n - G_n\}(-1)^n$$

$$- \frac{4}{a}\beta\sum_n\frac{\alpha(\alpha^2+\overline{2-\nu}\beta^2)}{(\alpha^2+\beta^2)^2}(-1)^n\{(-1)^m h_n - i_n\}$$

$$- \frac{4}{a^2}\sum_n\frac{\alpha(\alpha^2+\overline{2-\nu}\beta^2)}{(\alpha^2+\beta^2)^2}\,q_{mn}(-1)^n \tag{2e}$$

$$\frac{2B_{xa}}{D}\,a^2\beta^4C_m = -\frac{\beta^2a^2B_m}{\mathrm{S}^2}\{\overline{1-\nu}(2\mathrm{S} + \beta a\mathrm{C}) + \overline{1+\nu}\mathrm{S}\}$$

$$+ \frac{\beta^2a^2C_m}{\mathrm{S}^2}\{\overline{1-\nu}(2\mathrm{SC} + \beta a) + \overline{1+\nu}\mathrm{SC}\} + \frac{\beta d_m}{\mathrm{S}^2}\{\overline{1-\nu}\beta a\mathrm{C}$$

$$+ \overline{1+\nu}\mathrm{S}\} - \frac{\beta e_m}{\mathrm{S}^2}\{\overline{1-\nu}\beta a + \overline{1+\nu}\mathrm{SC}\}$$

$$+ 4\beta^2a\sum_n\frac{\alpha(\overline{2\nu+1}\alpha^2+\nu\beta^2)}{(\alpha^2+\beta^2)^2}\{(-1^m)F_n - G_n\}$$

$$- \frac{4\beta}{a}\sum_n\frac{\alpha(\alpha^2+\overline{2-\nu}\beta^2)}{(\alpha^2+\beta^2)^2}\{(-1)^m h_n - i_n\}$$

$$-\frac{4}{a^2}\sum_n \frac{\alpha(\alpha^2+\overline{2-\nu}\beta^2)}{(\alpha^2+\beta^2)^2}\,q_{mn} \quad (2f)$$

$$\frac{2B_{y^0}}{D}\,\alpha^4 aF_n = \frac{4\alpha^3a^2}{b}\sum_m \frac{\beta(\overline{2\nu+1}\,\beta^2+\nu\alpha^2)}{(\alpha^2+\beta^2)^2}\,(-1)^m$$

$$\{(-1)^n B_m - C_m\} - \frac{4\alpha}{ab}\sum_m \frac{\beta(\beta^2+\overline{2-\nu}\alpha^2)}{(\alpha^2+\beta^2)^2}\,(-1)^m$$

$$\{(-1)^n d_m - e_m\} - \frac{\alpha^3 aF_n}{\bar{S}^2}\{\overline{1-\nu}(2\bar{S}\bar{C}+\alpha b)+\overline{1+\nu}\,\bar{S}\bar{C}\}$$

$$+\frac{\alpha^3 aG_n}{\bar{S}^2}\{\overline{1-\nu}(2\bar{S}+\alpha b\bar{C})+\overline{1+\nu}\bar{S}\}$$

$$+\frac{\alpha h_n}{a\bar{S}^2}\{\overline{1-\nu}\alpha b+\overline{1+\nu}\bar{C}\bar{S}\}-\frac{\alpha i_n}{a\bar{S}^2}\{\overline{1-\nu}\alpha b\bar{C}-\overline{1+\nu}\bar{S}\}$$

$$-\frac{4}{a^2b}\sum_m \frac{\beta(\beta^2+\overline{2-\nu}\alpha^2)}{(\alpha^2+\beta^2)^2}\,q_{mn}(-1)^m \quad (2g)$$

$$\frac{4\alpha^3a^2}{b}\sum_m \frac{\beta(\overline{2\nu+1}\beta^2+\nu\alpha^2)}{(\alpha^2+\beta^2)^2}\{(-1)^n B_m - C_m\}$$

$$-\frac{4\alpha}{ab}\sum_m \frac{\beta(\beta^2+\overline{2-\nu}\alpha^2)}{(\alpha^2+\beta^2)^2}\{(-1)^n d_m - e_m\}$$

$$-\frac{\alpha^3 aF_n}{\bar{S}^2}\{\overline{1-\nu}(2\bar{S}+\alpha b\bar{C})+\overline{1+\nu}\bar{S}\}$$

$$+\frac{\alpha^3 aG_n}{\bar{S}^2}\{\overline{1-\nu}(2\overline{CS}+\alpha b)+\overline{1+\nu}\,\overline{CS}\}$$

$$+\frac{\alpha h_n}{a\bar{S}^2}\{\overline{1-\nu}\alpha b\bar{C}+\overline{1+\nu}\bar{S}\}-\frac{\alpha i_n}{a\bar{S}^2}\{\overline{1-\nu}\alpha b$$

$$+\overline{1+\nu}\bar{C}\bar{S}\}-\frac{4}{a^2b}\sum_m \frac{\beta(\beta^2+\overline{2-\nu}\alpha^2)}{(\alpha^2+\beta^2)^2}\,q_{mn}$$

$$=\frac{2B_{y^0}}{D}\,\alpha^4 aG_n \quad (2h)$$

Neglecting in each set of these unknowns all after a certain number, depending on the accuracy required, it is possible to solve for these unknowns. The convergence of a few cases, involving such a procedure, is discussed elsewhere.[2]

The solution may be easily extended to include that for a plate elastically restrained to different degrees on different edges. If the restraint is rotational (i.e., rotation = $\lambda \times$ moment acting on the edge,[2] (1*a*) has to be replaced by

$$\omega_{xx}(a, y) + \nu\omega_{yy}(a, y) = \frac{1}{\lambda_{xa}}\,\omega_x(a, y) \quad (3a)$$

which is equivalent to writing

$$T_{xa} = -\frac{1}{\lambda_{xa}\beta^2}$$

in equation (2*a*). A similar treatment is possible when the edges rest on elastic supports; i.e., with the condition, deflection = $\mu \times$ reaction on the edge.

[2] S. P. Timoshenko, "Theory of Plates and Shells," McGraw-Hill Book Company, Inc., New York, N. Y., 1940, p. 17.

The Effect of Turbulence on Slider-Bearing Lubrication[1]

M. LESSEN.[2] The effect of turbulence on bearing lubrication may be qualitatively evaluated in the following manner. For an idealized model of a gas, statistical mechanics yields the form of the stress tensor as

$$\tau_{ij} = \rho \overline{u_i u_j}$$

where ρ is density and u_i is the peculiar (random) velocity of the particles of the gas. In turbulence the form of the Reynolds stress is the same except that the random velocity is that of the continuum. In both cases the magnitude of the stress is affected by the scale of the transport phenomenon.

For the case of laminar flow, the scale of the transport phenomenon is the mean free path of a particle. In the case of turbulent flow, the approximate analog is the mixing length. Since the scale of the mixing length is much greater than that of the mean free path, the Reynolds stress is much greater than the viscous stress. Hence, qualitatively the turbulent situation should be and is roughly the same as a laminar situation with greater viscosity.

The finer differences in the laminar and turbulent situations may be explained in the following manner: The mixing length varies across the flow region and hence the velocity gradient must vary accordingly. Where the mixing length is greater, the velocity gradient is least. In the laminar case, the mean free path is substantially constant over the flow field and hence so is the velocity gradient.

The authors are to be commended for carrying out a forthright and definitive investigation.

J. M. ROBERTSON.[3] As the authors note, it is now necessary that we consider the possibility of turbulent, rather than laminar, flow in lubrication problems. Their essay into this uncharted field is to be commended. Unfortunately, their model of turbulence is questionable and the solution obtained may be irrelevant to the problem. Thus, assumption AIV in regard to the lateral mixing-length and shear distribution in this turbulent flow seems inappropriate while their justification for it is fallacious. Also, by inference from the velocity distributions shown, much too weak a turbulence has been assumed.

The authors consider Prandtl's assumptions for the mixing length $l \sim y$ and then base their model on erroneous comments concerning the shear. Apparently it is not realized that Prandtl's mixing-length model near a wall is independent of shear-stress considerations. Actually, near the wall Prandtl assumed that the shear stress, entering into his momentum-transfer equation, may be taken as a constant. This assumption is correct for the flat-plate boundary layer and yields satisfactory results for other flows, e.g., the wall region of a pipe, even though it is but an approximation. Following the Prandtl model therefore, the authors' statement of zero shear at $y = 0, h$ cannot be justified. It is true that the turbulent portion of the shear must pass to zero as one approaches a wall from a turbulent-flow region. However, boundary conditions inside the laminar film (or sublayer) cannot be applied to a turbulent-flow model since this can only hope to be rational outside of the film. Therefore near $y = 0, h$ the turbulent shear is finite.

The flow solutions shown in Fig. 3 of the paper indicate a slight curving of the turbulent velocity profile about the profiles that would occur if the flow were laminar. Since these latter are closely linear, comparison with the case of plane Couette flow is appropriate. In plane Couette flow, which represents the limiting lubrication case of h = const (or the flow at the x-station where $dp/dx = 0$), a linear velocity profile is predicted in the laminar-viscous flow case. Several solutions for the turbulent velocity profile have been developed for plane Couette flow since Th. von Karman [1][4] first attacked this case in 1937. All except one of these (S. I. Pai [2] in 1953 and modification by Yau Wu [3] in 1958) are based on the fact that in this case for turbulent, as for laminar-viscous, flow the shear stress is constant from $y = 0$ to h. Various assumptions concerning the mixing-length or eddy-viscosity distribution then lead to solutions for the velocity profile. The solution by H. Reichardt [4] was based in part on his experimental study of the velocity profile at Reynolds numbers (hU/ν) of 5800 and 36,000. The approach introduced by Pai involves a rigorous solution to the Reynolds equations of motion, Equation (1) of the paper, in series form, which solution, however, loses any hope of achieving physical rationality. It develops that Pai assumed too weak a turbulence in the main portion of the flow and Wu has attempted to correct for this. As part of a study [5] of homologous turbulence under a National Science Foundation grant, the writer has developed yet another solution for turbulent plane Couette flow and has compared all the solutions with the results of experimental measurements. Fig. 1 shows the type of velocity profile obtained, in comparison with the laminar-viscous case. The turbulent profile is rather closely predicted by von Karman's solution, if one chooses the proper skin friction, and by Reichardt's and the writer's solutions which include predictions for the skin friction coefficient.

[4] Numbers in brackets designate References at end of discussion.

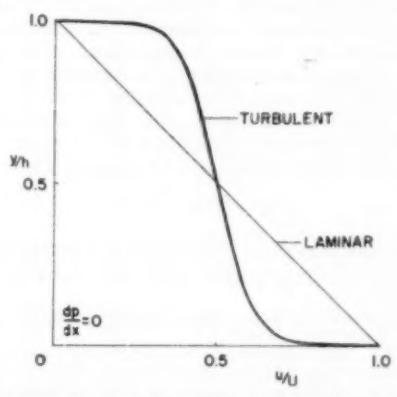

Fig. 1 Viscous-flow velocity profiles for plane Couette flow

[1] By Ye Tsang Chou and Edward Saibel, published in the March, 1959, issue of the JOURNAL OF APPLIED MECHANICS, vol. 26, TRANS. ASME, vol. 81, pp. 122–126.

[2] Professor, Engineering Mechanics Division, University of Pennsylvania, Philadelphia, Pa. Mem. ASME.

[3] Professor of Theoretical and Applied Mechanics, University of Illinois, Urbana, Ill. Mem. ASME.

DISCUSSION

Comparison of the turbulent plane Couette-flow velocity profile with the profiles of the authors' **Fig. 3** strongly suggests that they have assumed much too weak a turbulence. Extension of the plane Couette-flow approach to the more general slider-bearing case is apparently rather straightforward, since all that is required is an appropriate relation for the lateral (y-wise) shear-stress distribution at various x-stations. Owing to the obvious interest in the lubrication problem, the writer is currently performing this exercise but the calculations are not yet complete.

References

1 Th. von Karman, "The Fundamentals of the Statistical Theory of Turbulence," *Journal of The Aeronautical Sciences*, vol. 4, 1937, pp. 131–138.

2 S. I. Pai, "On Turbulent Flow Between Parallel Plates," JOURNAL OF APPLIED MECHANICS, vol. 20, TRANS. ASME, vol. 75, 1953, pp. 109–114.

3 Yau Wu, "A Study of Plane Turbulent Couette Flow," MS thesis in Theoretical and Applied Mechanics, University of Illinois, Urbana, Ill., 1958.

4 H. Reichardt, "Uber die Geschwindigkeitsverteilung in einer geradliniger turbulenten Couettestromung," *Zeitschrift für angewandte Mathematik und Mechanik*, Sonderheft, 1956, pp. 26–29.

5 J. M. Robertson, " A Study of Turbulent Plane Couette Flow," unpublished report 141, Department of Theretical and Applied Mechanics, University of Illinois, Urbana, Ill., January 1959.

L. N. TAO.[5] The authors are to be complimented for their rational analysis of the effect of turbulence on hydrodynamic lubrication. This investigation is of special interest to the writer. In a recent publication[6] and a submitted paper,[7] the writer also has analyzed bearing problems with turbulent flow.

In the present discussion, only the assumptions employed by the authors will be discussed. The writer intends to supplement few additional justifications on some of the assumptions.

The authors use the Reynolds equations of motion for turbulent flow and adopt the following assumptions:

(a) No side leakage.

(b) Order-of-magnitude approximation on account of the thinness of the oil film.

(c) Negligible laminar friction.

(d) An experimentally determined constant k.

(e) Negligible inertial effect.

On this basis they obtain a solution of a first-order approximation.

Within the scope of a two-dimensional bearing problem, the first two assumptions are certainly permissible. The third assumption is a common simplification in seeking solutions to the Reynolds equations of motion for turbulent flow. The justifications of these assumptions are well explained in the paper.

Adopting an experimentally determined constant in turbulent-flow problems is actually indispensable. In order to solve a dynamic problem it is necessary to have a stress-strain-rate relationship. In laminar flow it is the linear expression of Newton's law of viscosity. In view of the invalidity of Newton's law of viscosity in the turbulent regime, some other stress-strain-rate relationship must be used. The authors follow Prandtl's mixing-length concept in pipe flow and propose a simple form

$$\rho l^2 = k^2 y(h - y)$$

Though there is no experimental verification of the validity of the expression, the concept is quite logical and reasonable because of the zero turbulent shear stresses at the walls. However, a refinement may be suggested. Evidently, the value k^2 has a dimension of density, hence it is neither a constant nor a dimensionless quantity. Rewrite k^2 in the form

$$k^2 = \rho\lambda^2$$

Here λ^2 is a true dimensionless quantity, though it may or may not be a universal constant. Only experimental results can verify this unanswered question.

As to the last assumption that the inertial effect is negligible, the writer may use the argument of his own analyses. As just mentioned, in a dynamic problem it is necessary to have a stress-strain-rate relationship other than Newton's law of viscosity. Instead of expression (3) of the paper, Blasius' law of friction has been used. It is well known that in the laminar case the ratio of the inertial force to the viscous force is of the order

$$\frac{\text{Inertial force}}{\text{Viscous force}} = 0\left(\text{Re}\,\frac{h}{l}\right)$$

where Re is the Reynolds number and l is a physical linear dimension. By the adoption of Blasius' law of friction, it can be easily verified that

$$\frac{\text{Inertial force}}{\text{Viscous force}} = 0\left(\text{Re}^n\,\frac{h}{l}\right)$$

for turbulent flow. This expression includes the laminar-flow problem as a special case where $n = 1$. For fully developed turbulent flow the exponent n is small, having a value between 0 and 0.25. This indicates that for a Reynolds number of 10,000 in the turbulent regime the ratio of these forces will have, at most, the same order of magnitude as that of Re = 10 in the laminar case. Hence the assumption of ignoring the inertial effect in bearings with turbulent flow is justifiable.

[5] Department of Mechanics, Illinois Institute of Technology, Chicago, Ill. Assoc. Mem. ASME.

[6] L. N. Tao, "A Theory of Lubrication in Short Journal Bearings With Turbulent Flow," TRANS. ASME, vol. 80, 1958, pp. 1734–1740.

[7] L. N. Tao, "A Theory of Lubrication With Turbulent Flow and Its Application to Slider Bearings," ASME Paper No. 59—A-26.

Authors' Closure

We want to thank Professors Lessen, Robertson, and Tao for their discussions. We are in complete accord with the comments of Professors Lessen and Tao. With reference to Professor Robertson's comments, the authors are well aware that in his derivation of the universal velocity distribution law for pipe flow Prandtl assumed, in addition to $l = ky$, that the shearing stress remained constant in the entire flow field. This does not mean that the authors, in treating a different problem, must make the same assumption. Theirs is a finite convergence nonparallel plane Couette flow problem ($h = h(x)$, $dp/dx = 0$) and not a pipe or parallel plate flow problem (h = const, $dp/dx = 0$). They assumed $l^2 = k^2 y\,(h - y)$ in analogy with the first part of Prandtl's assumption $l = ky$, but believed it improper to introduce Prandtl's second assumption of constant shear.

Professor Robertson also states that, "following the Prandtl model, therefore, the authors' statement of zero shear at $y = 0$, h cannot be justified." Again, the authors only used Prandtl's mixing length concept in a general way and did not intend to follow Prandtl's treatment for pipe flow in their problem. In fact, the authors' assumption that the *turbulent* shear stress is zero *at* the walls has been used by many workers in the field, such as Schlichting and Pai.

The authors are very much interested in Professor Robertson's experimental results on Couette flow, but since these are as yet unpublished, are unable to comment. These experimental results could lead to further refinement of the author's work; however, the physical aspects of his experiments should be carefully checked against the case dealt with by the authors before a comparison can be made.

An Experimental Surface-Wave Method for Recording Force-Time Curves in Elastic Supports[1]

ENRICO VOLTERRA.[2] This paper is an important contribution in the field of stress-wave propagation. It furnishes a method for recording force-time curves when the well-known method, based on the use of the Hopkinson-Davies compression bar, fails because of dispersion effects connected with short pulses. In fact, this new method records Rayleigh surface waves propagated on the plane surface of a solid block, which waves are not affected by dispersion. For recording the short pulses produced by the impact of small hard-steel balls on the plane surface of the block, this method utilizes techniques already developed and used by one of the authors of this paper and described in previous papers [1, 2].[3] Another important feature of this paper is the experimental verification of Lamb's theory of propagation of surface waves on elastic solids [3].

Concerning the verification of Hertz's theory of impact, in addition to the works mentioned by the authors in their bibliography, two other papers could be mentioned. The first is by C. V. Raman [4] on transverse impact of elastic spheres on horizontally held infinitely extended plates of finite thickness. Raman derived a formula for the coefficient of restitution expressed as a function of the elastic constants and densities of the materials, the diameters of the spheres, the thicknesses of the plates, and the velocities of impact. In Raman's paper [4], experimental results of hard-steel balls dropped on glass plates were compared with the theoretical ones. The second paper is by C. Zener [5]. In Zener's paper a theory is developed for the study of short-duration impacts of spheres on large plates. Since the impacts were of short duration, the effects of the reflection from the boundaries of the plates were neglected.

Table 1 of this discussion shows the principal results of some experiments, carried on under the sponsorship of the Office of Naval Research, on the longitudinal elastic impact of steel balls on a very long cylindrical steel bar [6, 7]. Balls of diameters ranging from 1 to 2 in. were dropped from heights ranging from 7.5 to 30 cm to impact longitudinally a 1-in-diam bar. The stress-time curves produced during the impacts were obtained from an oscilloscope record of the pulse waves measured by strain gages fixed on the impacted bar. The experimental results are compared with the theoretical results obtained by applying Hertz's theory of impact. The nonlinear differential equation which was used in deriving the theoretical results to be compared with the experimental ones was the same as the one derived independently a year later by Goodier and Ripperger [6, 7]. The writer believes that the lack of agreement between theoretical and experimental results indicated in Fig. 6 of the paper is probably because of the fact that the heights of drops were much larger and the times of contact much shorter than those used in Table 1.

The writer wishes to congratulate the authors upon the work they have done in connection with this paper.

References

1 E. A. Ripperger, "The Propagation of Pulses in Cylindrical Bars—An Experimental Study," Proceedings of the First Midwestern Conference on Solid Mechanics, Urbana, Ill., 1953, pp. 29–39.

2 E. A. Ripperger, "A Piezoelectric Strain Gage," *Proceedings of the Society for Experimental Stress Analysis*, vol. 12, 1954, pp. 117–124.

3 H. Lamb, "On the Propagaton of Tremors Over the Surface of an Elastic Solid," *Philosophical Transactions of The Royal Society of London*, series A, vol. 203, 1904, pp. 1–12.

4 C. V. Raman, "On Some Applications of Hertz's Theory of Impact," *Physical Review*, vol. 15, 1920, pp. 277–284.

5 C. Zener, "The Intrinsic Inelasticity of Large Plates," *Physical Review*, vol. 59, 1951, pp. 669–673.

6 R. A. Eubanks, D. Muster, and E. G. Volterra, "An Investigation on the Dynamic Properties of Plastics and Rubberlike Materials," Contract No. N7 ONR-064369 with Illinois Institute of Technology, Chicago, Ill., June 1952.

7 C. S. Barton, E. G. Volterra, and S. Citron, "On Elastic Impacts of Spheres on Long Rods," Proceedings of the Third U. S. Congress of Applied Mechanics, ASME, 1958, pp. 89–94.

Authors' Closure

Professor Volterra's discussion carries further the question of the applicability of the Hertz theory of impact of elastic spheres to impacts of spheres on other bodies—plane surfaces of large blocks, thin plates, and ends of cylindrical bars. In all these cases the conditions of the Hertz theory are not met for the reason pointed out in the paper in connection with the block, and yet in some a close correspondence of durations is found experimentally, and a more or less close correspondence of force magnitudes. In view of the violation of the Hertz conditions, the authors have taken the view that it is this *agreement* which calls for explanation,

Table 1 Comparison between experimental and theoretical results for impact tests

Ball diam, in.	Ball height, cm	Duration of pulse, microsec: Theoretical	Duration of pulse, microsec: Experimental	Duration of pulse, microsec: Difference	Maximum amplitude, megadynes/cm²: Theoretical	Maximum amplitude, megadynes/cm²: Experimental	Maximum amplitude, megadynes/cm²: Difference	Peak times, microsec: Theoretical	Peak times, microsec: Experimental	Peak times, microsec: Difference
1.00	30	75	78	+4.0	141	153	+8.5	35	37	+5.7
	22.5	77	79	+2.6	119	120	+0.1	36	37	+2.8
	15	80	82	+2.5	92	97	+5.4	42	40	−4.8
	7.5	86	86	0.0	62	59	−4.8	41	40	−2.4
1.25	30	95	97	+2.1	202	212	+5.0	43	46	+7.0
	22.5	98	102	+4.1	171	181	+5.9	42	46	+8.7
	15	102	105	+2.9	135	141	+4.5	46	47	+2.2
	7.5	108	110	+1.9	90	94	+4.4	50	51	2.0
1.50	30	120	124	+3.3	270	284	+5.2	51	54	+5.9
	22.5	121	123	+1.7	226	229	+1.2	52	54	+3.8
	15	126	129	+2.4	178	187	+5.1	55	59	+7.3
	7.5	134	136	+1.5	120	122	+1.7	59	59	0.0
1.75	30	141	142	+0.1	330	353	+6.1	58	61	+5.2
	22.5	146	147	+0.1	280	302	+7.9	59	63	+6.8
	15	151	151	0.0	223	256	+14.8	62	65	+4.8
	7.5	161	158	−1.9	150	164	+9.3	67	68	+1.5
2.00	30	170	168	−1.2	392	401	+2.3	65	68	+4.6
	22.5	174	172	−1.2	335	349	−4.2	67	69	+3.0
	15	180	180	0.0	267	290	+8.6	70	74	+5.7
	7.5	190	198	+4.2	181	183	+1.1	76	79	+3.9

[1] By J. N. Goodier, W. E. Jahsman, and E. A. Ripperger, published in the March, 1959, issue of the JOURNAL OF APPLIED MECHANICS, vol. 26, TRANS. ASME, vol. 81, pp. 3–7.

[2] Professor, Department of Engineering Mechanics, The University of Texas, Austin, Tex. Mem. ASME.

[3] Numbers in brackets designate References at end of discussion.

rather than any lack of agreement. Hunter (Ref. [11] of the paper) has thrown some light on this for the block, and through his paper connection is made with the earlier work of Zener and Raman.

It may be, as Professor Volterra believes and as the experimental values he gives suggest, that experimental curves of the type shown in Fig. 6 of the paper would be in closer agreement with the Hertz curve if plastic flow did not occur. Yet the fact that the results actually obtained were closely repeatable in a large number of successive impacts on the same target seems to mean that plastic flow was not an important factor. A more extended investigation would be required to resolve these difficulties. The main purpose of the paper is to present the new method, with its present imperfections, in order that its potentialities as an adjunct to the Hopkinson pressure bar may be assessed. The authors thank Professor Volterra for his contribution to such an assessment.

A Mathematical Model Depicting the Stress-Strain Diagram and the Hysteresis Loop[1]

JoDEAN MORROW.[2] This paper is of great interest to the writer. About a year ago, in the course of a study of mechanical hysteresis as a criterion for fatigue failure, the writer expressed mathematically a curvilinear stress-strain curve as the integrated behavior of a set of "domains" each having different flow-stress properties. The subject was discussed subsequently at a graduate seminar on flow and fracture under the title, "Yield by Domains." The concepts involved are basically the same as presented by the author. The approach, however, is from the opposite direction; that is, a mathematical expression for a curvilinear stress-strain curve of a polydomain mass is manipulated to obtain the frequency-distribution curve of the domain strengths. The development follows:

Yield by Domains. The assumption is made that a body is composed of small discrete domains each having a stress-strain response like the author's Fig. 3. The elastic modulus, E, is assumed to be the same for each domain, but each has a different yield point. It is presumed that as load is applied to a polydomain mass, all domains experience the same strain in the direction of loading. As the weaker domains yield, the distribution of stress across the body is not uniform. The weaker domains continue to deform without increase in stress while the stronger domains still strain elastically. For any given average stress on a polydomain mass of unit area, there will be a certain fraction, k, of the cross section which is composed of fully plastic domains. Under these conditions the stiffness of the body or the tangent modulus, E_t, will be

$$E_t = E(1 - k) \tag{1}$$

The total strain in the direction of loading, ϵ, of a body may be expressed as the sum of the elastic strain, ϵ_e, and the plastic strain, ϵ_p:

$$\epsilon = \epsilon_e + \epsilon_p \tag{2}$$

The strains ϵ_e and ϵ_p may be written as functions of stress, σ, as follows:

$$\epsilon = \frac{\sigma}{E} + \epsilon_f \left(\frac{\sigma}{\sigma_f}\right)^{1/n} \tag{3}$$

where ϵ_f and σ_f are known corresponding values of plastic strain and stress and where n is the slope of the log σ − log ϵ_f curve.[3]

Differentiating Equation (3) with respect to σ, the reciprocal of the tangent modulus is obtained.

$$\frac{1}{E_T} = \frac{d\epsilon}{d\sigma} = \frac{1}{E} + \frac{\epsilon_f}{n\sigma_f}\left(\frac{\sigma}{\sigma_f}\right)^{\frac{1}{n}-1} \tag{4}$$

Solving for E_T, substituting in Equation (1), and solving explicitly for k, the following is obtained:

$$k = \frac{1}{\dfrac{\sigma_f n}{E\epsilon_f}\left(\dfrac{\sigma}{\sigma_f}\right)^{1-1/n} + 1} \tag{5}$$

Since k is defined as the fraction of domains which have yielded at a particular stress, Equation (5) represents the cumulative frequency-distribution curve of the domain strengths.

The frequency-distribution curve may be obtained by differentiating Equation (5) once with respect to σ:

$$\frac{dk}{d\sigma} = \frac{\dfrac{(1-n)}{E\epsilon_f}\left(\dfrac{\sigma}{\sigma_f}\right)^{-1/n}}{\left[\dfrac{\sigma_f n}{E\epsilon_f}\left(\dfrac{\sigma}{\sigma_f}\right)^{1-1/n} + 1\right]^2} \tag{6}$$

The types of cumulative frequency and frequency curve obtained for Equations (5) and (6) for two types of materials are shown in Fig. 1 of this discussion.

Work is continuing on this subject. Space does not permit details, but in closing the writer wishes to make a few comments concerning the promise of such an approach.

For many years the concept of domain behavior has been a

[3] The plastic-strain function, $\epsilon_f\left(\dfrac{\sigma}{\sigma_f}\right)^{1/n}$ is empirical. It presumes that a plot of log σ versus log ϵ_p is linear for the polydomain body.

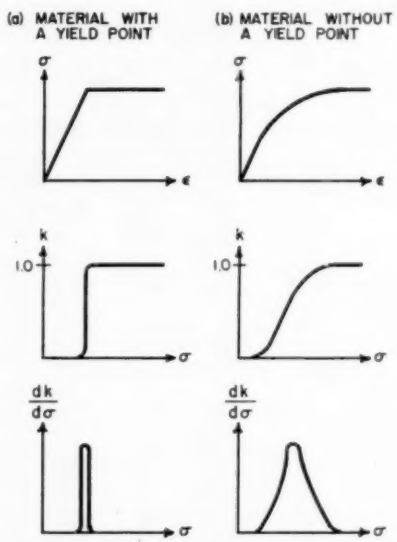

Fig. 1 Domain strength distribution for two types of materials

[1] By I. R. Whiteman, published in the March, 1959, issue of the JOURNAL OF APPLIED MECHANICS, vol. 26, TRANS. ASME, vol. 81, pp. 95–100.

[2] Assistant Professor, Department of Theoretical and Applied Mechanics, College of Engineering, University of Illinois, Urbana, Ill.

part of the thinking of people working in the field of flow and fracture. To physicists, the concept of a domain applies to dislocations and other atomic imperfections; to a metallurgist the concept may bring to mind slip bands, the random distribution of grain size and orientation in a metal, or possibly microresidual stresses.

A materials engineer may think of "internal stress concentrations," regions of nonuniform stress, and at least qualitatively be able to explain why there is such a thing as "size effect."

If solid-state physics and metallurgy concepts are ever successfully "married" to engineering design, it is the writer's opinion that the vows will be spoken in the language of statistical probability based on a domain or single-element model. The author is to be congratulated for contributing to the vocabulary of this language.

Author's Closure

It is a pleasure to read the comments of Professor Morrow. Many attempts have been made to obtain a suitable formula to describe the stress-strain diagram in a form that lends itself to the study of fatigue failure. It is to be hoped through use of concepts such as domains or elements or whatever else is developed that eventually a better understanding will result.

A model is of interest because its behavior is similar to that which occurs in reality. Assumptions are made which are probably not or are not fully realized in nature. However, if a better understanding of reality is obtained, this is more than sufficient justification for using the model.

Attempts to correlate the fatigue limit with points or combinations of points of the stress-strain curve have not proved too fruitful; it is felt that if success is to be obtained that the curve in its entirety must be considered.

Certain advantages accrue by describing the stress-strain curve in terms of some frequency distribution and being able to describe resulting hysteresis loops in terms of this same frequency distribution. As changes take place, the state at any time is reflected in the distribution; the frequency distribution at any time is some function of its past history. By the same token, starting with a known stress-strain diagram and a known history of the change of the hysteresis-loop width, the function which produces the history from the initial frequency distribution can be determined. At hand, then, is a method for describing the changes which take place with time in a measurable fashion; this is what is required for a quantitative description of fatigue phenomenon.

Theory of Flight of the Sounding Rocket[1]

R. A. STRUBLE.[2] This paper generalizes a closed-form solution of Blatz[3] apparently unknown to the author. The generalization, however, is superficial as the variable-drag-coefficient case treated by the author may be inferred from Blatz's constant-drag-coefficient case. In fact, the term $C_2\mathbf{M}^{-2}$ in $C_D = C_1 + C_2\mathbf{M}^{-2}$ corresponds to a constant in the general equation of motion, (2) of the paper, and thus may be absorbed (notationally) into the constant-thrust term. The mathematical solution of the more general case is then effected by the constant-drag-coefficient solution.

The author contributes materially to the usefulness of these closed-form solutions by a judicious choice of dimensionless performance parameters. His plots of these parameters versus altitude greatly facilitate trajectory calculations based on the analytical results.

The restriction to constant atmospheric density in the power-flight analysis limits the closed-form solution to small changes in altitude. This is a serious handicap in sounding rockets and somewhat annuls the acute treatment of the variable drag coefficient. In many cases, the variations in the drag term due to the density may be far more signifiant than those resulting from the drag coefficient! The writer suggests that both effects might be incorporated in the author's solutions. In fact, the empirical constants C_1 and C_2 impart very little physical significance and are merely selected to yield a good numerical representation of measured drag data. Thus, since the drag force

$$D = \frac{1}{2}\rho A v^2 C_D$$

itself is required in the equation of motion, one might better choose C_1 and C_2 so as to obtain a good numerical representation of the complete drag term D and not just C_D. For accelerating rockets (the only atmospheric case for which an approximate treatment of the drag term is justified) the velocity v increases with altitude. Hence the density ρ, which decreases with altitude, will decrease with increasing velocity. A numerical representation depicting the decay of both ρ and C_D with v thus appears feasible and will yield better engineering results within the same mathematical framework.

Such a procedure requires an *a priori* estimate of the density ρ as a function of v (or $\mathbf{M}$),[4] in addition to the measured drag data. Since the former ostensibly entails the trajectory solution itself, an iterative procedure is suggested. For example, one might obtain a preliminary estimate of the density-velocity relationship from a drag-free solution and plot $(\rho/\rho_0)C_D$ versus Mach number $\mathbf{M}$. The decay of the latter with $\mathbf{M}$ is then depicted by appropriate choices of the empirical constants C_1 and C_2 in the equation

$$\frac{\rho}{\rho_0} C_D = C_1 + C_2\mathbf{M}^{-2}$$

A drag-free solution has been suggested as a starting point since the corresponding trajectories[5] are readily available[6] and are inexact only as the drag becomes pronounced.[7] Thus if the foregoing preliminary estimate is used, then the author's solution can be expected to yield a similar representation and in most cases no further adjustment of the empirical constants will be required. In any event, iteration may be employed to yield the best possible representation of the complete drag term.

The free-flight analysis of the author appropriately includes variation of density with altitude. Interestingly enough, the latter closed-form solution has also been anticipated.[8]

[1] By V. C. Liu, published in the March, 1959, issue of the JOURNAL OF APPLIED MECHANICS, vol. 26, TRANS. ASME, vol. 81, pp. 127–129.

[2] Associate Professor of Mathematics, North Carolina State College of Agriculture and Engineering, Raleigh, N. C.

[3] P. H. Blatz, "Kinematics of a Vertical Booster," *Jet Propulsion*, vol. 24, 1954, p. 37.

[4] The dependence of sound speed on altitude may also be incorporated so that Mach-number dependence becomes more realistic.

[5] Note that a displacement, i.e., altitude, versus velocity relationship is required.

[6] H. D. Black, "Characteristics of the Vertical Trajectory," The Johns Hopkins University Applied Physics Laboratory Report No. CM-9444, August, 1958.

[7] R. A. Struble and H. D. Black, "A Generalized Closed Form for Burnt Velocity," *Jet Propulsion*, vol. 27, 1957, pp. 151–155, 168.

[8] H. G. L. Krause, "Strenge Integration der Bewegungsgleichung einer senkrecht aufsteingenden Rakete nach Brennschluss in der Erdatmosphar," *Space-Flight Problems*, Switzerland Astronautical Society, Biel, Switzerland (lectures held during Fourth Astronautical Congress, Zurich, 1953), p. 171.

Author's Closure

The author[3] is indebted to Professor Struble for calling his attention to the work of Blatz.[4]

The suggestion made by Professor Struble to take into account the variable density effect by using an iteration process in the power-flight analysis is a useful one. In fact, I might mention that in Ref. [3] of the paper under discussion the idea of using a preliminary estimate of the density-velocity relationship, as suggested by Professor Struble in the present discussion, had been incorporated in numerically integrating the equation of motion of a power-flight rocket. The difficulty in such an iteration method lies in determining in advance a *suitable* density-velocity relationship that is useful for a *long*-range power flight. One must keep in mind the fact that the most accurate method of treating the power-flight trajectory problem is available. This is by means of numerical integration of the equation of motion for the rocket. The purpose of my original paper under discussion is to present a simple labor-saving and useful approximation to this trajectory problem. For a multi-variable problem such as this, there are always numerous combinations of iteration processes that one can use to approximate the solution required. The degree of precision of the solution obtained often depends on the time one can afford to spend.

Forced Torsional Vibration of Systems With Distributed Mass and Internal and External Damping[1]

J. D. SWANNACK.[2] The distributed-damping paper has been studied with interest. An exact solution for the distributed-mass torsional system seems to round out the practical calculating schemes.

Some years ago, the writer's company used viscous dampers. Experience indicated the viscous-damper effect was so great that all internal damping in the engine could be neglected. At that time, complex Holzer methods were used even though distributed systems were used for undamped calculations.

As a practical matter, if one has IBM equipment available, the Holzer method still would seem preferable. With a desk computer, the distributed-damping scheme should save time.

Torsiograph tests have convinced the writer that engine damping might be well approximated by external damping only. The algebra would be somewhat relieved to drop the internal-damping term.

The author has contributed a number of useful methods for those who actually must carry out numerical vibration studies. As a last thought, even though it violates the spirit of the present paper, it would be interesting to see the damping concentrated at the location of the torque impulses (for the case of a multicylinder engine). One then has a simple system between torques. Should the writer again have to make engine-damping calculations, he would work out this last idea. The author's comment on this would be appreciated.

Author's Closure

Mr. Swannack's comments are much appreciated. In reference to his suggestion that the damping be concentrated at the sections where the torque impulses are applied, one can readily deduce this solution from the results of the paper. For intermediate sections between torque impulses, $\kappa_1 = \kappa_2 = 0$, hence $q = 0$, and Equations (8*a*) and (8*b*) reduce to

$$u(x) = C_1 \cos px + C_4 \sin px$$
$$v(x) = C_2 \cos px - C_2 \sin px$$

and similar simplifications follow in Equations (12) and (13). After working out the details of the analysis, one finds for the illustrative example discussed in the paper that

$$C_2' = \frac{\Gamma_{\xi l}\lambda_\xi + \mu_\xi}{\Delta} \cos p\xi$$

$$C_4' = \frac{\lambda_\xi - \Gamma_{\xi l}\mu_\xi}{\Delta} \cos p\xi$$

$$C_1' = -\gamma_l C_4'$$
$$C_2' = \gamma_l C_2'$$
$$C_1 = C_1' + C_4' \tan p\xi$$
$$C_2 = 0$$
$$C_3 = C_3' - C_2' \tan p\xi$$
$$C_4 = 0$$

Holzer Table 1

Mass No.	$\frac{I\omega^2}{10^6}$	θ	$\frac{I\omega^2}{10^6}\theta$	$\frac{M}{10^6}$	$\frac{\Sigma}{10^6}$	$\frac{C}{10^6}$	$\frac{\Sigma}{C} = \Delta\theta$
1	38.055	θ_1	38.025 θ_1	0	38.025 θ_1	84.5	0.45000 θ_1
2	2.535	0.55000 θ_1	1.39425 θ_1	0	39.41925 θ_1	42.25	0.93300 θ_1
3	2.535	−0.38300 θ_1	−0.970905 θ_1	0	38.44835 θ_1	42.25	0.91002 θ_1
4	2.535	−1.29302 θ_1	−3.27781 θ_1	0	35.17054 θ_1	42.25	0.83244 θ_1
5	2.535	−2.12546 θ_1	−5.38804 θ_1	$1 - 8.28929i\ \theta_1$	(29.78250 −8.28929i) θ_1 +1	42.25	(0.70491 −0.19620i) θ_1 +0.236
6	2.535	(−2.83037 +0.19620i) θ_1 −0.02367	(−7.17499 +0.49737i) θ_1 −0.059999	0	(22.60751 −7.79192i) θ_1 +0.94000	42.25	(0.53509 −0.18442i) θ_1 +0.02225
7	2.535	(−3.36546 +0.38062i) θ_1 −0.04598	(−8.53144 +0.96487i) θ_1 −0.11640	0	(14.07607 −6.82705i) θ_1 +0.82360		

[3] Now Professor of Aeronautical Engineering, The University of Michigan, Ann Arbor, Mich.

[4] By K. E. Bisshopp, published in the March, 1959, issue of the JOURNAL OF APPLIED MECHANICS, vol. 26, TRANS. ASME, vol. 81, pp. 8–12.

[1] Chief Design Analyst, Fairbanks, Morse and Company, Beloit, Wis. Mem. ASME.

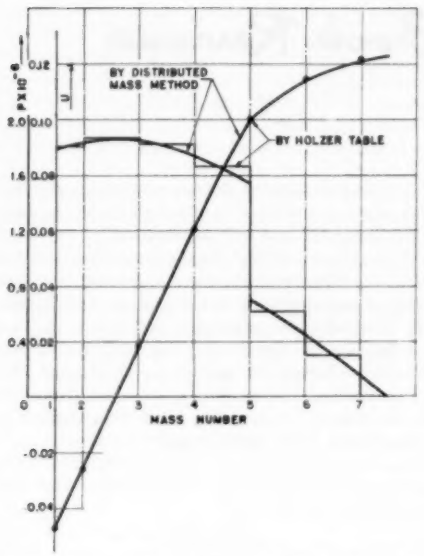

Fig. 1 Torque and displacement distribution for normal phase of motion

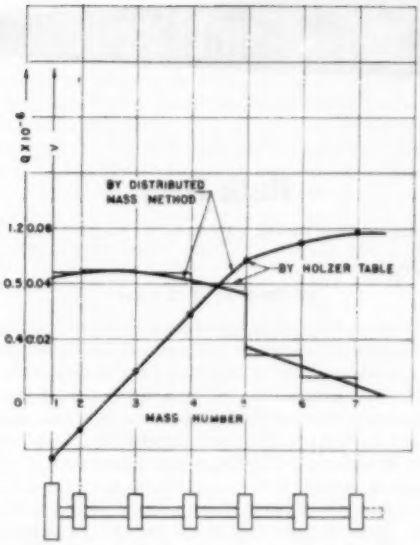

Fig. 2 Torque and displacement distribution for damping phase of motion

Holzer Table 2

Mass No.	$\frac{I\omega^2}{10^8}$	θ	$\frac{I\omega^2}{10^8}\theta$	$\frac{M}{10^8}$	$\frac{\Sigma}{10^8}$	$\frac{C}{10^8}$	$\frac{\Sigma}{C} = \Delta\theta$
1	38.055	−0.04737 −0.02297i	−0.80124 −0.87343i	0	−1.80124 −0.87343i	84.5	−0.02132 −0.01034i
2	2.535	−0.02605 −0.01263i	−0.6604 −0.3202i	0	−1.86728 −0.90545i	42.25	−0.04420 −0.02143i
3	2.535	0.01815 +0.0880i	0.04601 +0.02231i	0	−1.82127 −0.88314i	42.25	−0.04311 −0.02090i
4	2.535	0.06125 +0.02970i	0.15527 +0.07529i	0 0	−1.6660 −0.80785i	42.25	−0.03943 −0.01912i
5	2.535	0.10068 +0.04883i	0.25522 +0.1238i	+0.80956 +0.39265i	−0.60122 −0.29140i	42.25	−0.01423 −0.00690i
6	2.535	0.11491 +0.5575i	0.29130 +0.14133i	0	−0.30992 −0.15007i	42.25	−0.00734 −0.00355i
7	2.535	0.12225 +0.05930i	0.30990 +0.15033i	0	−0.00002 +0.00026i		

where

$$-\Delta = 1 + (\Gamma_{\xi l})^2$$

$$\gamma_l = \frac{\sin pl - \alpha p \cos pl}{\cos pl + \alpha p \sin pl}$$

$$\Gamma_{\xi l} = \kappa \cos p\xi \frac{\alpha p \cos (l - \xi) - \sin (l - \xi)}{\cos pl + \alpha p \sin pl}$$

$$\kappa = \eta\omega/pGI_p$$

$$\alpha = GI_p/I\omega^2$$

A comparative recalculation of the example given in the paper with $\kappa_1 = \kappa_2 = 0$ and all remaining parameters the same except $\eta = 6000$ gives the following Holzer tables and curves (Figs. 1 and 2).

Acknowledgment. The author is indebted to Mr. Ho Chong Lee of the Mechanical Engineering Department of Rensselaer Polytechnic Institute for aid in preparation of this reply.

Plastic Theory

Plastic Design of Steel Frames. By Lynn S. Beedle. John Wiley & Sons, Inc., New York, N. Y., 1958. Cloth, 9¼ × 6¼ in., xiii and 406 pp., illus. $13.

REVIEWED BY W. J. HALL[1]

THE theme of this recently published textbook is the application of the simple plastic theory to practical steel building design. The first two chapters are devoted to a presentation of the simple plastic theory. This is followed by a description of two of the more common methods of limit analysis in this area, namely, the statical and mechanism methods. Axial loads, shear, buckling, and other miscellaneous topics are discussed briefly in Chap. 4. Next comes a chapter devoted exclusively to the design of connections, followed by a short chapter on deflections and rotation capacity. There are problems at the end of each of the first six chapters. The last three chapters, Design Guides, Continuous Beam Design, and Steel Frame Design, occupy almost one half of the book and contain a summary of design provisions and procedures as well as a number of completely detailed illustrative designs. The emphasis on practical design should make this book of particular interest and use to design engineers. The book also serves as a practical companion reference to some of the more rigorous theoretical works recently published in this field in this country and abroad.

Nuclear Engineering

Introduction to Nuclear Engineering. Second Edition. By Richard Stephenson. McGraw-Hill Book Co., Inc., New York, N. Y., 1958. Cloth, 9¼ × 6¼ in., xi and 491 pp., illus. $9.50.

REVIEWED BY GLENN MURPHY[2]

THE second edition of "Introduction to Nuclear Engineering" differs from the first edition principally in the inclusion of information that has become available in the intervening four years. The new chapter that has been added on reactor core design is largely devoted to heat transfer with the inclusion of formulas on thermal stresses and four pages on hardware. It is rather unfortunate that the treatment in this chapter is not tied in with the chapter on reactor theory in such a way that it gives the reader a feeling for the influence of changes in the mechanical features upon the nuclear feasibility of the core.

The author has added a new chapter on thermonuclear power "in case fusion should ever replace fission as a source of energy," as he states in the preface. The treatment serves to give the reader a good introduction to the subject, and a number of references are included to assist those who are interested in more details of specific portions.

The second edition appears to be designed more for the practicing engineer who has some background in the field than it does for the nuclear engineering student. The book has a decidedly practical tone and contains an abundance of descriptive material; about fifty pages are devoted to descriptions of reactors. The book is well illustrated and well documented.

The book touches on most of the topics associated with reactor engineering, but falls somewhat short of serving as an introduction to nuclear engineering in that it does not include indications of the extensive industrial radioisotope utilization; the treatment of instrumentation is cursory, and the discussion of biological damage from radiation is scattered. The terms "health," "safety," "protection," "damage," or "biological damage" do not appear in the index. On the other hand, "hot channel factors" rates twelve entries in the index in various places.

The second edition is definitely an improvement over the first edition and contains much to interest the reader who is interested in an introduction to reactors.

Gas Dynamics

Mathematical Aspects of Subsonic and Transonic Gas Dynamics. By Lipman Bers. John Wiley & Sons, Inc., New York, N. Y., 1958. Cloth, 9¼ × 6 in., xv and 164 pp., illus. $7.75.

REVIEWED BY K. G. GUDERLEY[3]

THE BOOK by Dr. Bers is one of a series of survey articles in applied mathematics. According to the preface, "they are aimed not so much at the research specialist . . . as . . . at a broader mathematically literate audience looking for contemporary information . . . whether it be for the use in classrooms and seminars, or for the sake of possible applications to problems in other fields of science and engineering or simply for reasons of personal interest." These remarks may be supplemented by some sentences of the introduction: "This report on subsonic and transonic gas flows is written from the point of view of the mathematician. The choice of the material was greatly influenced by this point of view and the author's personal interest . . . we shall confine ourselves to problems which have been treated with a certain degree of sophistication."

A reader, particularly with the background of the physicist or engineer, will do well to keep these limitations in mind. The language *is* that of the mathematician, and no pretense is made to motivate the work done by its applicability. But this should not be considered as a drawback, for this approach is completely in keeping with the subject. An exception are the last twenty pages, which show examples of transonic-flow patterns. Seen from a mathematical point of view (without a physical motivation), these problems are rather uninteresting. Quite likely, this feeling is shared by the author. Inaccuracies in certain historical remarks, in details of many figures and gaps in the material presented, would thus find their explanation.

The first chapter gives the basic differential equations of the gas flow and of the hodograph and a rather complete survey of modifications which one may use to make the equations more tractable. A section on particular solutions of the hodograph method goes far beyond the standard tools of the aerodynamicist. The second chapter, mathematical background of subsonic flow theory, is concerned with the basic properties of the flow differen-

[1] Associate Professor, Department of Civil Engineering, University of Illinois, Urbana, Ill.

[2] Anson Marston Distinguished Professor of Engineering; Head, Department of Theoretical and Applied Mechanics; Chairman, Nuclear Engineering Administrative Committee, Iowa State College, Ames, Iowa.

[3] Chief, Applied Mathematics Branch, Aeronautical Research Laboratory, Wright Air Development Center, Wright-Patterson Air Force Base, Ohio.

tial equation. Besides some less esoteric subjects, such questions as smoothness of the solutions, unique continuation, maximum principle, quasiconformal mapping, pseudoanalytic function, and solutions in function space are treated. Chap. 3 gives some applications to problems in subsonic flow. Chap. 4 shows the mathematical background of transonic gas dynamics. The important discussions of the proper formulation of mixed subsonic-supersonic boundary-value problems is its main concern. Chap. 5 treats, first, subsonic flows with local supersonic regions and the important mathematical question of existence of such flows. This part will be of great interest to the aerodynamicist who may not be familiar with the original papers. Finally, there is a discussion of a number of transonic-flow problems.

The author has a great gift of presenting the essential ideas—in particular the more abstract mathematical questions—in a very lucid form. Naturally, the study of his book cannot replace the study of the original papers, but the book enables the reader to see the various methods in a perspective which would be very difficult to obtain by a direct study of the voluminous literature. Thus the aim of this article has been accomplished in an excellent manner.

Physics

Handbook of Physics. Edited by E. U. Condon and Hugh Odishaw. McGraw-Hill Book Co., Inc., New York, Toronto, London, 1958. Cloth, $10^1/_8$ in. × $7^1/_2$ in., xxvi and 1458 pp., illus. $25.

REVIEWED BY D. C. DRUCKER[4]

A most distinguished list of almost 90 contributors guarantee a very interesting and valuable book for the research engineer who must make more and more of physics his working tool. Dr. Condon sets the tone for much of the work by the very appropriate device of writing the introductory chapters of six of the nine parts of the Handbook: atomic physics, optics, heat and thermodynamics, electricity and magnetism, mechanics of deformable bodies, and mechanics of particles and rigid bodies. He contributes also to Part 1 on mathematics and is acknowledged in Parts 8 and 9, on the solid state, and nuclear physics.

As may be proper for a book written for physicists, the treatment of applied mechanics of solids is on the level of introductory lessons to graduate students. In this area it does not contain a compilation of useful results for the specialist nor are the references in general to the most modern or advanced work as in the chapter by Dr. Seeger on fluid mechanics.

Jet Propulsion Engines

Jet Propulsion Engines. Edited by O. E. Lancaster. Princeton University Press, Princeton, N. J., 1959. Cloth, $9^1/_2$ × $6^1/_2$ in., xvii and 799 pp., illus. $20.

REVIEWED BY B. H. GOETHERT[5]

This book is one of the well-known volumes of the "High Speed Aerodynamics and Jet Propulsion Series" published by Princeton University Press. It gives an extensive treatment of the wide field of jet propulsion ranging from the primitive historic forms of jets to the various forms of air-breathing jet engines and finally to the modern rocket engines of various types. This book is written in the language of the engineer and assumes as a prerequisite the knowledge of the fundamental laws of physics and chemistry as presented, for example, in the various other volumes of the high-speed aerodynamics series. It is notable that for each major chapter of this book a separate literature list is assembled.

The individual chapters of this volume are written by well-known engineers and scientists in the particular field; for example, turbojet engines by C. A. Meyer; turboprop engines by Ivan H. Driggs and Otis E. Lancaster; ramjets by DeMarquis D. Wyatt and Bruce T. Lundin; intermittent jet engines by Joseph F. Foa; liquid-propellant rockets by Martin Summerfield; solid-propellant rockets by C. E. Bartley and Mark M. Mills; ram-rockets by Irvin Glassman and Joseph V. Charyk; jet rotors by A. Gail; nuclear engines by Ralph Zirkind; and future prospects of jet propulsion by F. Zwicky.

First, a very informative chapter on the history of jet propulsion is presented. The most important milestones in the development of air-breathing engines and rocket engines from the first modest attempts to the present-day sophisticated engines are described. Extensive chapters of the book are devoted to the various types of air-breathing engines, like turbojets and their various modifications, ramjets, intermittent jets, etc. Emphasis is placed on the analysis of the gas cycles involved, deriving the various forms of efficiencies and investigating which type of engine offers the most favorable conditions for high efficiencies or high specific thrust output. It allows the reader to obtain a quick and fundamentally correct over-all picture of the merits of the various propulsion systems for different applications. A selected group of quantitative values for specific engine parameters, like unit mass flow, unit weight, specific fuel consumption, etc., are summarized in graphs for a large number of specific engines in the past 20 years.

In a similar manner, the performance of liquid-propellant as well as solid-propellant rockets are analyzed. Starting with the equations for an ideal rocket engine, the numerous departures from ideal behavior are covered in detail. Particularly, the various types of combustion instability and hot starts are discussed and suitable rules for suppressing these detrimental phenomena are reviewed.

A jet propulsion review would be incomplete when the potential of atomic energy for propulsion purposes would not be considered. Due to security restrictions, however, only the basic principles as far as are covered in the published literature could be discussed. This section presents a condensed valuable review of the problems associated with the design of nuclear reactors without being specifically restricted to jet propulsion. The book concludes with a comparative discussion of the potential of numerous possible propulsion systems on the basis of the fundamental laws of science.

In summary, the volume "Jet Propulsion Engines" with its extensive review of present-day propulsion techniques and potential of new principles, backed up by a large list of references, is a valuable book for the practical engineer engaged in engine development and testing, and the student as an introduction to the propulsion field.

Stress and Strain

Introduction to the Theoretical and Experimental Analysis of Stress and Strain. By A. J. Durelli, E. A. Phillips, and C. H. Tsao. McGraw-Hill Book Co., Inc., New York, N. Y., 1958 (Series in Mechanical Engineering). 498 pp. $12.50.

REVIEWED BY D. H. PLETTA[6]

This book is intended to introduce engineering seniors or first-year graduate students to the theory of elasticity (Part I) and to experimental stress analysis (Part II). The first six chapters

[4] Professor and Chairman, Division of Engineering, Brown University, Providence, R. I.

[5] Chief, Engine Test Facility, ARO, Inc., Tullahoma, Tenn.

[6] Professor and Head, Department of Applied Mechanics, Virginia Polytechnic Institute, Blacksburg, Va.

develop the elasticity equations for the three-dimensional state and apply this theory mainly to two-dimensional problems. There is an excellent discussion of the various methods for representing stress and strain graphically. These include the stress ellipse, Cauchy's stress quadric, Mohr's circle, the diadic circle, and so on. This treatment will prove helpful to a beginner. A chapter is devoted to the properties of families of curves encountered in experimental analysis, such as isoclinics, isobars, etc.

Part II deals with strain measurements and gives an excellent treatment of the application of statistical methods in experimental analysis, and of dimensional analysis as well. Photoelasticity and bonded electrical strain gages are mentioned briefly. The main emphasis is placed on grid methods, brittle coatings, and stress coat. A chapter on mechanical strain gages is also included.

The book has a lucid style and treats topics so thoroughly that individuals wholly unfamiliar with this subject should have little difficulty following the text material or problems. On the other hand, even an expert will find a study of much of Part II worth while. A series of exercises is included for most of the chapters which should make it valuable as a text. References are cited in only a few of the chapters, but this omission in the remaining portion of the book is probably not serious.

Nuclear Engineering

Nuclear Engineering Handbook. Edited by H. Etherington. McGraw-Hill Book Co., Inc., New York, 1958. 1872 pp. $25.

REVIEWED BY R. J. GOLDSTEIN[7]

This latest and without doubt most ambitious compilation of nuclear technology by some 70 contributors falls in the category of a general reference work. It follows the trend in present-day handbooks toward greater emphasis on presentation of formally written articles rather than primarily a collection of tables. Considerable tabulated data are of course requisite in a work of this type and are present in the various sections. The diversity of technical fields that converge into nuclear engineering is amply shown by the coverage extended to such subjects as mathematical analysis, nuclear physics, isotope separation, chemistry, health physics, reactor control, heat transfer, reactor materials, and mechanical design among others.

Of particular interest to readers of this journal are the sections on fluid flow, heat removal, and thermal stresses. The first two of these contain a large amount of information in a very handy presentation. They do, however, lack a certain freshness, essentially being abridgments of similar material recently presented by the same author in a separate book. The section on thermal stresses is quite brief. Physical properties of heat-transport fluids are tabulated, and the thermal properties of solids often encountered in reactors or associated equipment are presented in various sections.

The editor and the authors have concentrated on a logical presentation of a tremendous amount of information including theory, experimental data and properties, empirical correlations, and descriptive material. The lack of rigor is understandable, in fact, desirable in such a handbook. Adequate references are given to aid in the pursuit of further information.

[7] Assistant Professor of Engineering, Brown University, Providence, R. I.

Classical Mechanics

Classical Mechanics. By J. W. Leech. Methuen & Company, Ltd., London, 1958, and John Wiley & Sons, Inc., New York, N. Y., 1959. Cloth, 149 pp. $2.50.

REVIEWED BY R. B. LINDSAY[8]

The appearance of this new volume in the very useful "Methuen's Monographs on Physical Subjects" is a welcome indication of the realization of the importance of classical mechanics as a foundation for a large part of modern theoretical physics as well as its applications. There has grown up in some quarters a tendency to short circuit basic classical mechanics in order to enable the student to pass more quickly to quantum and statistical mechanics as well as the more advanced parts of applied mechanics for engineers and applied mathematicians. Though understandable in part from the exigencies of time, it is nevertheless an unfortunate attitude. It provides a challenge to the clever expositor to provide in relatively brief compass a treatment of those aspects of the subject which are of greatest importance for the future investigator. The author of the present volume has met this challenge rather well and has produced a well-written book which should be of value to students of physics, engineering, and applied mathematics.

Emphasis is properly placed on the prime position of the Lagrangian and Hamiltonian formulations. These are deduced in the first instance from Newton's laws, but are later shown to be derivable from a variational principle like that of Hamilton. The classical transformation theory is explained and Poisson brackets are introduced in order to smooth the transition to quantum mechanics. The Lagrangian and Hamiltonian methods are also applied to continuous systems and this gives a chance to discuss the classical mechanics of fields. There is a brief treatment of relativistic mechanics.

The analysis does not demand much beyond a working knowledge of calculus and differential equations. Though the reasoning is couched in very concise terms, methods and results are in most cases illustrated by well-chosen examples.

Sound Pulses

Sound Pulses. By F. G. Friedlander. Cambridge University Press, New York, N. Y., 1958. Cloth, $8^3/_4 \times 5^3/_4$ in., xi and 202 pp., illus. $7.50.

REVIEWED BY R. B. LINDSAY[9]

The term "sound pulse" as used by the author of this book refers to an aperiodic disturbance in an elastic fluid medium, which has a clearly defined front. The book is devoted to a mathematical discussion of such pulse fronts treated as characteristics of the acoustical wave equation. The treatment is restricted to the linearized case, but shock-front propagation is discussed as an example of geometrical acoustics.

The author gives detailed analysis of such problems as the reflection of a pulse by surfaces of revolution and the diffraction of a pulse by a wedge. The book is primarily a mathematical exercise in the theory of linear partial differential equations of the hyperbolic type, but many of the results obtained will be of use to workers in the field of practical wave propagation.

[8] Dean of the Graduate School and Hazard Professor of Physics, Brown University, Providence, R. I.

[9] Dean of the Graduate School and Hazard Professor of Physics, Brown University, Providence, R. I.

Journal of APPLIED MECHANICS

Information for Authors

• Manuscripts should be submitted in final form to the Technical Editors. Each manuscript must be accompanied by a statement that it has not been published elsewhere nor has it been submitted for publication elsewhere. A paper which would occupy more than five pages of the Journal may be returned to the author for abridgment.

• The author should state his business connection, the title of his position, and his mailing address. A short abstract (50 to 100 words) should be included on the first page immediately preceding the introductory paragraph of the paper.

• Three copies of the manuscript are required. One of these must be a carefully prepared printer's copy, typed in double spacing, on one side of the page only, with wide margins, on $8^1/_2$ by 11-in. opaque white paper. Mimeographed manuscripts, if prepared with exceptional care, can be accepted provided they are completely edited.

• As far as possible, all mathematical expressions should be typewritten. Greek letters and other symbols not available on the typewriter should be carefully inserted in ink. Care should be taken to distinguish between capital and lowercase letters, between zero (0) and the letter (*O*), between the numeral (1) and the letter (*l*), etc. A letter representing a vector cannot be printed with an arrow above or below it. The letter should be underscored with a single wavy line, wherever it appears in the text, to designate boldface type. A list of symbols carefully marked for the use of the editor (thus: κ, Greek l.c. kappa), if it has not been included in the body of the paper, should accompany the manuscript on a separate page.

• Before preparing a manuscript the author should study printed articles in the Journal, with special attention to the form and style of mathematical expressions, tables, footnotes, references, and abstract. Numbers that identify mathematical expressions should be enclosed in parentheses. Numbers that identify references at the end of the paper should be enclosed in brackets. Care should be taken to arrange all tables and mathematical expressions in such a way that they will fit into a single column when set in type. Equations that might extend beyond the width of one column (fractions that should not be broken or long expressions enclosed in parentheses) should be rephrased to go on two or more lines within column width. Fractional powers are preferred to root signs and should always be used in more elaborate formulas. The solidus should be used instead of the horizontal line for fractions wherever possible.

• A normal paper should not exceed five pages in the Journal. It is about 6000 words or twenty to twenty-five double-spaced typewritten pages inclusive of drawings. A Brief Note should not exceed 750 words or about one column in the Journal inclusive of drawings.

• Originals and two copies of figures must accompany the manuscript. Line drawings should not be larger than $8^1/_2 \times 11$ inches and should be planned for reduction to column width. Lettering should be large enough to be clearly legible when the illustration is reduced. The originals of line drawings must be in India ink on white or pale blue tracing paper or tracing cloth. Photographs of equipment or test specimens must be glossy prints and should be used sparingly. Captions for figures should be typed double-spaced and included as the last page of the manuscript. The figure number and author's name should be written in the margin or on the back of each illustration.

• Titles of papers should be brief.

• Authors can obtain copies of the ASME Manual MS-4, "An ASME Paper," from the Technical Editors and are urged to do so before drafting their papers in final form.

• Papers published in the Journal of Applied Mechanics must be presented at a Meeting, either in person or by title. Scheduling of papers is in the hands of the Secretary of the Applied Mechanics Division. Authors should indicate their preference in this respect to the Technical Editors when submitting a paper.

• An author is entitled to 25 preprints free of charge (in the case of two authors, 15 each; three or more authors, 10 each). Larger quantities of preprints or reprints can be ordered from Editorial Department, The American Society of Mechanical Engineers, 29 West 39th Street, New York 18, N. Y. Quotations will be sent on request.

ASME Publications Committee

Please address all communications to:

Technical Editors

Journal of Applied Mechanics, ASME

Division of Engineering

Brown University

Providence 12, R. I.

TENTH INTERNATIONAL CONGRESS OF APPLIED MECHANICS

Stresa, Italy, August 31–September 7, 1960

The technical sessions of the Congress, apart from a number of invited general lectures, will be held in two sections:

Section 1: Fluid dynamics (hydrodynamics and aerodynamics)

Section 2: Mechanics of solids (rigid-body dynamics, vibrations. elasticity, plasticity, and theory of structures)

It should be noted that thermodynamics and computational methods as such are not included, although specific applications of computational methods to pertinent problems of one of the two sections mentioned are acceptable subjects for papers to be read at the Congress.

Abstracts of papers should be submitted in four copies to Dr. W. C. Koiter, Secretary of the International Committee, Prof. Mekelweg 2, Delft, The Netherlands, before January 1, 1960.

The abstracts should not exceed two typewritten double-spaced pages, but in no case should they exceed four pages. It is recommended that abstracts be in two of the official Congress languages (English, French, German, and Italian). Authors are urged to make their abstracts as clear as possible, since selection of papers has to be based upon them. Decisions of the Program Committee are final, and it will be understood that it is impossible to enter into correspondence about them with authors of papers. Authors will be informed promptly of the decision on each paper.

Day-by-day organization of the Congress is effected by the Italian Organizing Committee (President: Prof. G. Colonnetti. Secretary: Dr. F. Rolla). Information on accommodations, also registration forms, should be addressed to: Dr. F. Rolla, Consiglio Nazionale delle Ricerche, Uffizio relazioni internationali, Piazza della Scienza 7, Rome, Italy.

The Proceedings of the Congress will contain the invited general lectures at full length and abstracts of papers accepted for presentation at one of the sections. Authors are therefore permitted to submit their papers for publication in a scientific journal provided that such publication should not occur before the presentation of the paper at the Congress.

Executive Committee of the International Committee for the Congresses of Applied Mechanics:

C. B. Biezeno, President;
Richard V. Southwell;
W. T. Koiter, Secretary.